Netherlands Enterprise Agency

Metocean Assessment Modelling Report

IJmuiden Ver Wind Farm Zone

>> *Sustainable. Agricultural. Innovative. International.*

Netherlands Enterprise Agency

RVO Approval for Publication

Document Characteristics

Version	Title	Date of Publication	Reference Contractor	Reference RVO
1.0	Metocean Assessment Modelling report IJmuiden Ver Wind Farm Zone	December 22nd , 2023	11827690	WOZ2220015

Approval

Approval for public disclosure	Position
Daniëlle Gerritsma	Project Manager RVO Offshore Wind Energy
Matté Brijder	Senior Project Manager RVO Offshore Wind Energy

Statement RVO

The underlying report presents normal- and extreme design values for wind, waves, water levels and currents as derived by DHI using proprietary methods at one analysis location in the IJmuiden Ver Beta wind farm zone. DHI have stated that the presented values represent their most accurate estimates based on the most advanced methods known and available to them during the study and that during the estimation process no choices were made that lead to conservatism.

These results are updates to RVO's previously published precedents. Users should make their own decisions on what values to use for preliminary and/or detailed engineering design. RVO has decided in discussion with DHI to publish a non-certified, concise metocean assessment report due to time constraint related to the permit tender. A complete and final certified report pertaining to more analysis locations and maps of normal and extreme conditions will follow in 2024, after the IJmuiden Ver Alpha and Beta permit tender.

IJmuiden Ver Wind Farm Zone

Part A: Metocean Modelling

Rijksdienst voor Ondernemend Nederland

20.12.2023

Prepared for Rijksdienst voor Ondernemend Nederland (RVO)

The expert in **WATER ENVIRONMENTS**

IJmuiden Ver Wind Farm Zone

Part A: Metocean Modelling

Prepared for: Rijksdienst voor Ondernemend Nederland (RVO)
Represented by Ms. Danielle Gerritsma

Contact person: Ameya Sathe, amsa@dhigroup.com
Project Manager: Ameya Sathe
Quality Supervisor: Eduardo Gonzalez - Gorbena Eisenmann, Ameya Sathe
Author: Daniel Caichac, Joana Mendes, Helene Syneva Wellm Resende de Paiva, Cecilie Borch Devantier

Project No.: 11827690
Approved by: Jesper Ulrik Fuchs
Approval date: 20.12.2023
Revision: Final 1.0
Classification: **Open:** This document may be shared inside and outside the DHI Group entities without the client's prior approval.
File name: 11827690_IJV_DHI_Metocean_Modelling.docx

DHI A/S • Agern Allé 5 • • DK-2970 Hørsholm • Denmark
Telephone: +45 4516 9200 • dhi@dhigroup.com • www.dhigroup.com • Company Reg. No.: DK36466871

Contents

Figures

Tables

Appendices

Revision History

Revision	Date	Reviewer	Approver	Comments
Draft 0.1	29-11-2023	AMSA	JUF	First draft
Draft 0.2	12-12-2023	AMSA	JUF	Second draft incorporating comments from RVO
Final 1.0	20-12-2023	AMSA	JUF	Final revision incorporating revised comments from RVO

Nomenclature

Abbreviations	
BSH	Federal Maritime and Hydrographic Agency of Germany - Bundesamt für Seeschifffahrt und Hydrographie
CMEMS	Copernicus Marine Environment Monitoring Service
DWF	Dutch Wind Farm
DA	Data Assimilation
DTM	Digital Terrain Model
ECMWF	European Centre for Medium-Range Weather Forecasts
EMODnet	European Marine Observation and Data Network
ERA5	ECMWF Reanalysis 5
FM	Flexible Mesh
GWM	Global Wave Model
HD	Hydrodynamic
HKN	Hollandse Kust (noord)
HKW	Hollandse Kust (west)
HKZ	Hollandse Kust (zuid)
IJV	IJmuiden Ver
IOS	Institute of Oceanographic Sciences
KNMI	Koninklijk Nederlands Meteorologisch Instituut
LAT	Lowest Astronomical Tide
MSL	Mean Sea Level
MOOD	DHI's Metocean-On-Demand Portal
NE	North Europe
OWF	Offshore Wind Farm
QA	Quality Assurance
QQ	Quantile-Quantile
RVO	Rijksdienst voor Ondernemend Nederland
RWS	Rijkswaterstaat
SW	Spectral Wave
TNW	Ten noorden van de Waddeneilanden
UTC	Coordinated Universal Time (Universal Time Coordinated)

UTM	Universal Transverse Mercator
WL	Water Level
WOZ	Wind op Zee
WRF	Weather Research & Forecasting Model
WGS84	World Geodetic System 1984

Subscripts	
2DH	2D Depth Averaged
NE	North Europe
DA	Data Assimilation
Total	Total signal of WL, CS and CD
Tide or Tid	Tidal component of WL, CS and CD
Res	Residual component of WL, CS and CD
z	WS, WD, CS and CD at specific vertical level z
Sea	Wind-sea component of wave spectrum
Swell	Swell component of wave spectrum

Definitions	
Time	Times are relative to UTC
Level	Levels are relative to MSL (if not specified otherwise)
Coordinate system	Project coordinate system is ETRS 89 UTM 31N (EPSG:25831) Numerical models are set up in Lon/Lat WGS84 (EPSG:4326)
Direction	Directions are 30 bins relative to true north, i.e., 12 bins covering: 30 deg: 0° = ÷15° -15°N, 30° = 15°-45°N, etc. Clockwise from North Wind and Waves: °N coming from Current: °N going to Nautical convention was used
Time averaging	All time averages are based on a central window rolling averaging

Symbols		Units
$AirDen_z$	Air Density @ z mMSL	Kg/m^3
$AirPres_z$	Air Pressure @ z mMSL	hPa
CD	Current Direction	°N (going to)
CS	Current Speed	m/s
WL	Water Level	m
WS_{10}	Wind speed at 10 mMSL	m/s
WD_{10}	Wind direction at 10 mMSL	°N (coming from)
WS_{30}	Wind speed at 30 mMSL	m/s
WD_{30}	Wind direction at 30 mMSL	°N (coming from)
DSD	Direction Standard Deviation	°
H_{m0}	Spectral Significant Wave Height	m
Max	Maximum	-
Min	Minimum	-
MSLP	Mean Sea Level Pressure	hPa
MWD	Mean Wave Direction	°N (coming from)
N	Sample count	-
PBL height	Planetary Boundary Layer Height	mMSL
Px	x% Percentiles	-
PWD	Peak Wave Direction	°N (coming from)
RH_z	Relative humidity @ z mMSL	
Std or σ	Standard deviation	-
SST	Sea Surface Temperature	°C
SWSR	Short Wave Solar Radiation	W/m^2
T_{01}	Spectral equivalent of mean wave period	s
T_{02}	Spectral equivalent of zero-down-crossing wave period	s
$T_{air,zm}$	Air Temperature @ z mMSL	°C
T_p	Peak Wave Period	s
T_z	Mean zero-crossing wave period	s
N, E, S, W	North, East, South and West	-
z	Vertical coordinate, positive up	mMSL
d	Water depth	m

Executive Summary

In English

This report provides background information on the numerical models set up to establish the meteorological and oceanographic (metocean) conditions for the IJmuiden Ver (IJV) Offshore Wind Farm Zone.

Under contract with Rijksdienst voor Ondernemend Nederland (RVO), DHI A/S (DHI) established dedicated high-resolution (down to ~400 m) state-of-the-art hydrodynamic and spectral wave numerical models (based on DHI's MIKE21 software package) covering the 44-year period from 1979 to 2022 to provide metocean conditions in the IJmuiden Ver (IJV) Offshore Wind Farm Zone. High-resolution wind and pressure fields downscaled from ERA5 with WRF were applied as model forcing to the wave and flow models.

A local hindcast 2D hydrodynamic model was set up to simulate water levels and currents using the MIKE 21 HD model. The model domain covers not only the IJV Offshore Wind Farm Zone, but also most of the Dutch Exclusive Economic Zone of the North Sea, thus comprising all the offshore wind farm search areas within Dutch maritime boundaries.

The waves were similarly simulated using the MIKE 21 SW spectral wave model, covering the same domain as the hydrodynamic model.

Extensive validation of the models was conducted using a comprehensive set of wind, water level, current, and wave measurement data. The validation showed very good model performance and thus ensured accurate high-quality metocean conditions not only at IJV but also across the whole feasibility domain area.

A comprehensive web-based digital database is provided, which enables users to access the modelling data and the analysis result at one location through a user-friendly web interface called MOOD[1].

Normal and extreme metocean conditions are described in detail in a separate report.

[1] https://www.metocean-on-demand.com/

In Dutch

Samenvatting

Dit rapport verschaft achtergrondinformatie over de numerieke modellen die zijn ontwikkeld om de meteorologische en oceanografische (metocean) condities voor de IJmuiden Ver (IJV) Offshore Windparkzone in kaart te brengen.

In opdracht van de Rijksdienst voor Ondernemend Nederland (RVO) heeft DHI A/S (DHI) hoge resolutie (tot ~400 m), state-of-the-art, hydrodynamische en spectrale numerieke golfmodellen ontwikkeld (gebaseerd op het DHI's MIKE21-softwarepakket). De modellen bestrijken een periode van 44 jaar (van 1979 tot en met 2022), met als doel de metoceanische omstandigheden in de IJmuiden Ver (IJV) Offshore Windparkzone vast te stellen. De golf- en stromingsmodellen zijn aangedreven door hoge resolutie wind- en luchtdrukgegevens die zijn gebaseerd op gedownscalede ERA5 en WRF-modellen.

Een lokaal 2D hydrodynamisch hindcastmodel (een model met historische simulaties) is opgezet om waterniveaus en zeestromingen te simuleren met behulp van het MIKE 21 HD-model. Het modeldomein bestrijkt niet alleen de IJV Offshore Windparkzone, maar ook het grootste deel van de Nederlandse Exclusieve Economische Zone van de Noordzee en omvat derhalve alle zoekgebieden voor offshore windparken binnen de Nederlandse maritieme grenzen.

De golven zijn op soortgelijke wijze gesimuleerd met behulp van het MIKE 21 SW spectrale golfmodel, dat hetzelfde domein bestrijkt als het hydrodynamische model.

De modellen zijn uitgebreid gevalideerd met behulp van een omvangrijke reeks aan wind-, waterniveau-, stromings- en golfmeetgegevens. De validatie laat een zeer goede prestatie van het model zien, wat de beschikbaarheid van accurate, kwalitatief hoge metocean gegevens garandeert, in zowel de IJV Offshore Windparkzone als het hele haalbaarheidsdomein.

Via de gebruiksvriendelijke webinterface genaamd MOOD[2], hebben gebruikers toegang tot een uitgebreide digitale database waar de modelleringsgegevens en de analyseresultaten in te vinden zijn.

Normale en extreme metocean condities worden gedetailleerd beschreven in een afzonderlijk rapport.

[2] https://www.metocean-on-demand.com/

1 Introduction

This study has been developed as a part of the metocean assessment for Dutch Wind Farm Zones. The assessment includes detailed modelling of the metocean conditions in the wind farm zones together with a comprehensive metocean analysis using the state-of-the-art modelling and analysis methods. This report presents detailed metocean modelling in the IJmuiden Ver Wind Farm Zone.

The Dutch government has developed a Routekaart Wind op Zee[3], which sets out the development of offshore wind energy up to a total capacity of approximately 21 GW by 2030, enough to supply 8.5% of all the energy in the Netherlands.

The IJmuiden Ver (IJV) Wind Farm Zone (IJVWFZ, Project sites) has been identified by Rijksdienst voor Ondernemend Nederland (RVO) as an area of potential wind energy development. The Project site is in the Dutch Exclusive Economic Zone on the Dutch shelf in the North Sea. It lies approximately 62 km from the west mainland coast of the Netherlands.

Within the IJVWFZ, RVO has identified three offshore wind farm sites (OWF) for development, labelled IJV Alpha OWF, IJV Beta OWF and IJV Gamma OWF. Two additional OWF zones have also been identified by RVO, namely Nederwiek and Doordewind, in the vicinity of IJVWFZ. Exact information on the location and shape of the project sites can be found through the online portal of RVO [1]. The locations of the project sites are presented in Figure 1.1.

RVO plays a central role in the tendering process for Dutch Offshore Wind Farm Zones. Preliminary investigations are carried out for suitable sites, and their results are published as part of the tendering process. As part of the bid calculation, the bidder needs as detailed information as possible to estimate the metocean conditions in the area. To address this requirement, DHI has carried out comprehensive metocean modelling and analyses. The results produced by DHI aim to provide the input required for the bidders to use in their preliminary front-end engineering design (Pre-FEED) and arrive at an optimal bid. The modelling is carried out for the feasibility domain. The analysis is carried out at one location (named IJV1) in IJVWFZ, as indicated in Figure 1.1.

One of the main requirements of RVO in this study was to have an alignment between the wind resource assessment (WRA) and the metocean analysis. To address this requirement, DHI A/S (DHI) formed and led a consortium with partners OWC and C2 Wind Aps. OWC, together with its partners ProPlanEn, ArcVera and Innosea, were responsible for the development of the mesoscale modelling and wind resource assessment [2]. DHI carried out the modelling of water levels, currents, and waves that is presented in this report. DHI is the overall responsible for all the deliveries in the project.

[3] https://windopzee.nl/onderwerpen/wind-zee/wanneer-hoeveel/wind-zee-rond-2030/

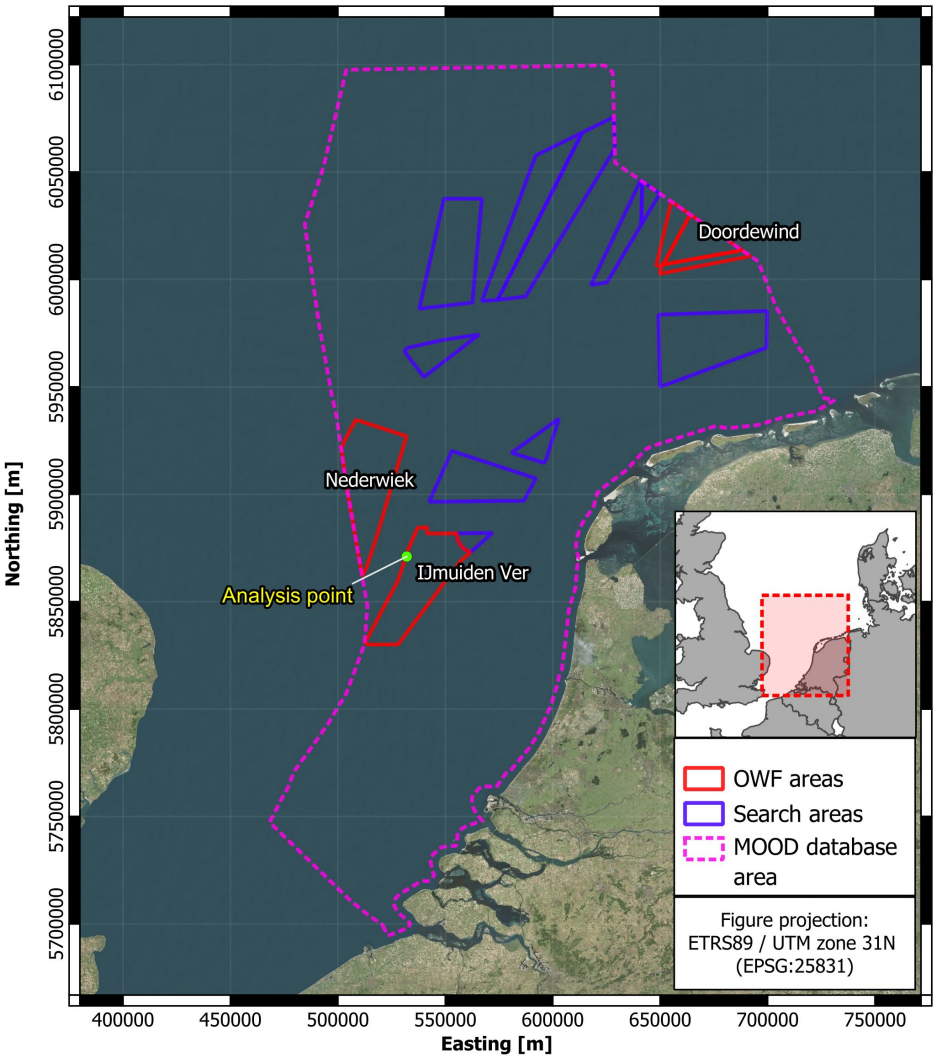

Figure 1.1 Area of coverage of this study by DHI shown in magenta called feasibility domain (MOOD database area).
The modelling is carried out for the feasibility domain. The analysis is carried out at one location (named IJV1) in the IJVWFZ.

1.1 Scope of the study

The scope of the study was twofold:

1. To perform comprehensive metocean modelling across the feasibility domain (see Figure 1.1) containing the IJVWFZ.
2. To perform detailed metocean analyses at one location in the IJVWFZ (see Figure 1.1 and Figure 1.2).

The study is presented in two separate reports tackling each scope. This report presents the former comprehensive metocean modelling, whereas [3] presents the latter detailed metocean analyses. It is noted that only the near-surface winds are considered in this report for forcing the metocean models. Winds at other heights are reported in [2] and [3].

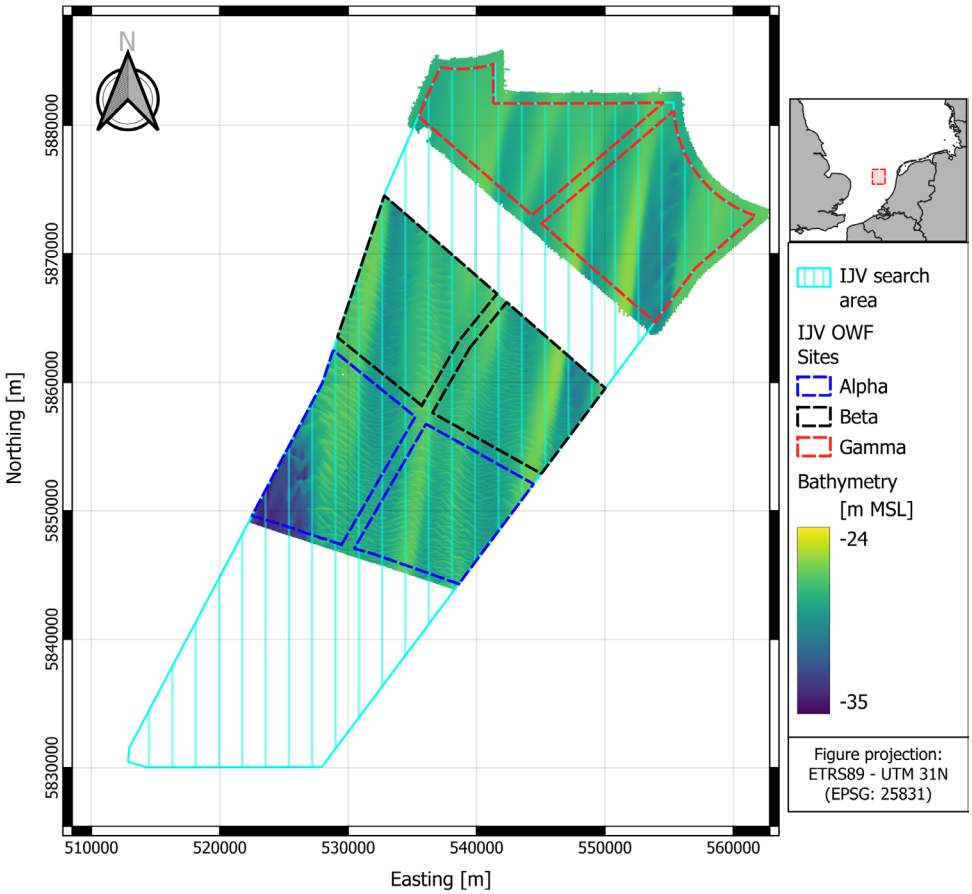

Figure 1.2 IJVWFZ comprising of three sub zones, Alpha, Beta, and Gamma.

1.2 Conventions

Unless noted otherwise, the following conventions are used throughout the study and this report (see Figure 1.3).

1. Elevations are given as distance above MSL.
2. Directions are relative to North (0°) with clockwise direction as positive (e.g., East is 90°).
3. Wind and wave directions are designated by the direction they come from.
4. Current directions are designated by the direction it is heading.
5. The reference coordinate system is ETRS 89 UTM 31N (EPSG:25831). The numerical models are set up in Lon/Lat WGS84 (EPSG:4326).
6. English Style Guide of the European Commission [4] is applicable throughout the document. Point is used as a decimal separator in this study. It is noted that no thousand grouping was used in this study deviating from the same guideline.

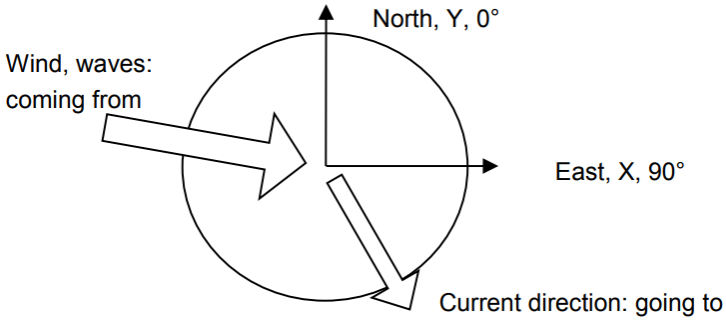

Figure 1.3 Conventions of directions.

1.3 Report structure

This report is arranged as follows:

- Section 2 presents the data that was used for establishing, calibrating and validating the numerical wind, hydrodynamic and wave models such as the measurements acquired from RVO and from other sources, e.g., bathymetry data, wind, wave, water level and current measurements. This section includes details about the different quality flags available in the measurements as well as description of different post-processing workflows applied to the raw data (data filtering, acceptable limits, depth-averaging of currents, etc.).
- Section 3 summarises the hydrodynamic and wave models used to establish the data for this project and provides details of the models' setup and validation against local measurements. Additionally, a short summary and validation is provided of the mesoscale atmospheric model developed specifically for this project, while the details of it are shown in a separate report that comprises the wind resource assessment [2].
- Section 4 presents the data sources that were used to retrieve other atmospheric variables, such as air temperature, pressure and density, lighting, and visibility.
- Section 5 presents the data sources that were used to retrieve other oceanographic variables, such as sea surface temperature, density and salinity, sea ice, and marine growth.
- Section 6 presents a brief comparison of the model performance when compared with the previous models developed for Dutch offshore windfarms.
- Section 7 briefly describes the web-based metocean database for IJmuiden Ver OWF provided as part of this study.
- Section 8 presents the list of references used in this study.

2 Measurement Data Basis

This section provides information about the measurement data provided by RVO or acquired by DHI and applied for calibration/validation of the numerical models that formed the basis for the metocean data analyses. It also presents the bathymetry data applied to make the high-resolution computational mesh for the modelling process.

2.1 Bathymetry data sources

This section provides information about the bathymetry data sources and processing applied to establish the computational meshes for the hydrodynamic (HD_{DWF23}) and spectral wave (SW_{DWF23}) modelling activities at IJmuiden Ver OWF.

The bathymetry datasets used in this study were EMODnet v2020's Digital Terrain Model[4] (DTM), Rijkswaterstaat's bathymetric measurements along the Dutch coasts (Vaklodingen[5]), FUGRO's bathymetric measurements at the HKZ, HKN and HKW wind farm zones, MMT SWEDEN AB's bathymetric survey for the TNW wind farm zone, GEOxyz's bathymetric survey of IJmuiden Ver wind farm zone (alpha and beta) and FUGRO's bathymetric survey of IJmuiden Ver Wind Farm Zone (gamma).

The site bathymetry is characterised by several north-south oriented sand banks with heights ranging from a few metres up to 10 m, and by smaller scale sand waves oriented perpendicularly to the sand banks. The bathymetry survey of sites alpha, beta and gamma is shown in Figure 2.1 along with an indication of the sand banks and sand waves.

[4] https://portal.emodnet-bathymetry.eu/
[5] https://publicwiki.deltares.nl/display/OET/Dataset+documentation+Vaklodingen

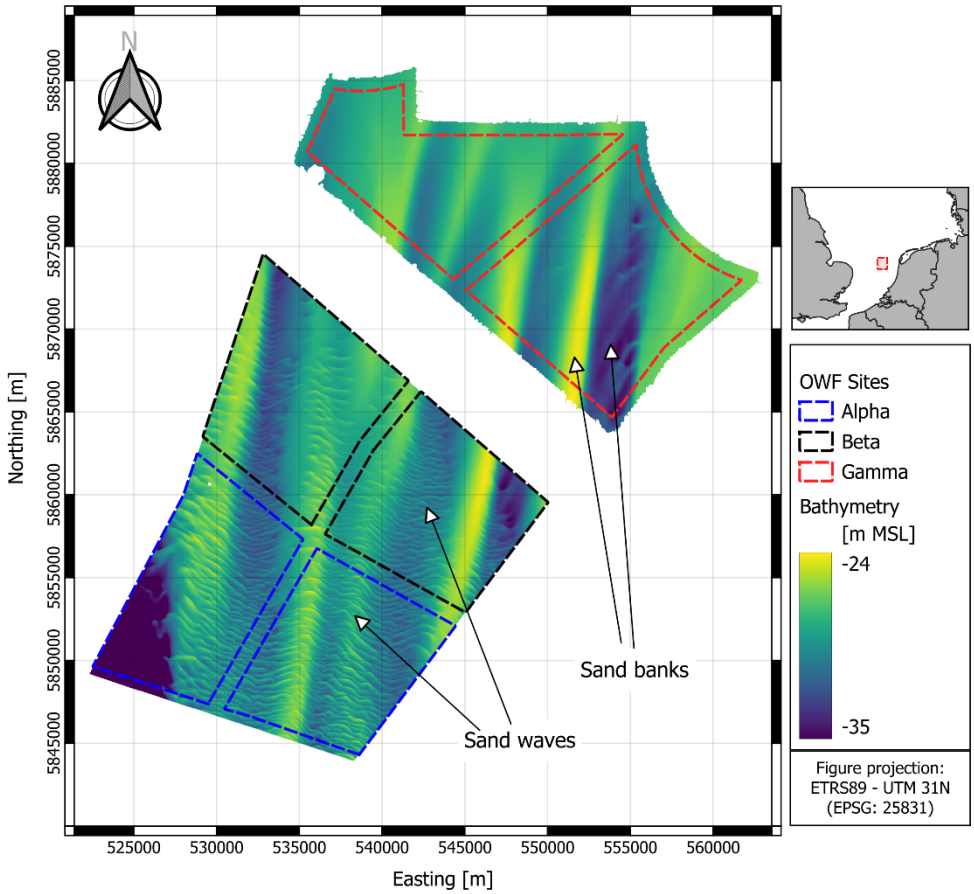

Figure 2.1 IJmuiden Ver OWFZ bathymetry survey.
Sites alpha, beta and gamma are indicated by blue, black and red polygons, respectively.

All datasets except EMODnet and Rijkswaterstaat's data were provided by RVO. These datasets are described in Table 2.1. The different datasets have been merged giving priority to the latest high-resolution site surveys above the more general datasets (EMODnet). An interpolation of the merged bathymetry has then been conducted onto the computational meshes used for SW_{DWF23} and HD_{DWF23} models. More details about the processing of bathymetric datasets can also be found in the previous HKN, HKZ, HKW and TNW reports [5-8], in FUGRO's geophysical site investigation surveys ([9], [10],[11] ,[12] ,[13] ,[14] , and [15]) in MMT's site survey ([16]) and in GEOxyz's site survey([17]).

The high-resolution wind farm zones bathymetry surveys (0.5 m resolution, corresponding to Fugro, MMT and GEOxyz's datasets) have been interpolated on 50 m resolution gridded datasets to be more easily handled in the creation of the meshes for numerical modelling. Vaklodingen data was available in a 20 m resolution grid; hence it was resampled (box-averaged) in a 60 m resolution grid for the same purpose. All bathymetric datasets are provided on the ETRS89-UTM31N projection except for EMODnet which is in WGS84 (Latitude/Longitude) projection.

All datasets were available in LAT and MSL vertical reference except for Vaklodingen dataset, which is only available in MSL. Merging of all the datasets (as well as resampling of high-resolution datasets to 50 m resolution)

was therefore performed in MSL vertical reference level, which is also the datum used in the numerical models.

The areas not covered by local bathymetry surveys were filled with the latest European Marine Observation and Data Network (EMODnet) Digital Terrain Model (DTM) data. This dataset consists of aggregated bathymetric surveys, composite DTMs, satellite derived bathymetry and information from the General Bathymetric Chart of the Oceans (GEBCO). The EMODnet bathymetric data is quality controlled. The portal also includes a metadata discovery service that provides information about the background survey data used to produce the DTM, its access restrictions, originators, and distributors. In this study, the version EMODnet v2020 was used, which is available on a 1/16 arc minutes grid (circa 115 m) in both MSL and LAT vertical datum.

An inconsistency in the EMODnet v2020 dataset (also present in previous versions of EMODnet) following the marine border between the Danish and German waters was identified, and DHI attributes this to the different origin of the underlying bathymetry ("*Danish Waters*" dataset in the Danish sector, by *Danish Geodata Agency – Danish Hydrographic Office,* and "*Deutsche Bucht 2*" in the German sector, by the German *Federal Maritime and Hydrographic Agency*). A corridor of 6 km was removed along the border and linearly interpolated to remove the discontinuity. The interpolated area is ~350 km away from the study area of this project, and the models mesh resolution at the corridor location is in the order of ~10 km; hence no impact on the model results within the study area is expected.

Figure 2.2 shows the extent of all the wind farm zones bathymetry surveys and Vaklodingen dataset, whereas Figure 2.3 shows the coverage of EMODnet 2020 within the North Sea. A comparison between EMODnet's data and IJmuiden Ver site survey is addressed in the following subsection.

Table 2.1 Bathymetry datasets implemented for SW_{DWF23} and HD_{DWF23} models.

Priority	Dataset	Horizontal reference	Vertical reference	Resolution
1	IJmuiden Ver (alpha and beta) by GEOxyz (2021)	ETRS89 – UTM 31N	MSL and LAT	0.5 m interpolated on 50 m grid by DHI
	IJmuiden Ver (gamma) by FUGRO (2022)	ETRS89 – UTM 31N	MSL and LAT	0.5 m interpolated on 50 m grid by DHI
2	TNW by MMT (2019)	ETRS89 – UTM 31N	MSL and LAT	0.5 m interpolated on 50 m grid by DHI
3	HKW by Fugro (2019)	ETRS89 – UTM 31N	MSL and LAT	0.5 m interpolated on 50 m grid by DHI

Priority	Dataset	Horizontal reference	Vertical reference	Resolution
4	HKN by Fugro (2019)	ETRS89 – UTM 31N	MSL and LAT	0.5 m interpolated on 50 m grid by DHI
5	HKZ by Fugro (2019)	ETRS89 – UTM 31N	MSL and LAT	0.5 m interpolated on 50 m grid by DHI
6	Vaklodingen by Rijkswaterstaat (2020)	ETRS89 – UTM 31N	MSL	20 m interpolated on 60 m grid by DHI
7	EMODnet v2020	WGS84 (Latitude/Longitude)	MSL and LAT	1/16 arc minutes (115 m)

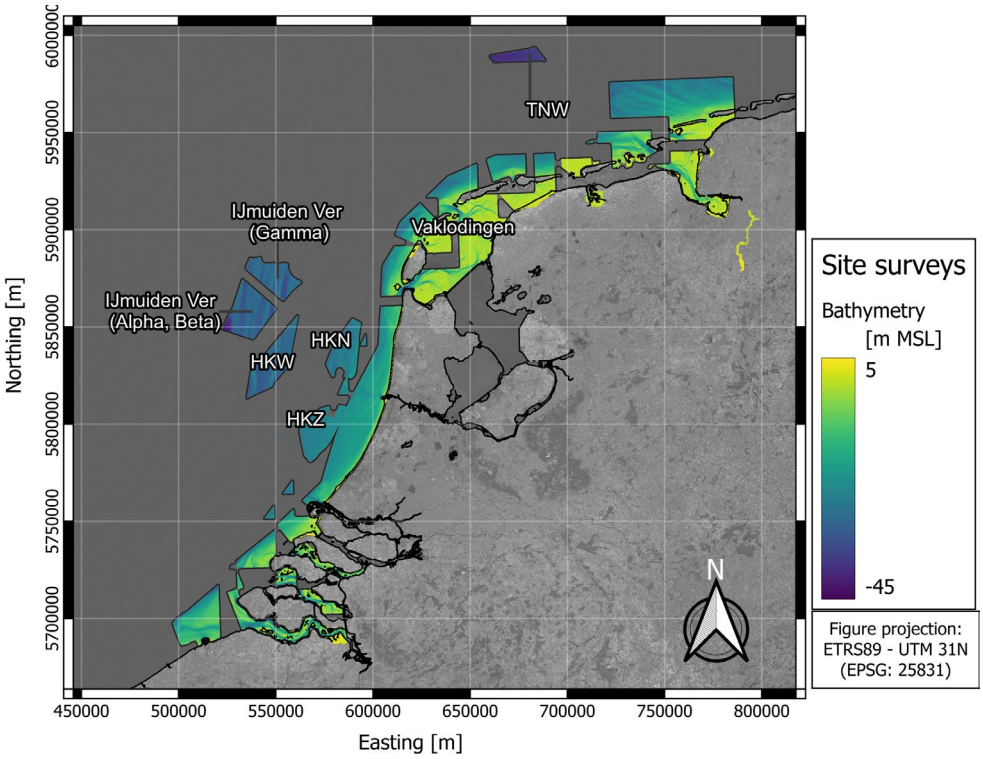

Figure 2.2 **Extent of wind farm zones site surveys and Vaklodingen data.** Compiled map of IJmuiden Ver, TNW, HKW, HKN, HKZ wind farm zones bathymetry surveys as well as Vaklodingen bathymetry.

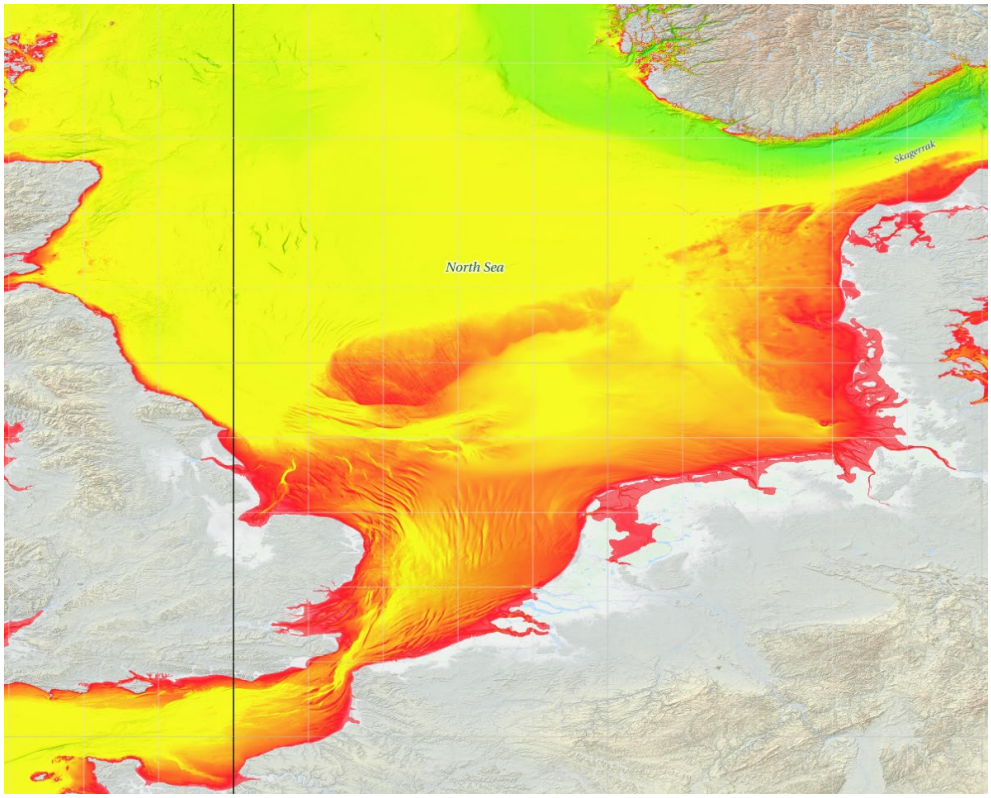

Figure 2.3 EMODnet v2020 bathymetry.
Map showing the EMODnet v2020 bathymetry in the North Sea. (Source: snapshot from https://portal.emodnet-bathymetry.eu/).

2.1.1 Comparison between survey and EMODnet

A comparison of the local IJmuiden Ver site bathymetry survey against EMODnet 2020 was carried out. For this purpose, three different approaches were undertaken:

- Overlay the local site survey on top of EMODnet to see how different they are and if any hard transitions (strong gradients between datasets) are found.
- Generate a difference map of the local survey minus EMODnet data to visualize the spatially variant bathymetry disagreements.
- Extract a total of 5 cross sections of both datasets to analyse how the bathymetries differ from each other. In this comparison, the interpolated numerical meshes were also included (SWDWF23 and HDDWF23 meshes).

In this section, the local surveys shown and analysed correspond to the datasets downsampled to 50 m, as was indicated in the previous section.

Figure 2.4 shows the local site survey (IJmuiden Ver, enclosed by white polygons) overlayed on top of EMODnet 2020 bathymetry, both bathymetries with the same colour scale. Both datasets show similar patterns, and no strong gradients or changes from one dataset to another are observed. Furthermore, the sand waves as well as the banks are present in both EMODnet and the local survey.

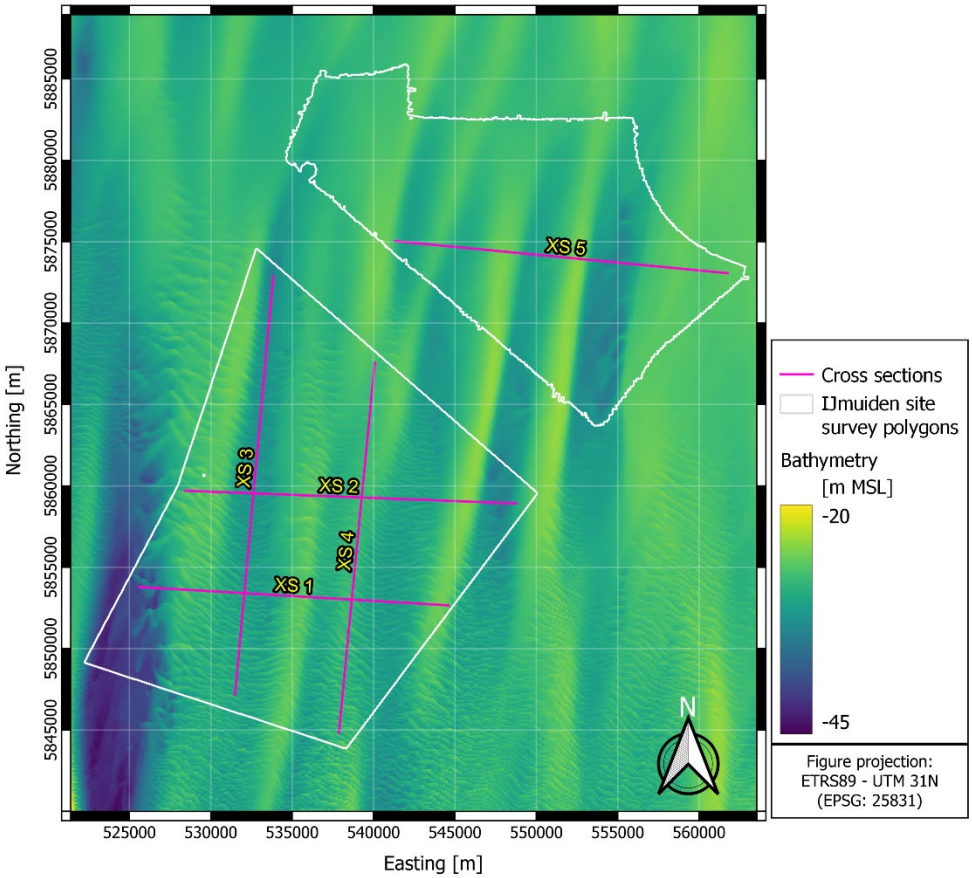

Figure 2.4 Local IJmuiden bathymetry overlayed on top of EMODnet bathymetry.
Both datasets are divided by the white polygons. The location of 5 cross sections is also depicted in the figure.

Figure 2.5 shows the bathymetry difference map when subtracting EMODnet data from the local survey data; hence positive values means that local survey has a higher elevation than EMODnet, and negative values the opposite. Almost no differences are seen in the northern survey area, whereas in the southern survey area some differences up to ±4 m are seen along the sand waves. This is expected as these bedforms migrate in time. The bias between both datasets is +0.1 m, which is considered negligible for the scale of the sand waves and for the purpose of the hydrodynamic and spectral wave modelling.

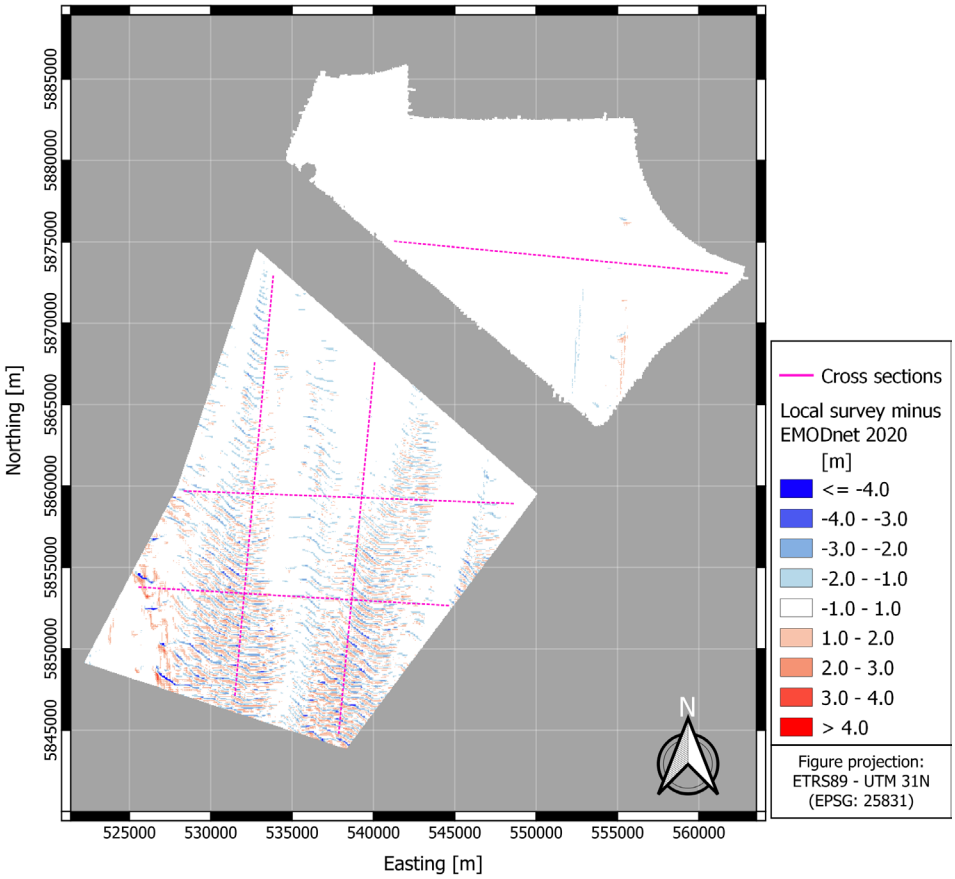

Figure 2.5 Difference between local IJmuiden bathymetry and EMODnet 2020 bathymetry.
Positive values (in red) mean that the local survey has a shallower bathymetry, and negative values (blue) mean the opposite.

Finally, Figure 2.6 and Figure 2.7 show the bathymetry comparison at the 5 cross sections (XS1 to XS5 as depicted in Figure 2.4). The sand waves migration is seen more clearly in cross sections XS3 and XS4, where sand waves of similar amplitude are seen out of phase between the local survey and EMODnet. In contrast, cross sections XS1, XS2 and XS5 show the sand banks, which are expected to have a slower migration celerity, and both datasets show a good match both in amplitude and phase.

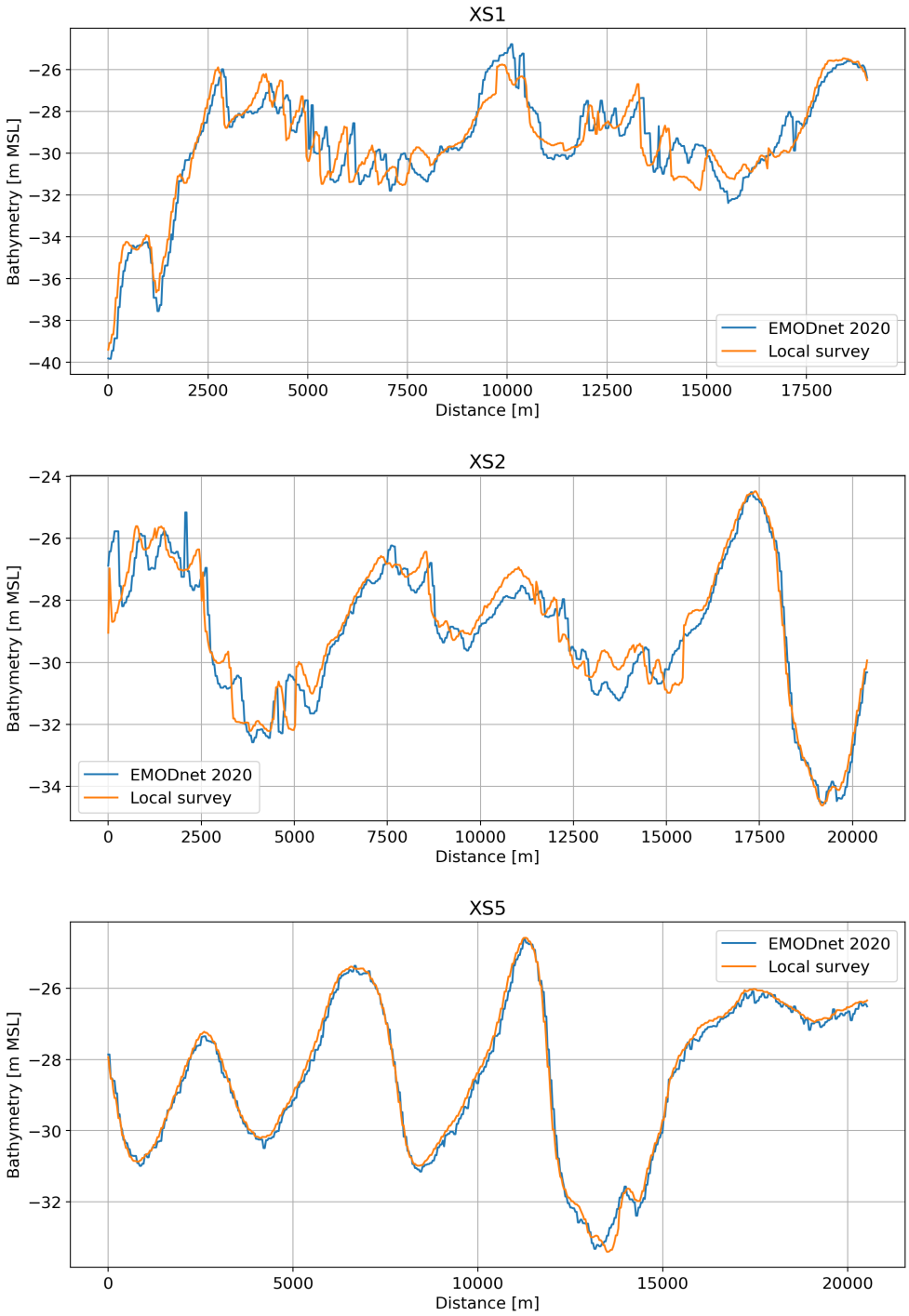

Figure 2.6 Bathymetry comparison in cross sections XS1, XS2 and XS5. Distances are given in metres from west to east. Initial and final coordinates in the cross sections are shown in Table 2.2.

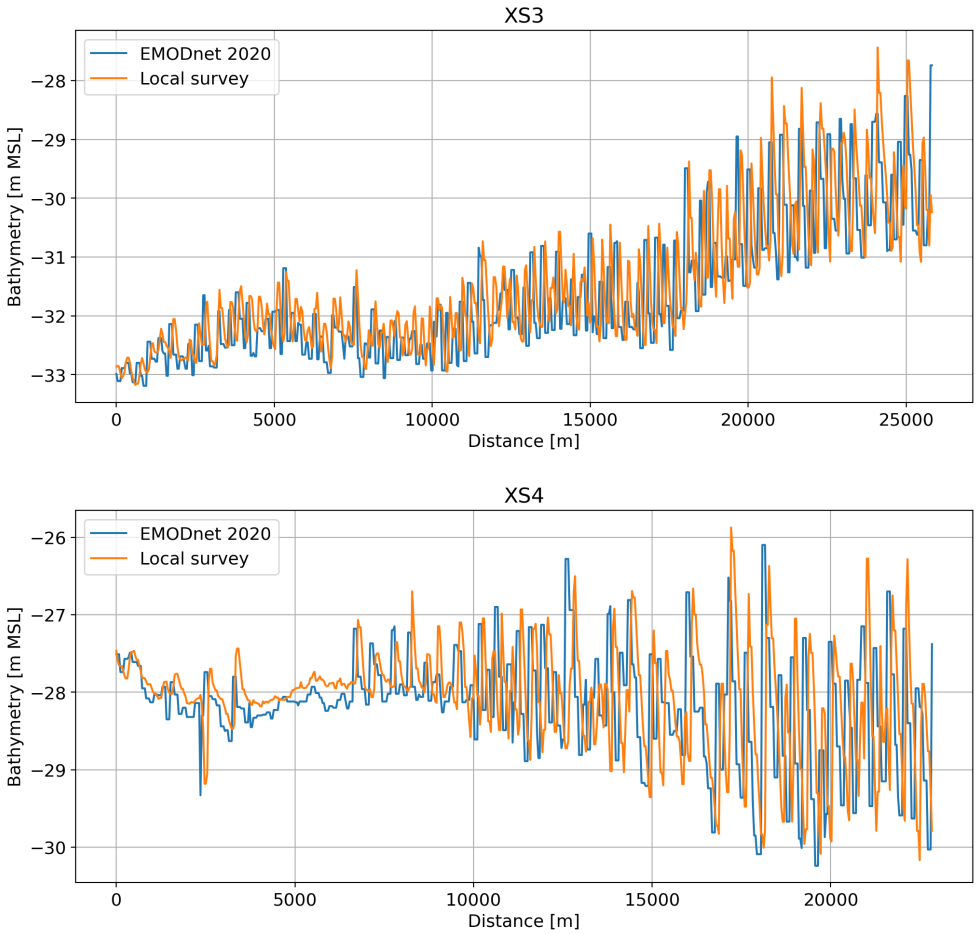

Figure 2.7 Bathymetry comparison in cross sections XS3, and XS4. Distances are given in metres from north to south. Initial and final coordinates in the cross sections are shown in Table 2.2.

Table 2.2 Coordinates of cross sections (XS1 to XS5) in WGS84.

Cross section	Initial longitude	Initial latitude	Final longitude	Final latitude
XS1	3.3800	52.8333	3.6617	52.8219
XS2	3.4218	52.8863	3.7246	52.8778
XS3	3.5042	53.0045	3.4667	52.7735
XS4	3.5964	52.9561	3.5610	52.7520
XS5	3.6159	53.0233	3.6159	53.0233

2.1.2 Conclusion on bathymetry

In conclusion, the considered bathymetric data sources are in reasonable agreement considering their origin and means of measure. Their vertical reference levels are acceptably close. The high-resolution bathymetries at IJmuiden Ver and the previous Dutch OWF sites were downsampled to 50 m resolution. The available bathymetric data was considered suitable to be used as input to the numerical models.

2.2 Metocean measurements

This section provides an overview of the in-situ measurements that were utilized to calibrate and validate the local hydrodynamic and spectral waves models of this study.

2.2.1 Overview

Figure 2.8 shows the locations of measurement stations within the metocean database area. The station names, coordinates, sources, and overview of available metocean parameters are further specified in Table 2.3.

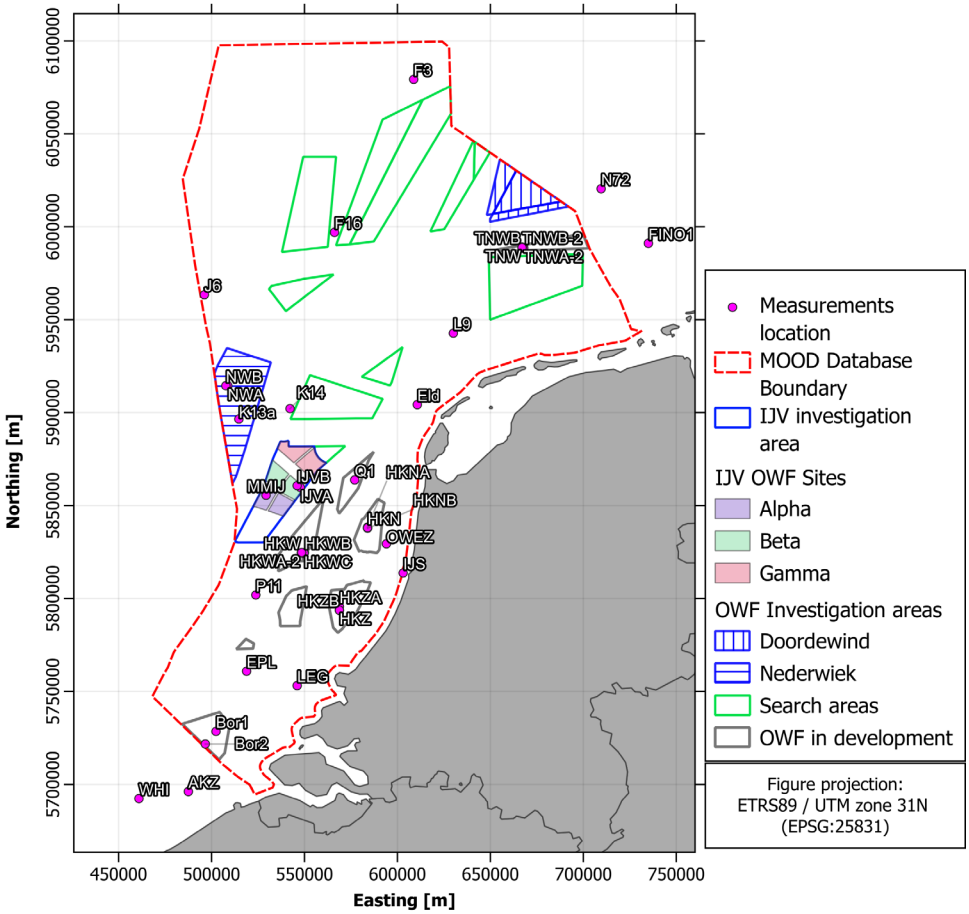

Figure 2.8 Locations of in-situ measurement stations.

Table 2.3 Overview of in-situ measurements.
Coordinates easting, northing in ETRS89 / UTM31N (EPSG:25831) and longitude, latitude in WGS84 (EPSG:4326); Water depths from EMODnet2020 and from the SW_{DWF23} mesh. Stations IJVA and IJVB are highlighted with bold text.

Name	Long name	Easting [m]	Northing [m]	Longitude [°E]	Latitude [°N]	Depth MSL EMODnet2020 [m]	Depth MSL SW_{DWF23} [m]	Wind	Water level	Current	Waves
AKZ	Akkaert Zuid	487538	5696114	2.8208	51.4161	21.9	22.1				X
Bor1	Borssele 1	502405	5728451	3.0348	51.7070	31.8	31.7			X	X
Bor2	Borssele 2	496658	5721712	2.9517	51.6464	25.3	31.8			X	X
Eld	Eierlandse	610707	5904282	4.6603	53.2762	28.3	27.0				X
EPL	Europlatform	518866	5760840	3.2748	51.9979	31.6	31.9	X	X		X
F16	F16	566162	5996979	4.0122	54.1167	47.8	47.6	X	X		X
F3	F3	608758	6079292	4.6939	54.8489	43.3	43.1	X	X		X
FINO1	FINO1	735044	5991071	6.5877	54.0143	29.9	30.2	X			X
HKNA	Hollandse Kust Noord A	583948	5838366	4.2420	52.6887	24.6	23.7	X(1)	X	X	X
HKNB	Hollandse Kust Noord B	583951	5837765	4.2419	52.6833	24.1	23.7	X(1)	X	X	X
HKWA	Hollandse Kust West A	548391	5824678	3.7140	52.5700	23.1	26.0	X(2)	X	X	X
HKWA-2	Hollandse Kust West A2	548358	5824600	3.7135	52.5693	23.1	26.0	X(2)		X	X
HKWB	Hollandse Kust West B	549950	5824693	3.7370	52.5700	32.5	27.2	X(2)	X	X	X
HKWC	Hollandse Kust West C	549819	5824247	3.7350	52.5660	33.5	26.3	X(2)	X	X	X
HKZA	Hollandse Kust Zuid A	568793	5795619	4.0090	52.3066	24.5	22.7	X	X	X	X
HKZB	Hollandse Kust Zuid B	568793	5793673	4.0086	52.2891	23.6	22.7	X	X	X	X
IJS	IJmuiden Stroomeetpaal	603087	5813697	4.5174	52.4637	14.7	16.2		X		X
IJVA	**IJmuiden Ver A**	**547802**	**5859703**	**3.7104**	**52.8849**	**33.8**	**33.5**	**X(3)**	**X**	**X**	**X**
IJVB	**IJmuiden Ver B**	**546049**	**5860698**	**3.6845**	**52.8940**	**24.4**	**24.7**	**X(3)**	**X**	**X**	**X**

J6	J6	496155	5963419	2.9416	53.8193	39.2	38.7	X	X		X
K13a	K13a	514710	5896511	3.2203	53.2177	29.1	29.1	X	X		X
K14	K14	542238	5902126	3.6333	53.2667	28.0	28.6	X	X		X
L9	L9	630090	5942675	4.9667	53.6167	25.2	24.7	X	X		X
LEG	Lichteiland Goeree	546078	5753098	3.6701	51.9267	25.0	24.6	X	X		X
MMIJ	Meteomast IJmuiden	529342	5855473	3.4357	52.8482	27.5	27.1	X			X
N72	N72	709604	6020433	6.2205	54.2887	39.5	39.3	X			
NWA	Nederwiek A	508783	5914441	3.1311	53.3790	31.5	31.4		X	X	X
NWB	Nederwiek B	507738	5914452	3.1161	53.3791	30.7	30.7		X	X	X
OWEZ	OWEZ	594100	5829394	4.3896	52.6064	20.1	17.5	X			
P11	P11	523831	5801883	3.3500	52.3667	32.0	33.0	X			
Q1	Q1	577053	5863764	4.1460	52.9180	27.9	27.2		X		X
TNWA	TNWA	667074	5988556	5.5502	54.0182	38.5	38.1	X[(4)]	X	X	X
TNWA-2	TNWA-2	667965	5988588	5.5638	54.0182	38.6	38.1	X[(4)]	X	X	X
TNWB	TNWB	667034	5988956	5.5498	54.0218	38.7	38.1	X[(4)]	X	X	X
TNWB-2	TNWB-2	667165	5988949	5.5518	54.0217	38.7	38.1	X[(4)]		X	X
WHI	Westhinder	460965	5692344	2.4391	51.3810	28.1	34.3		X		X

[(1,2,3,4,5):] As part of the preprocessing of data of the wind resource assessment, these stations (floating lidar systems located <1000 m apart) have been merged into a single station, as the difference in wind climate in such a horizontal scale far offshore is considered negligible.

2.2.1.1 Measurement sources

In-situ measurements have been obtained from the following sources. The temporal coverage and instrumentation of each station (if available) is shown in sections 0 to 2.2.5.

2.2.1.1.1 RVO – RPS

At IJV and NW, RPS is currently performing metocean measurement campaigns on behalf of RVO utilizing each a pair of floating LiDAR buoys. These LiDAR buoys also measure water levels, waves, and currents. For this study, the monthly datasets were utilized. The time series were quality controlled, cross validated and compared to independent datasets by RPS. The data was distributed by RVO and was downloaded from RVO's web pages[6].

References:

- IJV monthly reports
- NW monthly reports
- URL: https://offshorewind.rvo.nl/

The measurements at IJV (namely IJVA and IJVB, see details in following sections) are referenced throughout the rest of this report. Stations IJVA and IJVB are located in the trough and crest of a sandbank, respectively, and their location is shown in Figure 2.9.

[6] https://offshorewind.rvo.nl/

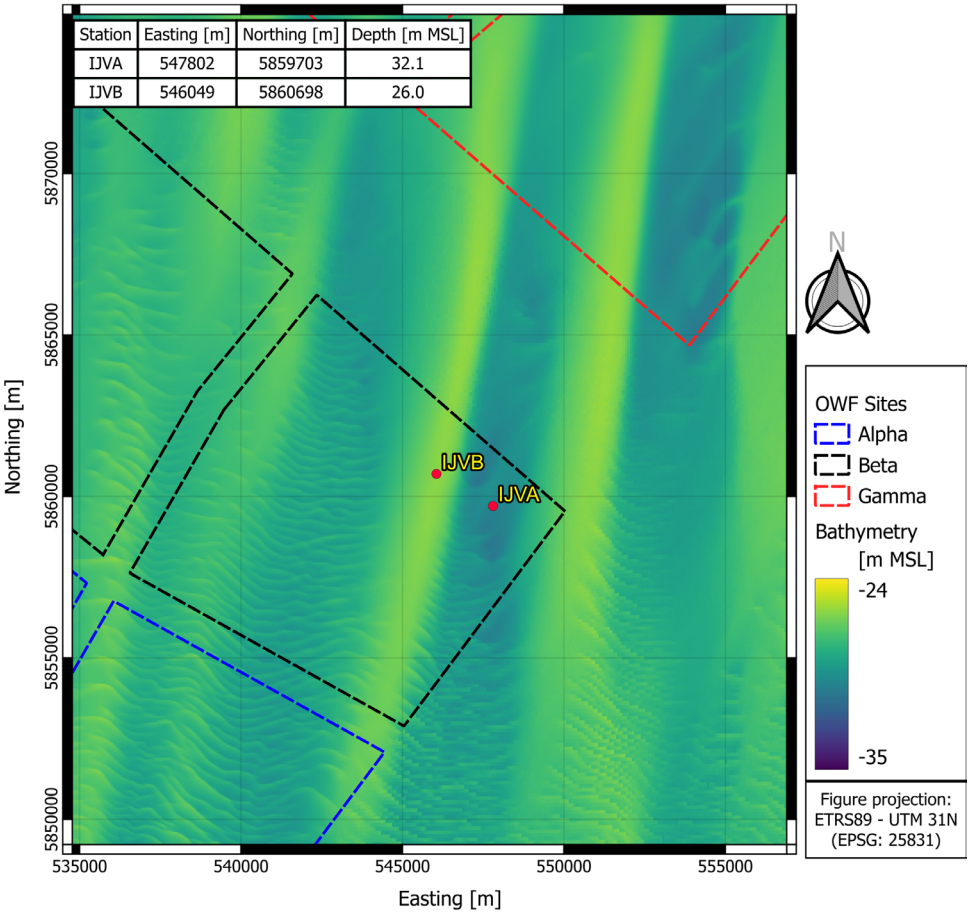

Figure 2.9 Location of stations IJVA and IJVB with IJV OWF.
The bathymetry at sites IJV alpha, beta and gamma corresponds to the local survey, whereas the surround bathymetry corresponds to EMODnet.

2.2.1.1.2 RVO – Fugro

At HKW, HKN, HKZ and TNW, Fugro has performed metocean campaigns for RVO with each a pair of floating LiDAR buoys. These LiDAR buoys also measure water levels, waves, and currents. For this study, the 2-year datasets were utilized. The provided data had already been filtered by Fugro, validated by Deltares, and quality checked by DNV-GL. The data was distributed by RVO and was downloaded from RVO's web pages[5].

References:

- HKW 2-year report [14]
- HKN 2-year report [13]
- HKZ 2-year report [12]
- TNW 2-year report [18]
- URL: https://offshorewind.rvo.nl/

2.2.1.1.3 CMEMS

The Copernicus Marine Environment Monitoring Service (CMEMS) distributes quality assured measurement data of wind, current and integral wave parameters from various data providers. The data is provided with a quality

flag. Data has been obtained from various stations via FTP from Copernicus' in-situ database.

References:

- URL: http://www.marineinsitu.eu/dashboard/

2.2.1.1.4 KNMI

The Royal Netherlands Meteorological Institute[7] (KNMI), the Dutch national weather service, provided wind measurements. No quality flags were available.

References:

- URL: https://www.knmi.nl/nederland-nu/klimatologie/uurgegevens_Noordzee

2.2.1.1.5 WOZ

The Dutch Ministry of Economic Affairs and Climate Policy provides measurement campaigns in the North Sea since 2014 at different strategically chosen locations under the program "Wind op Zee" (WOZ).

- https://www.windopzee.net/ ¨

2.2.1.1.6 RWS

Water level and significant wave height measurements were retrieved from Rijkswaterstaat (RWS) of the Dutch Ministry for Infrastructure and Waterways.

References:

- URL: https://waterinfo.rws.nl/#/nav/bulkdownload

2.2.1.1.7 BSH

Comprehensive metocean measurements are available from the research project FINO (Forschungsplattformen in Nord- und Ostsee – Research platforms in the North Sea and Baltic Sea). Data was requested at FINO1 from Bundesamt für Seeschiffahrt und Hydrographie (BSH), the German Maritime Agency. The data was provided with a quality flag.

References:

- URL: https://www.bsh.de/DE/DATEN/daten_node.html

2.2.1.2 Processing and quality control

The following data processing and QC was performed by DHI on the measured time series:

- Ingest and concatenate files in third party formats to DHI in-house format.
- Visually inspect and identify the parameters of the received measurements.
- Convert to UTC time, units and convention as used in this report.
- Remove data according to 3rd party quality flags as per Table 2.4.
- Remove data outside thresholds as per Table 2.5. These thresholds were defined based on DHI's experience in the feasibility domain area.

[7] https://www.knmi.nl/over-het-knmi/about

- Visually inspect and compare the filtered data with the raw data (before applying any DHI or 3rd party filters).

Table 2.4 3rd party quality flags and acceptance by DHI.

Source	3rd party quality flag meanings	Accepted
CMEMS	0=no_qc_performed; 1=good data; 2=probably_good_data; 3=bad_data_that_are_potentially_correctable; […]; 9=missing_value	1
BSH	9=Missing No data available; 0=Not checked Not subject to validation; 2=Formal pass Data within sensor limits; […]	2
RVO-RPS	0=unknown; 1=good; 2=suspect; 3=bad	1

Table 2.5 Applied sanity limits for in-situ measurements.

Parameter	Units	Lower limit	Upper limit
WS	m/s	0	40
WL	mMSL	-5	5
CS	m/s	0	5
H_{m0}	m	0.1	15
T_{02}	s	0	25
T_p	s	0	30
Directional data	°	0	360

2.2.2 Wind measurements

Wind measurement data is used for local validation of the WRF model (Section 3.1). The WRF data is subsequently used for forcing the hydrodynamic and spectral waves modelling. Wind measurements are listed in Table 2.6 and illustrated in Figure 2.10. The temporal coverage of the wind measurements is shown in Figure 2.11. Since the numerical models were forced by winds at 10 mMSL, only measurement stations with data at 10 m or near-surface data at 30 m (from LiDAR and floating LiDAR devices) were considered here.

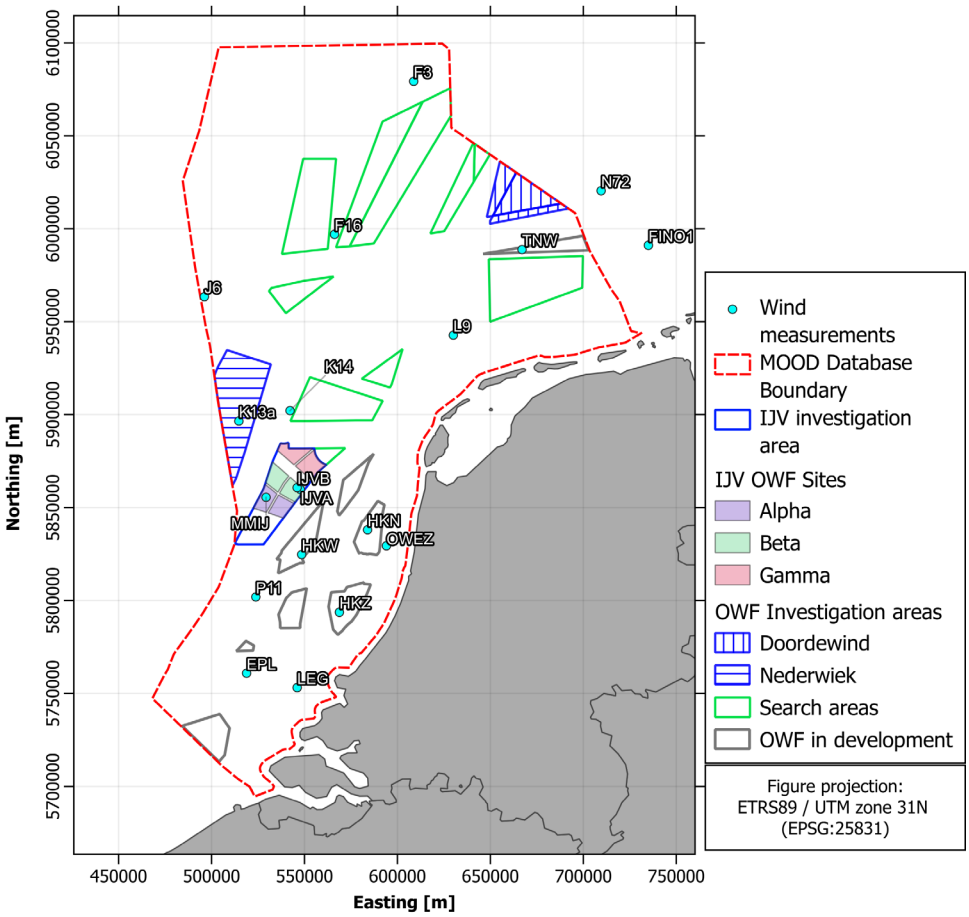

Figure 2.10 Locations of in-situ wind measurement stations.
Only stations with data at 10 or 30 mMSL were used for near-surface wind validation.

Table 2.6 Details of wind measurement stations used for wind validation.
Stations IJVA and IJVB are highlighted with bold text. Only stations with data at 10 or 30 mMSL were used for near surface wind validation.

Station Name	Longitude [°E]	Latitude [°N]	Measurement Height [mMSL]	Data coverage	Instrument type	Sampling interval [s]	Model	Data source or surveyor
EPL	3.2748	51.9979	10	1996-07-01 - 2022-10-19	Unknown	3600[1]	Unknown	KNMI
F16	4.0122	54.1167	10	2006-12-07 - 2020-08-31	Unknown	3600[1]	Unknown	KNMI
F3	4.6939	54.8489	10	1994-01-01 - 2022-10-19	Unknown	3600[1]	Unknown	KNMI
FINO1	6.5877	54.0143	30	2004-01-31 - 2008-12-31	Anemometers	600	Vector A100LK/PC3/WR cup anemometers	BSH
IJVA	**3.7104**	**52.8849**	**30**	**2022-05-01 - 2023-01-04**	**LiDAR**	**600**	**ZephIR ZX300**	**RPS/ FUGRO**
IJVB	**3.6845**	**52.8940**	**30**	**2022-05-01 - 2023-01-04**	**LiDAR**	**600**	**ZephIR ZX300**	**RPS/ FUGRO**
J6	2.9416	53.8193	10	2009-03-16 - 2022-10-19	Unknown	3600[1]	Unknown	KNMI
K13a	3.2203	53.2177	10	1996-07-01 - 2022-10-19	Unknown	3600[1]	Unknown	KNMI
K14	3.6333	53.2667	10	2008-09-12 - 2022-10-19	Unknown	3600[1]	Unknown	KNMI
L9	4.9667	53.6167	10	2008-09-12 - 2022-10-19	Unknown	3600[1]	Unknown	KNMI
LEG	3.6701	51.9267	10	1981-01-01 - 2022-10-19	Unknown	3600[1]	Unknown	KNMI
MMIJ	3.4357	52.8482	30	2012-01-01 - 2015-12-31	Anemometers	600	Unknown	WOZ

Station Name	Longitude [°E]	Latitude [°N]	Measurement Height [mMSL]	Data coverage	Instrument type	Sampling interval [s]	Model	Data source or surveyor
N72	6.2205	54.2887	30	2020-05-20 - 2021-05-04	LiDAR	600	ZephIR ZX300M	BSH
OWEZ	4.3896	52.6064	30	2005-06-30 - 2006-07-02	LiDAR	600	ZephIR ZX300M	WOZ
P11	3.3500	52.3667	10	2009-11-10 - 2022-10-19	Unknown	3600[1]	Unknown	KNMI
HKW	3.7156	52.5702	30	2019-02-05 - 2021-02-11	LiDAR	600	Gill Windsonic M ZephIR ZX300	RVO/ FUGRO
HKN	4.2419	52.6854	30	2017-04-10 - 2019-04-10	LiDAR	600	Gill Windsonic M ZephIR ZX300	RVO/ FUGRO
TNW	5.5500	54.0200	30	2019-06-19 - 2021-06-20	LiDAR	600	Gill Windsonic M ZephIR ZX300	RVO/ FUGRO
HKZ	4.0086	52.2891	30	2016-06-05 - 2018-06-04	LiDAR	600	Gill Windsonic M ZephIR ZX300	RVO/ FUGRO

[1] Data is averaged (representative) over the last 10 minutes of each hour, but it is available only with at a 1h interval in KNMI's website.

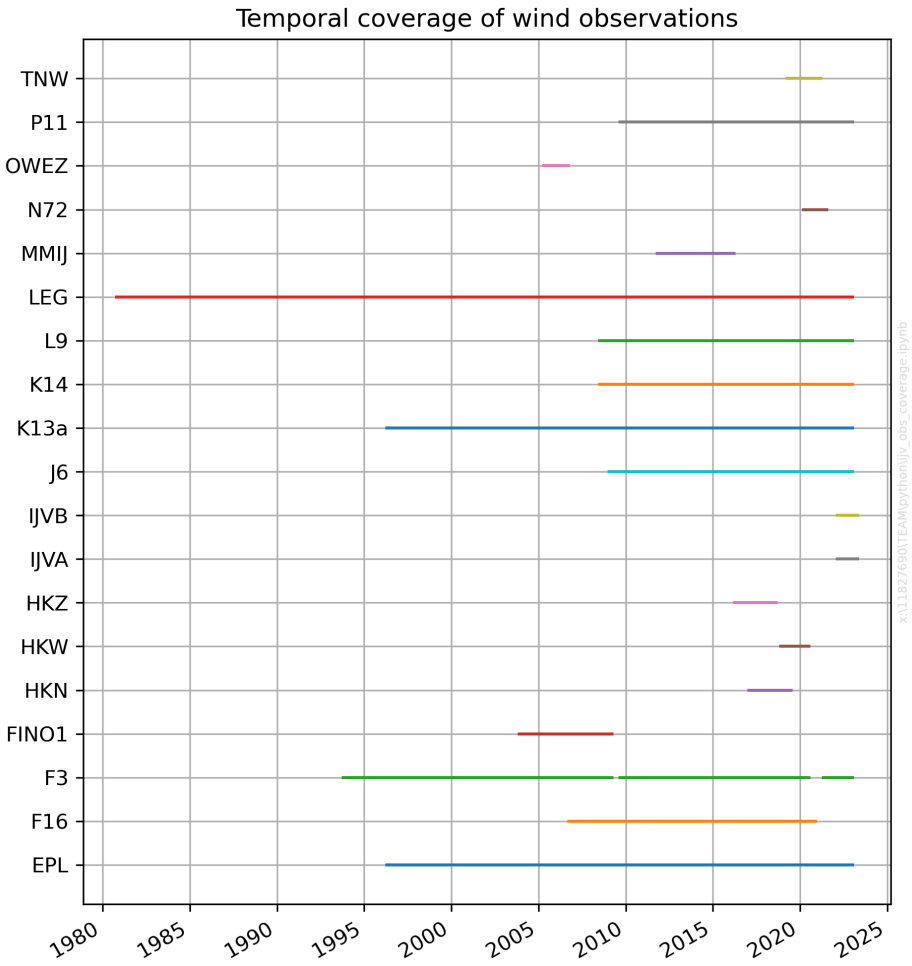

Figure 2.11 Temporal coverage of wind measurements.

2.2.3 Water level measurements

Water level measurement data used for validation of the hydrodynamic model are listed in Table 2.7 and illustrated in Figure 2.12. The temporal coverage of the water level measurements is shown in Figure 2.13.

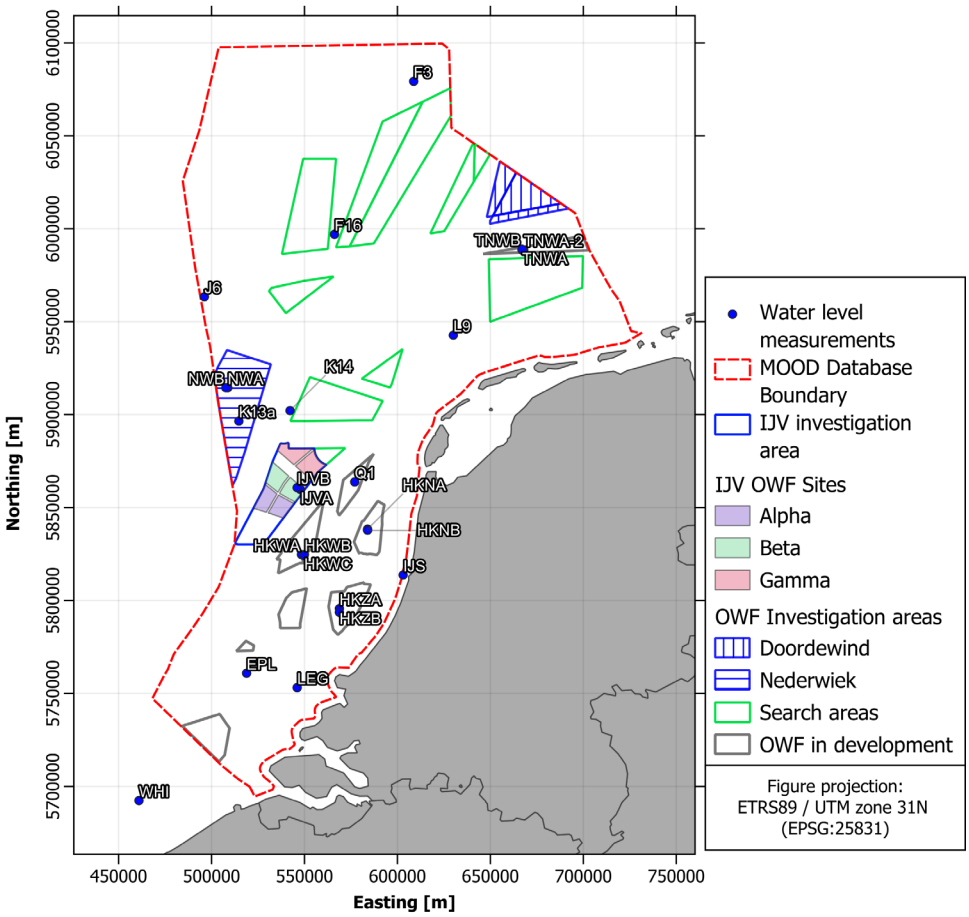

Figure 2.12 Locations of in-situ water level measurement stations.

Table 2.7 Details of water level measurement stations used for hydrodynamic model validation.
Stations IJVA and IJVB are highlighted with bold text.

Station Name	Longitude [°E]	Latitude [°N]	Modelled seabed elevation [mMSL][1]	Surveyed seabed elevation [mMSL]	Data coverage	Sampling interval [s]	Instrument	Data source or surveyor
EPL	3.2748	51.9979	31.6	31.6[2]	2014-01-06 - 2022-12-31	600	Unknown	CMEMS
F16	4.0122	54.1167	47.8	47.8[2]	2010-06-25 - 2019-12-31	600	Unknown	RWS
F3	4.6939	54.8489	43.3	43.3[2]	2014-08-01 - 2022-12-31	600	Unknown	CMEMS
HKNA	4.2420	52.6887	24.6	24.6[2]	2017-04-10 - 2018-10-13	600	Thelma (TBR 700)	RVO/ FUGRO
HKNB	4.2419	52.6833	24.1	24.1[2]	2017-04-10 - 2019-04-10	600	Thelma (TBR 700)	RVO/ FUGRO
HKWA	3.7140	52.5700	23.1	23.1[2]	2019-02-05 - 2020-04-24	600	Thelma (TBR 700)	RVO/ FUGRO
HKWB	3.7370	52.5700	32.5	32.5[2]	2020-05-09 - 2021-02-11	600	Thelma (TBR 700)	RVO/ FUGRO
HKWC	3.7350	52.5660	33.5	33.5[2]	2019-09-19 - 2019-11-24	600	Thelma (TBR 700)	RVO/ FUGRO
HKZA	4.0090	52.3066	24.5	24.5[2]	2016-10-30 - 2018-02-02	600	Thelma (TBR 700)	RVO/ FUGRO
HKZB	4.0086	52.2891	23.6	23.6[2]	2016-06-28 - 2018-03-04	600	Thelma (TBR 700)	RVO/ FUGRO
IJS	4.5174	52.4637	14.7	14.7[2]	2014-07-30 - 2022-12-31	600	Unknown	CMEMS
IJVA	**3.7104**	**52.8849**	**32.1**	**33.8**	**2022-05-01 - 2022-12-31**	**600**	**RPS Tide Sensor**	**RVO/ RPS**
IJVB	**3.6845**	**52.8940**	**26.0**	**24.4**	**2022-05-01 - 2022-12-31**	**600**	**RPS Tide Sensor**	**RVO/ RPS**
J6	2.9416	53.8193	39.2	39.2[2]	2017-01-19 - 2022-12-31	600	Unknown	CMEMS
K13a	3.2203	53.2177	29.1	29.1[2]	2015-06-28 - 2022-12-31	600	Unknown	CMEMS
K14	3.6333	53.2667	28.0	28.0[2]	2015-07-05 - 2022-12-31	600	Unknown	CMEMS
L9	4.9667	53.6167	25.2	25.2[2]	2015-06-28 - 2022-12-31	600	Unknown	CMEMS
LEG	3.6701	51.9267	25.0	25.0[2]	2015-01-01 - 2022-12-31	600	Unknown	CMEMS
NWA	3.1311	53.3790	29.1	31.4	2022-06-01 - 2022-12-31	600	RPS Tide Sensor	RVO/ RPS

Station Name	Longitude [°E]	Latitude [°N]	Modelled seabed elevation [mMSL][1]	Surveyed seabed elevation [mMSL]	Data coverage	Sampling interval [s]	Instrument	Data source or surveyor
NWB	3.1161	53.3791	29.6	30.7	2022-06-02 - 2022-12-31	600	RPS Tide Sensor	RVO/ RPS
Q1	4.1460	52.9180	27.9	27.9[2]	2015-06-28 - 2022-09-30	600	Unknown	CMEMS
TNWA	5.5502	54.0182	38.5	38.5[2]	2020-04-11 - 2021-06-20	600	Thelma (TBR 700)	RVO/ FUGRO
TNWA-2	5.5638	54.0182	38.6	38.6[2]	2021-01-16 - 2021-06-20	600	Thelma (TBR 700)	RVO/ FUGRO
TNWB	5.5498	54.0218	38.7	38.7[2]	2019-06-19 - 2020-10-25	600	Thelma (TBR 700)	RVO/ FUGRO
WHI	2.4391	51.3810	28.1	28.1[2]	2020-02-28 - 2022-09-30	300	Unknown	CMEMS

[1] Modelled seabed elevation based on the production mesh.
[2] Seabed elevation from EMODnet 2020.

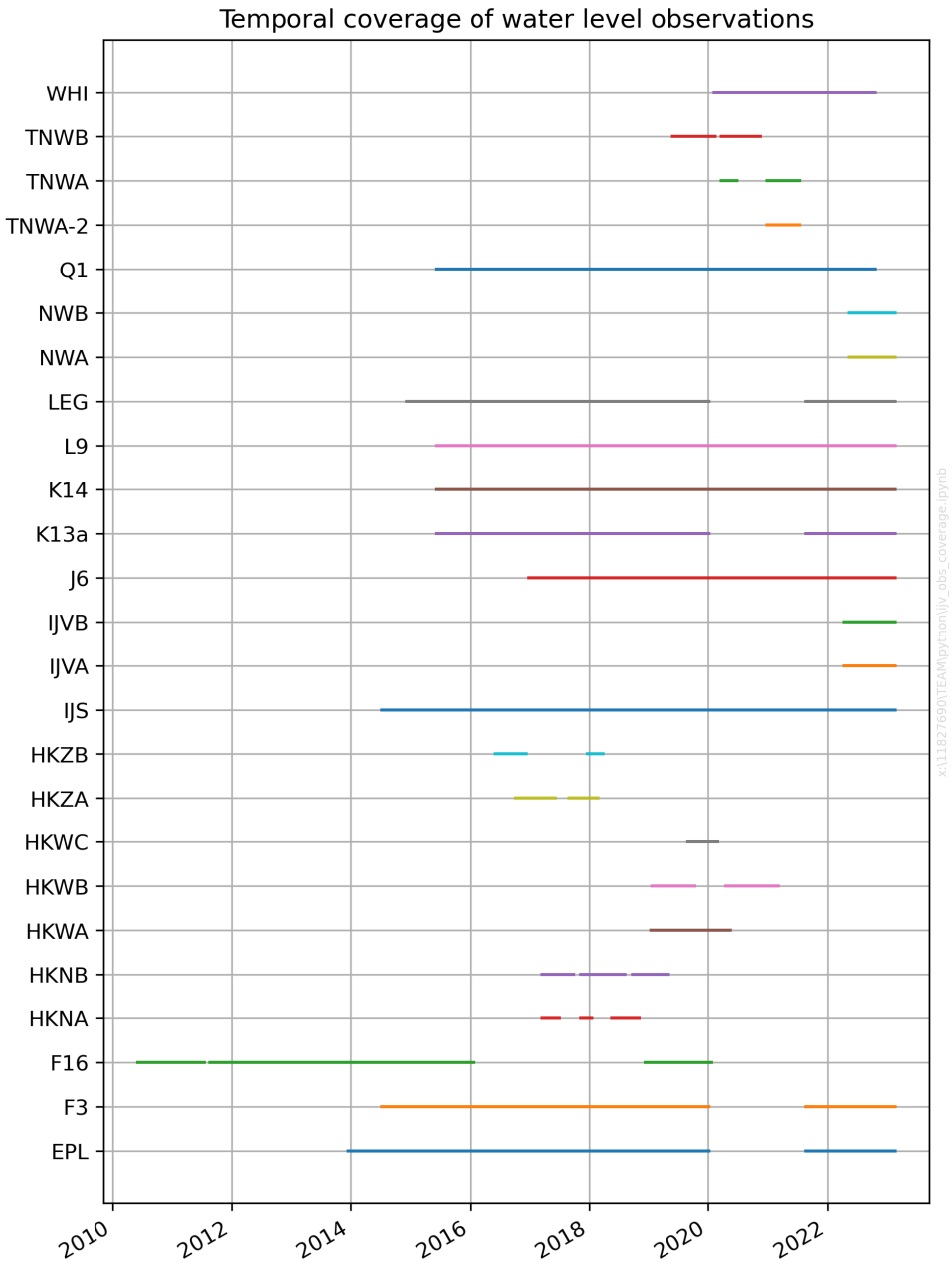

Figure 2.13 Temporal coverage of water level measurements.

2.2.3.1 Water level measurements post-processing

From the water level measurements retrieved from the various sources, after filtering by quality flags (if available), a different level of post-processing had to be applied depending on the quality of raw data. In some stations, no post-processing at all was applied, but in others, in particular the stations at the site (IJVA and IJVB), a moving average had to be performed before comparing with model results.

Figure 2.14 and Figure 2.15 show one week of raw water level measurements at IJVA and IJVB respectively, along with 1-hour and 3-hour moving averages of the same signal. What can be seen in these figures is that the raw signal has

short-frequency fluctuations, in the order of 10-minutes, that are not expected in a water level signal where short waves (wind-sea, swell) have been averaged out. This finding led to communications with RVO/RPS where it was confirmed that the water level measurements in IJVA/IJVB/NWA/NWB were indeed 1-minute averaged data, reported every 10-minutes, instead of the more common 10-minutes or 20-minutes averaged water level data, in which case these high frequency fluctuations are averaged out.

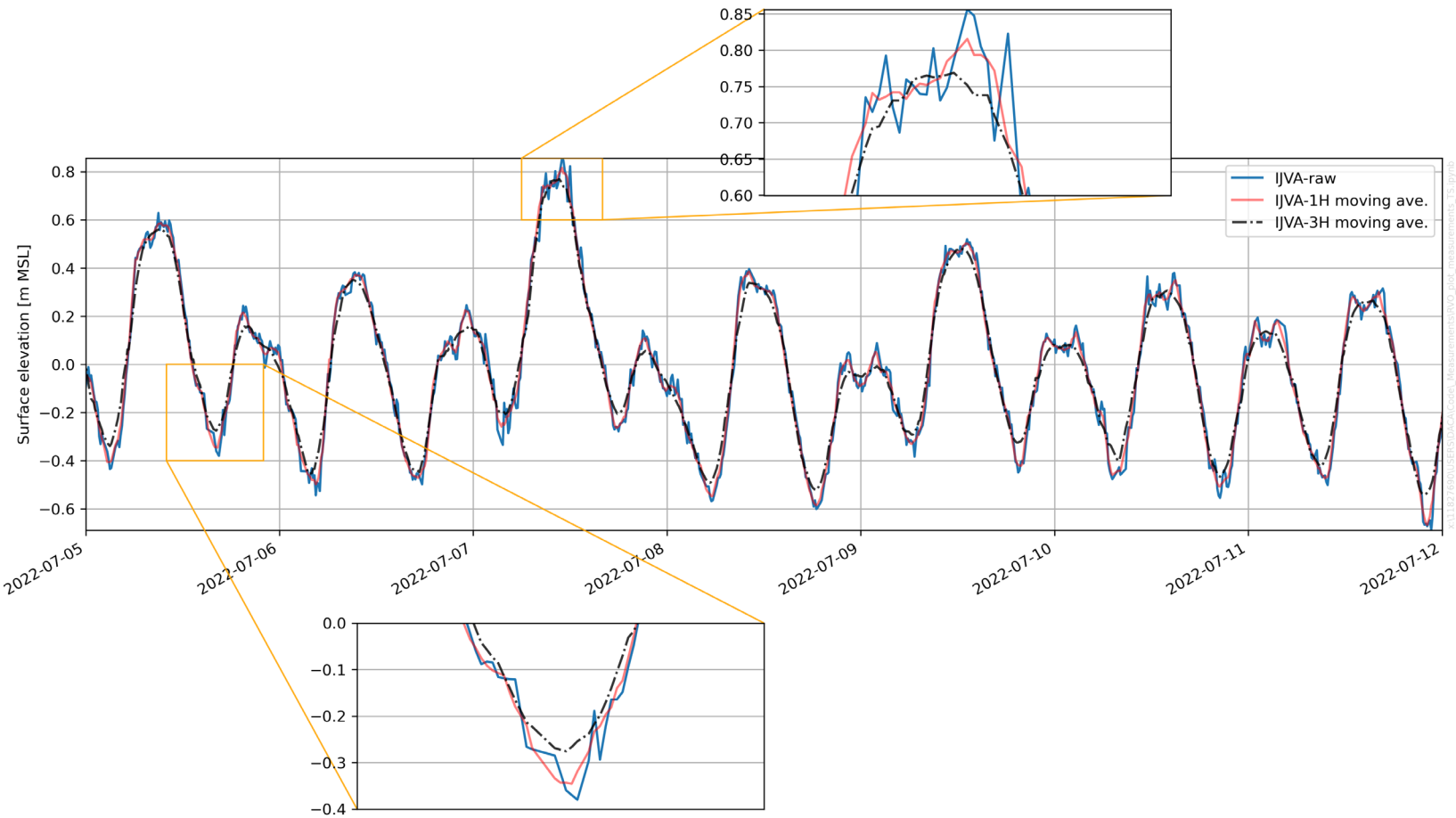

Figure 2.14 Water level measurement at IJVA for 1 week period in July-2022.
Raw signal, 1-hour moving average and 3-hour moving average are shown. Additionally, two zoom panels during a signal peak and trough are presented in sub-panels.

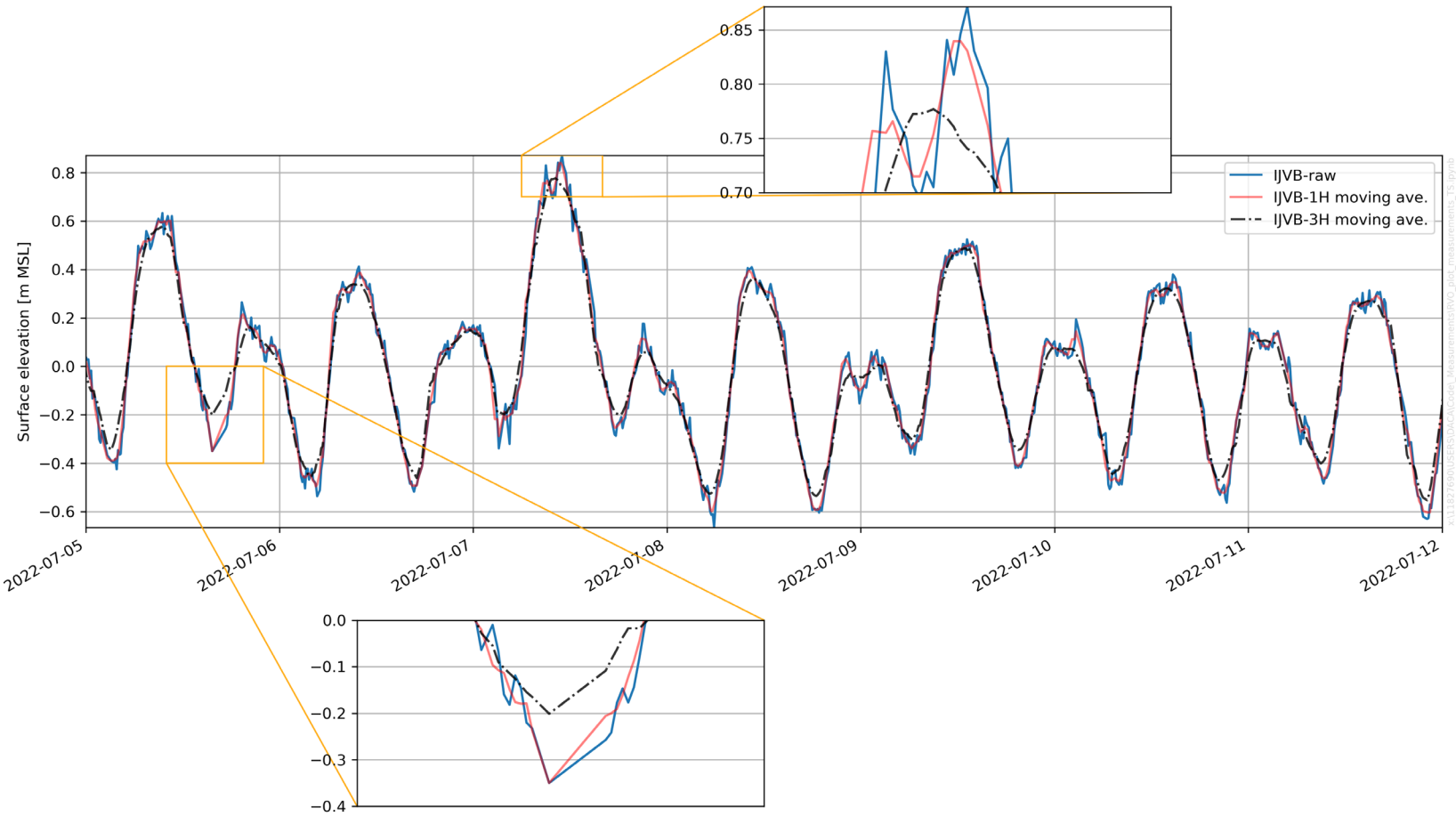

Figure 2.15 Water level measurement at IJVB for 1 week period in July-2022.
Raw signal, 1-hour moving average and 3-hour moving average are shown. Additionally, two zoom panels during a signal peak and trough are presented in sub-panels.

By comparing the raw, 1-hour moving average and the 3-hour moving average, it was concluded that the 1-hour moving average was sufficient to remove the high frequency (short waves) fluctuations of the signal while still retaining most of the peaks and troughs.

In other stations, a long-term trend of the mean value was observed, or sometimes different deployments had apparently different datums, hence a detrending of the signal was applied. This was done by subtracting the 1-month moving average to the raw signal. Just as an example of this procedure, Figure 2.16 shows the raw water depth signal from station HKNB along with the 1-month moving average, where different datums and trends are clearly identified. In the bottom panel, the resulting surface elevation after the detrending procedure has been undertaken is shown.

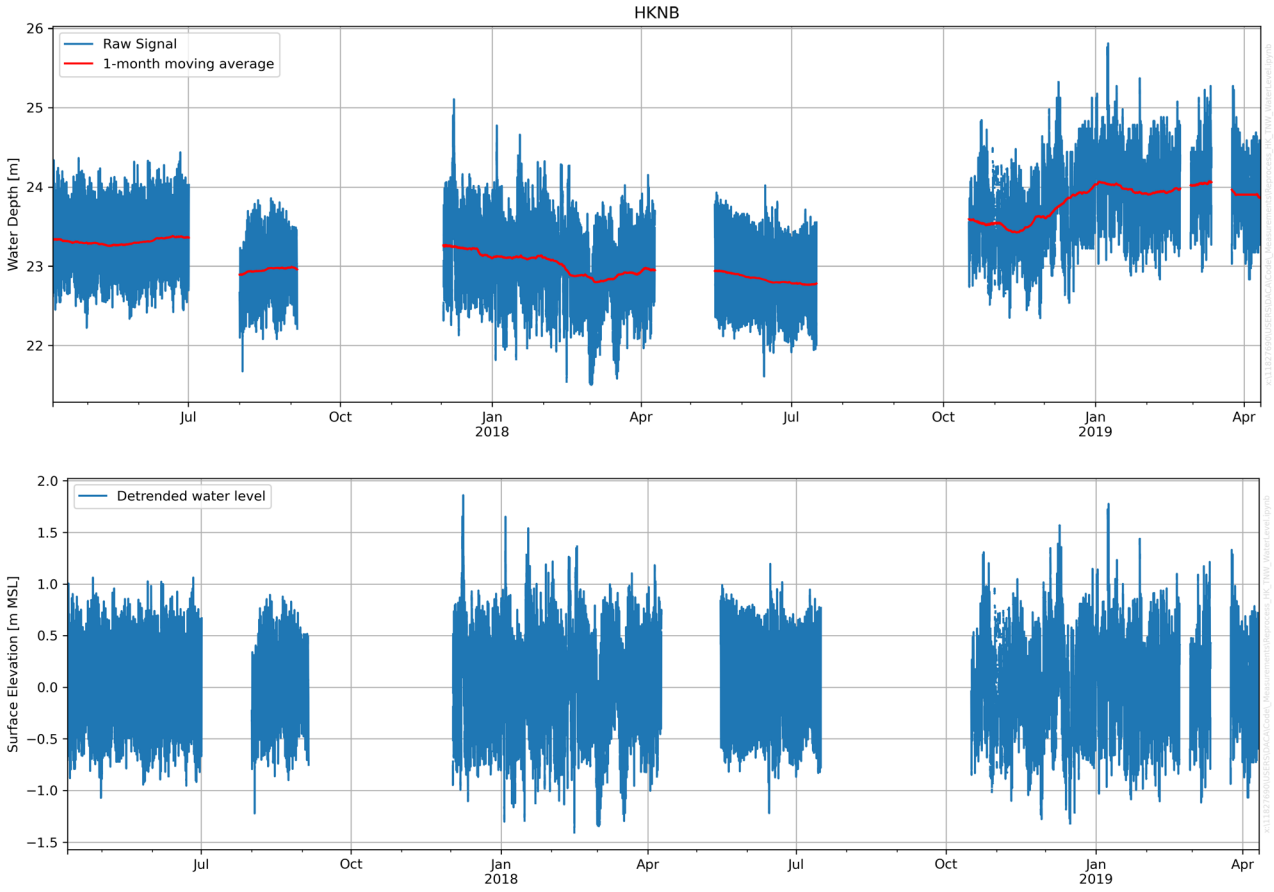

Figure 2.16 Water level measurement at HKNB.
Top: example of the raw signal with different datums and trends along with the 1-month moving average.
Bottom: resulting surface elevation after performing the detrending of the signal.

Table 2.8 presents the summary of the different post-processing procedure applied to the different water level stations.

Table 2.8 Details of post-processing applied to raw water level measurement before comparing to model results.
Stations IJVA and IJVB are highlighted with bold text.

Station Name	Post-processing applied to raw signal
EPL	None
F16	None
F3	None
HKNA	Detrend of signal
HKNB	Detrend of signal
HKWA	Detrend of signal
HKWB	Detrend of signal
HKWC	Detrend of signal
HKZA	Detrend of signal
HKZB	Detrend of signal
IJS	None
IJVA	**1-hour moving average**
IJVB	**1-hour moving average**
J6	None
K13a	Detrend of signal
K14	None
L9	None
LEG	None
NWA	1-hour moving average
NWB	1-hour moving average
Q1	Detrend of signal
TNWA	Detrend of signal
TNWA-2	Detrend of signal
TNWB	Detrend of signal
WHI	None

2.2.4 Currents measurements

Currents measurement data used for validation of the hydrodynamic model are listed in Table 2.9 and illustrated in Figure 2.17. The temporal coverage of the currents measurements is shown in Figure 2.18.

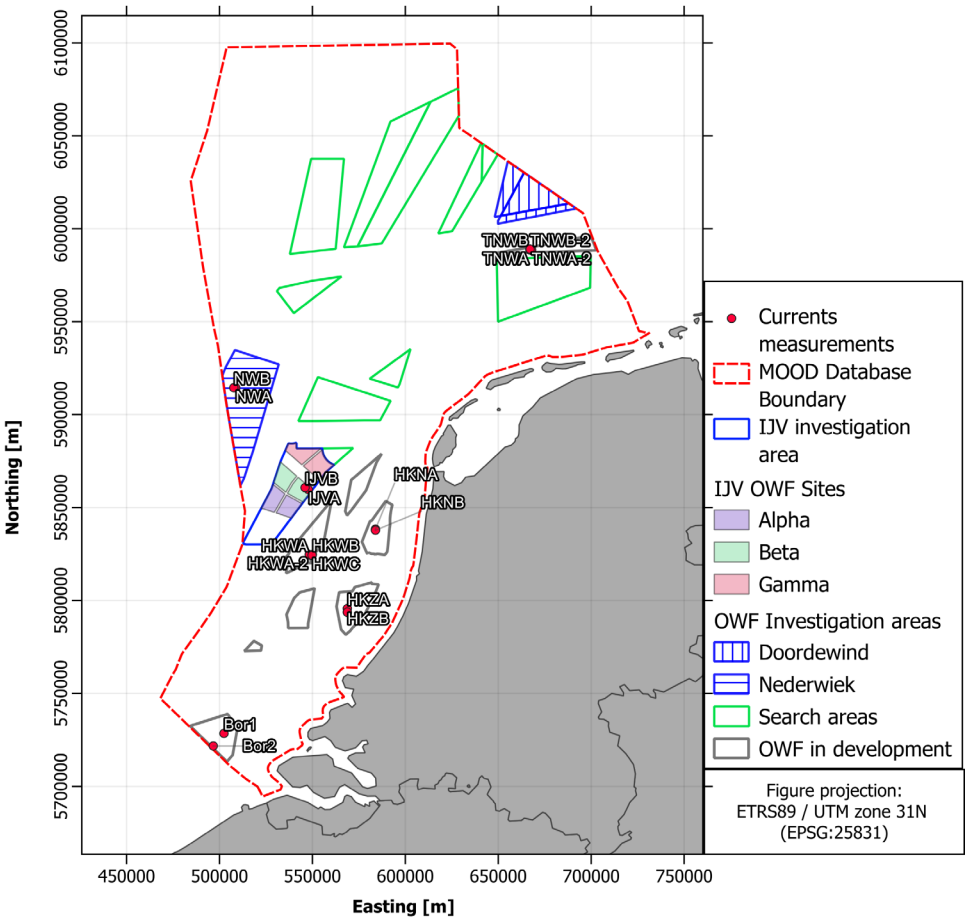

Figure 2.17 Locations of in-situ currents measurement stations.

Table 2.9 Details of currents measurement stations used for hydrodynamic model validation.
Stations IJVA and IJVB are highlighted with bold text.

Station Name	Longitude [°E]	Latitude [°N]	Modelled seabed elevation [mMSL][1]	Surveyed seabed elevation [mMSL]	Data coverage	Sampling interval [s]	Instrument	Data source or surveyor
Bor1	3.0348	51.7070	31.8	31.7[2]	2015-06-11 - 2017-02-27	600	Nortek Aquadopp 600kHz	RVO/ FUGRO
Bor2	2.9517	51.6464	25.3	31.8[2]	2016-02-12 - 2016-07-07	600	Nortek Aquadopp 600kHz	RVO/ FUGRO
HKNA	4.2420	52.6887	24.6	23.7[2]	2017-04-10 - 2019-04-10	600	Nortek Aquadopp 600kHz	RVO/ FUGRO
HKNB	4.2419	52.6833	24.1	23.7[2]	2017-04-10 - 2019-04-10	600	Nortek Aquadopp 600kHz	RVO/ FUGRO
HKWA	3.7140	52.5700	23.1	26.0[2]	2019-02-05 - 2020-04-24	600	Nortek Aquadopp 600kHz	RVO/ FUGRO
HKWA-2	3.7135	52.5693	23.1	26.0[2]	2020-05-09 - 2021-02-11	600	Nortek Aquadopp 600kHz	RVO/ FUGRO
HKWB	3.7370	52.5700	32.5	27.2[2]	2019-02-10 - 2021-02-11	600	Nortek Aquadopp 600kHz	RVO/ FUGRO
HKWC	3.7350	52.5660	33.5	26.3[2]	2019-08-01 - 2020-02-07	600	Nortek Aquadopp 600kHz	RVO/ FUGRO
HKZA	4.0090	52.3066	24.5	22.7[2]	2016-10-30 - 2018-06-05	600	Nortek Aquadopp 600kHz	RVO/ FUGRO
HKZB	4.0086	52.2891	23.6	22.7[2]	2016-06-05 - 2018-06-05	600	Nortek Aquadopp 600kHz	RVO/ FUGRO
IJVA	**3.7104**	**52.8849**	**33.8**	**33.5**	**2022-05-01 - 2022-12-31**	**600**	**Nortek Signature 500 kHz**	**RVO/ RPS**
IJVB	**3.6845**	**52.8940**	**24.4**	**24.7**	**2022-05-01 - 2022-12-31**	**600**	**Nortek Signature 500 kHz**	**RVO/ RPS**

Station Name	Longitude [°E]	Latitude [°N]	Modelled seabed elevation [mMSL][1]	Surveyed seabed elevation [mMSL]	Data coverage	Sampling interval [s]	Instrument	Data source or surveyor
NWA	3.1311	53.3790	29.1	31.4	2022-06-01 - 2022-12-31	600	Nortek Signature 500 kHz	RVO/ RPS
NWB	3.1161	53.3791	29.6	30.7	2022-06-02 - 2022-12-31	600	Nortek Signature 500 kHz	RVO/ RPS
TNWA	5.5502	54.0182	38.5	38.1[2]	2019-06-19 - 2020-12-30	600	Nortek Aquadopp 600kHz	RVO/ FUGRO
TNWA-2	5.5638	54.0182	38.6	38.1[2]	2021-01-16 - 2021-06-20	600	Nortek Aquadopp 600kHz	RVO/ FUGRO
TNWB	5.5498	54.0218	38.7	38.1[2]	2019-06-19 - 2021-02-15	600	Nortek Aquadopp 600kHz	RVO/ FUGRO
TNWB-2	5.5518	54.0217	38.7	38.1[2]	2021-03-03 - 2021-06-20	600	Nortek Aquadopp 600kHz	RVO/ FUGRO

[1] Modelled seabed elevation based on the production mesh.
[2] Seabed elevation from EMODnet 2020.

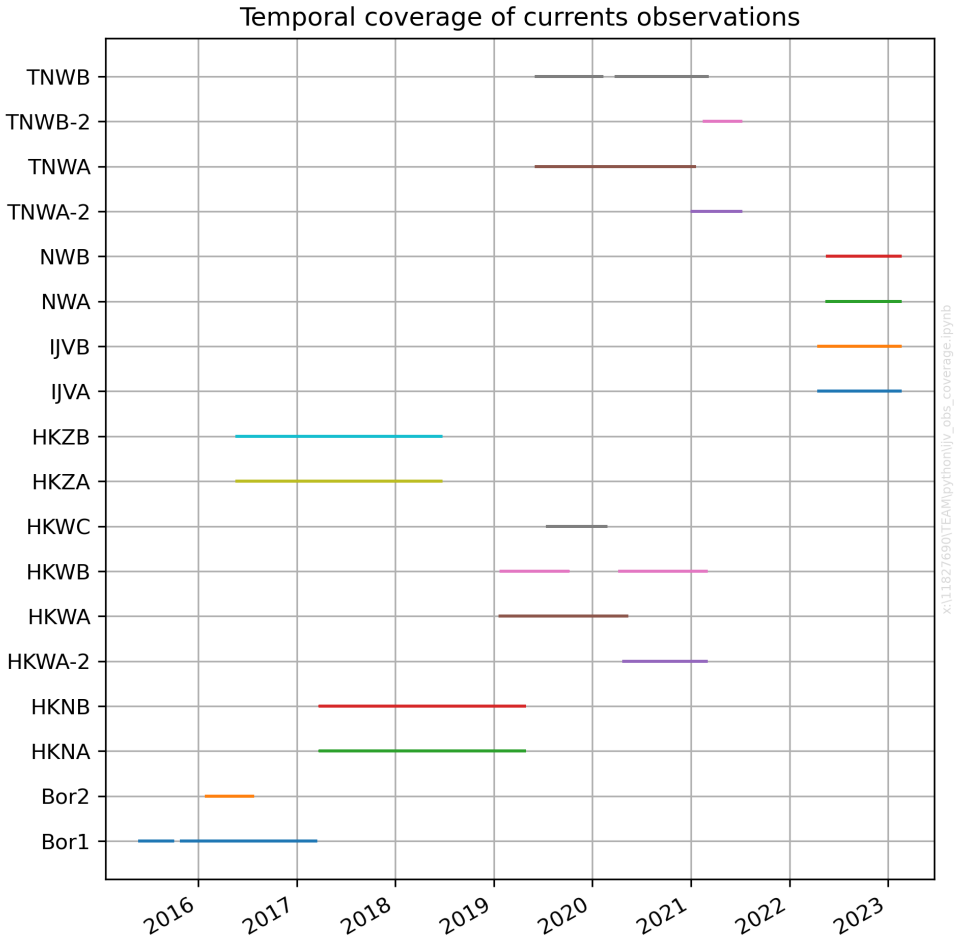

Figure 2.18 Temporal coverage of current measurements.

2.2.4.1 Current profiles

The current profiles at the IJV site were initially assessed based on the local measurements. To compare measured current data against the hydrodynamic model, the measured currents had to be depth-averaged, as the hydrodynamic model is a depth-averaged model (see Section 3.2). Figure 2.19 and Figure 2.20 show the measured current profiles for both stations IJVA and IJVB. In these figures, only the data flagged as “good” is considered.

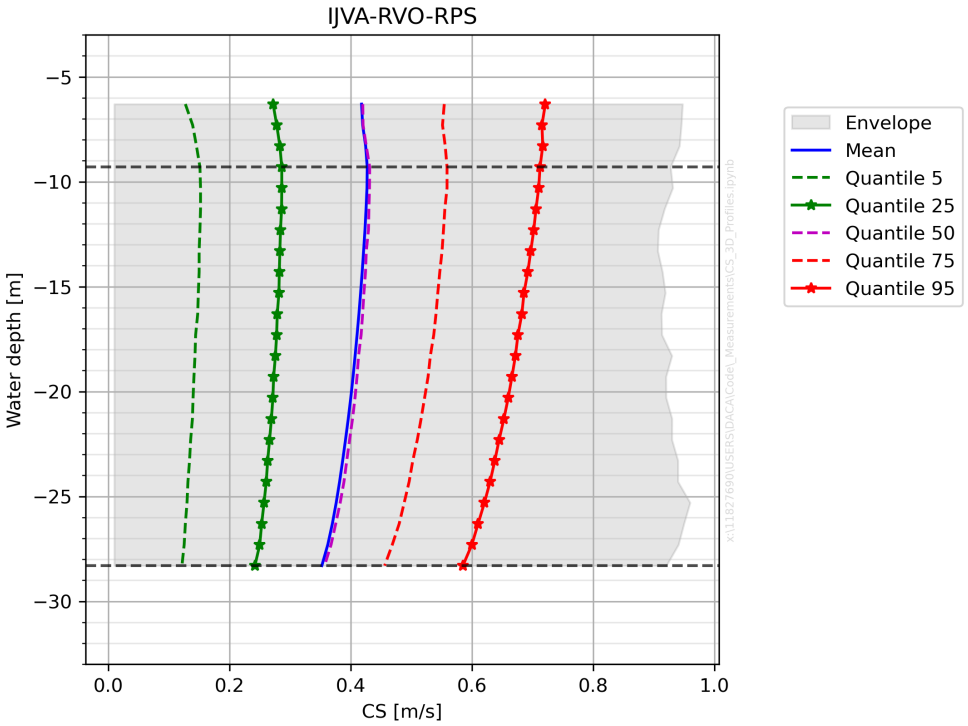

Figure 2.19 Measured current speed profiles at IJVA.
Horizontal lines represent the minimum and maximum water depth that were considered to derive the depth-averaged currents. Surveyed water depth: 33.5 m.

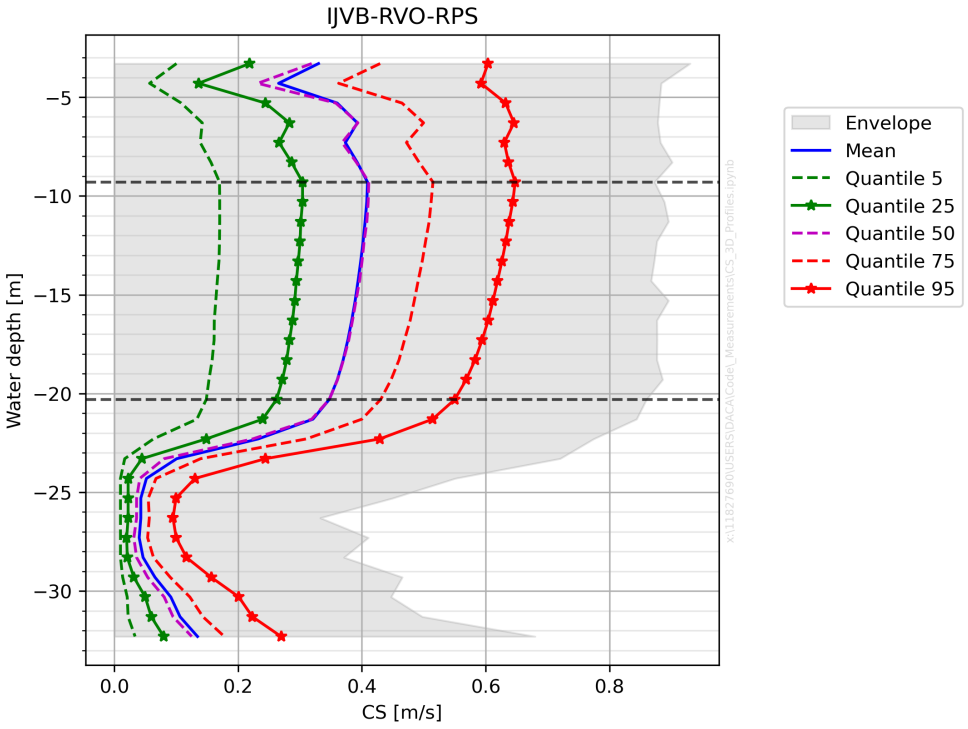

Figure 2.20 Measured current speed profiles at IJVB.
Horizontal lines represent the minimum and maximum water depth that were considered to derive the depth-averaged currents. Surveyed water depth: 24.4 m.

For IJVA, some near-surface layers were discarded to obtain the depth-averaged currents, to be in consistency with the monthly measurement campaigns by RPS; thus, for profile integration, water depths between 9.3 and 28.3 m were considered.

For IJVB, several layers, both near the water surface and close to the seabed, were not representative of the depth-averaged profile, despite being flagged as "good" data. There is data down to ~32 m, despite the surveyed water depth at that location being ~24.7 m only. Hence, before doing the depth-average integration, several layers near the surface and seabed were discarded; thus, for profile integration, only water depths between 9.3 and 20.3 m were considered. The data used for depth-integration of current speeds in IJVA and IJVB corresponds to the data comprised between the horizontal dashed lines in Figure 2.19 and Figure 2.20.

The same procedure (visual inspection of profile shapes and its different quantiles) was performed for all the currents stations indicated in Table 2.9. The selected layers for depth-integration are presented in Table 2.10. The profiles are shown in Appendix B.

Table 2.10 Selected layers for depth-averaging of current speed profiles.

Station	Minimum depth [m]	Maximum depth [m]	Model water depth [m]
Bor1-RVO-FUGRO	4.0	30.0	31.8
Bor2-RVO-FUGRO	4.0	24.0	25.3
HKNA-RVO-FUGRO	4.0	20.0	24.6
HKNB-RVO-FUGRO	4.0	20.0	24.1
HKWA-2-RVO-FUGRO	3.0	20.0	23.1
HKWA-RVO-FUGRO	3.0	20.0	23.1
HKWB-RVO-FUGRO	3.0	27.0	32.5
HKWC-RVO-FUGRO	4.0	27.0	33.5
HKZA-RVO-FUGRO	4.0	20.0	24.5
HKZB-RVO-FUGRO	4.0	18.0	23.6
IJVA-RVO-RPS	9.3	28.3	33.8
IJVB-RVO-RPS	9.3	20.3	24.4
NWA-RVO-RPS	9.3	25.3	29.1
NWB-RVO-RPS	9.3	25.3	29.6
TNWA-RVO-FUGRO	3.0	36.0	38.5
TNWA-2-RVO-FUGRO	3.0	36.0	38.6
TNWB-RVO-FUGRO	3.0	36.0	38.7
TNWB-2-RVO-FUGRO	3.0	36.0	38.7

2.2.5 Wave measurements

Wave measurement data used for validation of the spectral wave model are listed in Table 2.11 and illustrated in Figure 2.21. The temporal coverage of the wave measurements is shown in Figure 2.22.

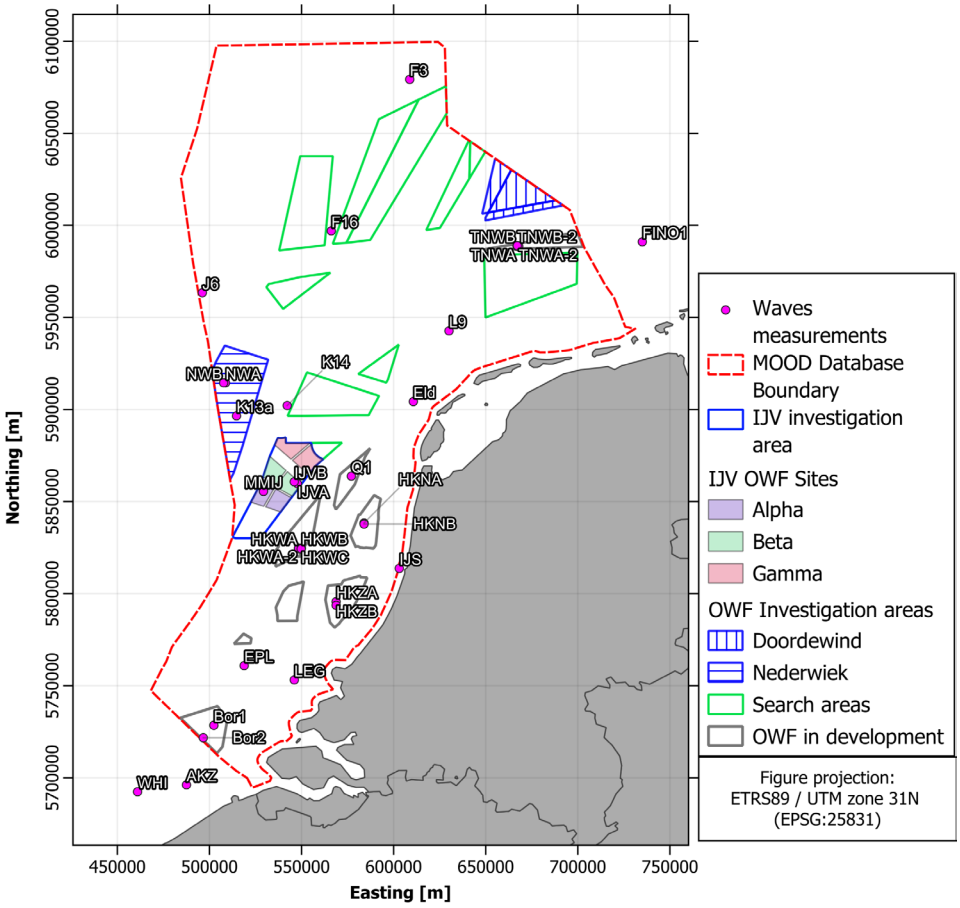

Figure 2.21 Locations of in-situ wave measurement stations.

Table 2.11 Details of wave measurement stations used for wave model validation.
Stations IJVA and IJVB are highlighted with bold text.

Name	Longitude [°E]	Latitude [°N]	Modelled seabed elevation [mMSL][1]	Surveyed seabed elevation [mMSL]	Data coverage	Parameters	Averaging period [s]	Sampling interval [s]	Instrument (type)	Data source or surveyor
AKZ	2.8208	51.4161	21.9	22.1[2]	2014-01-24 - 2022-01-13	Hm0 [m], Tz [s]	~3,600[3]	3,600	Not known	CMEMS
Bor1	3.0348	51.7070	31.8	31.7[2]	2015-06-11 - 2017-02-27	Hm0 [m], TP [s], Tz [s], Tm01 [s], Tm02 [s], MWD [°], PWD [°], DSD [°]	1,024	600	Wave buoy (Wavesense 3)	RVO/ FUGRO
Bor2	2.9517	51.6464	25.3	31.8[2]	2016-02-12 - 2016-07-07	Hm0 [m], TP [s], Tz [s], Tm01 [s], Tm02 [s], MWD [°], PWD [°], DSD [°]	1,024	600	Wave buoy (Wavesense 3)	RVO/ FUGRO
Eld	4.6603	53.2762	28.3	27.2[2]	2011-05-19 - 2022-12-31	Hm0 [m], TP [s], Tz [s], MWD [°]	~3,600[3]	3,600	Not known	CMEMS
EPL	3.2748	51.9979	31.6	31.9[2]	2011-05-19 - 2022-11-30	Hm0 [m], TP [s], Tz [s]	~3,600[3]	3,600	Not known	CMEMS
F16	4.0122	54.1167	47.8	47.6[2]	2011-05-19 - 2020-08-31	Hm0 [m], TP [s], Tz [s]	~3,600[3]	3,600	Not known	CMEMS
F3	4.6939	54.8489	43.3	43.1[2]	2014-01-06 - 2022-09-30	Hm0 [m], TP [s], Tz [s]	~3,600[3]	3,600	Not known	CMEMS
FINO1	6.5877	54.0143	29.9	30.2[2]	2003-07-30 - 2022-09-30	Hm0 [m], TP [s], Tz [s]	~3,600[3]	3,600	Not known	CMEMS
HKNA	4.2420	52.6887	24.6	23.7[2]	2017-04-10 - 2019-04-10	Hm0 [m], TP [s], Tz [s], Tm01 [s], Tm02 [s], MWD [°], PWD [°], DSD [°]	1,024	600	Wave buoy (Wavesense 3)	RVO/ FUGRO
HKNB	4.2419	52.6833	24.1	23.7[2]	2017-04-10 - 2019-04-10	Hm0 [m], TP [s], Tz [s], Tm01 [s], Tm02 [s], MWD [°], PWD [°], DSD [°]	1,024	600	Wave buoy (Wavesense 3)	RVO/ FUGRO
HKWA	3.7140	52.5700	23.1	26.2[2]	2019-02-05 - 2020-04-24	Hm0 [m], TP [s], Tz [s], Tm01 [s], Tm02 [s], MWD [°], PWD [°], DSD [°]	1,024	600	Wave buoy (Wavesense 3)	RVO/ FUGRO
HKWA-2	3.7135	52.5693	23.1	26.2[2]	2020-05-09 - 2021-02-11	Hm0 [m], TP [s], Tz [s], Tm01 [s], Tm02 [s], MWD [°], PWD [°], DSD [°]	1,024	600	Wave buoy (Wavesense 3)	RVO/ FUGRO

Name	Longitude [°E]	Latitude [°N]	Modelled seabed elevation [mMSL][1]	Surveyed seabed elevation [mMSL]	Data coverage	Parameters	Averaging period [s]	Sampling interval [s]	Instrument (type)	Data source or surveyor
HKWB	3.7370	52.5700	32.5	27.2[2]	2019-02-10 - 2021-02-11	Hm0 [m], TP [s], Tz [s], Tm01 [s], Tm02 [s], MWD [°], PWD [°], DSD [°]	1,024	600	Wave buoy (Wavesense 3)	RVO/ FUGRO
HKWC	3.7350	52.5660	33.5	26.3[2]	2019-08-01 - 2020-02-07	Hm0 [m], TP [s], Tz [s], Tm01 [s], Tm02 [s], MWD [°], PWD [°], DSD [°]	1,024	600	Wave buoy (Wavesense 3)	RVO/ FUGRO
HKZA	4.0090	52.3066	24.5	22.7[2]	2016-06-05 - 2018-06-05	Hm0 [m], TP [s], Tz [s], Tm01 [s], Tm02 [s], MWD [°], PWD [°], DSD [°]	1,024	600	Wave buoy (Wavesense 3)	RVO/ FUGRO
HKZB	4.0086	52.2891	23.6	22.7[2]	2016-06-05 - 2018-06-05	Hm0 [m], TP [s], Tz [s], Tm01 [s], Tm02 [s], MWD [°], PWD [°], DSD [°]	1,024	600	Wave buoy (Wavesense 3)	RVO/ FUGRO
IJS	4.5174	52.4637	14.7	16.2[2]	2011-05-19 - 2018-12-13	Hm0 [m], TP [s], Tz [s]	~3,600[3]	3,600	Not known	CMEMS
IJVA	**3.7104**	**52.8849**	**33.8**	**33.5**	**2022-05-01 - 2022-12-31**	**Hm0 [m], TP [s], Tz [s], Tm01 [s], Tm02 [s], MWD [°], PWD [°], DSD [°], Spectra**	**~1,800[3]**	**1,800**	**Wave buoy (Kongsberg MRU-5)**	**RVO/ RPS**
IJVB	**3.6845**	**52.8940**	**24.4**	**24.7**	**2022-05-01 - 2022-12-31**	**Hm0 [m], TP [s], Tz [s], Tm01 [s], Tm02 [s], MWD [°], PWD [°], DSD [°], Spectra**	**~1,800[3]**	**1,800**	**Wave buoy (Kongsberg MRU-5)**	**RVO/ RPS**
J6	2.9416	53.8193	39.2	38.7[2]	2011-05-19 - 2022-09-30	Hm0 [m], TP [s], Tz [s]	~3,600[3]	3,600	Not known	CMEMS
K13a	3.2203	53.2177	29.1	29.1[2]	2011-05-19 - 2022-09-30	Hm0 [m], TP [s], Tz [s], MWD [°]	~3,600[3]	3,600	Not known	CMEMS
					1979-01-18 - 2021-02-01	Hm0 [m]	~3,600[3]	3,600	Not known	RWS
K14	3.6333	53.2667	28	28.6[2]	2011-05-19 - 2022-09-30	Hm0 [m], TP [s], Tz [s]	~3,600[3]	3,600	Not known	CMEMS
L9	4.9667	53.6167	25.2	24.7[2]	2011-05-19 - 2022-09-30	Hm0 [m], TP [s], Tz [s]	~3,600[3]	3,600	Not known	CMEMS
LEG	3.6701	51.9267	25	24.6[2]	2011-05-19 - 2022-09-30	Hm0 [m], TP [s], Tz [s]	~3,600[3]	3,600	Not known	CMEMS

Name	Longitude [°E]	Latitude [°N]	Modelled seabed elevation [mMSL][1]	Surveyed seabed elevation [mMSL]	Data coverage	Parameters	Averaging period [s]	Sampling interval [s]	Instrument (type)	Data source or surveyor
					1979-01-01 - 2022-10-25	Hm0 [m]	~3,600[3]	3,600	Not known	RWS
MMIJ	3.4357	52.8482	27.5	27.1[2]	2011-11-02 - 2016-03-09	Hm0 [m], TP [s], Tm02 [s], MWD [°]	~3,600[3]	3,600	Wave buoy (Triaxys)	WOZ
NWA	3.1311	53.3790	29.1	31.4	2022-06-01 - 2022-12-31	Hm0 [m], TP [s], Tz [s], Tm01 [s], Tm02 [s], MWD [°], PWD [°], DSD [°], Spectra	~1,800[3]	1,800	Wave buoy (Kongsberg MRU-5)	RVO/ RPS
NWB	3.1161	53.3791	29.6	30.7	2022-06-02 - 2022-12-31	Hm0 [m], TP [s], Tz [s], Tm01 [s], Tm02 [s], MWD [°], PWD [°], DSD [°], Spectra	~1,800[3]	1,800	Wave buoy (Kongsberg MRU-5)	RVO/ RPS
Q1	4.1460	52.9180	27.9	27.2[2]	2015-06-02 - 2022-09-30	Hm0 [m], TP [s], Tz [s]	~3,600[3]	3,600	Not known	CMEMS
TNWA	5.5502	54.0182	38.5	38.1[2]	2019-06-19 - 2020-12-30	Hm0 [m], TP [s], Tz [s], Tm01 [s], Tm02 [s], MWD [°], PWD [°], DSD [°]	1,024	600	Wave buoy (Wavesense 3)	RVO/ FUGRO
TNWA-2	5.5638	54.0182	38.6	38.1[2]	2021-01-16 - 2021-06-20	Hm0 [m], TP [s], Tz [s], Tm01 [s], Tm02 [s], MWD [°], PWD [°], DSD [°]	1,024	600	Wave buoy (Wavesense 3)	RVO/ FUGRO
TNWB	5.5498	54.0218	38.7	38.1[2]	2019-06-19 - 2021-02-15	Hm0 [m], TP [s], Tz [s], Tm01 [s], Tm02 [s], MWD [°], PWD [°], DSD [°]	1,024	600	Wave buoy (Wavesense 3)	RVO/ FUGRO
TNWB-2	5.5518	54.0217	38.7	38.1[2]	2021-03-03 - 2021-06-20	Hm0 [m], TP [s], Tz [s], Tm01 [s], Tm02 [s], MWD [°], PWD [°], DSD [°]	1,024	600	Wave buoy (Wavesense 3)	RVO/ FUGRO
WHI	2.4391	51.3810	28.1	34.3[2]	2011-05-19 - 2022-09-30	Hm0 [m], Tz [s]	~3,600[3]	3,600	Not known	CMEMS

[1] Modelled seabed elevation based on the production mesh
[2] Seabed elevation from EMODnet 2020
[3] Averaging period is not known but assumed to be the same as the sampling interval

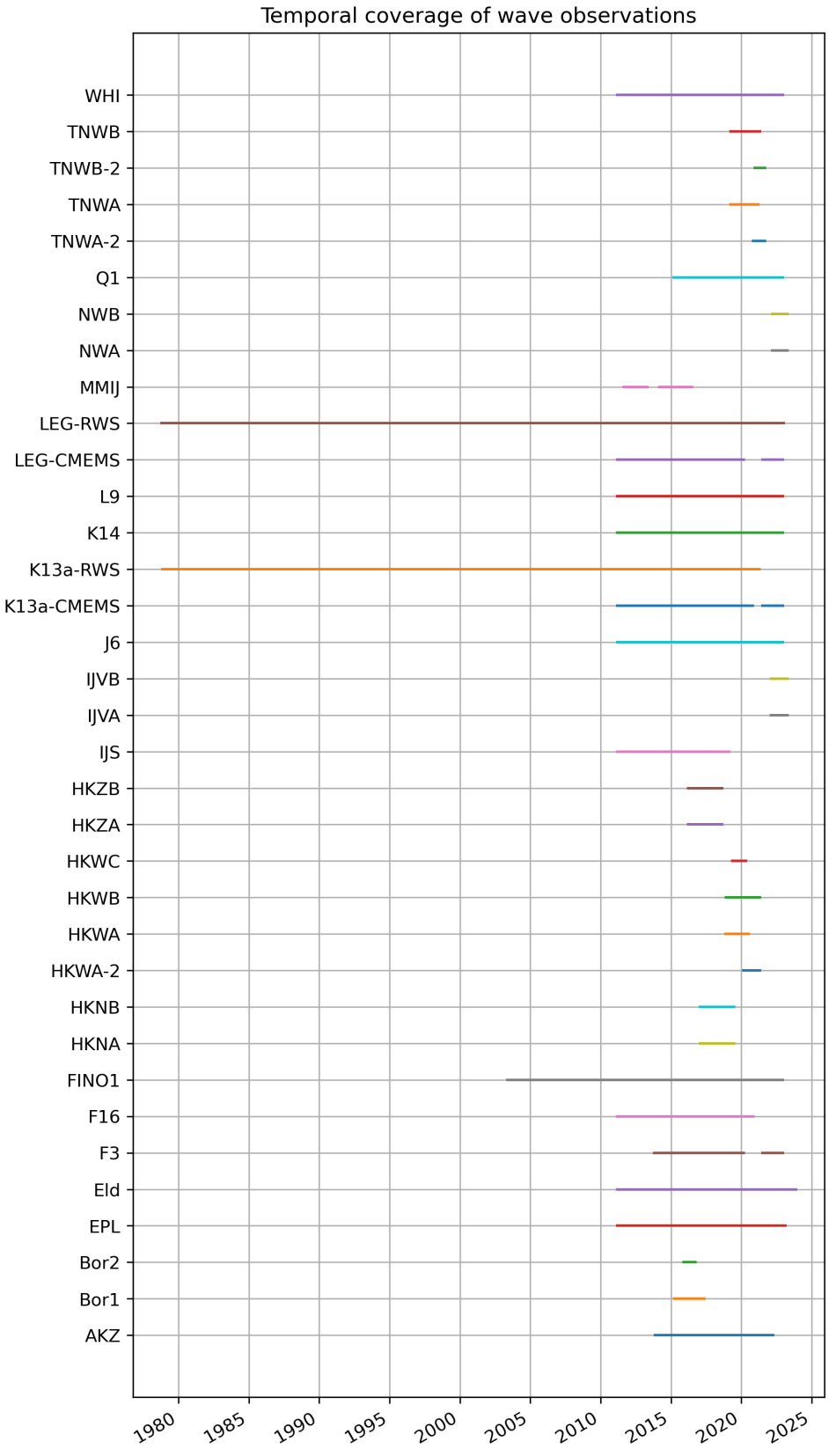

Figure 2.22 Temporal coverage of wave measurements.

3 Metocean Modelling

This section provides information about the different numerical models developed as part of the metocean study. This includes the atmospheric WRF model used to force DHI's local hydrodynamic and spectral wave models as well as these models.

3.1 Weather Research Forecasting (WRF) model

Atmospheric data used as forcing of the numerical hydrodynamic and wave models and for analyses purposes was adopted from the dedicated Weather Research Forecasting (WRF) model developed exclusively for this project.

A full description of the WRF model is shown in the combined Wind Resource Assessment (WRA) and WRF report [2]. For the sake of the simplicity of this report, only a short summary of the WRF model is presented in the following bullet points. For further details, the reader is referred to [2]:

- WRF model was downscaled from ECMWF's ERA5 dataset.
- Temporal resolution was 10 minutes.
- Variable spatial resolution, with a ~1.67 km resolution in all the delivered datasets, and ~5 km resolution near the hydrodynamic and spectral wave model boundaries.
- Data available at several heights between 10 and 300 mMSL.
- Data from the WRF model spans the years 1979 to 2022 (both years included).

Model validation at several heights is also presented in the WRA/WRF report. For ocean modelling purposes, only winds near the water surface are relevant since both the spectral wave and hydrodynamic models are forced with winds at 10 mMSL. In Figure 2.10 and Table 2.6 a list of wind measurement stations with near-surface data is provided. Most of LiDAR or Floating LiDAR stations have data at approx. 30 mMSL, whereas only the data retrieved from KNMI is provided at 10 mMSL.

Figure 3.1 and Figure 3.2 present comparisons of measured and modelled wind data at the 30 mMSL in terms of scatter plots and wind roses for stations IJVA and IJVB, respectively. The figures demonstrate a very good agreement between the datasets of both wind speed and wind direction. For the sake of the readability of this report, in this section, only validation plots of the stations at the IJmuiden Ver site are provided. The remainder of the validation plots are shown in Appendix C.

Table 3.1 shows the summary of the model validation at all wind measurement stations previously introduced in Table 2.6. From these results it can be concluded that the WRF data compares very well to the local measurements and is considered excellent as wind forcing for the hindcast hydrodynamic and spectral wave models to produce accurate waves, currents, and water levels at the IJmuiden Ver site.

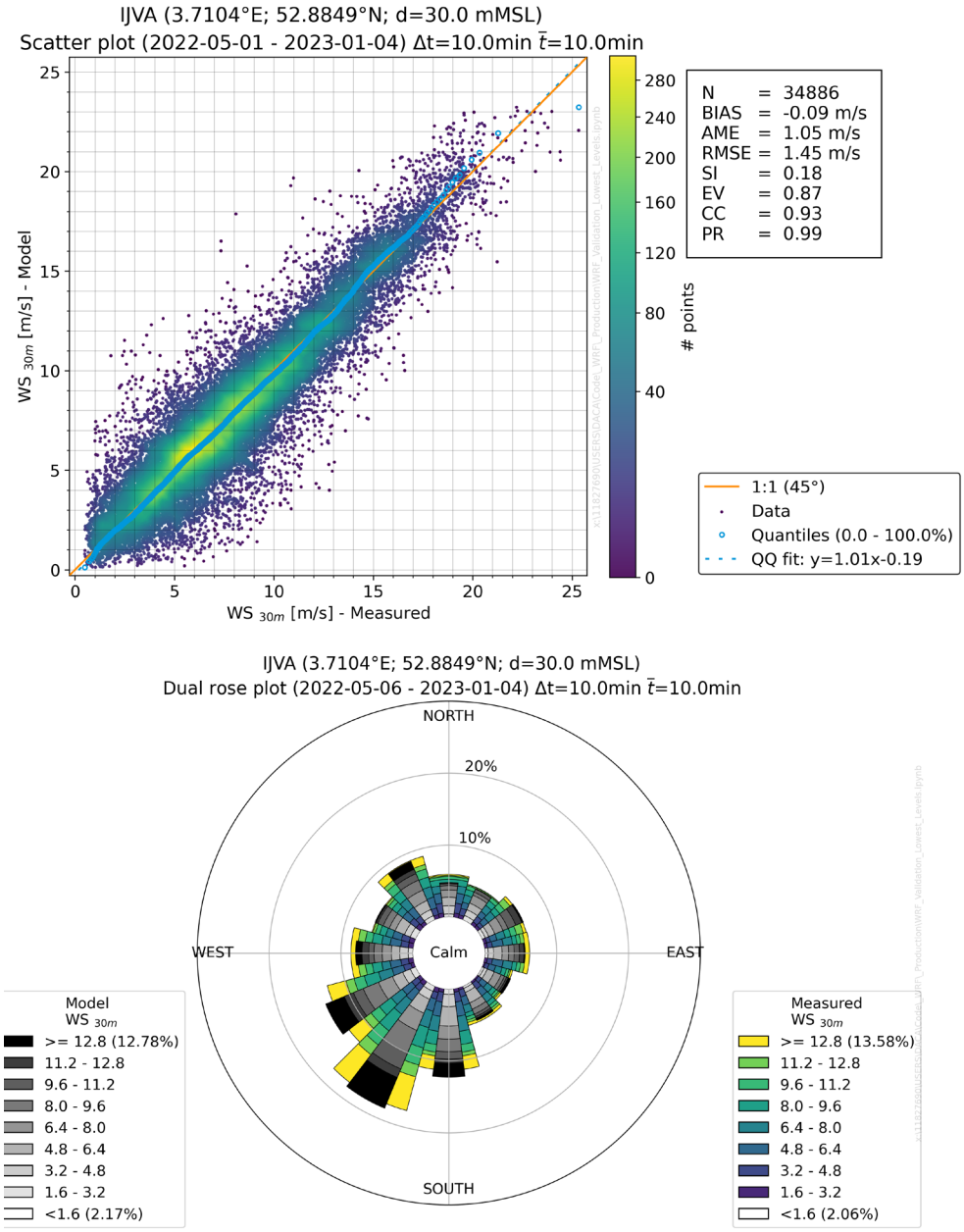

Figure 3.1 Comparison of measured and modelled (WRF) winds at IJVA station. Comparison at 30 mMSL.
Top: Scatter plot comparison. Bottom: Dual wind rose comparison.

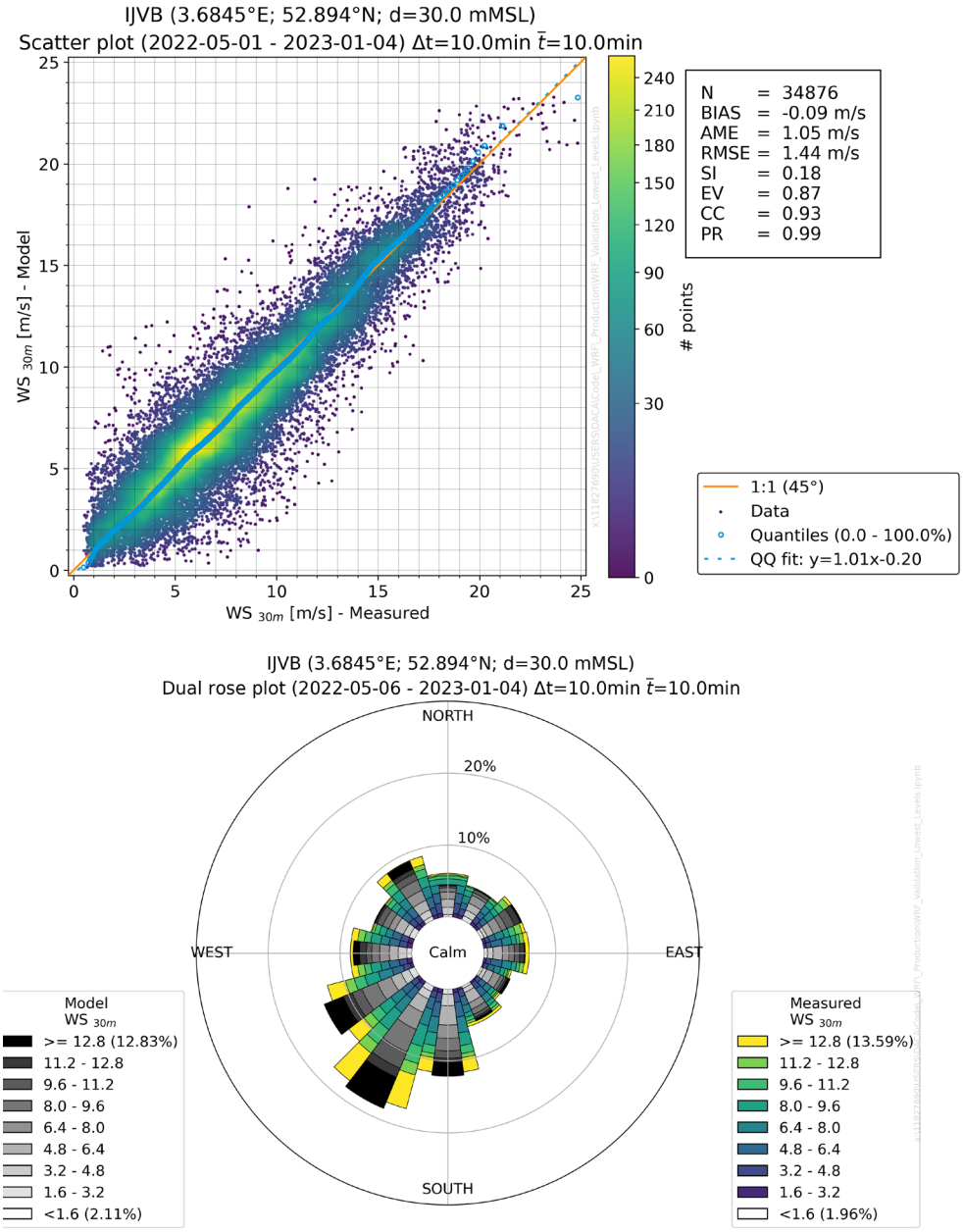

Figure 3.2 Comparison of measured and modelled (WRF) winds at IJVB station. Comparison at 30 mMSL.
Top: Scatter plot comparison. Bottom: Dual wind rose comparison.

Table 3.1 Summary table of WRF model wind validation.
Comparison statistics between WRF model and measurements at near-surface height. Stations IJVA and IJVB are highlighted with bold text.

Station Name	Number of data points	Bias [m/s]	AME [m/s]	RMSE [m/s]	SI [-]	EV [m]	CC [-]	PR [-]
EPL	226933	0.17	1.05	1.40	0.18	0.86	0.93	1.03
F16	113417	0.41	1.44	1.86	0.23	0.78	0.89	0.98
F3	223949	0.33	1.15	1.59	0.19	0.85	0.92	0.99
FINO1	166191	0.05	1.44	1.95	0.23	0.76	0.88	0.98
HKN	92765	-0.08	1.02	1.41	0.16	0.88	0.94	0.97
HKW	99414	0.01	1.02	1.40	0.15	0.89	0.95	1.01
HKZ	92274	-0.02	1.05	1.45	0.18	0.86	0.93	0.99
IJVA	**34886**	**-0.09**	**1.05**	**1.45**	**0.18**	**0.87**	**0.93**	**0.99**
IJVB	**34876**	**-0.09**	**1.05**	**1.44**	**0.18**	**0.87**	**0.93**	**0.99**
J6	116592	0.10	1.24	1.62	0.20	0.81	0.91	0.96
K13a	226046	-0.03	1.11	1.48	0.18	0.85	0.92	1.00
K14	119746	-0.02	1.23	1.62	0.20	0.83	0.91	0.95
L9	119980	-0.07	1.31	1.75	0.21	0.81	0.90	0.95
LEG	360069	0.05	1.16	1.55	0.20	0.83	0.91	0.96
MMIJ	194828	-0.02	1.02	1.39	0.15	0.89	0.95	1.00
N72	42180	-0.05	1.06	1.44	0.16	0.86	0.93	1.01
OWEZ	43092	0.10	1.05	1.44	0.18	0.85	0.93	0.97
P11	111451	0.43	1.36	1.81	0.23	0.80	0.90	1.01
TNWA	92760	0.00	1.01	1.37	0.15	0.89	0.95	0.99
AVERAGE	**132182**	**0.06**	**1.15**	**1.55**	**0.19**	**0.84**	**0.92**	**0.99**

3.1.1 Averaging period of winds

Mean wind measurements commonly represent 10-minute averages at a single point, while atmospheric modelled wind data represent an area and duration determined by a combination of the applied forcing and the model grid. One may therefore expect the measurements to exhibit higher variability (more variance) compared to model data. Correspondingly, the model data may be regarded as somewhat 'smoothed' (in space and time) compared to the observations. Meaning that the model data does not show the small (or even larger events like gusts) and rapid changes compared to reality and are thus considered smooth.

In this section, the effect of 'smoothing' is estimated by comparing WRF model spectra to spectra from measured time series. The averaging period or 'temporal scale' was assessed by comparing power spectra of the measured wind speeds at IJVA and IJVB stations. The comparison was performed for the

wind speed at 30 mMSL (WS_{30}), which is the lowest layer available in the measurements.

The frequency power spectra of the WRF model and the measurements with applied moving averages of 10-minute (i.e., no averaging), 20-minute, 30-minute, 1-hour and 2-hour are shown in Figure 3.3. The measured spectra for different averaging periods are plotted until a Nyquist frequency of 20-minute, since the sampling frequency of the measurements is 10-minute. Similarly, the modelled spectra are plotted until a Nyquist frequency of 20-minute.

For the spectra of the averaged measurement time series wriggles are observed for frequencies below the Nyquist frequency times the ratio of averaging time to 10-minute due to the averaging filter applied. Therefore, only frequencies lower than these frequencies are used for comparing model to measurements. The best agreement of slopes is found between the WRF model spectrum and the spectrum of the 10min time series, and hence “we say” that WRF represents 10-min averaged wind speeds.

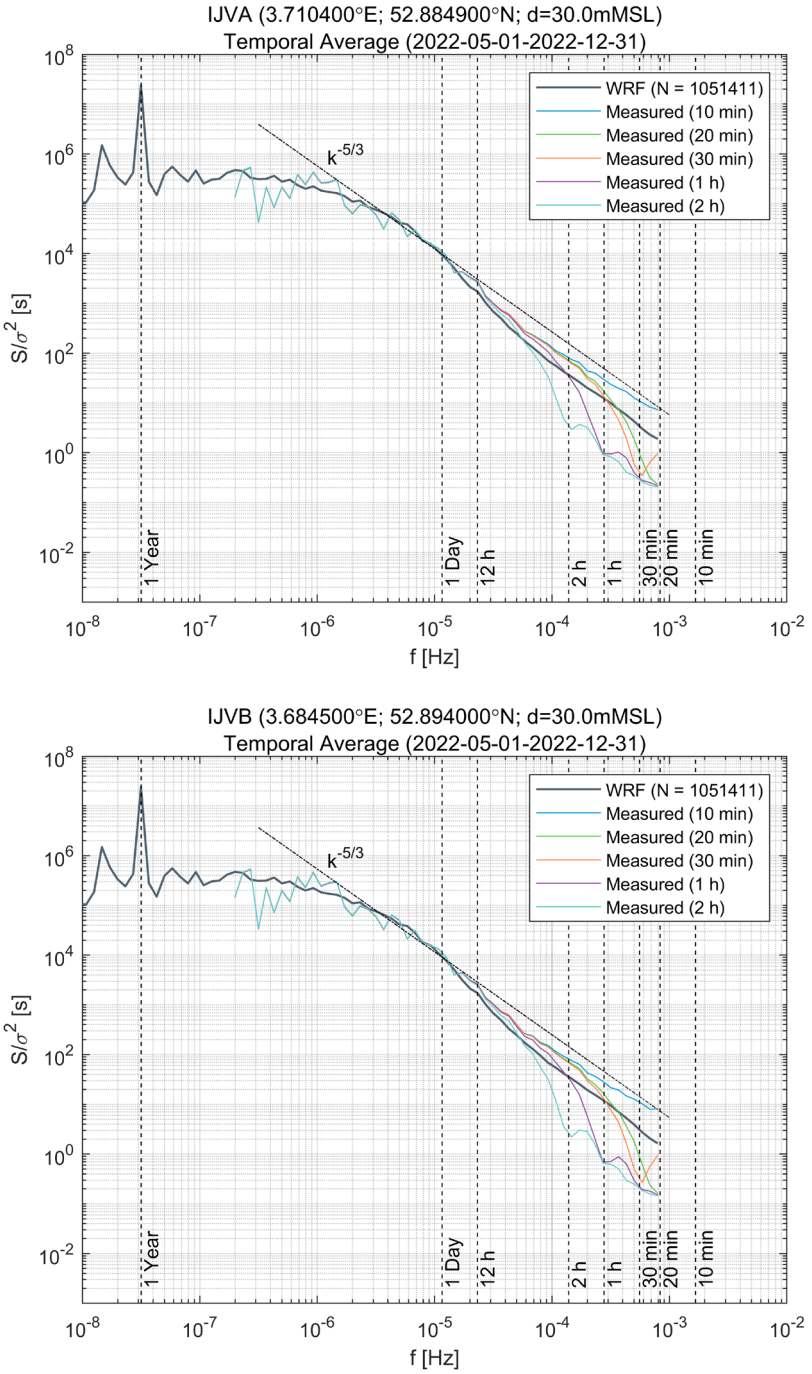

Figure 3.3 Frequency power spectra of wind speed at 30 mMSL (WS_{30}) at IJVA (top) and IJVB (bottom).

3.1.2 Wind gusts (3-second wind gusts)

A 3-second gust wind speed may be required for design purposes. This section describes common factors for conversion between 10-minute wind and 3-second gust and arrives at recommended temporal conversion factors for 3-second gust.

Table 3.2 lists common temporal conversion factors to convert between

10-minute and 3-second gusts of extreme wind speeds. The factors are developed specifically for storm conditions. Thus, the factors are not applicable to convert time series of wind speeds (as this would increase the mean value).

The factors are adopted from IEC, CEM, WMO, and DNV/ISO. The IEC, CEM, and WMO factors are independent of wind speed (fixed surface roughness). Hence, when using a wind speed independent vertical profile (such as the power profile), the factors become independent of height. The WMO factors are recommended specifically for tropical cyclones.

The DNV/ISO (Frøya) factors [19] consider the variation in turbulence intensity as a function of speed and height. The Frøya profile also uses a 1-hour average wind speed as a reference. Table 3.2 provides three examples using 20, 30, and 40 m/s wind speed as reference 1-hour average wind speeds at 10 m height using Frøya profile[19]. To get the conversion factors relative to 10-minute wind speeds, first, the factors are calculated relative to 1-hour wind speeds, and subsequently the factors relative to 10-minute wind speeds are calculated. Table 3.2 also provides factors from IEC, CEM and WMO standards.

Table 3.2 Common temporal conversion factors of extreme wind speed. 10-minute is the representative averaging period of the WRF wind data.

Reference	Remark	10-min	3-s
DNV [19], ISO [20] (Frøya)	20m/s, 10m height	1.0	1.22
	30m/s, 10m height	1.0	1.26
	40m/s, 10m height	1.0	1.30
IEC [21]	All speeds/heights	1.0	-
CEM [22]	All speeds/heights	1.0	1.44
WMO[8] [23]	All speeds/heights	1.0	1.26

For the design of an OWF, the IEC standard is one of the main standards used. However, the IEC standards do not provide a conversion factor for 3-second gusts. On the other hand, the DNV standards [19] are also widely used. The Frøya profile provides a reasonably conservative method for converting the 10-minute wind to 3-second gust. **Therefore, it is recommended to adopt the DNV factors for converting between 10-minute extreme wind speed and 3-second gusts**.

3.2 DHI's Hydrodynamic model

Hindcast water level and current data were established from a dedicated high-resolution local hydrodynamic model developed specifically for this study. This model is referred to as HD_{DWF23} (Hydrodynamic model for the Dutch Wind Farm zones 2023) herein.

This version of the hydrodynamic model differs from its 2020 predecessors (HKZ, HKN, DWF_{2020} [5, 6]) by its bathymetry and mesh resolution within IJmuiden Ver wind farm zone as well as by its atmospheric forcing and the

[8] WMO is recommended specifically for tropical cyclones.

inclusion of data assimilation in the HD model. More details about these modifications are given in the subsequent subsections.

The HD_{DWF23} was forced by boundary conditions extracted from DHI's high-resolution regional hydrodynamic model covering Northern Europe, HD_{NE-DA} [24].

The hydrodynamic modelling includes both astronomical tide and surge forced by the atmospheric data from the WRF model. The hindcast covers a period of 44 years between 1979 and 2022 and has a 30-minute temporal resolution output (time step).

The model is based on DHI's MIKE 21 Flow Model FM (Flexible Mesh) module which includes:

- Water level
- Depth-averaged zonal and meridional current components.

3.2.1 MIKE 21 Flow Model FM

The MIKE 21 Flow Model FM is a modelling system for 2D free-surface, depth-integrated flows that is developed and maintained by DHI and offered as part of MIKE Powered by DHI[9].

The model system is based on the numerical solution of the two-dimensional (2D) incompressible Reynolds-averaged Navier-Stokes equations subject to the assumptions of Boussinesq and of hydrostatic pressure. The model is applicable for the simulation of hydraulic and environmental phenomena in lakes, estuaries, bays, coastal areas, and seas, wherever stratification can be neglected. The model can be used to simulate a wide range of hydraulic and related items, including tidal exchange, currents, and storm surges.

The hydrodynamic (HD) module is the basic module in the MIKE 21 Flow Model FM. The HD module simulates water level variations and flows in response to a variety of forcing functions in lakes, estuaries, and coastal regions. The effects and facilities include:

- Bottom shear stress
- Wind shear stress
- Barometric pressure gradients
- Sources and sinks (e.g., rivers, intake, and outlets from power plants) (not applied here)
- Flooding and drying
- Momentum dispersion
- Coriolis force
- Tidal potential (not applied in this study)
- Precipitation/Evaporation (not applied in this study)
- Ice coverage (not applied in this study)

9 https://manuals.mikepoweredbydhi.help/2023/Coast_and_Sea/M21HDFST_Scientific_Doc.pdf

- Wave radiation stresses (not applied in this study)

The model uses a flexible mesh (FM) based on unstructured triangular or quadrangular elements and applies a finite volume numerical solution technique[25]. The version 2022 of MIKE 21 Flow Model FM was used in the present study.

3.2.2 North Europe HD model ($HD_{NE\text{-}DA}$)

The North Europe hydrodynamic model previously developed by DHI, $HD_{NE\text{-}DA}$, was used to provide boundary data for the local hydrodynamic model of this study, HD_{DWF23}.

Figure 3.4 shows the $HD_{NE\text{-}DA}$ model domain along with its bathymetry and the location of the local HD_{DWF23} model boundaries. The $HD_{NE\text{-}DA}$ model includes tide (boundaries extracted from DHI's global tide model) and surge forced by wind fields and air pressure from the ERA5 dataset. Furthermore, the model was optimised by using data assimilation of measured water levels. The assimilation was applied for the period from 1993-01-01 to 2022-12-31 using the available data from most of the stations. Figure 3.5 shows stations used for assimilation or validation of the $HD_{NE\text{-}DA}$ model in the North Sea area. The results of $HD_{NE\text{-}DA}$ have been successfully applied in many projects in the North Sea, the English Channel, the Baltic Sea, and the Inner Danish waters. The regional $HD_{NE\text{-}DA}$ model (including the details of the data assimilation scheme) is fully explained in[24], which is also attached in Appendix H.

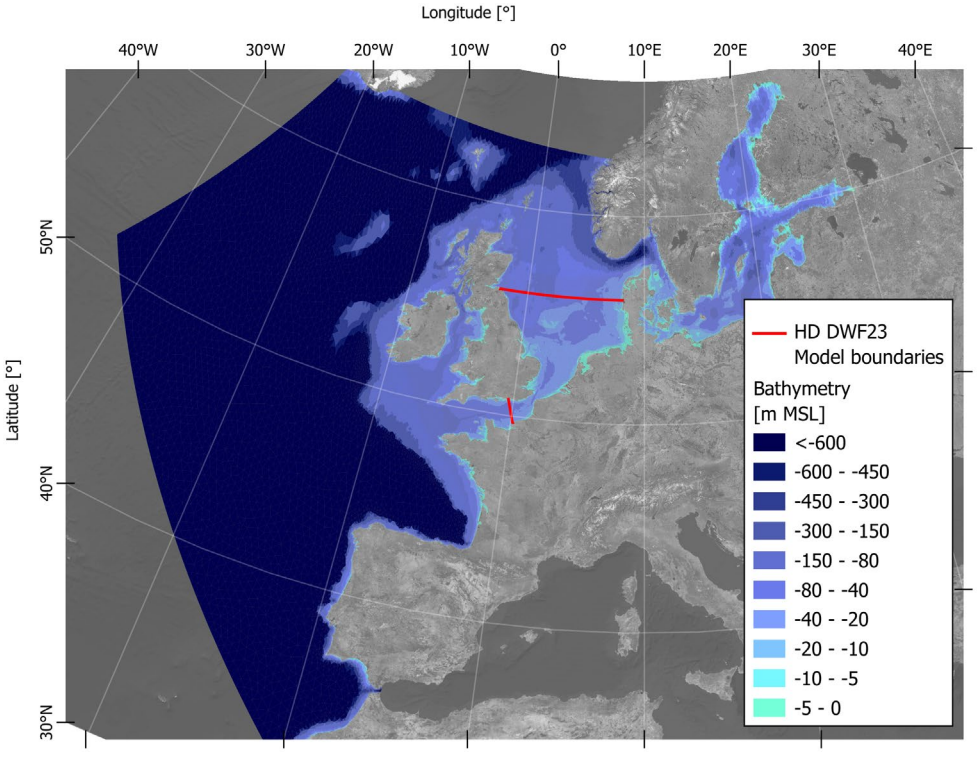

Figure 3.4 North Europe hydrodynamic model ($HD_{NE\text{-}DA}$) coverage and bathymetry.
Red lines indicate the boundaries of the local HD_{DWF23} model.

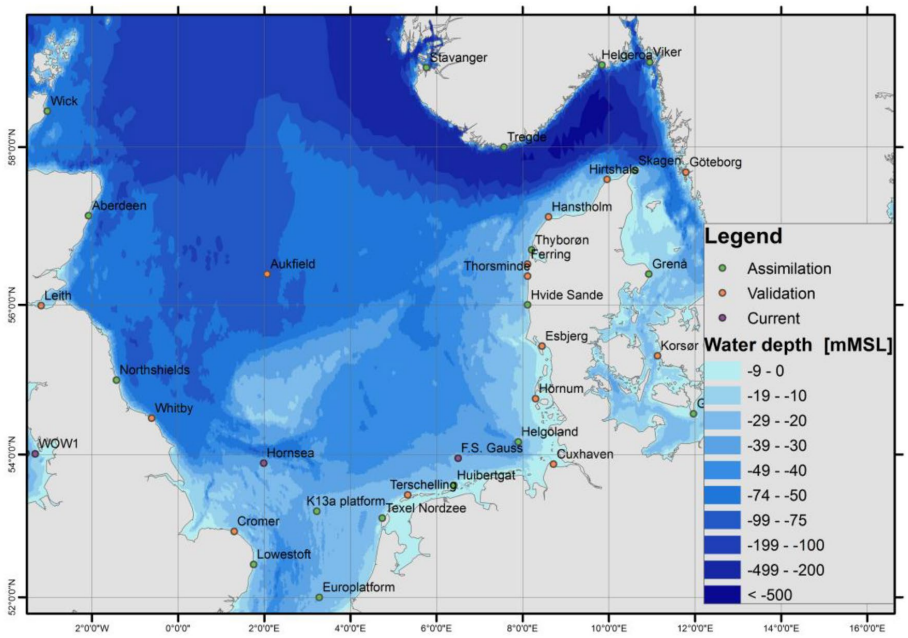

Figure 3.5 Water level and current measurement stations used for assimilation and validation of $HD_{NE\text{-}DA}$.

3.2.3 Hydrodynamic model for the Dutch Wind Farm area (HD_{DWF23})

The following sections describe the establishment of the hydrodynamic model (HD) data developed and used in this project. To achieve high-quality results, a dedicated high-resolution local HD model (HD_{DWF23}) using the latest bathymetric surveys and available data listed in Section 2.1 was set up for the Dutch Wind Farms area.

3.2.4 Model domain, bathymetry, and resolution

The dedicated high-resolution local HD_{DWF23} model was set up to provide the highest quality results at IJmuiden Ver, Doordewind and Nederwiek OWFZs. Additionally, a total of 10 search areas were defined as areas of semi-high resolution.

The local model uses an unstructured mesh with progressively increasing spatial resolution towards the Dutch Wind Farm area. The model domain and bathymetry used for the present study is shown in Figure 3.6 and Figure 3.7 with highest resolution of about 400 m at IJmuiden Ver, Doordewind and Nederwiek, whereas a resolution of about 1000 m was set in the search areas. Outside these refined areas, the mesh resolution varied from 3 km up to 3.5 km close to the model boundaries.

The model bathymetry was generated based on the bathymetric datasets described in Section 2.1, with the vertical datum corresponding to mean sea level (MSL)

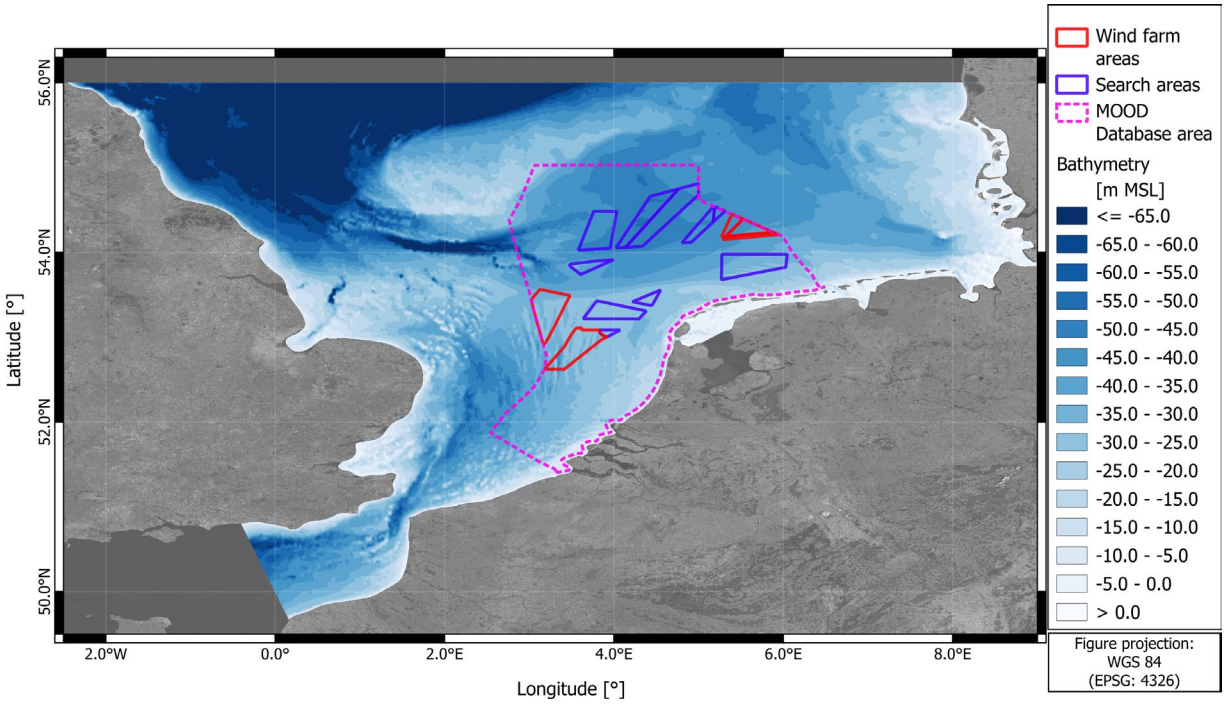

Figure 3.6 Domain and bathymetry of the local hydrodynamic model, HD_{DWF23}.

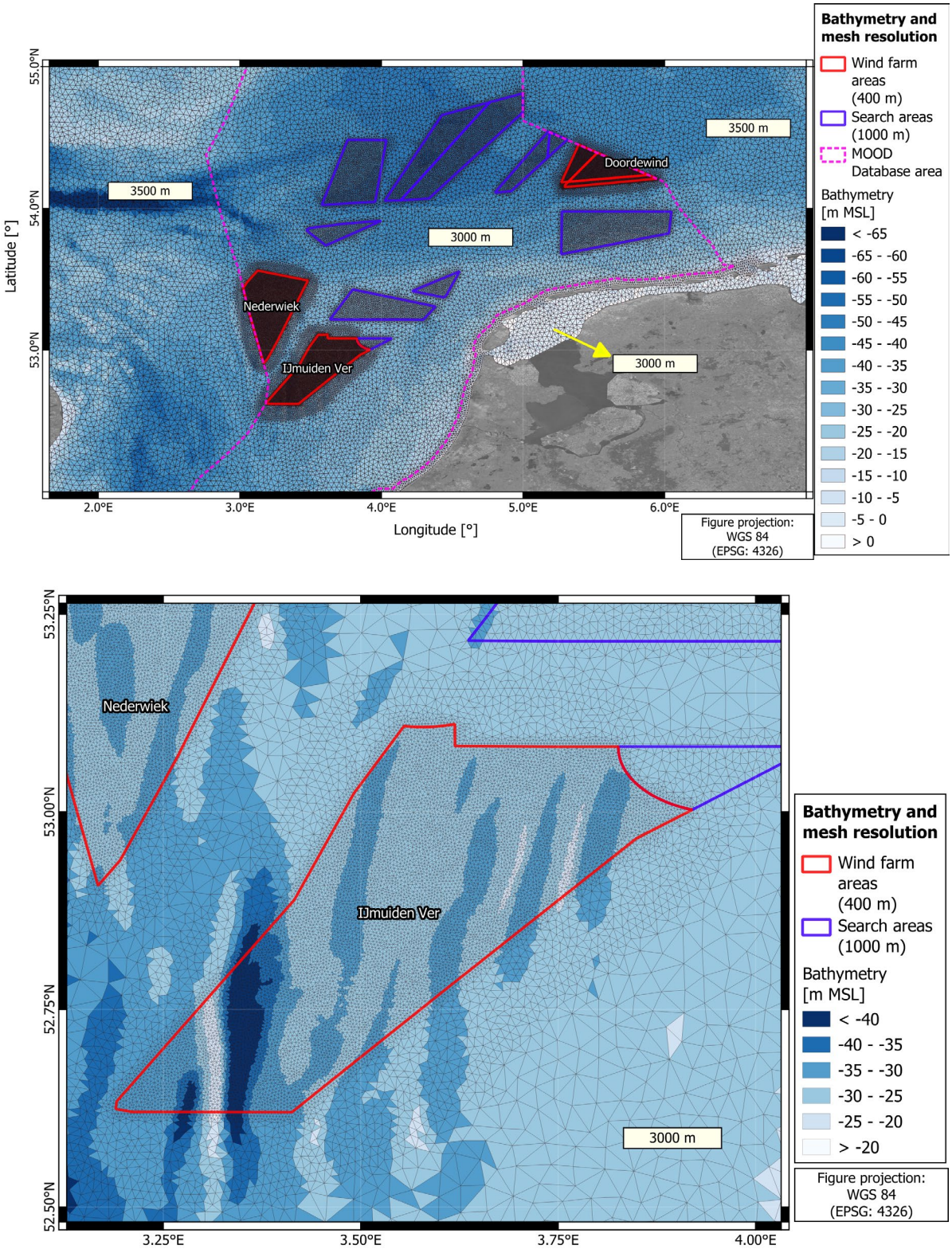

Figure 3.7 Zoom of the final mesh used in HD$_{DWF23}$ close to the Dutch offshore wind farm areas. Top: Zoom comprising all the search areas. Bottom: Zoom at IJmuiden Ver.

3.2.5 Model setup and parameters

The HD_{DWF23} model was defined with two open boundaries. The model relied on the boundary information from the regional HD_{NE-DA} model[24]. So-called 'Flather' boundary conditions technique that includes both the surface elevation and the currents from the regional HD model is implemented into the local HD model.

The HD_{DWF23} flow model was set up with the specifications listed in Table 3.3.

Table 3.3 Summary of the $HD_{DWF2023}$ model settings applied for production.
Settings considered after the calibration exercise.

Setting	Value
MIKE Engine	MIKE 21 Flow Model FM Release 2022
Mesh resolution	Element size around IJmuiden Ver, Doordewind and Nederwiek of ~400m
Simulation period	1979-01-01 – 2022-12-31
Output time step	30-minute
Density	Barotropic
Eddy viscosity	Smagorinsky formulation with a constant value of 0.28
Bed resistance	Manning number varying in domain M=35 $m^{1/3}/s$ if depth>25m (deeper areas) M=38 $m^{1/3}/s$ elsewise (shallower areas).
Atmospheric forcing	WRF wind and pressure fields downscaled from ERA5 [2], with a 1.67 km resolution Friction varying with wind speed: Linear variation from 0.001255 at 7m/s to 0.002425 at 25m/s wind speed (uniform value for wind speeds >25 m/s)
Tidal potential	Not included
Boundary conditions	Flather boundary conditions[10], extracted from HD_{NE-DA} [24], varying in time and along the boundaries: • Current velocity components • Water level
Data assimilation	Assimilation of water level in 7 stations See details in section 3.2.6.

3.2.6 Data assimilation

Data assimilation (DA) is a method that utilises observed measurements to improve the skills and accuracy of a model. In this project, assimilation of in-situ water level data was considered. The observations included were in-situ measurements obtained from either CMEMS or Rijkswaterstaat data portal.

[10] Details on flather boundary conditions shown in [25] DHI, "MIKE 21 Flow Model FM, Hydrodynamic Module, User Guide," 2022. .

The main difference of a model that incorporates data assimilation, compared to a model without it, is that when data assimilation is included, the measurements are not only used for model calibration/validation but are used when the model is running as a target function, i.e., the model results are nudged towards the measurement values. This generates overall a significant improvement of the model results.

For the sake of the simplicity of this report, the full explanation of the data assimilation procedure is shown in the $HD_{NE\text{-}DA}$ report [24], since the same setup was used in the HD_{DWF23} model; hence, only a summary is presented in this section.

A very relevant component of the data assimilation workflow is indicating the stations that were used to assimilate the HD_{DWF23} model. Most of these stations are located outside the data delivery area (MOOD Database Area) as shown in Figure 3.8. The stations used for data assimilation, except for K13a and Europlatform, were not considered as part of the model calibration nor validation. Having independent measurements for assimilation adds robustness to the modelling procedure, because it means that most of the water level measurements listed previously in Table 2.7 were not incorporated in the data assimilation framework but were only used for model validation. The number of assimilation/validation stations is summarised in the following bullet points:

- Number of assimilation stations used in HD_{DWF23} model: 7 stations.
- Number of validation stations used in HD_{DWF23} model: 23 stations.

The list of stations used for data assimilation is shown in Table 3.4. It is important to stress that current measurements were not assimilated.

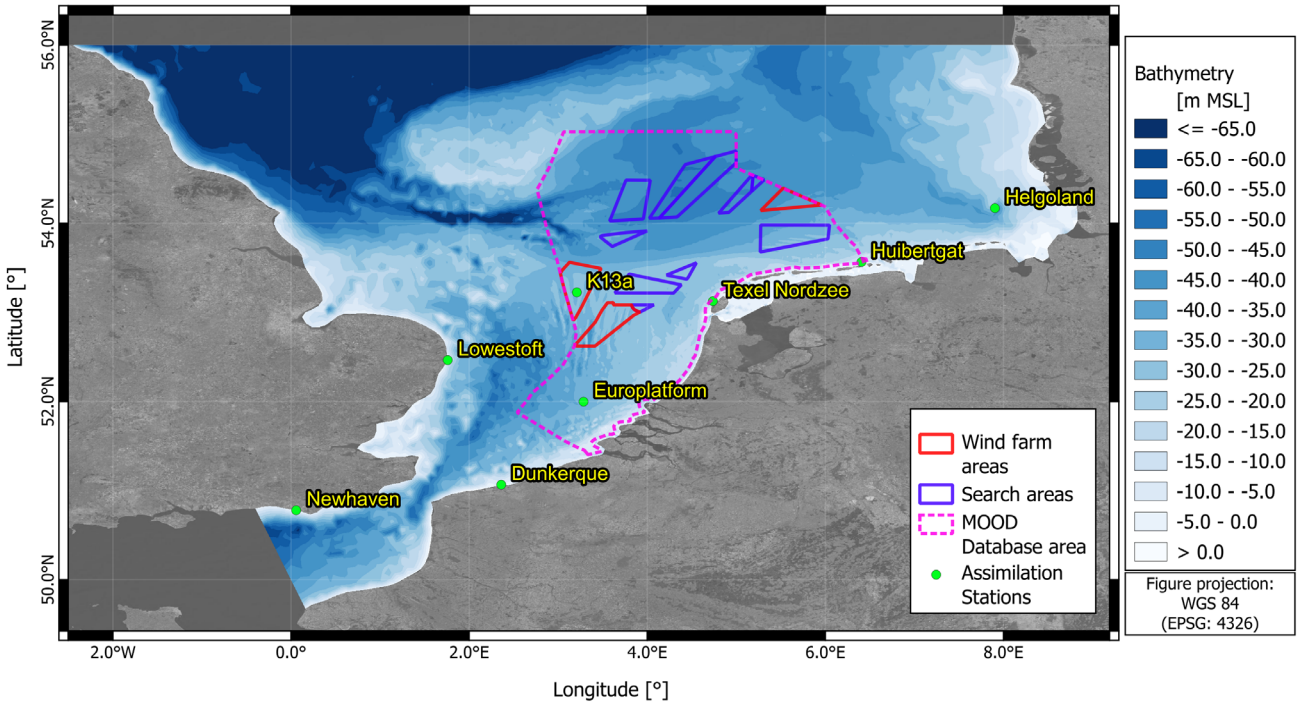

Figure 3.8 Location of stations used for data assimilation of water levels in HD_{DWF23} model.

Table 3.4 Details of water level measurement stations used for data assimilation in HD_{DWF23} model.
Stations Europlatform (EPL) and K13a are the only stations used both in assimilation and validation of HD_{DWF23} model results.

Station Name	Longitude [°E]	Latitude [°N]	Modelled seabed elevation[1] [mMSL]	Surveyed seabed elevation[2] [mMSL]	Data coverage	Instrument	Data source or surveyor
EPL	3.2748	51.9979	31.6	31.6	1994-01-01 - 2022-12-31	Unknown	RWS
K13a	3.2203	53.2177	29.1	29.1	1994-01-01 - 2022-12-31	Unknown	RWS
Dunkerque	2.3665	51.0482	4.7	12.5	1995-07-09 - 2022-04-30	Unknown	CMEMS
Newhaven	0.0667	50.7833	8.8	4.6	1993-01-01 - 2022-12-31	Unknown	CMEMS
Texel Nordzee	4.7400	53.1200	11.8	11.0	1993-01-01 - 2022-12-31	Unknown	RWS
Huibertgat	6.4000	53.5700	5.0	4.5	1993-12-31 - 2022-12-31	Unknown	RWS
Helgoland	7.8900	54.1789	12.8	9.9	1997-10-14 - 2022-12-31	Unknown	CMEMS

[1] Modelled seabed elevation based on the production mesh.
[2] Seabed elevation from EMODnet 2020.

3.2.7 Convergence study

The mesh convergence study was performed to decide upon the optimal mesh resolution of the model, which ensures the highest accuracy and enhanced computational schemes combined with reasonable computational time. The tests were conducted on three different spatial resolutions (200 m, 300 m, and 400 m) within the IJmuiden Ver Wind Farm. The water depths and element resolution of the three meshes are presented in Figure 3.9.

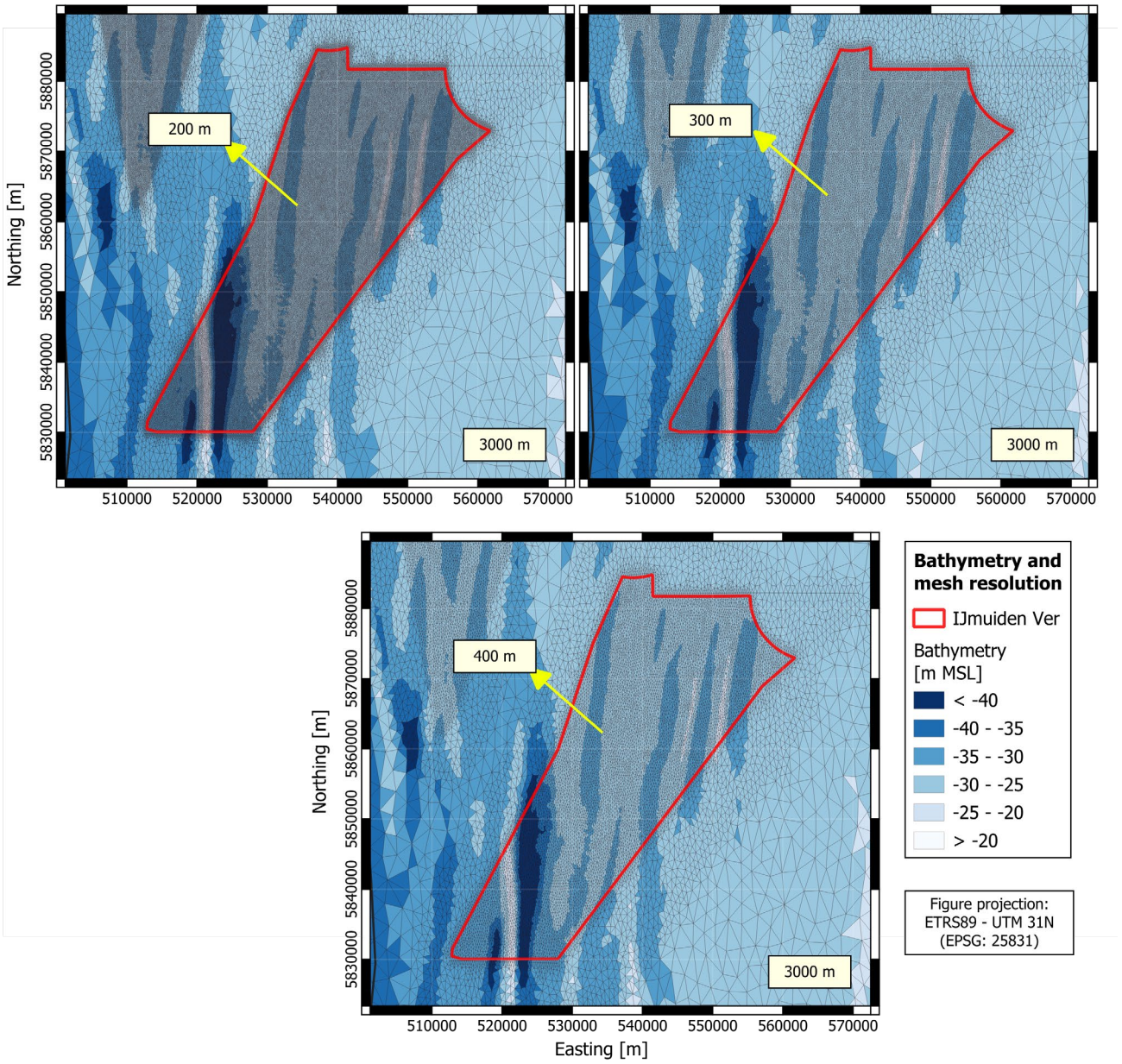

Figure 3.9 Different mesh resolutions at the project location used for the HD mesh convergence study.
Top left panel: 200 m mesh resolution at IJmuiden Ver area.
Top right panel: 300 m mesh resolution at IJmuiden Ver area.
Bottom panel: 400 m mesh resolution at IJmuiden Ver area.
Same resolutions were applied at Doordewind and Nederwiek OWF areas.

To assess the level of representation of the processed bathymetry at the IJmuiden Ver site, some profile comparisons were conducted between the generated bathymetry for the numerical meshes and the bathymetric surveys. The comparison of seabed elevation is presented in Figure 3.10 and Figure 3.11 for computational meshes of 200 m, 300 m and 400 m in 5 different cross sections, which are the same cross sections that were previously defined when comparing the survey data with EMODnet data (Figure 2.4). The bathymetry from the computational meshes follows the trend of the observations quite well.

What can be seen from this comparison is that the sand banks are well represented by all resolutions' meshes (200, 300 and 400 m), whereas the sand waves are averaged out and cannot be properly captured by any of these resolutions. This was expected since the wavelength of the sand waves is in the order of 10-100 m, which is smaller than what the mesh resolution can capture. A very high-resolution mesh would be required to properly capture all these sand waves, but the computation effort required to solve such a mesh is not warranted. Therefore, it is accepted at this stage that only the sand banks will be properly solved by the HD_{DWF23} model.

Overall, the bathymetry from all three computational meshes follows the trend of the observations with sufficient accuracy.

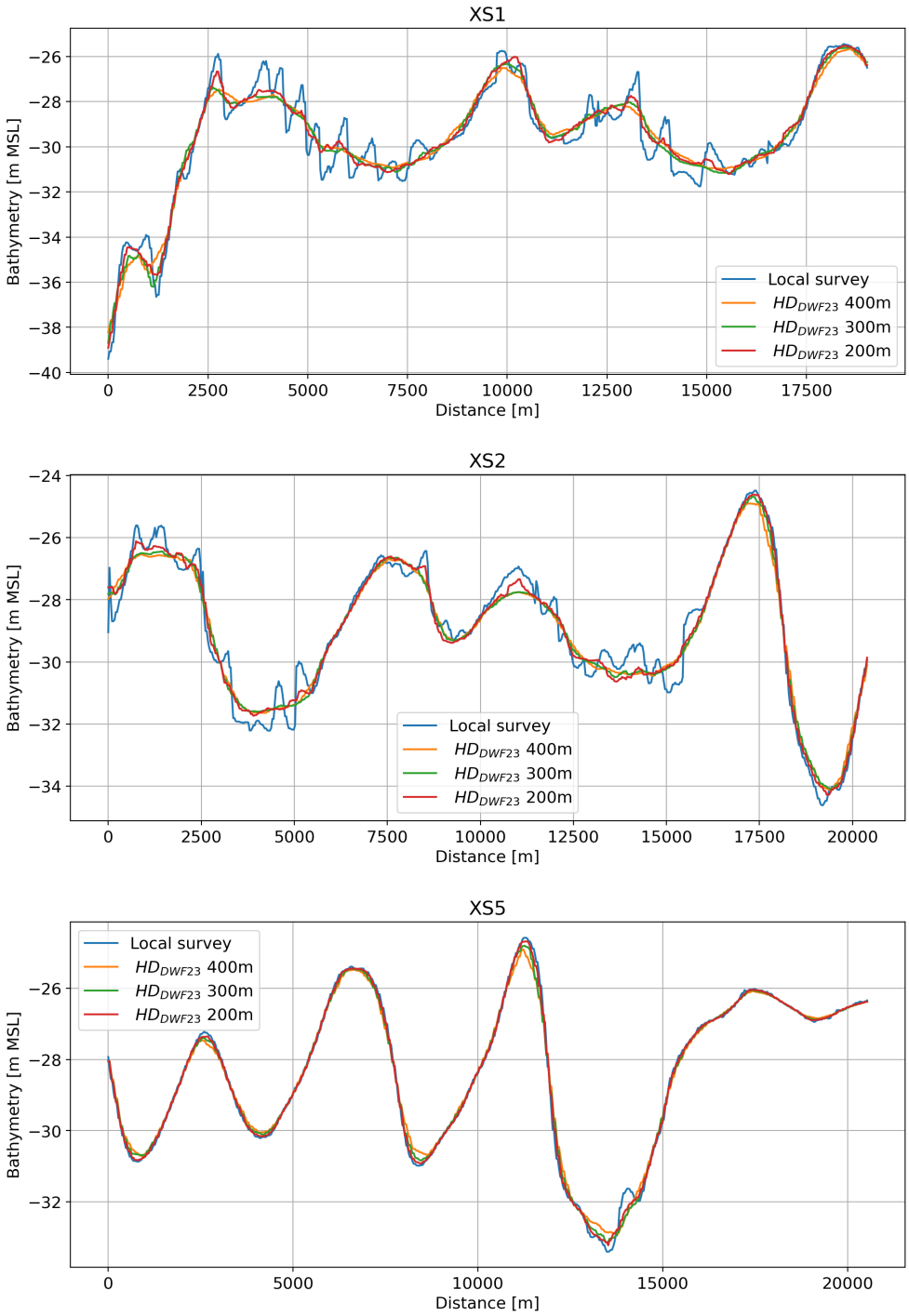

Figure 3.10 Bathymetry comparison in cross sections XS1, XS2 and XS5 between local survey and HD_{DWF23}.
Distances are given in metres from west to east. Initial and final coordinates of the cross sections are shown in Table 2.2.

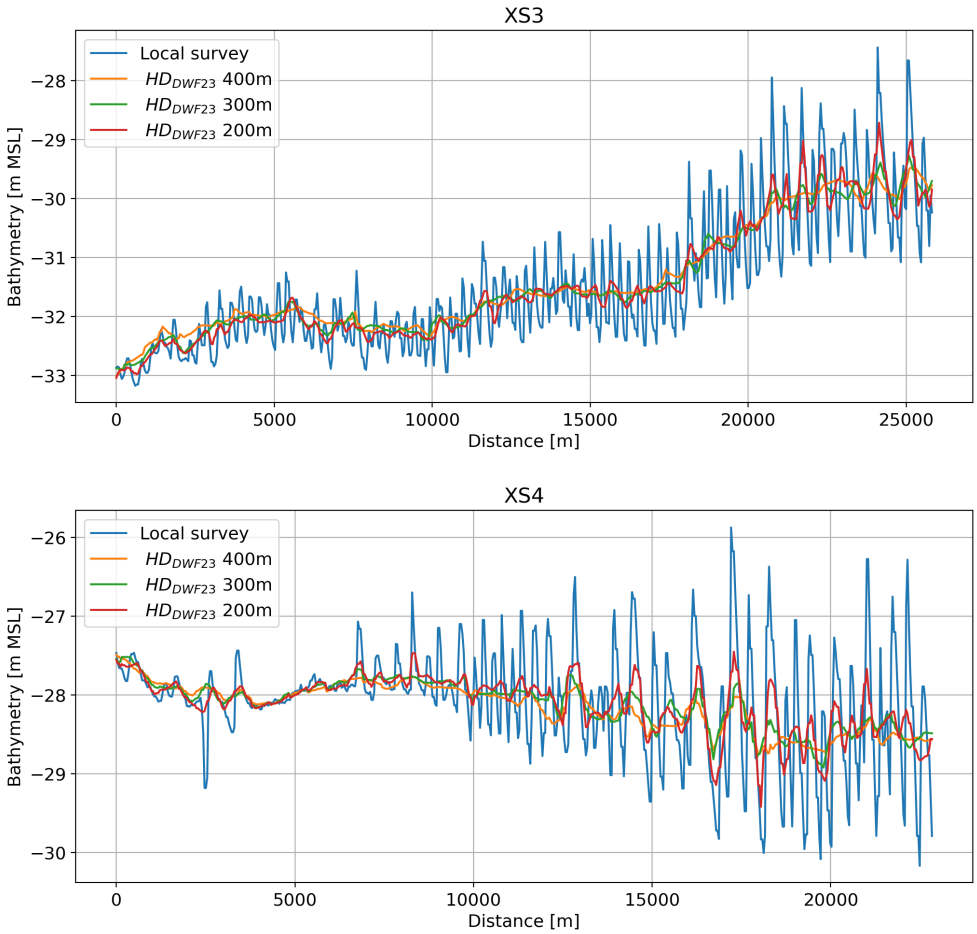

Figure 3.11 Bathymetry comparison in cross sections XS3 and XS4 between local survey and HD_{DWF23}.
Distances are given in metres from north to south. Initial and final coordinates of the cross sections are shown in Table 2.2.

3.2.7.1 Selection of events

The first step of the convergence study was to select a set of scenarios regarding water level and current speeds that could be sensitive to different mesh resolutions. For this purpose, a sample point inside the IJmuiden Ver domain was defined (Point 1), which was located also inside the bathymetry survey area. Additionally, a second point (Point 2) was defined in the north surveyed area of IJmuiden Ver. The location of both points is shown in Figure 3.12.

A 44-year time series of water level and current speeds was extracted at Point 1 from the $HD_{NE\text{-}DA}$ model. From this time series, four events were selected, considering the following criteria:

1. Maximum water level: 1989-02-14 10:00
2. Maximum current speed: 1999-12-24 04:00
3. Maximum combined current speed/water level: 2013-12-05 21:30
4. Minimum water level: 1995-01-31 12:00

A scatter plot of water level vs current speed of the 44-year time series at Point 1 is shown in Figure 3.13, highlighting the four events selected for the convergence study.

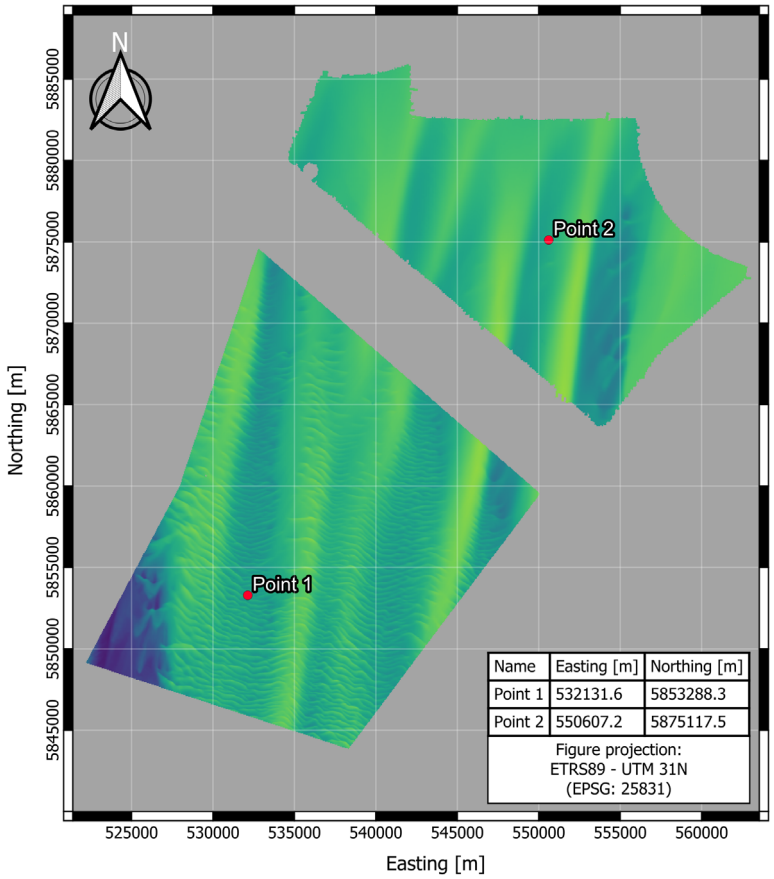

Figure 3.12 Location of the sample points for time series extraction in HD_{DWF23} mesh convergence study.
Points are overlayed on top of the surveyed bathymetry areas in IJmuiden Ver for reference.

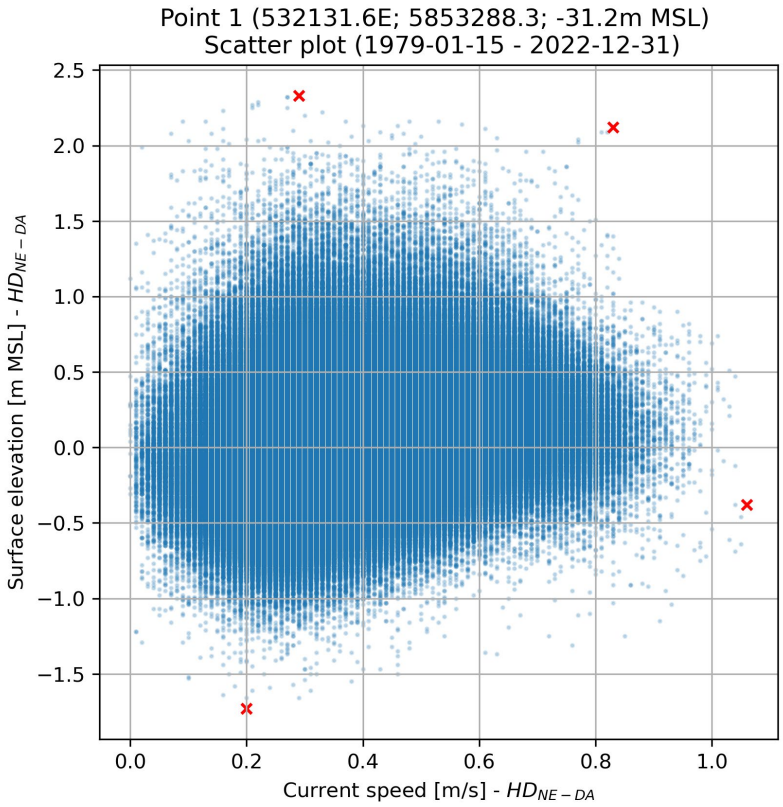

Figure 3.13 Surface elevation vs current speed scatter plot at Point 1 (HD_{NE-DA}) for events selection of HD_{DWF23} convergence study.
The four selected events are shown as red crosses.

It is important to stress that the regional model used for the selection of these events is not relevant since that model was not calibrated for the IJmuiden Ver area, and the sole purpose of the convergence study was to define the optimal mesh resolution for the HD_{DWF23} model production, as the results from the convergence tests were not compared against measurements.

3.2.7.2 Time series comparisons at sample points (1D analysis - Points)

A time series comparison of modelled water level and current speed was carried out at the location of the sample points Point 1 and Point 2 for a 5-day period in each of the four events previously defined.

From all the events, the one that showed the largest differences between models was Event 4, corresponding to the minimum water level (January 1995).

The time series of modelled water level and current speed for all meshes, as well as the time series of the difference between the meshes for Event 4, are shown in Figure 3.14 and Figure 3.15 for Point 1 and Point 2, respectively. In these time series, the first 2 days of the simulation were removed to discard any effect during the model spin-up time. The time series of all the other events assessed during the mesh convergence study are shown in Appendix D.

The differences found between the 200 m, 300 m and 400 m meshes were negligible, with the maximum differences being less than ± 3.0 cm in surface elevation and less than ± 2.0 cm/s in current speed. To assess the differences in the whole IJmuiden Ver area and not just at these two sample points, 2D spatial comparison of the model differences was carried out as presented in the next section.

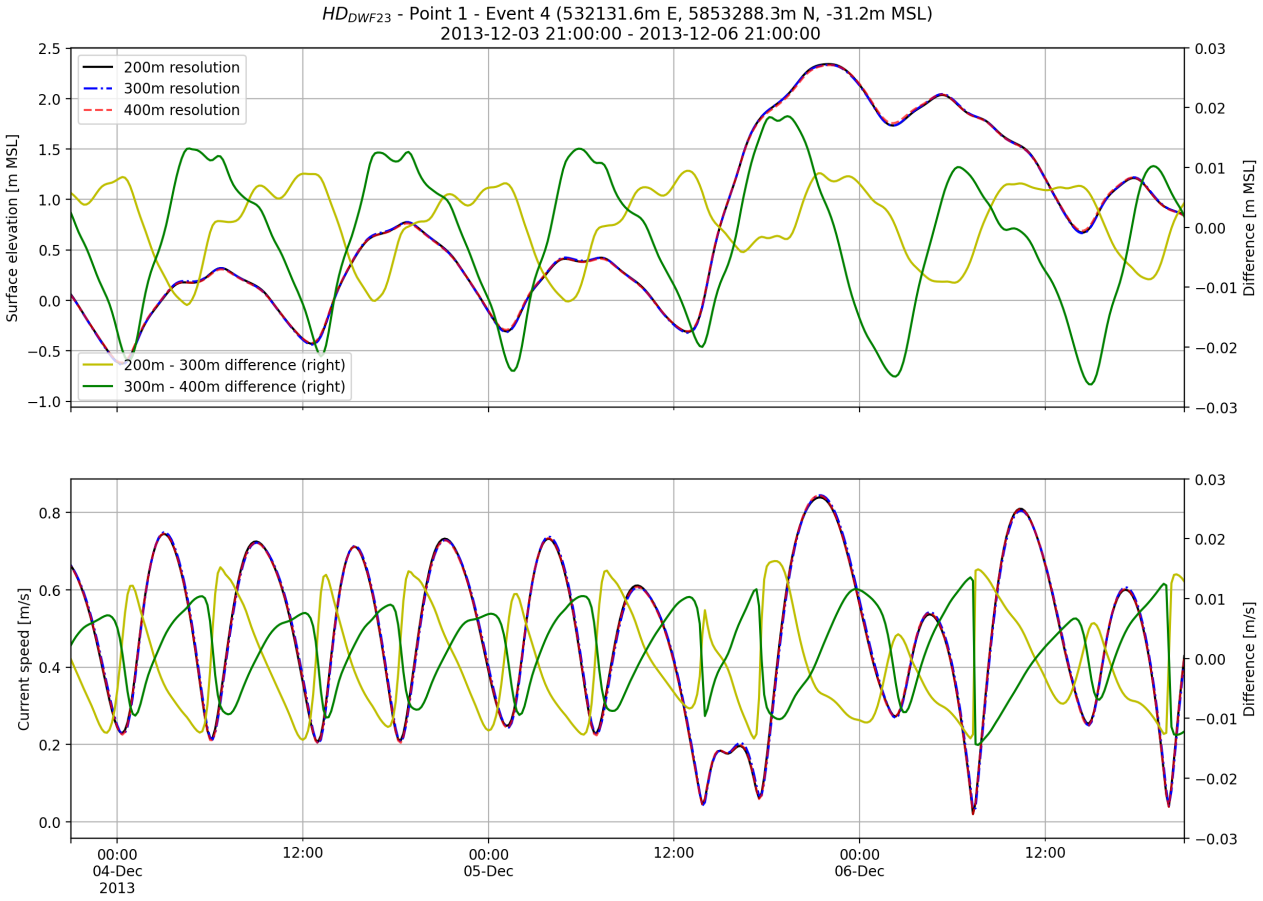

Figure 3.14 Surface elevation and depth-averaged current speed time series comparison between 200 m, 300 m and 400 m mesh resolutions (HD_{DWF23} model) at Point 1 during Event 4. Absolute values are shown on the left axis (black, blue, and red lines), and time series difference between 200-300 m and 300-400 m is shown on the right axis (green and yellow lines).

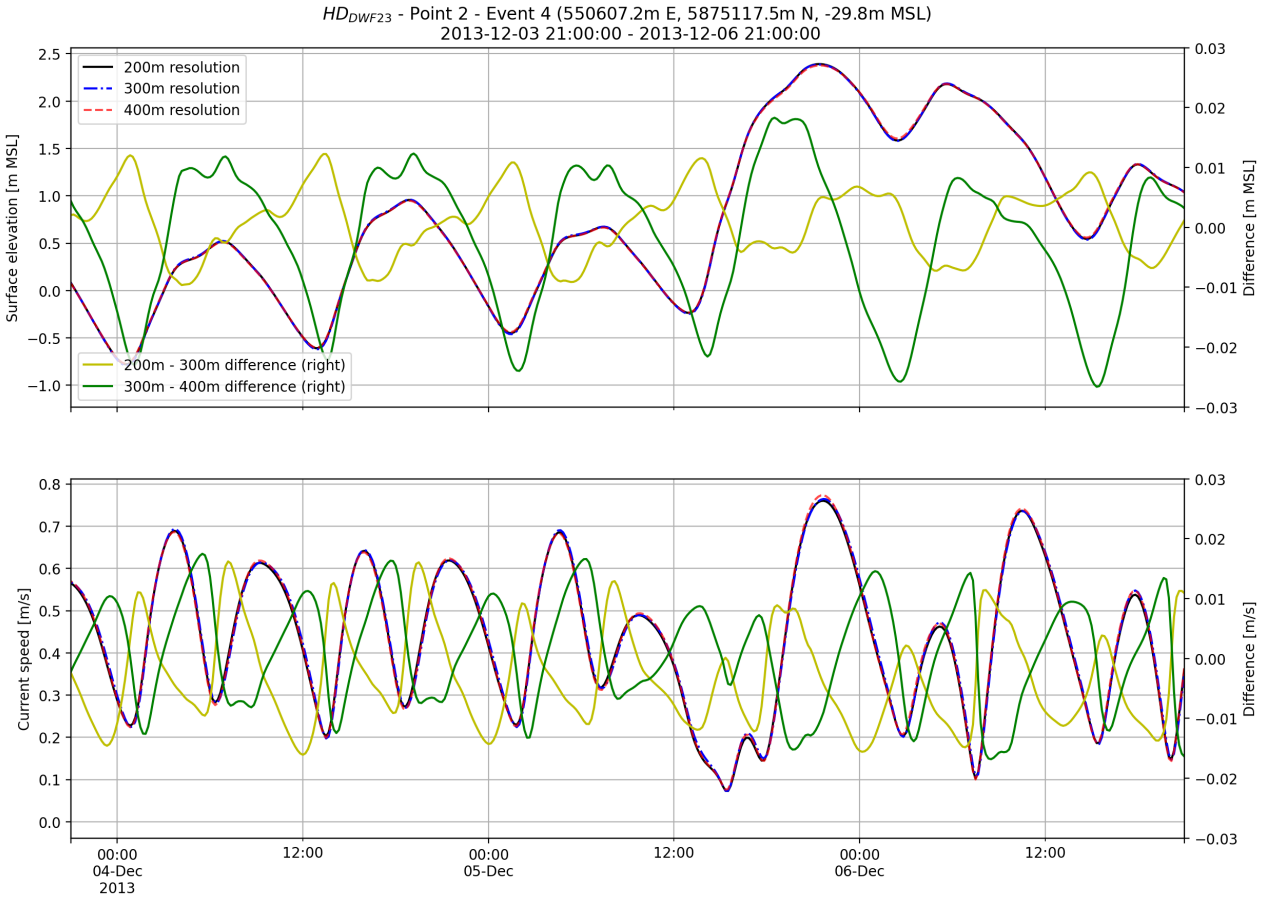

Figure 3.15 Surface elevation and depth-averaged current speed time series comparison between 200 m, 300 m, and 400 m mesh resolutions (HD_{DWF23} model) at Point 2 during Event 4. Absolute values are shown on the left axis (black, blue, and red lines), and time series difference between 200-300 m and 300-400 m is shown on the right axis (green and yellow lines).

3.2.7.3 Spatial comparisons (2D analysis - Maps)

A spatial comparison was carried out for the modelled minimum water level, maximum water level, and maximum depth-averaged current speed on all three mesh resolutions for all four events.

When looking at all the points within the IJmuiden Ver area, the maximum differences were seen in Event 3. The difference maps of minimum surface elevation, maximum surface elevation and maximum current speed for this event are shown in Figure 3.16, Figure 3.17 and Figure 3.18, respectively. The difference maps of all the other events assessed during the mesh convergence study are shown in Appendix D.

Differences in minimum water level of less than 1 cm were found between the different meshes. Minor differences were also found for the maximum water level and the depth-averaged currents, where the maximum difference reaches 2 cm and 5 cm/s, respectively.

Differences were considered negligible and confirmed that the model predictions are insensitive to further refinement of the mesh. Therefore, a 400 m mesh resolution was chosen for the HD_{DWF23} model production.

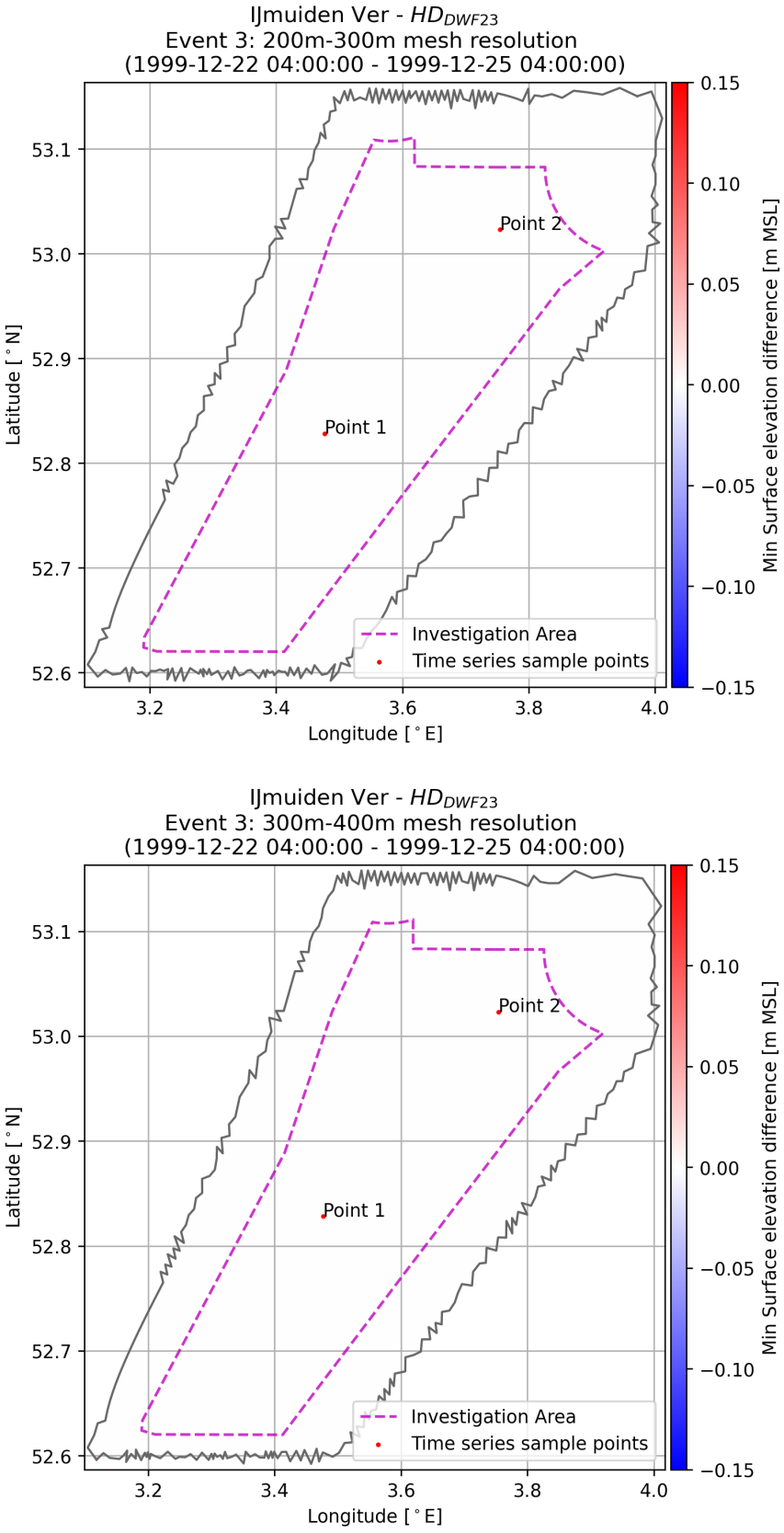

Figure 3.16 Difference map of minimum surface elevation.
Top: Difference between 200 m and 300 m mesh resolutions.
Bottom: Difference between 300 m and 400 m mesh resolutions.

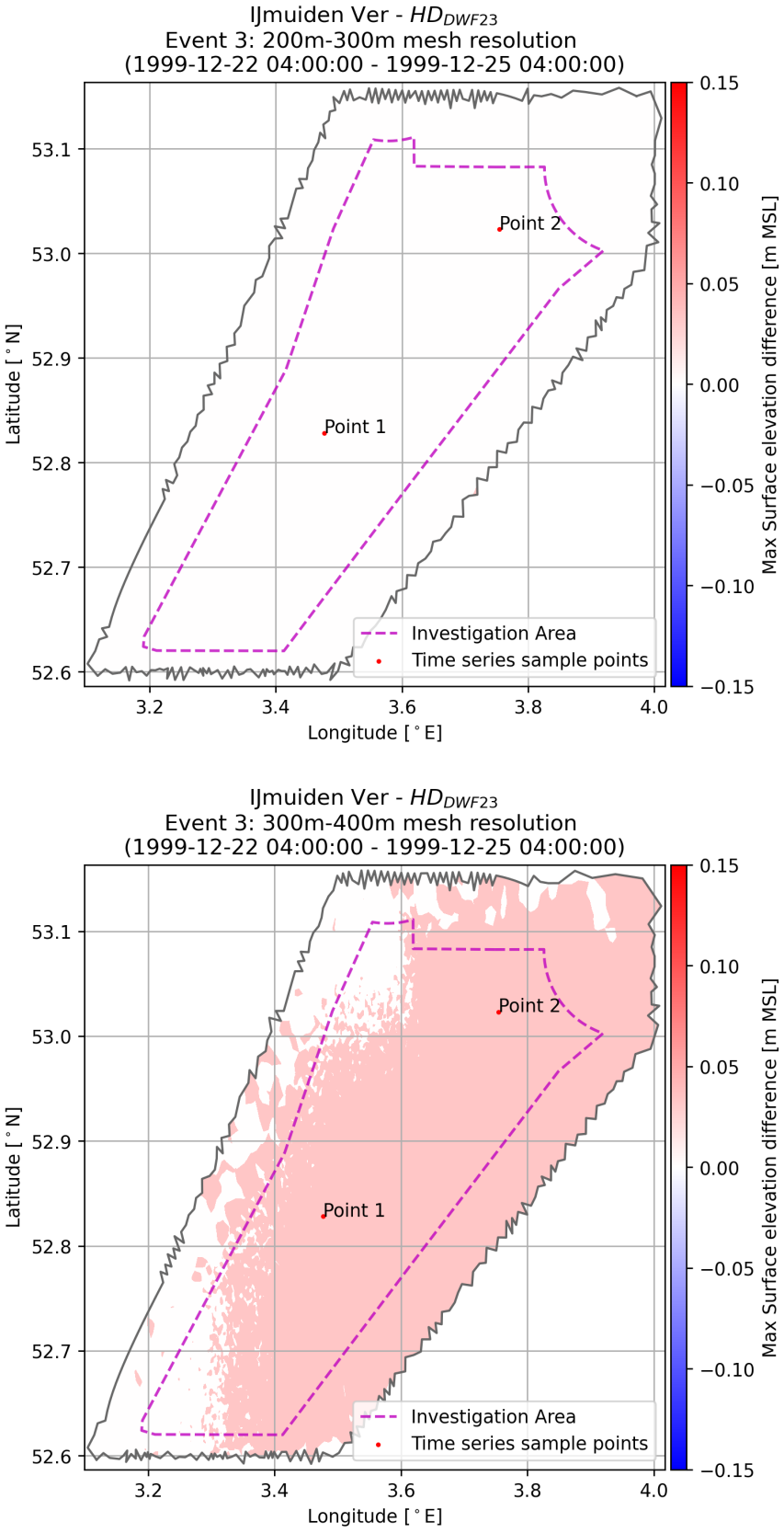

Figure 3.17 Difference map of maximum surface elevation.
Top: Difference between 200 m and 300 m mesh resolutions.
Bottom: Difference between 300 m and 400 m mesh resolutions.

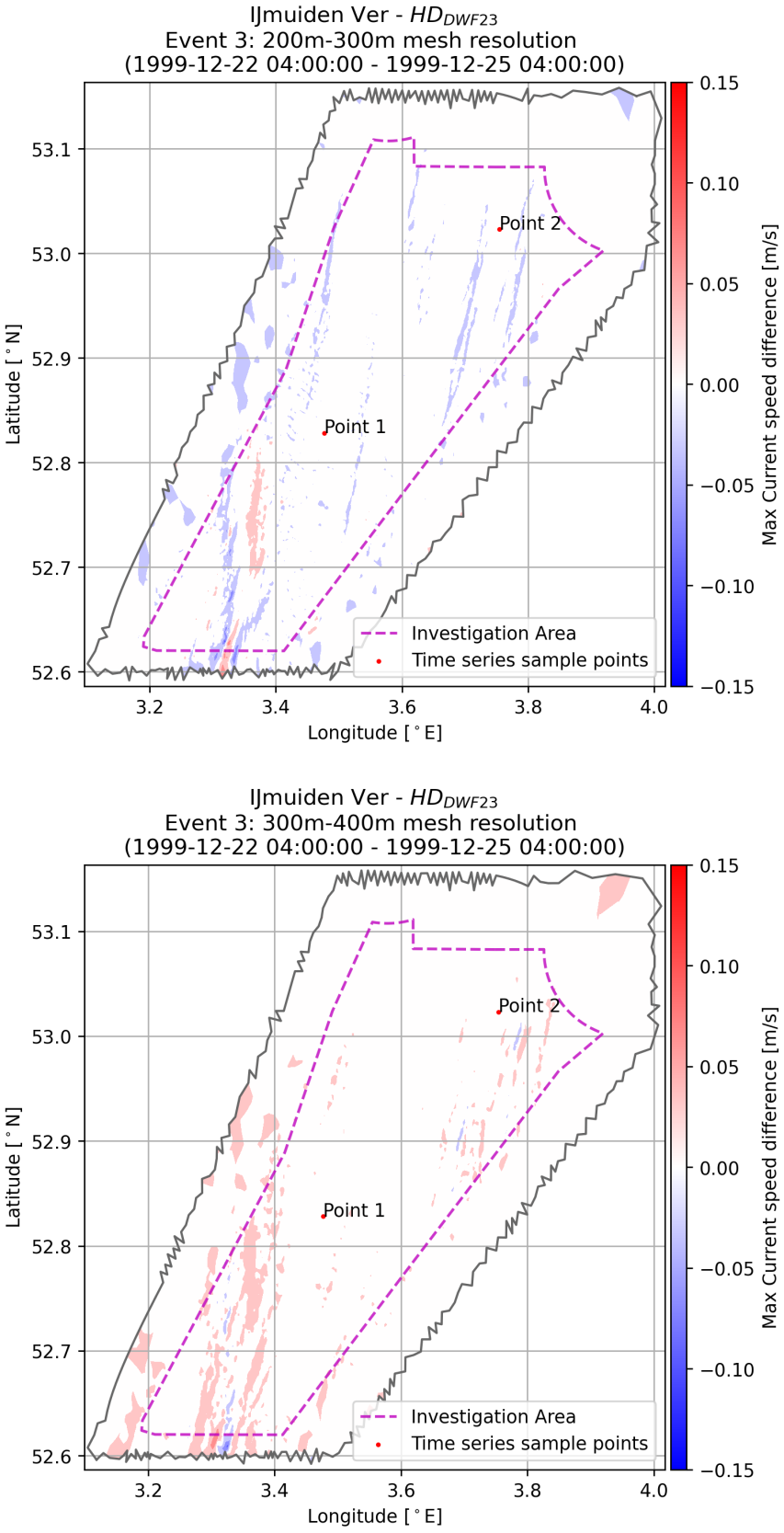

Figure 3.18 Difference map of maximum depth-averaged current speed.
Top: Difference between 200 m and 300 m mesh resolutions.
Bottom: Difference between 300 m and 400 m mesh resolutions.

3.2.8 Calibration

For the calibration, measurements at stations IJVA and IJVB were used as a target, and the remainder of the stations shown in Table 2.7 (water level stations) and Table 2.9 (current stations) were used to confirm that the calibration procedure was giving good results in all the domain. Different bed roughness, wind friction, neutral pressure, and mesh resolutions were tested.

The following table comprises the ranges of the calibration parameters tested along with the final setup selected for each parameter.

Table 3.5 Summary of the $HD_{DWF2023}$ model calibration parameters.

Setting	Range of values tested	Final value selected
Mesh resolution near model boundaries	3.5 to 10 km	3.5 km
Mesh resolution at OWF areas	200 m, 300 m, 400 m	400 m
Bed resistance	Manning number varying in domain, ranging between 31 $m^{1/3}/s$ and 42 $m^{1/3}/s$	Manning number varying in domain. M=35 $m^{1/3}/s$ if depth<-25m M=38 $m^{1/3}/s$ elsewise
Wind forcing	Friction varying with wind speed: Linear variation from 0.001569 at 7m/s to 0.0036375 at 25m/s wind speed	Friction varying with wind speed: Linear variation from 0.0018825 at 7m/s to 0.0033 at 25m/s wind speed
Neutral pressure	1010 to 1015 hPa	1013 hPa

3.2.9 Validation

In this section, the validation of the HD_{DWF23} model (water level and currents) is shown, considering the final model setup as indicated in Table 3.3, which is the setup obtained after model calibration. For the sake of simplicity of this report, only figures at stations IJVA and IJVB are presented in this section. The validation plots of the remainder of the stations presented in Table 2.7 (water level stations) and Table 2.9 (current stations) are shown in Appendix E.

Comparisons of model versus measured water levels, current speeds, and current roses for stations IJVA and IJVB are shown in Figure 3.19 and Figure 3.20, respectively. Overall, results show an excellent performance of the local HD_{DWF23} model in both stations, with a bias close to 0 in water level and current speeds, a correlation coefficient (CC) close to 1.0, SI lower than 0.2 and a QQ alignment close to the 1:1 line. The only distinguishable difference is seen in IJVB for the highest current speeds (of approx. ~80 cm/s), where a small bias of ~5 cm/s is seen (approx. 6% bias), which is considered a small deviation. This difference is probably due to some localized effect of the bathymetry (the sand banks, sand waves, and related complex 3D local flow). Current directions are also well aligned between the model and the measurements for both stations.

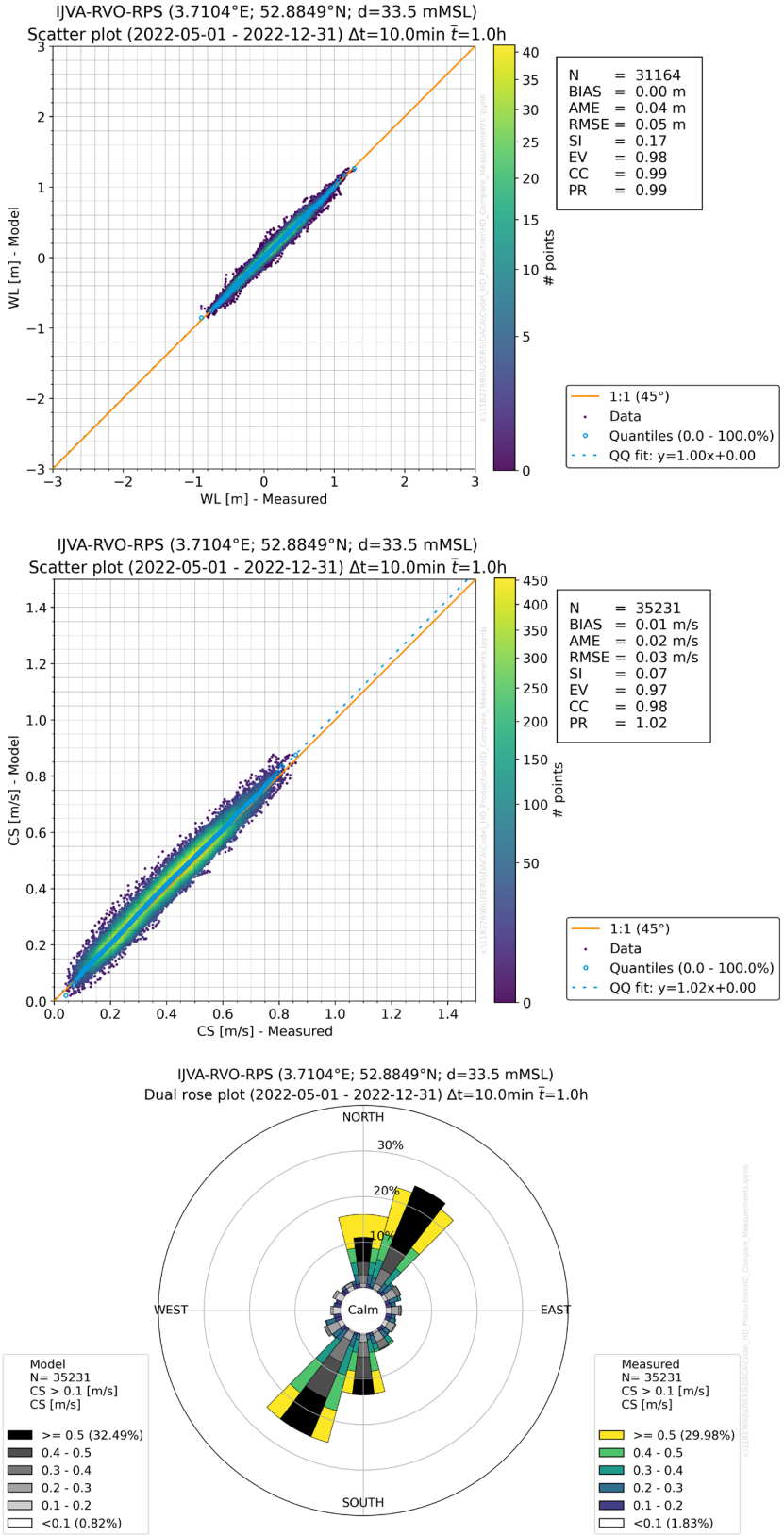

Figure 3.19 HD_{DWF23} model validation at IJVA.
Top figure: Water level validation results.
Middle figure: Depth-averaged current speed validation results.
Bottom figure: Depth-averaged current rose validation results.

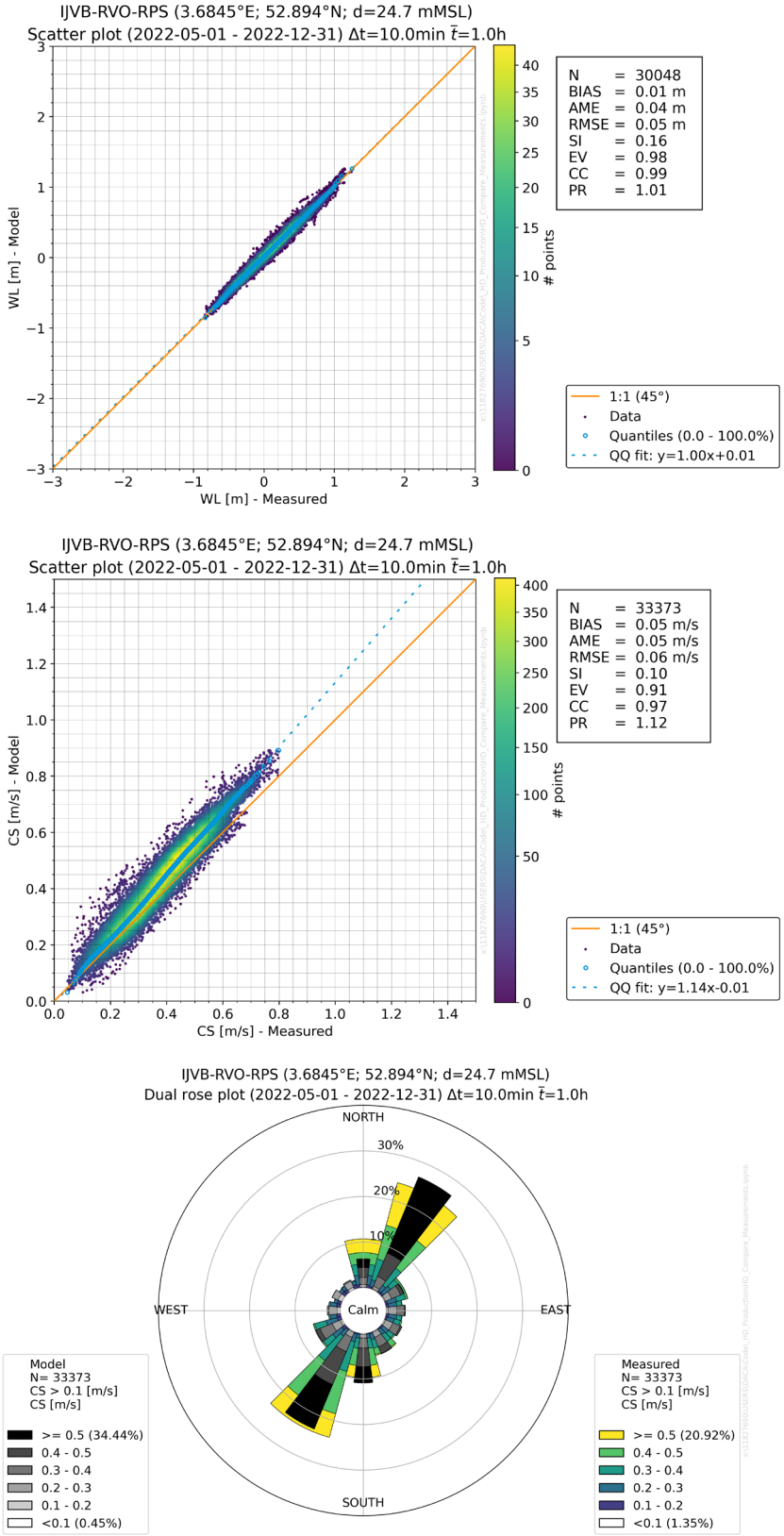

Figure 3.20 HD_{DWF23} model validation at IJVB.
Top figure: Water level validation results.
Middle figure: Depth-averaged current speed validation results.
Bottom figure: Depth-averaged current rose validation results.

Summary tables with the validation statistics at each station are shown in Table 3.6 for water level results and in Table 3.7 for current speed results. For both parameters (water level and currents), the model has an excellent performance with results that have low bias, with low RMSE, SI and high CC for all validation stations.

Table 3.6 HD_{DWF23} model validation statistics against measurements. Water level results. Stations IJVA and IJVB are highlighted with bold text.

Station Name	No data points	BIAS [m]	AME [m]	RMSE [m]	SI [-]	EV [-]	CC [-]	PR [-]
EPL	357592	0.03	0.04	0.05	0.08	1.00	1.00	1.03
F16	318026	0.07	0.09	0.11	0.22	0.96	0.98	1.10
F3	337837	-0.06	0.09	0.11	0.39	0.88	0.94	1.03
HKNA	26133	0.05	0.09	0.12	0.28	0.94	0.97	1.21
HKNB	61974	0.05	0.12	0.16	0.38	0.90	0.95	1.12
HKWA	59131	0.08	0.12	0.14	0.41	0.88	0.95	1.26
HKWB	30496	0.08	0.10	0.11	0.28	0.94	0.97	1.12
HKWC	9132	-0.05	0.07	0.08	0.21	0.96	0.98	1.06
HKZA	34376	0.11	0.17	0.21	0.45	0.86	0.94	1.12
HKZB	27986	0.05	0.13	0.17	0.40	0.88	0.96	1.11
IJS	402368	0.02	0.05	0.07	0.14	0.99	0.99	1.03
IJVA	**31164**	**0.00**	**0.04**	**0.05**	**0.17**	**0.98**	**0.99**	**0.99**
IJVB	**30048**	**0.01**	**0.04**	**0.05**	**0.16**	**0.98**	**0.99**	**1.01**
J6	301166	-0.07	0.09	0.11	0.18	0.98	0.99	0.97
K13a	291677	-0.03	0.03	0.04	0.08	0.99	1.00	0.98
K14	373273	0.05	0.06	0.07	0.15	0.99	0.99	1.05
L9	380251	0.04	0.06	0.07	0.11	0.99	1.00	1.04
LEG	320440	0.04	0.06	0.07	0.10	0.99	1.00	1.03
NWA	21585	0.00	0.04	0.06	0.14	0.99	0.99	1.02
NWB	28156	-0.01	0.04	0.05	0.13	0.99	0.99	1.02
Q1	367812	0.08	0.08	0.09	0.10	0.99	1.00	1.02
TNWA-2	21379	0.04	0.08	0.10	0.22	0.97	0.98	1.05
TNWA	28969	0.02	0.06	0.08	0.18	0.98	0.99	1.05
TNWB	50706	0.10	0.11	0.13	0.24	0.96	0.98	1.16
WHI	264751	-0.02	0.05	0.06	0.05	1.00	1.00	1.01
AVERAGE	**167057**	**0.03**	**0.08**	**0.09**	**0.21**	**0.96**	**0.98**	**1.06**

Table 3.7 **HD_{DWF23} model validation statistics against measurements. Depth-averaged current speed results.**
Stations IJVA and IJVB are highlighted with bold text.

Station Name	No data points	BIAS [m/s]	AME [m/s]	RMSE [m/s]	SI [-]	EV [-]	CC [-]	PR [-]
Bor1	25123	0.05	0.08	0.12	0.23	0.60	0.86	1.08
Bor2	6940	0.02	0.07	0.09	0.17	0.76	0.93	1.03
HKNA	30478	0.02	0.05	0.07	0.15	0.88	0.95	0.96
HKNB	22749	0.03	0.06	0.08	0.17	0.86	0.93	0.90
HKWA-2	9138	0.04	0.06	0.06	0.12	0.93	0.98	1.05
HKWA	21276	0.05	0.06	0.07	0.13	0.92	0.98	1.09
HKWB	23394	0.04	0.06	0.07	0.15	0.89	0.95	1.03
HKWC	7725	0.01	0.07	0.08	0.18	0.85	0.92	0.90
HKZA	24002	0.04	0.06	0.08	0.17	0.87	0.95	0.98
HKZB	32925	0.01	0.05	0.07	0.16	0.89	0.95	0.91
IJVA	**35231**	**0.01**	**0.03**	**0.03**	**0.07**	**0.97**	**0.98**	**1.02**
IJVB	**33373**	**0.05**	**0.05**	**0.06**	**0.10**	**0.91**	**0.97**	**1.12**
NWA	28102	0.02	0.03	0.04	0.09	0.92	0.96	0.98
NWB	30496	0.02	0.03	0.04	0.08	0.94	0.97	1.03
TNWA-2	7470	-0.02	0.06	0.07	0.23	0.76	0.88	0.77
TNWA	26518	-0.01	0.05	0.07	0.23	0.76	0.88	0.88
TNWB-2	2465	0.00	0.04	0.05	0.17	0.87	0.94	0.86
TNWB	21583	-0.01	0.05	0.07	0.23	0.77	0.89	0.90
AVERAGE	**21610**	**0.02**	**0.05**	**0.07**	**0.16**	**0.85**	**0.94**	**0.97**

3.2.10 De-tiding of water levels and currents

The modelled water levels were subjected to a harmonic tidal analysis to separate the tidal and non-tidal (residual) components. This “de-tiding” was conducted using the U-tide method[26]. This method builds on the IOS tidal analysis method defined by the Institute of Oceanographic Sciences as described by [27] and integrates the approaches defined in [28] and [29].

The tidal analyses were performed for the whole hindcast period (44-years). The residual water level/current was found by subtracting the predicted tidal level/current from the total water level/current. This approach ensured a consistent tidal signal for the entire hindcast.

3.2.11 HD_{DWF23} output specification

The output of the HD_{DWF23} model included water level and depth-averaged u- and v-velocity components covering the entire model area (all grid cells) at 30-minute intervals.

The water level and current data were de-tided applying the IOS method (see the description of the method in the Section 3.2.10) to obtain time series of total, tidal and residual water levels and currents.

Water level and current data are considered representative of instantaneous data. The output specifications are summarised in Table 3.8. The current speeds at different water depths are calculated based on the depth-averaged data CS_{Tot}, CS_{Tid}, CS_{Res}, applying the vertical profiles presented in section 3.3.1 of [3].

Table 3.8 Output specifications of HD_{DWF23}.
Parameters saved at all grid elements at 30-minute intervals.

Abbreviation	Unit	Description	Comment
WL_{Tot}, WL_{Tid}, WL_{Res}	mMSL	Total, tidal and residual water level	De-tided via IOS
CS_{Tot}, CS_{Tid}, CS_{Res}	m/s	Total, tidal and residual current speed	Depth-averaged De-tided via IOS
CD_{Tot}, CD_{Tid}, CD_{Res}	°N (going to)	Total, tidal and residual current direction	
CS_{zTot}, CS_{zTid}, CS_{zRes}	m/s	Total, tidal and residual current speed at Z% of the water depth	Data at Z% of the water depth with Z=[5,25,50,75,100], where Z=5%~ near seabed and Z=100%~ surface. De-tided via IOS
CD_{zTot}, CD_{zTid}, CD_{zRes}	°N (going to)	Total, tidal and residual current direction Z% of the water depth	

3.3 DHI's Spectral Wave model

To quantify waves for normal and extreme conditions and to provide long-term wave data at the IJmuiden Ver site, the numerical spectral wave model from the MIKE modelling software, MIKE 21 Spectral Wave (SW) Flexible Mesh (FM), was used[30].

A dedicated high-resolution local spectral waves model was developed for this study. This model is referred to as SW_{DWF23} (Spectral Waves model for the Dutch Wind Farm zones 2023) herein. The SW_{DWF23} model was forced by wave boundary conditions extracted from DHI's Global Wave Model (GWM) and winds from the local WRF model (Section 3.1).

The following subsections give a detailed description of the model's setup, calibration, and validation.

3.3.1 MIKE 21 SW Spectral Wave FM Model

MIKE 21 Spectral Wave (SW) Flexible Mesh (FM) model is developed and maintained by DHI. Like the other modules included in the FM series of MIKE Powered by DHI, the spectral wave model is based on an unstructured, cell-centred finite volume method and uses an unstructured mesh in

geographical space. This approach allows the mesh resolution to be varied and optimised according to the requirements in the different parts of the studied domain.

The MIKE 21 SW version 2022 was used in the present study. A summary of the model description and abilities is given below[11].

MIKE 21 SW is a third-generation spectral wind-wave model based on unstructured meshes. The model simulates the growth, decay, and transformation of wind and swell-waves in offshore and coastal areas. MIKE 21 SW includes the following physical processes:

- Wave growth by wind.
- Non-linear wave interaction.
- Dissipation due to white-capping.
- Dissipation due to bottom friction.
- Dissipation due to depth-induced wave breaking.
- Refraction and shoaling due to depth variations.
- Wave-current interaction.
- Effect of time-varying water depth and currents.
- Effect of ice coverage (not applicable).
- Diffraction (not applicable).
- Reflection.
- Influence of structures e.g., piers, wind turbine foundations, Wave Energy Converted (WEC), Tidal Energy Converter (TEC) – Not applied in this study.

The main computational features in MIKE 21 SW are:

- Source functions based on state-of-the-art 3rd generation formulations.
- Fully spectral and directionally decoupled parametric formulations.
- In-stationary and quasi-stationary solutions.
- Optimal degree of flexibility in describing the bathymetry and the ambient flow conditions using depth-adaptive and boundary-fitted unstructured mesh.
- Coupling with hydrodynamic flow module for modelling of wave-current interaction and time-varying water depth.
- Flooding and drying in connection with time-varying water levels.
- Extensive range of model output parameters (e.g. wind sea, swell, air-sea interaction parameters, radiation stress, spectra, etc.).
- Parallelization using Open MP and MPI techniques.

Further details are provided in [31].

[11] https://manuals.mikepoweredbydhi.help/2022/Coast_and_Sea/M21SW_Scientific_Doc.pdf

3.3.2 Global Wave Model (GWM)

The DHI Global Wave Model (GWM) is forced by ERA5 wind and ice coverage data. The model has been validated against wave and satellite altimetry observations and has proven successful when applied as boundary conditions for several models around the globe. The GWM uses a computational mesh with a varying element size resulting in a resolution of ~50 km in offshore areas up to ~15 km near the coastline (snapshot of the mesh in Figure 3.21). The GWM was established with MIKE SW Release 2022. The GWM model hindcast was run, including the following:

- Cap on wind friction.
- Stability corrected wind fields.
- Temporal and spatially varying ratio of air/sea density (based on ERA5).

The GWM was used to get directional spectral boundaries for the local SW_{DWF23} model. A detailed description of the GWM is given in [32].

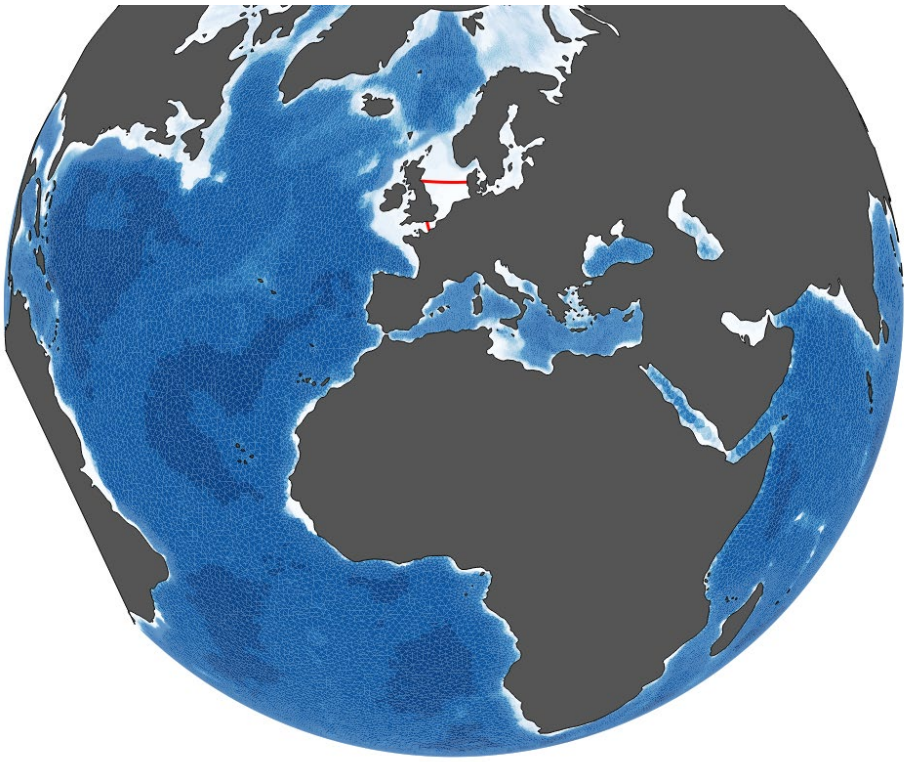

Figure 3.21 DHI's Global Wave Model (GWM) coverage and bathymetry.
Red lines indicate the boundaries of the local SW_{DWF23} model.

3.3.3 Spectral wave model for the Dutch Wind Farm area (SW_{DWF23})

The following sections describe the establishment of the spectral wave (SW) data developed and used in this project. To achieve high-quality results, a dedicated high-resolution local SW model using the latest bathymetric surveys and available data listed in Section 2 was set up for the Dutch Wind Farm area.

3.3.4 Wave model domain, bathymetry and resolution

The local wave model uses unstructured mesh with progressive increasing spatial resolution towards the Dutch Wind Farm area. The model domain and bathymetry used for the present study is shown in Figure 3.22 and Figure 3.23 with highest resolution of about 400 m at IJmuiden Ver, Doordewind and Nederwiek, whereas a resolution of about 1000 m was set in the search areas. Outside the refined areas, the mesh resolution varies from 3 km up to 10 km close to the model boundaries.

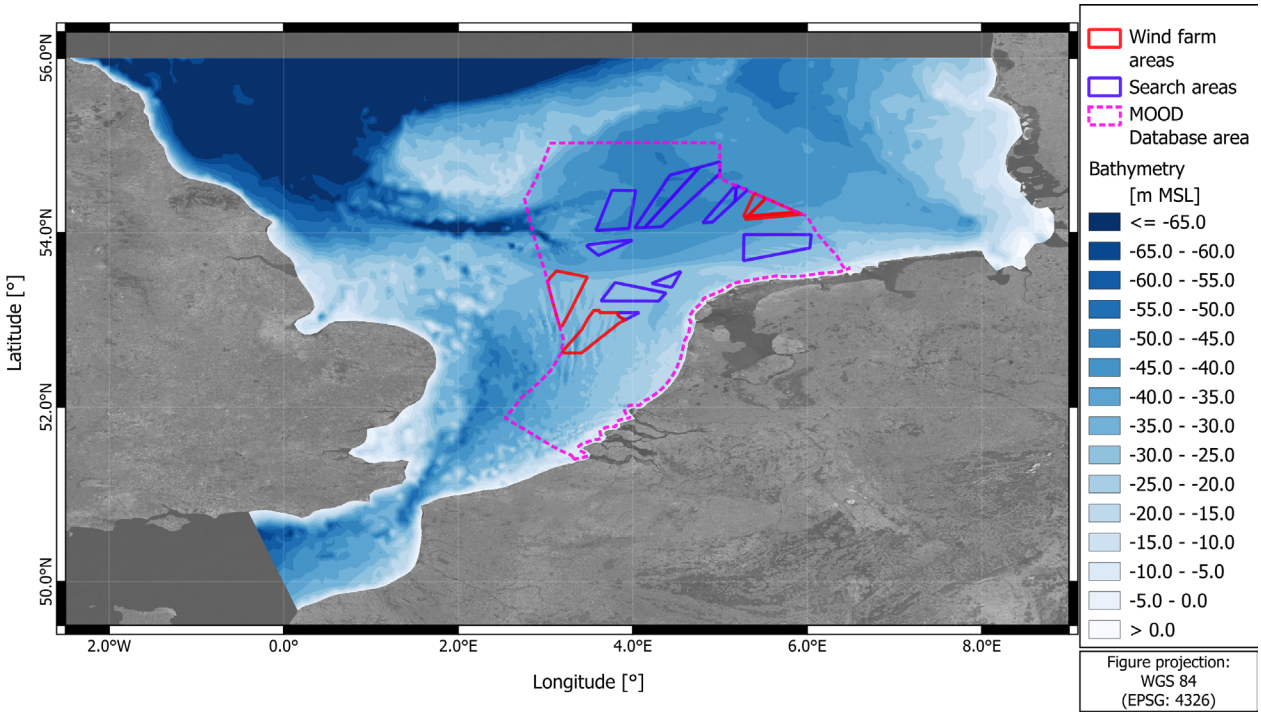

Figure 3.22 Domain and bathymetry of the local spectral waves model, SW_{DWF23}.

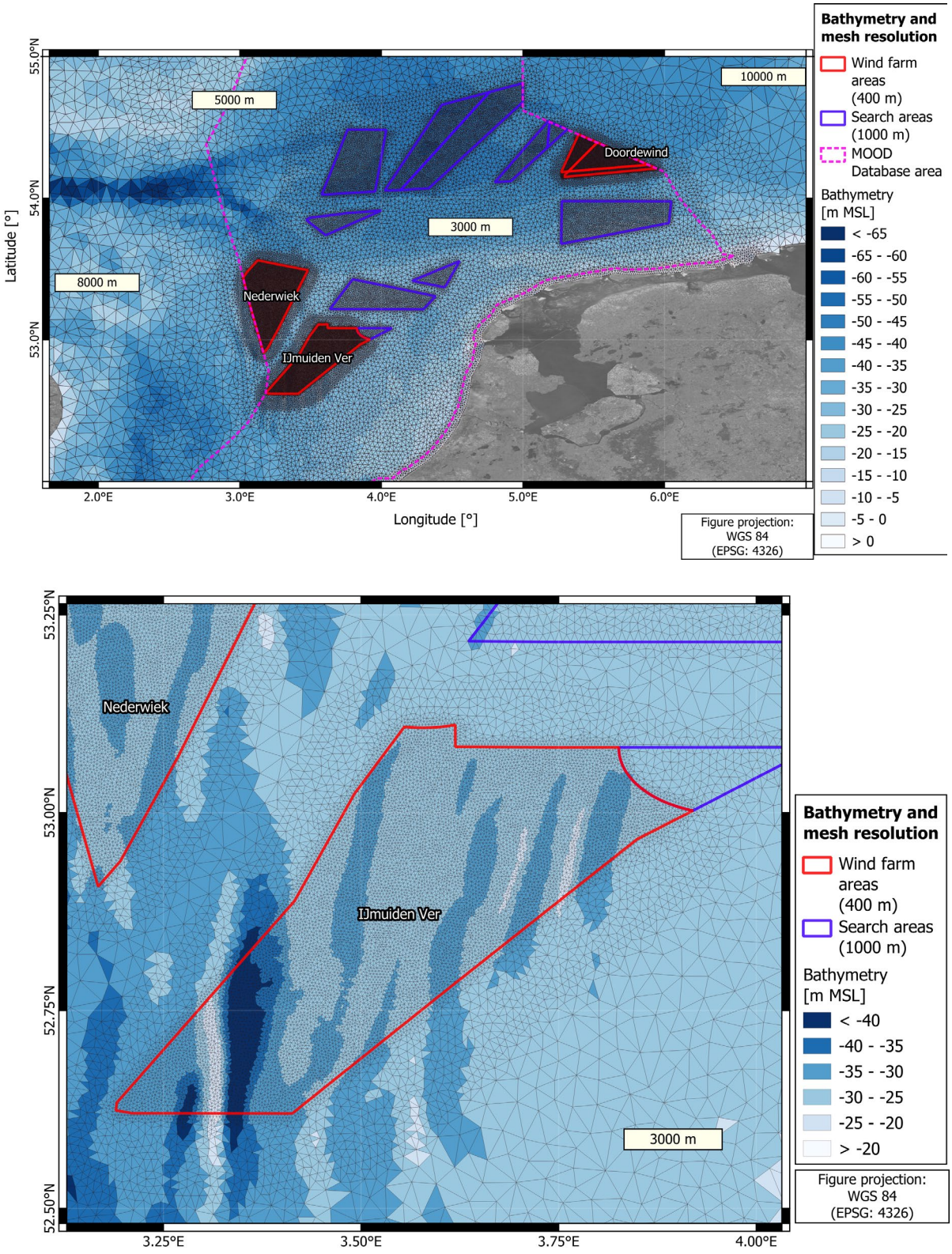

Figure 3.23 Zoom of the final mesh used in SW$_{DWF23}$ close to the Dutch Offshore Wind Farm area.
Top: Zoom comprising all the search areas. Bottom: Zoom at IJmuiden Ver.

3.3.5 Model setup and parameters

The SW_{DWF23} model was defined with two open boundaries. The local SW_{DWF23} model used in the present study relies on the boundary information from the GWM. Directional spectral in-stationary boundary conditions were applied at both the north and the south boundaries.

The SW_{DWF23} model was set up with the specifications listed in Table 3.9.

Table 3.9 Summary of the SW_{DWF23} model settings applied for production.

Setting	Value
Engine	DHI's MIKE 21 Spectral Wave (SW) Flexible Mesh (FM) 2022
Mesh resolution	Element size around IJmuiden Ver, Doordewind and Nederwiek of ~400m
Simulation period	1979-01-01 – 2022-12-31
Output time step	60-minute
Basic equations	Directional spectral in-stationary (frequency & direction)
Discretisation	36 frequencies (0.78–30.3 s (0.033-1.273 Hz) 36 directions (10° resolution)
Time step (adaptive)	0.01-120 s with a maximum time-step factor of 16
Water level	From HD_{DWF23} (temporally and spatially varying)
Current conditions	From HD_{DWF23} (temporally and spatially varying)
Wind forcing	WRF wind fields downscaled from ERA5, see Section 3.1 and [2].
Air-sea interaction	Coupled Background Charnock 0.02
Calculation of neutral winds	True (varying in time and domain calculated from WRF winds)
Correction of friction velocity	Cap value of 0.06
Air/water density ratio	Varying in time and domain calculated from WRF
Energy transfer	Include quadruplet-wave interaction (no triads)
Wave breaking	Included, Specified Gamma, γ=0.8, α= 1 ([33])
Bottom friction	Nikuradse roughness Varying in space between k_n = 0.001 m and k_n = 0.05 m
Boundary conditions	2D spectra varying in time and along line; from GWM

3.3.5.1 Averaging period of waves

The significant wave heights, H_{m0}, from the SW_{DWF23} model are essentially instantaneous 'snapshots' of the wave field that are saved at 1-hour time intervals from the model. The time scales resolved in the numerical models underpinning the hindcast data are affected by the spatial resolution and the wind forcing, and hence the data represents wave heights that are implicitly averaged over some time averaging period, T_{avg}. One may therefore expect measurements to exhibit higher variability compared to model data. Correspondingly, the model data may be regarded as somewhat 'smoothed' (in space and time) compared to the observations.

A simple and frequently used approach for assessing the representative temporal scale (or smoothing) of the wave models is to compare the power spectra of modelled wave heights with the power spectra of measurements that have been smoothed using various averaging windows (30-minutes, 60-minutes, 120-minutes, and 180-minutes). The spectral analysis was performed to the measured datasets from IJVA and IJVB buoys as well as to their corresponding datasets from the SW_{DWF23}. The resulting frequency power spectra for H_{m0} are shown in Figure 3.24, where the frequency power spectra follow the 180-minutes line the most closely.

Interpretation of the comparison of the modelled and the measured spectra for different averaging periods is provided in section 3.1.1. The same interpretation is also applicable to waves. Therefore, for the purposes of this study, 180 minutes has been adopted as the representative temporal averaging period of H_{m0} of the SW_{DWF23} model, i.e., T_{avg} = 180 minutes.

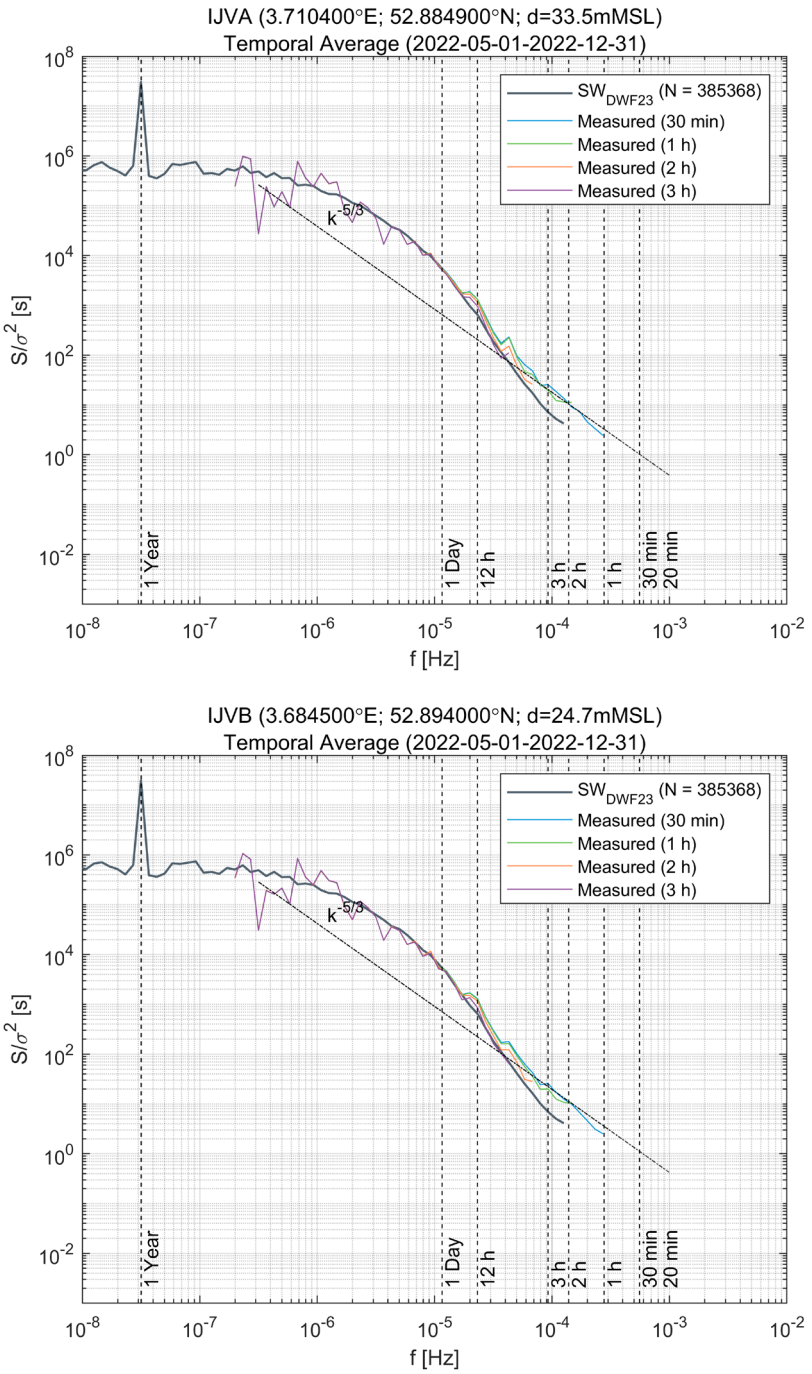

Figure 3.24 Frequency power spectra of H_{m0} at IJVA (top) and IJVB (bottom).
Comparison of measurements and model data.

3.3.6 Convergence study

The mesh convergence study was performed to decide upon the optimal mesh resolution, which ensures the highest accuracy and enhanced computational schemes combined with reasonable computational time. The tests were conducted on three different spatial resolutions (300 m, 400 m and 600 m) within the IJmuiden Ver wind farm. The water depths and element resolution of the three meshes are presented in Figure 3.25.

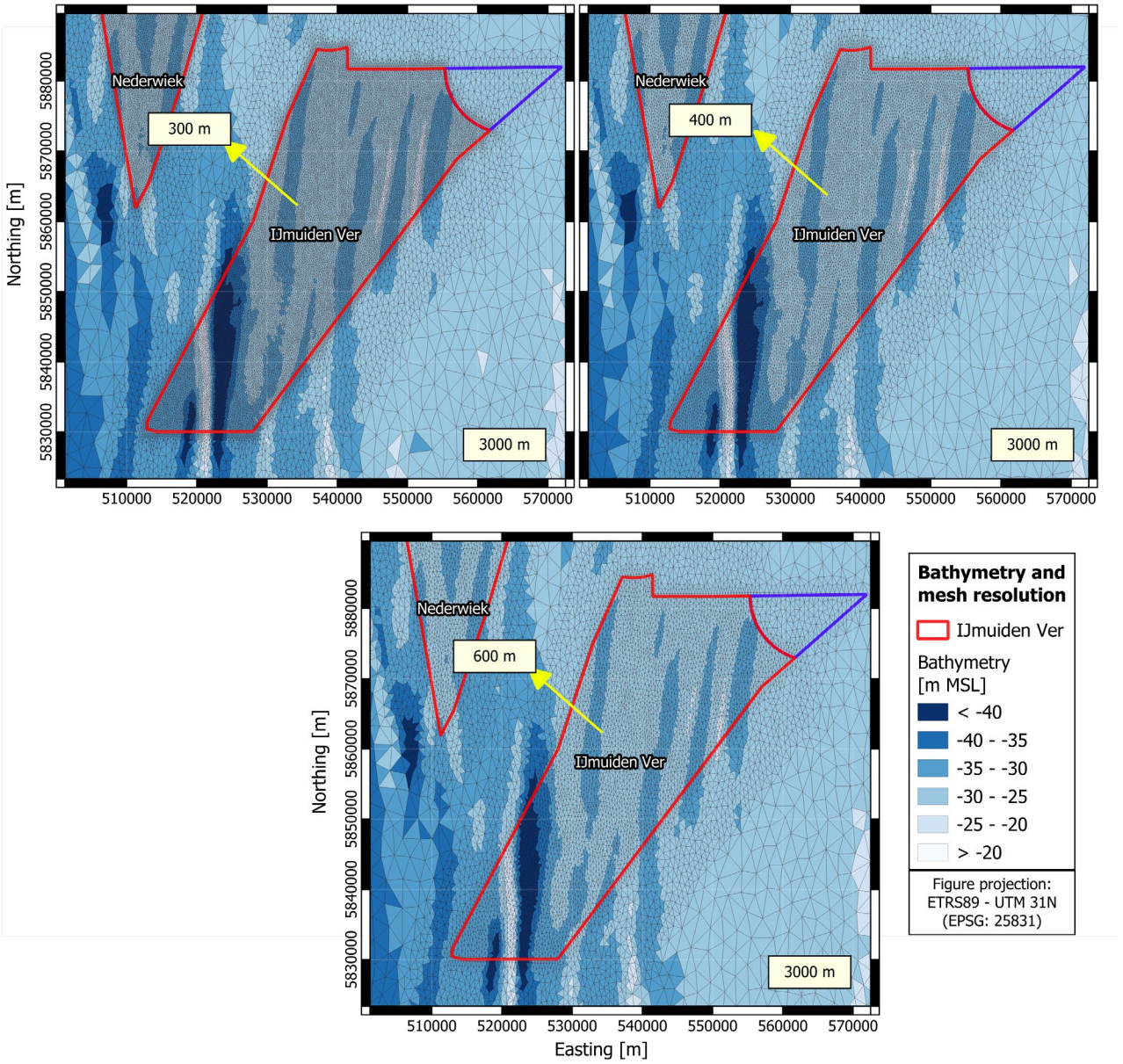

Figure 3.25 Different mesh resolutions at the project location for the SW_{DWF23} mesh convergence study.
Top left panel: 300 m mesh resolution at IJmuiden Ver area.
Top right panel: 400 m mesh resolution at IJmuiden Ver area.
Bottom panel: 600 m mesh resolution at IJmuiden Ver area.
Same resolutions were applied at Doordewind and Nederwiek OWF areas.

To assess the level of representation of the processed bathymetry at the IJmuiden Ver site, some profile comparisons were conducted between the generated bathymetry for the numerical meshes and the bathymetric surveys. The comparison of seabed elevation between the meshes is presented in Figure 3.26 and Figure 3.27 in 5 different cross sections, which are the same cross sections that were previously defined when comparing the survey data with EMODnet data (Figure 2.4). The bathymetry from the computational meshes follows the trend of the observations quite well, although some difference in the crest and troughs of the sand banks are observed for the coarser mesh (600 m resolution).

The conclusions from analysing these profiles align with the conclusions obtained from the HD mesh convergence study, presented previously in section 3.2.7, which in summary are:

- The sand banks are well represented by both the 300 m and 400 m mesh bathymetries, and in general also well represented by the 600 m mesh (only showing some difference in some crests/troughs).
- In all meshes the sand waves are averaged out and cannot be captured by the model. This was expected since the wavelength of the sand waves is in the order of ~10-100 m, which is smaller than what the mesh resolution can capture. Nevertheless, given the water depths at the site, it is expected that the sand waves will have a minimal effect (negligible) on the spectral wave model results.

Overall, the bathymetry from the computational meshes follows the trend of the observations quite well.

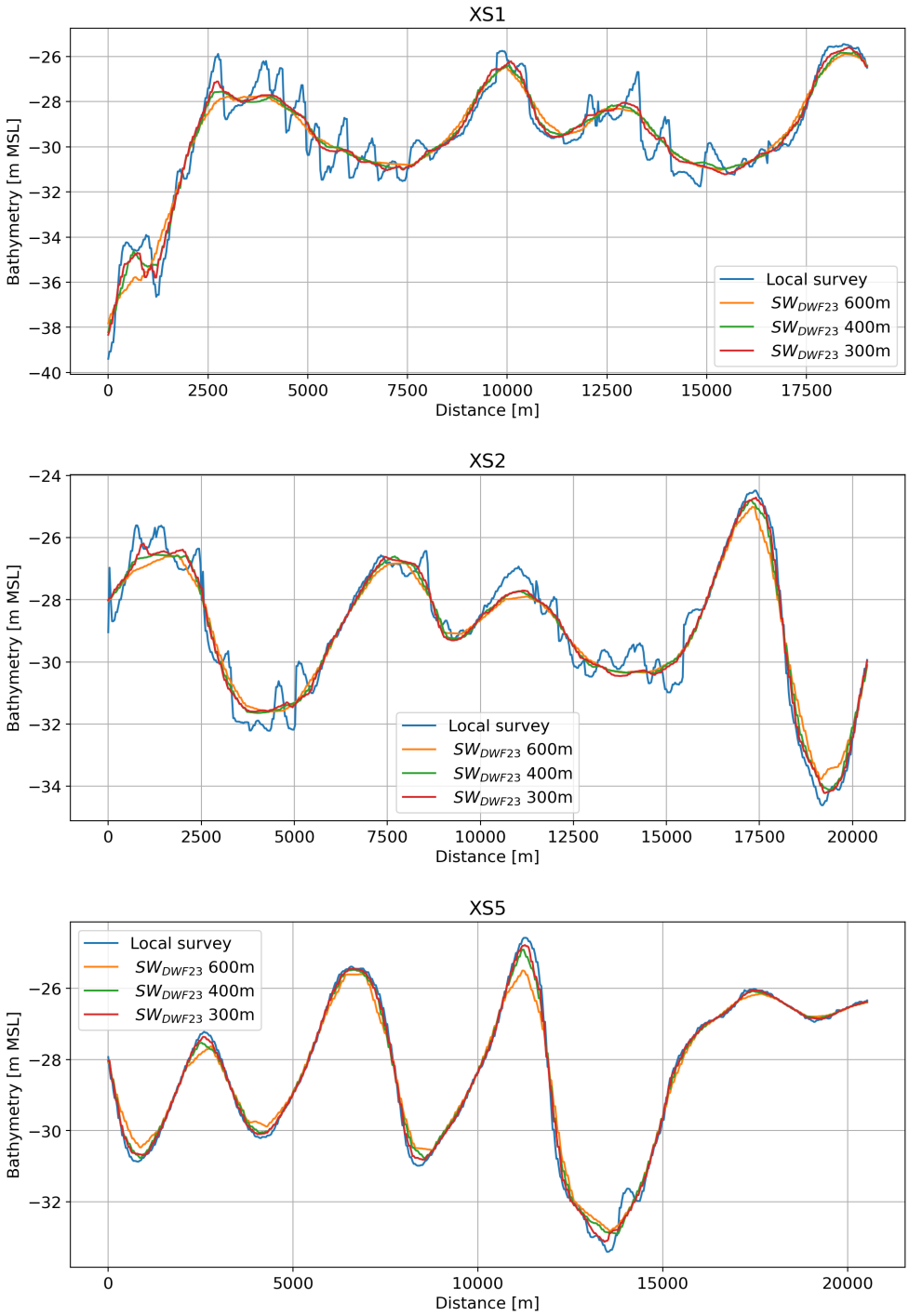

Figure 3.26 Bathymetry comparison in cross sections XS1, XS2 and XS5 between local survey and SW_{DWF23}.
Distances are given in metres from west to east. Initial and final coordinates of the cross sections are shown in Table 2.2.

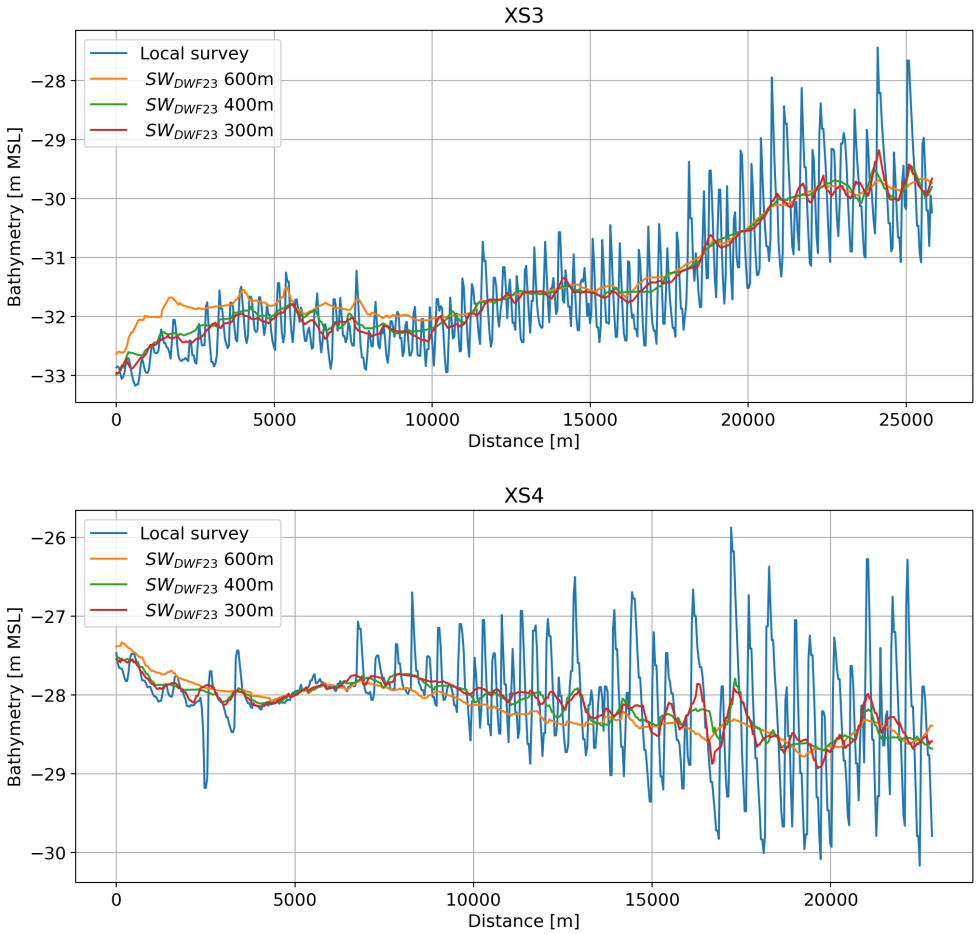

Figure 3.27 Bathymetry comparison in cross sections XS3 and XS4 between local survey and SW_{DWF23}.
Distances are given in metres from north to south. Initial and final coordinates of the cross sections are shown in Table 2.2.

3.3.6.1 Selection of storms

The first step of the convergence study was to select a set of scenarios regarding significant wave height that could be sensitive to different mesh resolutions. For this purpose, the same sample points as used in the HD_{DWF23} mesh convergence study were selected, i.e., Point 1 and 2 as shown in Figure 3.12.

A 44-year time series of wave parameters was extracted at Point 1 from DHI's regional North Europe spectral waves model (SW_{NE})[12], which runs from 1979 to 2022 (both years included). From this time series, five (5) storms were selected, considering the following criteria (directions in degrees from north):

1. Largest storm (max H_{m0}) from the east (90° ±45°): 2021-02-07 10:00
2. Largest storm (max H_{m0}) from the west (270° ±45°): 1990-01-25 21:00
3. Largest storm (max H_{m0}) from the north (0° ±45°): 1993-11-14 17:00

[12] At this stage of the project, the local SW model (SW_{DWF23}) had not been developed nor undergone production; hence a time series from a different model (SW_{NE}) was used to select storms for the mesh convergence study.

4. Largest storm (max H_{m0}) from the south (180° ±45°): 2000-10-30 09:00
5. Maximum H_{m0} combined with the lower water level: 1982-12-19 15:00

A scatter plot of H_{m0} versus mean wave direction and H_{m0} vs water level of the 43-year time series at Point 1 is shown in Figure 3.28, highlighting the five storms selected for the convergence study.

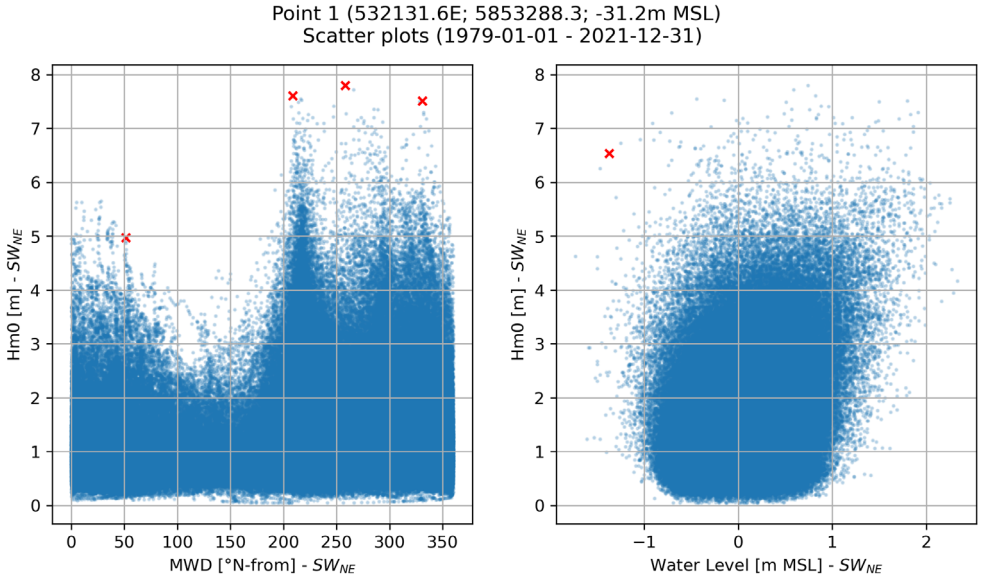

Figure 3.28 H_{m0} vs MWD (left) and H_{m0} vs water level (right) scatter plots at Point 1 (SW_{NE}) for storm selection of SW_{DWF23} convergence study.
The five selected storms are shown as red crosses.

It is important to stress that the regional model used for the selection of these events, i.e., DHI's regional North Europe spectral waves model (SW_{NE}), has not been calibrated for the IJmuiden Ver area, and the sole purpose of the convergence study was to define the optimal mesh resolution for model production (SW_{DWF23}), as the results from the convergence tests were not compared against measurements at this stage. The SW_{NE} model was selected as it comprises water levels and currents from DHI's HD_{NE} model. Since the SW_{NE} model is not used neither for calibration nor production of boundary conditions, no further details of that model are given.

3.3.6.2 Time series comparisons at sample points (1D analysis - Points)

A time series comparison of modelled integral wave parameters (H_{m0}, T_{02}, MWD, Directional Spreading-DSD) was carried out at the location of the sample points Point 1 and Point 2 for a 5-day period in each of the five storms previously defined.

From all the storms, the one that showed the largest differences between models was Storm 2, corresponding to the largest storm coming from the west (January 1990).

The time series of modelled integral wave parameters for the three meshes as well as the time series of the difference between model results during storm 2 are shown in Figure 3.29 and Figure 3.30 for Point 1 and Point 2, respectively. In these time series, the first two days of the simulation were removed to discard any effect during the models' spin-up time. The time series of all the

other storms assessed during the mesh convergence study are shown in Appendix F.

The differences found between 300-400 m and 400-600 m meshes were negligible, with the maximum differences being less than ±2.0 cm in H_{m0}, less than ±0.1 s in T_{02}, and less than 0.4° in both MWD and DSD. To assess the differences in the whole IJmuiden Ver area and not just these two sample points, 2D spatial comparisons of the model differences were carried out as presented in the next section.

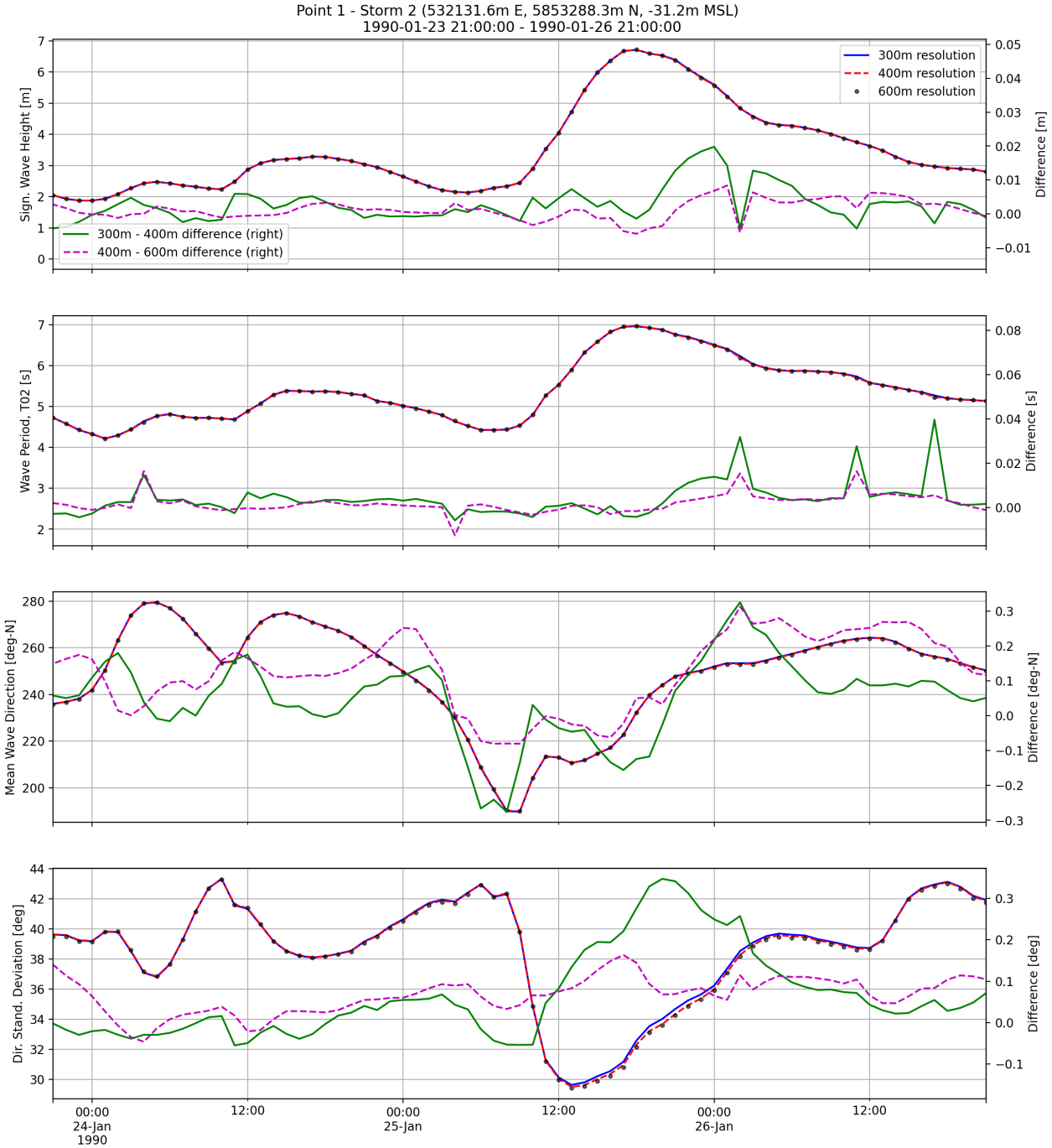

Figure 3.29 Time series comparison of H_{m0}, T_{02}, MWD, and DSD between 300 m, 400 m, and 600 m mesh resolutions (SW model) at Point 1.
Absolute values are shown on the left axis (black, blue, and red lines), and time series difference between 300-400m and 400-600m is shown on the right axis (green and magenta lines).

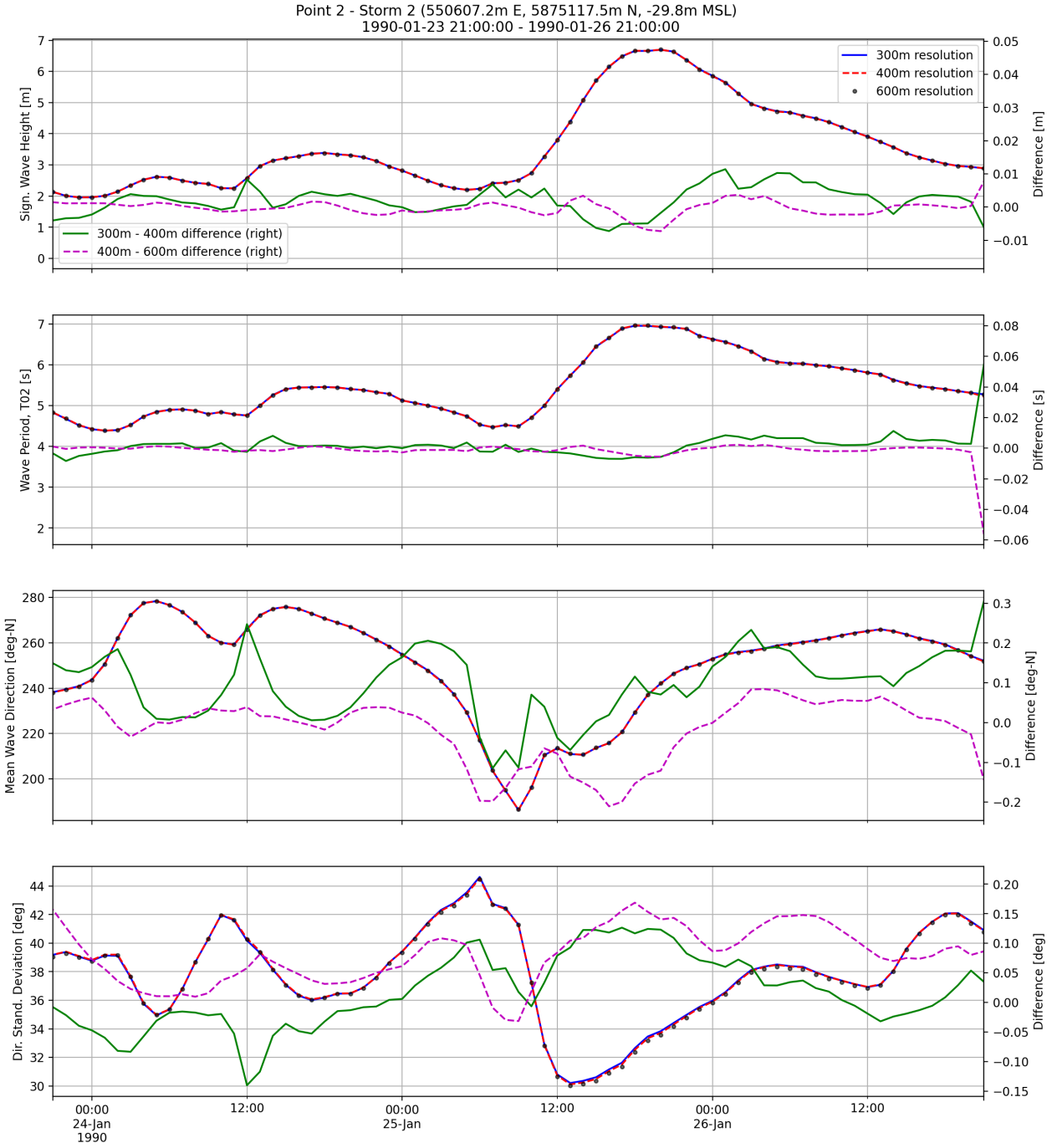

Figure 3.30 Time series comparison of H_{m0}, T_{02}, MWD, and DSD between 300 m, 400 m and 600 m mesh resolutions (SW model) at Point 2.
Absolute values are shown on the left axis (black, blue, and red lines), and time series difference between 300-400m and 400-600m is shown on the right axis (green and magenta lines).

3.3.6.3 Spatial comparisons (2D analysis - Maps)

A spatial comparison was carried out for the modelled maximum H_{m0} on the three mesh resolutions for all 5 storms. The maximum differences were found in Storm 2, even though all the storms showed similar results. The H_{m0} difference maps of Storm 2 are shown in Figure 3.31.

The H_{m0} difference maps of all the other storms assessed during the mesh convergence study are shown in Appendix F.

Differences of less than $\pm$3 cm were found in most of the IJmuiden Ver area between the 300 and 400 m meshes, and in the order of $\pm$5 cm between the 400 and 600 m meshes. Only at the southernmost location of the investigation area larger differences are found in the order of $\pm$8 cm, which are nevertheless considered small, since the maximum H_{m0} at this location is approx. H_{m0}=6.7 m for this storm; hence the maximum H_{m0} difference between the different mesh resolutions is less than 2% of the total significant wave height.

It can be seen from the maps that when comparing the 300 m and 400 m resolution meshes, the H_{m0} differences are small, which confirms that the model predictions are insensitive to further mesh refinement. Therefore, a 400 m mesh resolution was chosen for the SW_{DWF23} model production, which also aligns with the mesh resolution of the hydrodynamic HD_{DWF23} model.

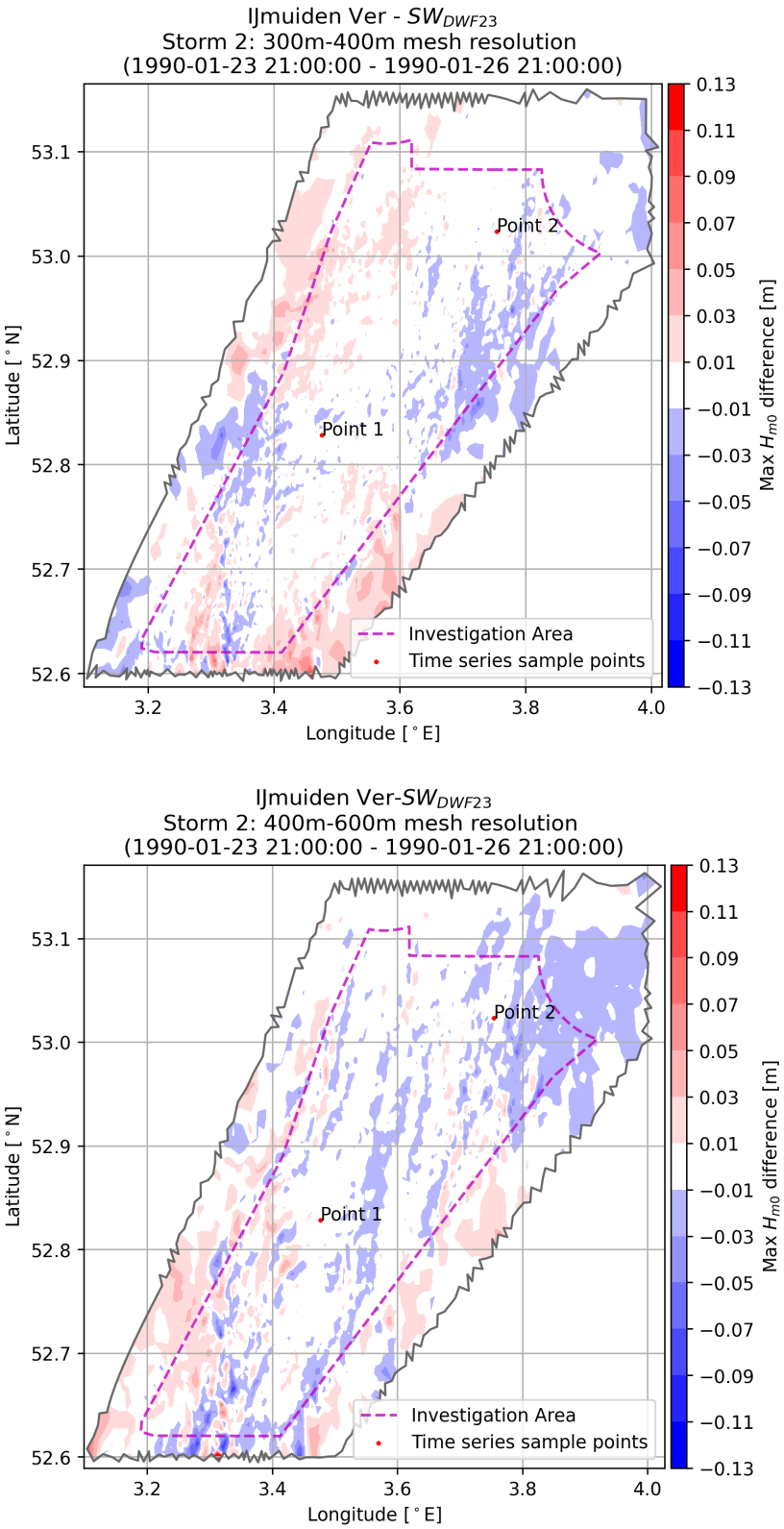

Figure 3.31 Difference map of maximum H_{m0} between different mesh resolutions (SW model).
Top: Difference between 300 m and 400 m mesh resolutions.
Bottom: Difference between 400 m and 600 m mesh resolutions.

3.3.7 Calibration

For the calibration period, a set of 44 storms in the period 1979-2022 was selected. The selection was based on a heuristic approach considering the following criteria:

- Select storms that overlap with both wind and wave measurements as much as possible.
- Select storms where the waves come from different directions, such that MWD covers all possible directions.
- Select some of the largest storms (based on H_{m0} only) covered by wave measurements (even if no wind measurement were available).

The rationale behind including the wind measurements for the storm selection lies on the fact that one of the most important inputs to the SW model is the wind field. Hence it was important to ensure that the storms modelled in the wave model were also being well represented (and not under/overpredicted) in the WRF wind model.

Like the mesh convergence study, DHI's North Europe regional spectral wave model (SW_{NE}) was used for the storm selection only[13], since a 44-year hindcast from this model was available before the SW_{DWF23} model had been finished.

Figure 3.32 shows a 44-year time series of H_{m0} at the location of K13a, which is a station with a long series of measurements near the IJmuiden Ver site, along with the selected storms which are highlighted in red. The time frames of the modelled storms are also shown in

Table 3.10.

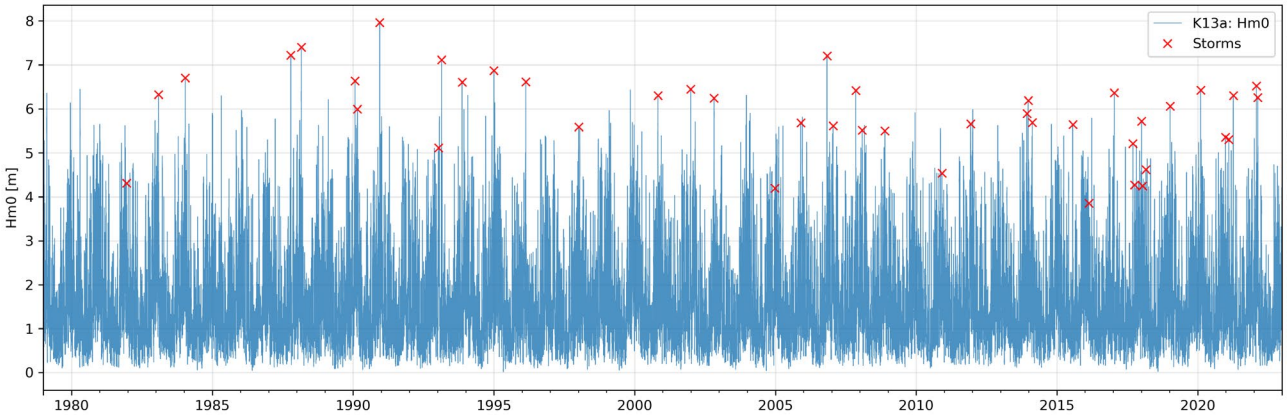

Figure 3.32 Storms selected for SW_{DWF23} model calibration.
Data shown corresponds to station K13a.

[13] SW_{NE} was used only for storm selection, i.e., selection of time periods for calibration of SW_{DWF23}. Therefore, no more details on this model (SW_{NE}) are given.

Table 3.10 List of storms selected for SW_{DWF23} model calibration.

Storm number	Start date	End date	Storm number	Start date	End date
1	1981-12-05	1981-12-15	**23**	2008-01-23	2008-02-02
2	1983-01-24	1983-02-03	**24**	2008-11-13	2008-11-23
3	1984-01-04	1984-01-19	**25**	2010-11-23	2010-12-03
4	1987-10-10	1987-10-20	**26**	2011-12-03	2011-12-13
5	1988-02-22	1988-03-03	**27**	2013-11-27	2013-12-07
6	1990-01-17	1990-01-27	**28**	2013-12-17	2013-12-27
7	1990-02-21	1990-03-03	**29**	2014-02-05	2014-02-20
8	1990-12-08	1991-01-07	**30**	2015-07-20	2015-07-30
9	1993-01-06	1993-01-16	**31**	2016-02-15	2016-02-25
10	1993-02-15	1993-02-25	**32**	2016-12-31	2017-01-15
11	1993-11-07	1993-11-17	**33**	2017-09-07	2017-09-17
12	1994-12-27	1995-01-06	**34**	2017-09-27	2017-10-07
13	1996-02-15	1996-02-25	**35**	2017-12-26	2018-01-05
14	1997-12-31	1998-01-10	**36**	2018-01-10	2018-01-20
15	2000-10-21	2000-10-31	**37**	2018-02-24	2018-03-06
16	2001-12-20	2001-12-30	**38**	2018-12-26	2019-01-10
17	2002-10-21	2002-10-31	**39**	2020-02-04	2020-02-19
18	2004-12-14	2004-12-24	**40**	2020-12-20	2020-12-30
19	2005-11-19	2005-11-29	**41**	2021-01-29	2021-02-13
20	2006-10-25	2006-11-04	**42**	2021-03-30	2021-04-09
21	2007-01-13	2007-01-23	**43**	2022-01-24	2022-02-03
22	2007-11-04	2007-11-14	**44**	2022-02-13	2022-02-23

None of the storms shown in

Table 3.10 are covered by the measurements at the site (stations IJVA, IJVB). Therefore, the data at the site was used just for model validation, and the remainder of the wave measurements stations shown in Table 2.11 were used for the SW_{DWF23} model calibration. The calibration workflow included testing/modifying different values for bed roughness, wave growth, background Charnock, wave age coefficient, source terms coefficients (from Ardhuin et. al formulation [31]), and drag-formulation of the wind fields (as explained in WRA report [2]). The following table comprises the ranges of the calibration parameters tested along with the final setup selected for each parameter.

Table 3.11 Summary of the $SW_{DWF2023}$ model calibration parameters.

Setting	Range of values tested	Final value selected
Mesh resolution at OWF areas	300 m, 400 m, 600 m	400 m
Bed resistance	Nikuradse roughness k_N, ranging between 0.001m and 0.05m, constant and varying in domain	Nikuradse roughness k_N varying in domain, ranging between 0.001m to 0.05m
Wind forcing	WRF winds with low drag, high drag and hybrid drag [2]	WRF winds with hybrid drag [2]
Wave growth coefficient	1.2 to 1.7	1.65
Wave age coefficient	0.004 to 0.008	0.008
Background Charnock coefficient	0.0062 to 0.03	0.02
Swell dissipation[14] coefficient s_1	0.66 to 1.4	0.66
Swell dissipation[12] coefficient s_2	-0.018 to -0.009	-0.018
Swell dissipation[12] coefficient s_3	0.011 to 0.066	0.05
Friction velocity[12] sheltering coefficient s_u	0.06 to 0.55	0.25
Air saturation[12] dissipation constant C_{ds}^{sat}	-6E-6 to -2.2E-5	-2.2E-5

3.3.8 Validation of integral wave parameters

In this section, the validation of the SW_{DWF23} model (integrated wave parameters) is shown, considering the final setup as indicated in Table 3.9, which is the setup obtained after model calibration. For the sake of the simplicity of this report, only figures at stations IJVA and IJVB are presented in this section. The validation plots of the remainder of the stations previously presented in Table 2.11 are shown in Appendix G.

Comparisons of model versus measured parameters (H_{m0}, T_P, T_{02}) and wave roses for stations IJVA and IJVB are shown in Figure 3.33 and Figure 3.34, respectively. The SW_{DWF23} model shows an excellent comparison with measurements of H_{m0}. This is shown through the bias being close to 0 m, RMSE <21 cm, SI <0.2, and CC >0.96 in both locations. The model performance across all the measurement stations is summarized in Table 3.12, showing an excellent performance overall, with a mean bias of 2 cm, RMSE of 20 cm, SI of 0.15, and CC of 0.97. DHI notes that if the user wishes to perform metocean analysis at a point that lies on the crest of the sand banks, then extra care should be taken to ensure that local effects are captured sufficiently. So far, sufficient measurements are not available to quantify the local effects due to sand banks.

[14] See details in Ardhuin formulation [31].

Regarding directions, as shown in the wave roses, the modelled MWD follows the measured directional pattern very well for all stations.

With respect to wave periods, there is a tendency by SW_{DWF23} to slightly overestimate T_p, but this may be partly due to scatter in the measured data. Results from all stations are summarized in Table 3.13, where all the stations show a mean bias of 0.2 s, SI of 0.18, RMSE of 1.36 b and CC of 0.70.

Mean wave period, T_{02}, is shown to compare reasonably with measurements, albeit it appears to slightly underestimate T_{02} by ~0.3 s. However, such slight underestimation may well be caused by differences in the definition of T_{02} from model and measurements, respectively. T_{02} depends on the second order moment of the wave spectra and is thus very sensitive to the shape of the spectral tail (high frequencies, short waves) which may not be well recorded by a large instrument. In the comparisons shown in Figure 3.33 and Figure 3.34, the model spectra were cut at 0.5 Hz (2 s), since that value gives an overall good fit for most of the stations, as shown in Table 3.14. Across all the stations, a mean bias of -0.08 s is seen, RMSE of 0.47 s, SI of 0.09 and CC of 0.87. A closer agreement between measurements and model in stations IJVA and IJVB may be obtained by cropping the model spectra accordingly and reprocessing T_{02}.

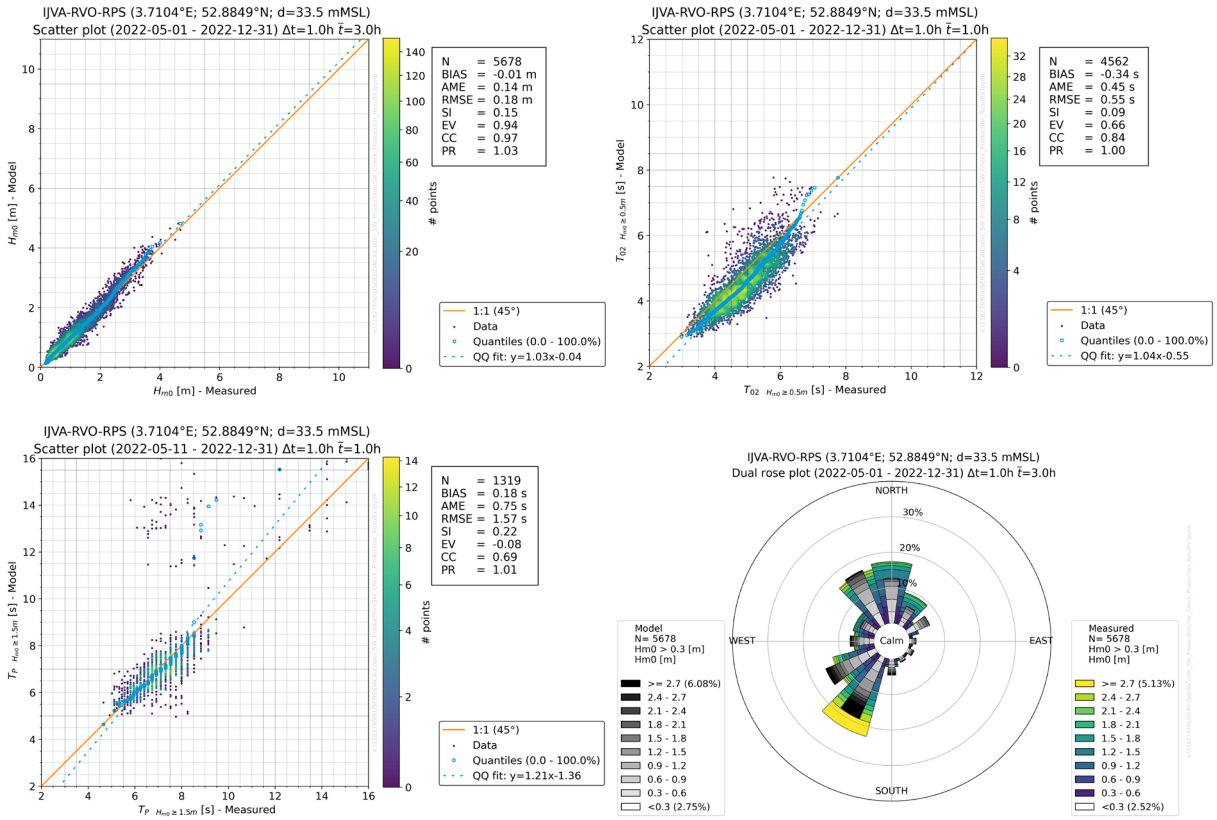

Figure 3.33 SW_{DWF23} model validation at IJVA.
Top-left figure: H_{m0} validation results.
Top-right figure: T_{02} validation results.
Bottom-left figure: T_P validation results.
Bottom-right figure: Wave rose validation results.

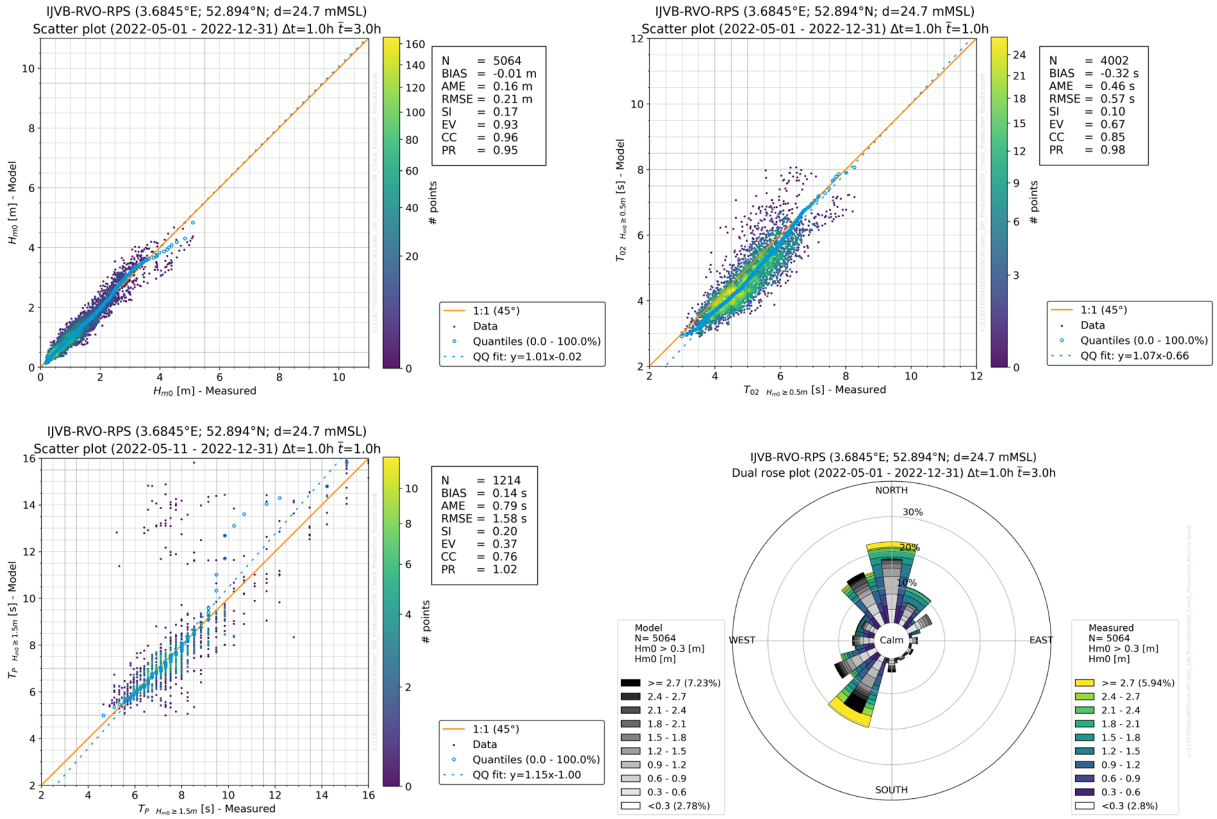

Figure 3.34 SW_{DWF23} model validation at IJVB.
Top-left figure: H_{m0} validation results.
Top-right figure: T_{02} validation results.
Bottom-left figure: T_P validation results.
Bottom-right figure: Wave rose validation results.

Table 3.12 SW_{DWF23} model validation statistics against measurements. H_{m0} results.

Station Name	No data points	BIAS [m]	AME [m]	RMSE [m]	SI [-]	EV [-]	CC [-]	PR [-]
AKZ	64244	0.09	0.15	0.21	0.19	0.90	0.97	1.07
Bor1	12549	0.04	0.13	0.17	0.15	0.94	0.97	0.97
Bor2	3463	0.07	0.13	0.18	0.15	0.93	0.97	1.20
EPL	93922	0.03	0.14	0.19	0.16	0.94	0.97	1.10
Eld	88513	0.00	0.15	0.20	0.15	0.94	0.97	0.96
F16	75635	0.10	0.17	0.24	0.14	0.95	0.98	1.04
F3	58483	0.00	0.15	0.21	0.12	0.96	0.98	1.03
FINO1	16440	0.01	0.14	0.19	0.13	0.96	0.98	0.97
HKNA	17076	0.02	0.13	0.18	0.14	0.95	0.98	0.92
HKNB	16049	0.02	0.13	0.19	0.14	0.95	0.98	0.92
HKWA-2	6675	-0.01	0.16	0.22	0.16	0.92	0.97	1.02
HKWA	10637	0.02	0.16	0.23	0.16	0.93	0.97	1.05
HKWB	11808	0.00	0.14	0.19	0.15	0.95	0.97	1.05
HKWC	3985	0.01	0.15	0.21	0.14	0.92	0.96	1.05
HKZA	17022	0.03	0.13	0.18	0.16	0.95	0.97	0.97
HKZB	17262	0.03	0.13	0.18	0.16	0.95	0.97	0.97
IJS	58787	-0.11	0.14	0.19	0.15	0.95	0.98	0.89
IJVA	**5678**	**-0.01**	**0.14**	**0.18**	**0.15**	**0.94**	**0.97**	**1.03**
IJVB	**5064**	**-0.01**	**0.16**	**0.21**	**0.17**	**0.93**	**0.96**	**0.95**
J6	91218	0.04	0.16	0.22	0.14	0.94	0.98	1.04
K13a	283203	0.07	0.17	0.25	0.17	0.92	0.97	1.03
K14	69522	0.10	0.17	0.24	0.16	0.94	0.97	0.98
L9	84130	0.10	0.16	0.22	0.14	0.95	0.98	1.03
LEG	306226	0.03	0.16	0.22	0.20	0.90	0.96	1.03
MMIJ	26456	-0.01	0.15	0.21	0.14	0.94	0.97	1.02
NWA	3954	0.02	0.14	0.19	0.16	0.92	0.96	1.01
NWB	5072	0.01	0.15	0.20	0.15	0.94	0.97	1.01
Q1	54132	-0.02	0.14	0.20	0.14	0.95	0.98	0.93
TNWA-2	3735	0.03	0.14	0.19	0.13	0.97	0.98	0.98
TNWA	13428	0.02	0.15	0.22	0.13	0.95	0.98	1.03
TNWB-2	2627	0.01	0.14	0.19	0.14	0.96	0.98	0.97
TNWB	12267	0.00	0.14	0.20	0.13	0.95	0.98	1.05
WHI	80933	0.04	0.13	0.19	0.18	0.92	0.97	1.11
AVERAGE	**49097**	**0.02**	**0.15**	**0.20**	**0.15**	**0.94**	**0.97**	**1.01**

Table 3.13 SW_{DWF23} model validation statistics against measurements. T_P results.
Only sea states with H_{m0}>1.5 m considered for T_P comparison.

Station Name	No data points	BIAS [s]	AME [s]	RMSE [s]	SI [-]	EV [-]	CC [-]	PR [-]
Bor1	2921	0.07	0.49	0.64	0.10	0.64	0.80	0.88
Bor2	641	0.07	0.49	0.61	0.09	0.60	0.77	0.92
EPL	23663	0.08	0.50	0.73	0.11	0.53	0.75	0.99
Eld	26696	0.23	0.77	1.41	0.19	0.10	0.68	1.14
F16	31080	0.30	0.73	1.43	0.18	0.20	0.71	1.16
F3	27380	0.36	0.81	1.64	0.20	0.10	0.69	1.12
FINO1	95038	0.40	0.86	1.61	0.20	0.24	0.71	0.73
HKNA	5047	0.34	0.80	1.50	0.20	-0.11	0.59	1.23
HKNB	4816	0.35	0.81	1.52	0.20	-0.16	0.59	1.27
HKWA-2	2301	0.05	0.58	1.06	0.15	0.42	0.71	1.08
HKWA	3541	0.11	0.58	0.94	0.13	0.56	0.79	1.02
HKWB	3211	0.11	0.59	1.11	0.16	0.35	0.68	0.80
HKWC	1578	0.11	0.48	0.86	0.12	0.41	0.75	1.01
HKZA	4166	0.15	0.69	1.23	0.18	0.26	0.66	1.07
HKZB	4149	0.13	0.68	1.24	0.18	0.27	0.66	1.03
IJS	10399	-0.16	0.63	1.02	0.14	0.44	0.70	0.99
IJVA	**1319**	**0.18**	**0.75**	**1.57**	**0.22**	**-0.08**	**0.69**	**1.01**
IJVB	**1214**	**0.14**	**0.79**	**1.58**	**0.20**	**0.37**	**0.76**	**1.02**
J6	34253	0.38	0.75	1.48	0.19	0.21	0.69	1.20
K13a	24579	0.36	0.75	1.44	0.19	0.13	0.67	1.14
K14	23187	-0.53	1.37	2.29	0.26	0.25	0.55	0.78
L9	27950	-0.22	1.28	2.18	0.26	0.04	0.49	0.80
LEG	16104	-0.03	0.50	0.73	0.11	0.49	0.71	0.92
MMIJ	9993	0.17	0.67	1.36	0.19	0.15	0.66	0.92
NWA	730	0.49	0.97	1.95	0.25	-0.24	0.65	1.02
NWB	1462	0.37	0.81	1.70	0.22	-0.01	0.68	1.02
Q1	18273	0.32	0.79	1.49	0.20	0.20	0.69	1.12
TNWA-2	1260	0.46	0.79	1.42	0.17	0.63	0.85	0.98
TNWA	5787	0.28	0.72	1.35	0.17	0.28	0.72	1.19
TNWB-2	834	0.62	0.93	1.69	0.19	0.59	0.83	0.98
TNWB	5064	0.31	0.75	1.50	0.19	0.17	0.69	1.15
AVERAGE	**13504**	**0.19**	**0.75**	**1.36**	**0.18**	**0.26**	**0.70**	**1.02**

Table 3.14 SW_{DWF23} model validation statistics against measurements. T_{02} results.
Only sea states of H_{m0}>0.5 m considered for T_{02} comparison. Model spectra cut-off at 0.5 Hz.

Station Name	No data points	BIAS [s]	AME [s]	RMSE [s]	SI [-]	EV [-]	CC [-]	PR [-]
AKZ	49327	0.12	0.33	0.42	0.10	0.71	0.84	1.04
Bor1	101116	-0.06	0.31	0.40	0.09	0.74	0.86	0.96
Bor2	2777	0.00	0.31	0.40	0.09	0.66	0.83	1.10
EPL	73317	-0.28	0.37	0.46	0.08	0.77	0.88	0.97
Eld	76814	-0.28	0.40	0.51	0.09	0.75	0.88	1.03
F16	69299	-0.27	0.40	0.50	0.08	0.81	0.91	1.00
F3	54678	-0.13	0.33	0.44	0.08	0.81	0.92	0.98
FINO1	226585	0.15	0.33	0.49	0.10	0.77	0.90	1.03
HKNA	14010	-0.01	0.32	0.43	0.09	0.74	0.87	0.92
HKNB	13383	0.00	0.32	0.44	0.10	0.73	0.87	0.93
HKWA-2	5802	-0.07	0.33	0.44	0.09	0.69	0.84	1.03
HKWA	9403	-0.07	0.33	0.44	0.09	0.74	0.87	1.11
HKWB	9869	-0.02	0.33	0.44	0.10	0.68	0.84	1.11
HKWC	3748	-0.03	0.31	0.43	0.09	0.64	0.82	1.09
HKZA	13332	-0.02	0.33	0.44	0.10	0.71	0.86	0.95
HKZB	13475	-0.05	0.33	0.44	0.10	0.72	0.86	0.95
IJS	40320	-0.12	0.34	0.48	0.10	0.56	0.80	1.09
IJVA	**4562**	**-0.34**	**0.45**	**0.55**	**0.09**	**0.66**	**0.84**	**1.00**
IJVB	**4002**	**-0.32**	**0.46**	**0.57**	**0.10**	**0.67**	**0.85**	**0.98**
J6	82863	0.01	0.33	0.50	0.10	0.66	0.87	1.10
K13a	62224	-0.22	0.38	0.48	0.09	0.75	0.89	1.03
K14	46080	-0.51	0.56	0.67	0.08	0.81	0.90	0.72
L9	59446	-0.20	0.36	0.46	0.08	0.79	0.91	0.97
LEG	61109	-0.16	0.29	0.38	0.08	0.78	0.89	1.02
MMIJ	24051	0.06	0.33	0.46	0.10	0.74	0.87	1.05
NWA	3307	-0.27	0.40	0.49	0.09	0.70	0.87	1.05
NWB	4387	-0.26	0.40	0.49	0.08	0.72	0.88	1.06
Q1	47042	0.00	0.33	0.46	0.10	0.74	0.88	1.04
TNWA-2	3300	0.16	0.37	0.54	0.10	0.72	0.89	0.93
TNWA	12324	0.03	0.30	0.45	0.09	0.76	0.89	1.09
TNWB-2	2256	0.27	0.42	0.62	0.11	0.68	0.88	1.06
TNWB	11231	0.03	0.29	0.43	0.09	0.77	0.90	1.05
WHI	61811	0.07	0.32	0.42	0.10	0.69	0.84	1.06
AVERAGE	**38402**	**-0.08**	**0.35**	**0.47**	**0.09**	**0.72**	**0.87**	**1.02**

3.3.8.1 Validation of extreme events

To assess the model performance during extreme events (storms), a longer time series than the ones available at the site are needed (both IJVA and IJVB overlap with the model for periods of less than one year). The closest stations to the IJVWFZ with several years of data are:

- MMIJ: Approx. 4 years of data
- K13a: Approx 44 years of data.

For these stations, peak-peak plots are made. In these plots (Figure 3.35 and Figure 3.36), peak values from both measurements and model were selected (2 events per year, on average) and plotted against each other (model versus measurement), both as independent series, and as joint events. The explanation of this type of plot is the following:

- The independent series corresponds to finding the value in the model (measurement) at the exact time time-step when the measurement (model) has a peak. These points correspond to the green triangles and grey crosses in the figure.
- The joint event corresponds to pairing peak events in time, if they occur withing 36-hour windows of each other (i.e., if the model peak is located between +/-18 h to the measured peak). These points correspond to the blue circles in the figure.

Peak-peak plot for MMIJ and K13a are shown in Figure 3.35 and Figure 3.36 respectively:

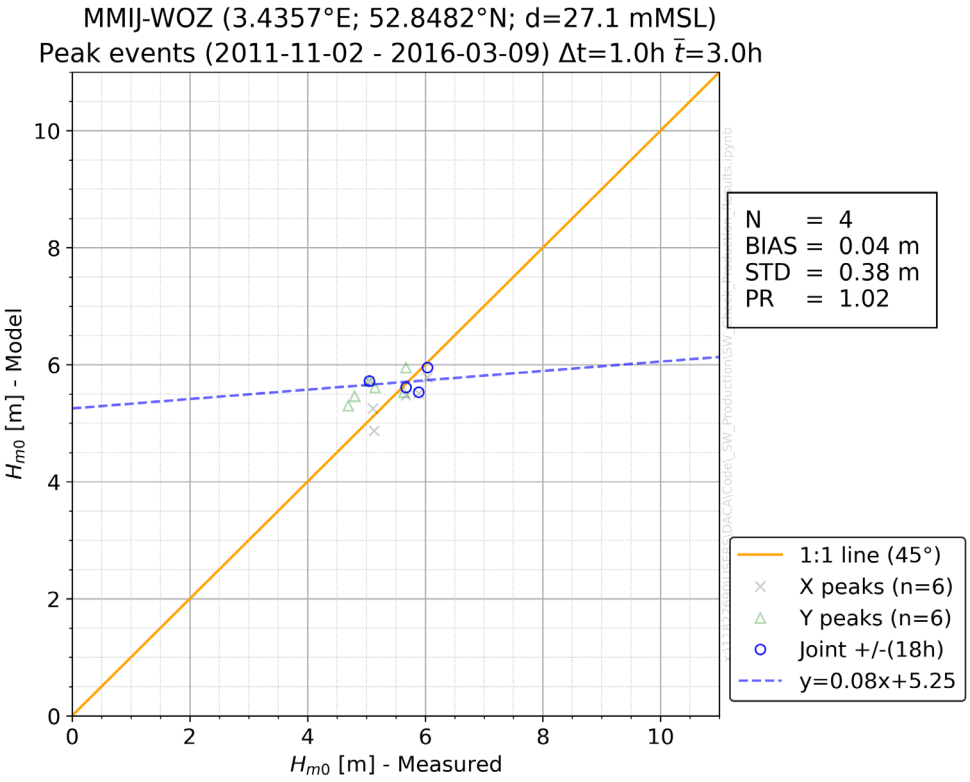

Figure 3.35 Comparisons of H_{m0} peaks between model and measurements at MMIJ
A positive bias and PR>1 indicate that the model is conservative when comparing storm peaks, and the opposite is also true (negative bias and PR<1 means model underpredicting peaks).

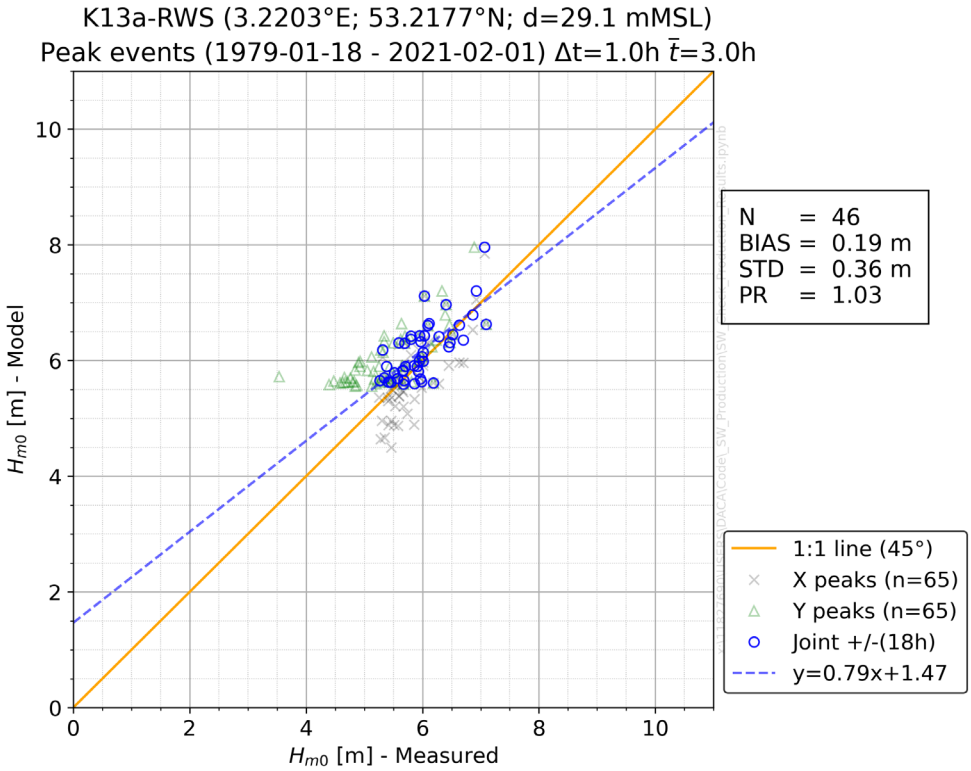

Figure 3.36 Comparisons of H_{m0} peaks between model and measurements at K13a

A positive bias and PR>1 indicate that the model is conservative when comparing storm peaks, and the opposite is also true (negative bias and PR<1 means model underpredicting peaks).

As an additional check, the time series of the four largest storms (selected from the measurements) were plotted and compared against the model results, both stations independently. Figure 3.37 and Figure 3.38 show the time series for stations MMIJ and K13a, respectively. It can be seen from both figures that in some storms, the model is overpredicting the peak value of H_{m0}, while in others, it is underpredicting the peaks. In general, the agreement is good.

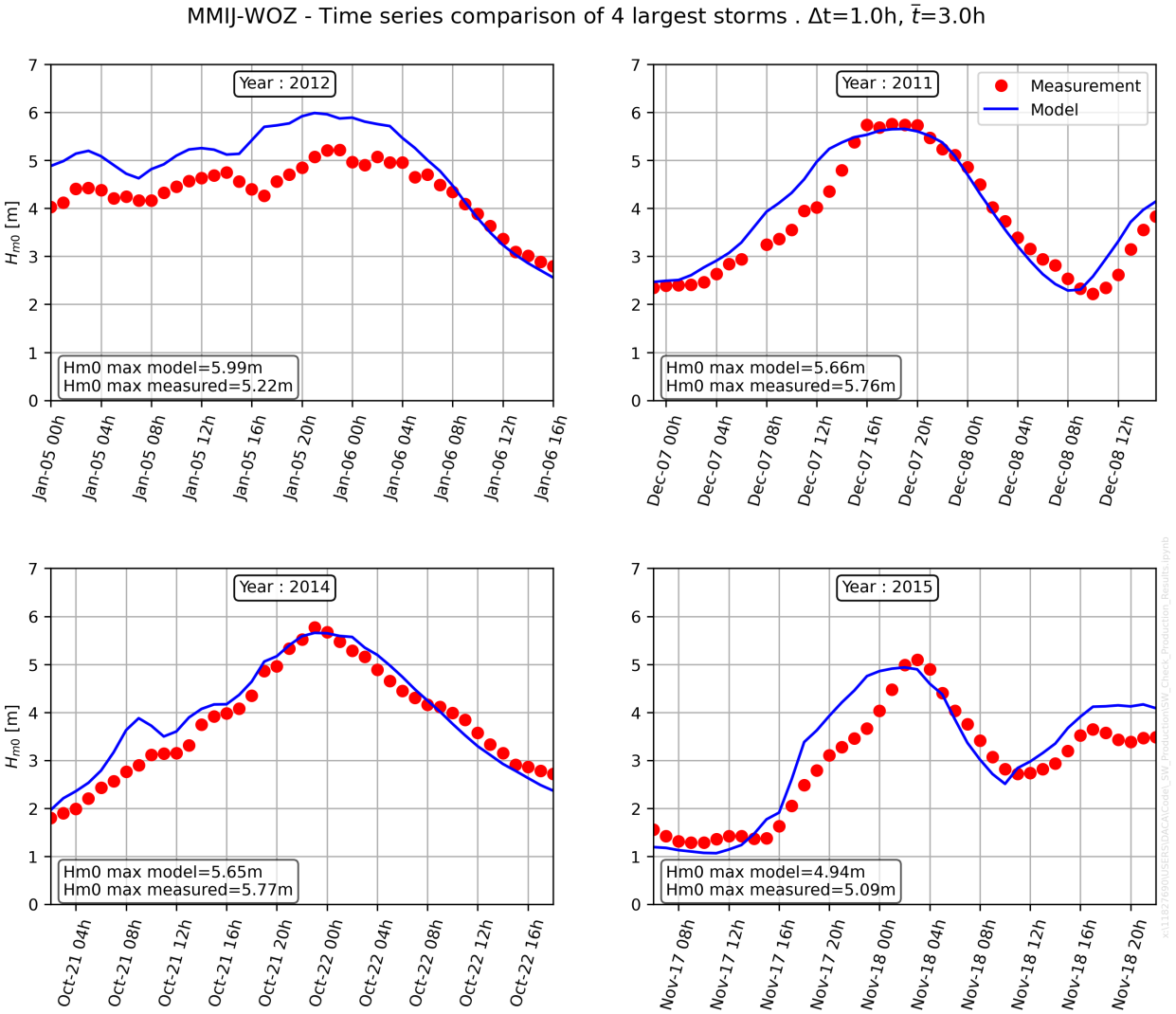

Figure 3.37 Time series comparison of model vs measured H_{m0} during the four (4) largest storms at station MMIJ.

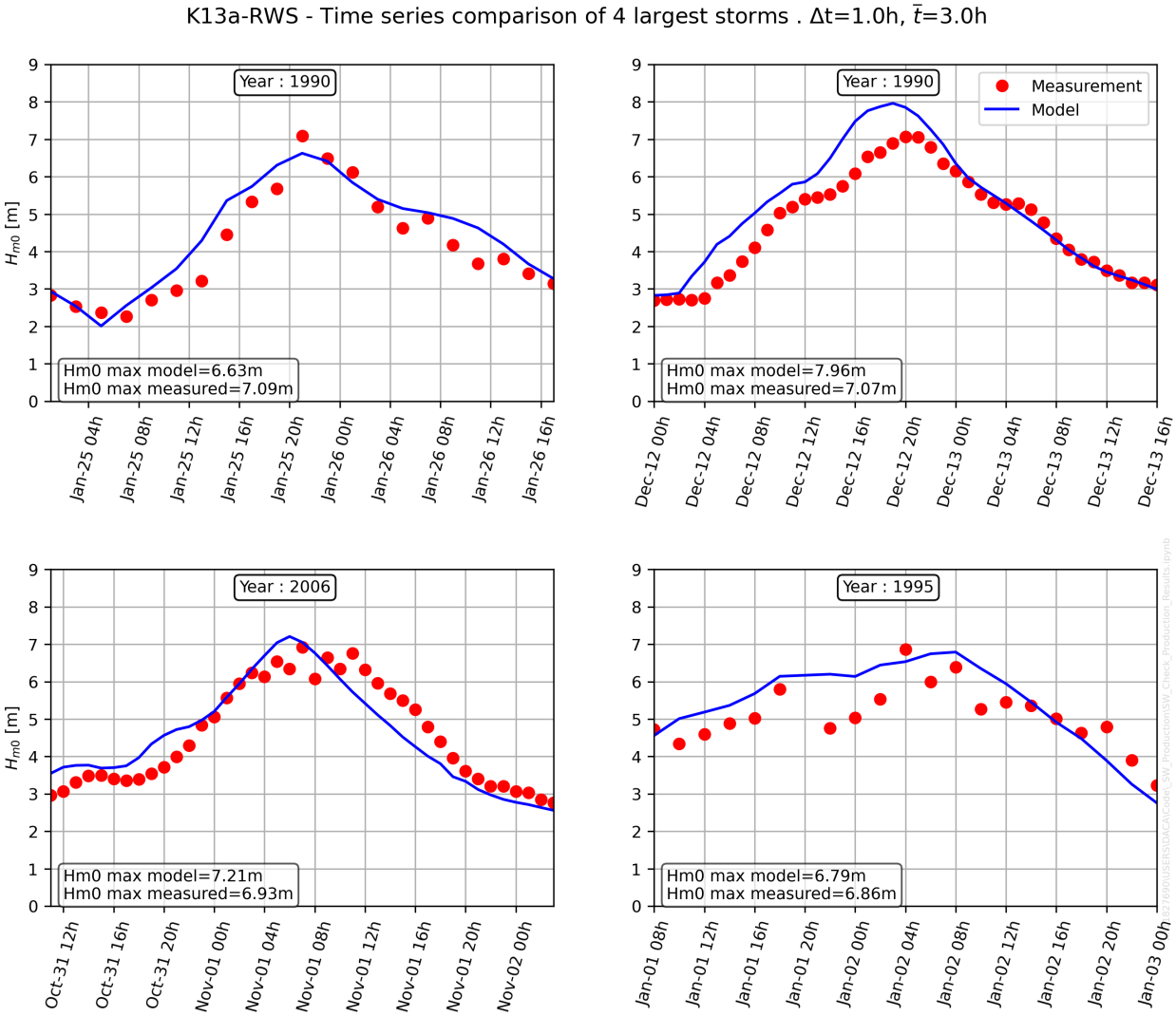

Figure 3.38 Time series comparison of model vs measured H_{m0} during the four (4) largest storms at station K13a.

3.3.9 Validation/comparison of wave spectra

Measured wave energy spectra were available at IJVA and IJVB from devices deployed at the IJmuiden Ver site, and modelled wave spectra from SW_{DWF23} were saved at the locations of these devices.

The measured spectral frequencies were adjusted during the measurement campaign with the following ranges:

- From 0.03 to 0.46 Hz (2.2 – 33 s) during the first three months (May-Jun-July 2022).
- From 0.004 to 1 Hz (1 – 250 s) from August 2022 onwards.

In contrast, the modelled spectral frequencies range from 0.033 to 1.273 Hz (0.8 - 30 s). Therefore, the validation considers the overlapping frequency range.

Figure 3.39 and Figure 3.40 present four frequency spectra comparisons at IJVA and IJVB, respectively. The first two spectral plots are dominated by a single (wind-sea) peak, and the last two have a bi-modal shape.

The figures demonstrate a good ability of the model to replicate the measured spectral shapes. The smoothed visual aspect of the model spectra when compared to the measured spectra is because the model spectra have a much coarser spectral resolution, of just 36 frequencies, in comparison with 256 frequencies of the measured spectra.

Figure 3.41 and Figure 3.42 show a stacked plot comparison of model versus measured spectra (IJVA and IJVB, respectively). Since the measured spectra discretization varies a lot from before to after August 2022, the figures were also split in these two periods. The similarity between the modelled and measured spectra demonstrates a good ability of the model to replicate the measured spectral distribution of energy.

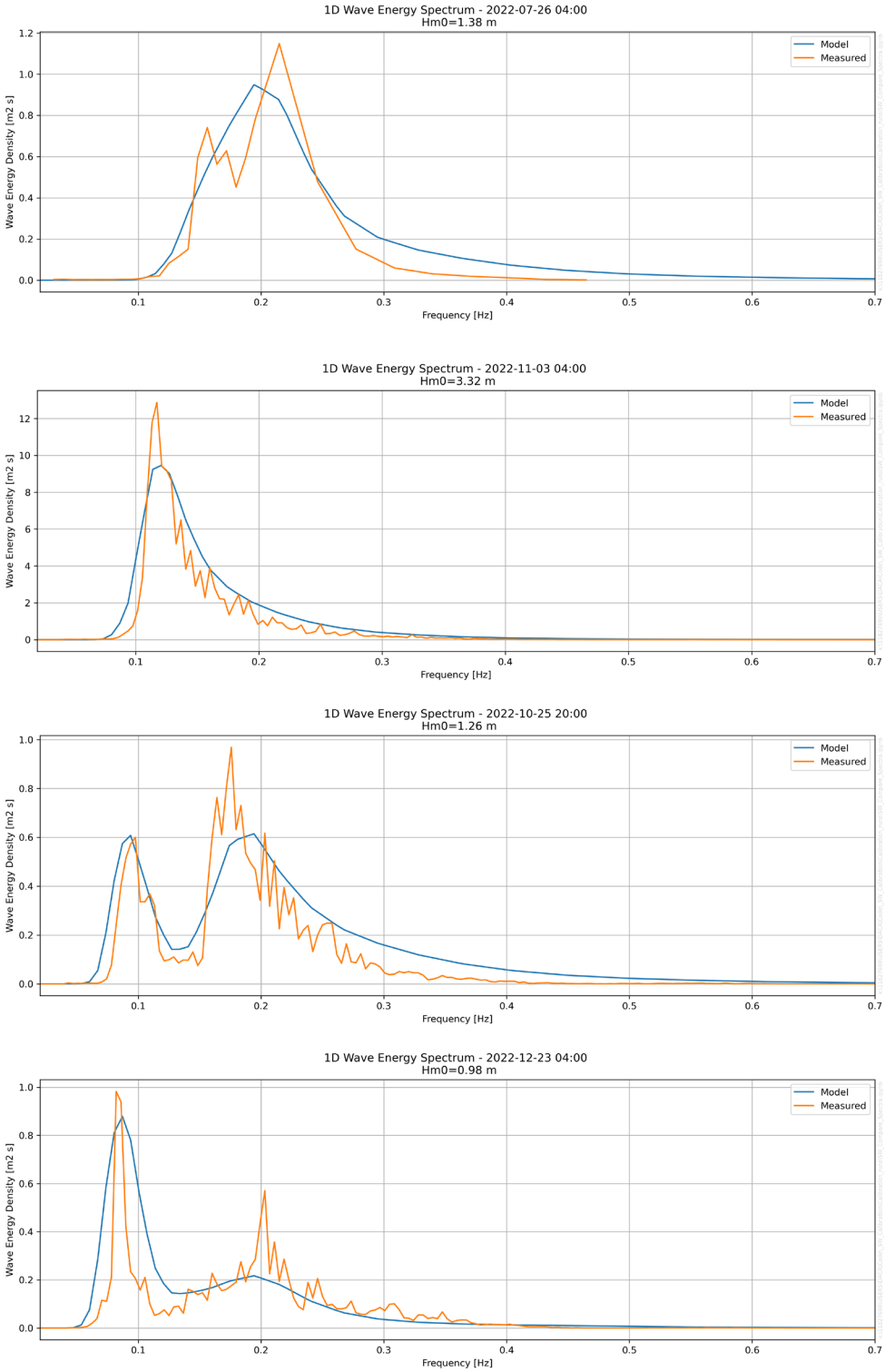

Figure 3.39 Comparisons of four measured /vs model frequency wave spectra at IJVA.
The figures demonstrate that the main shape of the measured spectra is followed by the (smoother) model spectra, both for single-peaked and bimodal spectra.

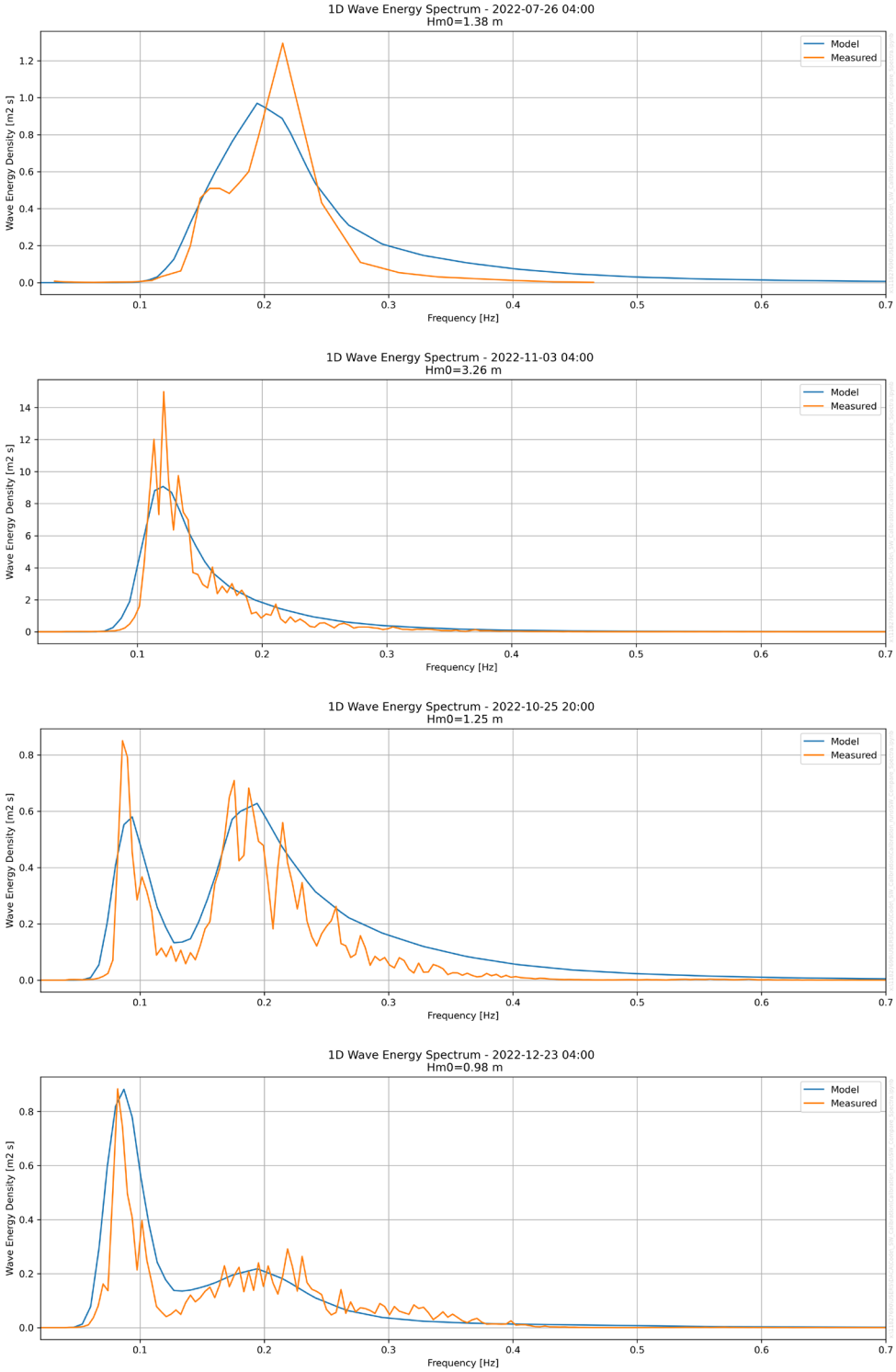

Figure 3.40 Comparisons of four measured /vs model frequency wave spectra at IJVB.
The figures demonstrate that the main shape of the measured spectra is followed by the (smoother) model spectra, both for single-peaked and bimodal spectra.

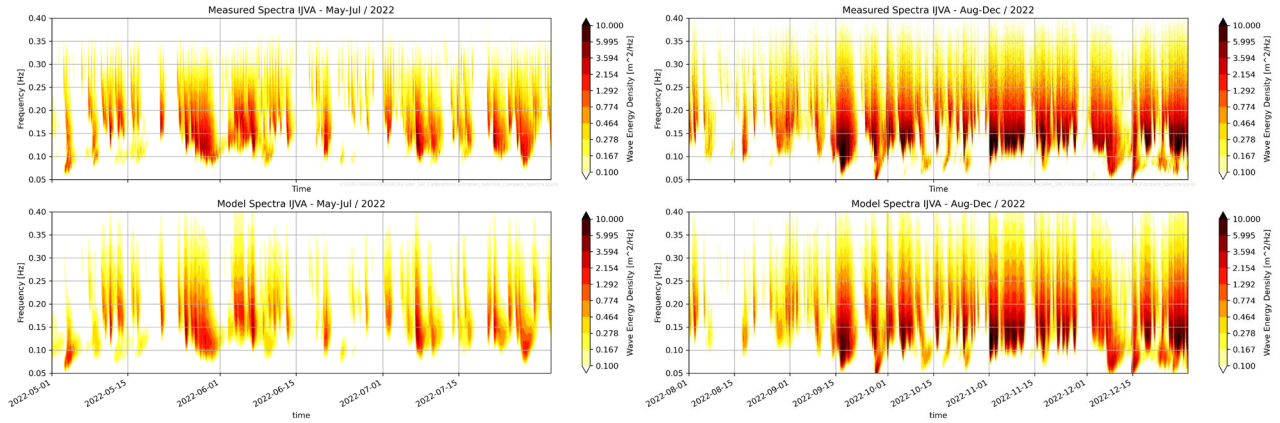

Figure 3.41 Comparisons of measured /vs model frequency wave spectra at IJVA.
Top-left figure: Measured spectra, period May-Jul 2022.
Top-right figure: Model spectra, period May-Jul 2022.
Bottom-left figure: Measured spectra, period Aug-Dec 2022.
Bottom-right figure: Model spectra, period Aug-Dec 2022.
The figures demonstrate a good ability of the model to replicate the distribution of energy along the spectral frequencies, when compared to the measured spectra.

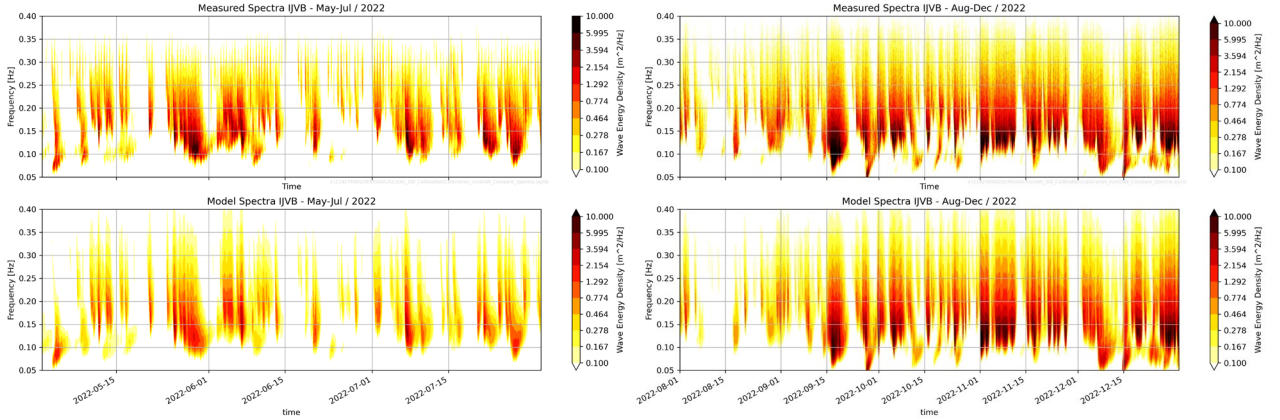

Figure 3.42 Comparisons of measured /vs model frequency wave spectra at IJVB.
Top-left figure: Measured spectra, period May-Jul 2022.
Top-right figure: Model spectra, period May-Jul 2022.
Bottom-left figure: Measured spectra, period Aug-Dec 2022.
Bottom-right figure: Model spectra, period Aug-Dec 2022.
The figures demonstrate a good ability of the model to replicate the distribution of energy along the spectral frequencies, when compared to the measured spectra.

In addition to the 1D frequency spectra, for each frequency the principal Fourier coefficients were available from the measurements (i.e., a1, a2, b1, b2). This allowed for a reconstruction of the 2D directional spectra by means of the Maximum Entropy Method (MeM), as explained in [34]. Directional spectra comparison of the same time steps previously shown in 1D spectra comparison (Figure 3.39 and Figure 3.40) are shown in Figure 3.43 and Figure 3.44 for locations IJVA and IJVB, respectively. What can be seen from these figures is that the model spectra agree well with the measured spectra in terms of frequency and directional distribution of the energy, with the model spectra being “smoother” or less noisy as they have a coarser frequency distribution of only 36 bins, compared to the 256 frequency bins of the measured spectra.

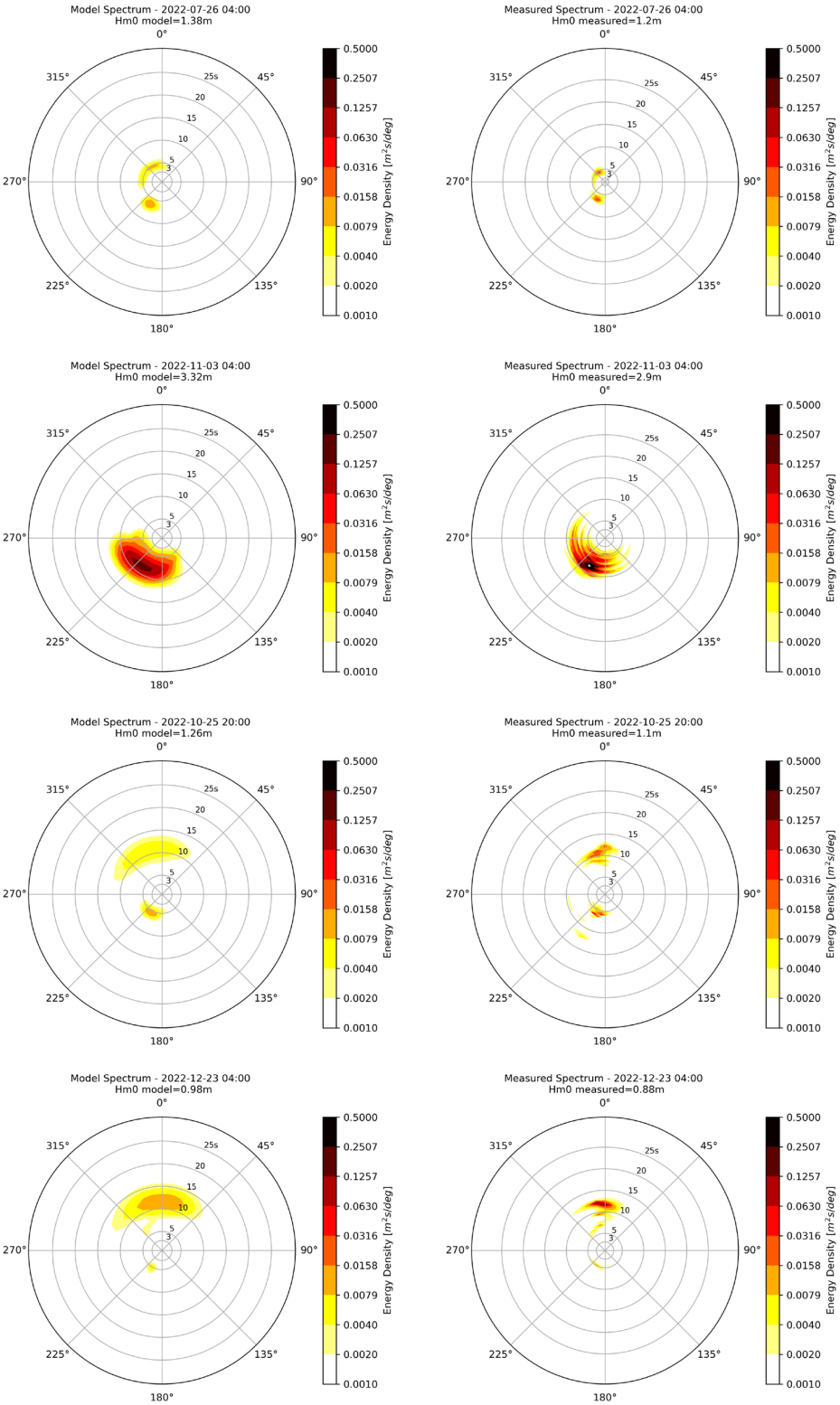

Figure 3.43 Comparisons of measured /vs model directional wave spectra at IJVA.
Left column figures: Model spectra.
Right column figures: Measured spectra.
The figures demonstrate a good ability of the model to replicate the measured spectral shapes both for single-peaked and bimodal spectra.

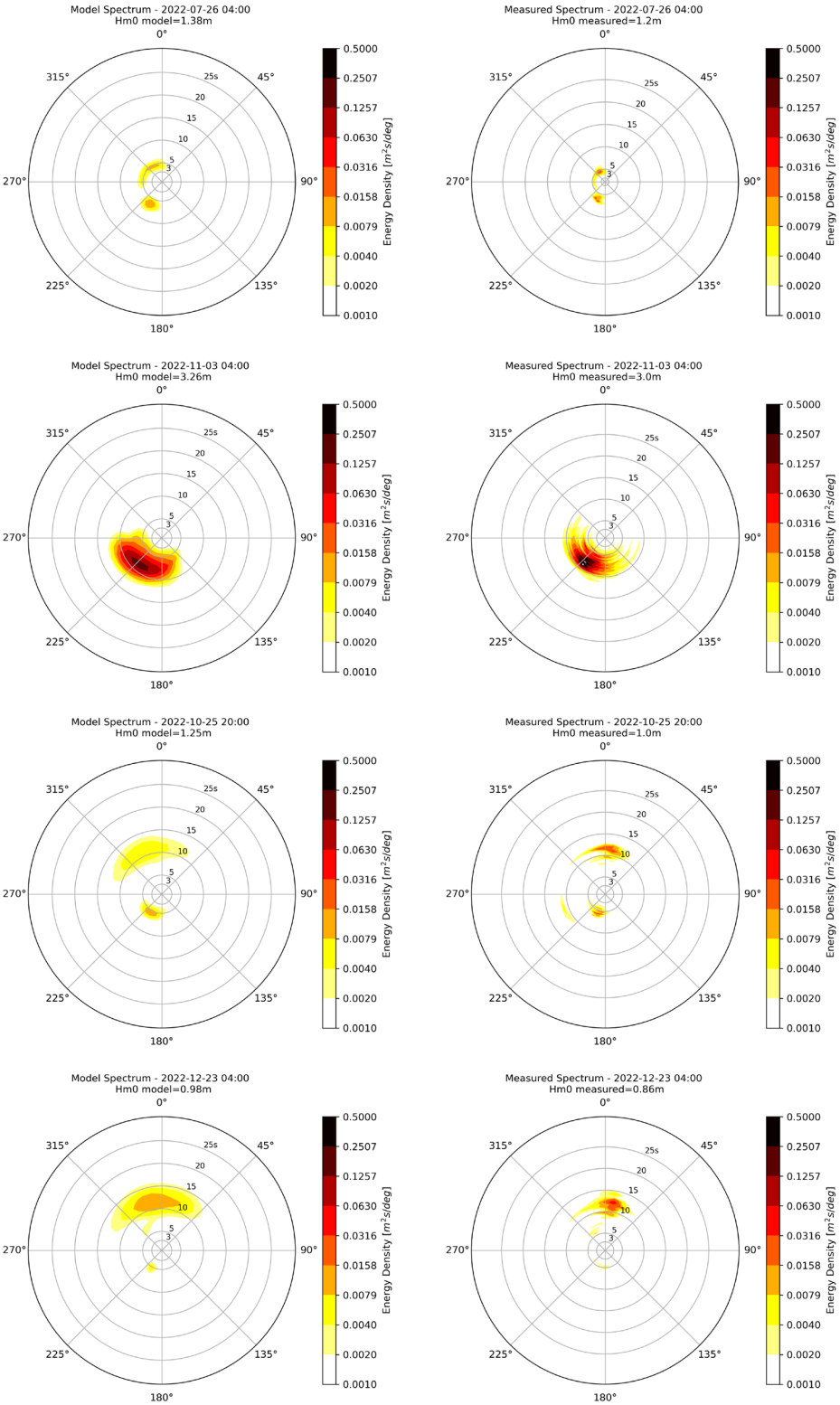

Figure 3.44 Comparisons of measured /vs model directional wave spectra at IJVB.
Left column figures: Model spectra.
Right column figures: Measured spectra.
The figures demonstrate a good ability of the model to replicate the measured spectral shapes both for single-peaked and bimodal spectra.

3.3.10 SW_{DWF23} output specification

Output from SW_{DWF23} was saved with a 60-minute interval and included the integral wave parameters listed in Table 3.15 at every mesh element inside the MOOD database area.

Each integral parameter was saved for the total sea state and for swell and wind-sea components, respectively. The wind-sea/swell partitioning was based on a wave-age criterion (see section 5.1 of [31]), where the swell components are defined as those components fulfilling:

$$\frac{U_{10}}{c}\cos(\theta - \theta_w)^{0.2} < 0.78$$

where U_{10} is the wind speed at 10 m above MSL, c is the wave phase speed, and θ and θ_w are the wave propagation direction and wind direction, respectively.

2D wave spectra (direction and frequency) were saved on a 5 km grid within the MOOD database area as shown in Figure 3.45.

Table 3.15 Output specifications of SW_{DWF23}.
Parameters saved at all grid elements with 60-minute interval.

Parameter (total, wind-sea, and swell)	Abbreviation	Unit
Spectral significant wave height	H_{m0}	m
Peak wave period	T_p	s
Spectral mean wave period	T_{01}	s
Spectral zero-crossing wave period	T_{02}	s
Peak wave direction	PWD	°N (clockwise from)
Mean wave direction	MWD	°N (clockwise from)
Direction standard deviation	DSD	°

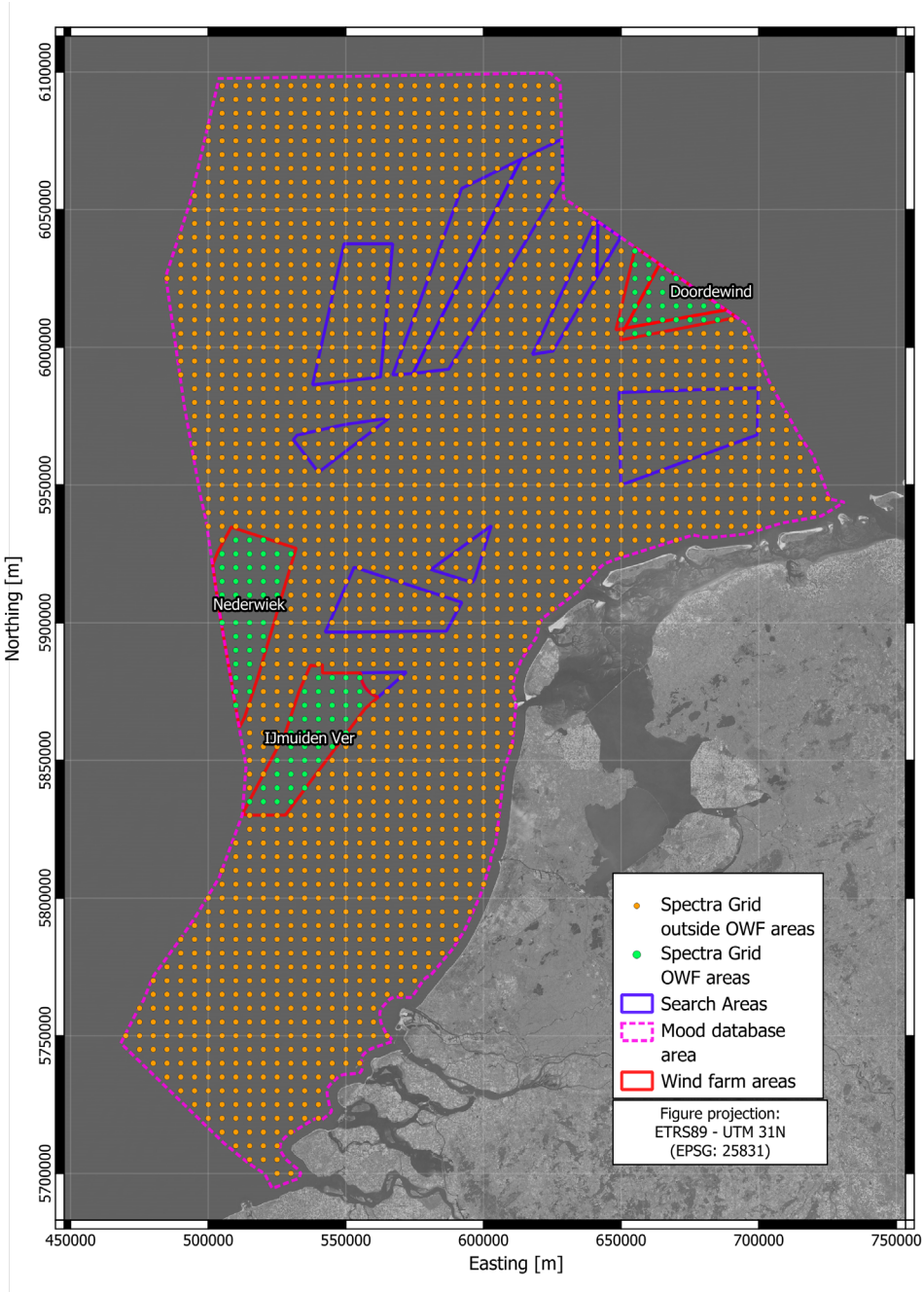

Figure 3.45 Locations of wave spectra saved from SW_{DWF23}.
Spectra inside IJmuiden Ver, Nederwiek and Doordewind OWF are highlighted with green points.

4 Other Atmospheric Parameters Model Data

This section presents other atmospheric parameters model data such as rainfall, air temperature, air pressure, air density, relative humidity, lightning, visibility, snow, and ice accretion. The data are used for analyses in the Part B Data Analysis report [3].

4.1 Rainfall, air temperature, air pressure, air density, humidity, snow, and ice accretion

Rainfall, air temperature, air pressure, air density and relative humidity time series data were adopted from the dedicated Weather Research Forecasting (WRF) model developed exclusively for this project. For the snow and ice accretion analysis, the parameters used (wind speed at 10 mMSL, sea surface temperature and air temperature at 2 mMSL) were also adopted from the WRF model. A full description of the WRF model is shown in the combined Wind Resource Assessment (WRA) and WRF report [2].

The WRF model was validated against on-site measured datasets at Met Mast IJmuiden (MMIJ) station located near the analysis point, IJV1, for air temperature, air pressure and relative humidity. More information on the MMIJ station and the analysis point IJV1, see table 2.5 in the WRA report [2] and the Part B Data Analysis report [3], respectively. Comparisons of modelled (100 mMSL) vs measured (90 mMSL) air temperature, air pressure and relative humidity for IJV1 station are shown in Figure 4.1, Figure 4.2 and Figure 4.3, respectively. Overall, results show an excellent performance of the WRF model for all 3 parameters, with a low bias, a correlation coefficient (CC) close to 1.0 (except for relative humidity with a CC of 0.77), SI equal or lower than 0.1 and a QQ alignment close to the 1:1 line.

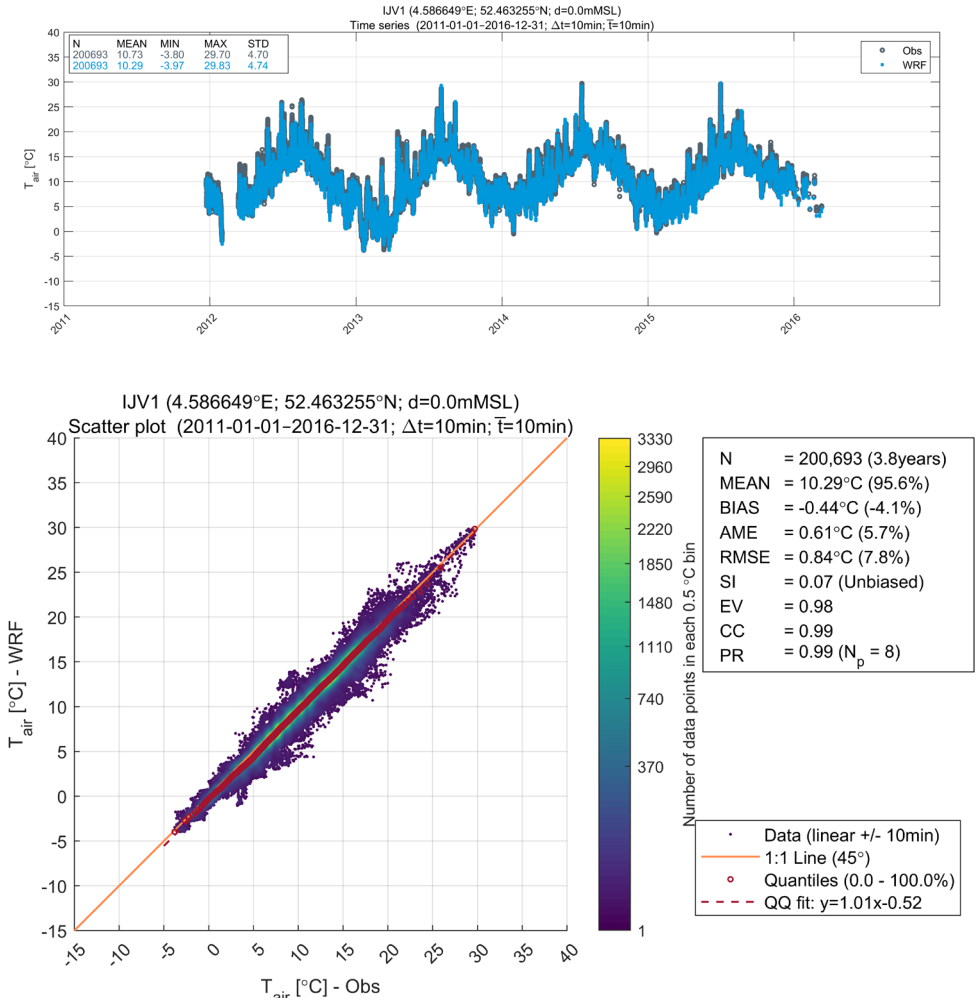

Figure 4.1 WRF model validation for air temperature at IJV1.
Top figure: Timeseries plot validation results.
Bottom figure: Scatter plot validation results.

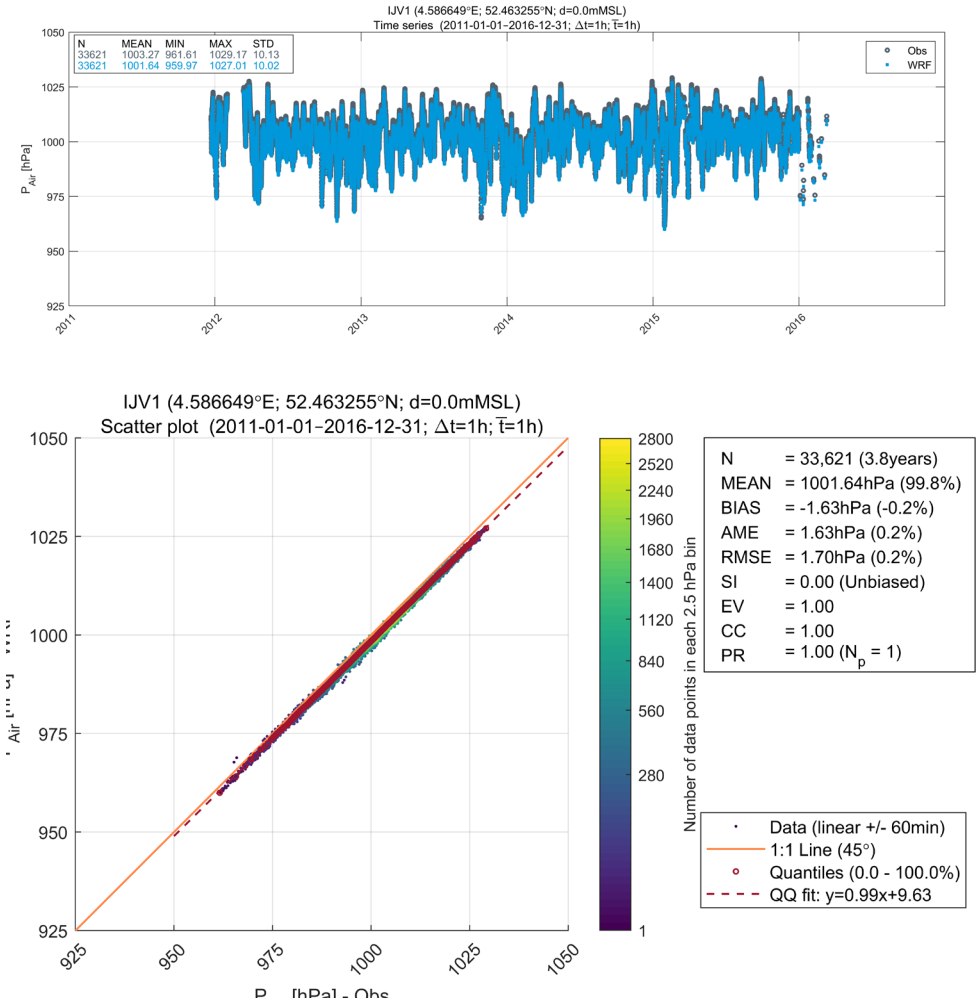

Figure 4.2 WRF model validation for air pressure at IJV1.
Top figure: Timeseries plot validation results.
Bottom figure: Scatter plot validation results.

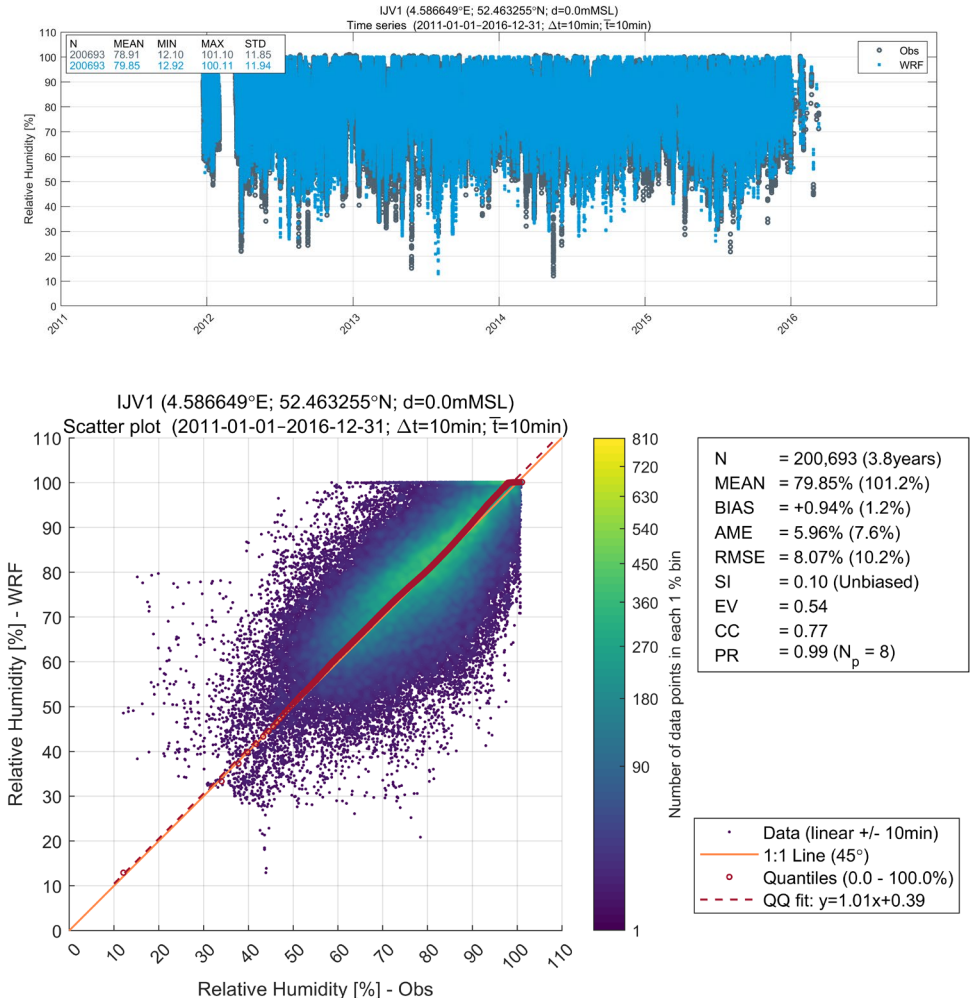

Figure 4.3 WRF model validation for relative humidity at IJV1.
Top figure: Timeseries plot validation results.
Bottom figure: Scatter plot validation results.

Furthermore, the WRA report includes an implicit validation of the main statistics for air temperature, air pressure, and humidity against MMIJ and FLS IJV B (see section 6.11.1 to 6.11.3 in [2]). The statistical mean of the model parameters compares very well with the measured data. For example, the WRF model air temperature (13-year period) at 10 mMSL has a mean of 10.9 °C at N4_Beta2 location (see Figure 6.2 and Table 6.12 in [2]), which is the nearest location to IJV1, whereas the measured mean air temperature (~ 4-year period) at MMIJ at 21 mMSL, 10.9 °C. Additionally, a short summary of the WRF model is presented previously in this report, cf. Section 3.1.

4.2 Lightning

Lightning data used for the lightning analysis in Part B Data Analysis report [3] was taken from the NASA's Global Hydrology Resource Centre (GHRC) and more precisely the LIS/OTD gridded Climatology datasets [35]. The LIS/OTD Gridded Climatology datasets consist of gridded climatology for total lightning flash rates seen by the spaceborne Optical Transient Detector (OTD) and Lightning Imaging Sensor (LIS) from 1995-05-04 to 2013-12-31. The dataset comprises a climatology of annual total lightning at both resolutions, the High-

Resolution Full Climatology (HRFC) on a 0.5° grid and the Low-Resolution Full Climatology (LRFC) on a 2.5° grid. Among others, it includes a 0.5° High-Resolution Monthly Climatology (HRMC) and a 2.5° Low Resolution Monthly Time Series (LRMTS) that are 30-days averages of the flash rate density. The description of the datasets can be found in [36]. The long LIS (equatorward of about 38°) record makes the merged climatology more robust in the tropics and subtropics, while the high latitude data are entirely from OTD. Figure 4.4 Figure 4.4 Global average flash rate density from the GHRC: (a) HRFC mean annual flash rate from combined LID and OTD 0.5° grid and (b) LRFC mean annual flash rate from combined LIS and OTD 2.5° grid (from [36]).shows the global average flash rate density (fl/km^2/yr) based on the high- and low-resolution data from the GHRC.

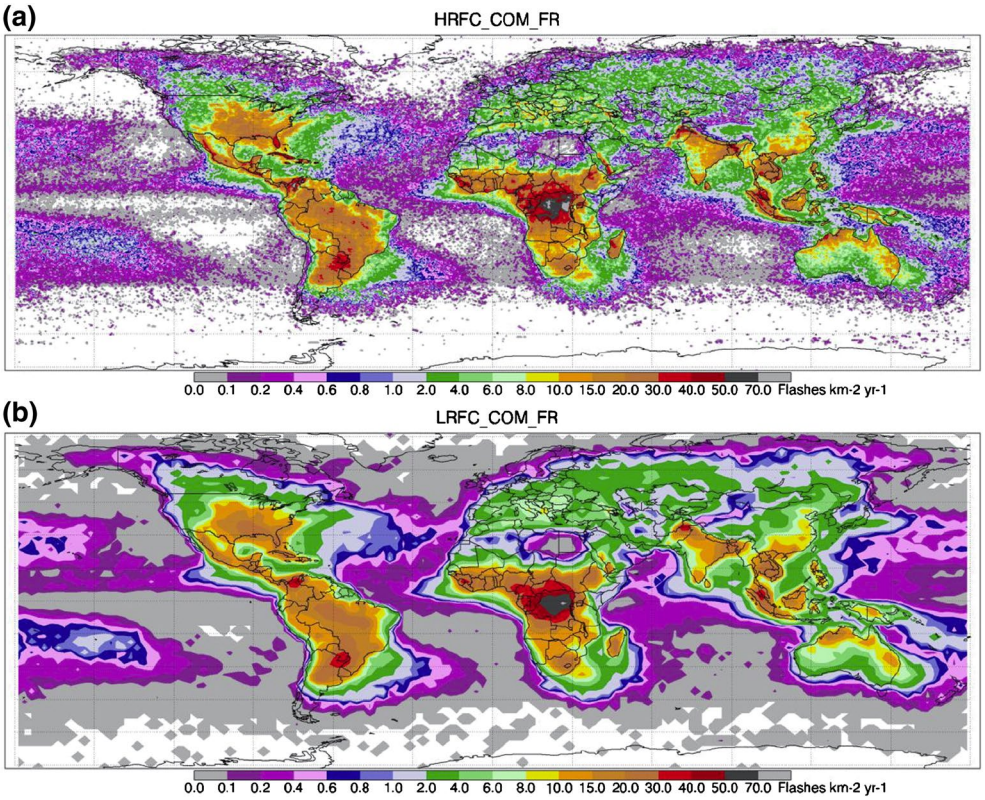

Figure 4.4 **Global average flash rate density from the GHRC: (a) HRFC mean annual flash rate from combined LID and OTD 0.5° grid and (b) LRFC mean annual flash rate from combined LIS and OTD 2.5° grid (from [36]).**

4.3 Visibility

The Royal Netherlands Meteorological Institute (KNMI) is the Dutch national weather service from which the visibility data is adopted[15]. KNMI collects observations from the automatic weather stations situated in the Netherlands and BES islands on locations such as aerodromes and North Sea platforms. The weather stations report every 10 minutes meteorological parameters such as temperature, relative humidity, wind, air pressure, visibility, precipitation, and cloud cover. For the visibility analysis in the Part B Data Analysis report [3], the following stations will be considered: EPL, F16, F3, J6, K14, L9, LEG

[15] https://dataplatform.knmi.nl/

and P11. A more detailed documentation of the KMNI stations data can be found on kmnidata.nl webpage[16].

[16] https://english.knmidata.nl/open-data/actuele10mindataknmistations

5 Other Oceanographic Parameters Model Data

This section provides information on oceanographic variables such as water temperature, salinity, density, sea ice and marine growth. The variables are used for analysis in the Part B Data Analysis report[3].

5.1 Water temperature, salinity, and density

Water temperature and salinity were adopted from the HD_{UKNS} model data from HD 3D UKNS model developed by DHI (see model description below) at the analysis location for the period 2013-01-01 to 2022-12-31 (see Part B Data Analysis report [3] for more information). The water density was calculated using the international one-atmosphere equation of state of seawater derived by Millero, F.J. and Poisson, A. [37], using the temperature and salinity from the HD_{UKNS} dataset. The sea water temperatures from the IJVA and IJVB have not been used for validation. They will be used when longer dataset is available (at least one year). Salinity measurements are not available at IJVA and IJVB.

The 3-dimensional salinity and seawater temperature data were established using the MIKE 3 Flow model FM by DHI. The model was forced by meteorological GFS model and boundary conditions from a combination of the Copernicus PSY3V3R1 global reanalysis model and the DTU10 satellite derived tidal model. The model was calibrated against water level, current, salinity and temperature observations, and later validated against 43 stations with 1 to 37 recording levels at each station giving a total of 677 recording levels. A detailed calibration report and a comprehensive validation report are available on MetOcean on Demand (MOOD)[17] (see section 3.3 for validation against measured salinity and water temperature at stations near analysis location).

The HD_{UKNS} model is based on the modelling software MIKE 3 FM (version 2017) developed by DHI. MIKE 3 FM is based on a flexible mesh approach, and it has been developed for applications within oceanographic, coastal, and estuarine environments.

The system is based on the numerical solution of the three-dimensional (3D) incompressible Reynolds averaged Navier-Stokes equations invoking the assumptions of Boussinesq and of hydrostatic pressure. Thus, the model consists of continuity, momentum, temperature, salinity, and density equations, and it is closed by a turbulent closure scheme. The free surface is considered using a sigma-coordinate transformation approach.

The scientific documentation of MIKE 3 FM is available online[18].

The HD_{UKNS} model domain covers the waters around the North Sea and the UK as illustrated in Figure 5.1. The model includes coastal sections of Ireland, UK, France, Belgium, Netherlands, Germany, Denmark, Sweden, and Norway and

[17] https://www.metocean-on-demand.com/metadata/waterdata-dataset-UKNS_HD3D_SGEO

[18] https://manuals.mikepoweredbydhi.help/latest/Coast_and_Sea/MIKE_3_Flow_FM_Scientific_Doc.pdf

has three open boundaries towards the North Atlantic and one open boundary in southern Kattegat.

The model bathymetry is based on [38]. The bathymetry refers to mean sea level (MSL).

The model resolution (Figure 5.1) varies from 3-6 km in the main part of the model domain to 8-12 km near the three ocean boundaries. The local resolution at project site is approximately 5 km. In a band along the west coast of Netherlands, Germany, and Denmark, the resolution is as fine as 2-3 km.

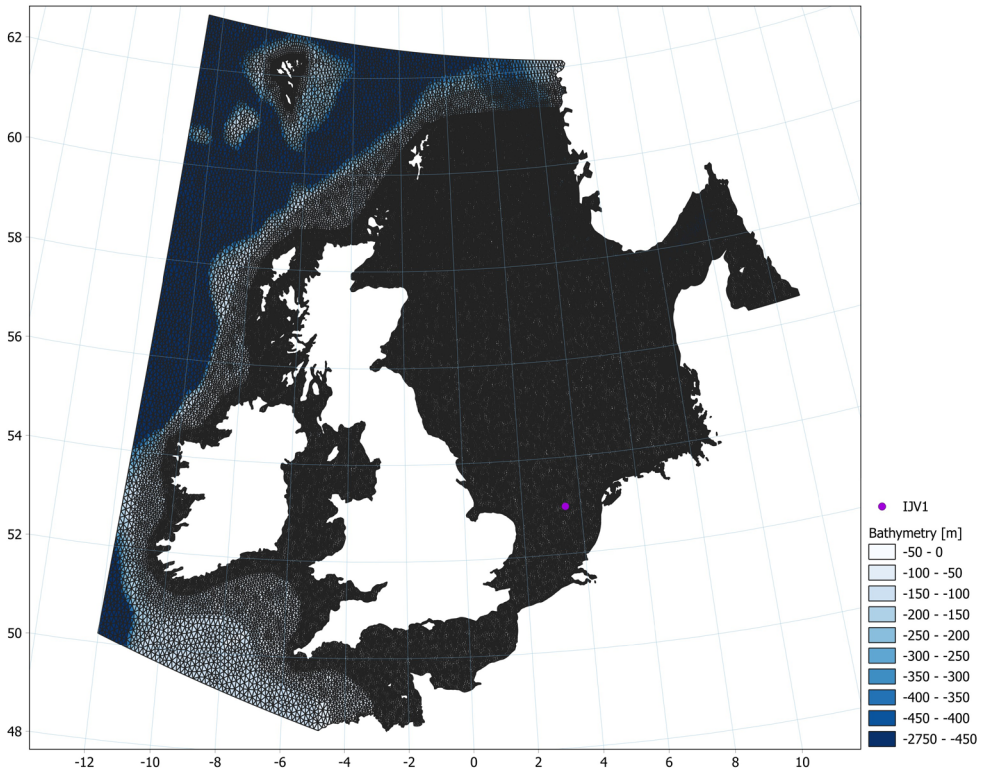

Figure 5.1 HD_{UKNS} model bathymetry and mesh.

The atmospheric forcing of the HD_{UKNS} model is provided by StormGeo in terms of temporally and spatially varying fields of:

- Wind
- Atmospheric pressure
- Precipitation
- Air temperature
- Cloud cover

The applied atmospheric data is from StormGeo's WRF meteorological model covering the North Atlantic. The data is provided in a resolution of 0.1° x 0.1° in hourly time steps.

In hindcast mode, the HD_{UKNS} model applies 'best-cast' meteorological fields and in forecast mode, it applies forecasted meteorological fields.

The StormGeo data is only available from 2009. Therefore, meteorological fields from Vejr2 of Denmark (0.15°, hourly) were applied for the period 2005-2009, and meteorological fields from Climate Forecast System Reanalysis (CFSR) (0.3-0.5°, hourly) were applied for the period 2000 - 2005.

The ocean data from HD_{UKNS} are available on half an hour basis from 2013-01-01 to 2021-12-31 extracted from model files. Before analysis, the data were re-sampled from half an hour to an hourly basis.

5.2 Sea ice cover

The ERA5 dataset is a reanalysis of hourly meteorological conditions back to 1940, established by the ECMWF and provided by Copernicus, the European Union's Earth Observation Programme from which the sea ice cover [%] data is adopted. ERA5 provides hourly estimates of many atmospheric, land and oceanic climate variables. The data cover the Earth on a 30km grid and resolve the atmosphere using 137 levels from the surface up to a height of 80km[19].

The sea ice parameter presents the fraction of a grid box which is covered by sea ice. Sea ice can only occur in a grid box which includes ocean or inland water according to the land-sea mask and lake cover, at the resolution being used. This parameter can be known as sea-ice (area) fraction, sea-ice concentration and more generally as sea-ice cover. In ERA5, sea-ice cover is given by two external providers. Before 1979 the HadISST2 dataset is used. From 1979 to August 2007 the OSI SAF (409a) dataset is used and from September 2007 the OSI SAF open dataset is used[20]. Sea ice does not include ice which forms on land such as glaciers, ice bergs and ice sheets.

5.3 Marine growth

The expected biofouling assessment is based upon scientific literature review where local studies were prioritized as well as existing recommendations for the area [39].

Additionally, expected species composition is based on a species list provided recently by a large-scale study [40]. Growth information is based on existing database with trait information on species found in the North Sea. Species which were not present in the database were further explored on a variety of well-known online databases.

[19] https://www.ecmwf.int/en/forecasts/dataset/ecmwf-reanalysis-v5
[20] https://cds.climate.copernicus.eu/cdsapp#!/dataset/reanalysis-era5-single-levels?tab=overview

6 Improvements in Ocean Modelling Compared to Previous Studies in the Area

This section presents a brief comparison between the model validation of the present HD and SW models (DWF23) and the previous models (DWF2020), with the purpose of quantifying the improvement of the new database resulting from this study. Additionally, a summary of the differences in model setups are presented.

It has been mentioned in this report that the hydrodynamic and spectra wave models (HD_{DWF23} and SW_{DWF23}) differ from their predecessors ($HD_{DWF2020}$ and $SW_{DWF2020}$) [5-7] in a certain number of aspects. In this section, these differences are quantified. For the sake of the readability of the report, the differences will be compared in three stations located far apart within the MOOD domain (see Figure 2.8). These stations were downloaded from the MOOD website where the DWF2020 model output are stored[21], and they were selected according to the following criteria:

- Station nearest to the site (IJV): Unfortunately, the stations from the present (undergoing) metocean measurement campaign, i.e., IJVA and IJVB, have data only from May-2022 onwards, hence do not overlap with the previous model DWF_{2020}, which ends in the year 2019. The closest stations to the site, which were selected for comparisons, are **MMIJ** (for comparing SW results) and **Q1** (for comparing HD results).
- Station farthest to the north: To compare against both the HD and SW model, station **F3** was selected.
- Stations farthest to the south: To compare against both the HD and SW model, station EPL22 was selected.

As a general picture, the comparison at these three stations shows the difference between the previous and present models' performances. The overall comparison was performed for most stations shown previously in Figure 2.8 to get a better understanding of the model improvements. However, the comparison at the three stations shown in this section provides a good summary, and comparing at more stations does not add significant value, since the same conclusions are achieved.

6.1 Comparison of HD models

Before comparing the differences in model performance, it is important to highlight the key differences between the models, as is shown in the following table.

[21] https://v1.metocean-on-demand.com/#/main - This database will no longer be available from the year 2024. Interested readers can contact RVO for the data.
[22] Other stations were slightly further to the south (e.g., Bor1), yet it is not available as part of the DWF_{2020} database.

Table 6.1 List of key differences between models $HD_{DWF2020}$ and HD_{DWF23}.

Parameter	$HD_{DWF2020}$	HD_{DWF23}
Number of local bathymetry surveys included	6	7
Background bathymetry dataset	EMODnet 2018	EMODnet 2020
Source of local model boundaries	HD_{NE-DA} forced with CFSR	HD_{NE-DA} forced with ERA5
End of data assimilation in model boundaries	2018-12-31	2022-12-31
Inclusion of data assimilation in local model	No	Yes
Atmospheric forcing in local model	CFSR (approx. resolution of ~20 to 30 km)	WRF (downscaled from ERA5, 1.67 km resolution)
Grid refinement	Finest resolution at HKW and TNW OWFs.	Finest resolution at IJmuiden Ver, Nederwiek and Doordewind OWFs.

Figure 6.1 to Figure 6.3 show the model performance at stations Q1, F3 and EPL, respectively. What can be seen from these results is that the new HD_{DWF23} model outperforms the previous $HD_{DWF2020}$ model in practically all the statistics, with the biggest improvements seen in RMSE and SI, where the new model shows an improvement in the order of a factor 2-3, followed by improvements in the CC (from 0.8-0.9 to ~1.0) and PR (from 1.1-1.2 to ~1.0).

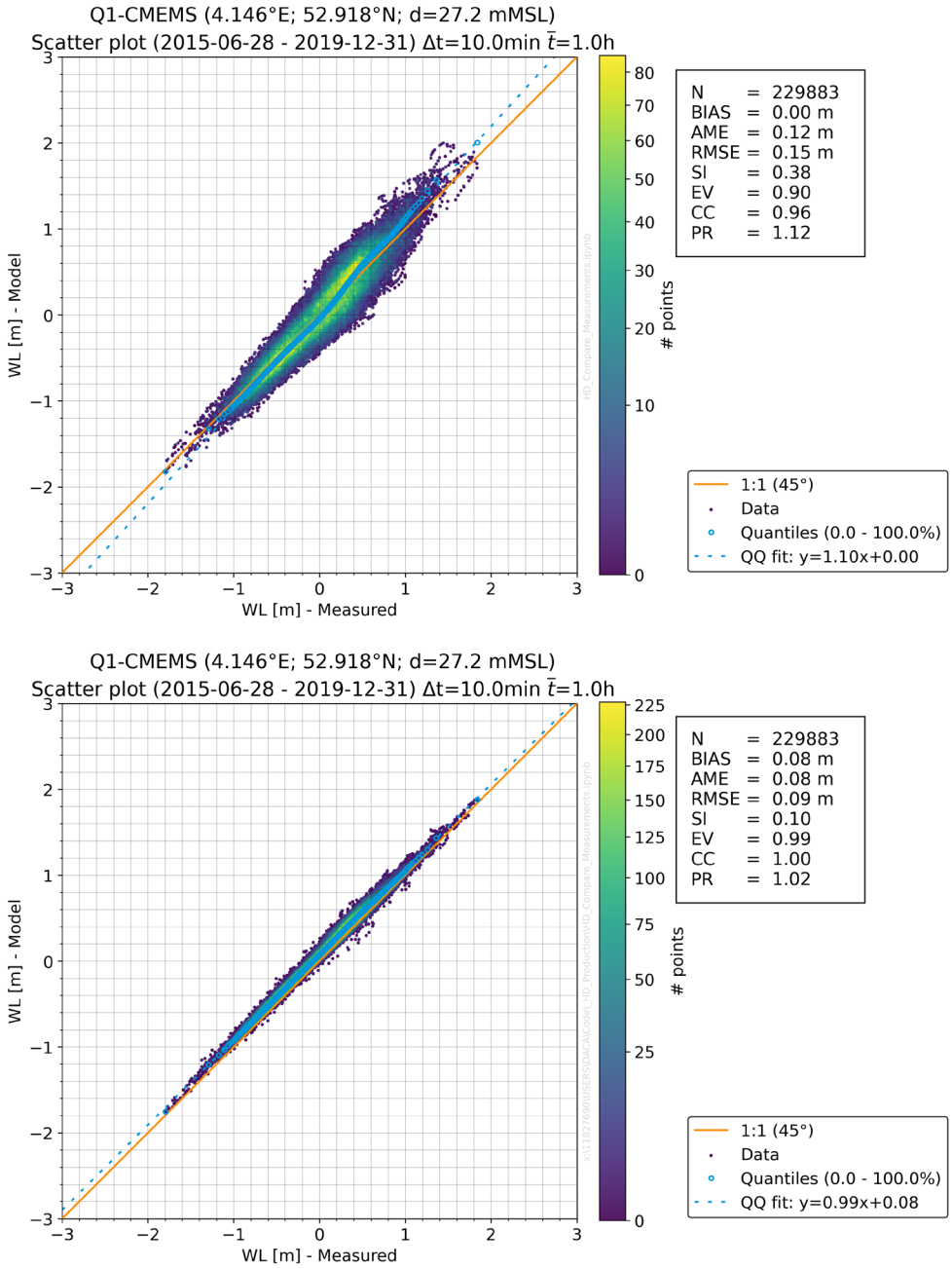

Figure 6.1 Model performance comparison (water level) against measurements at station Q1.
Top figure: $HD_{DWF2020}$ model. Bottom figure: HD_{DWF23} model.

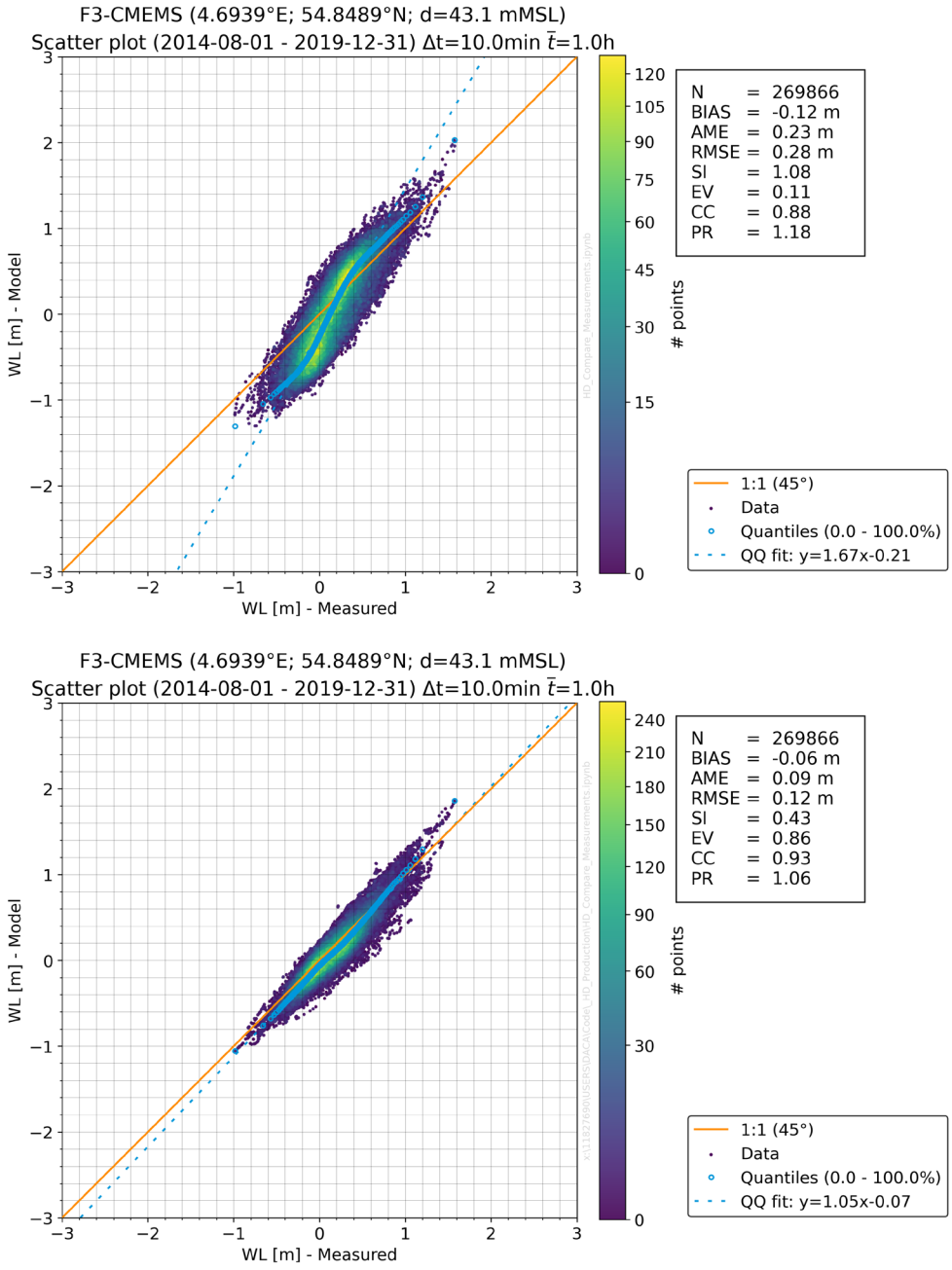

Figure 6.2 Model performance comparison (water level) against measurements at station F3.
Top figure: $HD_{DWF2020}$ model. Bottom figure: HD_{DWF23} model.

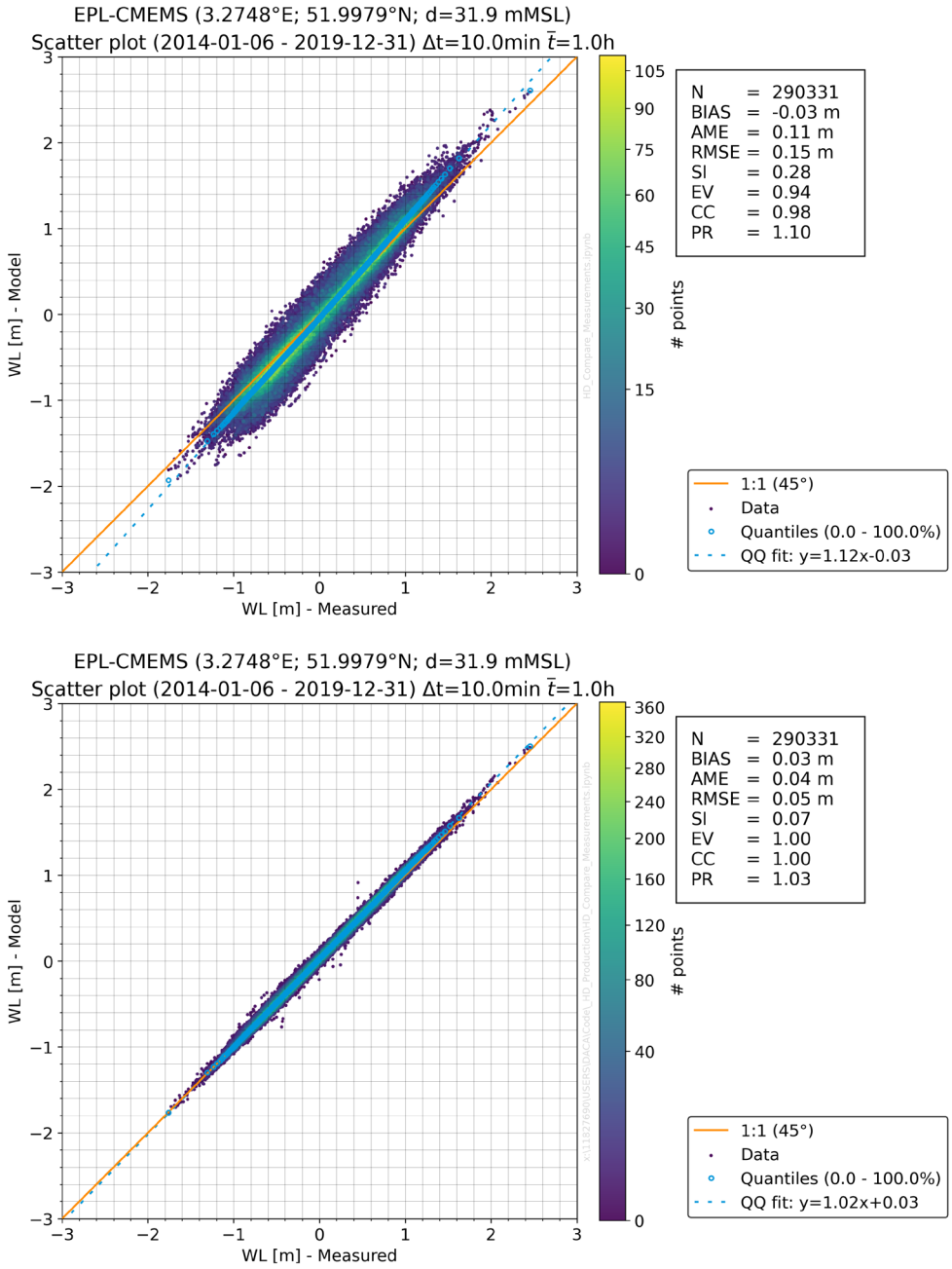

Figure 6.3 Model performance comparison (water level) against measurements at station EPL.
Top figure: $HD_{DWF2020}$ model. Bottom figure: HD_{DWF23} model.

6.2 Comparison of SW models

Before comparing the differences in models' performances, it is important to highlight the key differences between the models, as is shown in the following table.

Table 6.2 List of key differences between models $SW_{DWF2020}$ and SW_{DWF23}.

Parameter	$SW_{DWF2020}$	SW_{DWF23}
Number of local bathymetry surveys included	6	7
Background bathymetry dataset	EMODnet 2018	EMODnet 2020
Source of local model boundaries	SW_{NE} forced with CFSR	SW_{GWM} forced with ERA5
Atmospheric forcing in local model	CFSR (approx. resolution of ~20 to 30 km)	WRF (downscaled from ERA5, 1.67 km resolution)
Source terms formulation	WAM Cycle 4	Ardhuin et al.
Air-sea interaction	Uncoupled	Coupled
Spectral discretization	40 frequencies (1.03–28.57s (0.035-0.973Hz) 41 directions (8.8° resolution)	36 frequencies (0.78–30.3s (0.033-1.273 Hz) 36 directions (10° resolution)
Grid refinement	Finest resolution at HKW and TNW OWFs.	Finest resolution at IJmuiden Ver, Nederwiek and Doordewind OWFs.

Figure 6.4 to Figure 6.6 show the model performance at stations MMIJ, F3 and EPL, respectively. What can be seen from these results is that the new SW_{DWF23} model outperforms the previous $SW_{DWF2020}$ model in practically all the statistics for H_{m0} results, with a RMSE improvement between 2 and 10 cm, SI reduction in the range of 0.01-0.0.8, and a BIAS now closer to ~0 m.

With respect to the peak periods (T_p), what can be seen is that the previous model showed slightly better results, with a better RMSE in the order of 0.2 seconds and a better SI in the order of 0.02. However, considering the high scatter seen in peak periods given by the nature of the measurements (measured data is binned, as seen by the vertical lines in the figures), both models are considered comparable. Therefore, it can be concluded that the new model SW_{DWF23} gives similar results as the previous model $SW_{DWF2020}$, while still showing an improvement when it comes to significant wave height.

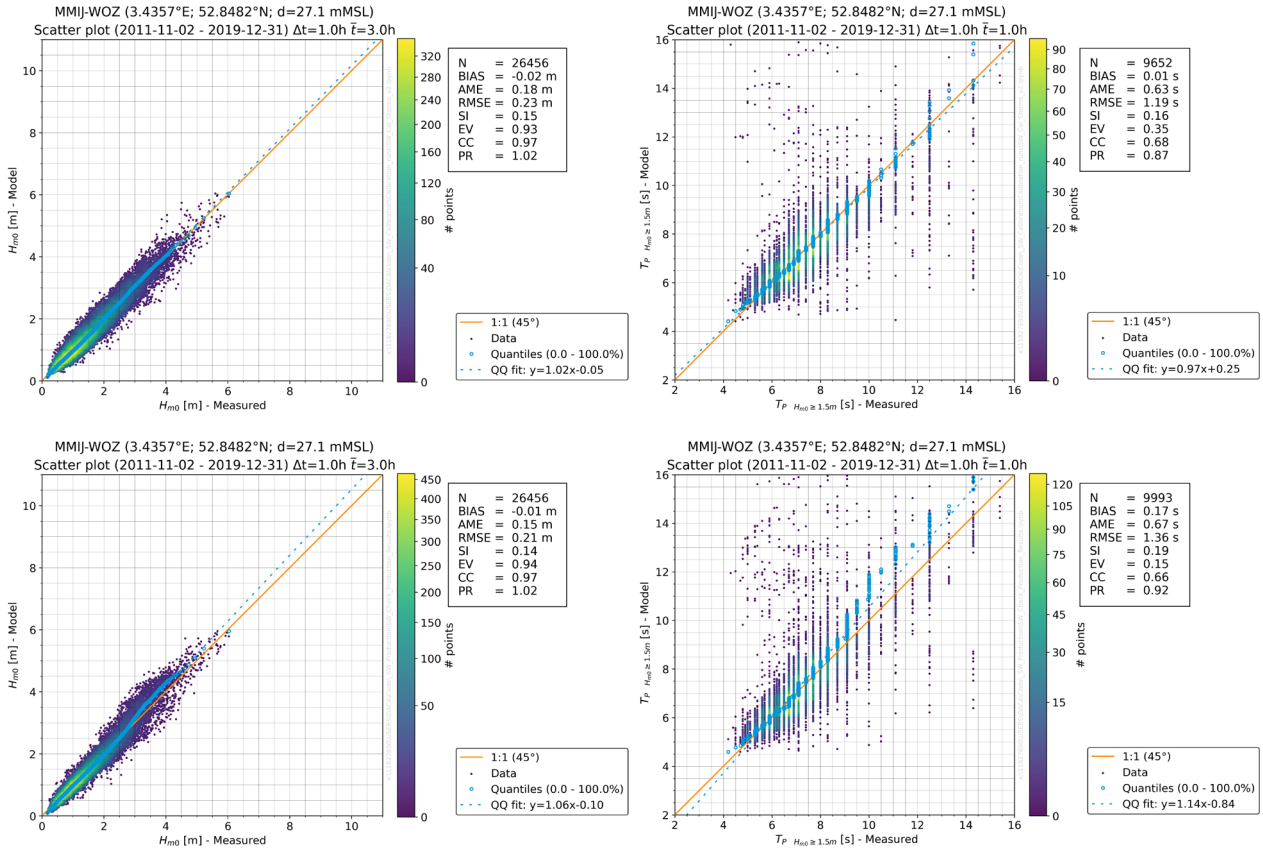

Figure 6.4 Model performance comparison against measurements at station MMIJ.
Top-left figure: $SW_{DWF2020}$ model, H_{m0}.
Top-right figure: $SW_{DWF2020}$ model, T_p.
Bottom-left figure: SW_{DWF23} model, H_{m0}.
Bottom-right figure: SW_{DWF23} model, T_p.

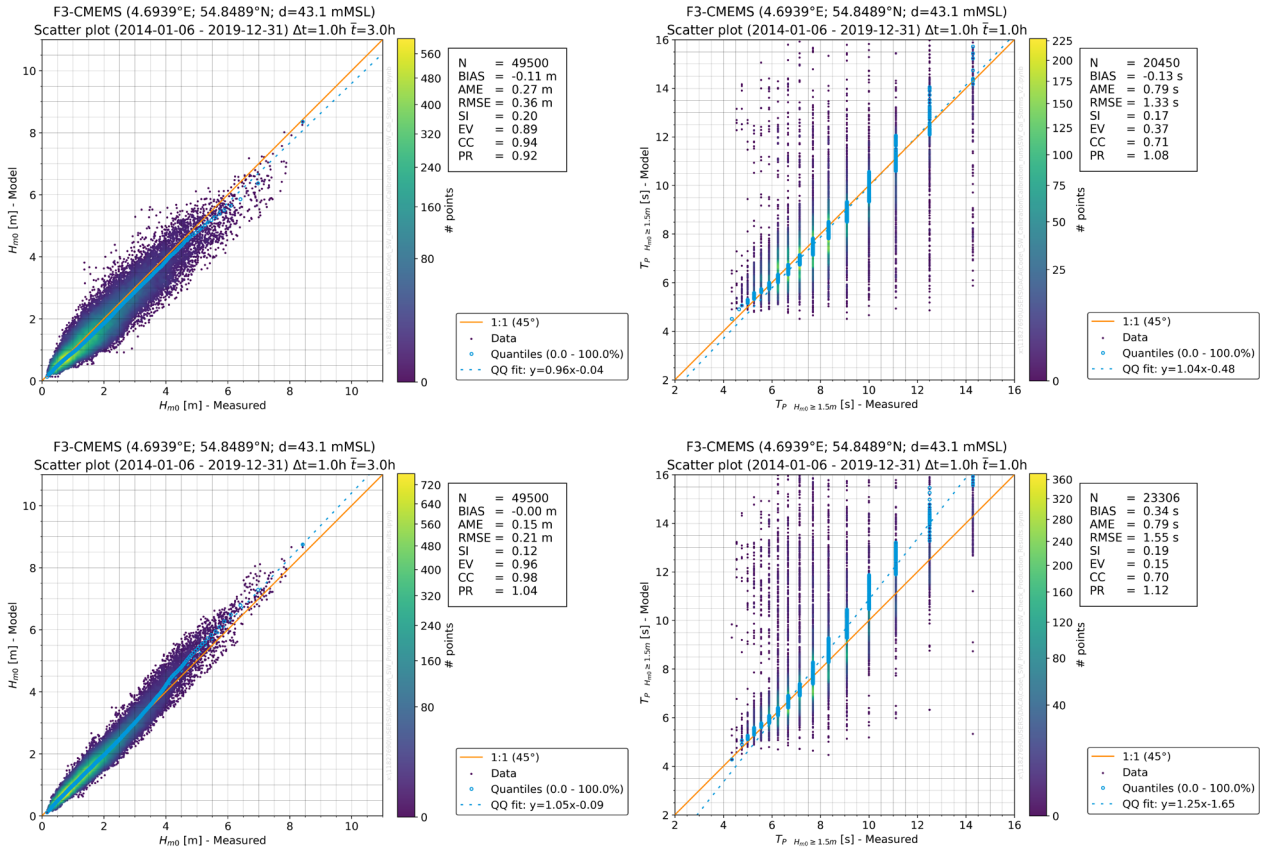

Figure 6.5 Model performance comparison against measurements at station F3.
Top-left figure: $SW_{DWF2020}$ model, H_{m0}.
Top-right figure: $SW_{DWF2020}$ model, T_p.
Bottom-left figure: SW_{DWF23} model, H_{m0}.
Bottom-right figure: SW_{DWF23} model, T_p.

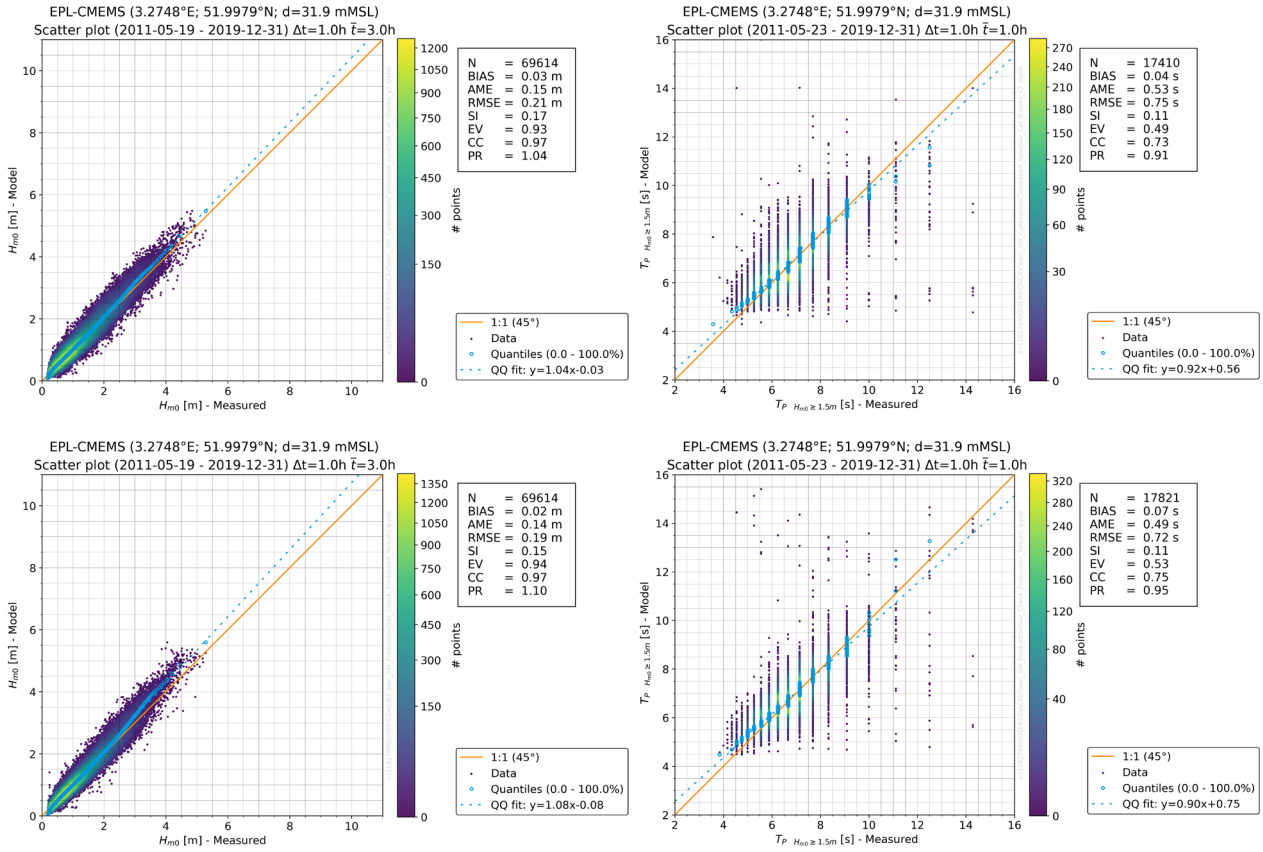

Figure 6.6 Model performance comparison against measurements at station EPL.
Top-left figure: $SW_{DWF2020}$ model, H_{m0}.
Top-right figure: $SW_{DWF2020}$ model, T_p.
Bottom-left figure: SW_{DWF23} model, H_{m0}.
Bottom-right figure: SW_{DWF23} model, T_p.

7 Accessing Metocean Data on the MOOD Web Database

This section provides a brief overview of the IJmuiden Ver online database, which is hosted on DHI's MetOcean-On-Demand (MOOD) online web data portal https://www.metocean-on-demand.com/.

7.1 Web based database and datasets

The datasets developed by this study and available in the MOOD platform are called DWF23 (from 'Dutch Wind Farms 2023').

It is important to note that the DWF23 dataset covers a large area within the Dutch North Sea sector but is currently only being certified for the IJmuiden Ver site. The HKN, HKZ, HKW and TNW datasets [5-8] also available in MOOD[23] (separate from DWF23) were already certified.

Figure 7.1 shows a screen shot of DWF23 datasets on MOOD. Once a point is selected within the database polygon, which comprises all investigation areas, the DWF23 datasets are automatically selected and shown in the dataset context menu on the right (Waves, Ocean, and Atmosphere). Points can be modified by drag-and-drop or by the provision of coordinates (in geographical or UTM coordinates). The point can be renamed, and multi-point selection is possible.

From the dataset context menu, the user has access to Metadata, Validation, Analytics and Reports for each dataset. Via the 'Add to Chart' button, the time series can be added for later download. The period 1979-01-01 07:00 to 2022-12-31 23:00 is available and selected by default. The selected period can be modified and will be applied to the analytics and to the download of data.

[23] Data available on https://v1.metocean-on-demand.com/#/main only until January 2024. The user is referred to RVO if data is required later.

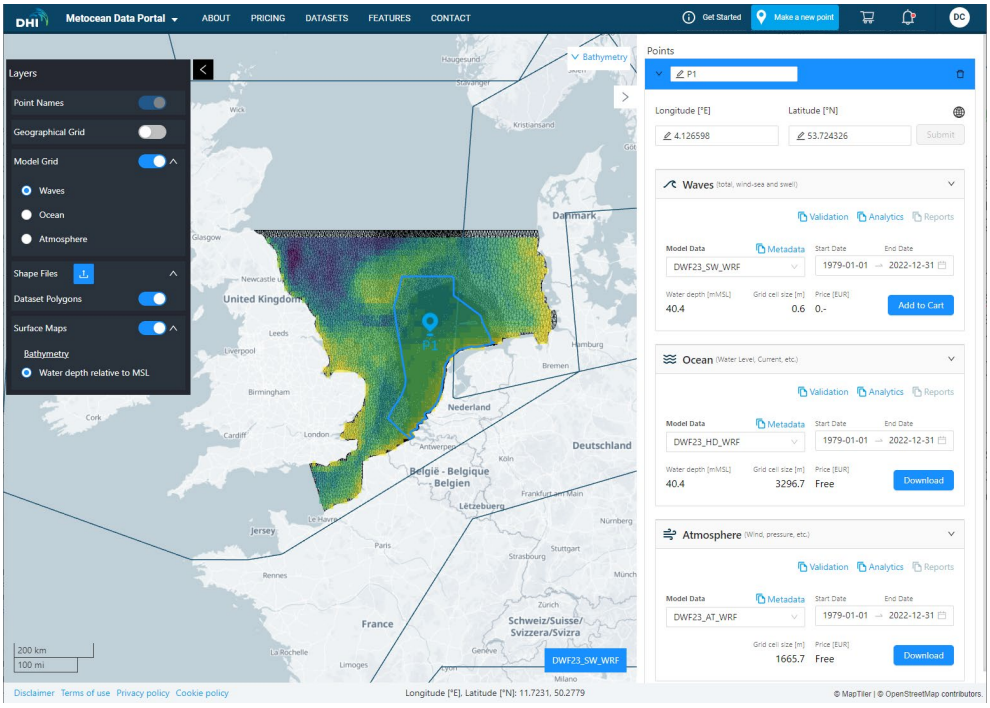

Figure 7.1 View of DWF23 datasets on the online data portal MOOD. Screen view of https://www.metocean-on-demand.com/ after selection of a point within the DWF23 dataset. The dataset context menu appears to the right and the layers context menu to the left.

7.2 Time series

The available time series are summarised in Table 7.1, which specifies the dataset names on MOOD, the underlying models, as well as post-processing steps. The time series are available at each grid point of the respective model mesh within the DWF23 area. This corresponds to 91,013 elements for the HD_{DWF23} (hydrodynamic) model, 89,410 elements for the SW_{DWF23} (wave) model, and 19,200 elements for the WRF (atmospheric) model.

Table 7.1 Available DWF23 datasets and time series.
MOOD dataset names, their underlying models and post-processing steps applied to the model outputs, reference for further details and included parameters.

MOOD dataset	Model	Details	Modelled and pre-processed parameters
DWF23_SW_WRF	SW_{DWF23}	Section 3.3	H_{m0}, T_p, T_{01}, T_{02}, PWD, MWD, DSD $H_{m0,Sea}$, $T_{p,Sea}$, $T_{01,Sea}$, $T_{02,Sea}$, $PWD_{,Sea}$, $MWD_{,Sea}$, $DSD_{,Sea}$ $H_{m0,Swell}$, $T_{p,\ Swell}$, $T_{01,\ Swell}$, $T_{02,\ Swell}$, $PWD_{,\ Swell}$, $MWD_{,\ Swell}$, $DSD_{,\ Swell}$ (wave-age sea/swell separation)
DWF23_HD_WRF	HD_{DWF23}	Section 3.2	WL_{tot}, $CS_{tot,2DH}$, $CD_{tot,2DH}$
DWF23_AT_10min	WRF	Section 3.1 and [2]	10-minute data: WS_z, WD_z, $Tair_z$, RH_z with Z=[10, 30, 60, 100, 120, 140, 160, 200, 250, 300] mMSL. MSLP, SST, DWSR, Precipitation, PBL height.
DWF23_AT_1h	WRF	Section 3.1 and [2]	1-hour data: $AirPres_z$, $AirDen_z$, @ Z=[10, 30, 60, 100, 120, 140, 160, 200, 250, 300] mMSL.

7.3 On-the-fly analytics

Various types of analyses (rose, scatter diagrams, occurrence tables, persistence, etc.) are available on-the-fly through the MOOD online database. Users can define their own set of thresholds for any given parameter and analysis. There is also a possibility for limiting the data coverage period to any given sub-period for specific analyses.

7.4 Surface maps

Surface maps of selected statistics of normal metocean conditions, tidal water levels and extreme metocean conditions will be provided in the database in the year 2024.

7.5 Reports

Two types of pre-processed reports (normal and extreme conditions) are available as .xlsx tables at the analysis point (IJV1). Details on the respective analyses can be found in the analysis report [3]. Normal and extreme conditions data for the entire feasibility domain area will be available in the year 2024.

8 References

[1] RVO. "IJmuiden Ver - General Information." https://offshorewind.rvo.nl/cms/view/5c06ac88-c12f-4903-89f3-27d66937b7e9/general-information-ijmuiden-ver (accessed 2023).

[2] OWC, "IJmuiden Ver Wind Farm Zones: Wind Resource Assessment," The Netherlands, 2023. [Online]. Available: https://offshorewind.rvo.nl/file/download/d61bb7ce-25eb-43dc-942f-60149f7d33b7/ijv_20231127_dhi_report-wind-resource-assessment-f.pdf

[3] DHI, "IJmuiden Ver, Nederwiek and Doordewind Detailed Metocean Study and Database: Part B, Metocean Analysis," 2023.

[4] E. Commission, "English Style Guide: A handbook for authors and translators in the European Commission," 2023.

[5] DHI, "Metocean desk study and database for Dutch Wind Farm Zones, Hollandse Kust (Noord)," RVO, NL, Project Nr. 11822658, Final 2.4, 2019.

[6] DHI, "MetOcean Study - Wind farm zone Hollandse Kust (zuid) and Hollandse Kust (noord) v2.3," RVO.nl, Utrecht, 2017.

[7] DHI, "Metocean desk study and database for Dutch Wind Farm Zones, Hollandse Kust (West)," Project Nr. 11822658, Final 0.5, 2020.

[8] DHI, "Ten noorden van de Waddeneilanden (TNW) Wind Farm Zone: Metocean Desk Study," The Netherlands, 2022. [Online]. Available: https://offshorewind.rvo.nl/file/download/4878bc26-52b4-43e3-b5d0-a77837de1a21/tnw_20220706_dhi_mds-report_final.pdf

[9] Fugro, "Geophysical Site Investigation Survey - Hollandse Kust (zuid) Wind Farm Development Zone Wind Farm Site I," Fugro Survey B.V., The Netherlands, 2016.

[10] Fugro, "Geophysical Site Investigation Survey - Hollandse Kust (zuid) Wind Farm Development Zone Wind Farm Site II," Fugro Survey B.V., The Netherlands, 2016.

[11] Fugro, "Geophysical Site Investigation Survey - Hollandse Kust (zuid) Wind Farm Development Zone Wind Farm Site III," Fugro Survey B.V., The Netherlands, 2016.

[12] Fugro, "Geophysical Site Investigation Survey - Hollandse Kust (zuid) Wind Farm Development Zone Wind Farm Site IV," Fugro Survey B.V., The Netherlands, 2016.

[13] Fugro, "Geophysical Site Investigation Survey - Hollandse Kust (noord) Wind Farm Zone Survey 2017," Fugro The Netherlands, 2017.

[14] Fugro, "Geophysical Results Report - Hollandse Kust (west) Wind Farm Zone Survey 2019," Fugro, The Netherlands, 2019.

[15] Fugro, "Geophysical Rersults Report - Geophysical Survey at the IJmuiden Ver Wind Farm Sites V and VI (IJ56) | Dutch Sector, The Netherlands," Fugro, The Netherlands, 2022.

[16] MMT, "Ten Noorden van de Waddeneilanden (TNW) wind farm zone geophysical survey," RVO, Utrecht, 2019.

[17] GeoXYZ, "Geophysical Survey - Ijmuiden Ver Wind Farm Zone - Final Survey Report," GeoXYZ, The Netherlands, 2021.

[18] "Supply of Meteorological and Oceanographic data at Ten noorden van de Waddeneilanden, 24-month summary campaign report, F," RVO, Utrecht, 2022.

[19] *Environmental Conditions and Environmental Loads*, DNV-RP-C205, DNV, 2021. [Online]. Available: http://rules.dnvgl.com/docs/pdf/DNV/codes/docs/2014-04/RP-C205.pdf

[20] *Petroleum and natural gas industries — Specific requirements for offshore structures — Part 1: Metocean design and operating considerations*, ISO 19901-1:2015, ISO, 2015.

[21] *Wind energy generation systems – Part 3-1: Design Requirements for fixed offshore wind turbines. Ed. 1.0*, IEC-61400-3-1, 2019.

[22] CEM, "Coastal Engineering Manual, Meteorology and Wave Climate," 2008. [Online]. Available: http://www1.frm.utn.edu.ar/laboratorio_hidraulica/Biblioteca_Virtual/Coastal%20Engineering%20Manual%20-%20Part%20II/Part_II-Chap_2.pdf

[23] *Guidelines for converting between various wind averaging periods in tropical cyclone conditions*, WMO/TD- No. 1555, W. M. O. (WMO), J. D. Kepert, J. David, and J. D. Ginger, Geneva, 2010.

[24] DHI, "DHI North Europe Hydrodynamic Model forced with ERA5 Validation Report," 2023.

[25] DHI, "MIKE 21 Flow Model FM, Hydrodynamic Module, User Guide," 2022.

[26] D. L. Codiga, "Unified Tidal Analysis and Prediction Using the UTide Matlab Functions. Technical Report 2011-01," Graduate School of Oceanography, University of Rhode Island, Narragansett, RI. 59pp, 2011.

[27] R. Pawlowicz, B. Beardsley, and S. Lentz, "Classical tidal harmonic analysis including error estimates in MATLAB using T-TIDE," *Computers & Geosciences 28,* pp. 929-937, 2002.

[28] K. E. Leffler and D. A. Jay, "Enhancing tidal harmonic analysis: Robust (hybrid L-1/L-2) solutions," *Cont. Shelf Res. 29,* pp. 78-88. DOI: 10.1016/j.csr.2008.1004.1011, 2009.

[29] M. G. G. Foreman, J. Y. Cherniawsky, and V. A. Ballantyne, "Versatile Harmonic Tidal Analysis: Improvements and Applications.," *J. Atmos. Oceanic Tech. 26,* pp. 806-817. DOI: 810.1175/2008JTECHO1615.1171, 2009.

[30] DHI, "MIKE 21 Spectral Waves FM: User Guide," 2022.

[31] DHI, "MIKE 21 Spectral Wave Module; Scientific Documentation," DHI, 2022.

[32] DHI, "EUDP. Global Atlas of Siting Parameters Offshore. D5.3 Automated modelling report/manual (part 1). M5.1 Global model data for automated modelling in portal. DHI Global Wave Model: Set-up, Calibration and Validation Report.," 2023. [Online]. Available: https://www.metocean-on-demand.com/metadata/waterdata-dataset-Global_SW_ERA5

[33] J. A. Battjes and a. J.P.F.M., "Energy loss and set-up due to breaking of random waves," in *16th Int. Conf. On Coastal Eng.*, NY, 1978: ASCE, pp. 569-587.

[34] J. H. G. d. M. Alves and E. Melo, "On the measurement of directional wave spectra at the southern Brazilian coast," *Applied Ocean Research,* vol. 21, no. 6, pp. 295-309, 1999.

[35] D. J. Cecil. *LIS/OTD Gridded Lightning Climatology Data Collection, Version 2.3.2015*, NASA EOSDIS Global Hydrology Resource Center Distributed Active Archive Center, Huntsville, Alabama, U.S.A., doi: http://dx.doi.org/10.5067/LIS/LIS-OTD/DATA311.

[36] D. J. B. Cecil, D. E.; Blackeslee, R. J., "Gridded lightning climatology from TRMM-LIS and OTD: Dataset description," *Atmospheric Research,* vol. 135-136, pp. 404-414, 2014.

[37] F. J. Millero and A. Poisson, "International one-atmosphere equation of state of seawater," *Deep Sea Research Part A. Oceanographic Research Papers,* vol. 28, no. 6, pp. 625-629, 1981/06/01/ 1981, doi: https://doi.org/10.1016/0198-0149(81)90122-9.

[38] *Bathymetry Consortium EMODnet. EMODnet Digital Bathymetry (DTM)*. 2016.

[39] *Loads and site conditions for wind turbines*, DNV-ST-0437, DNV, 2021.

[40] R. Ter Hofstede, F. Driessen, P. Elzinga, M. Van Koningsveld, and M. Schutter, "Offshore wind farms contribute to epibenthic biodiversity in the North Sea," *Journal of Sea Research,* vol. 185, p. 102229, 2022.

Appendix A Quality Indices

See next pages.

DHI Model Quality Indices (QI's)

Contents

Revisions

Date	Description	Initials
2021-08-13	Version 1.0.	PDG
2022-11-24	Version 1.1; table formatting updated.	SJA

Nomenclature

Abbreviation	Explanation
QI	Quality Index
POT	Peak-Over-Threshold

1 Model Quality Indices

To obtain an objective and quantitative measure of how well the model data compared to the observed data, several statistical parameters, so-called quality indices (QI's), are calculated.

Prior to the comparisons, the model data is synchronised to the time stamps of the observations so that both time series had equal length and overlapping time stamps. For each valid observation, measured at time t, the corresponding model value is found using linear interpolation between the model time steps before and after t. Only observed values that had model values within ± the representative sampling or averaging period of the observations are included (e.g., for 10-min observed wind speeds measured every 10 min compared to modelled values every hour, only the observed value every hour is included in the comparison).

The comparisons of the synchronised observed and modelled data are illustrated in (some of) the following figures:

- Time series plot including general statistics
- Scatter plot including quantiles, QQ-fit and QI's (density-coloured dots)
- Histogram of occurrence vs. magnitude or direction
- Histogram of bias vs. magnitude
- Histogram of bias vs. direction
- Dual rose plot (overlapping roses)
- Peak event plot including joint (coinciding) individual peaks

The quality indices are described below, and their definitions are listed in Table 1.1. Most of the quality indices are based on the entire dataset, and hence the quality indices should be considered averaged measures and may not be representative of the accuracy during rare conditions.

The MEAN represents the mean of modelled data, while the bias is the mean difference between the modelled and observed data. AME is the mean of the absolute difference, and RMSE is the root-mean-square of the difference. The MEAN, BIAS, AME and RMSE are given as absolute values and relative to the average of the observed data in percent in the scatter plot.

The scatter index (SI) is a non-dimensional measure of the difference calculated as the unbiased root-mean-square difference relative to the mean absolute value of the observations. In open water, an SI below 0.2 is usually considered a small difference (excellent agreement) for significant wave heights. In confined areas or during calm conditions, where mean significant wave heights are generally lower, a slightly higher SI may be acceptable (the definition of SI implies that it is negatively biased (lower) for time series with high mean values compared to time series with lower mean values (and same scatter/spreading), although it is normalised).

EV is the explained variation and measures the proportion [0 - 1] to which the model accounts for the variation (dispersion) of the observations.

The correlation coefficient (CC) is a non-dimensional measure reflecting the degree to which the variation of the first variable is reflected linearly in the variation of the second variable. A value close to 0 indicates very limited or no (linear) correlation between the two data sets, while a value close to 1 indicates a very high or perfect correlation. Typically, a CC above 0.9 is considered a high correlation (good agreement) for wave heights. It is noted that CC is 1 (or -1) for any two fully linearly correlated variables, even if they are not 1:1. However, the slope and intercept of the linear relation may be different from 1 and 0, respectively, despite CC of 1 (or -1).

The QQ line slope and intercept are found from a linear fit to the data quantiles in a least-square sense. The lower and uppermost quantiles are not included on the fit. A regression line slope different from 1 may indicate a trend in the difference.

The peak ratio (PR) is the average of the Npeak highest model values divided by the average of the Npeak highest observations. The peaks are found individually for each dataset through the Peak-Over-Threshold (POT) method applying an average annual number of exceedances of 4 and an inter-event time of 36 hours. A general underestimation of the modelled peak events results in a PR below 1, while an overestimation results in a PR above 1.

An example of a peak plot is shown in Figure 1.1. 'X' represents the observed peaks (x-axis), while 'Y' represents the modelled peaks (y-axis), based on the POT methodology, both represented by circles ('o') in the plot. The joint (coinciding) peaks, defined as any X and Y peaks within ±36 hours[1] of each other (i.e., less than or equal to the number of individual peaks), are represented by crosses ('x'). Hence, the joint peaks ('x') overlap with the individual peaks ('o') only if they occur at the same time exactly. Otherwise, the joint peaks ('x') represent an additional point in the plot, which may be associated with the observed and modelled individual peaks ('o') by searching in the respective X and Y-axis directions, see example with red lines in Figure 1.1. It is seen that the 'X' peaks are often underneath the 1:1 line, while the 'Y' peaks are often above the 1:1 line.

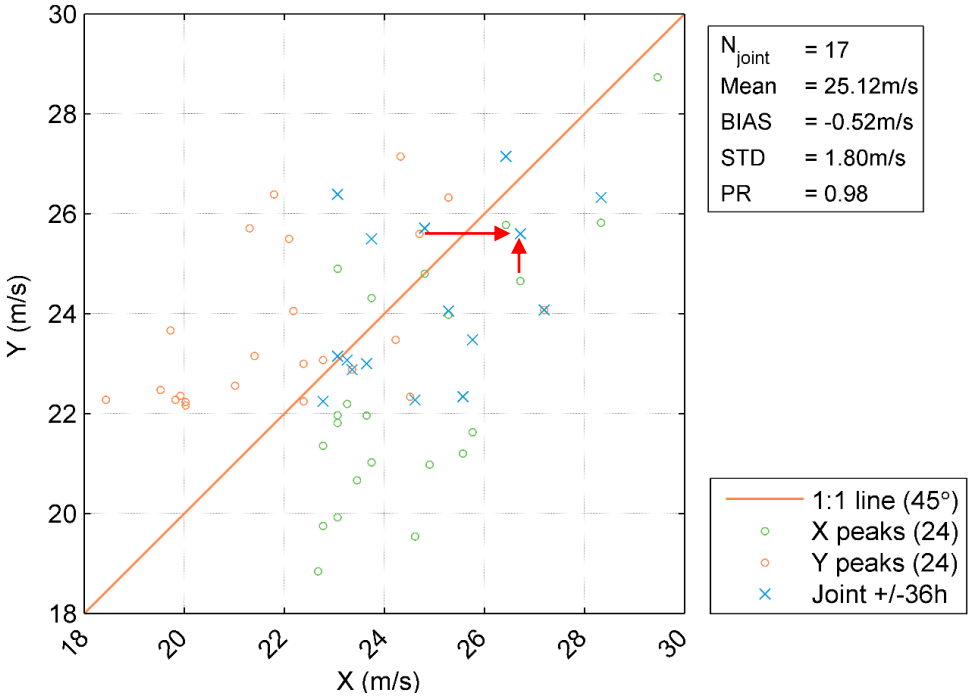

Figure 1.1 Example of peak event plot (wind speed)

[1] 36 hours is chosen arbitrarily as representative of an average storm duration. Often the measured and modelled peaks are within 1-2 hours of each other.

Table 1.1 Definitions of model quality indices (X = Observation, Y = Model)

Abbreviation	Description	Definition
N	Number of data (synchronised)	–
MEAN	Mean of Y data Mean of X data	$\frac{1}{N}\sum_{i=1}^{N} Y_i \equiv \overline{Y}$, $\frac{1}{N}\sum_{i=1}^{N} X_i \equiv \overline{X}$
STD	Standard deviation of Y data Standard deviation of X data	$\sqrt{\frac{1}{N-1}\sum_{i=1}^{N}(Y-\overline{Y})^2}$, $\sqrt{\frac{1}{N-1}\sum_{i=1}^{N}(X-\overline{X})^2}$
BIAS	Mean difference	$\frac{1}{N}\sum_{i=1}^{N}(Y-X)_i = \overline{Y}-\overline{X}$
AME	Absolute mean difference	$\frac{1}{N}\sum_{i=1}^{N}(\lvert Y-X\rvert)_i$
RMSE	Root-mean-square difference	$\sqrt{\frac{1}{N}\sum_{i=1}^{N}(Y-X)_i^{\,2}}$
SI	Scatter index (unbiased)	$\frac{\sqrt{\frac{1}{N}\sum_{i=1}^{N}(Y-X-\mathrm{BIAS})_i^{\,2}}}{\frac{1}{N}\sum_{i=1}^{N}\lvert X_i\rvert}$
EV	Explained variance	$\frac{\sum_{i=1}^{N}(X_i-\overline{X})^2-\sum_{i=1}^{N}[(X_i-\overline{X})-(Y_i-\overline{Y})]^2}{\sum_{i=1}^{N}(X_i-\overline{X})^2}$
CC	Correlation coefficient	$\frac{\sum_{i=1}^{N}(X_i-\overline{X})(Y_i-\overline{Y})}{\sqrt{\sum_{i=1}^{N}(X_i-\overline{X})^2\sum_{i=1}^{N}(Y_i-\overline{Y})^2}}$
QQ	Quantile-Quantile (line slope and intercept)	Linear least square fit to quantiles
PR	Peak ratio (of N_{peak} highest events)	$PR=\frac{\sum_{i=1}^{N_{peak}}Y_i}{\sum_{i=1}^{N_{peak}}X_i}$

Appendix B Current speed vertical profiles at measurement stations

See next pages.

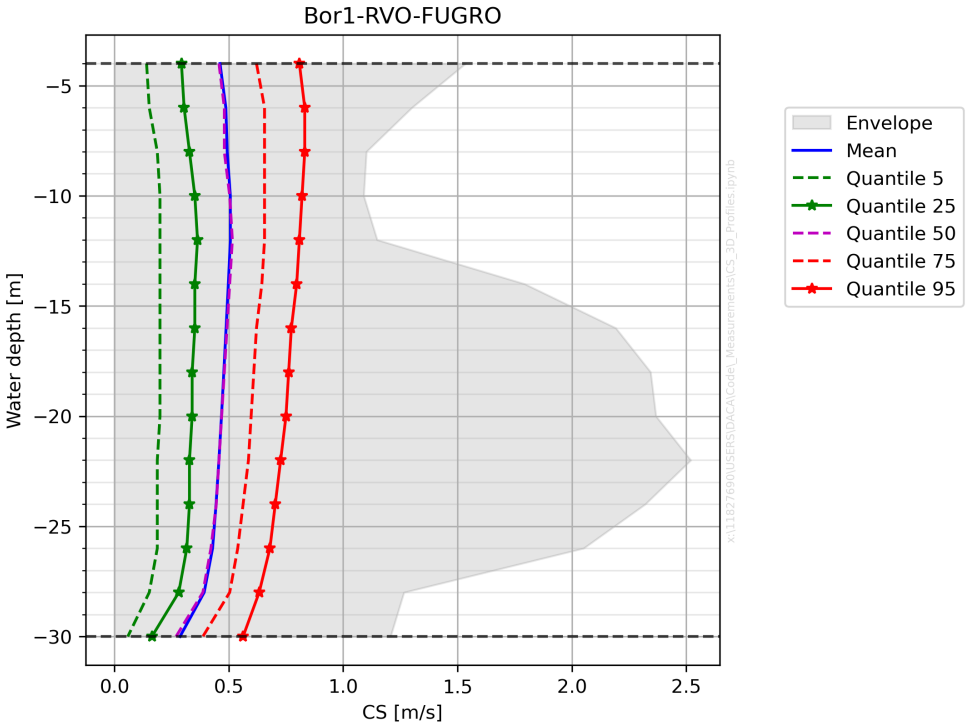

Figure B-1: Measured current speed profiles at Bor1

Horizontal lines represent the minimum and maximum water depth that were considered to derive the depth-averaged currents.

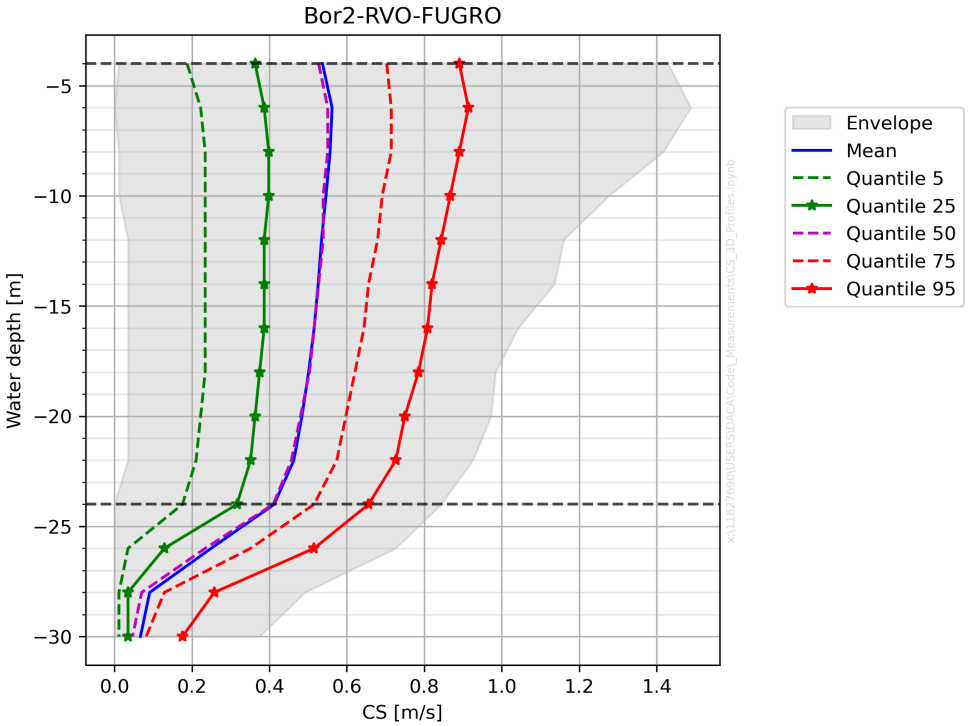

Figure B-2: Measured current speed profiles at Bor2.

Horizontal lines represent the minimum and maximum water depth that were considered to derive the depth-averaged currents.

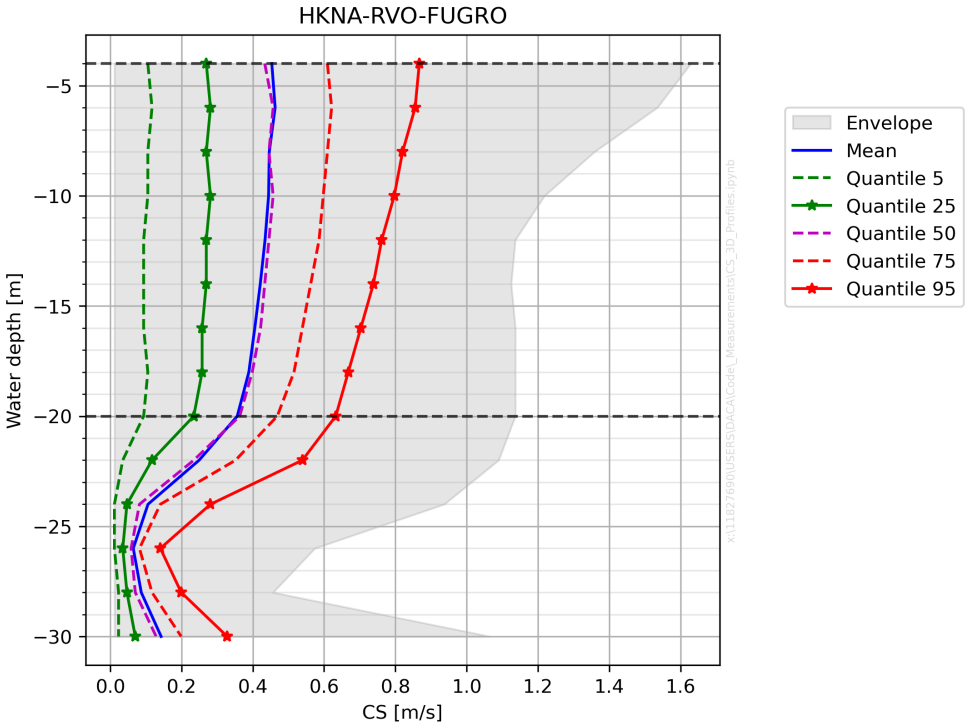

Figure B-3: Measured current speed profiles at HKNA.

Horizontal lines represent the minimum and maximum water depth that were considered to derive the depth-averaged currents.

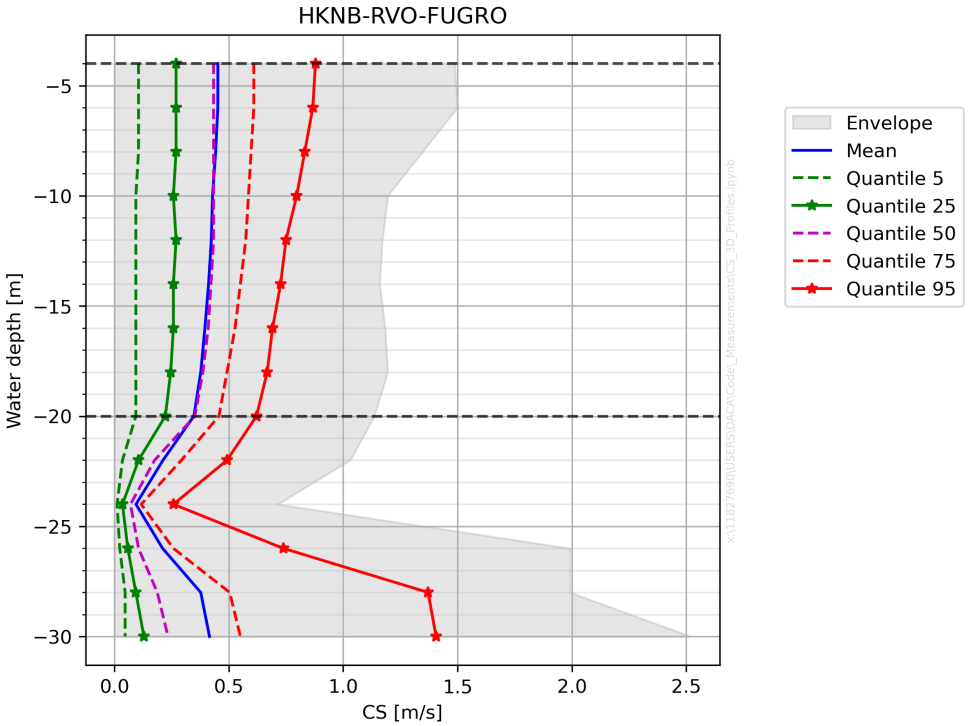

Figure B-4: Measured current speed profiles at HKNB.

Horizontal lines represent the minimum and maximum water depth that were considered to derive the depth-averaged currents.

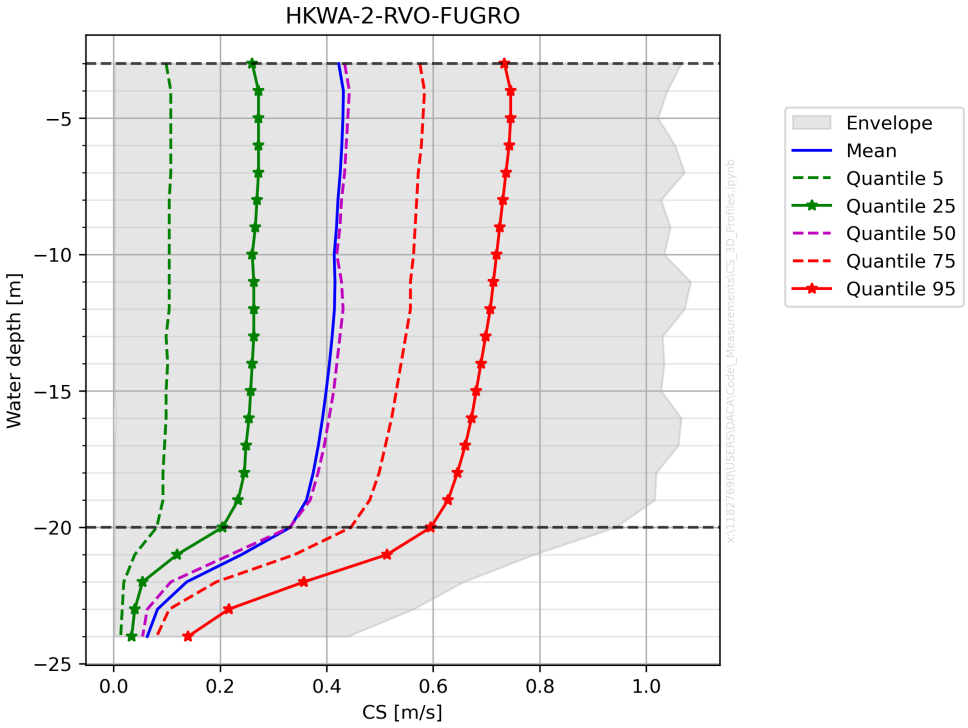

Figure B-5: Measured current speed profiles at HKWA-2.

Horizontal lines represent the minimum and maximum water depth that were considered to derive the depth-averaged currents.

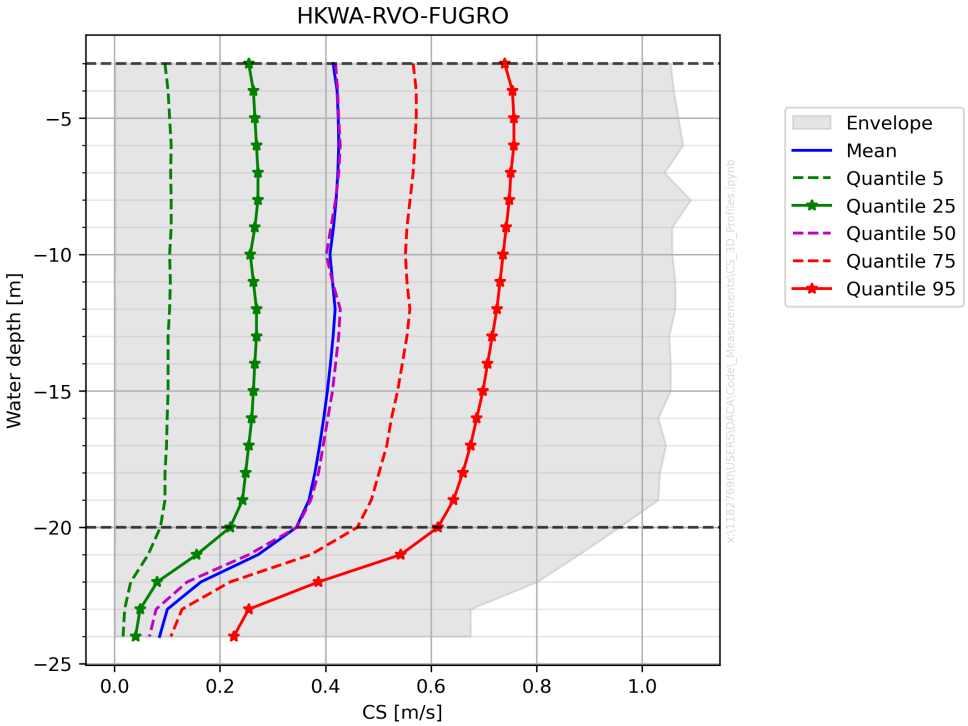

Figure B-6: Measured current speed profiles at HKWA.

Horizontal lines represent the minimum and maximum water depth that were considered to derive the depth-averaged currents.

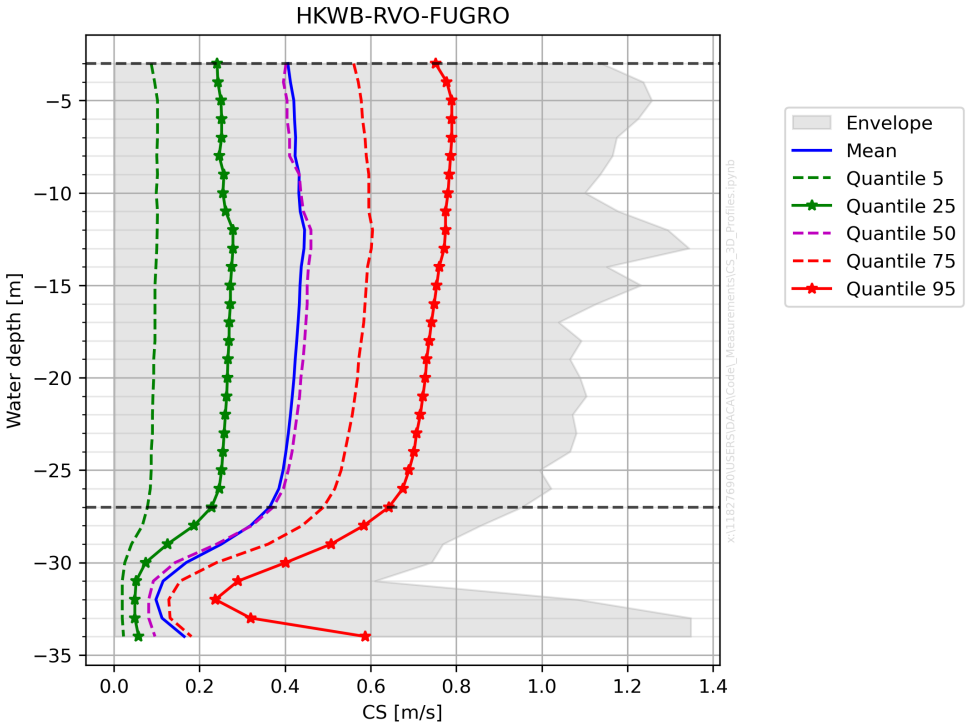

Figure B-7: Measured current speed profiles at HKWB.

Horizontal lines represent the minimum and maximum water depth that were considered to derive the depth-averaged currents.

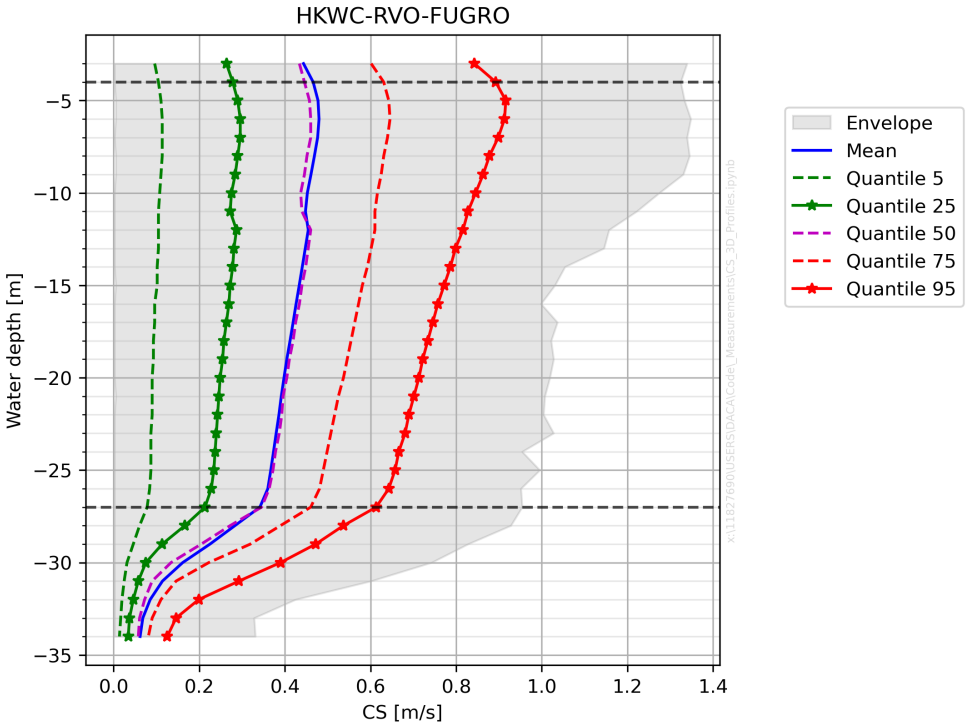

Figure B-8: Measured current speed profiles at HKWC.

Horizontal lines represent the minimum and maximum water depth that were considered to derive the depth-averaged currents.

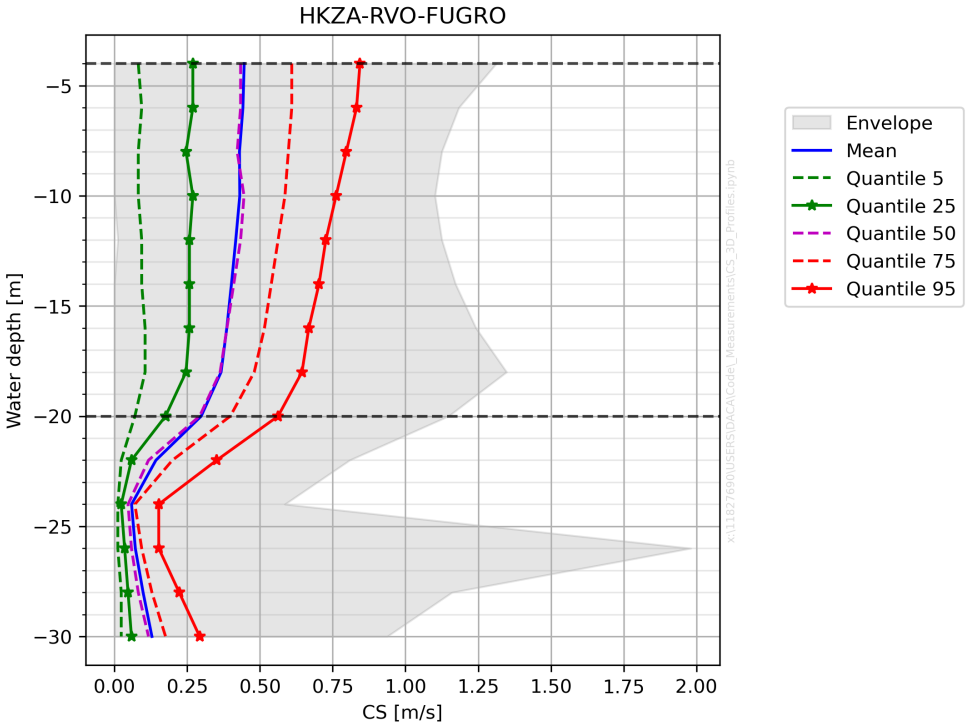

Figure B-9: Measured current speed profiles at HKZA.

Horizontal lines represent the minimum and maximum water depth that were considered to derive the depth-averaged currents.

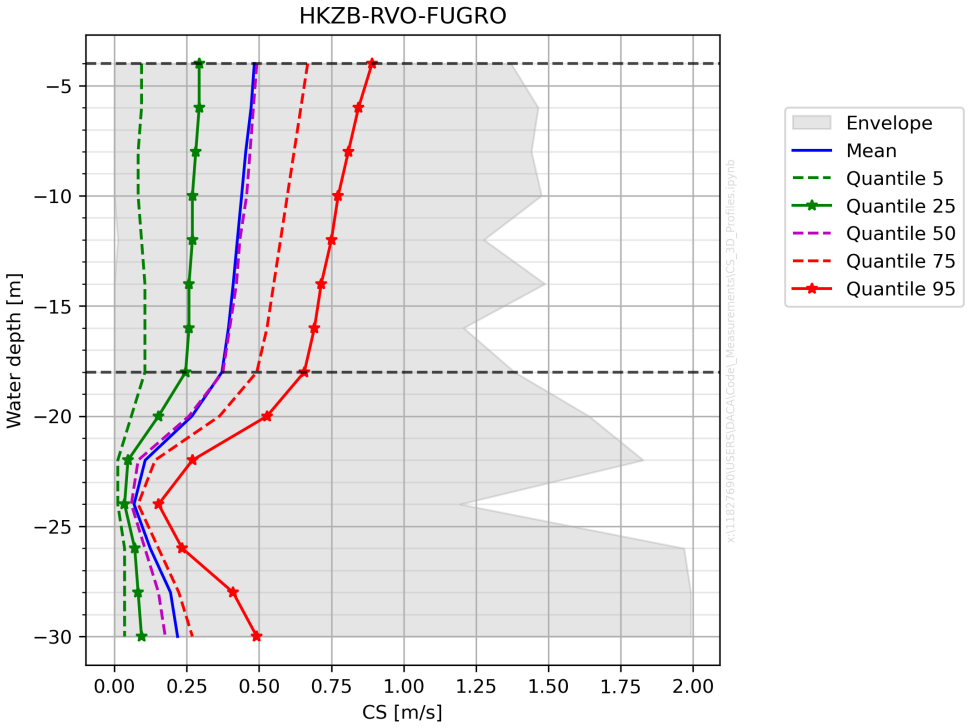

Figure B-10: Measured current speed profiles at HKZB.

Horizontal lines represent the minimum and maximum water depth that were considered to derive the depth-averaged currents.

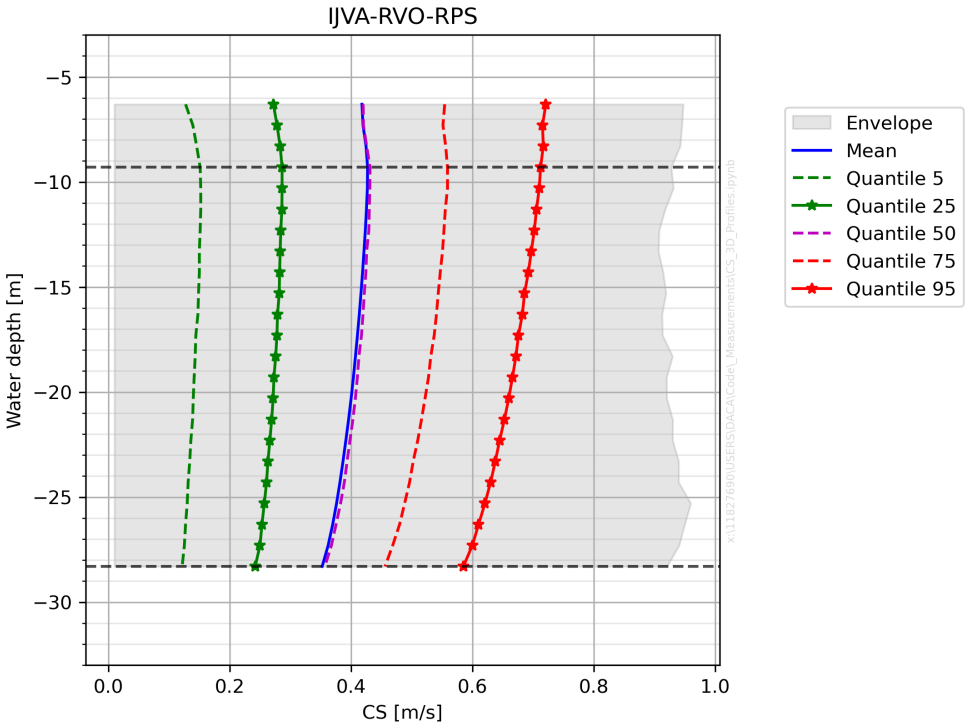

Figure B-11: Measured current speed profiles at IJVA.
Horizontal lines represent the minimum and maximum water depth that were considered to derive the depth-averaged currents.

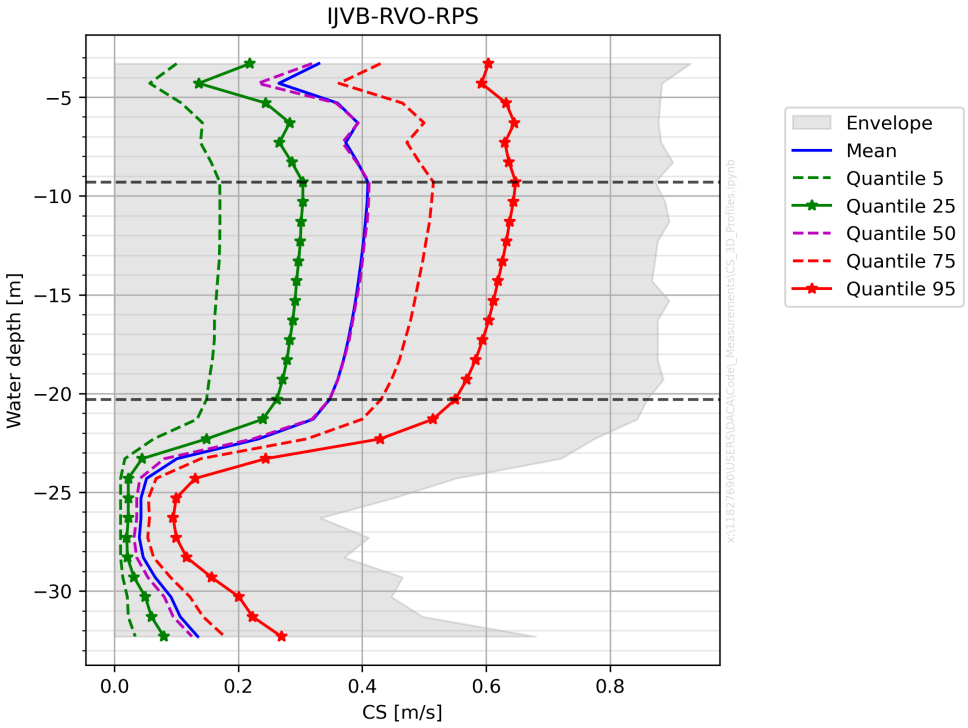

Figure B-12: Measured current speed profiles at IJVB.
Horizontal lines represent the minimum and maximum water depth that were considered to derive the depth-averaged currents.

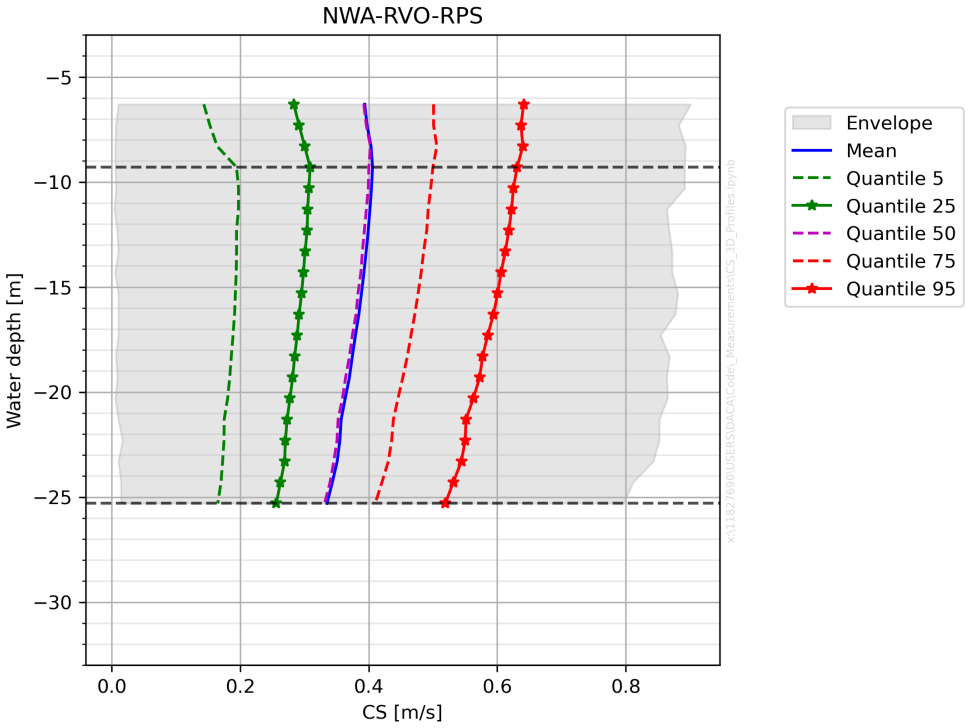

Figure B-13: Measured current speed profiles at NWA.

Horizontal lines represent the minimum and maximum water depth that were considered to derive the depth-averaged currents.

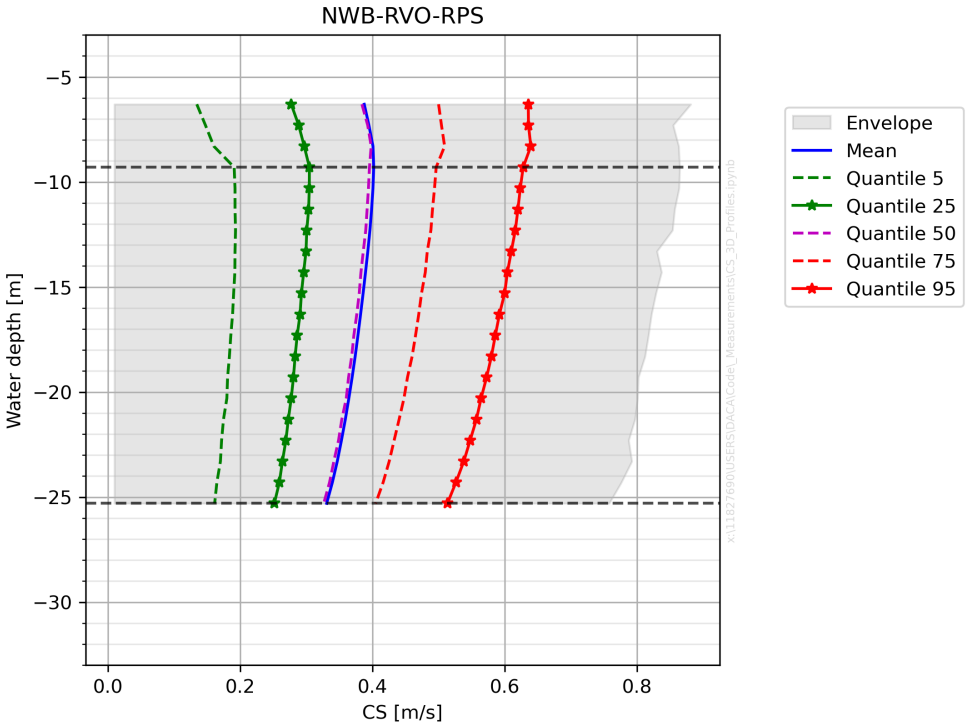

Figure B-14: Measured current speed profiles at NWB.

Horizontal lines represent the minimum and maximum water depth that were considered to derive the depth-averaged currents.

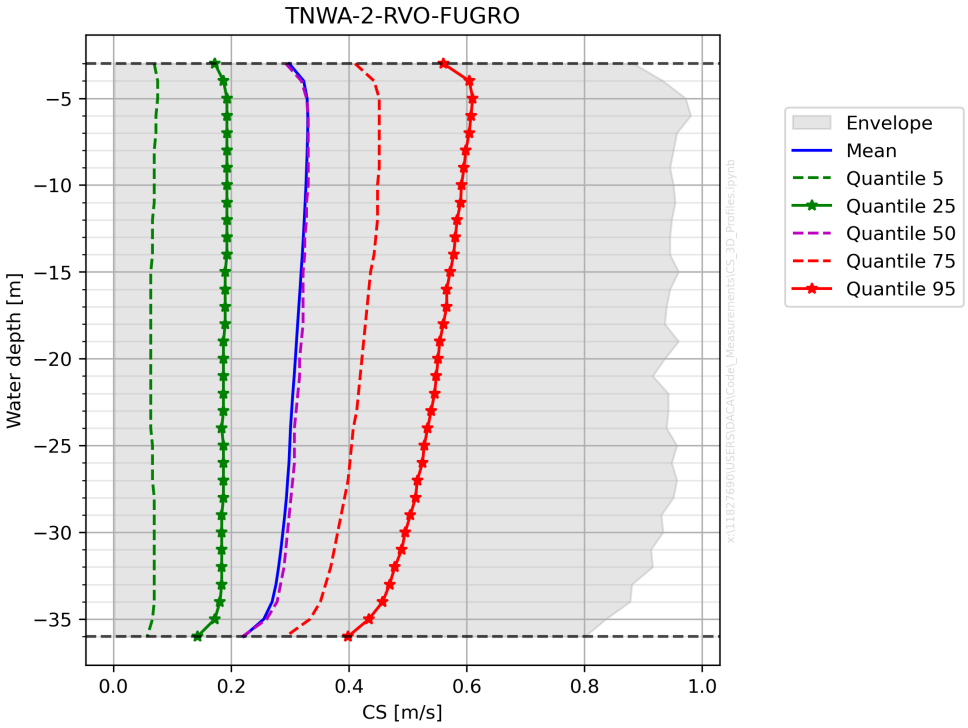

Figure B-15: Measured current speed profiles at TNWA-2.

Horizontal lines represent the minimum and maximum water depth that were considered to derive the depth-averaged currents.

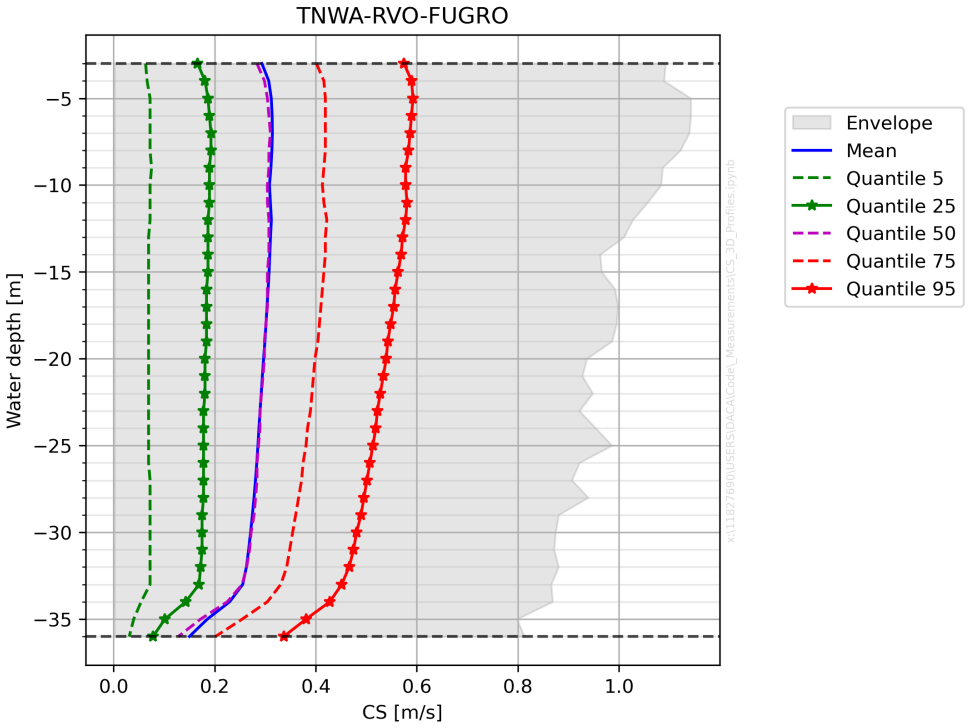

Figure B-16: Measured current speed profiles at TNWA.

Horizontal lines represent the minimum and maximum water depth that were considered to derive the depth-averaged currents.

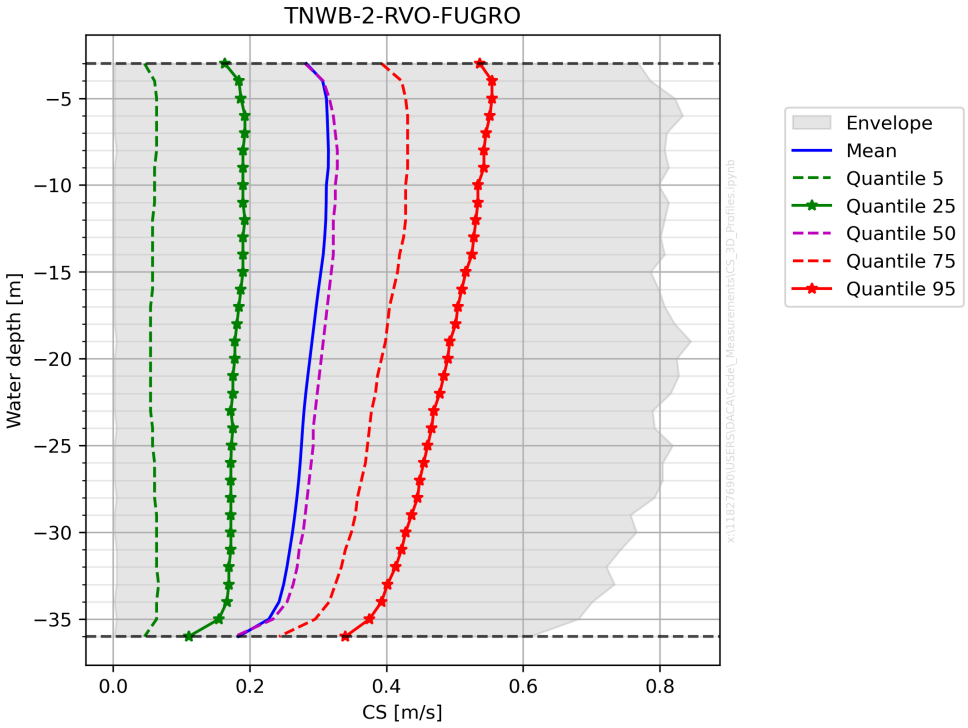

Figure B-17: Measured current speed profiles at TNWB-2.

Horizontal lines represent the minimum and maximum water depth that were considered to derive the depth-averaged currents.

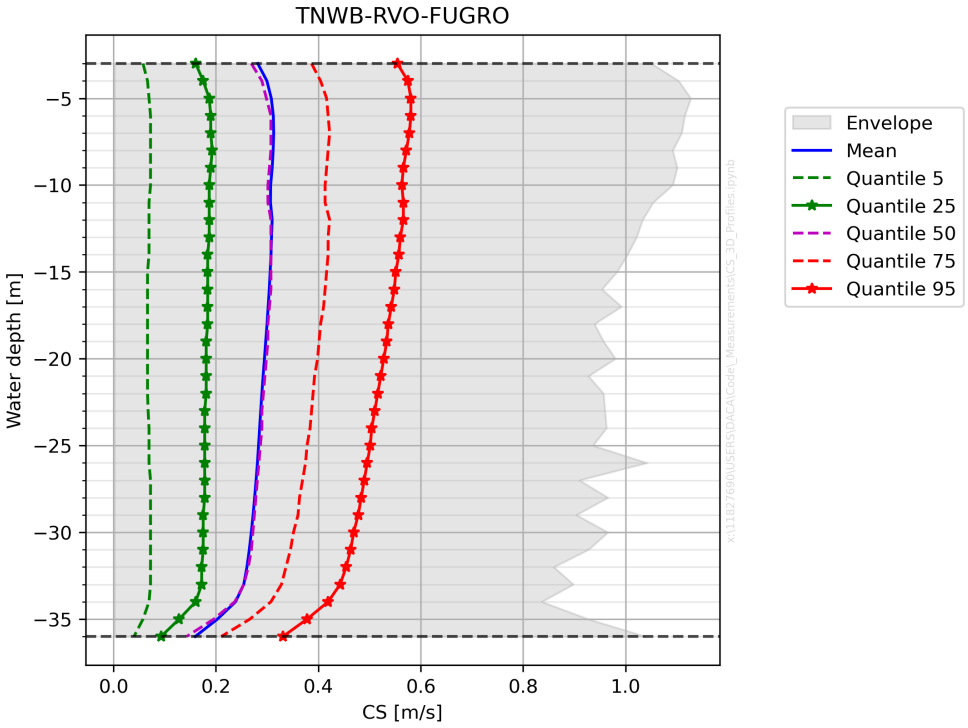

Figure B-18: Measured current speed profiles at TNWB.

Horizontal lines represent the minimum and maximum water depth that were considered to derive the depth-averaged currents.

Appendix C WRF model validation at near surface heights

See next pages.

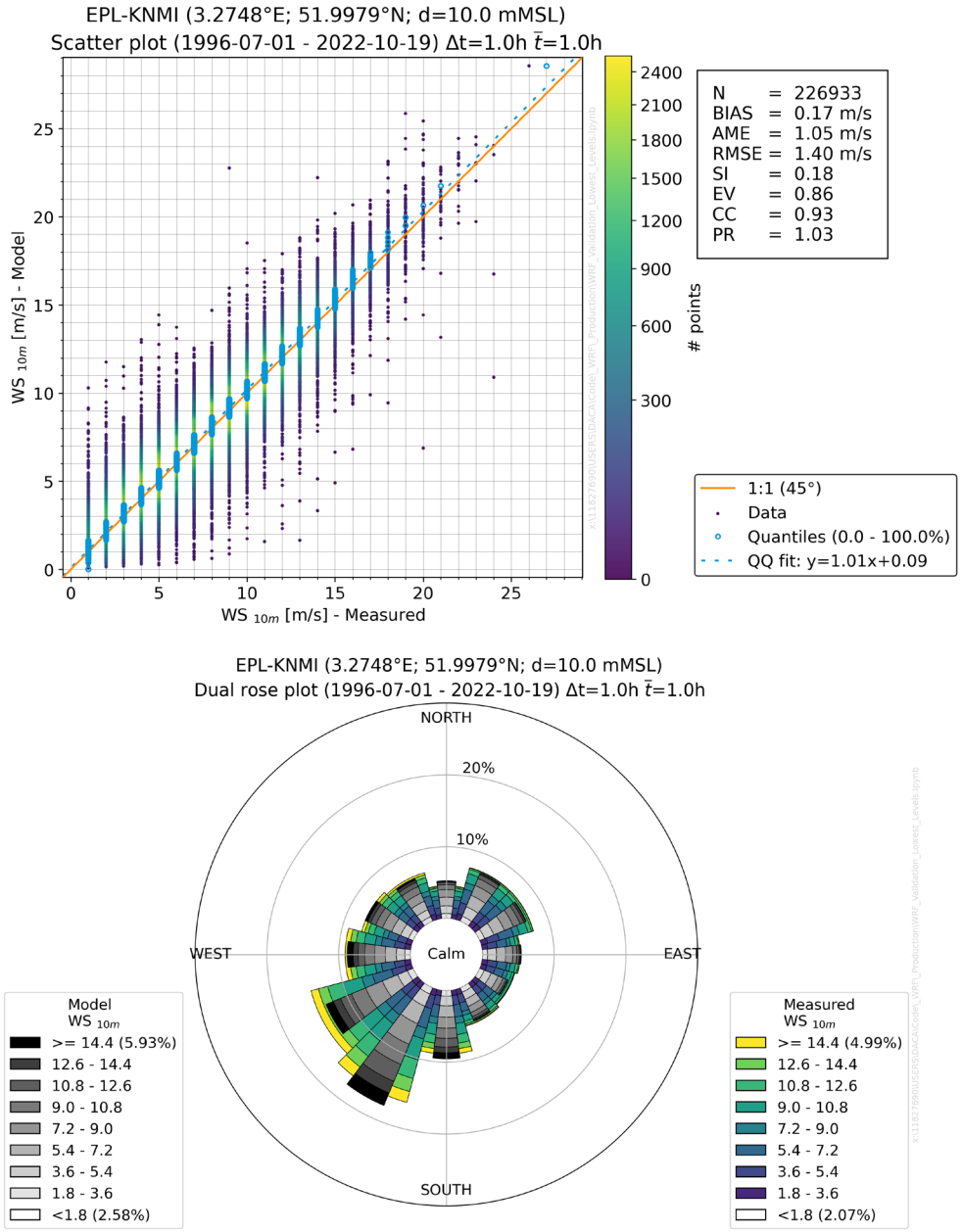

Figure C-1: Comparison of measured and modelled (WRF) winds at EPL station.
Top: Scatter plot comparison. Bottom: Dual wind rose comparison.

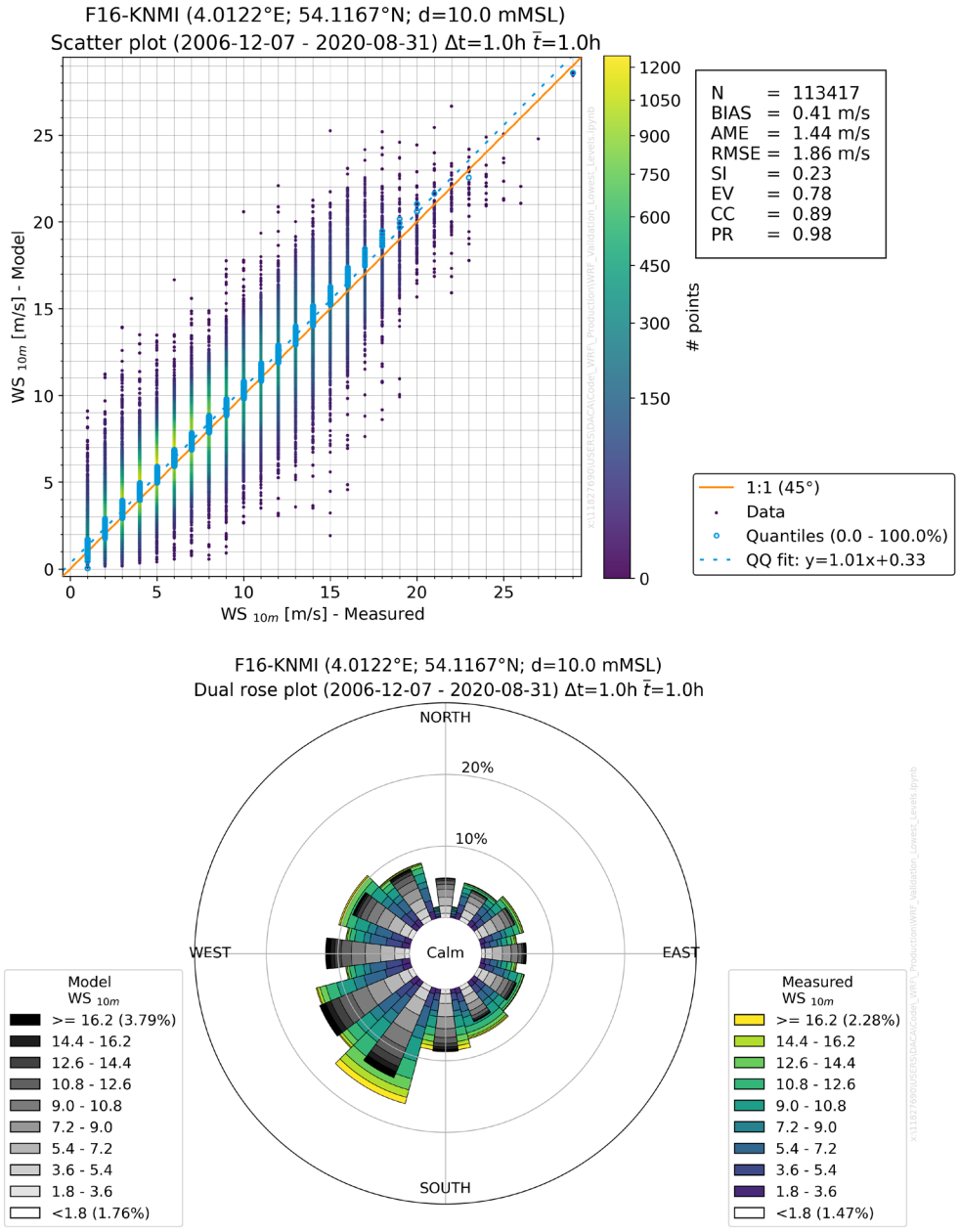

Figure C-2: Comparison of measured and modelled (WRF) winds at F16 station.
Top: Scatter plot comparison. Bottom: Dual wind rose comparison.

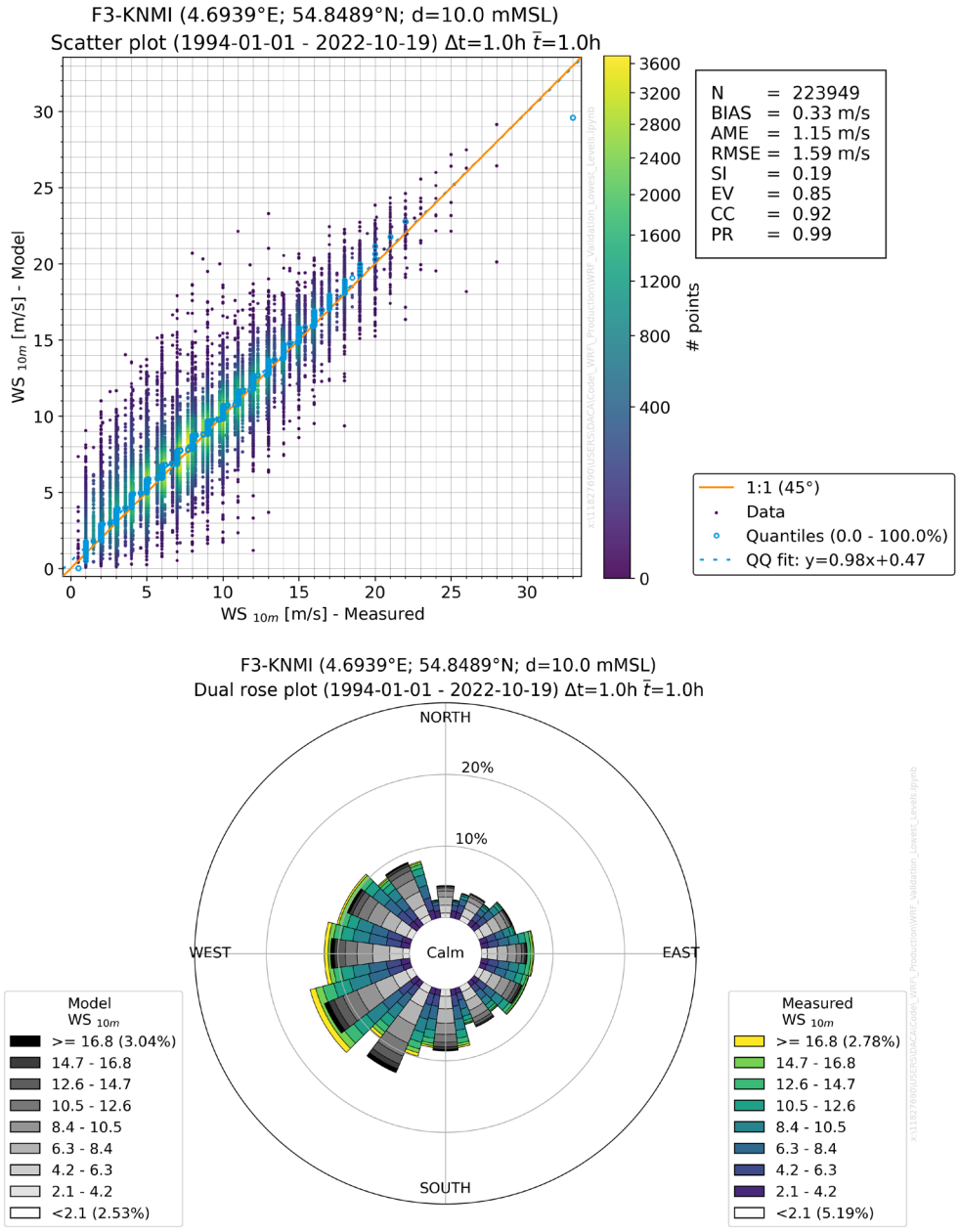

Figure C-3: Comparison of measured and modelled (WRF) winds at F3 station.
Top: Scatter plot comparison. Bottom: Dual wind rose comparison.

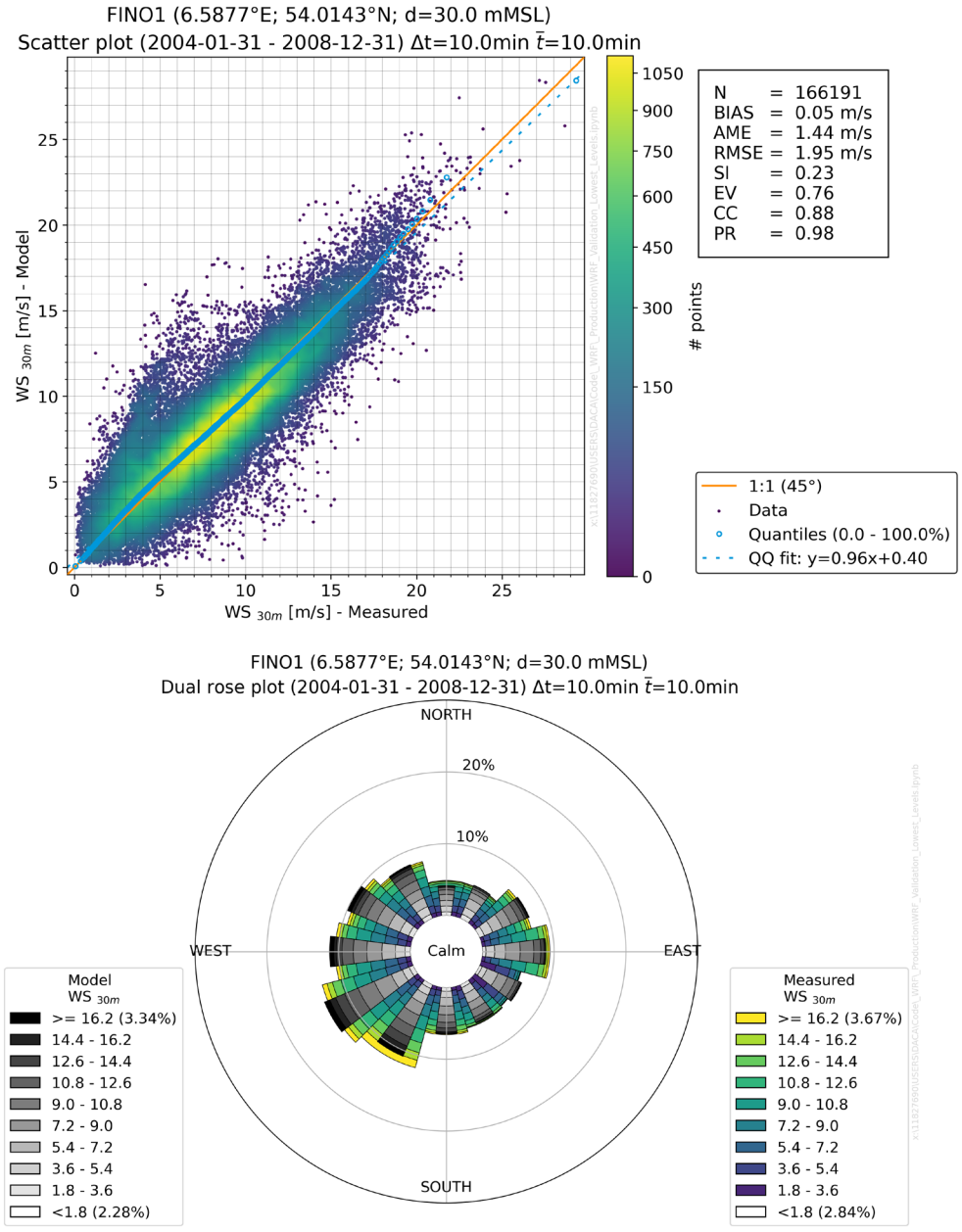

Figure C-4: Comparison of measured and modelled (WRF) winds at FINO1 station.
Top: Scatter plot comparison. Bottom: Dual wind rose comparison.

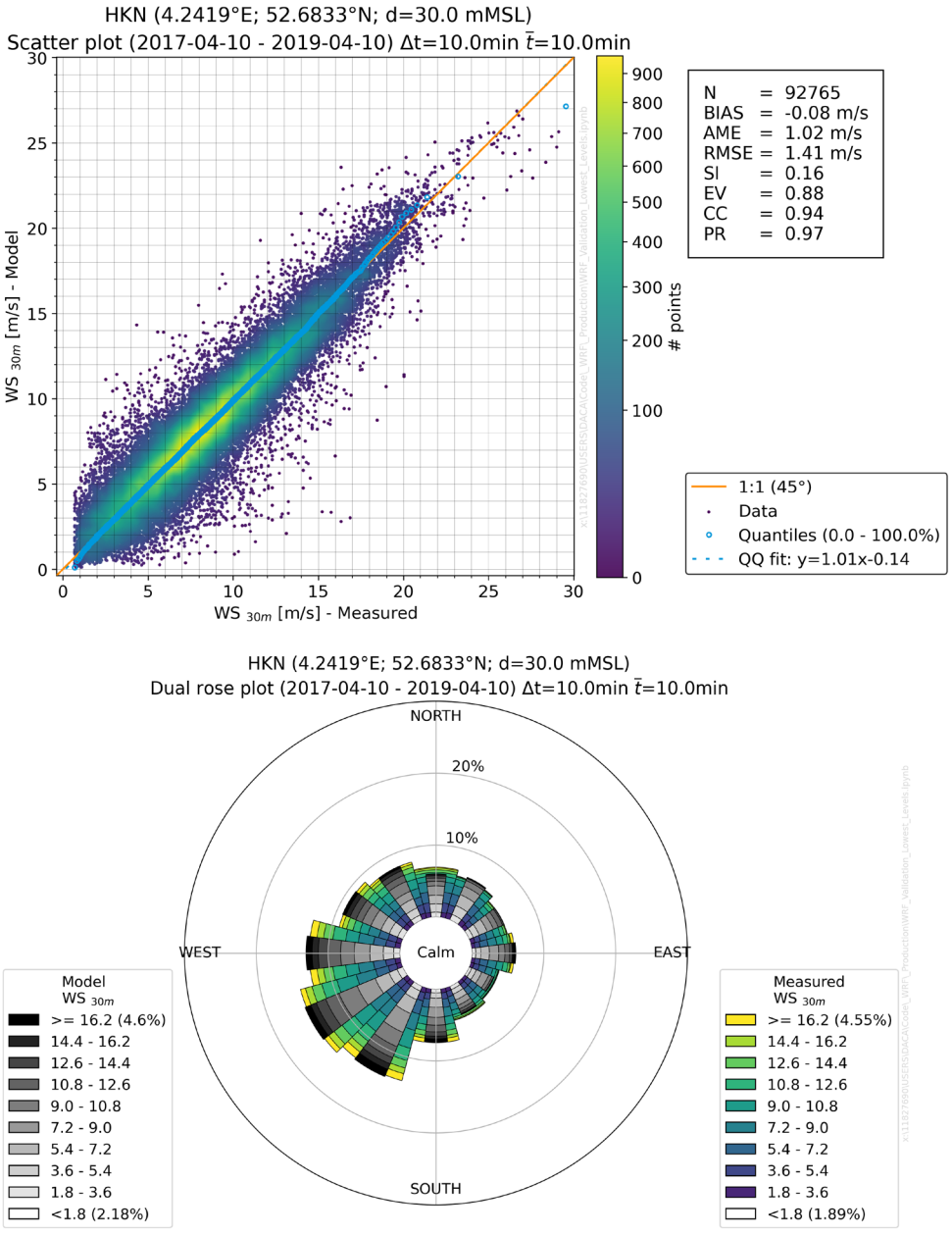

Figure C-5: Comparison of measured and modelled (WRF) winds at HKNB station.
Top: Scatter plot comparison. Bottom: Dual wind rose comparison.

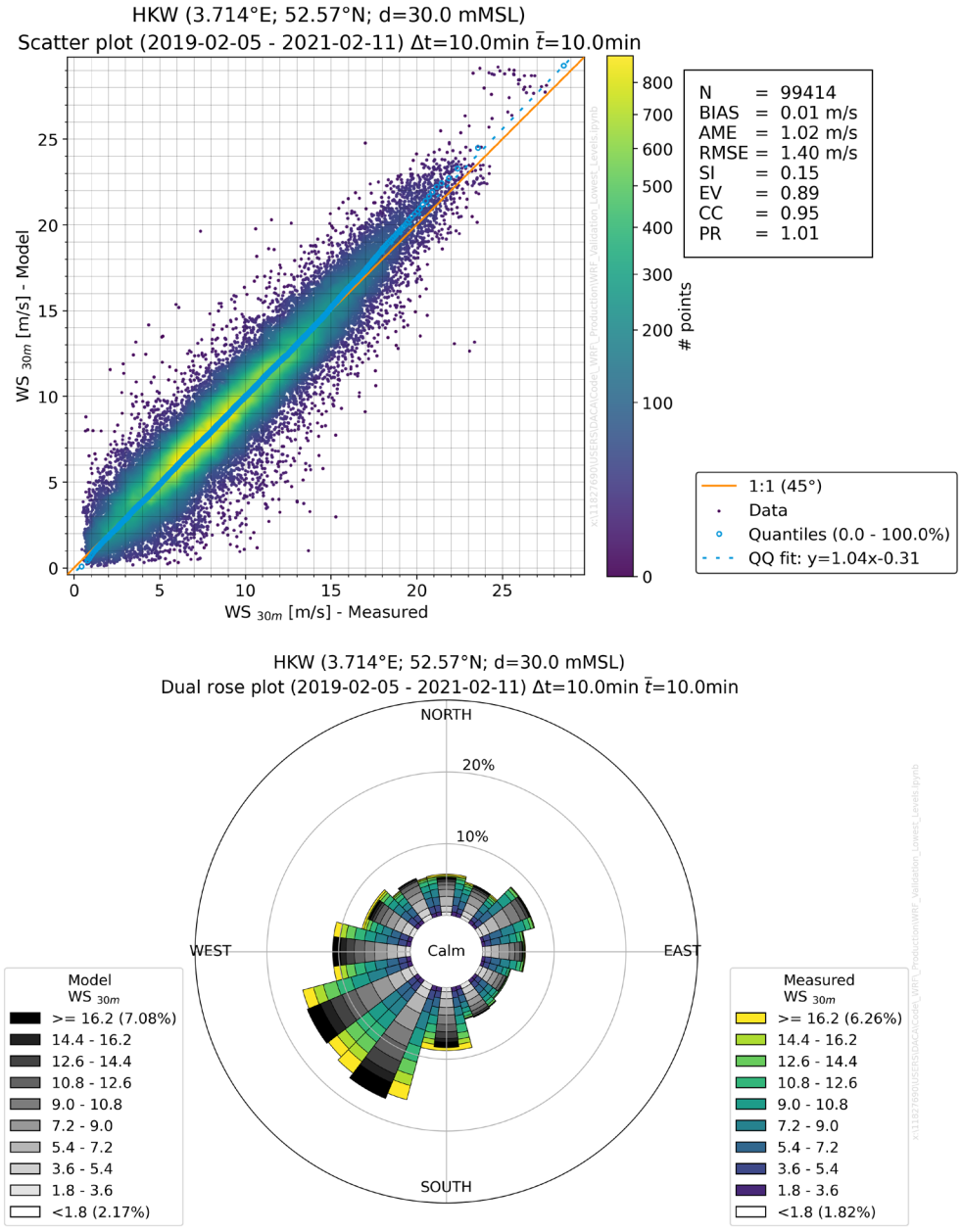

Figure C-6: Comparison of measured and modelled (WRF) winds at HKWA station.
Top: Scatter plot comparison. Bottom: Dual wind rose comparison.

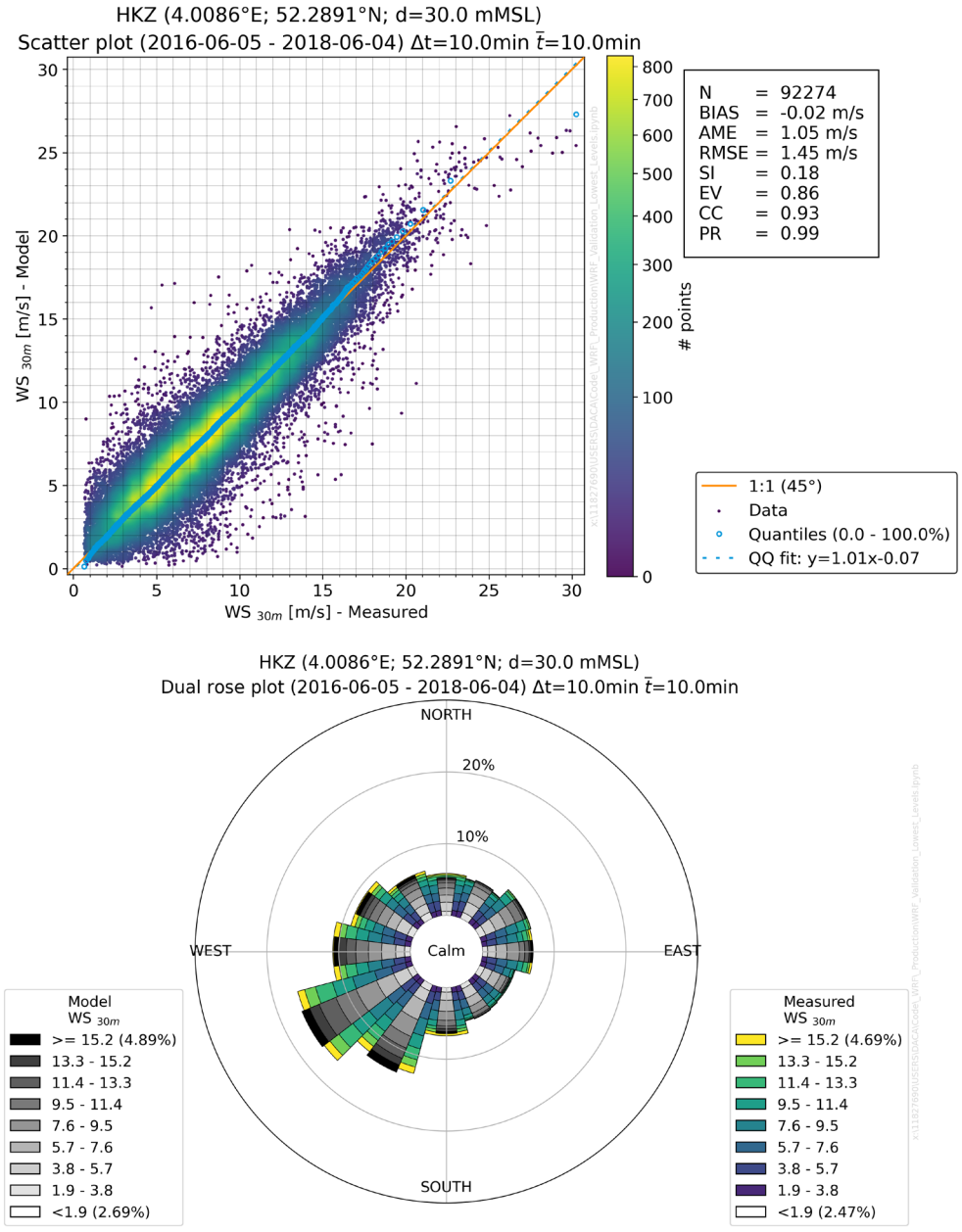

Figure C-7: Comparison of measured and modelled (WRF) winds at HKZB station.
Top: Scatter plot comparison. Bottom: Dual wind rose comparison.

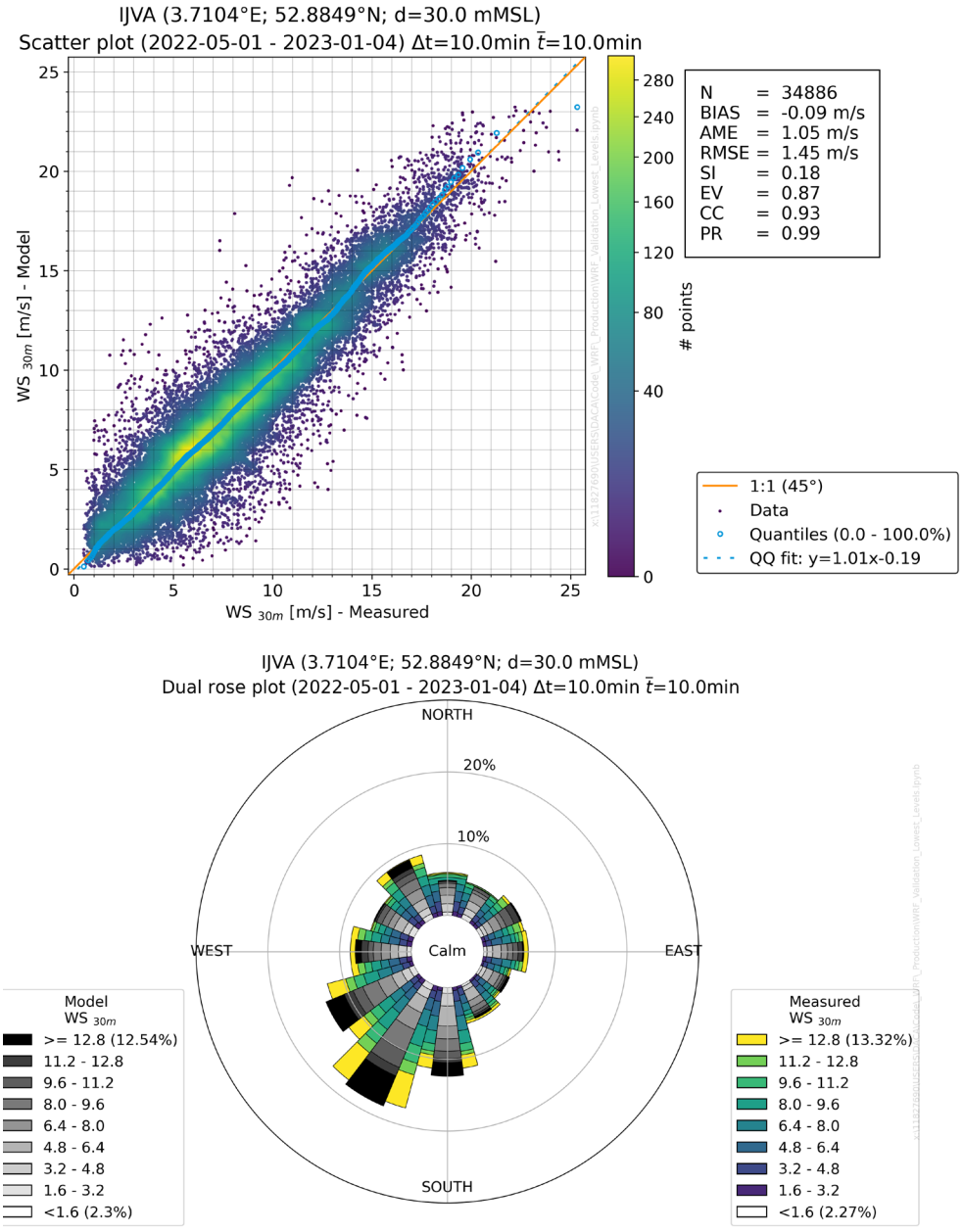

Figure C-8: Comparison of measured and modelled (WRF) winds at IJVA station.
Top: Scatter plot comparison. Bottom: Dual wind rose comparison.

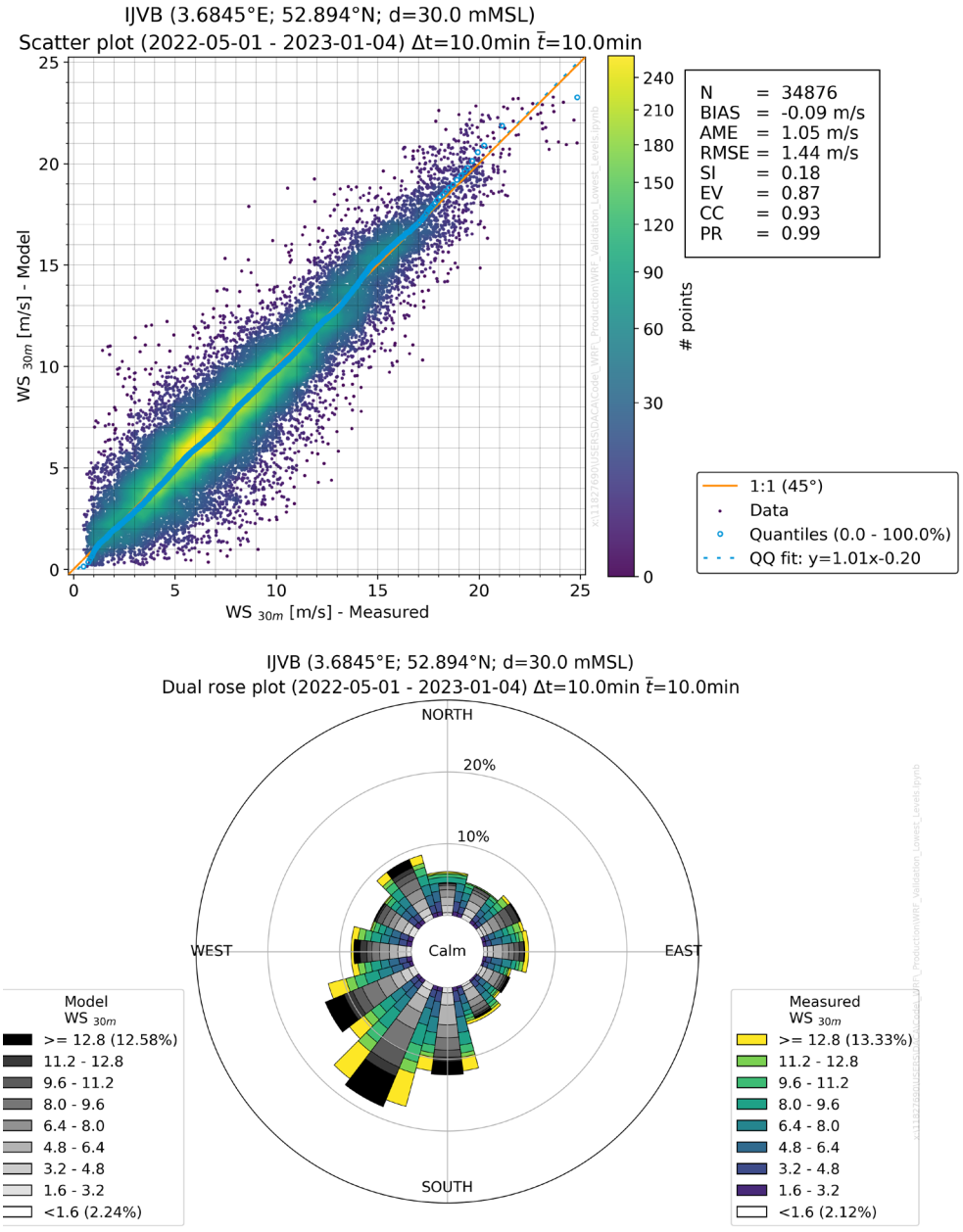

Figure C-9: Comparison of measured and modelled (WRF) winds at IJVB station.
Top: Scatter plot comparison. Bottom: Dual wind rose comparison.

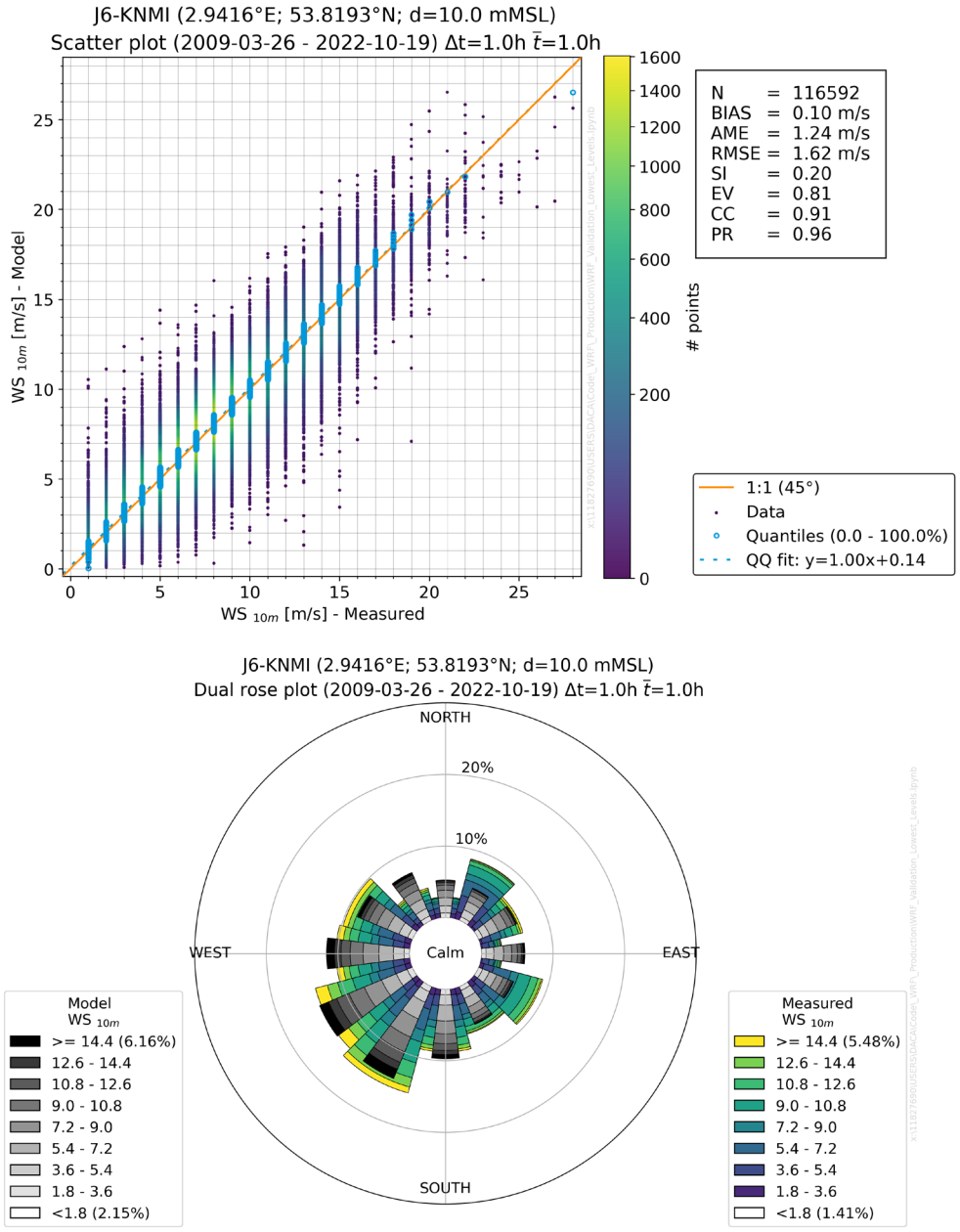

Figure C-10: Comparison of measured and modelled (WRF) winds at J6 station.
Top: Scatter plot comparison. Bottom: Dual wind rose comparison.

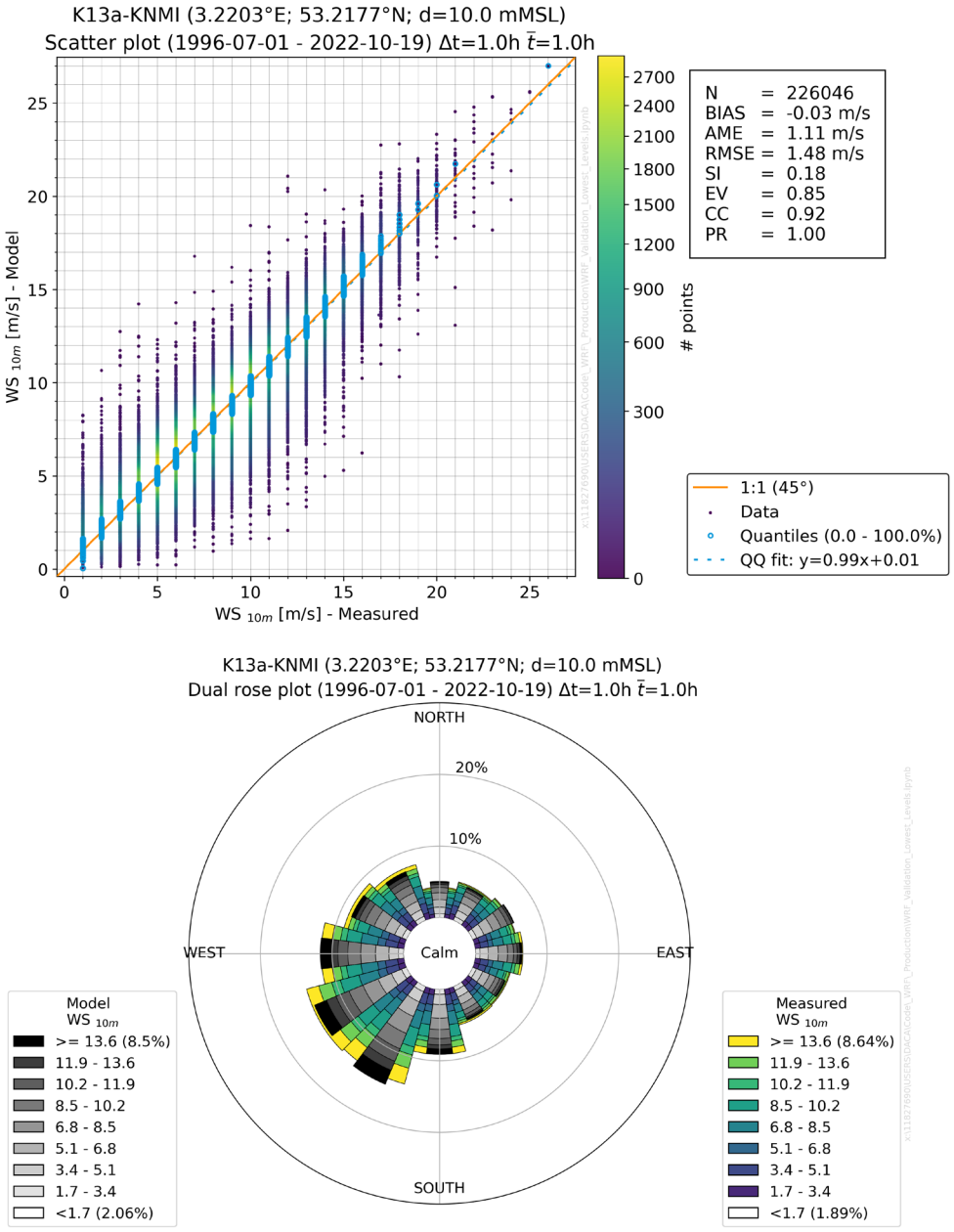

Figure C-11: Comparison of measured and modelled (WRF) winds at K13a station.
Top: Scatter plot comparison. Bottom: Dual wind rose comparison.

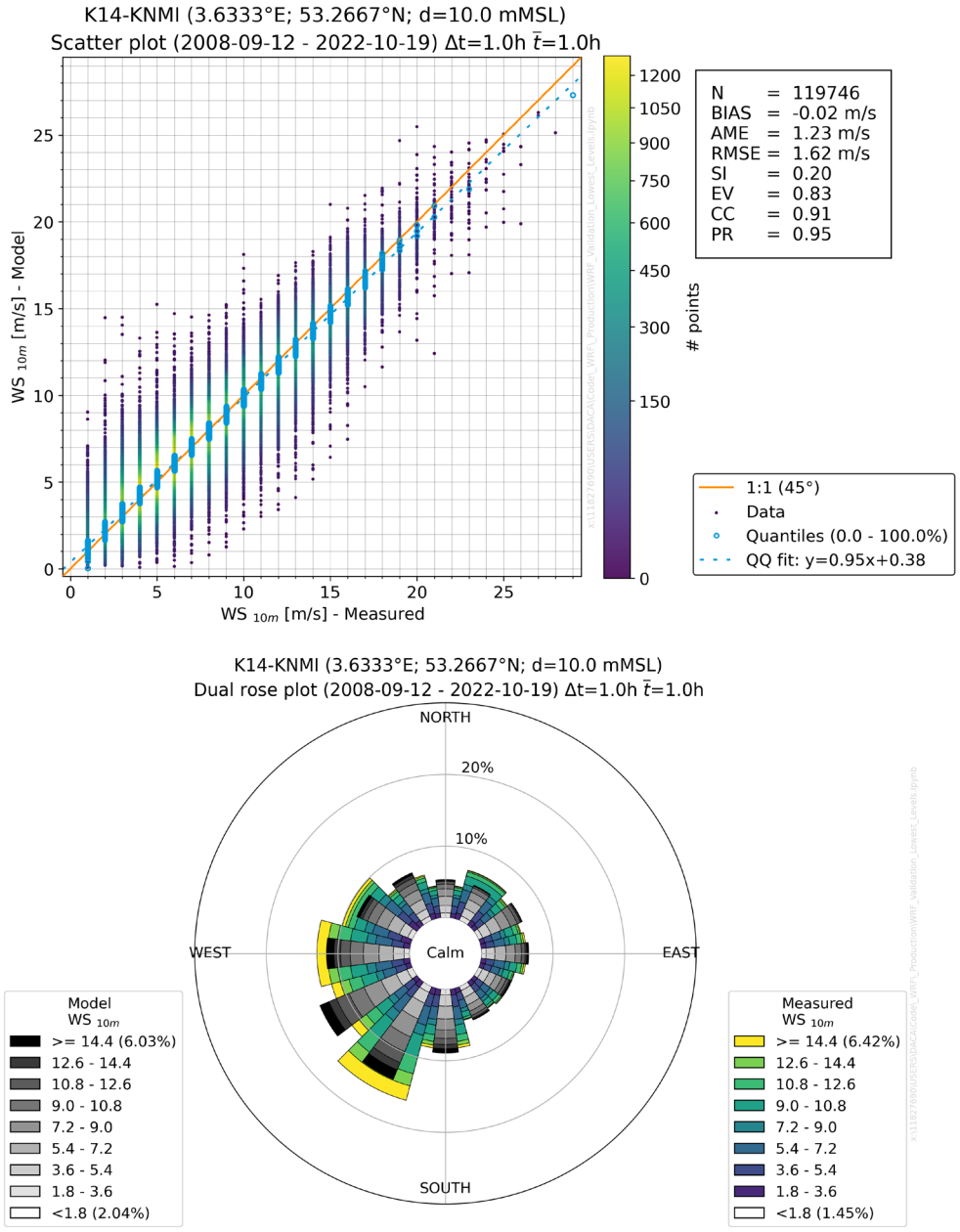

Figure C-12: Comparison of measured and modelled (WRF) winds at K14 station.
Top: Scatter plot comparison. Bottom: Dual wind rose comparison.

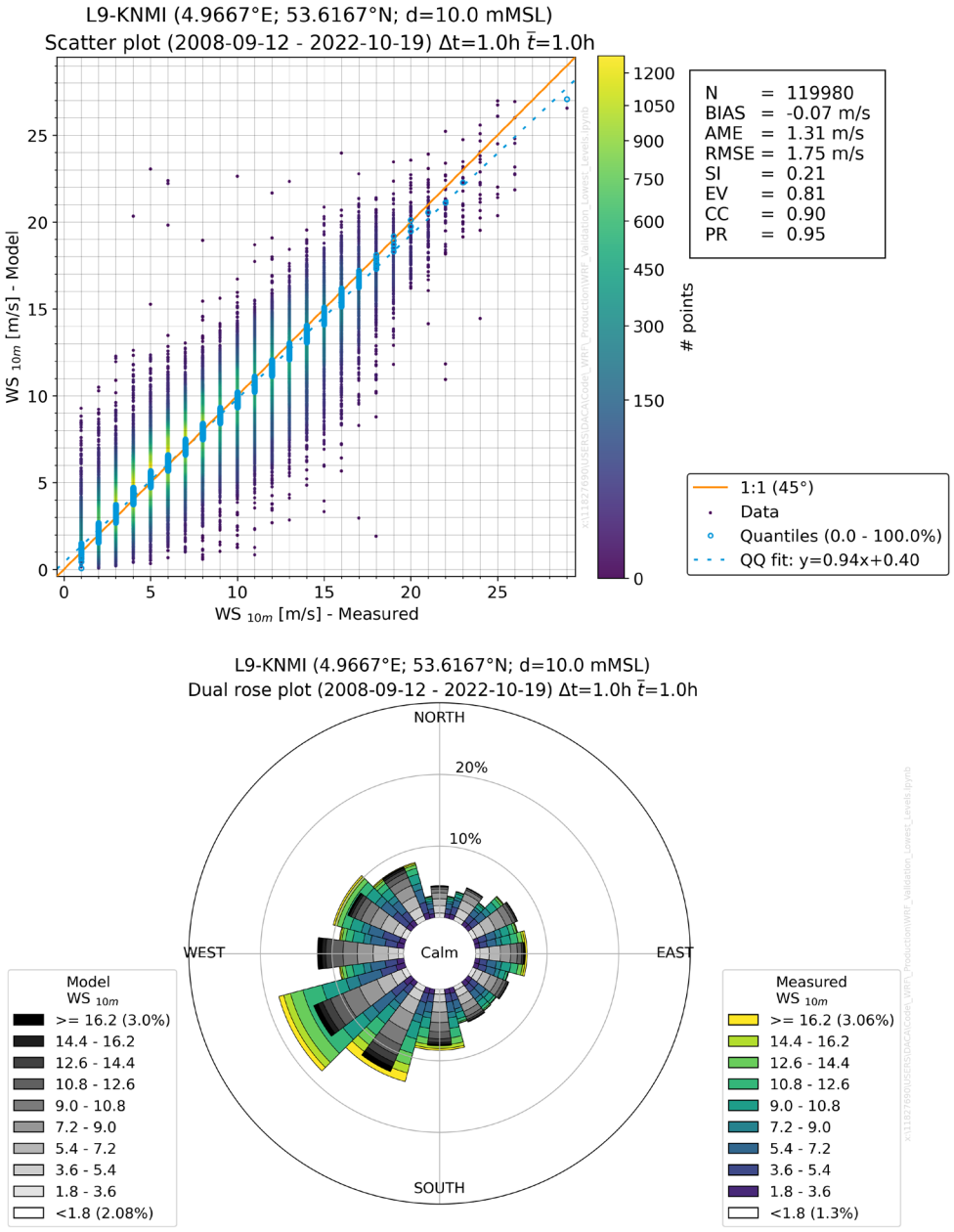

Figure C-13: Comparison of measured and modelled (WRF) winds at L9 station.
Top: Scatter plot comparison. Bottom: Dual wind rose comparison.

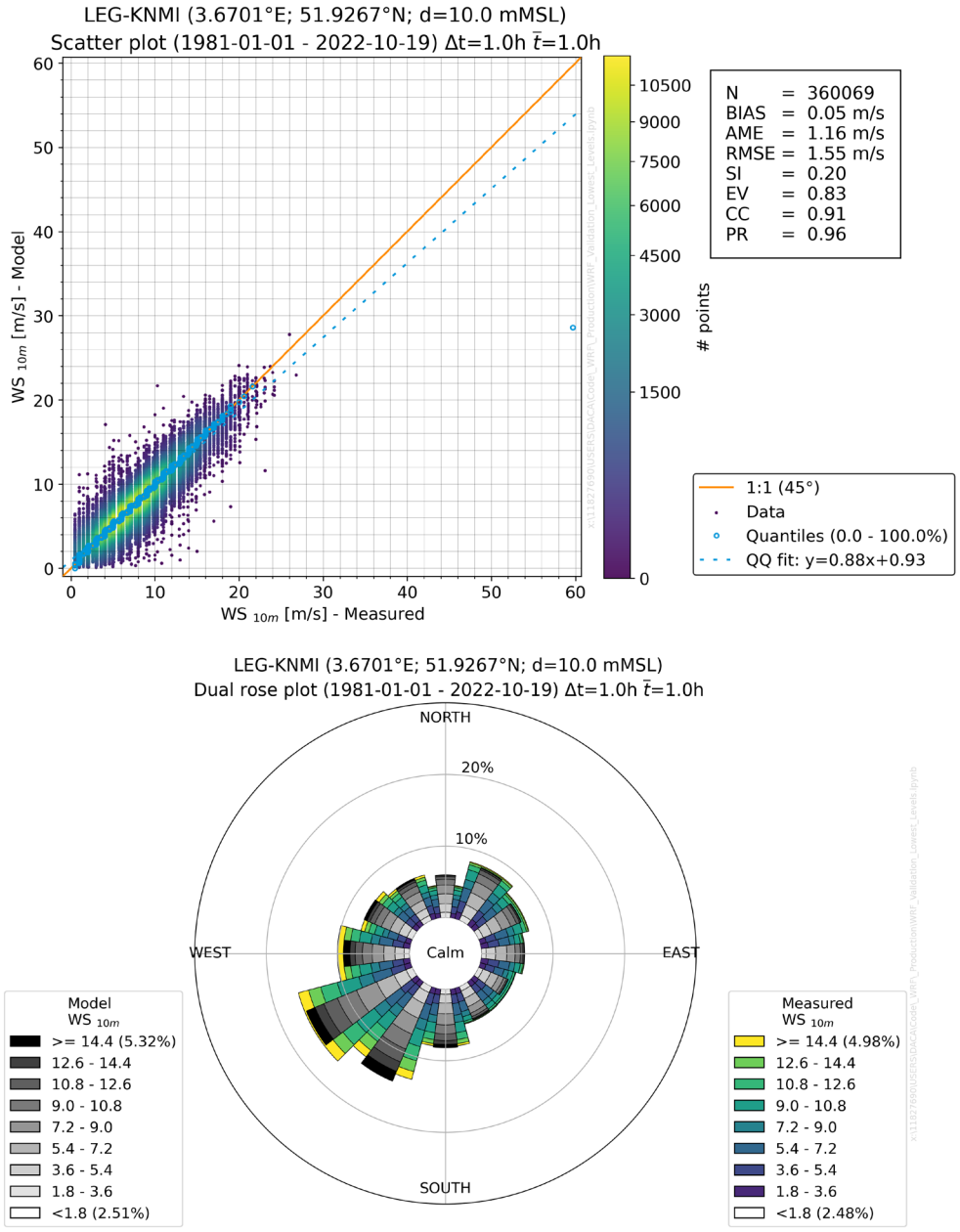

Figure C-14: Comparison of measured and modelled (WRF) winds at LEG station.
Top: Scatter plot comparison. Bottom: Dual wind rose comparison.

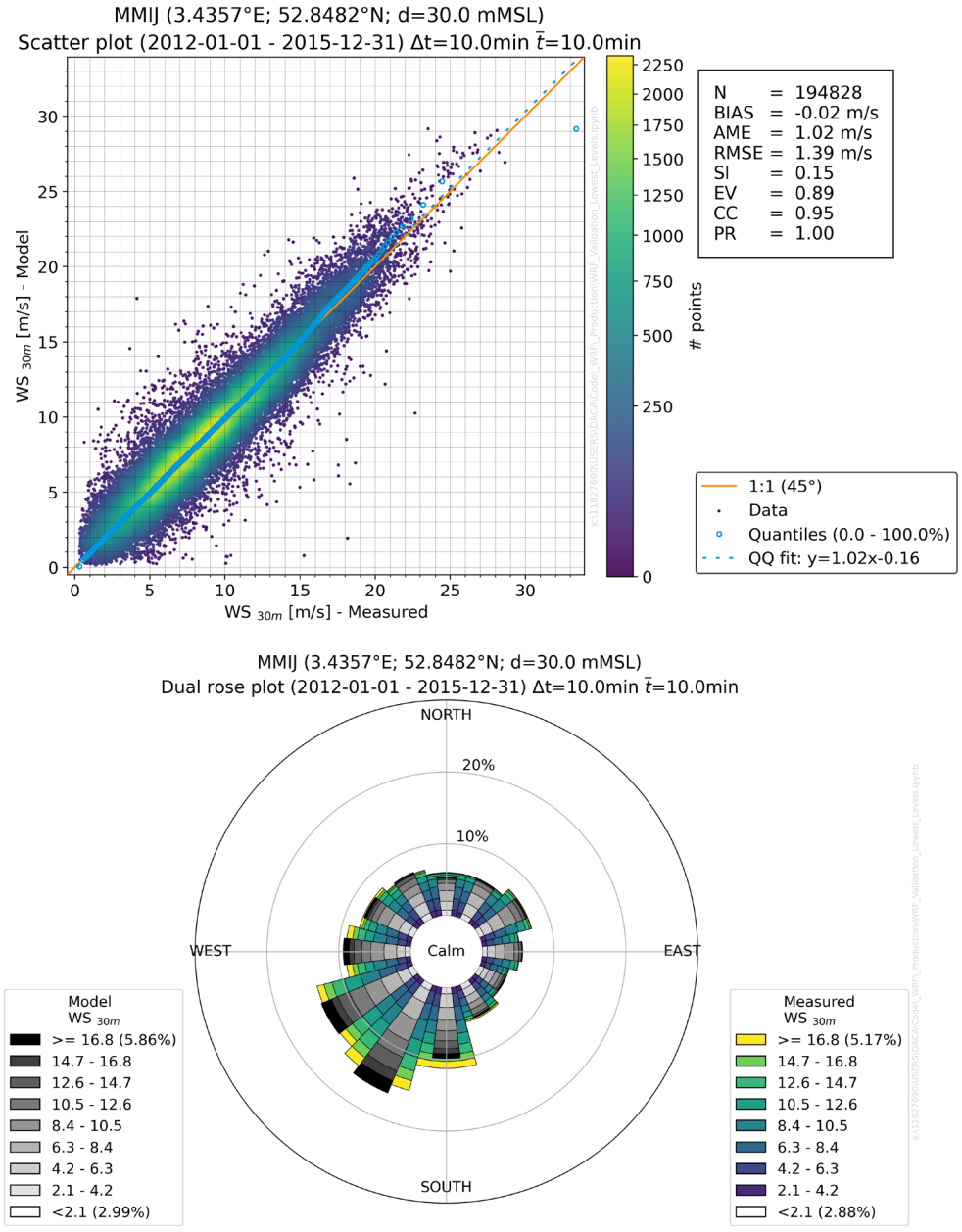

Figure C-15: Comparison of measured and modelled (WRF) winds at MMIJ-WOZ_Scatter.png station.
Top: Scatter plot comparison. Bottom: Dual wind rose comparison.

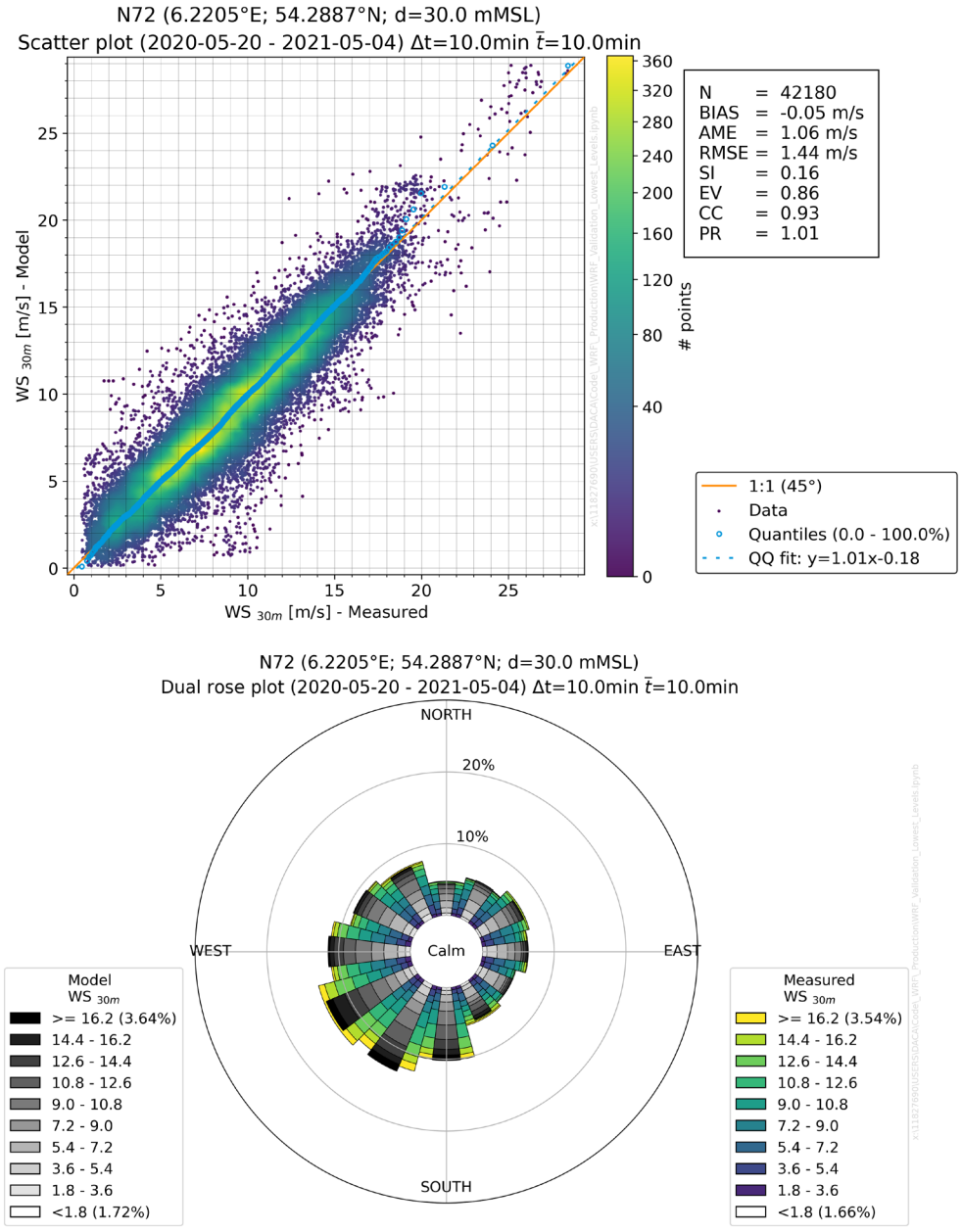

Figure C-16: Comparison of measured and modelled (WRF) winds at N72 station.
Top: Scatter plot comparison. Bottom: Dual wind rose comparison.

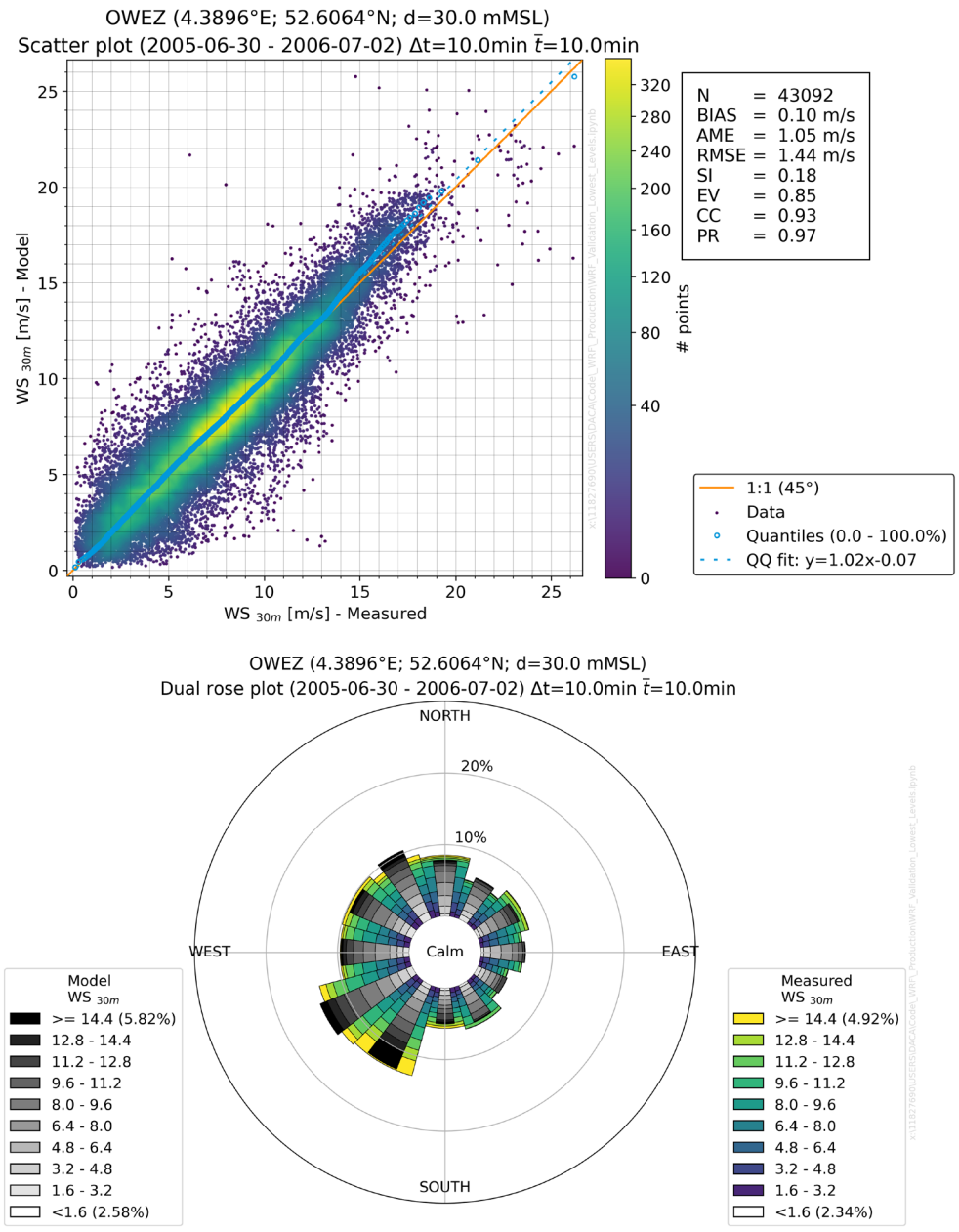

Figure C-17: Comparison of measured and modelled (WRF) winds at OWEZ station.
Top: Scatter plot comparison. Bottom: Dual wind rose comparison.

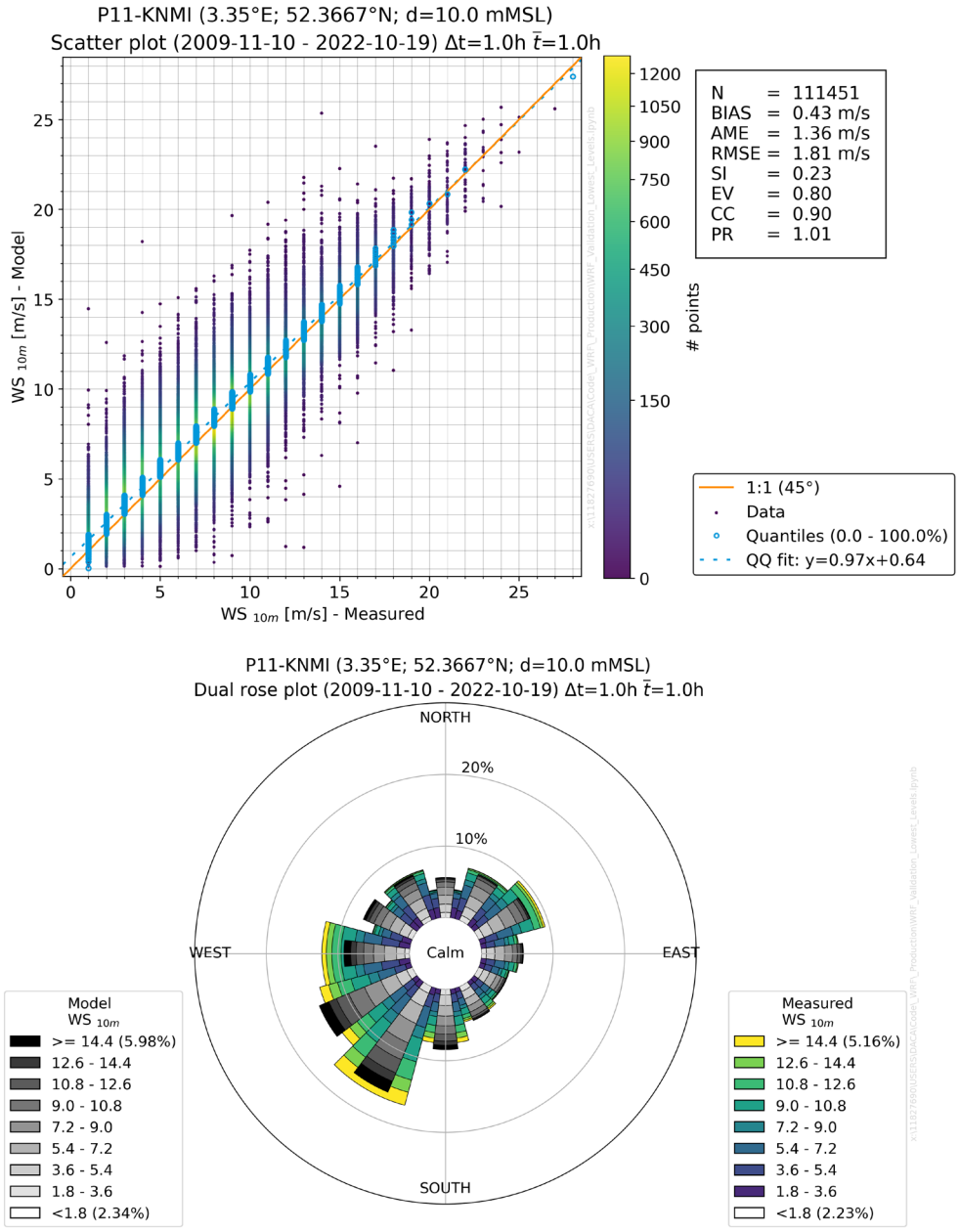

Figure C-18: Comparison of measured and modelled (WRF) winds at P11 station.
Top: Scatter plot comparison. Bottom: Dual wind rose comparison.

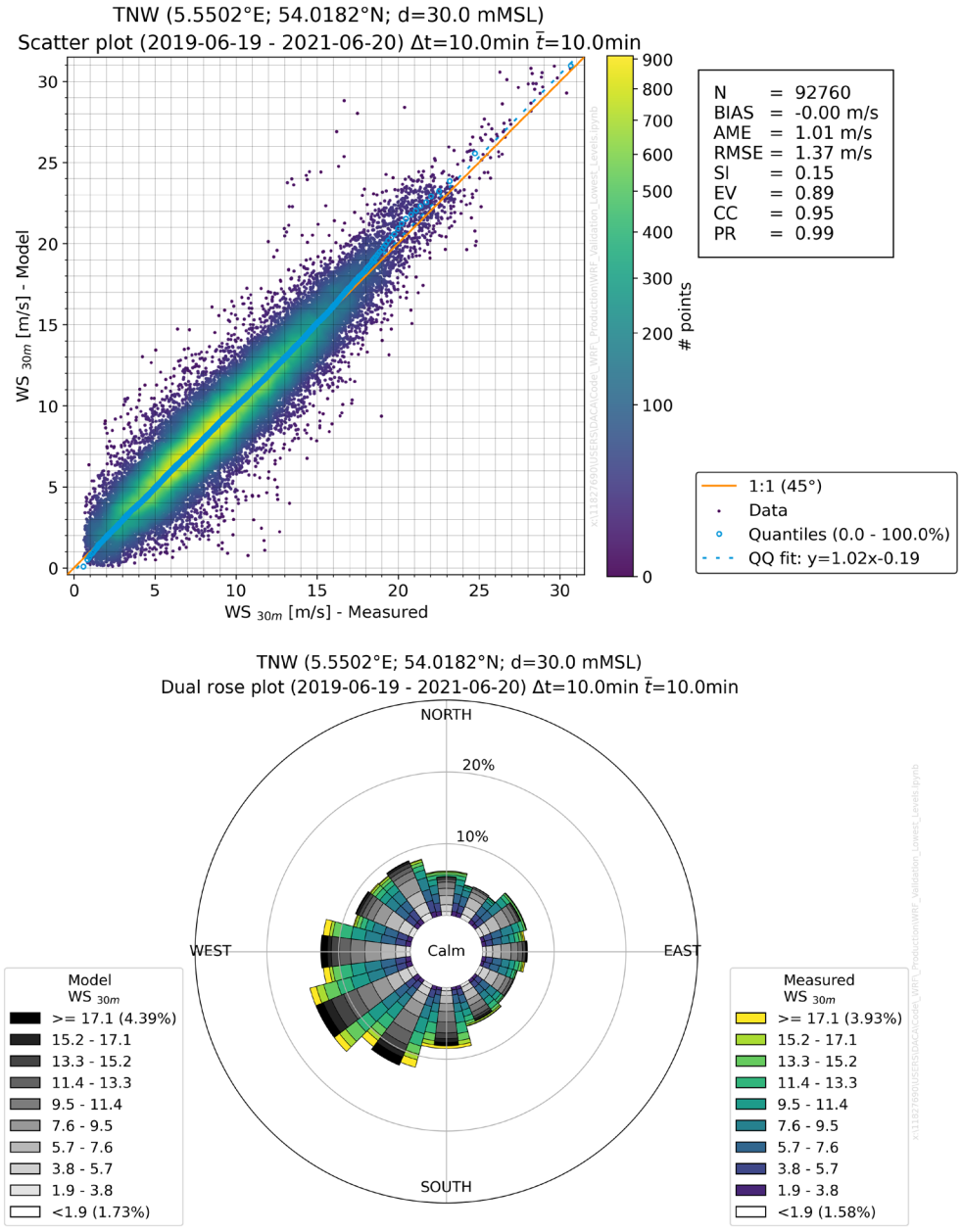

Figure C-19: Comparison of measured and modelled (WRF) winds at TNWA station.
Top: Scatter plot comparison. Bottom: Dual wind rose comparison.

Appendix D Hydrodynamic model mesh convergence results

See next pages.

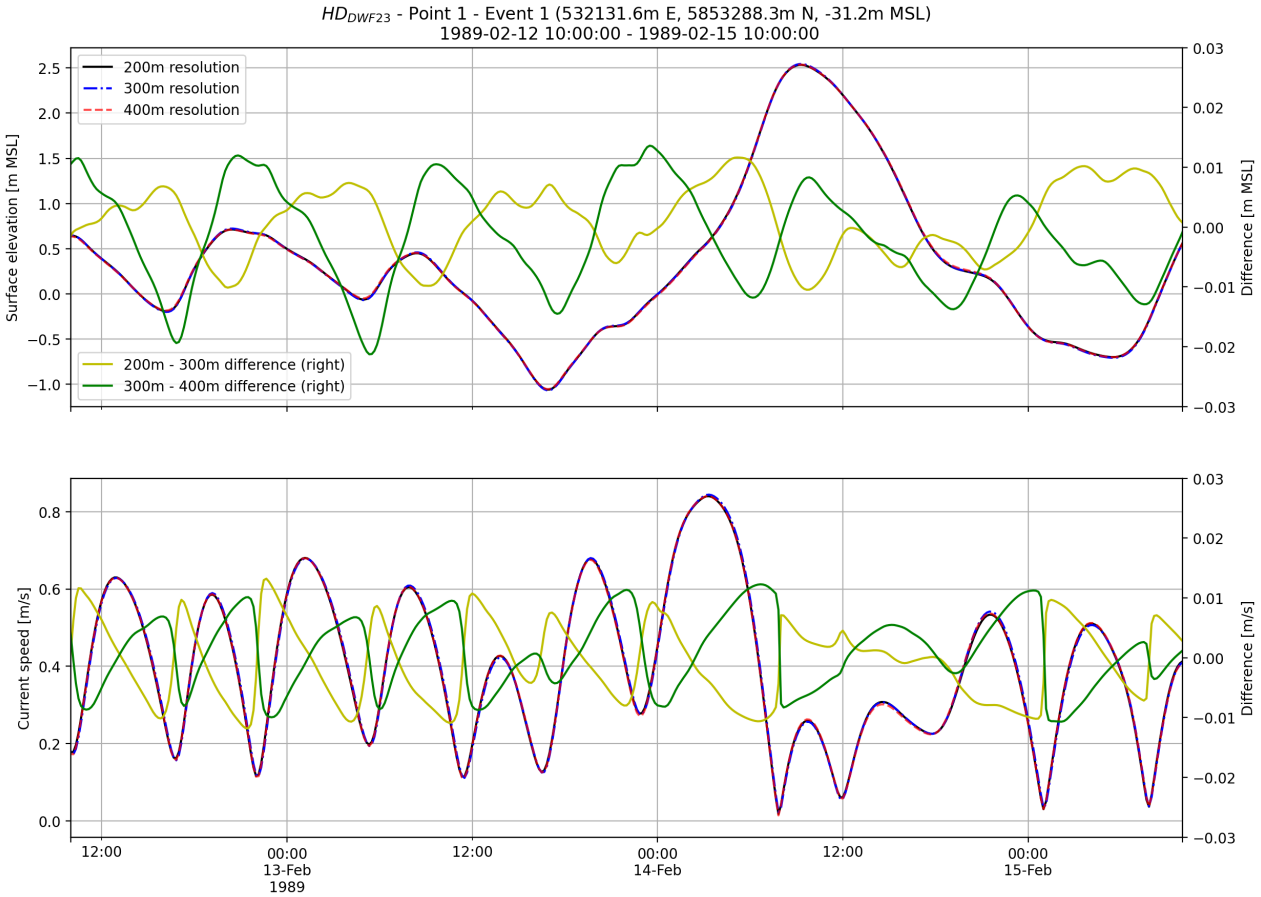

Figure D-1: Surface elevation and depth-averaged current speed time series comparison between 200 m, 300 m and 400 m mesh resolutions (HD model) during Event 1 at Point 1.
Absolute values are shown on the left axis (black, blue, and red lines), and time series difference between 200-300m and 300-400m is shown on the right axis (green and yellow lines).

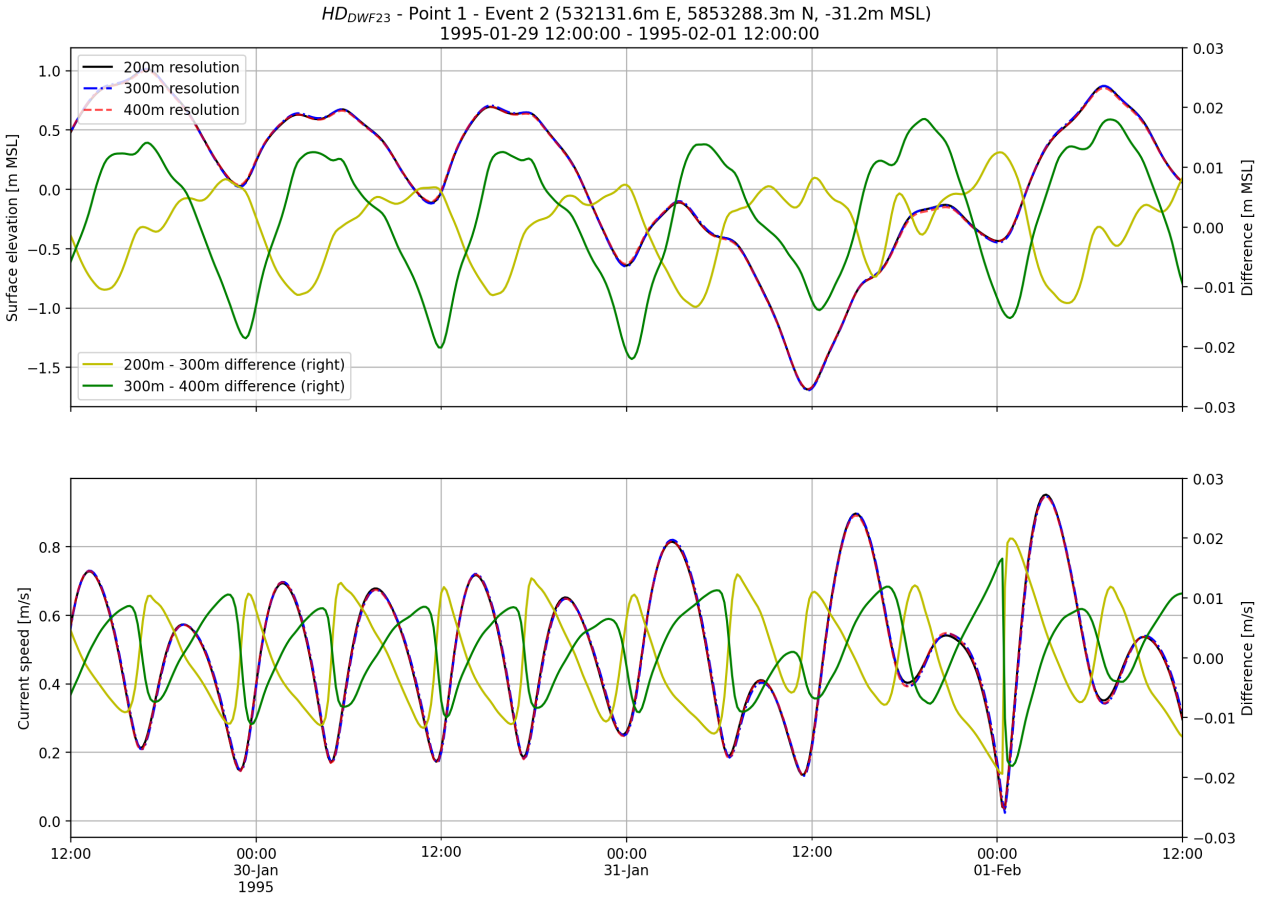

Figure D-2: Surface elevation and depth-averaged current speed time series comparison between 200 m, 300 m and 400 m mesh resolutions (HD model) during Event 2 at Point 1.
Absolute values are shown on the left axis (black, blue, and red lines), and time series difference between 200-300m and 300-400m is shown on the right axis (green and yellow lines).

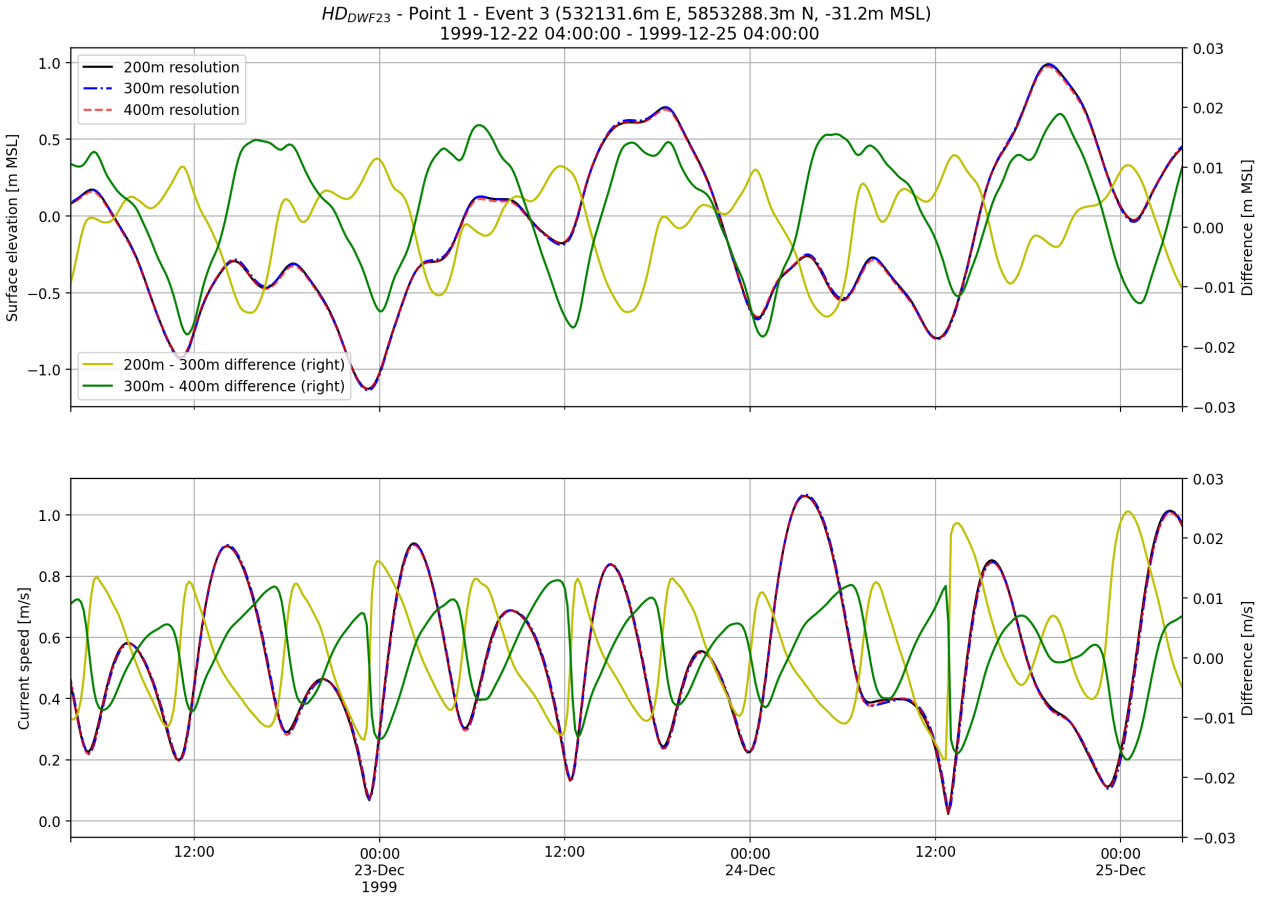

Figure D-3: Surface elevation and depth-averaged current speed time series comparison between 200 m, 300 m and 400 m mesh resolutions (HD model) during Event 3 at Point 1.
Absolute values are shown on the left axis (black, blue, and red lines), and time series difference between 200-300m and 300-400m is shown on the right axis (green and yellow lines).

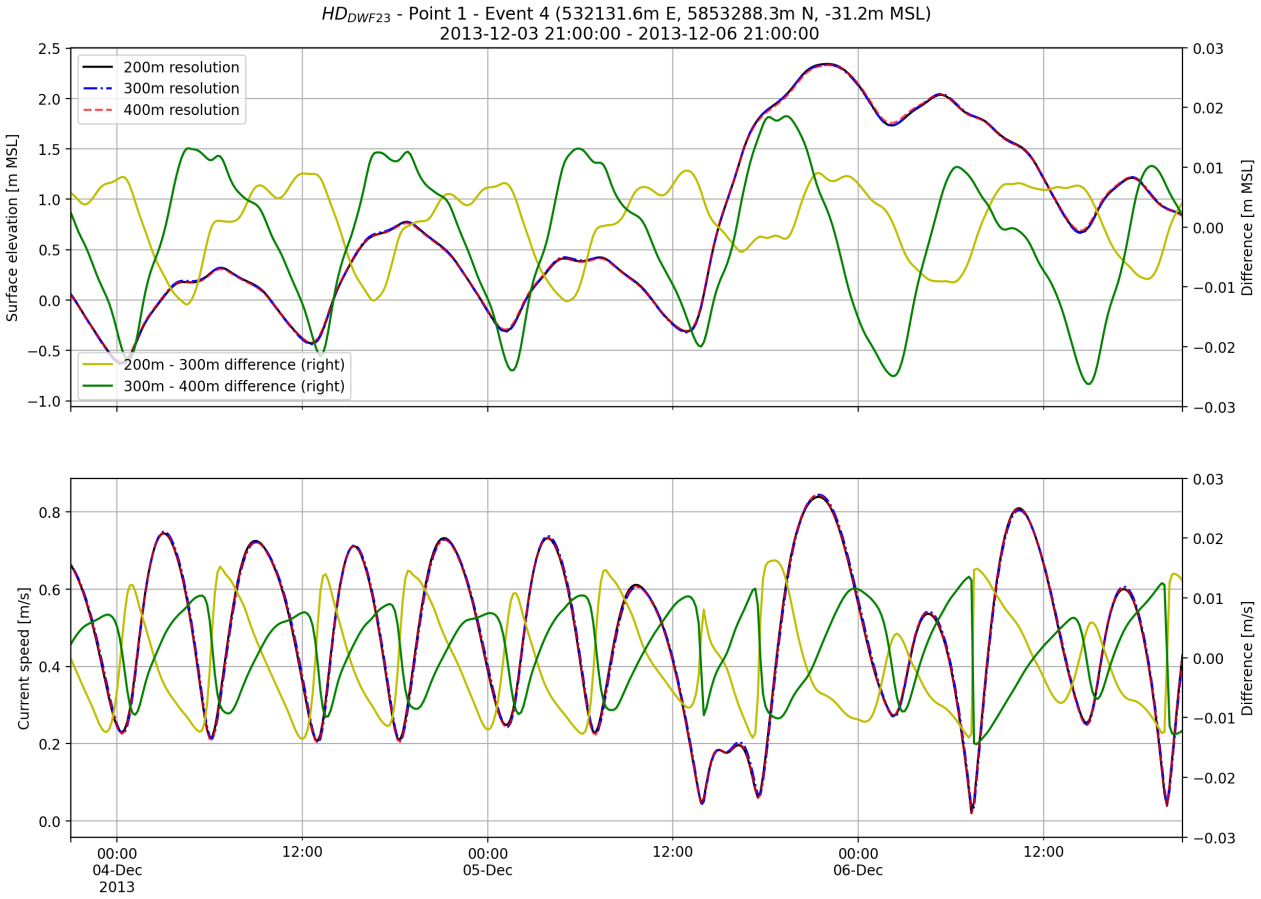

Figure D-4: Surface elevation and depth-averaged current speed time series comparison between 200 m, 300 m and 400 m mesh resolutions (HD model) during Event 4 at Point 1.
Absolute values are shown on the left axis (black, blue, and red lines), and time series difference between 200-300m and 300-400m is shown on the right axis (green and yellow lines).

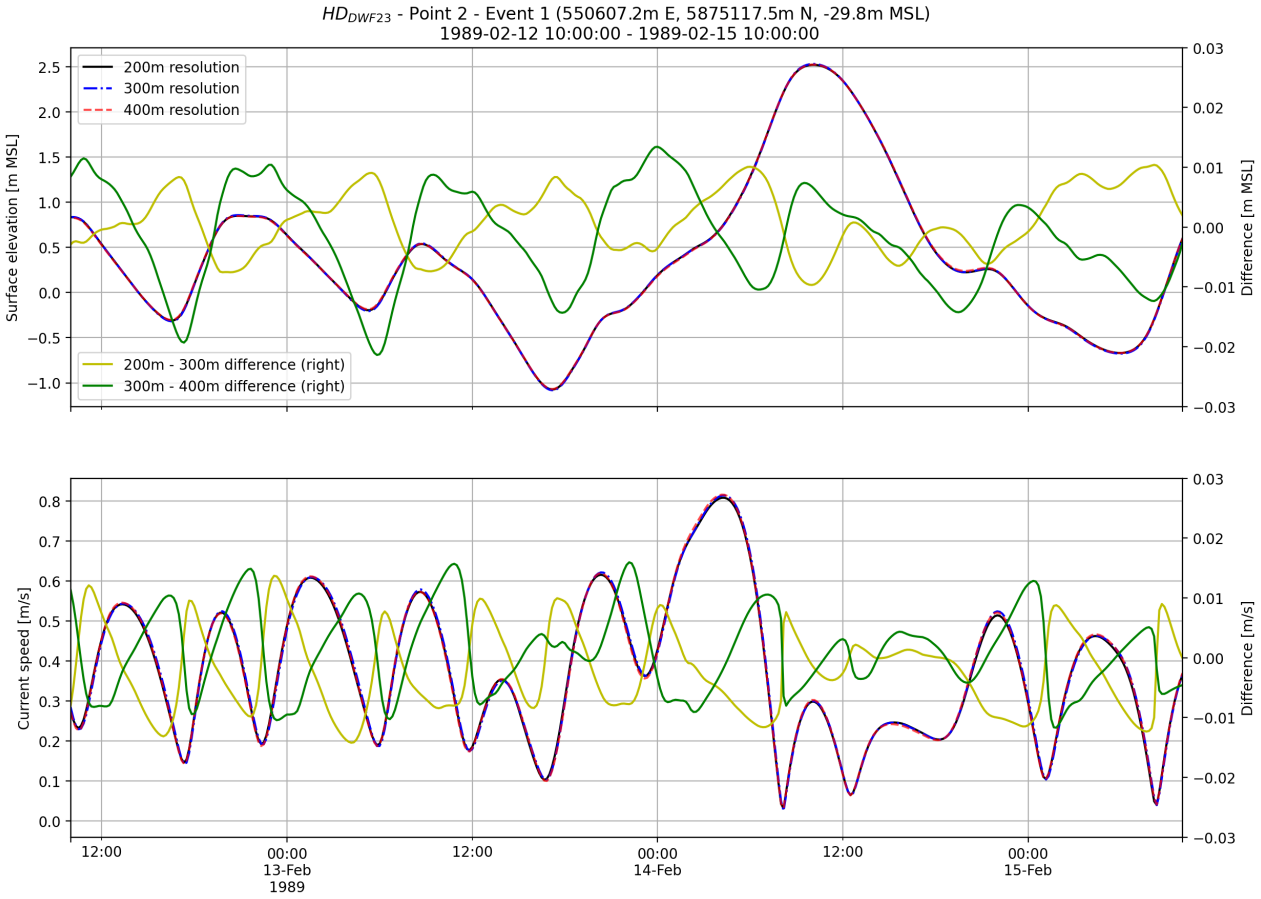

Figure D-5: Surface elevation and depth-averaged current speed time series comparison between 200 m, 300 m and 400 m mesh resolutions (HD model) during Event 1 at Point 2.
Absolute values are shown on the left axis (black, blue, and red lines), and time series difference between 200-300m and 300-400m is shown on the right axis (green and yellow lines).

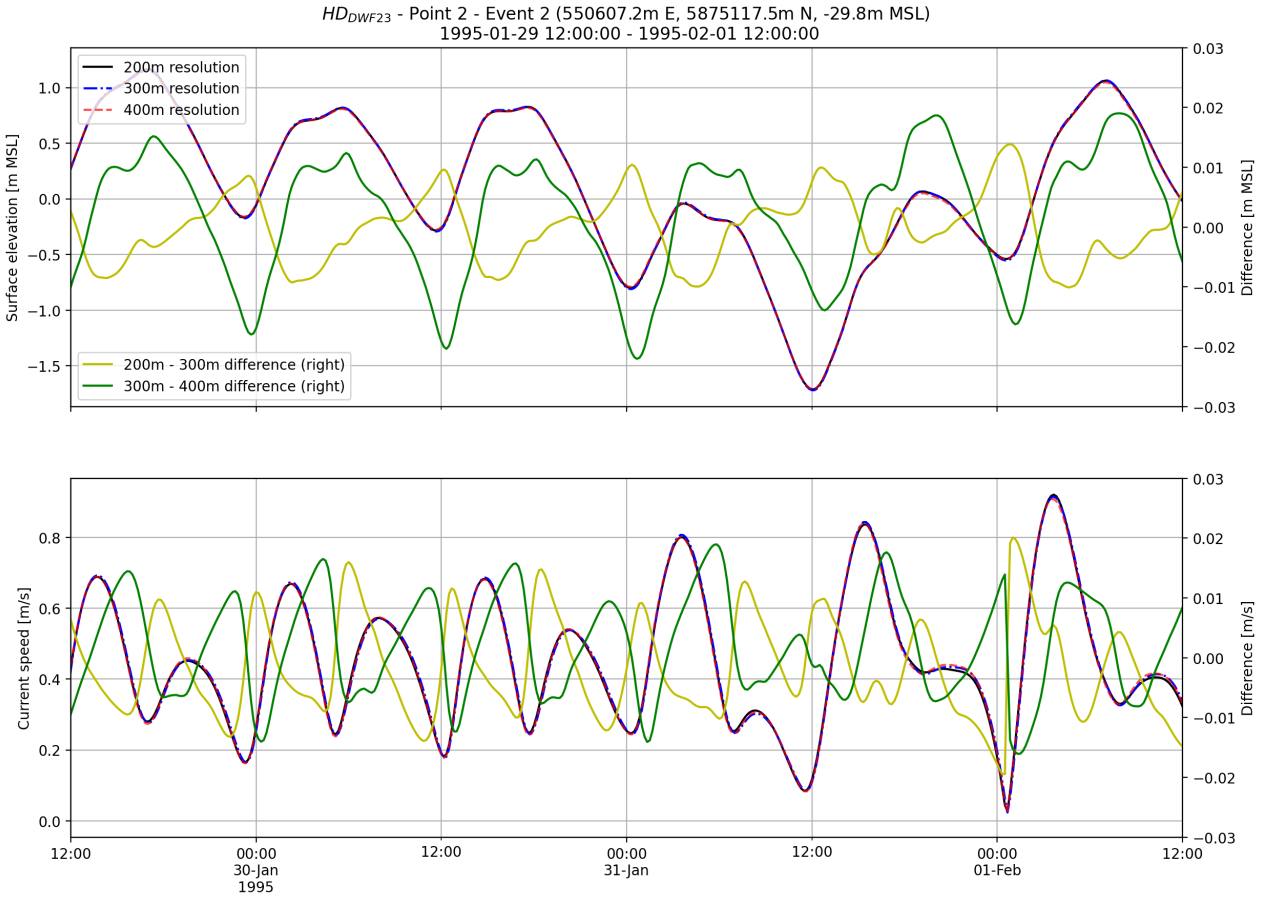

Figure D-6: Surface elevation and depth-averaged current speed time series comparison between 200 m, 300 m and 400 m mesh resolutions (HD model) during Event 2 at Point 2.
Absolute values are shown on the left axis (black, blue, and red lines), and time series difference between 200-300m and 300-400m is shown on the right axis (green and yellow lines).

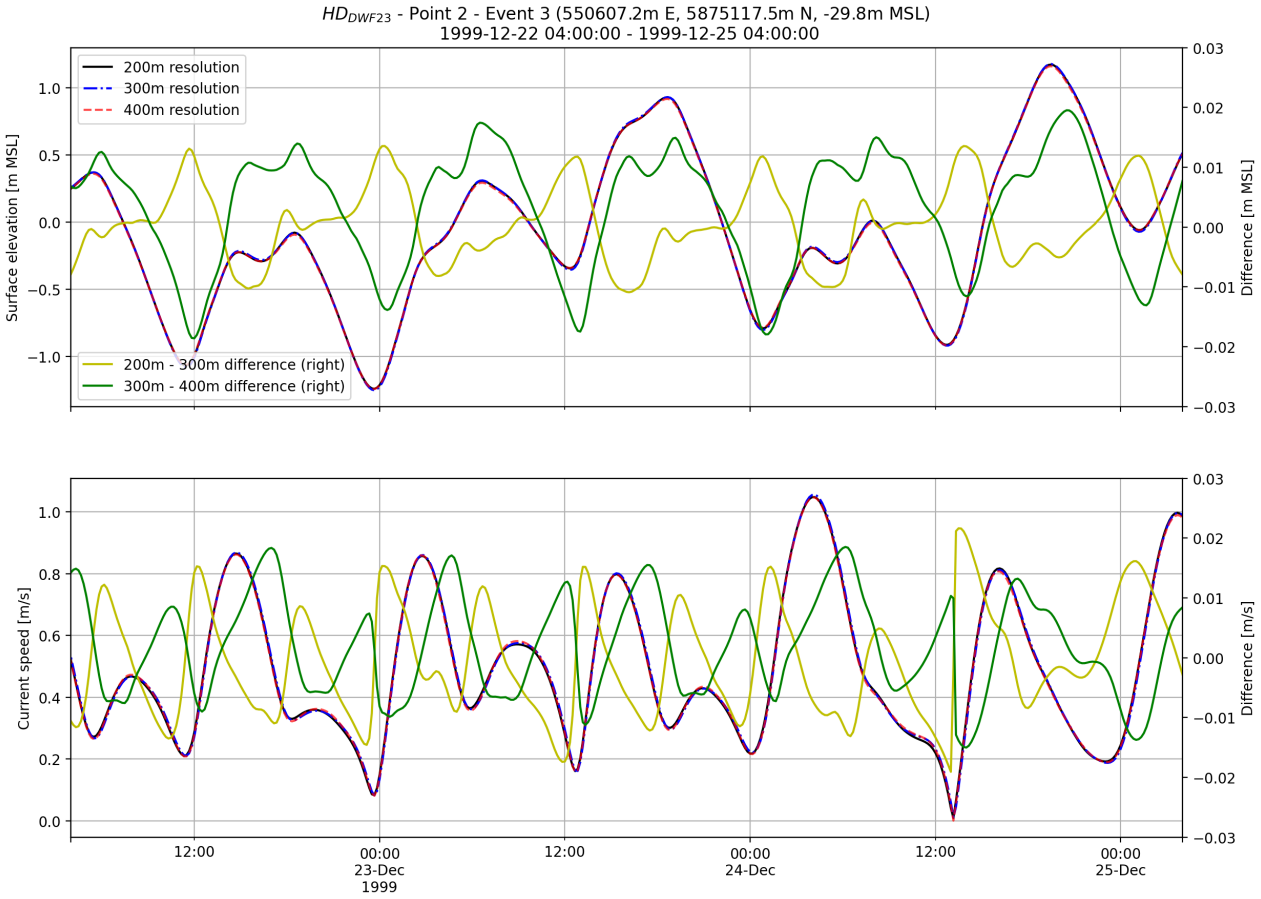

Figure D-7: Surface elevation and depth-averaged current speed time series comparison between 200 m, 300 m and 400 m mesh resolutions (HD model) during Event 3 at Point 2.
Absolute values are shown on the left axis (black, blue, and red lines), and time series difference between 200-300m and 300-400m is shown on the right axis (green and yellow lines).

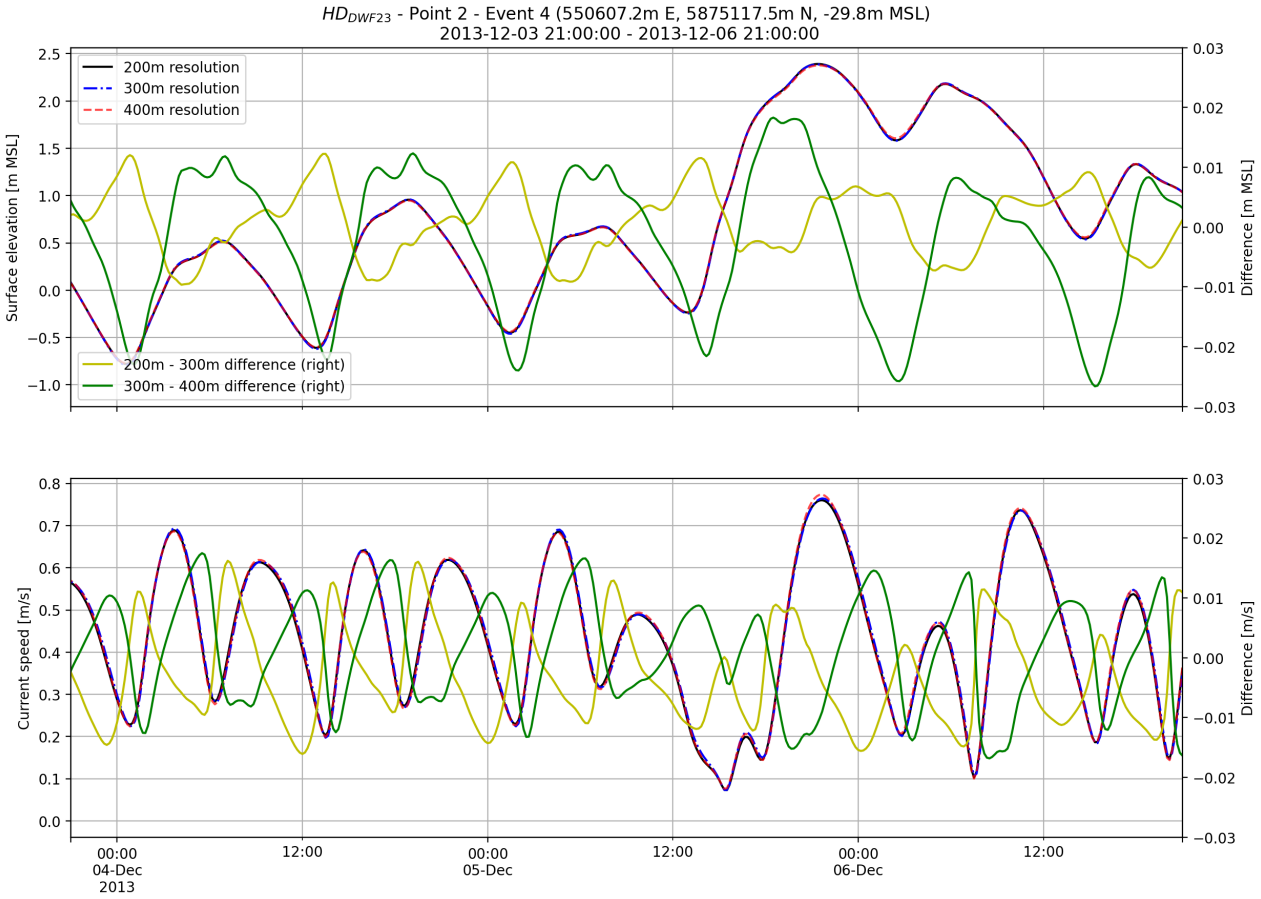

Figure D-8: Surface elevation and depth-averaged current speed time series comparison between 200 m, 300 m and 400 m mesh resolutions (HD model) during Event 4 at Point 2.
Absolute values are shown on the left axis (black, blue, and red lines), and time series difference between 200-300m and 300-400m is shown on the right axis (green and yellow lines).

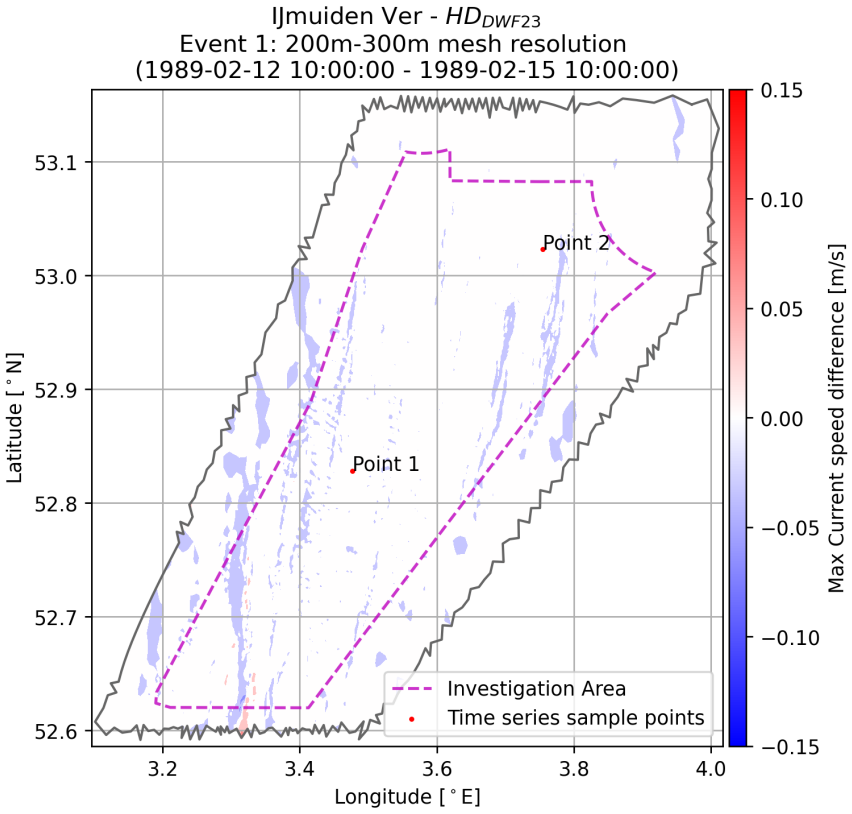

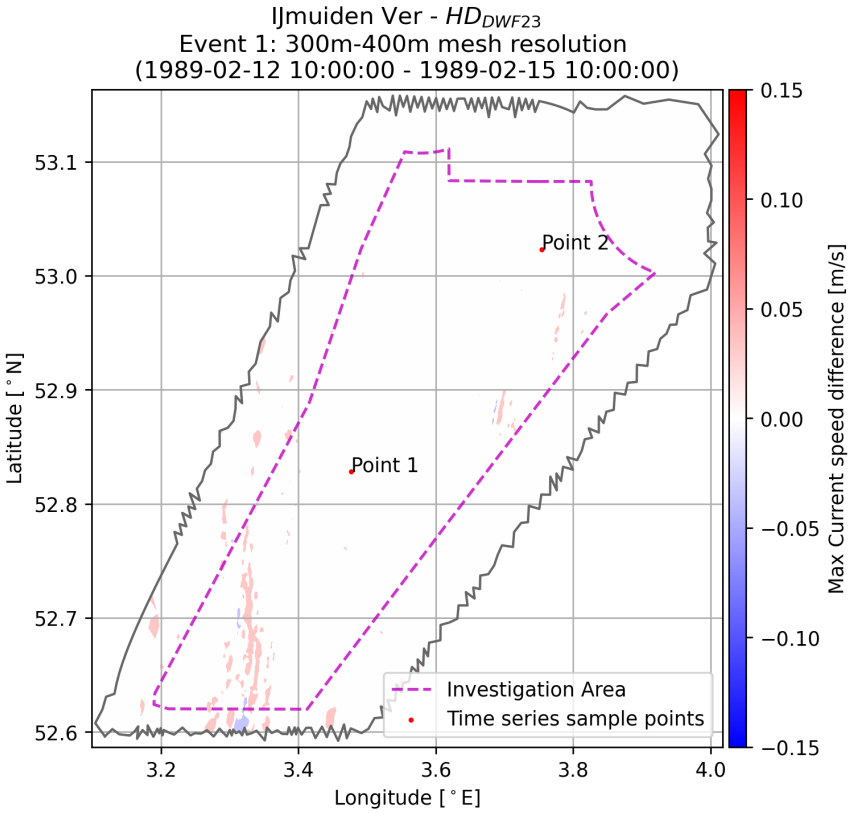

Figure D-9: Difference map of event.

Top: Difference between 200 m and 300 m mesh resolutions
Bottom: Difference between 300 m and 400 m mesh resolutions

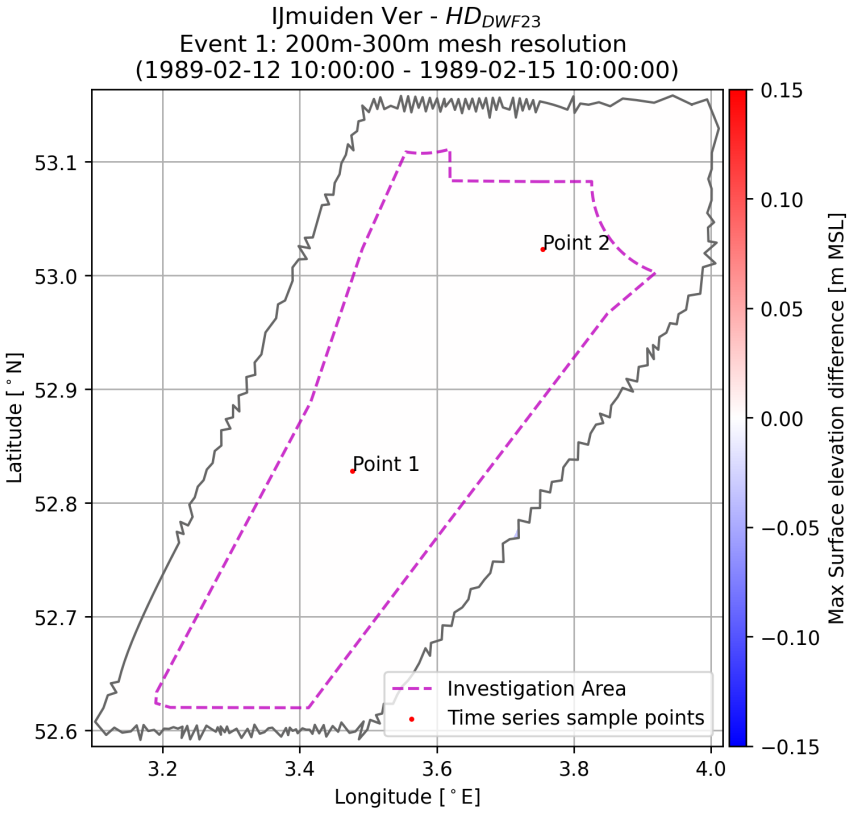

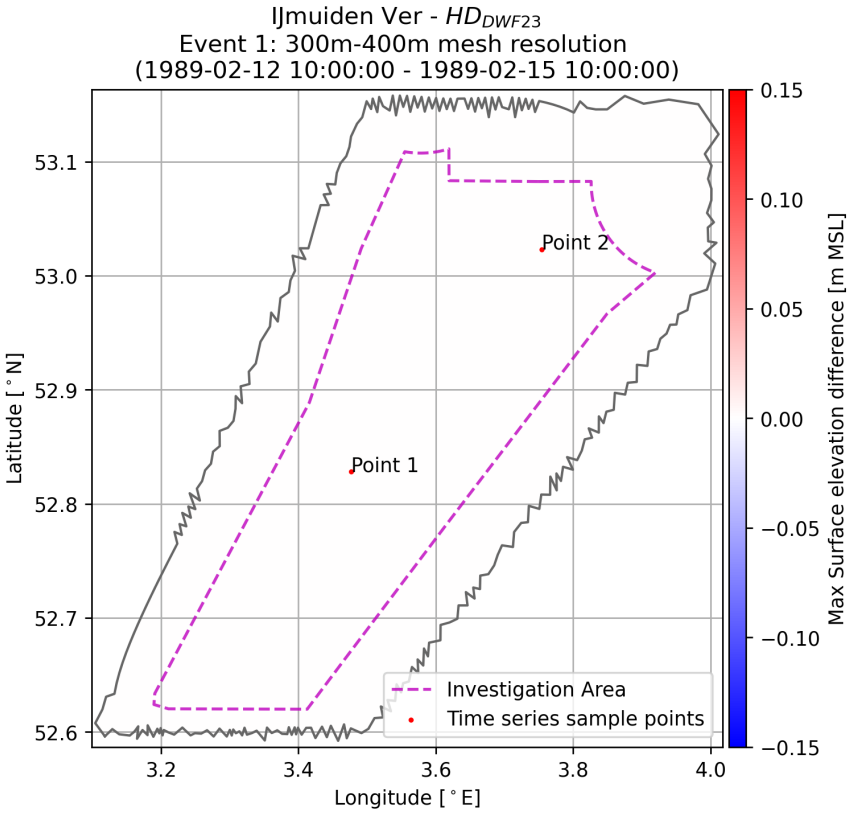

Figure D-10: Difference map of event.

Top: Difference between 200 m and 300 m mesh resolutions
Bottom: Difference between 300 m and 400 m mesh resolutions

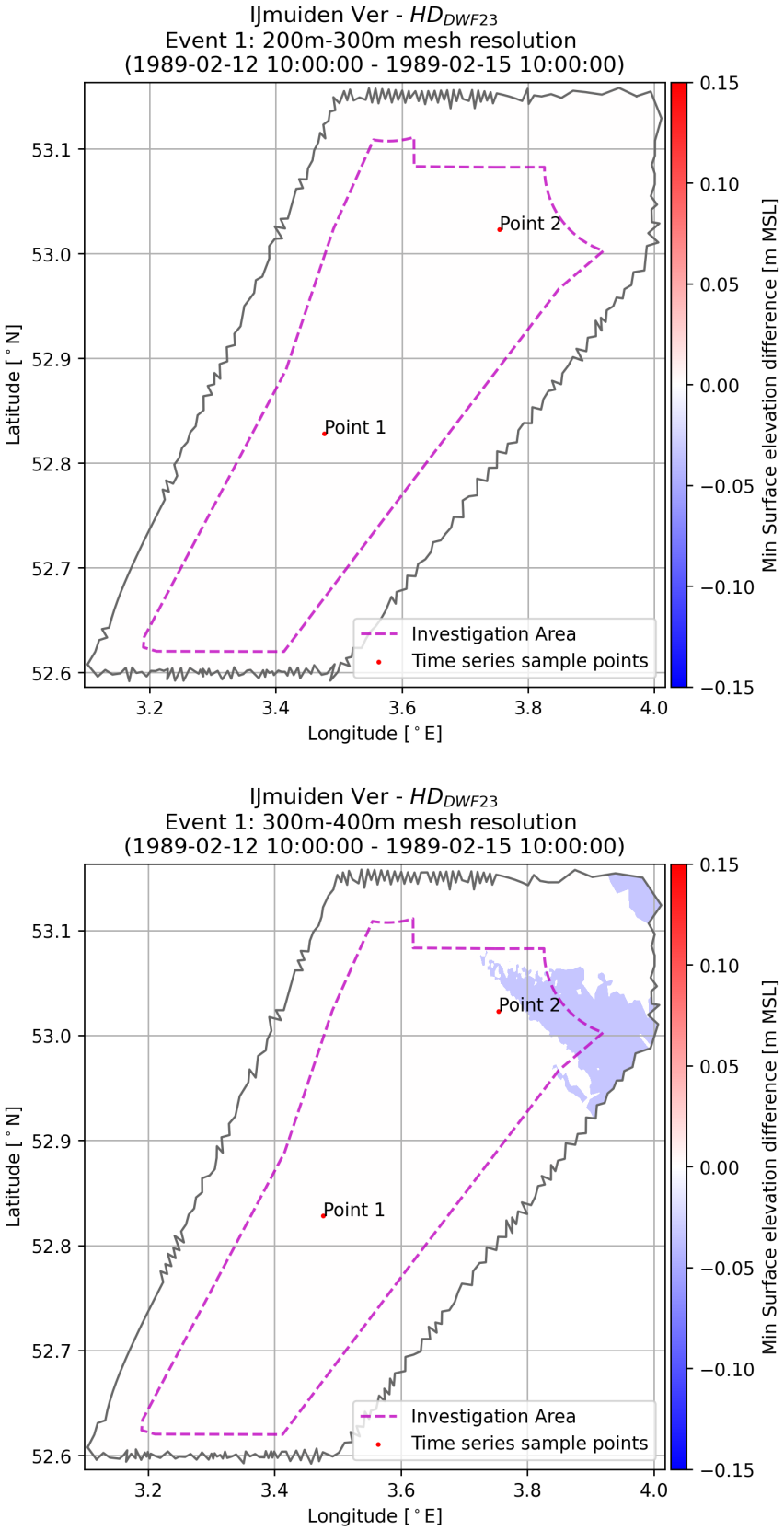

Figure D-11: Difference map of event.

Top: Difference between 200 m and 300 m mesh resolutions
Bottom: Difference between 300 m and 400 m mesh resolutions

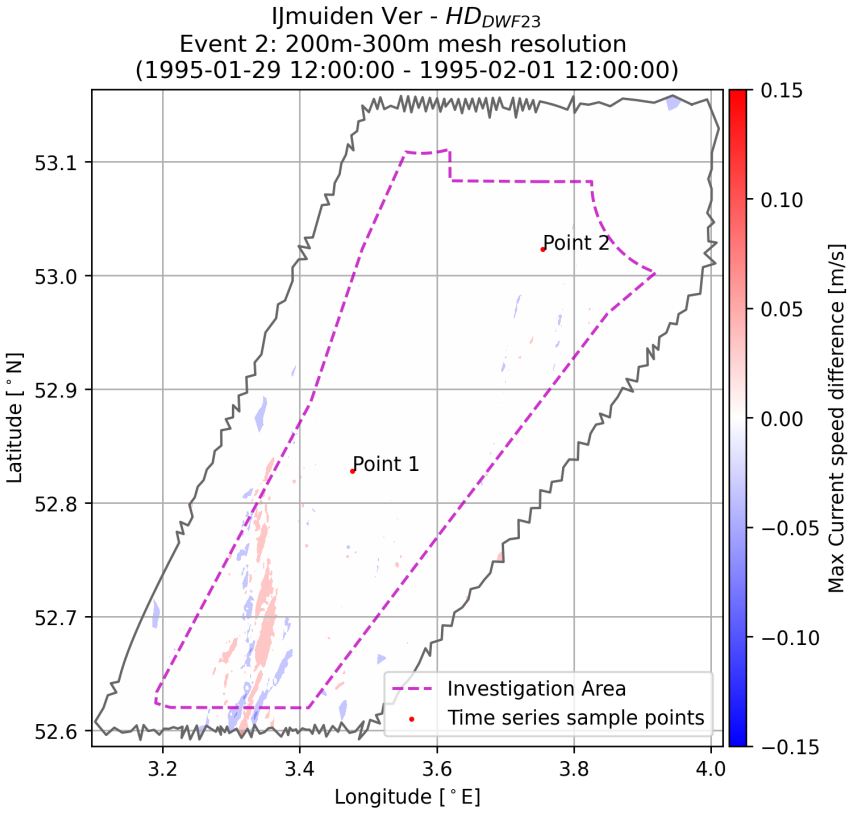

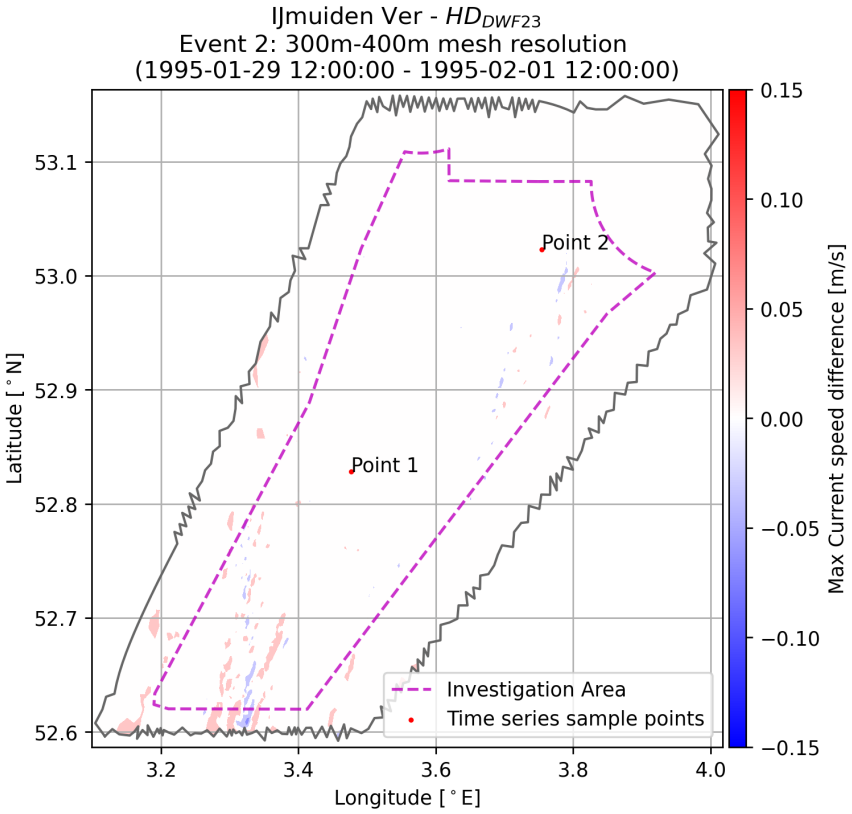

Figure D-12: Difference map of event.

Top: Difference between 200 m and 300 m mesh resolutions
Bottom: Difference between 300 m and 400 m mesh resolutions

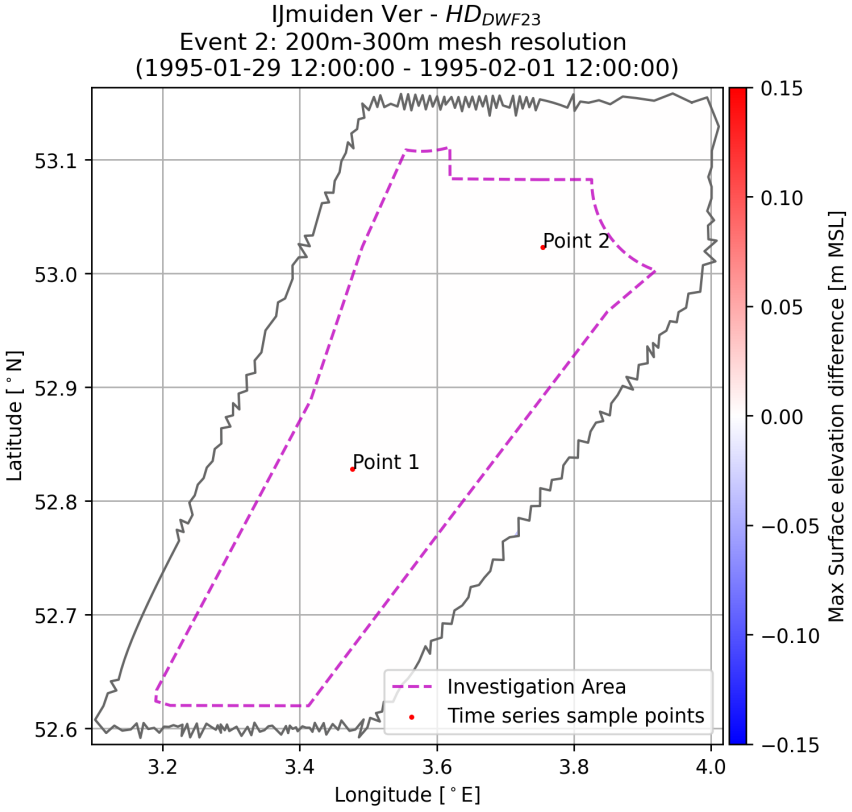

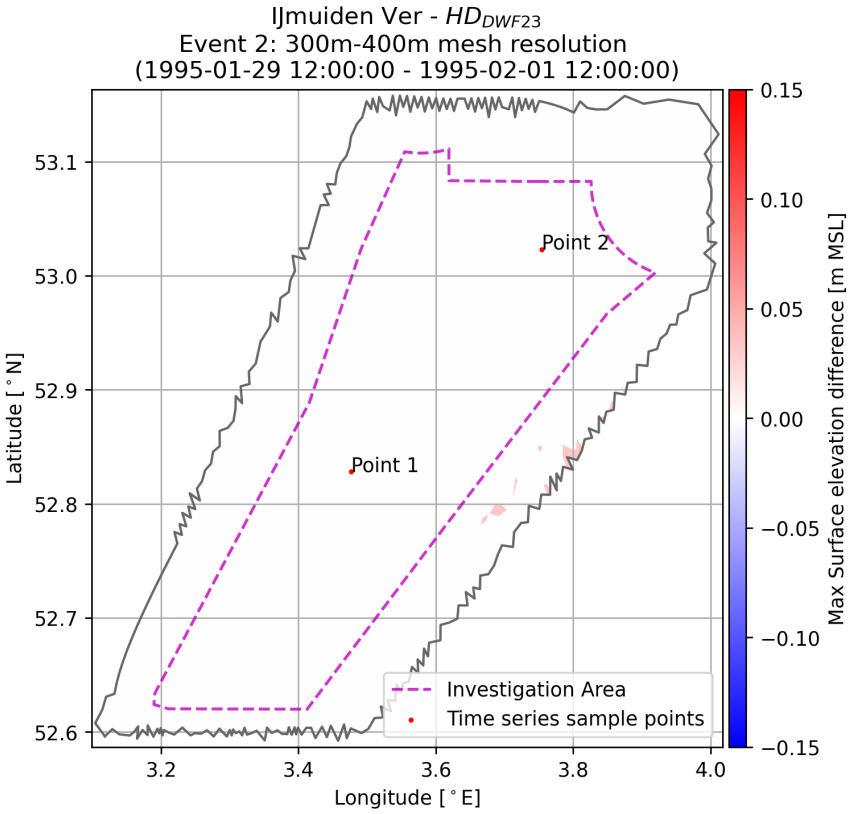

Figure D-13: Difference map of event.

Top: Difference between 200 m and 300 m mesh resolutions
Bottom: Difference between 300 m and 400 m mesh resolutions

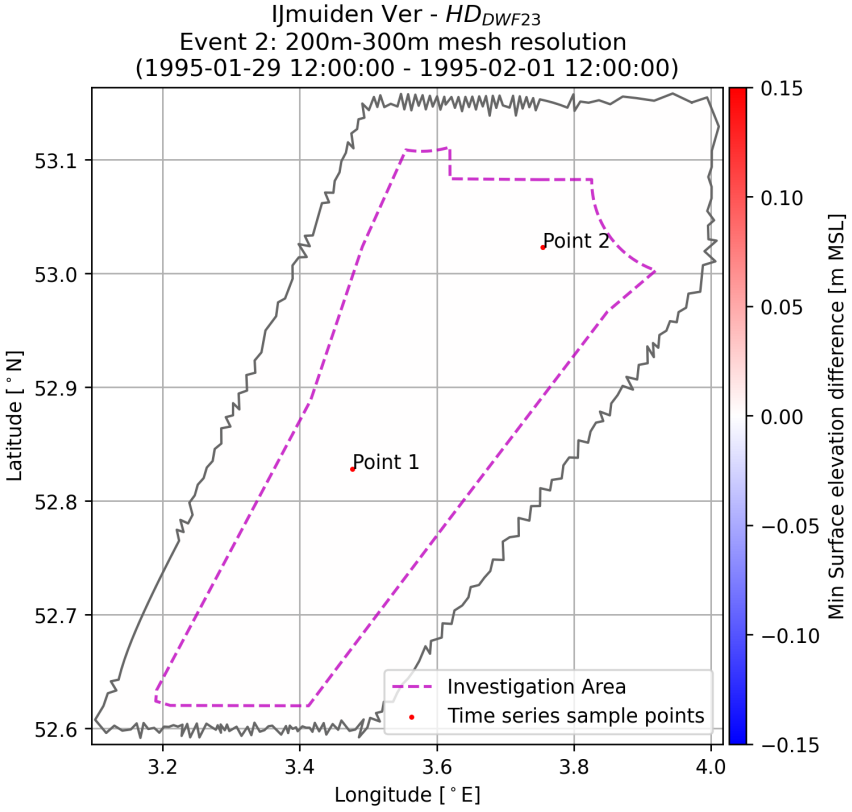

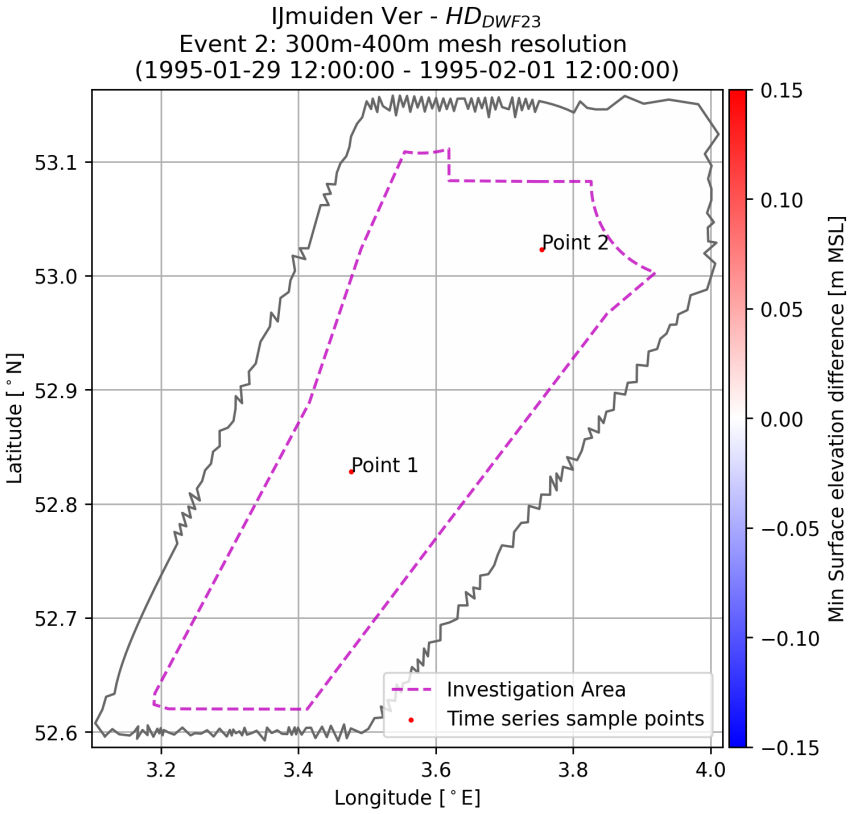

Figure D-14: Difference map of event.

Top: Difference between 200 m and 300 m mesh resolutions
Bottom: Difference between 300 m and 400 m mesh resolutions

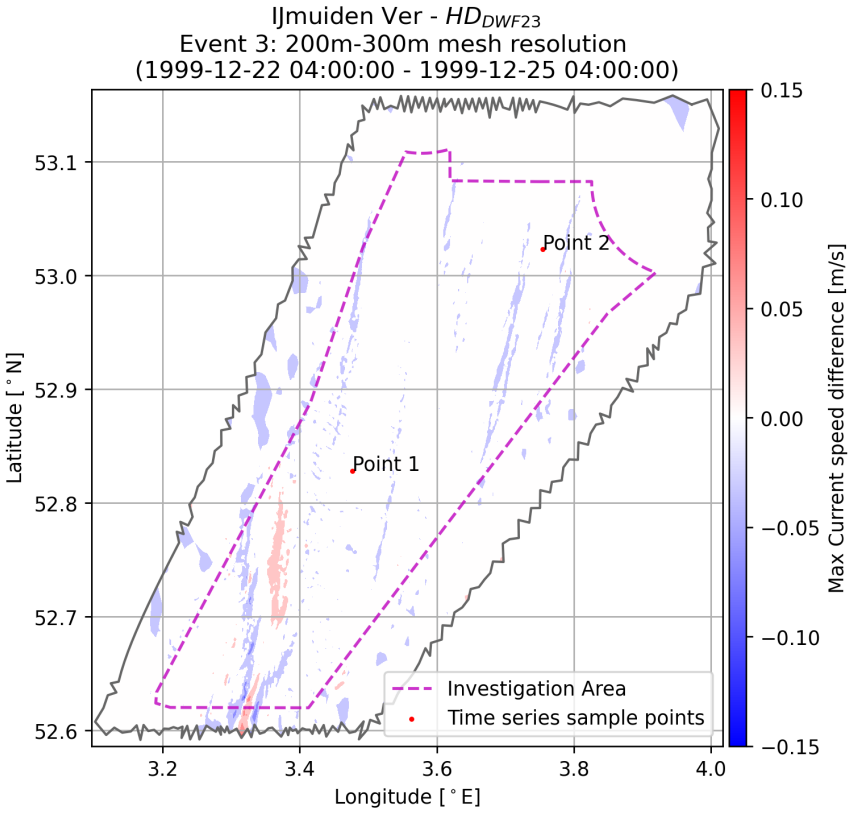

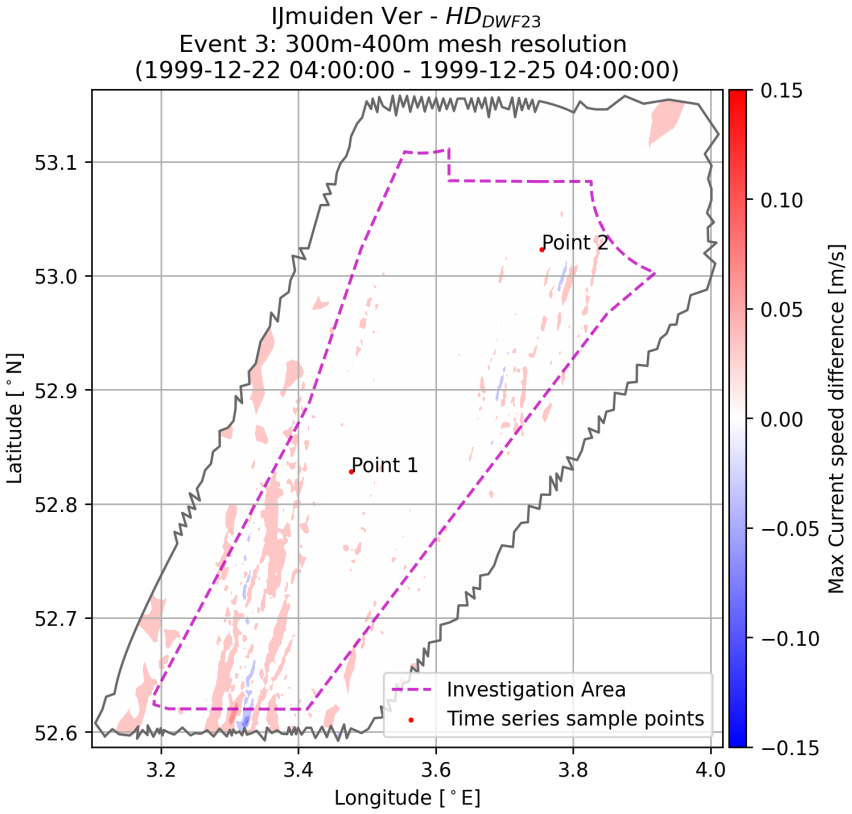

Figure D-15: Difference map of event.

Top: Difference between 200 m and 300 m mesh resolutions
Bottom: Difference between 300 m and 400 m mesh resolutions

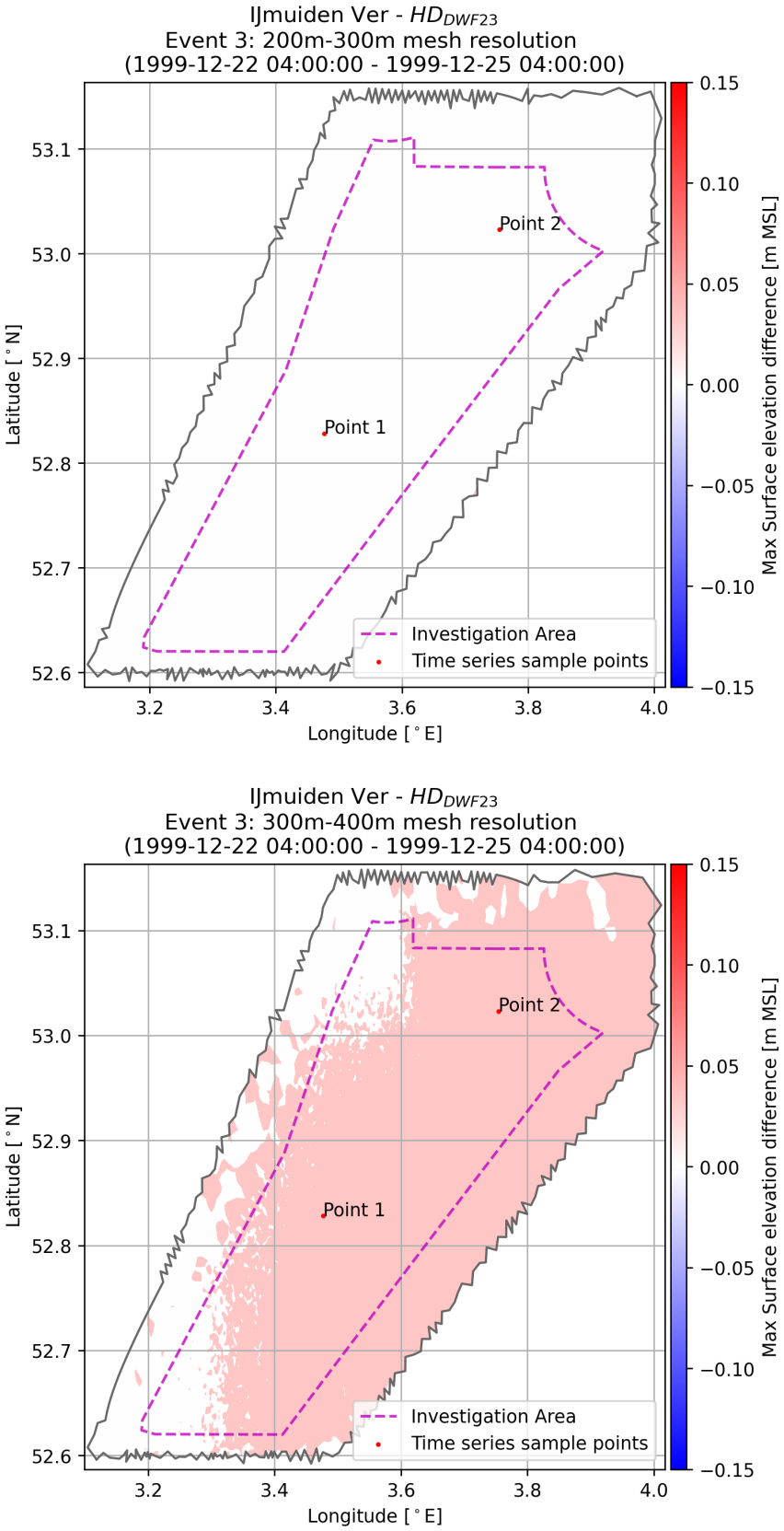

Figure D-16: Difference map of event.

Top: Difference between 200 m and 300 m mesh resolutions

Bottom: Difference between 300 m and 400 m mesh resolutions

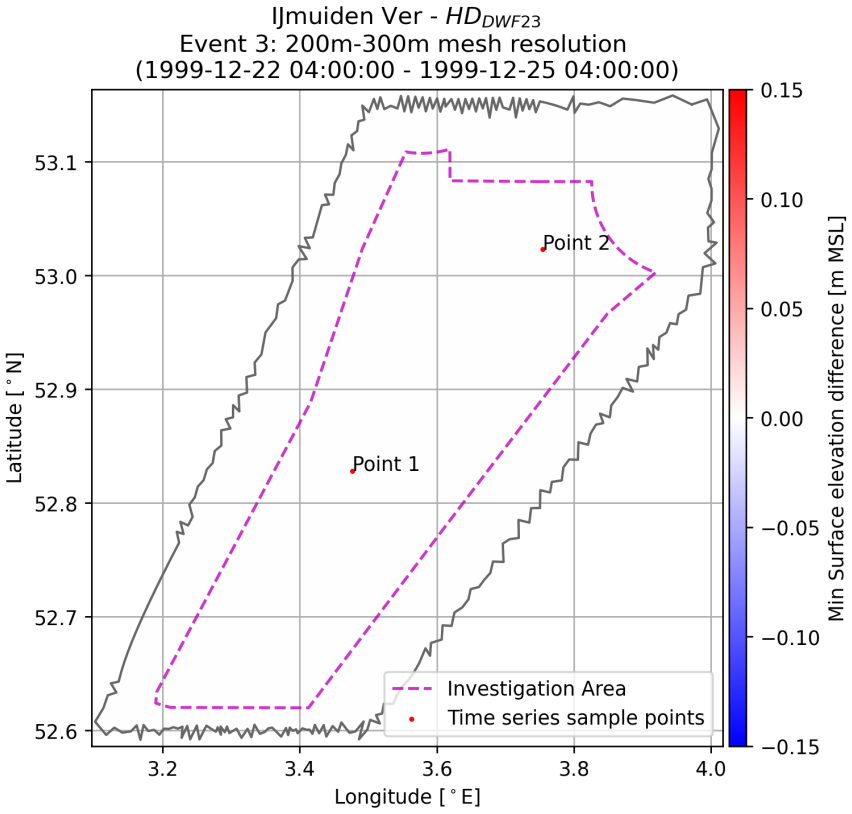

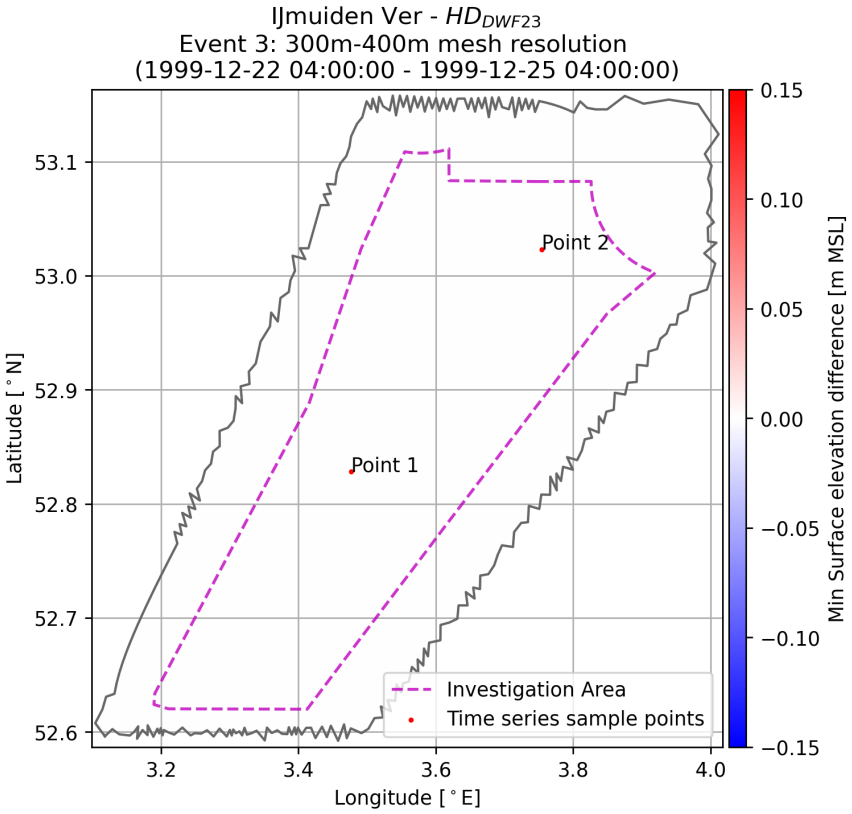

Figure D-17: Difference map of event.

Top: Difference between 200 m and 300 m mesh resolutions
Bottom: Difference between 300 m and 400 m mesh resolutions

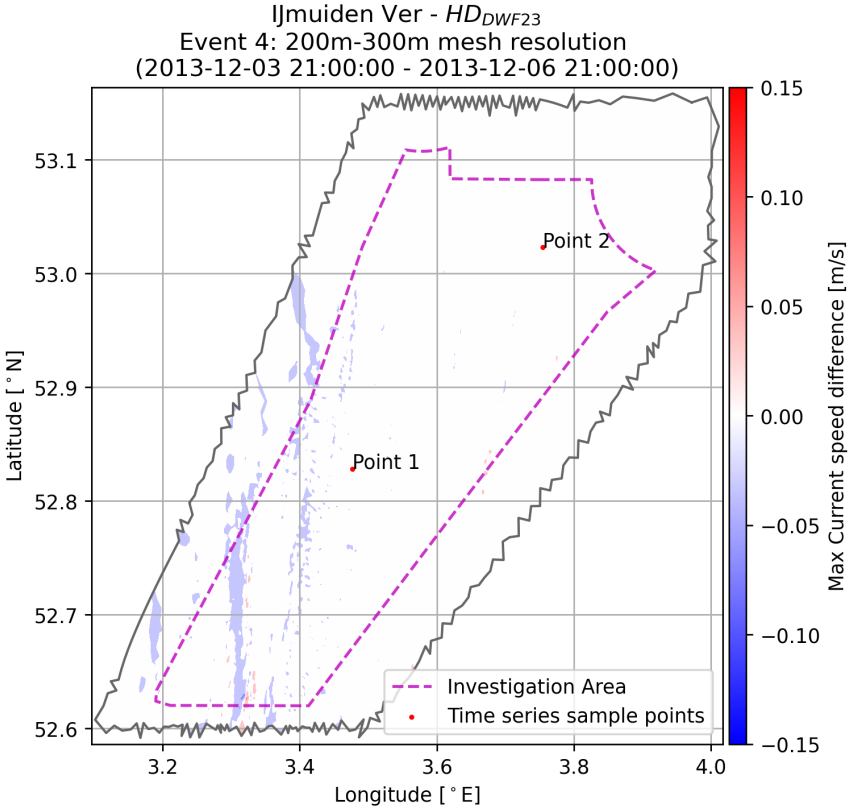

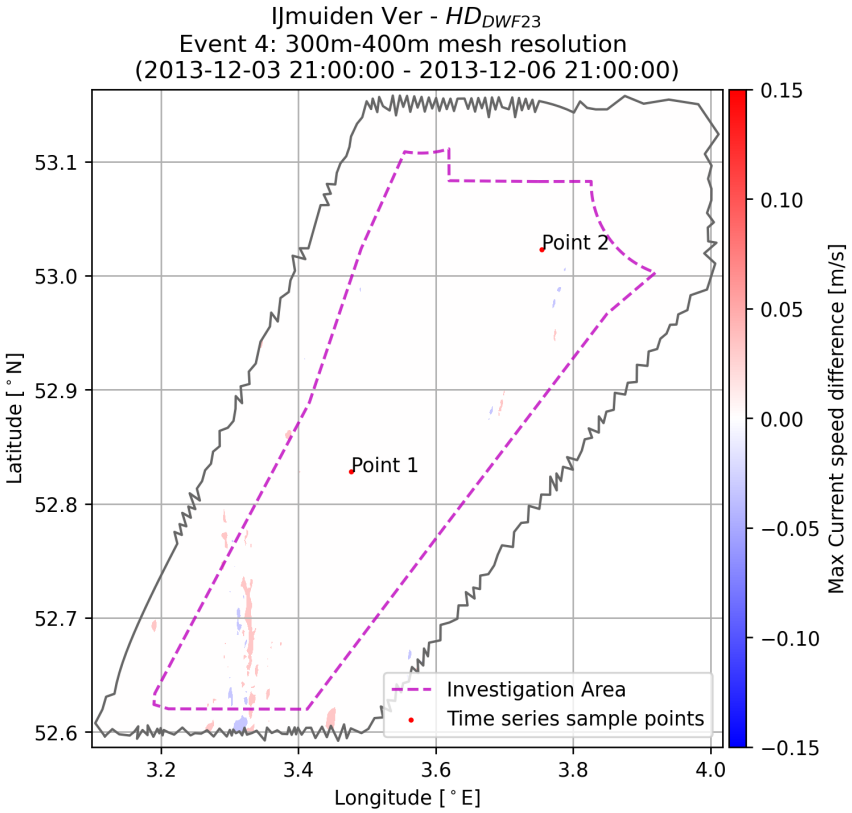

Figure D-18: Difference map of event.

Top: Difference between 200 m and 300 m mesh resolutions
Bottom: Difference between 300 m and 400 m mesh resolutions

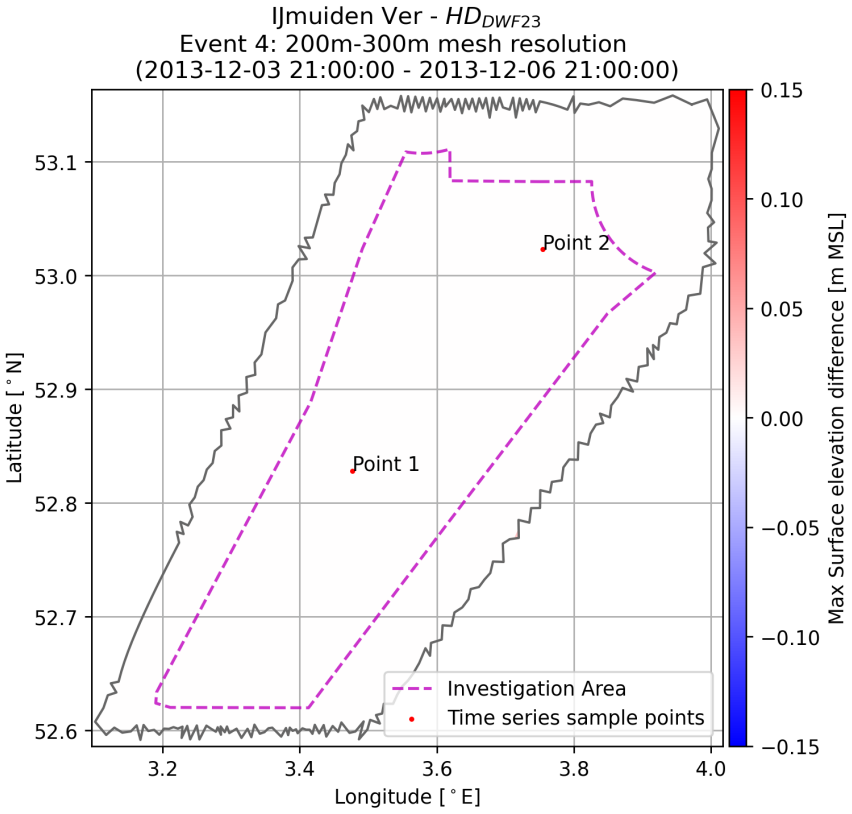

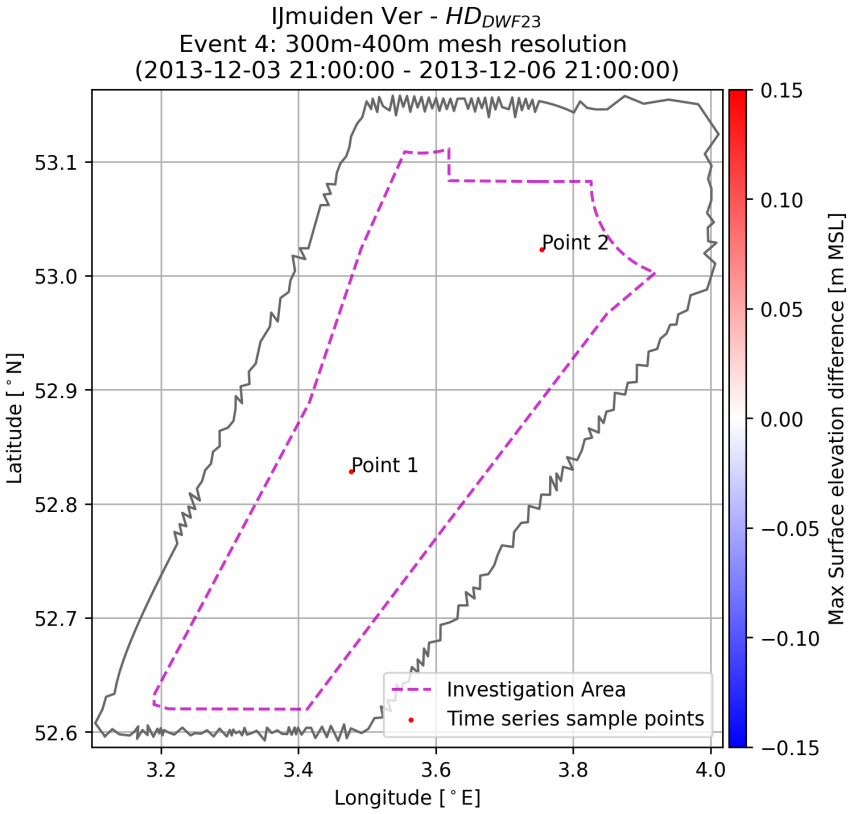

Figure D-19: Difference map of event.

Top: Difference between 200 m and 300 m mesh resolutions
Bottom: Difference between 300 m and 400 m mesh resolutions

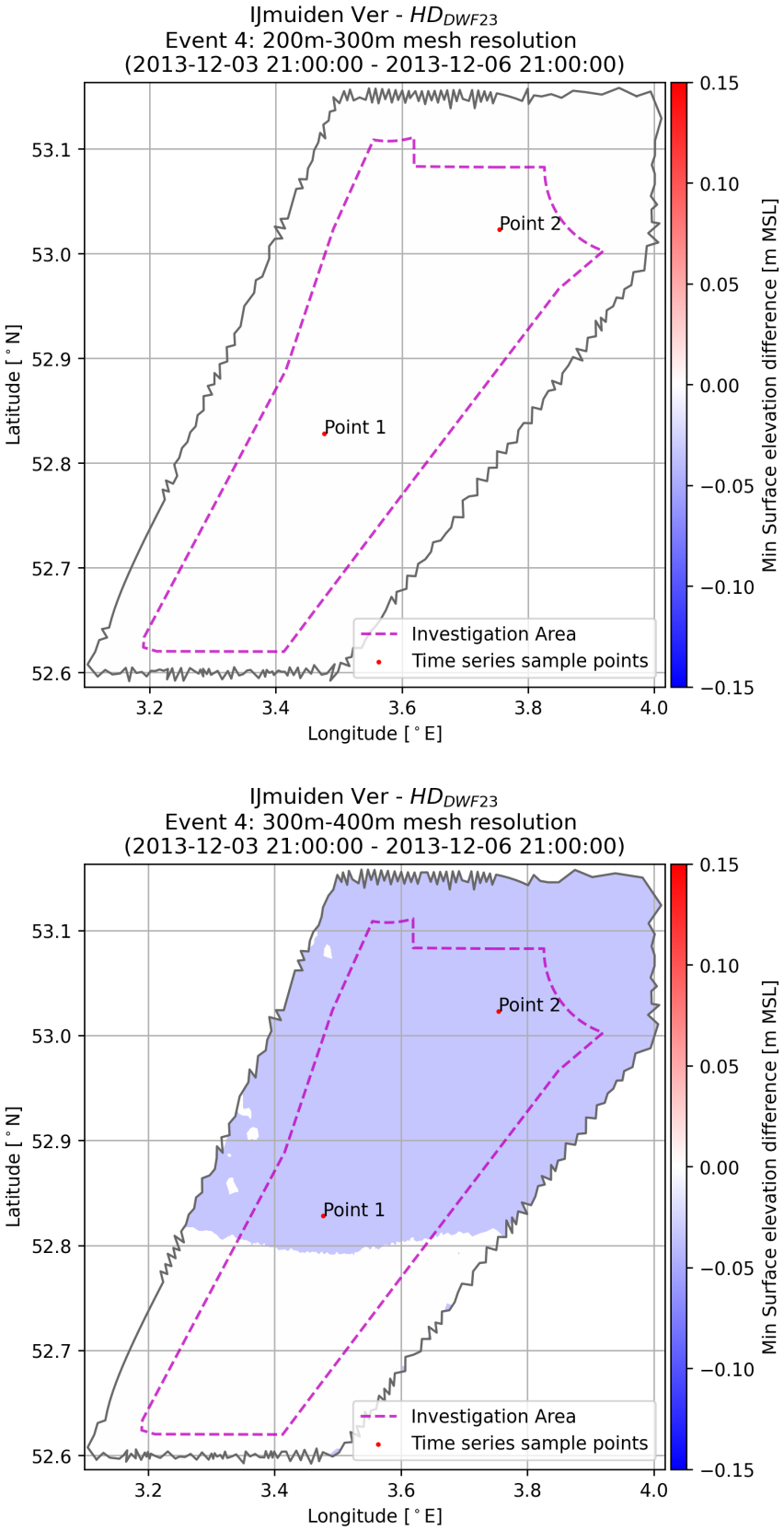

Figure D-20: Difference map of event.

Top: Difference between 200 m and 300 m mesh resolutions
Bottom: Difference between 300 m and 400 m mesh resolutions

Appendix E Hydrodynamic model validation results at all measurement stations

See next pages.

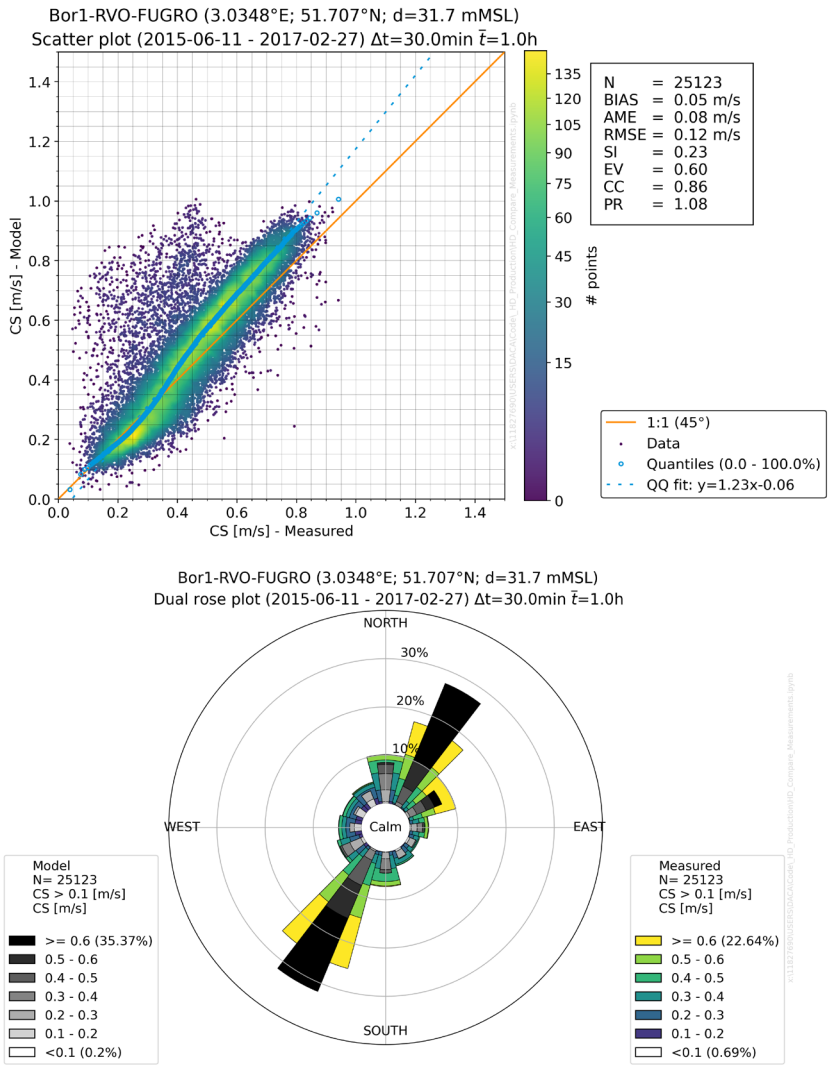

Figure E-1: HD_{DWF23} model validation at station Bor1.
Top figure: Depth-averaged current speed validation results
Bottom figure: Depth-averaged current rose validation results.

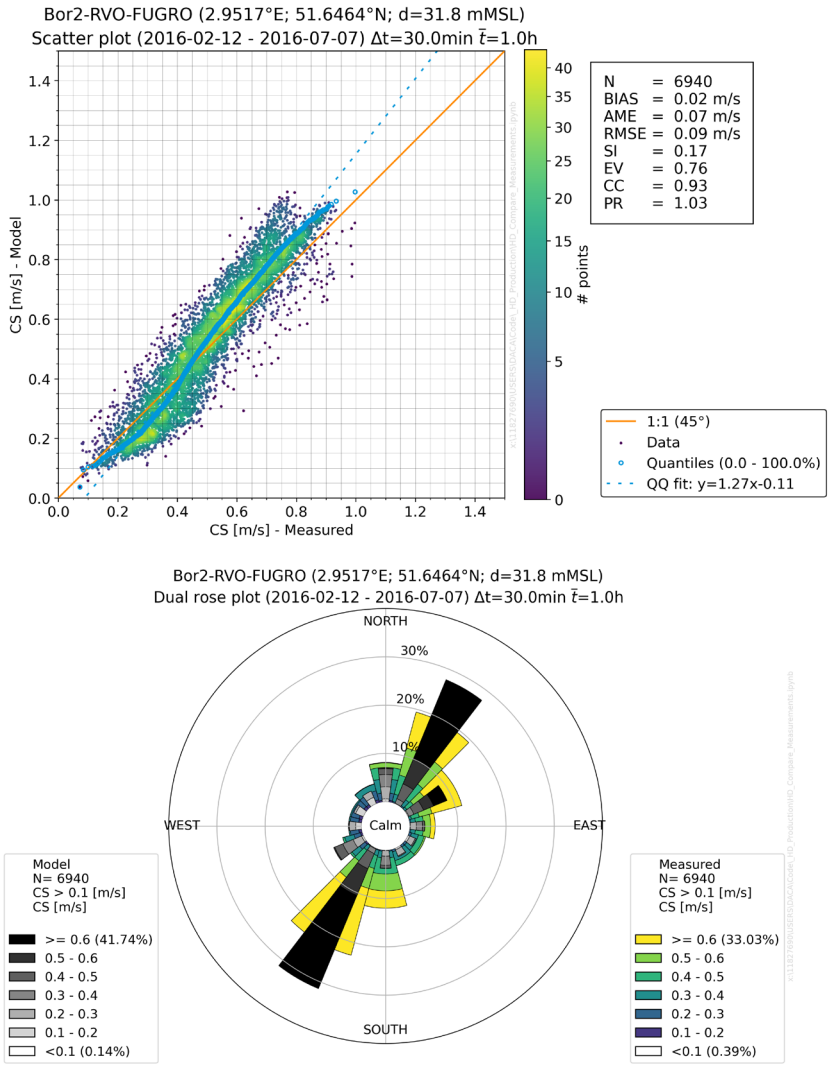

Figure E-2: HD_{DWF23} model validation at station Bor2.
Top figure: Depth-averaged current speed validation results
Bottom figure: Depth-averaged current rose validation results.

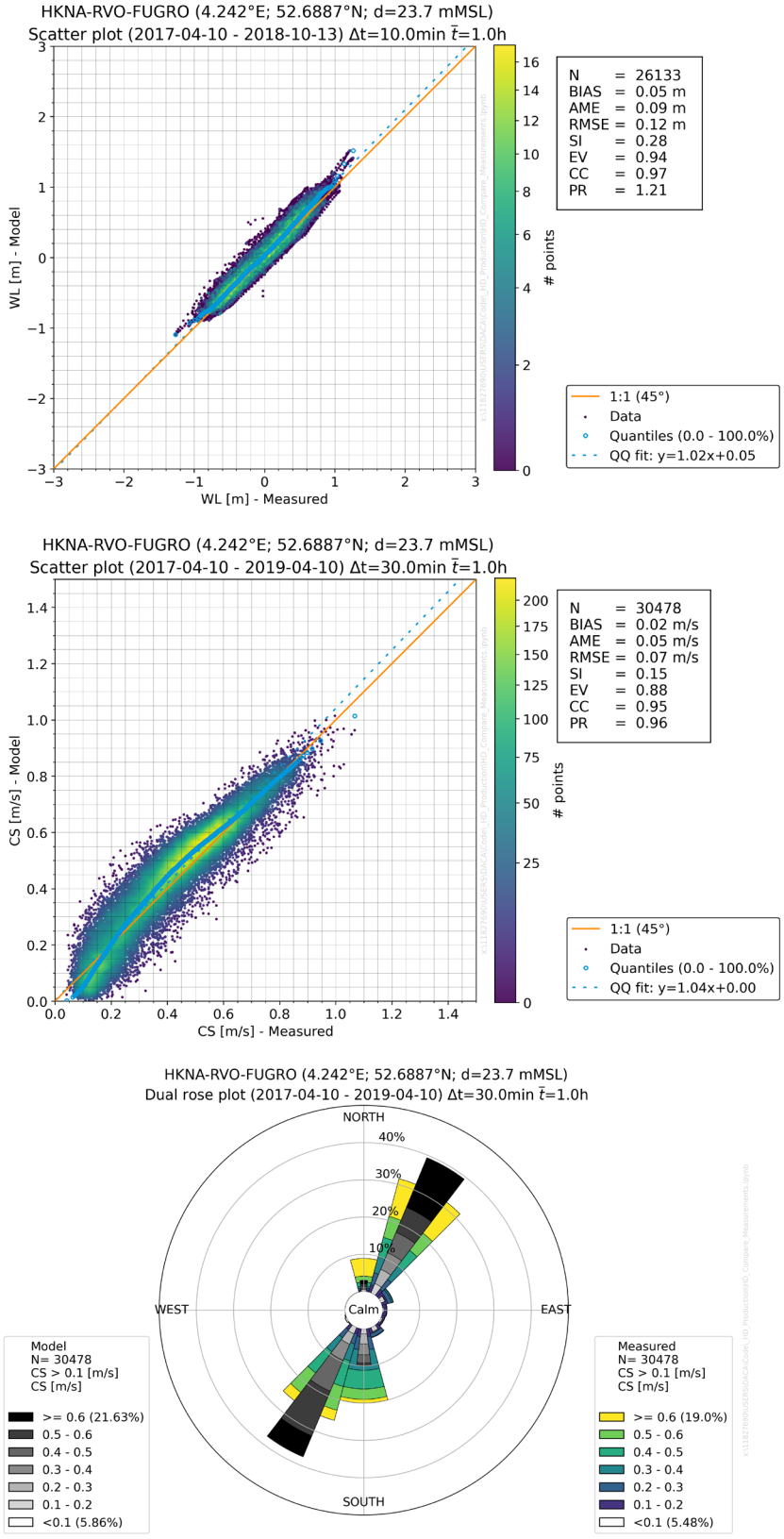

Figure E-3: HD_{DWF23} model validation at station HKNA.

Top figure: Water level validation results
Middle figure: Depth-averaged current speed validation results
Bottom figure: Depth-averaged current rose validation results.

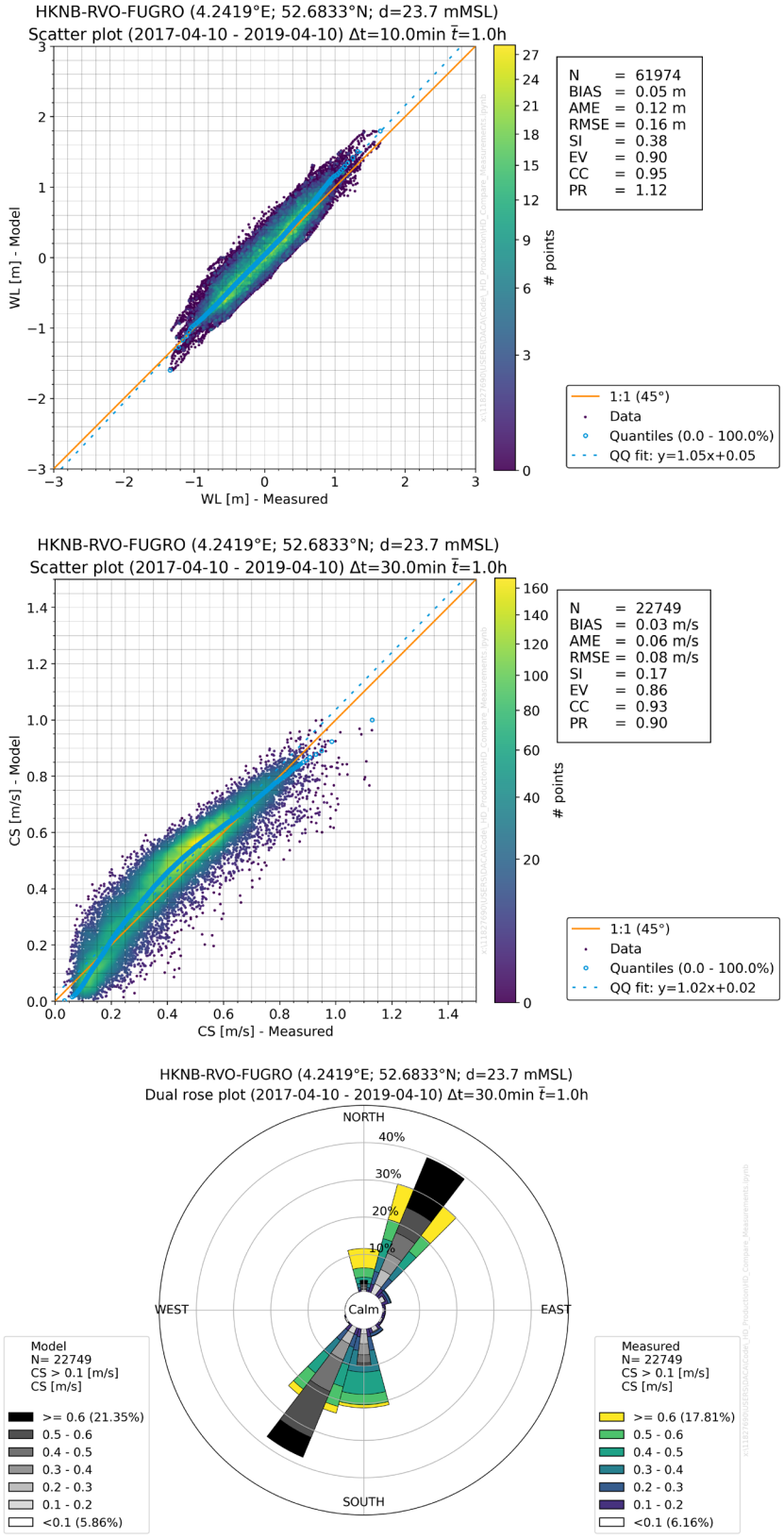

Figure E-4: HD_{DWF23} model validation at station HKNB.

Top figure: Water level validation results
Middle figure: Depth-averaged current speed validation results
Bottom figure: Depth-averaged current rose validation results.

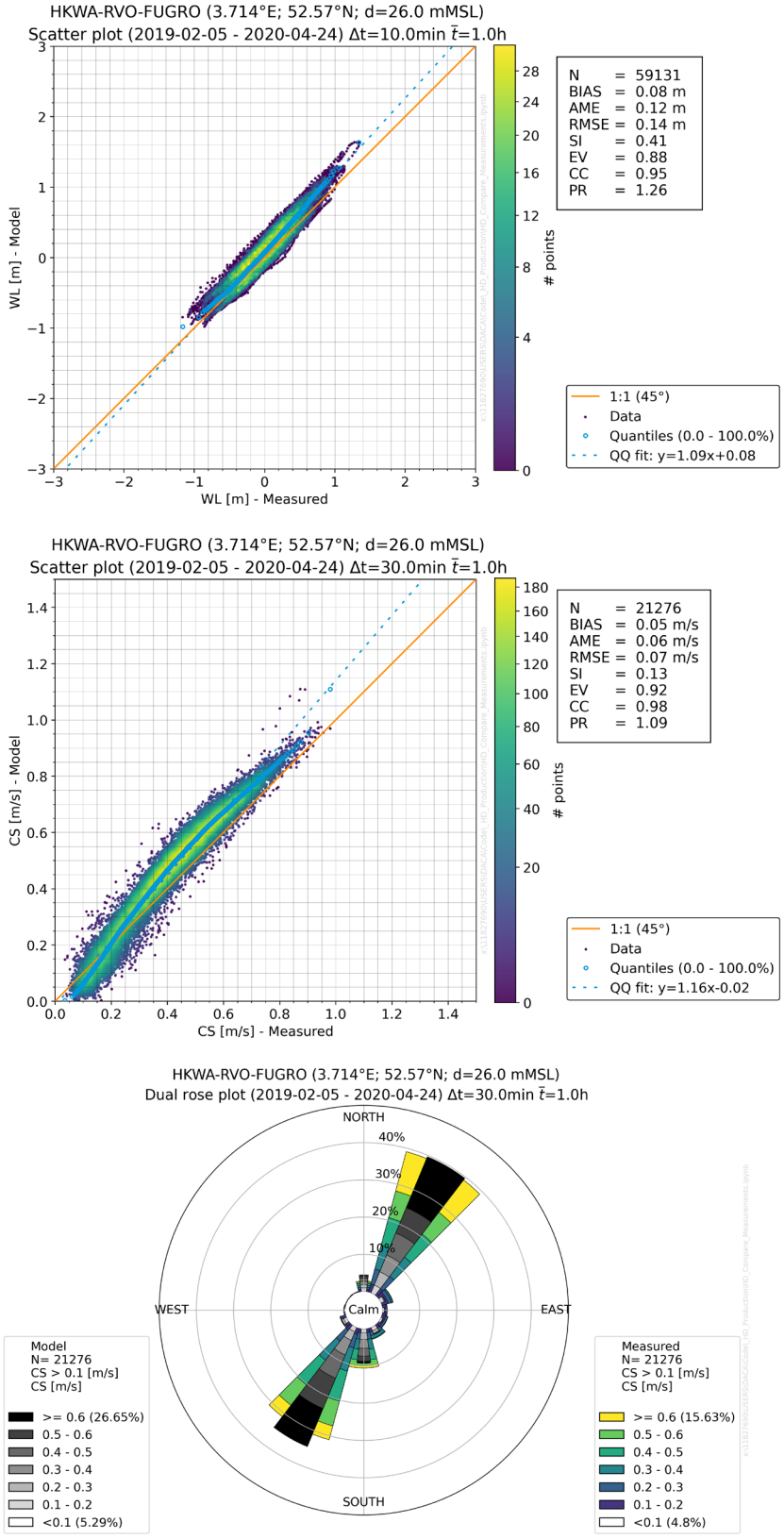

Figure E-5: HD_{DWF23} model validation at station HKWA.

Top figure: Water level validation results
Middle figure: Depth-averaged current speed validation results
Bottom figure: Depth-averaged current rose validation results.

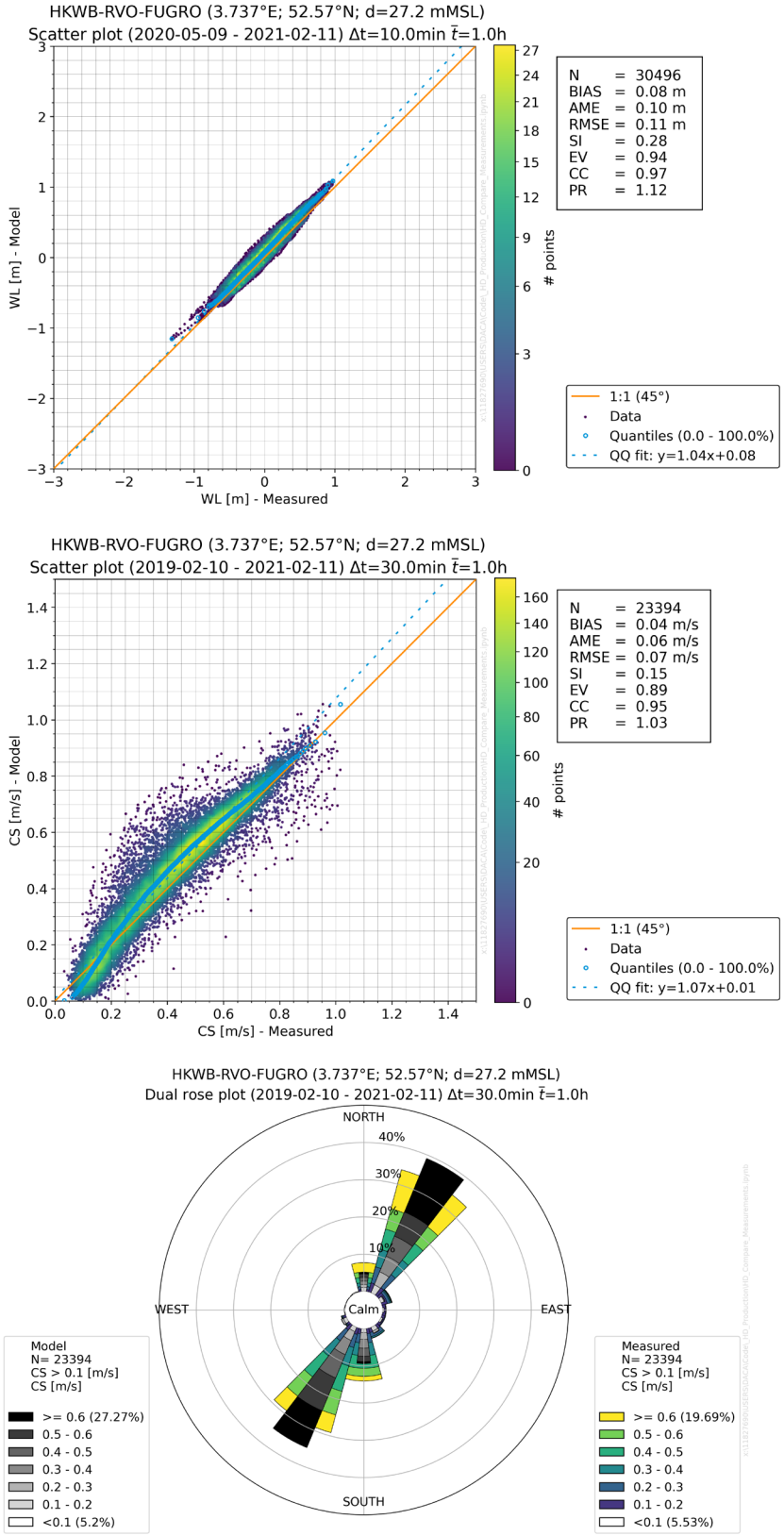

Figure E-6: HD_{DWF23} model validation at station HKWB.

Top figure: Water level validation results
Middle figure: Depth-averaged current speed validation results
Bottom figure: Depth-averaged current rose validation results.

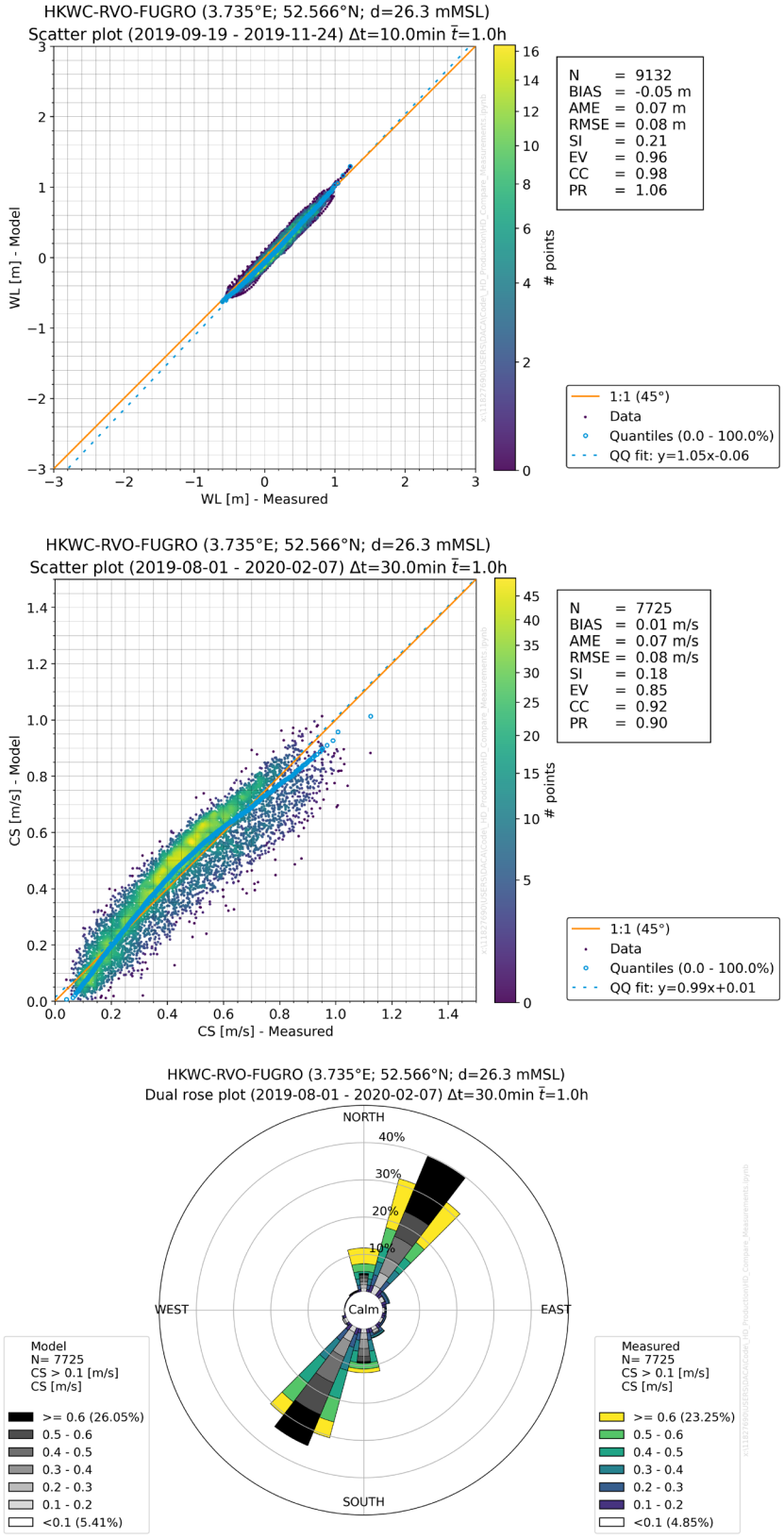

Figure E-7: HD_{DWF23} model validation at station HKWC.

Top figure: Water level validation results
Middle figure: Depth-averaged current speed validation results
Bottom figure: Depth-averaged current rose validation results.

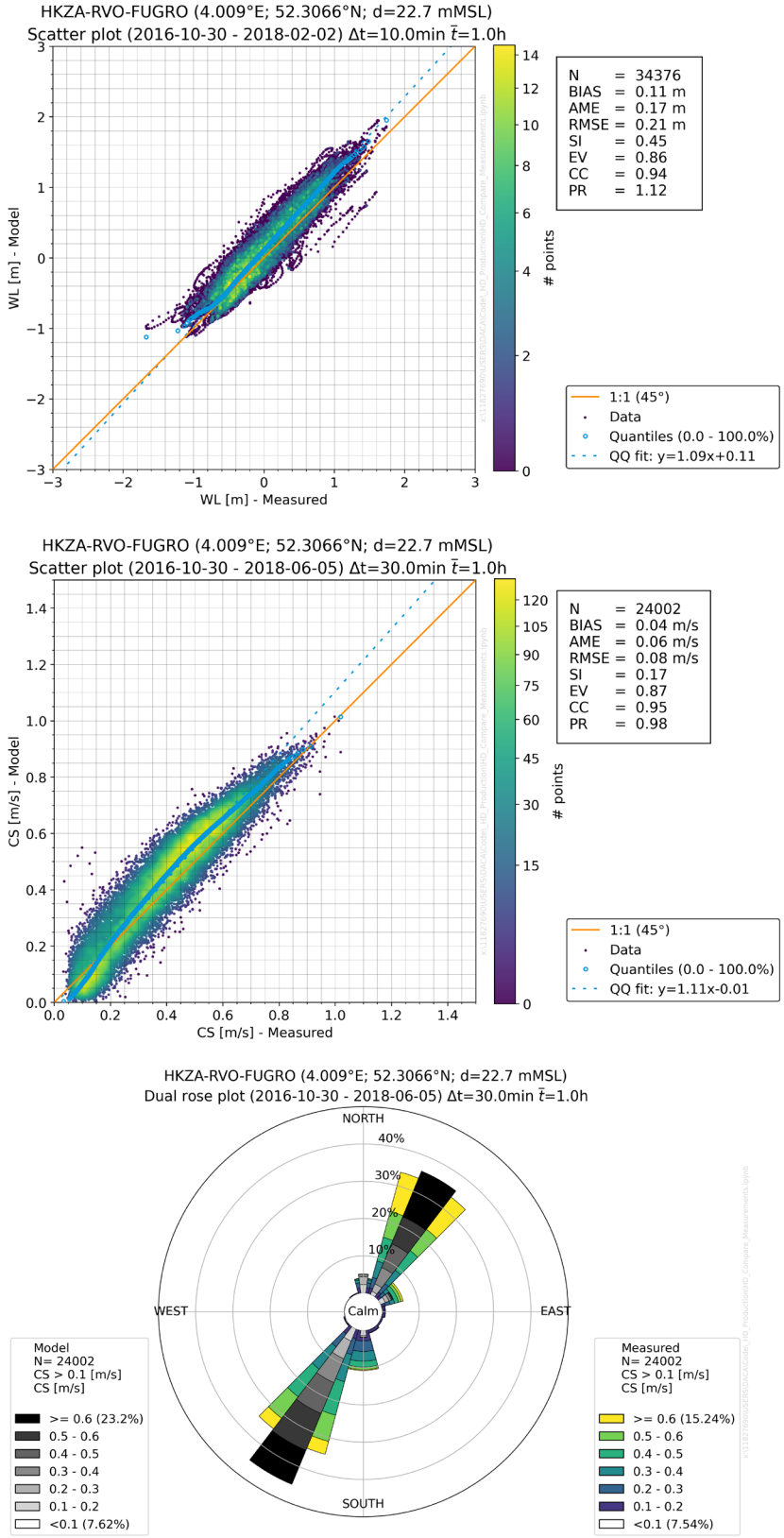

Figure E-8: HD_{DWF23} model validation at station HKZA.

Top figure: Water level validation results
Middle figure: Depth-averaged current speed validation results
Bottom figure: Depth-averaged current rose validation results.

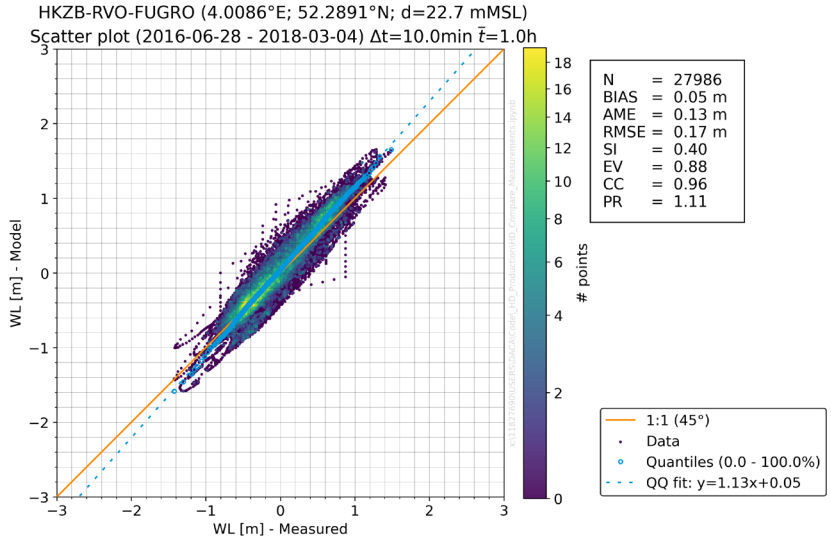

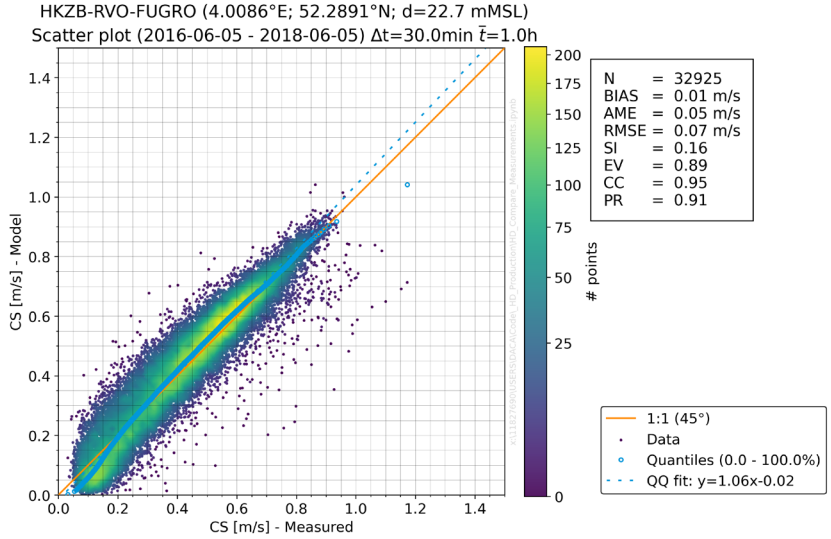

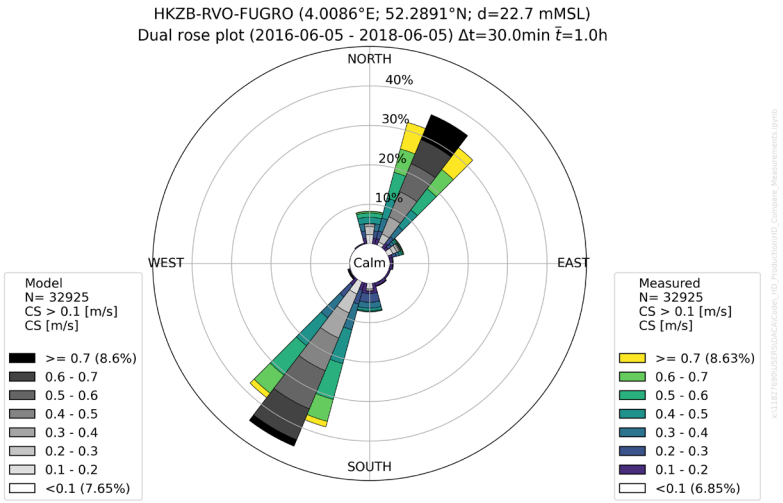

Figure E-9: HD_{DWF23} model validation at station HKZB.

Top figure: Water level validation results
Middle figure: Depth-averaged current speed validation results
Bottom figure: Depth-averaged current rose validation results.

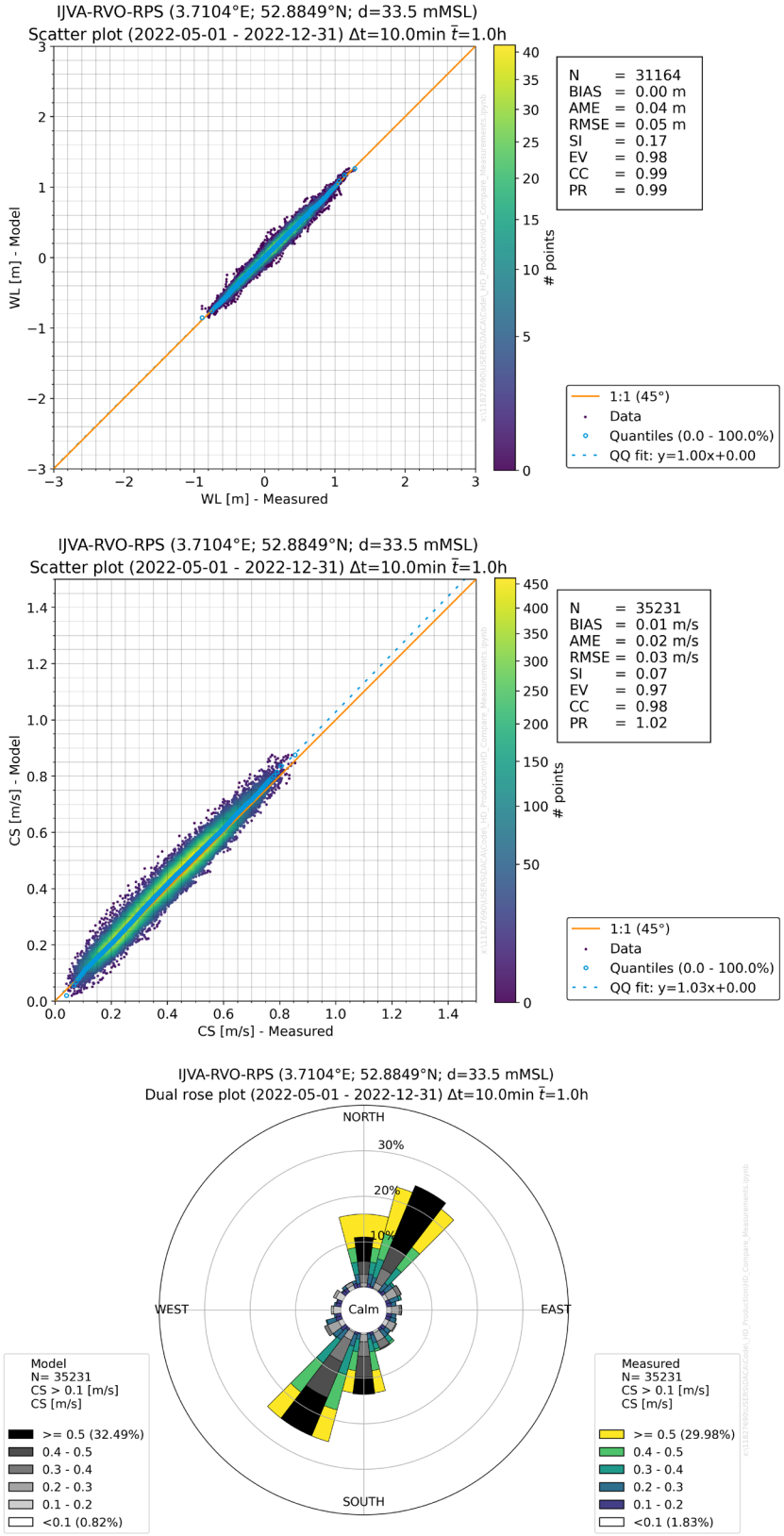

Figure E-10: HD_{DWF23} model validation at station IJVA.

Top figure: Water level validation results
Middle figure: Depth-averaged current speed validation results
Bottom figure: Depth-averaged current rose validation results.

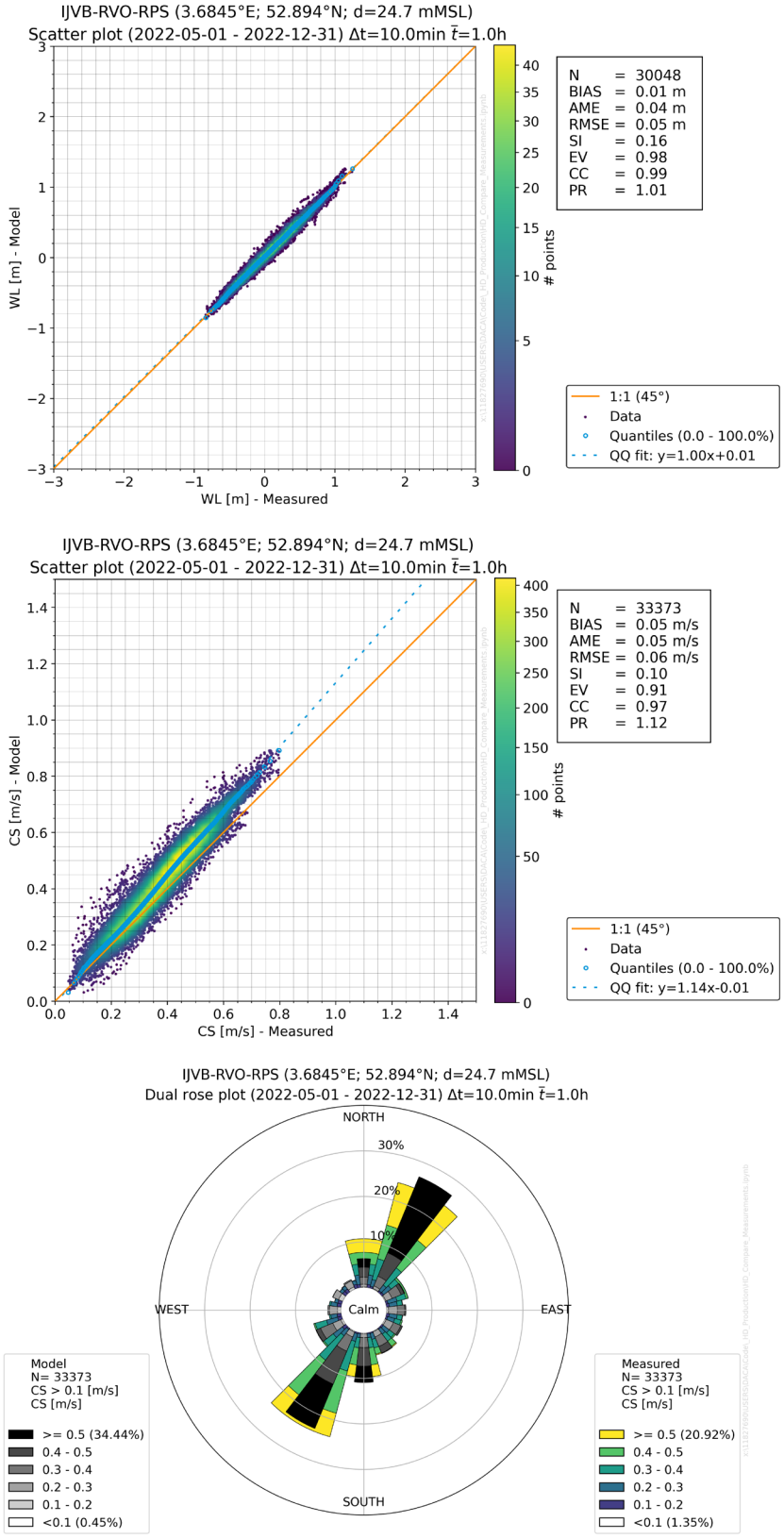

Figure E-11: HD_{DWF23} model validation at station IJVB.

Top figure: Water level validation results
Middle figure: Depth-averaged current speed validation results
Bottom figure: Depth-averaged current rose validation results.

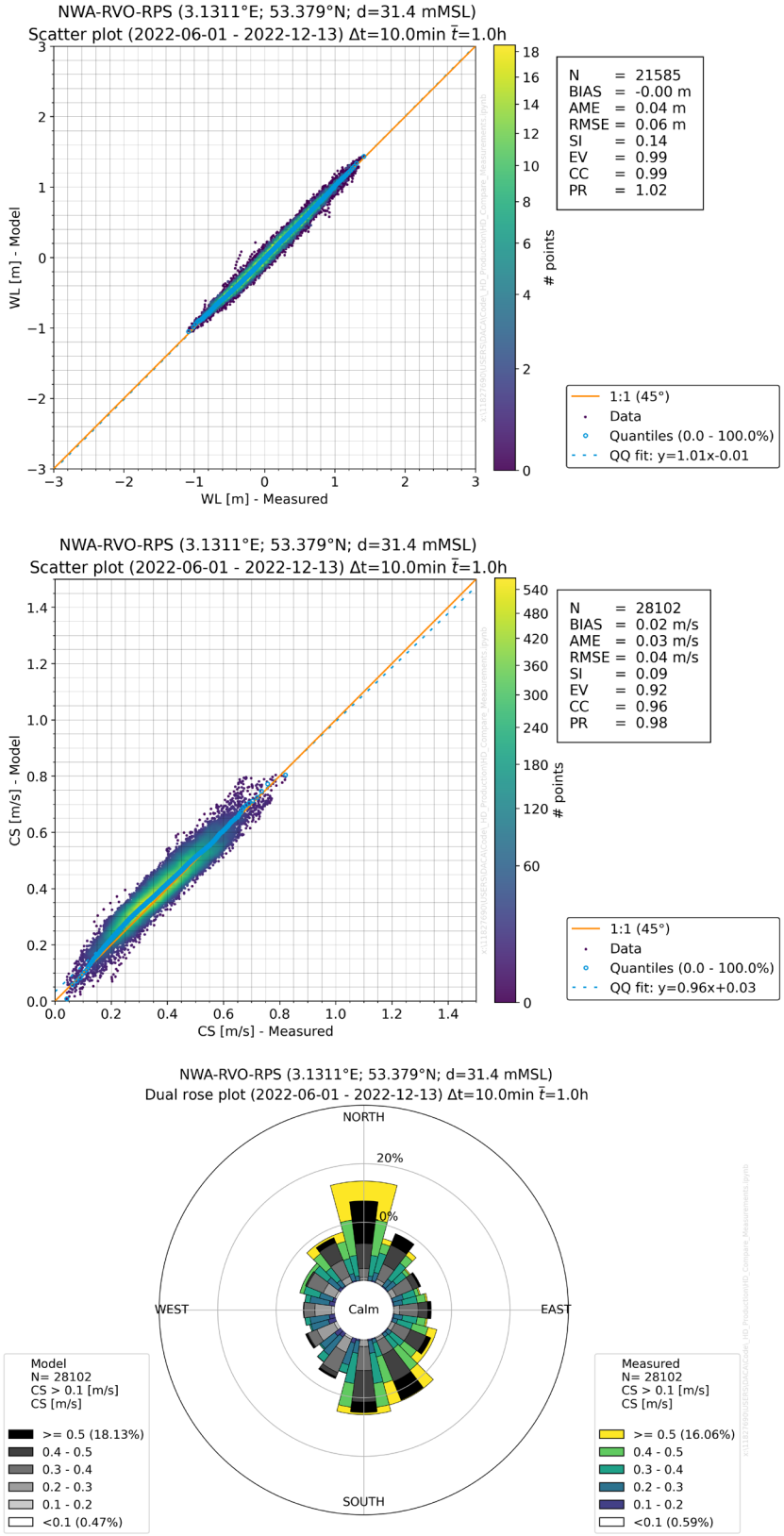

Figure E-12: HD_{DWF23} model validation at station NWA.

Top figure: Water level validation results
Middle figure: Depth-averaged current speed validation results
Bottom figure: Depth-averaged current rose validation results.

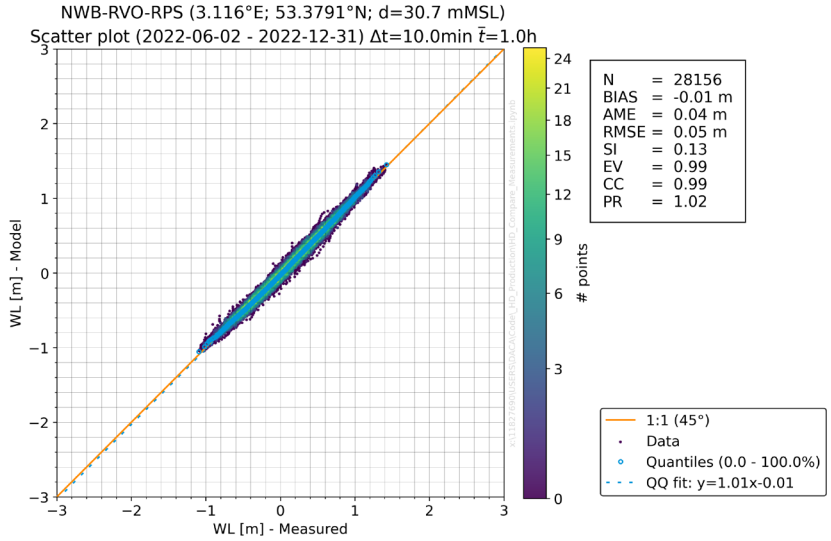

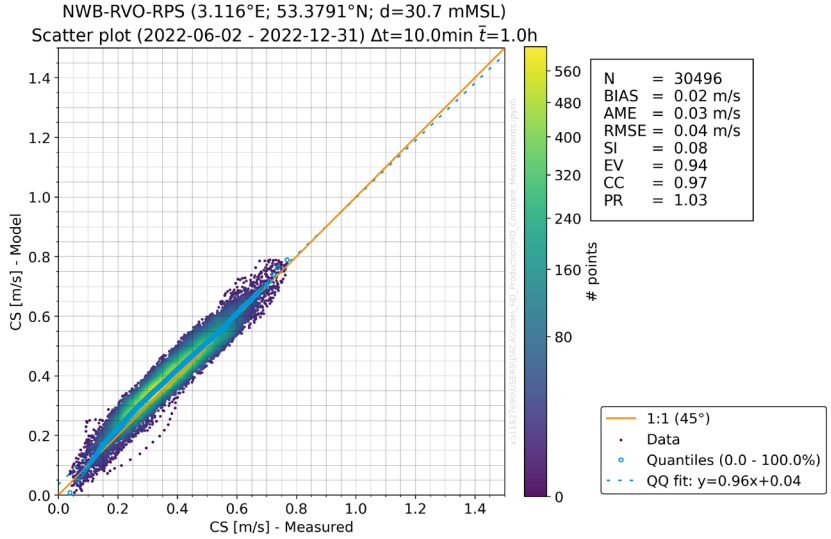

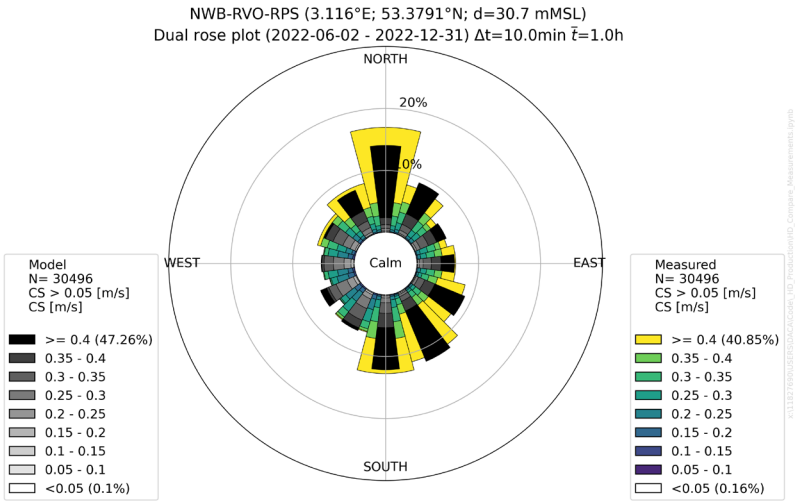

Figure E-13: HD_{DWF23} model validation at station NWB.

Top figure: Water level validation results
Middle figure: Depth-averaged current speed validation results
Bottom figure: Depth-averaged current rose validation results.

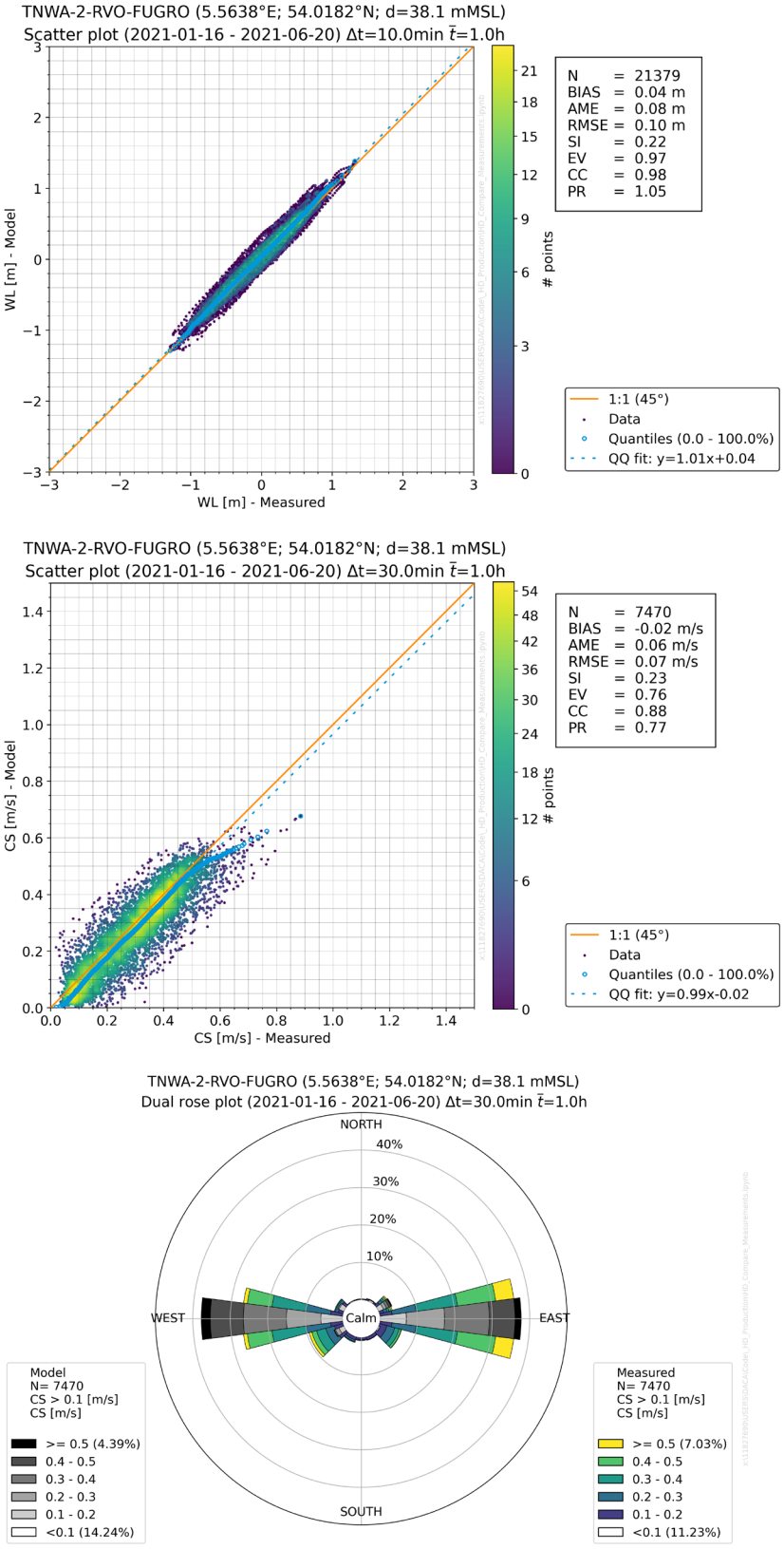

Figure E-14: HD_{DWF23} model validation at station TNWA-2.
Top figure: Water level validation results
Middle figure: Depth-averaged current speed validation results
Bottom figure: Depth-averaged current rose validation results.

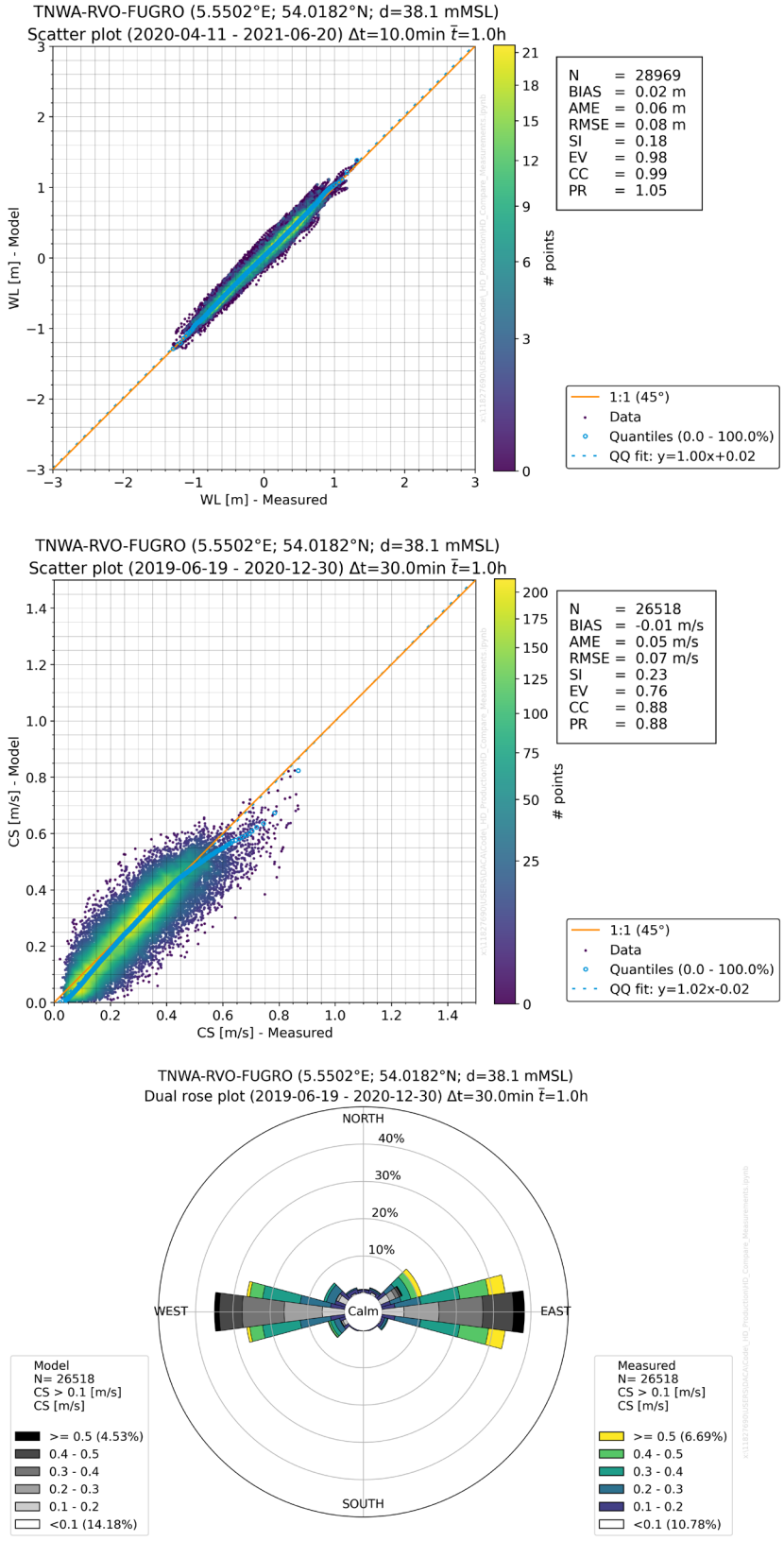

Figure E-15: HD_{DWF23} model validation at station TNWA.

Top figure: Water level validation results
Middle figure: Depth-averaged current speed validation results
Bottom figure: Depth-averaged current rose validation results.

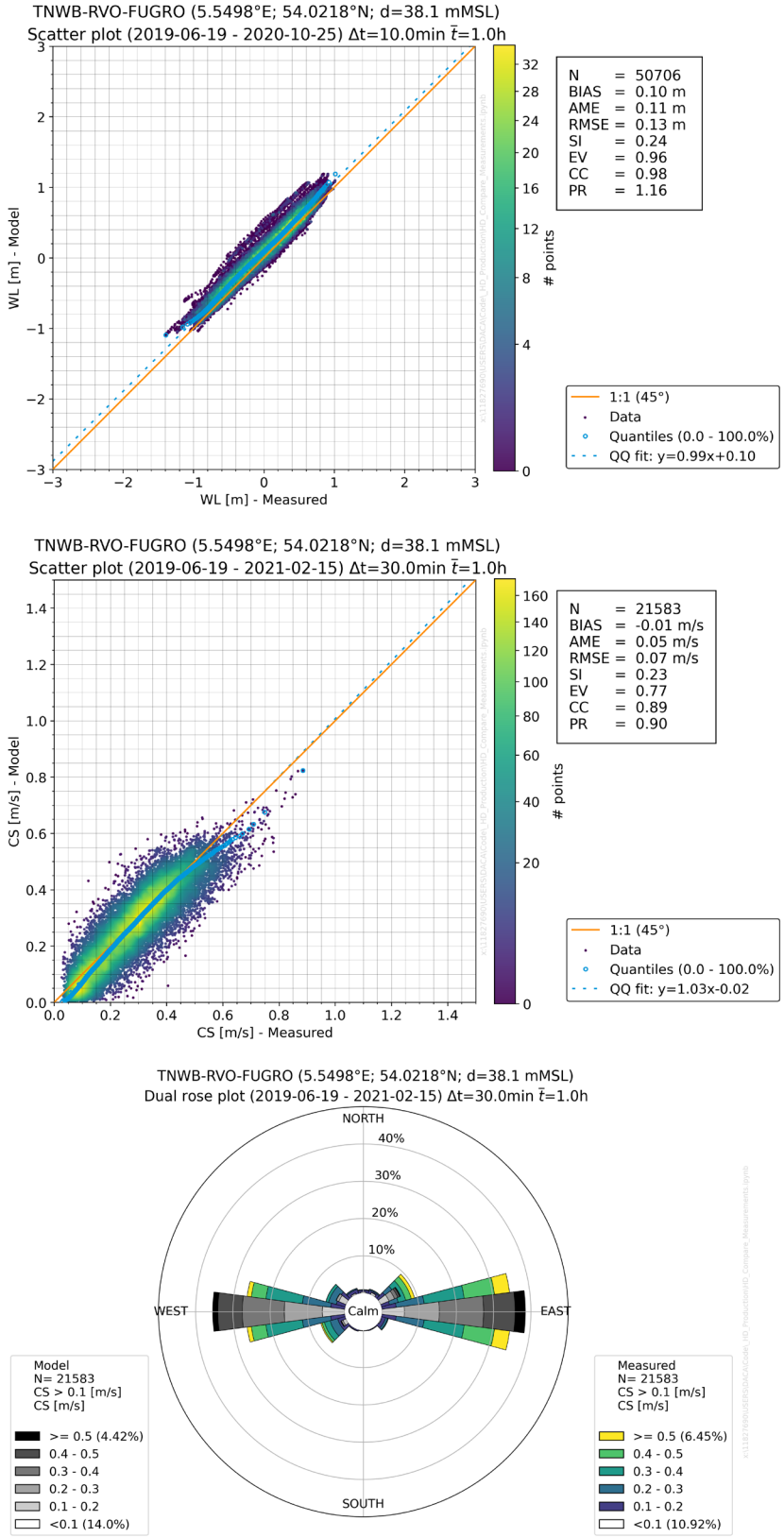

Figure E-16: HD_{DWF23} model validation at station TNWB.
Top figure: Water level validation results
Middle figure: Depth-averaged current speed validation results
Bottom figure: Depth-averaged current rose validation results.

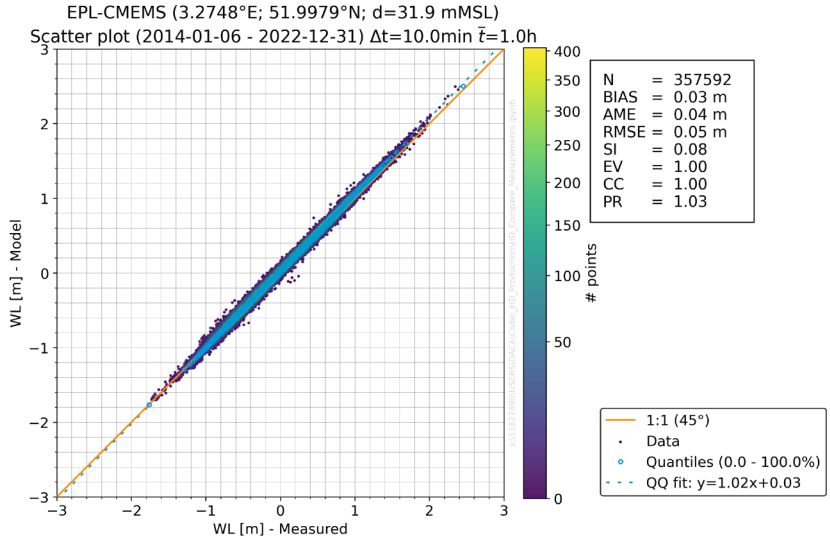

Figure E-17: HD_{DWF23} model validation at station EPL.
Water level validation results

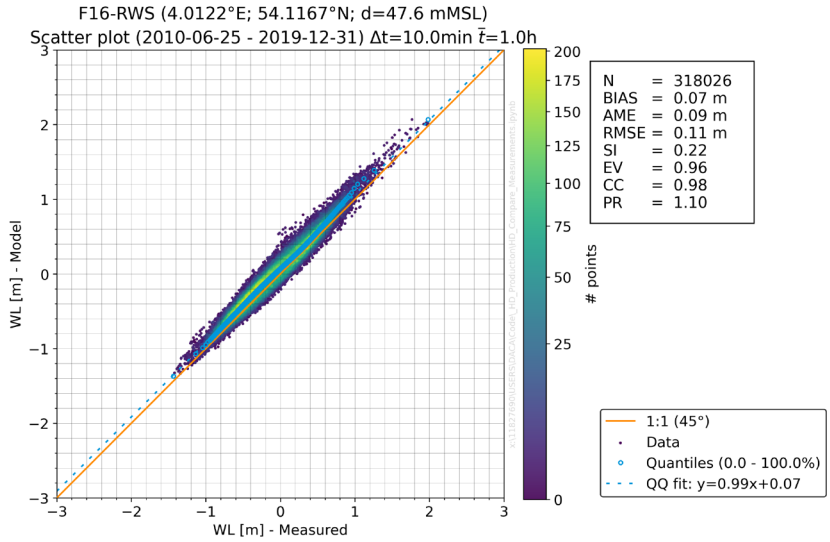

Figure E-18: HD_{DWF23} model validation at station F16.
Water level validation results

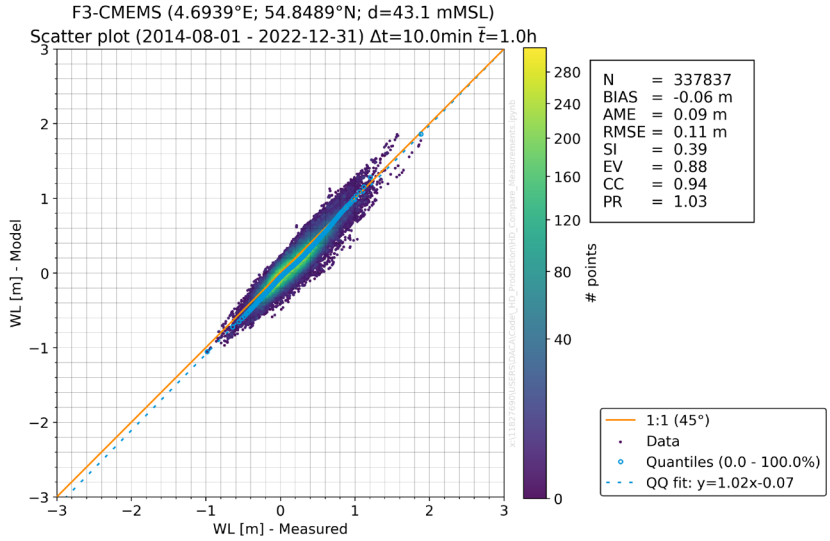

Figure E-19: HD_{DWF23} model validation at station F3.
Water level validation results

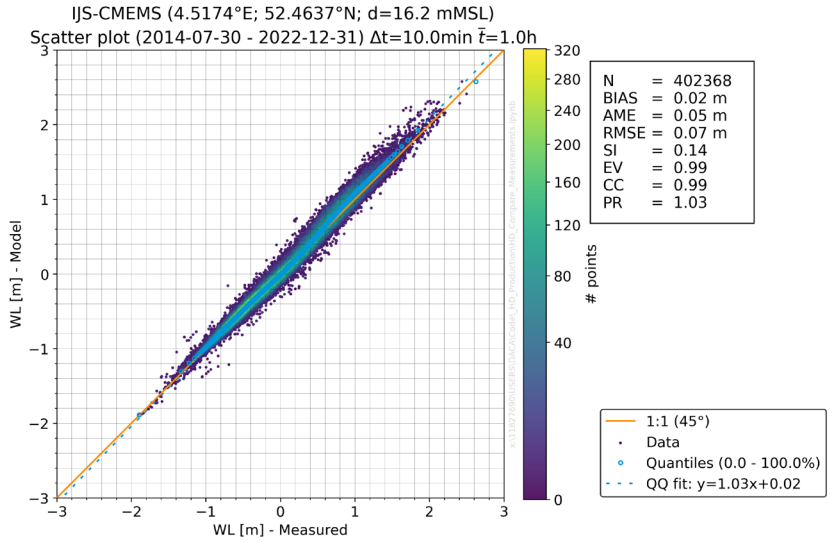

Figure E-20: HD_{DWF23} model validation at station IJS.
Water level validation results

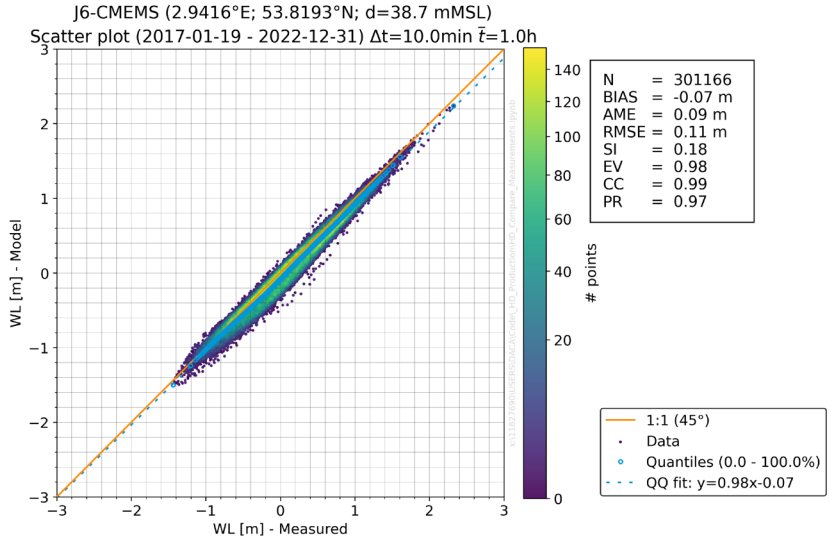

Figure E-21: HD_{DWF23} model validation at station J6.
Water level validation results

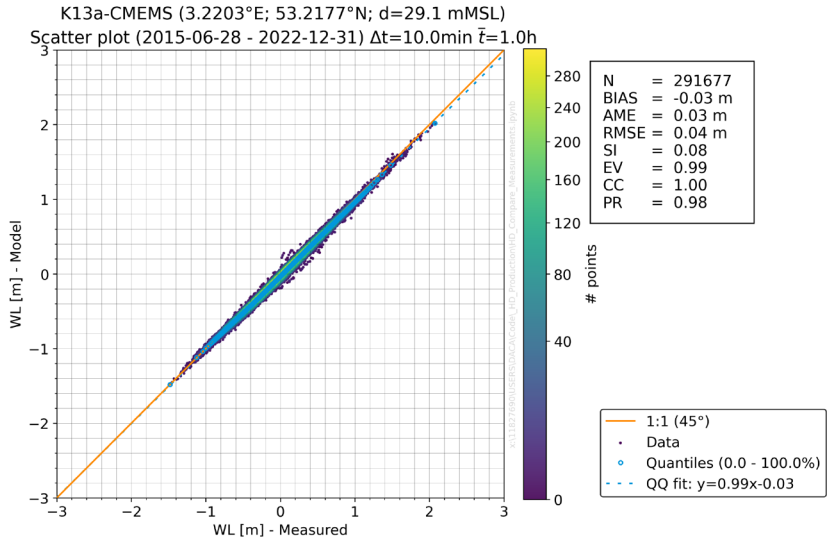

Figure E-22: HD_{DWF23} model validation at station K13a.
Water level validation results

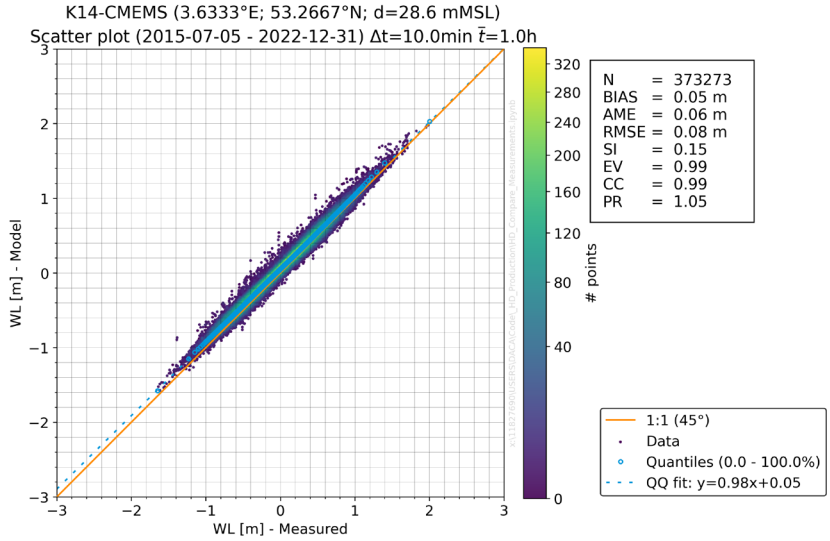

Figure E-23: HD_{DWF23} model validation at station K14.
Water level validation results

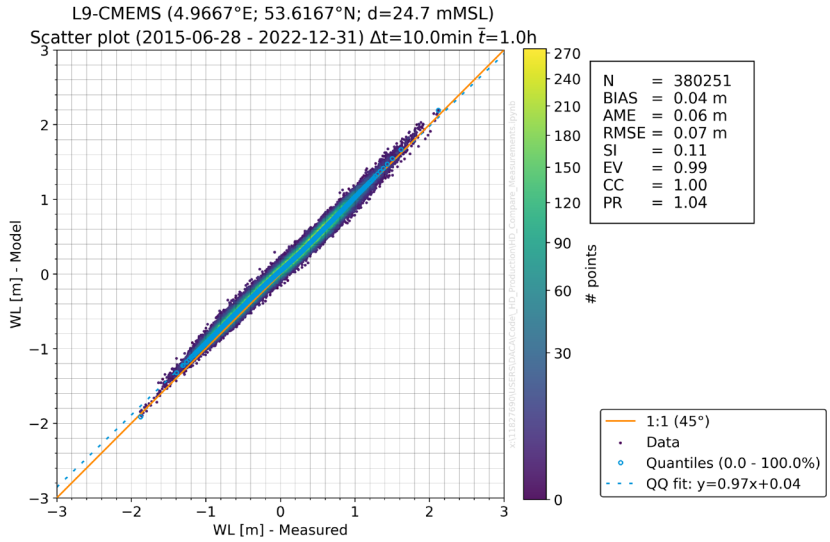

Figure E-24: HD_{DWF23} model validation at station L9.
Water level validation results

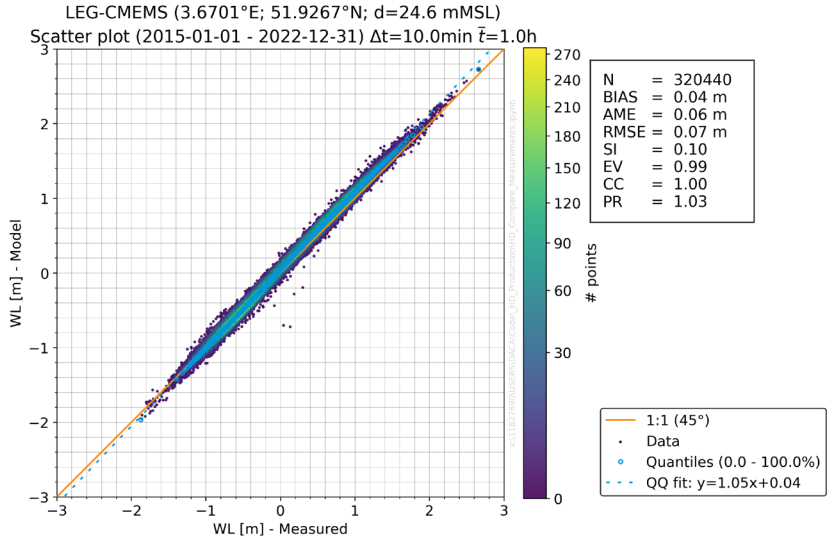

Figure E-25: HD_{DWF23} model validation at station LEG.
Water level validation results

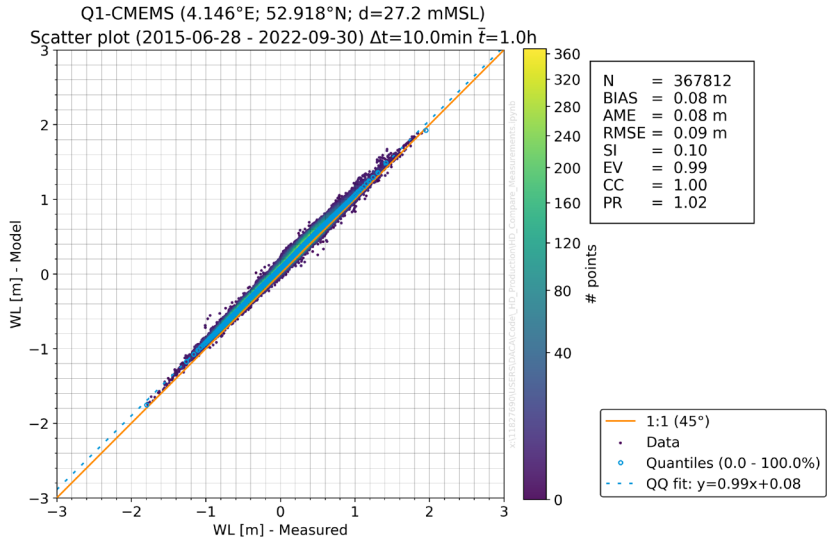

Figure E-26: HD_{DWF23} model validation at station Q1.
Water level validation results

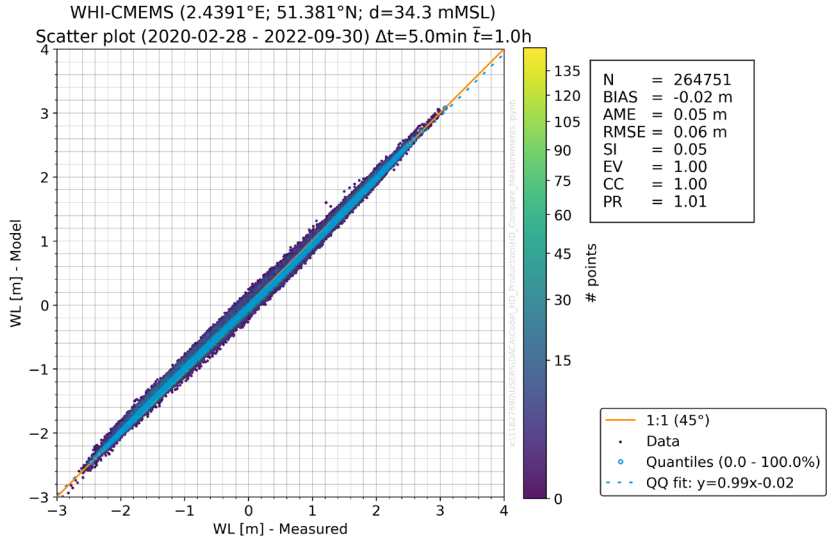

Figure E-27: HD_{DWF23} model validation at station WHI.
Water level validation results

Appendix F Spectral wave model mesh convergence results

See next pages.

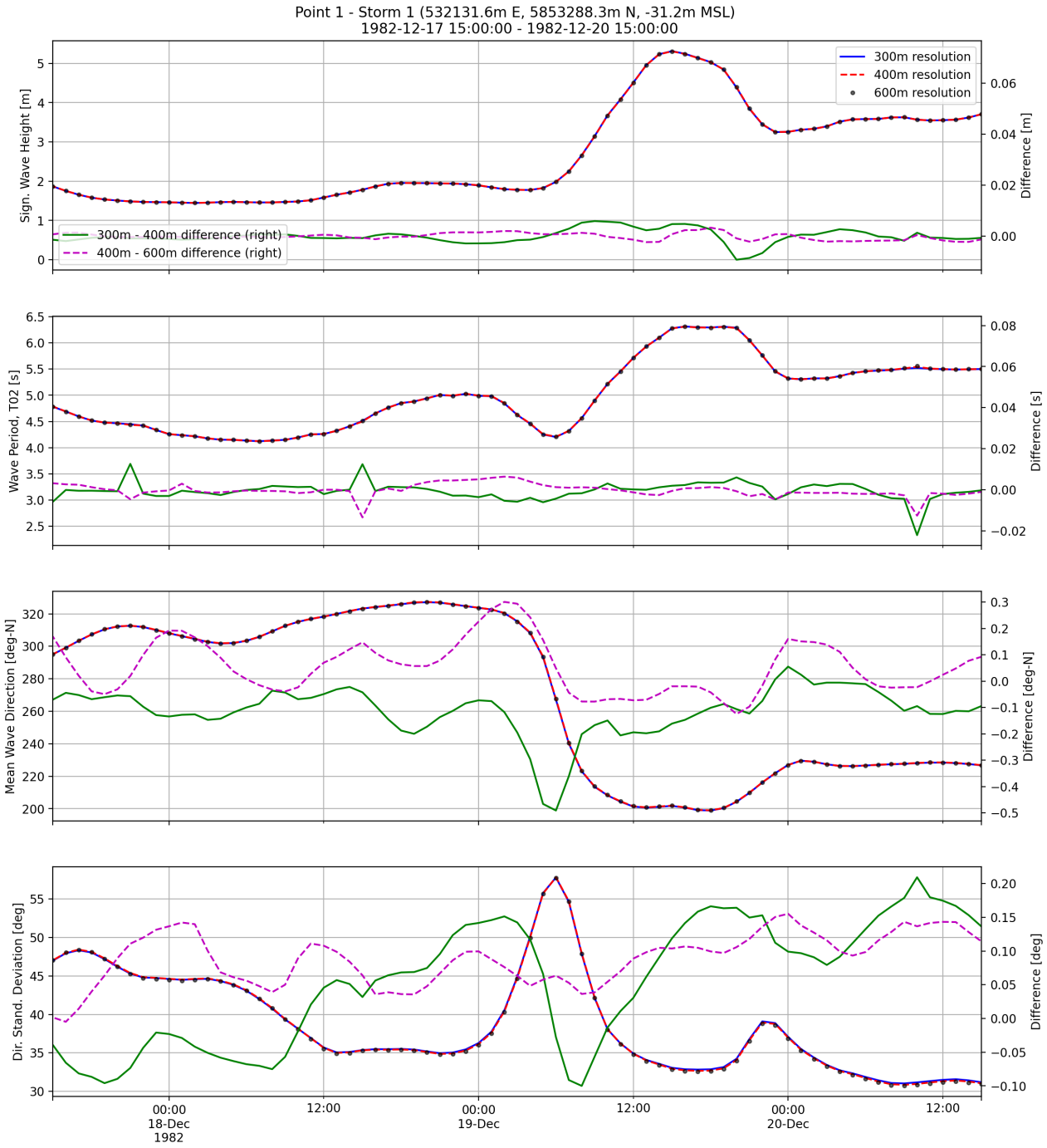

Figure F-1: Time series comparison of Hm0, T02, MWD, and DSD between 300m, 400m and 600m mesh resolutions (SW model) during Storm 1 at Point 1.
Absolute values are shown on the left axis (black, blue, and red lines), and time series difference between 300-400m and 400-600m is shown on the right axis (green and magenta lines).

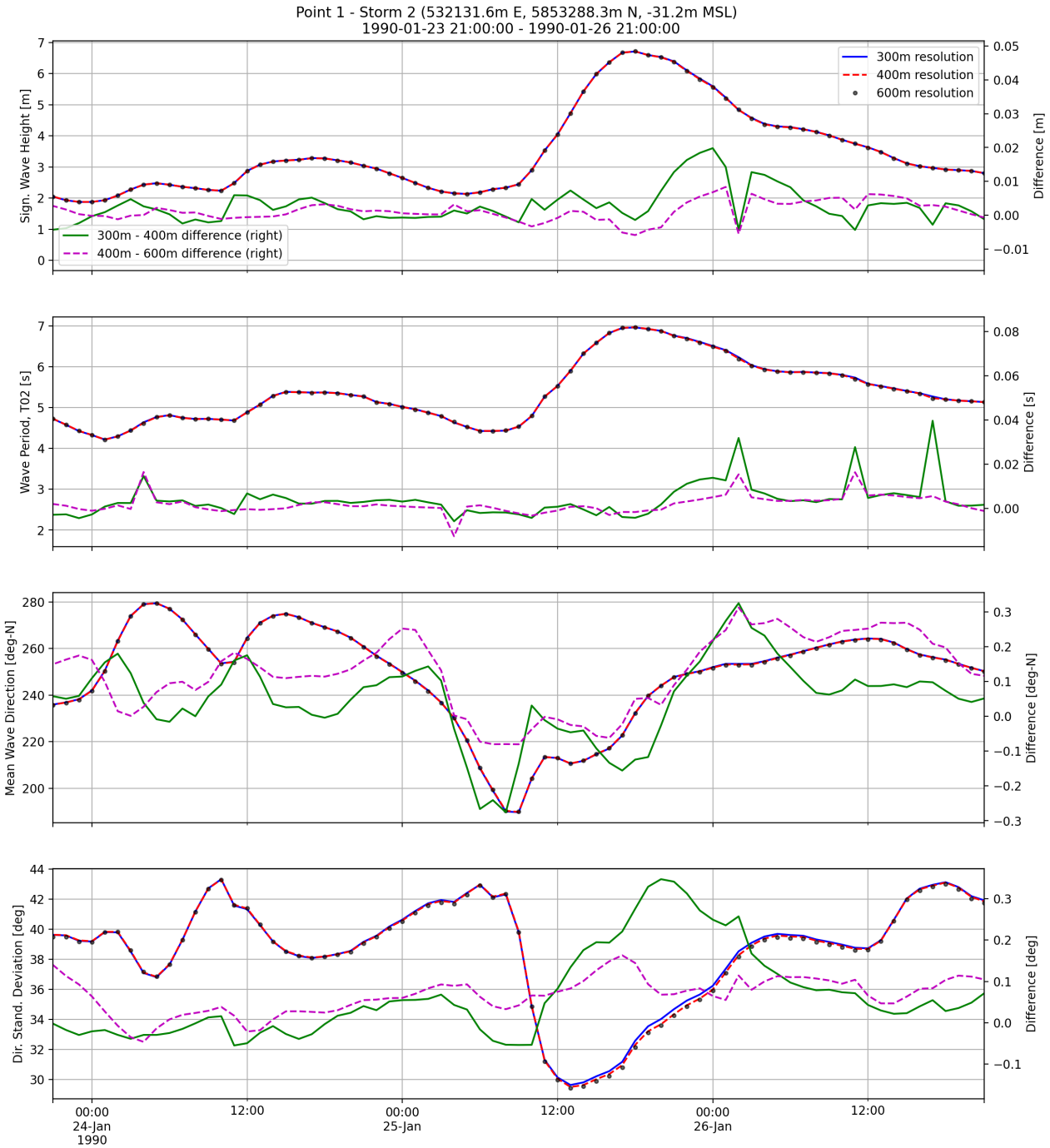

Figure F-2: Time series comparison of Hm0, T02, MWD, and DSD between 300m, 400m and 600m mesh resolutions (SW model) during Storm 2 at Point 1.

Absolute values are shown on the left axis (black, blue, and red lines), and time series difference between 300-400m and 400-600m is shown on the right axis (green and magenta lines).

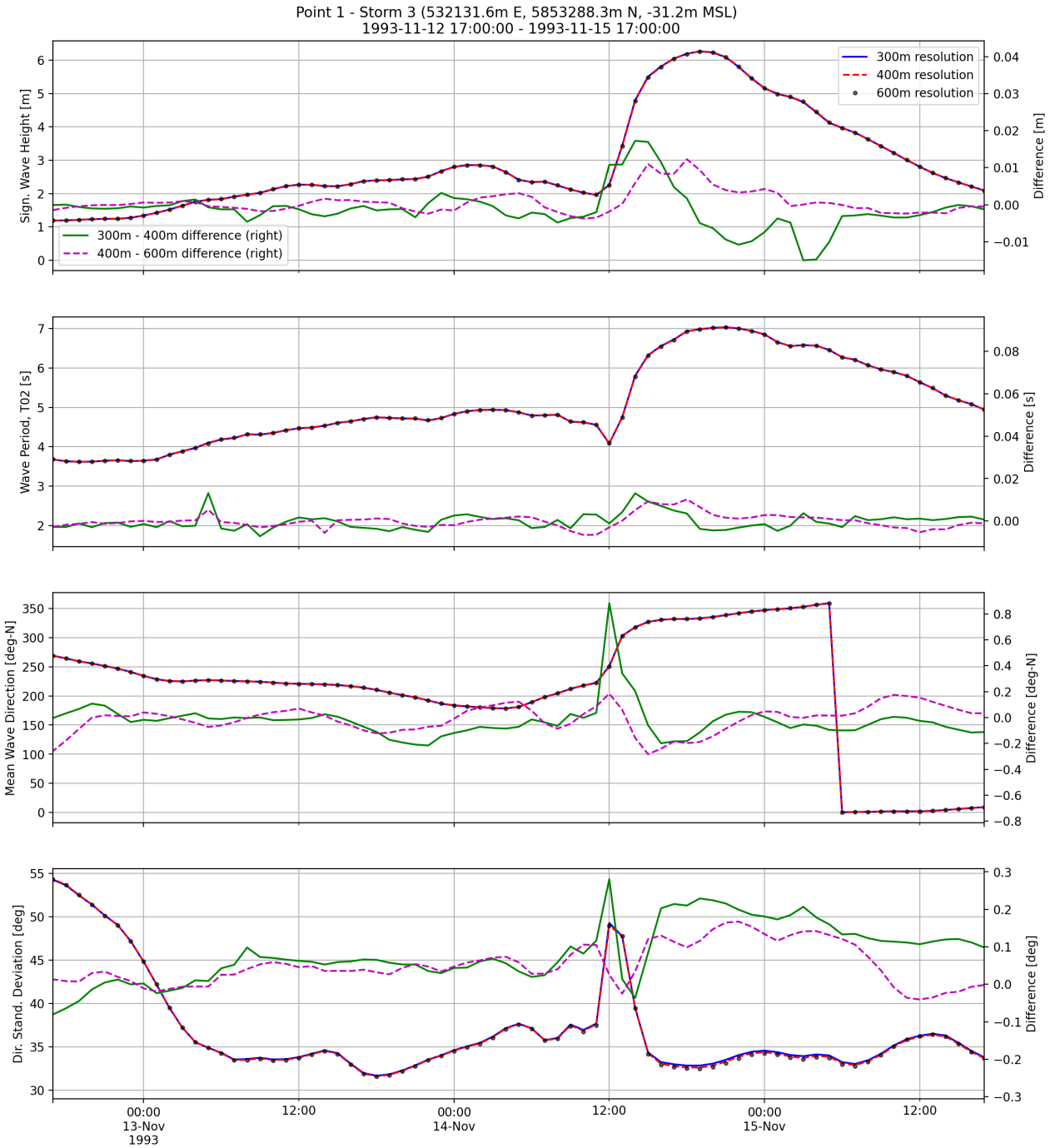

Figure F-3: Time series comparison of Hm0, T02, MWD, and DSD between 300m, 400m and 600m mesh resolutions (SW model) during Storm 3 at Point 1.

Absolute values are shown on the left axis (black, blue, and red lines), and time series difference between 300-400m and 400-600m is shown on the right axis (green and magenta lines).

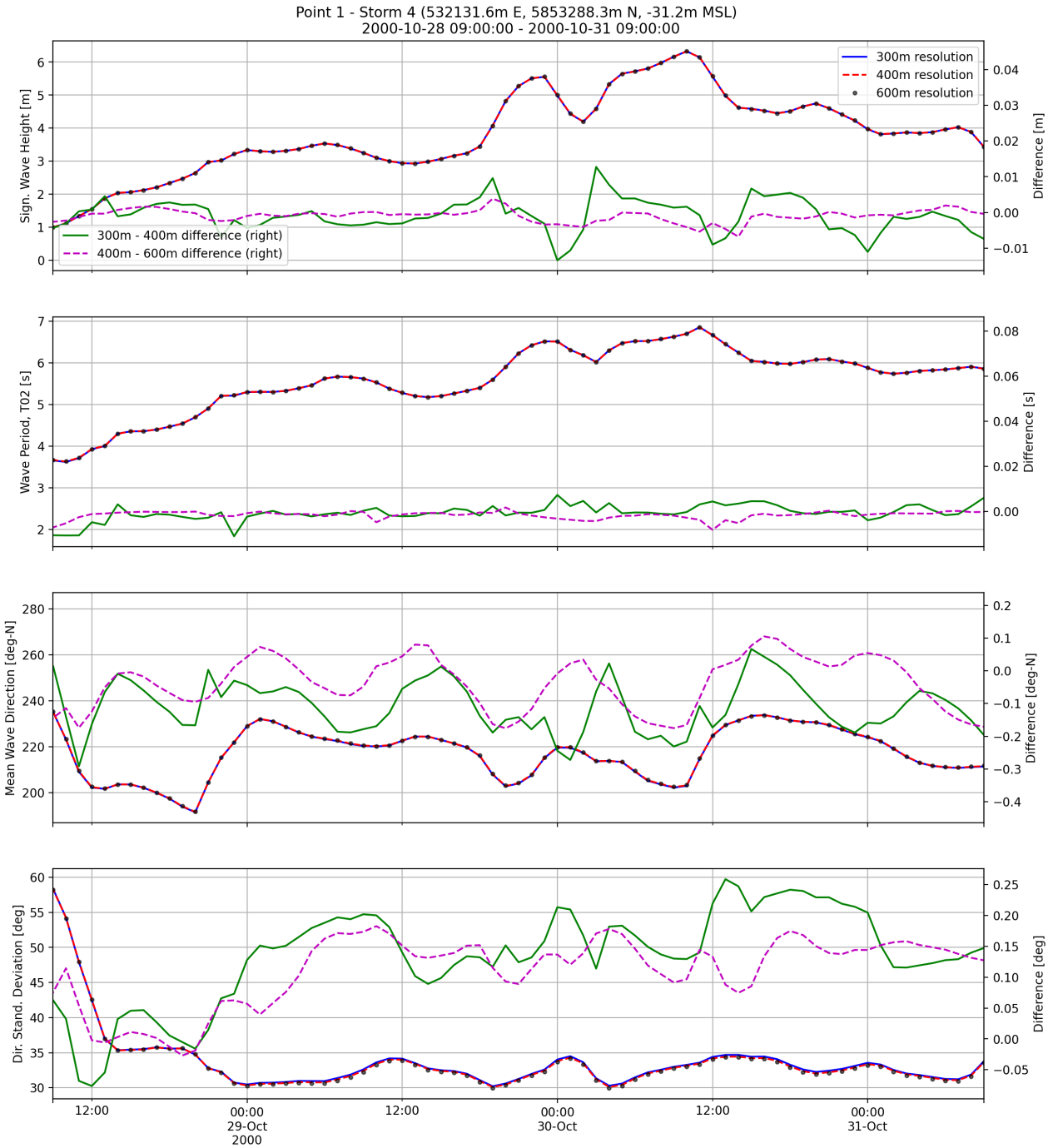

Figure F-4: Time series comparison of Hm0, T02, MWD, and DSD between 300m, 400m and 600m mesh resolutions (SW model) during Storm 4 at Point 1.

Absolute values are shown on the left axis (black, blue, and red lines), and time series difference between 300-400m and 400-600m is shown on the right axis (green and magenta lines).

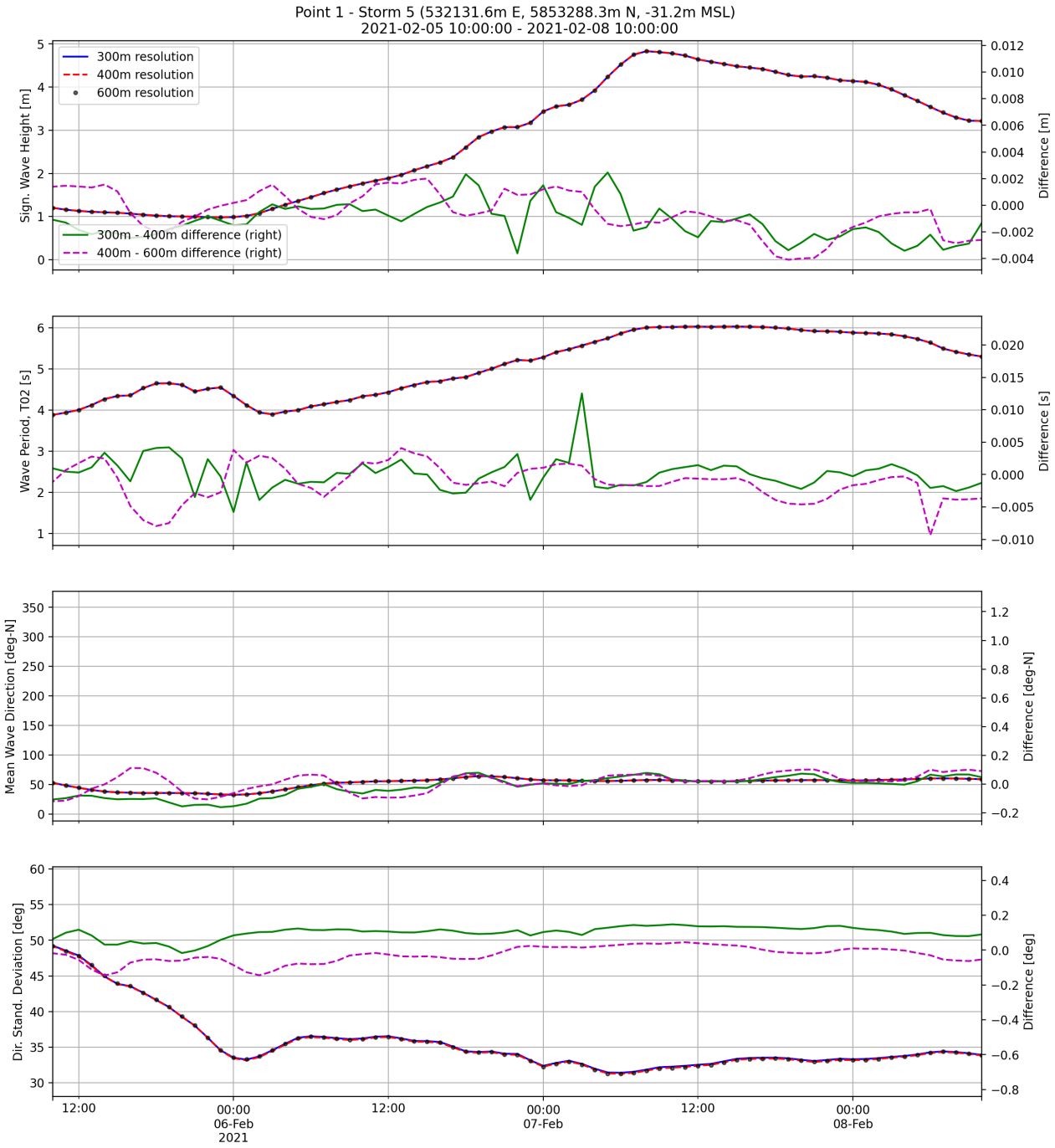

Figure F-5: Time series comparison of Hm0, T02, MWD, and DSD between 300m, 400m and 600m mesh resolutions (SW model) during Storm 5 at Point 1.

Absolute values are shown on the left axis (black, blue, and red lines), and time series difference between 300-400m and 400-600m is shown on the right axis (green and magenta lines).

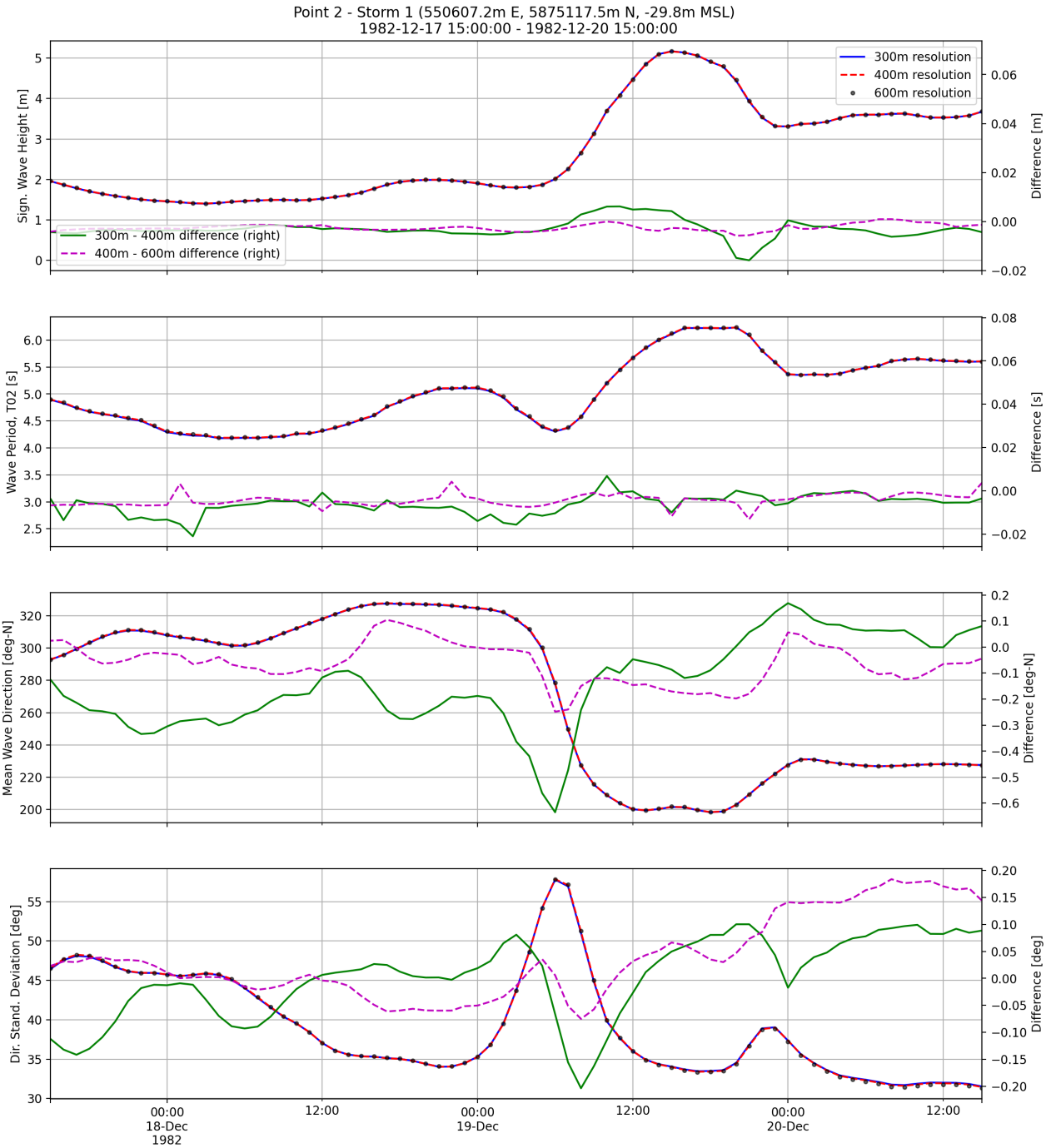

Figure F-6: Time series comparison of Hm0, T02, MWD, and DSD between 300m, 400m and 600m mesh resolutions (SW model) during Storm 1 at Point 2.

Absolute values are shown on the left axis (black, blue, and red lines), and time series difference between 300-400m and 400-600m is shown on the right axis (green and magenta lines).

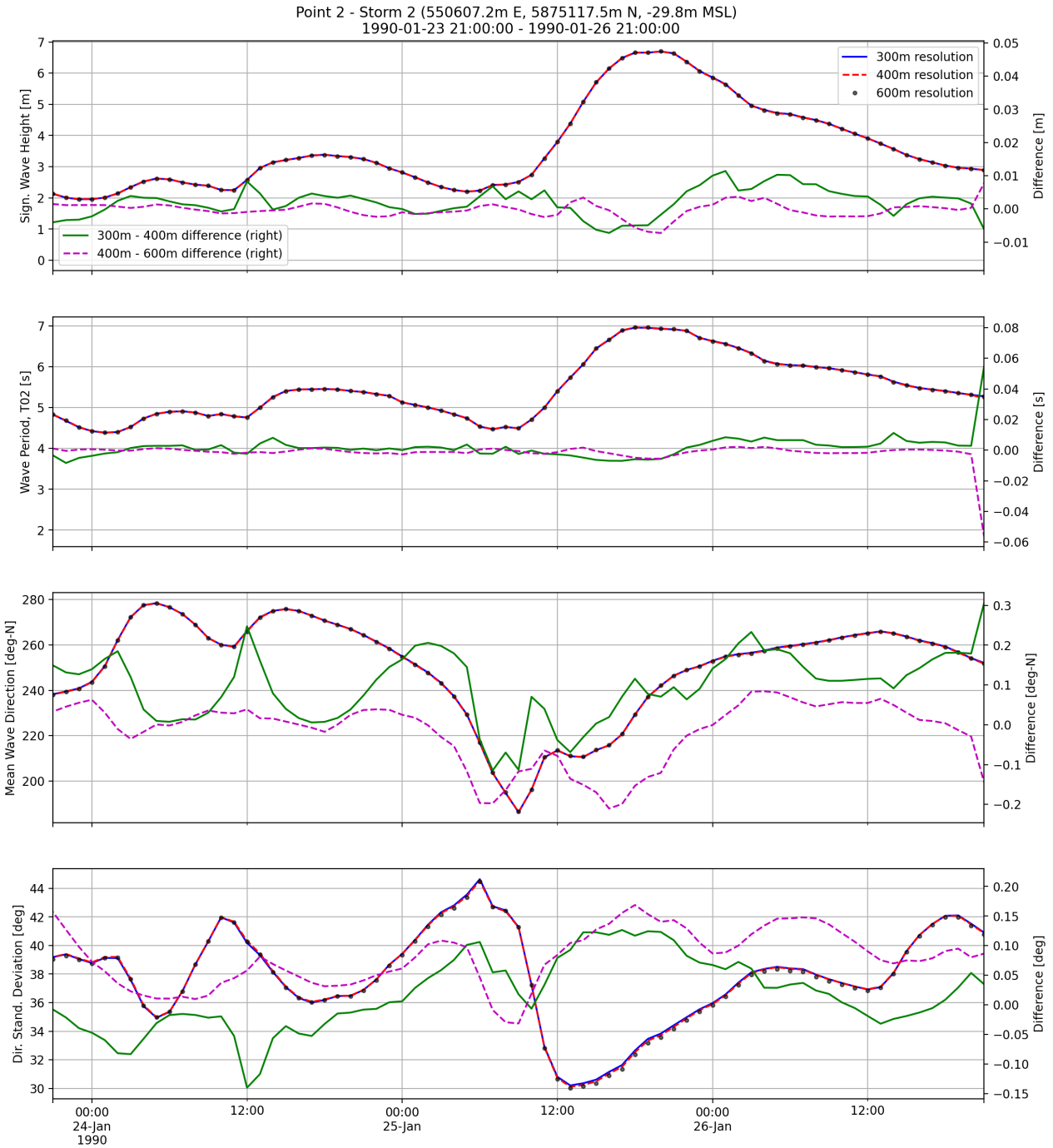

Figure F-7: Time series comparison of Hm0, T02, MWD, and DSD between 300m, 400m and 600m mesh resolutions (SW model) during Storm 2 at Point 2.

Absolute values are shown on the left axis (black, blue, and red lines), and time series difference between 300-400m and 400-600m is shown on the right axis (green and magenta lines).

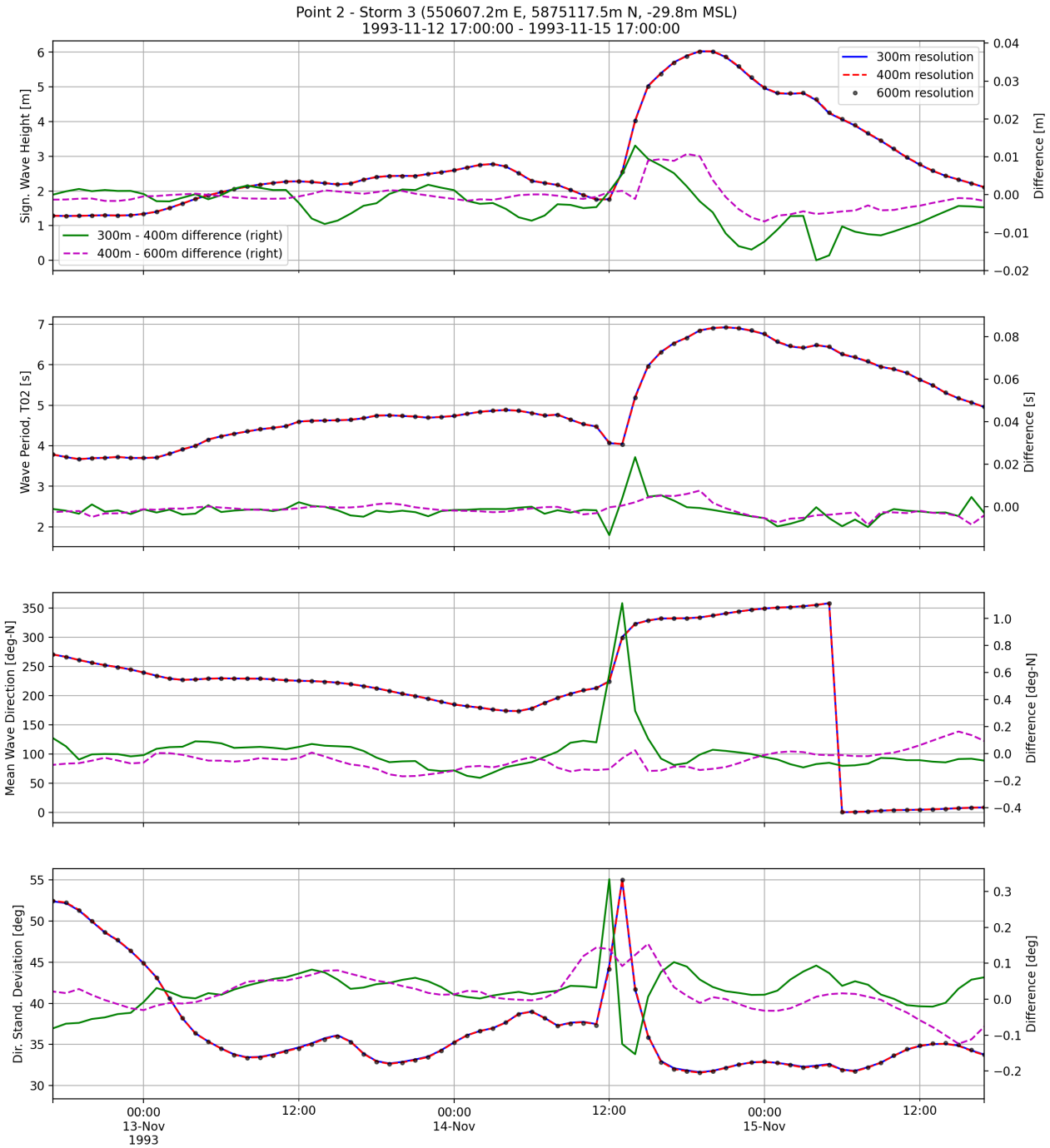

Figure F-8: Time series comparison of Hm0, T02, MWD, and DSD between 300m, 400m and 600m mesh resolutions (SW model) during Storm 3 at Point 2.

Absolute values are shown on the left axis (black, blue, and red lines), and time series difference between 300-400m and 400-600m is shown on the right axis (green and magenta lines).

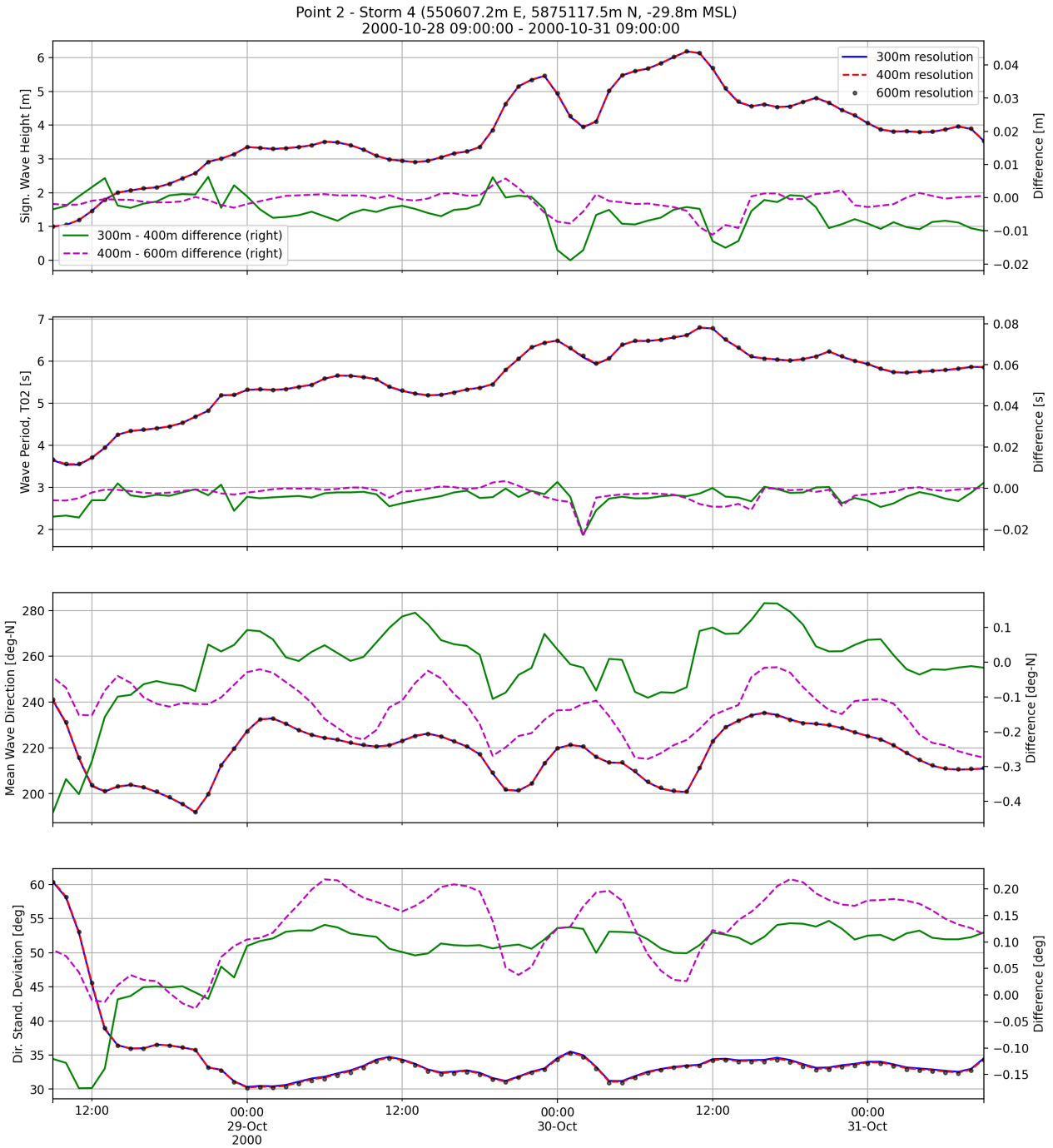

Figure F-9: Time series comparison of Hm0, T02, MWD, and DSD between 300m, 400m and 600m mesh resolutions (SW model) during Storm 4 at Point 2.

Absolute values are shown on the left axis (black, blue, and red lines), and time series difference between 300-400m and 400-600m is shown on the right axis (green and magenta lines).

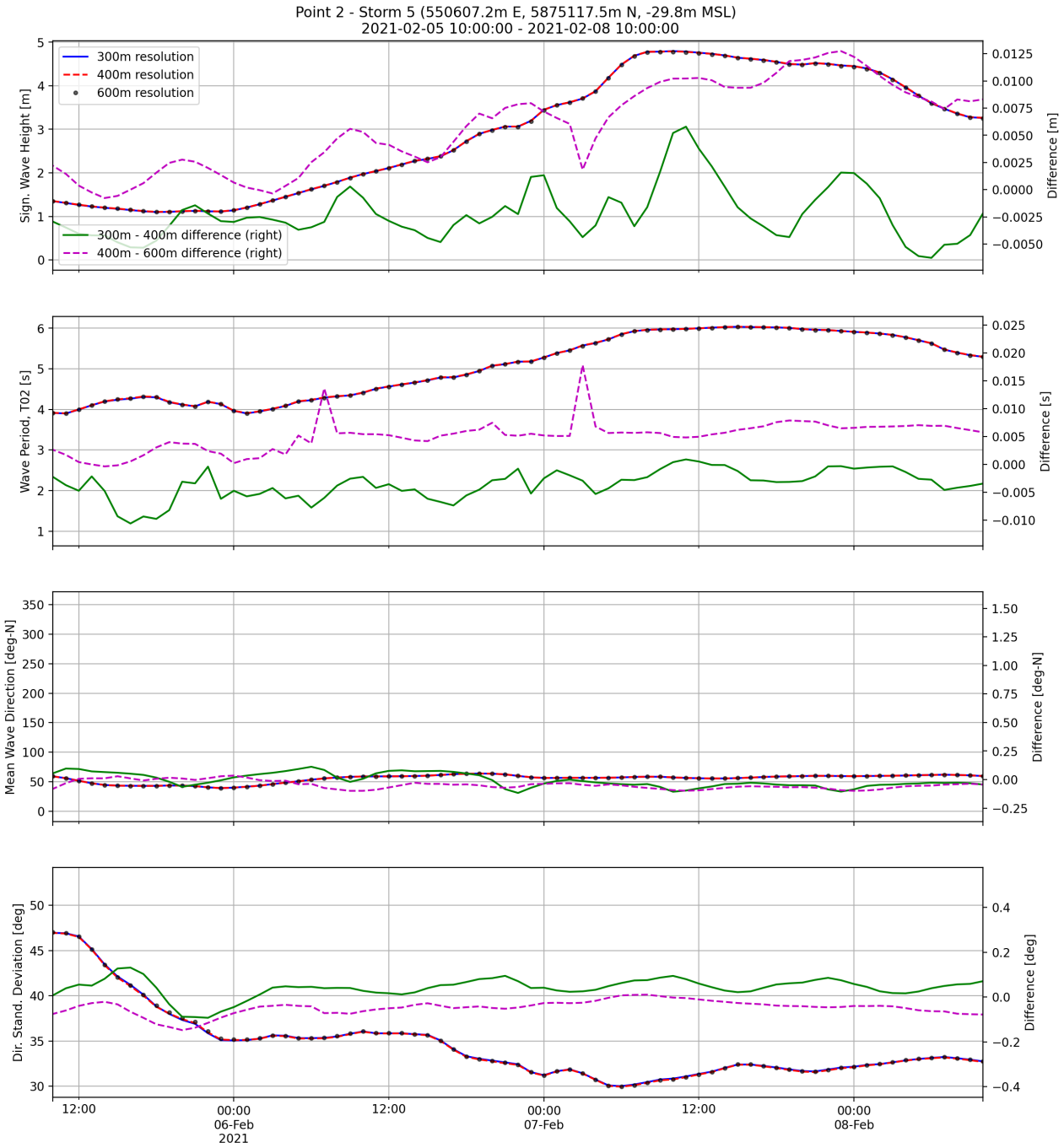

Figure F-10: Time series comparison of Hm0, T02, MWD, and DSD between 300m, 400m and 600m mesh resolutions (SW model) during Storm 5 at Point 2.

Absolute values are shown on the left axis (black, blue, and red lines), and time series difference between 300-400m and 400-600m is shown on the right axis (green and magenta lines).

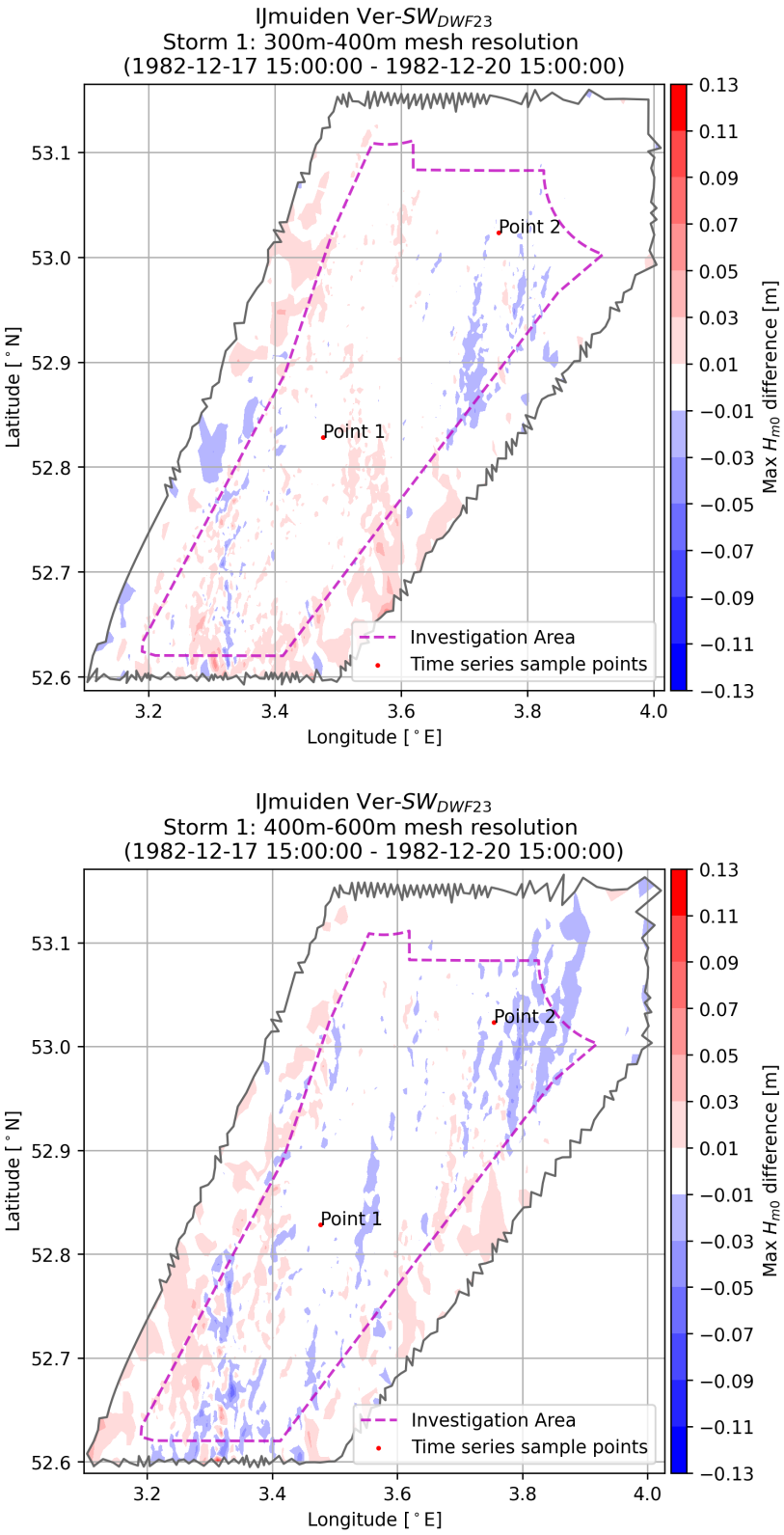

Figure F-11: Difference map of maximum Hm0 between different mesh resolutions (SW model) during storm 1.
Top: Difference between 300m and 400m mesh resolutions
Bottom: Difference between 400m and 600m mesh resolutions

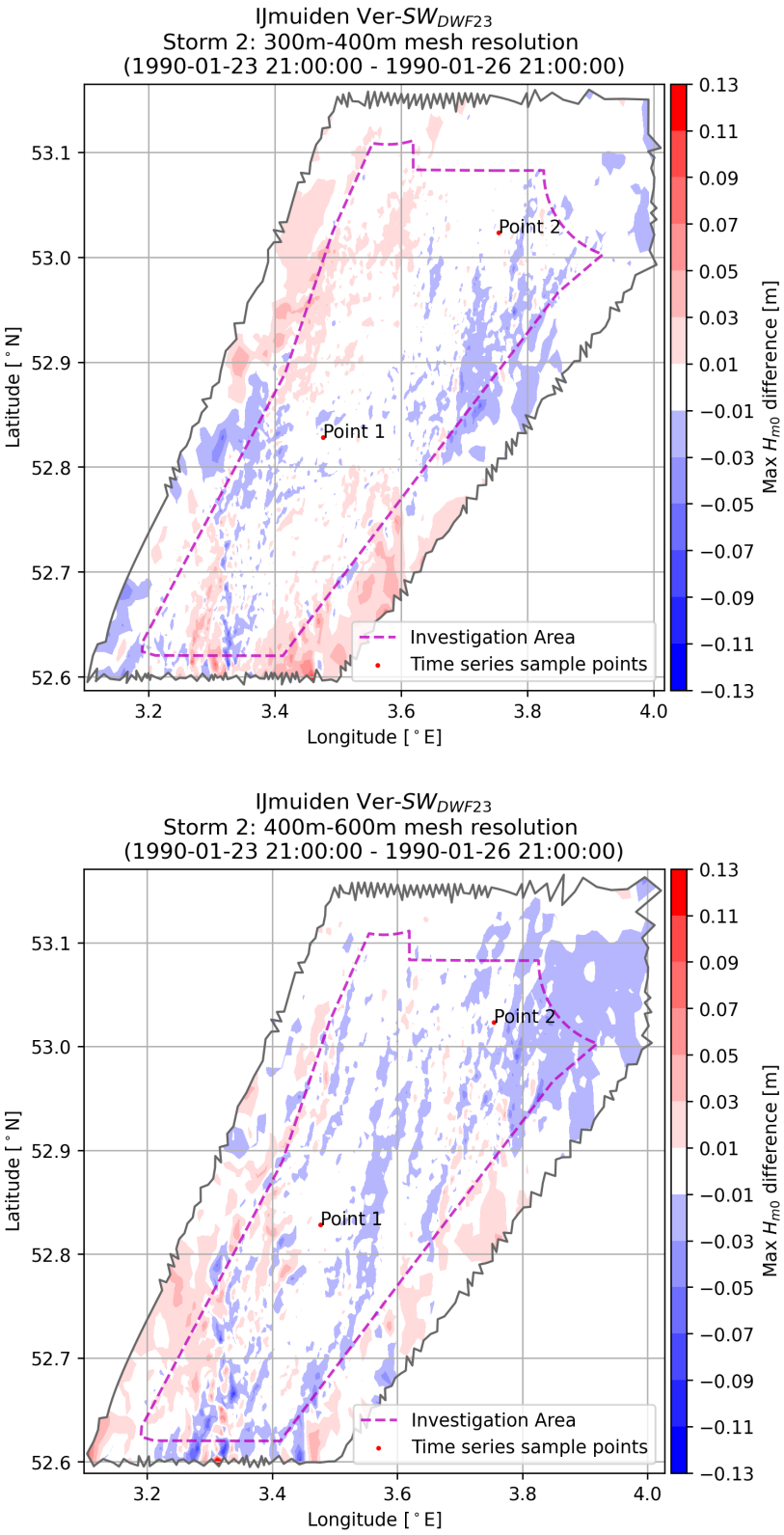

Figure F-12: Difference map of maximum Hm0 between different mesh resolutions (SW model) during storm 2.
Top: Difference between 300m and 400m mesh resolutions
Bottom: Difference between 400m and 600m mesh resolutions

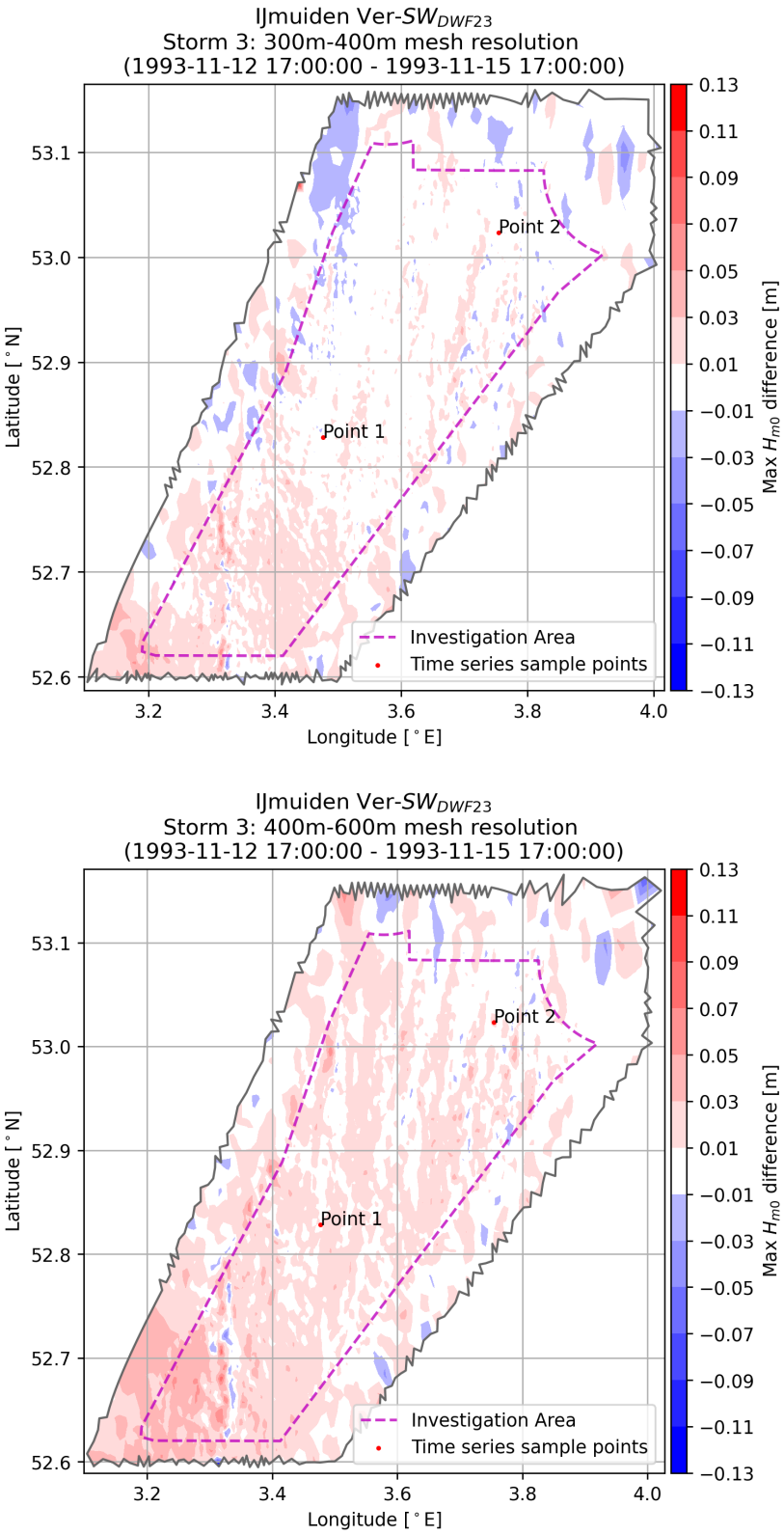

Figure F-13: Difference map of maximum Hm0 between different mesh resolutions (SW model) during storm 3.
Top: Difference between 300m and 400m mesh resolutions
Bottom: Difference between 400m and 600m mesh resolutions

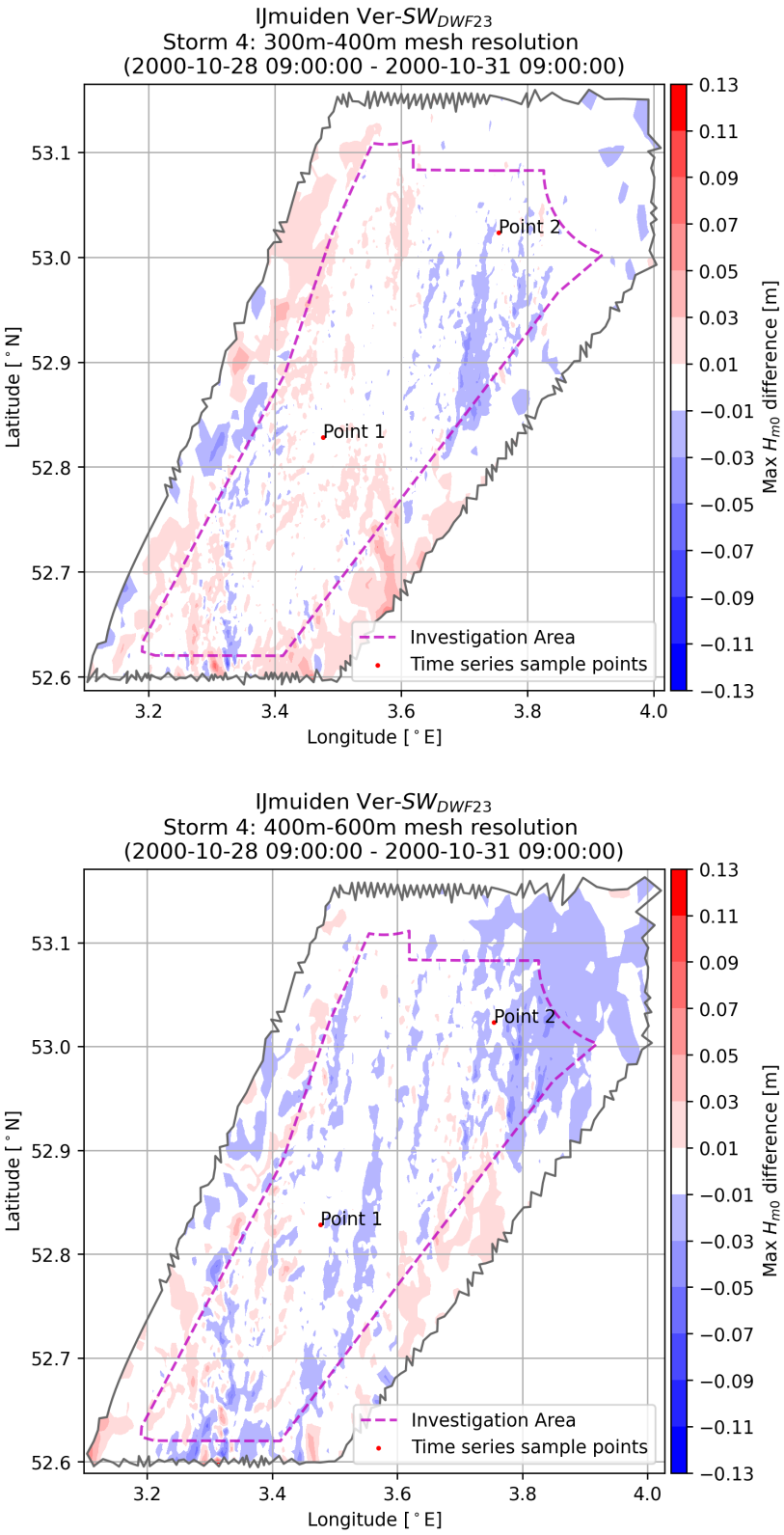

Figure F-14: Difference map of maximum Hm0 between different mesh resolutions (SW model) during storm 4.
Top: Difference between 300m and 400m mesh resolutions
Bottom: Difference between 400m and 600m mesh resolutions

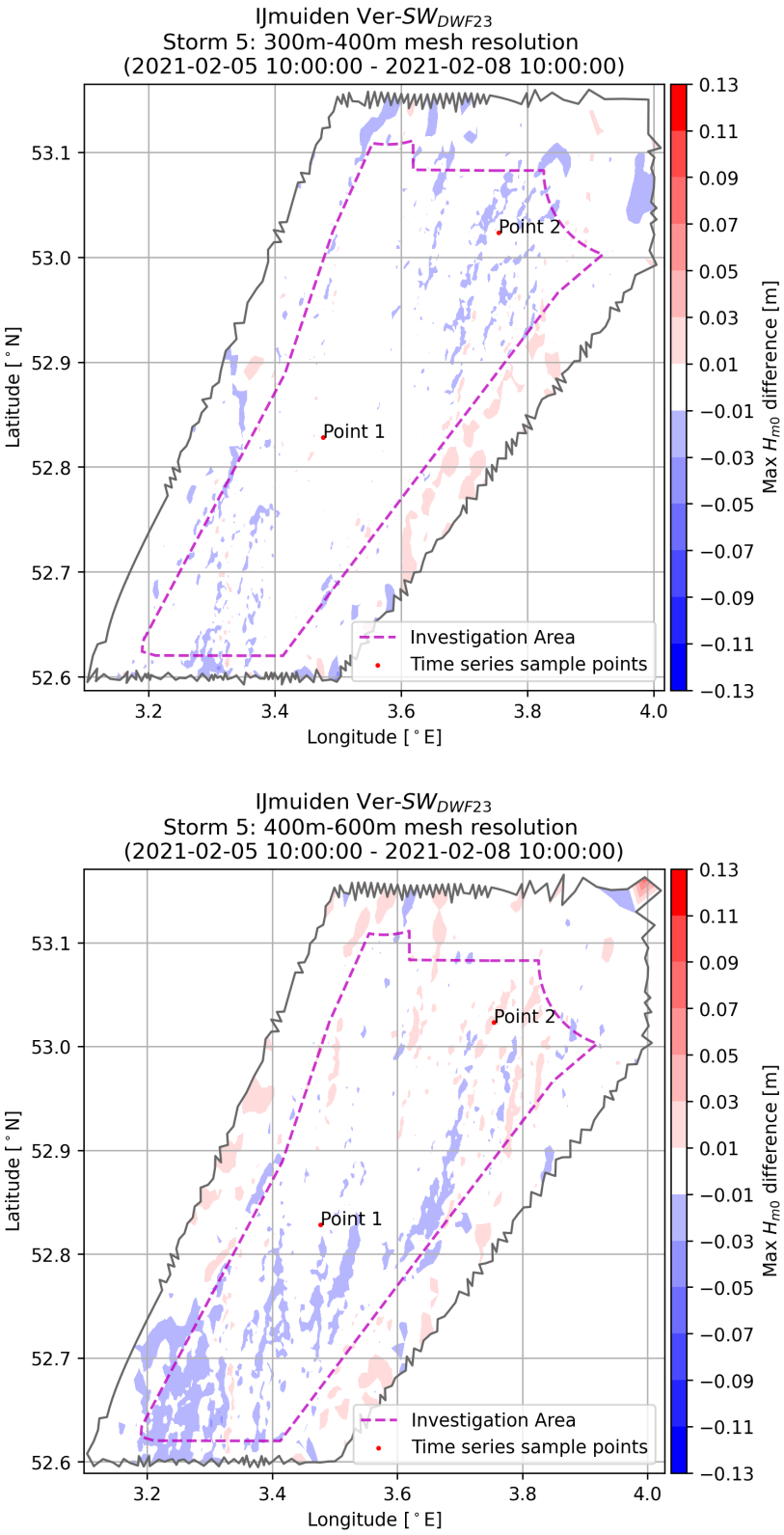

Figure F-15: Difference map of maximum Hm0 between different mesh resolutions (SW model) during storm 5.
Top: Difference between 300m and 400m mesh resolutions
Bottom: Difference between 400m and 600m mesh resolutions

Appendix G Spectral wave model validation results at all measurement stations

See next pages.

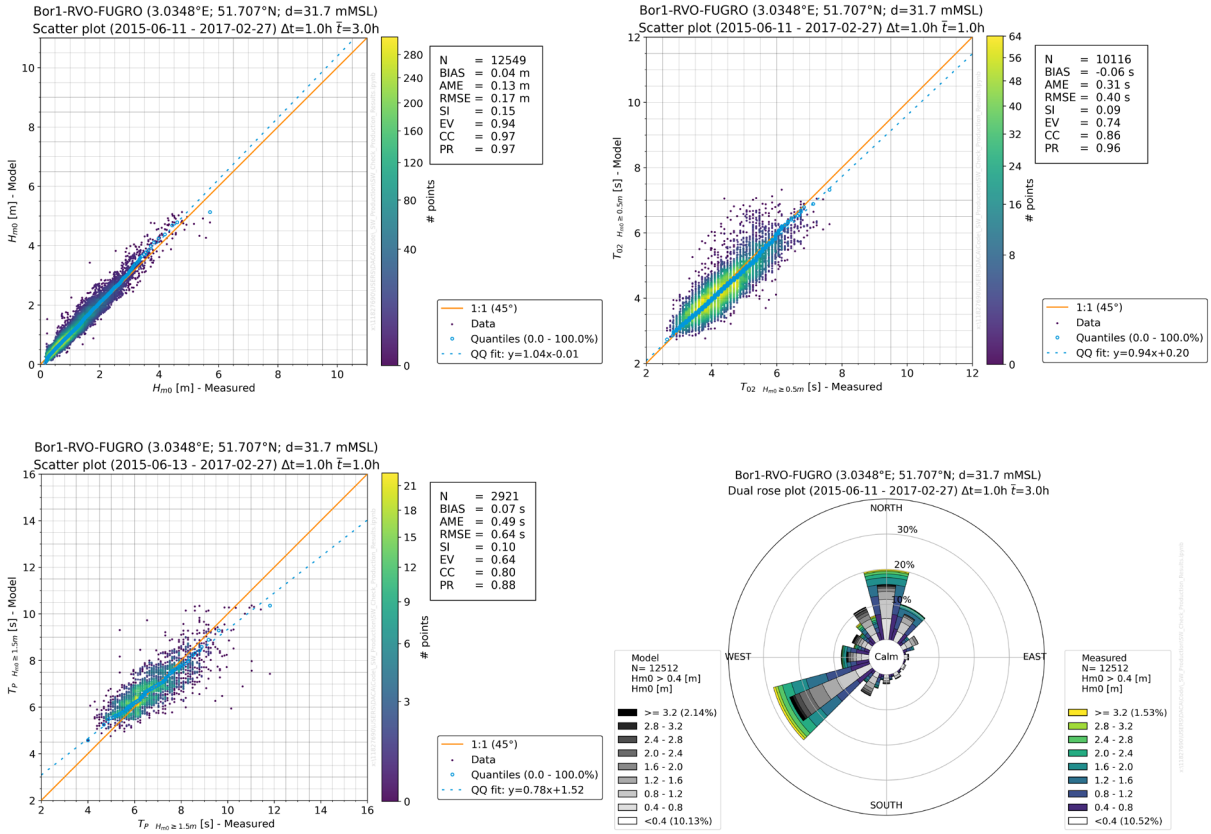

Figure G-1: SW_{DWF23} model validation at station Bor1-RVO.

Top-left figure: Hm0 validation results
Top-right figure: T02 validation results
Bottom-left figure: Tp validation results
Bottom-right figure: Wave rose validation results.

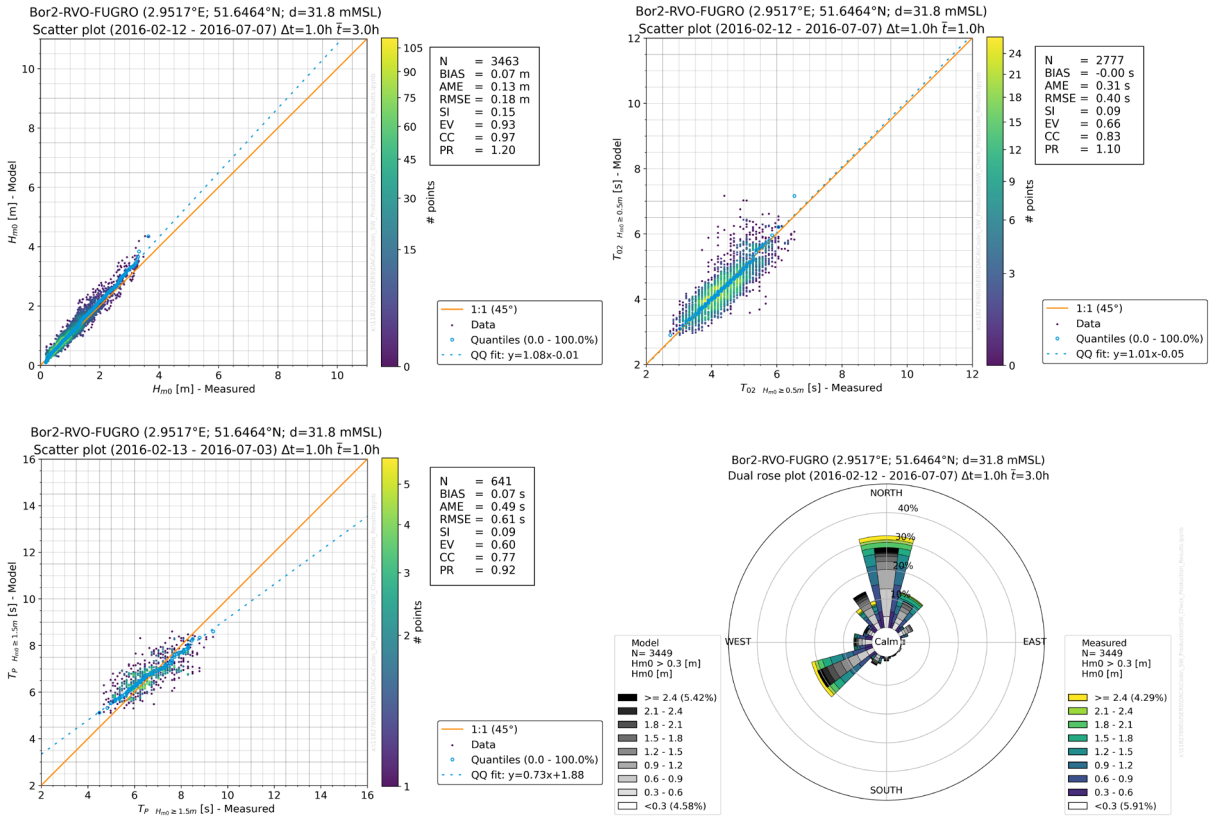

Figure G-2: SW_{DWF23} model validation at station Bor2-RVO.

Top-left figure: Hm0 validation results
Top-right figure: T02 validation results
Bottom-left figure: Tp validation results
Bottom-right figure: Wave rose validation results.

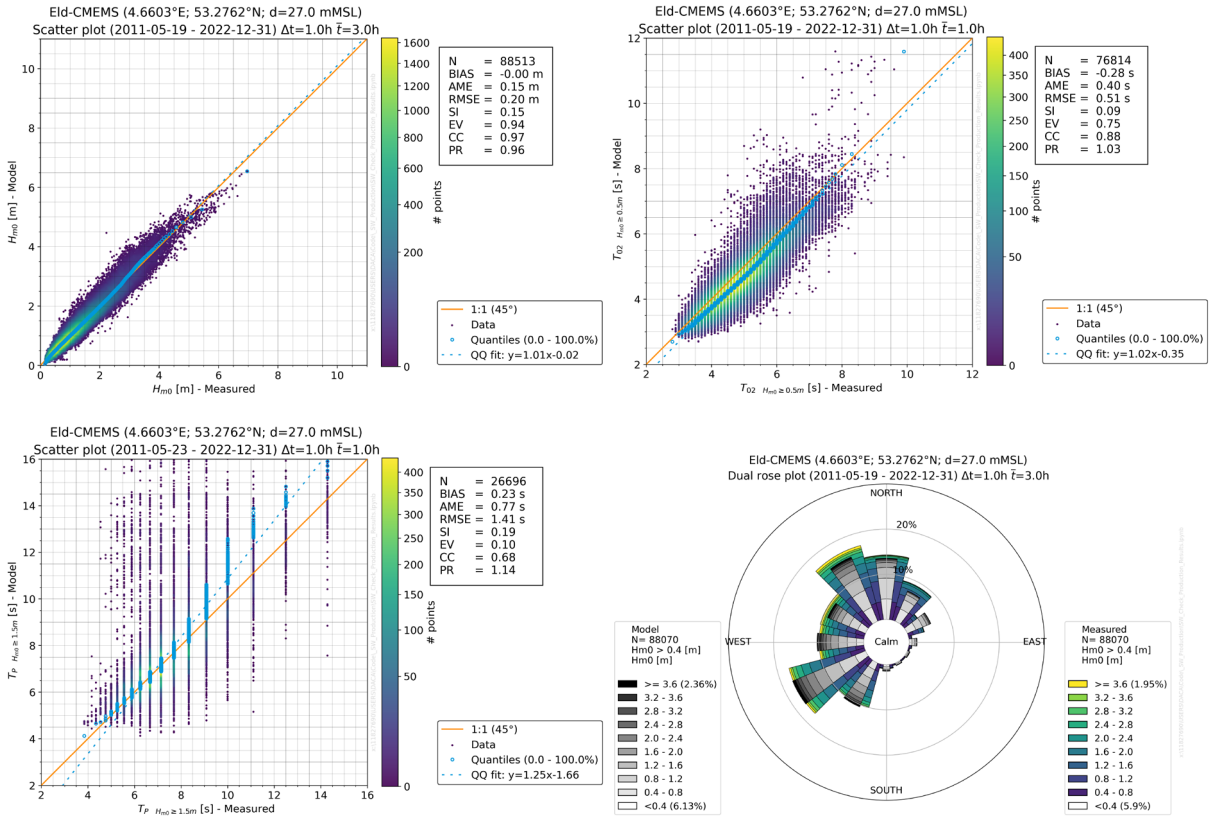

Figure G-3: SW_{DWF23} model validation at station Eld-CMEMS.

Top-left figure: Hm0 validation results
Top-right figure: T02 validation results
Bottom-left figure: Tp validation results
Bottom-right figure: Wave rose validation results.

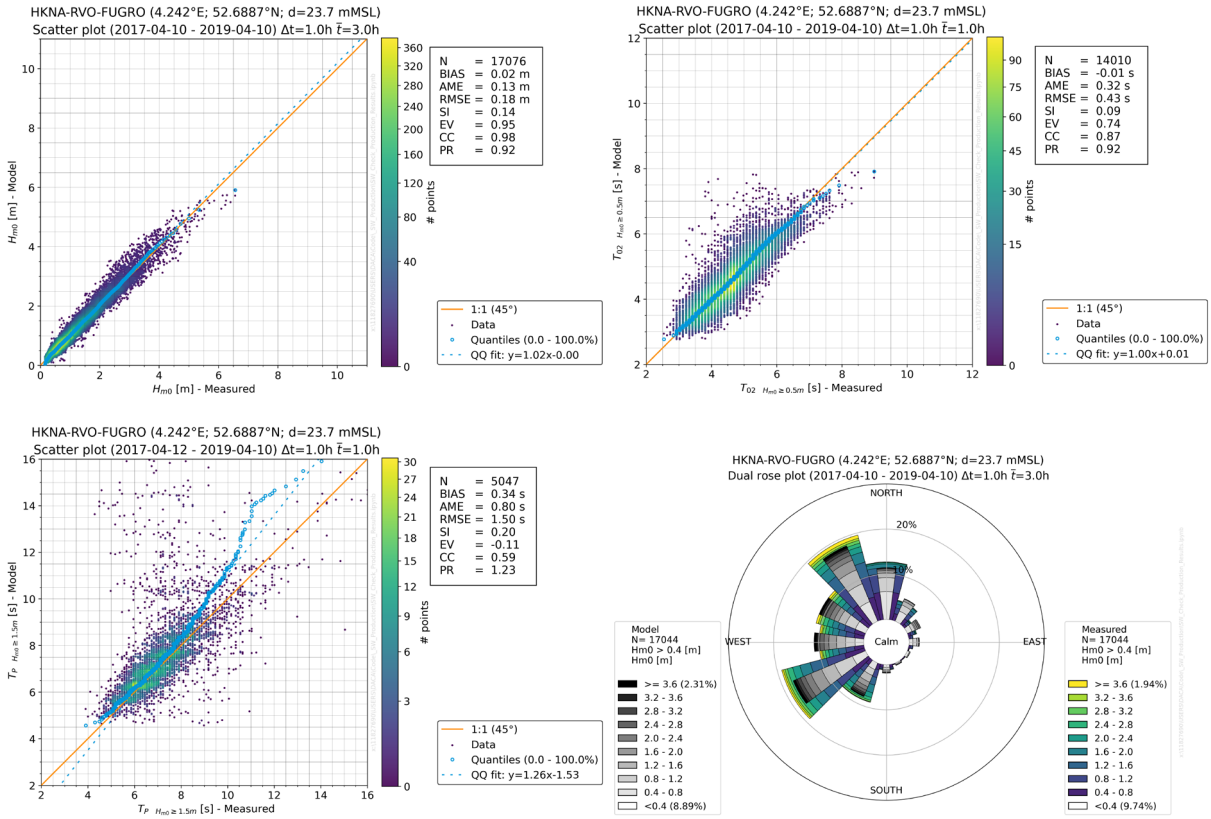

Figure G-4: SW_{DWF23} model validation at station HKNA-RVO.

Top-left figure: Hm0 validation results
Top-right figure: T02 validation results
Bottom-left figure: Tp validation results
Bottom-right figure: Wave rose validation results.

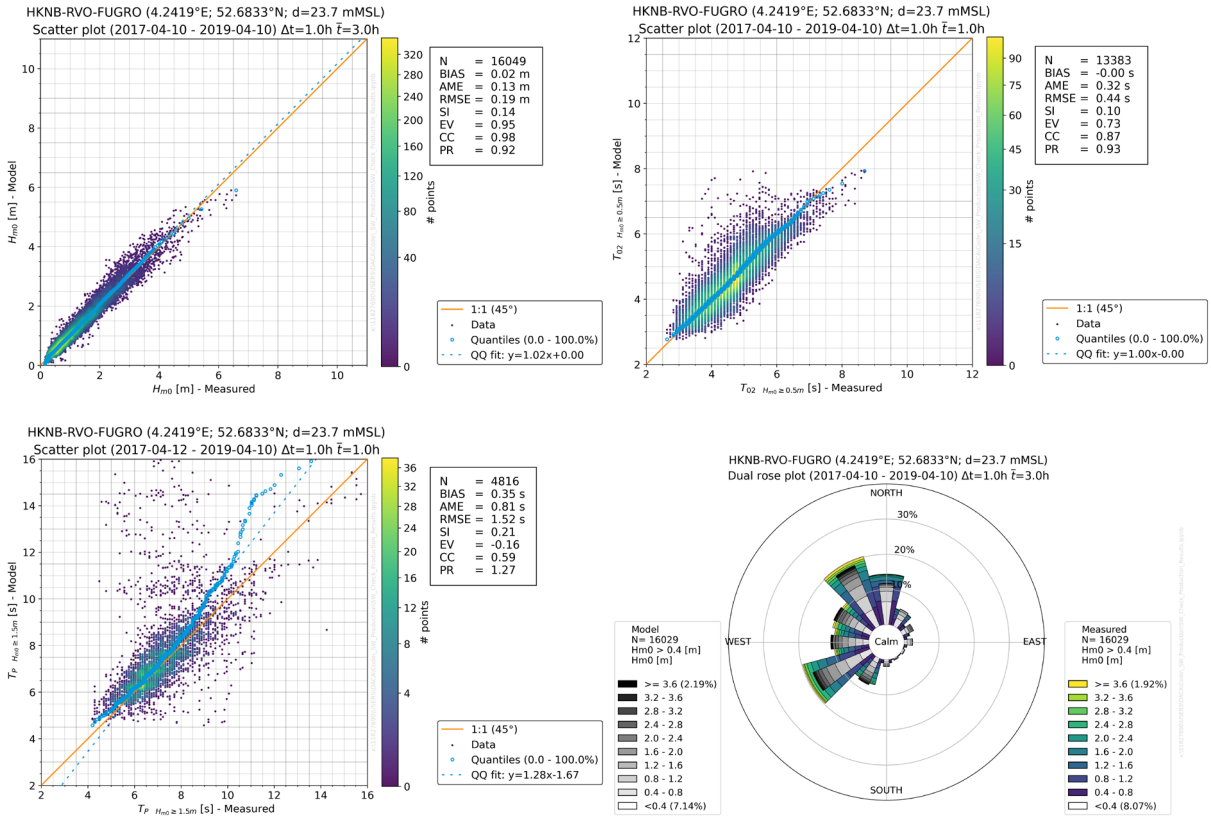

Figure G-5: SW_{DWF23} model validation at station HKNB-RVO.

Top-left figure: Hm0 validation results
Top-right figure: T02 validation results
Bottom-left figure: Tp validation results
Bottom-right figure: Wave rose validation results.

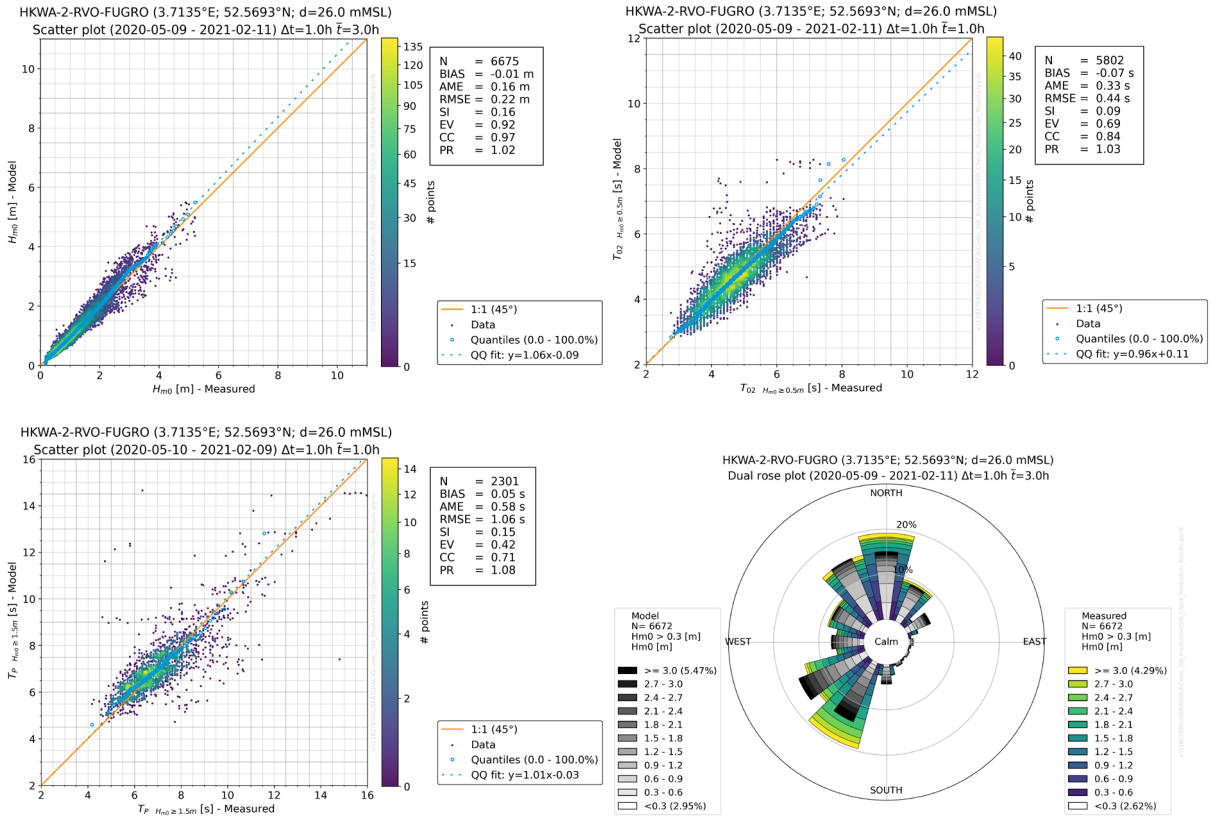

Figure G-6: SW_{DWF23} model validation at station HKWA-2-RVO.
Top-left figure: Hm0 validation results
Top-right figure: T02 validation results
Bottom-left figure: Tp validation results
Bottom-right figure: Wave rose validation results.

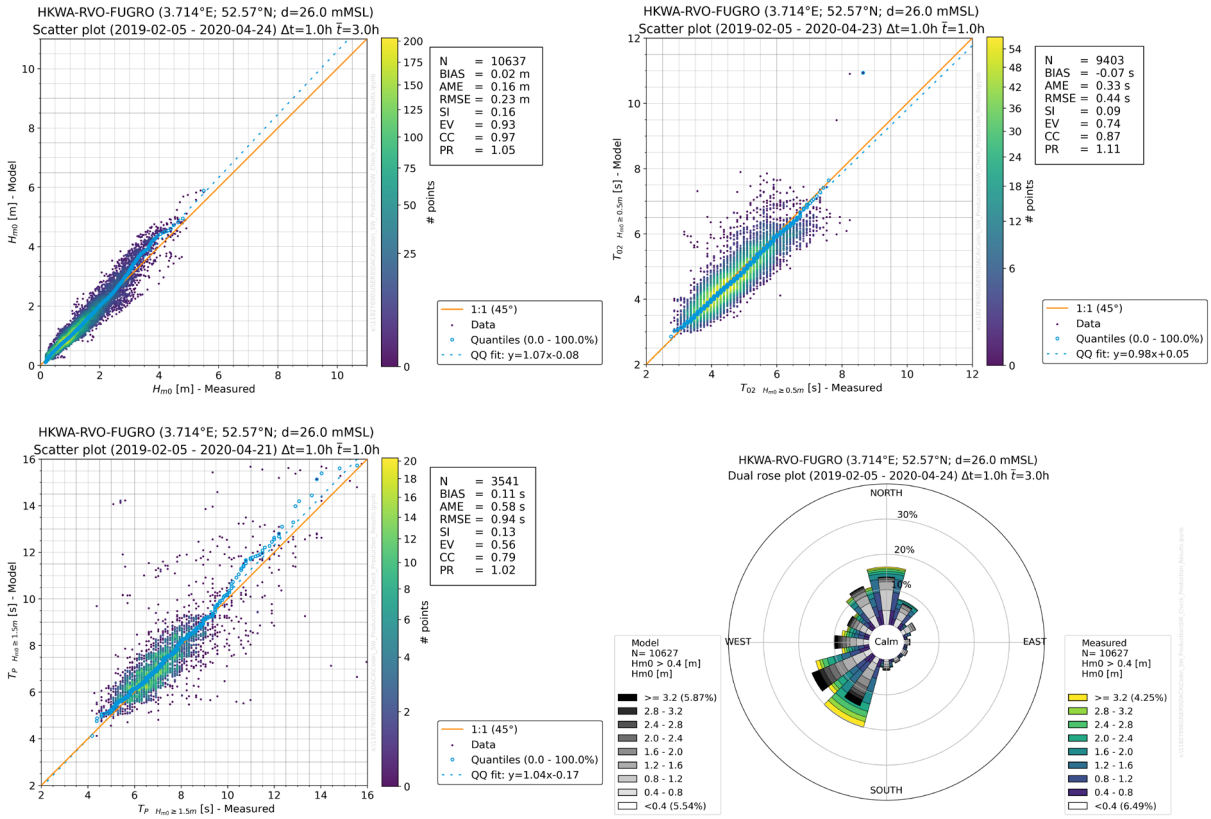

Figure G-7: SW_{DWF23} model validation at station HKWA-RVO.

Top-left figure: Hm0 validation results
Top-right figure: T02 validation results
Bottom-left figure: Tp validation results
Bottom-right figure: Wave rose validation results.

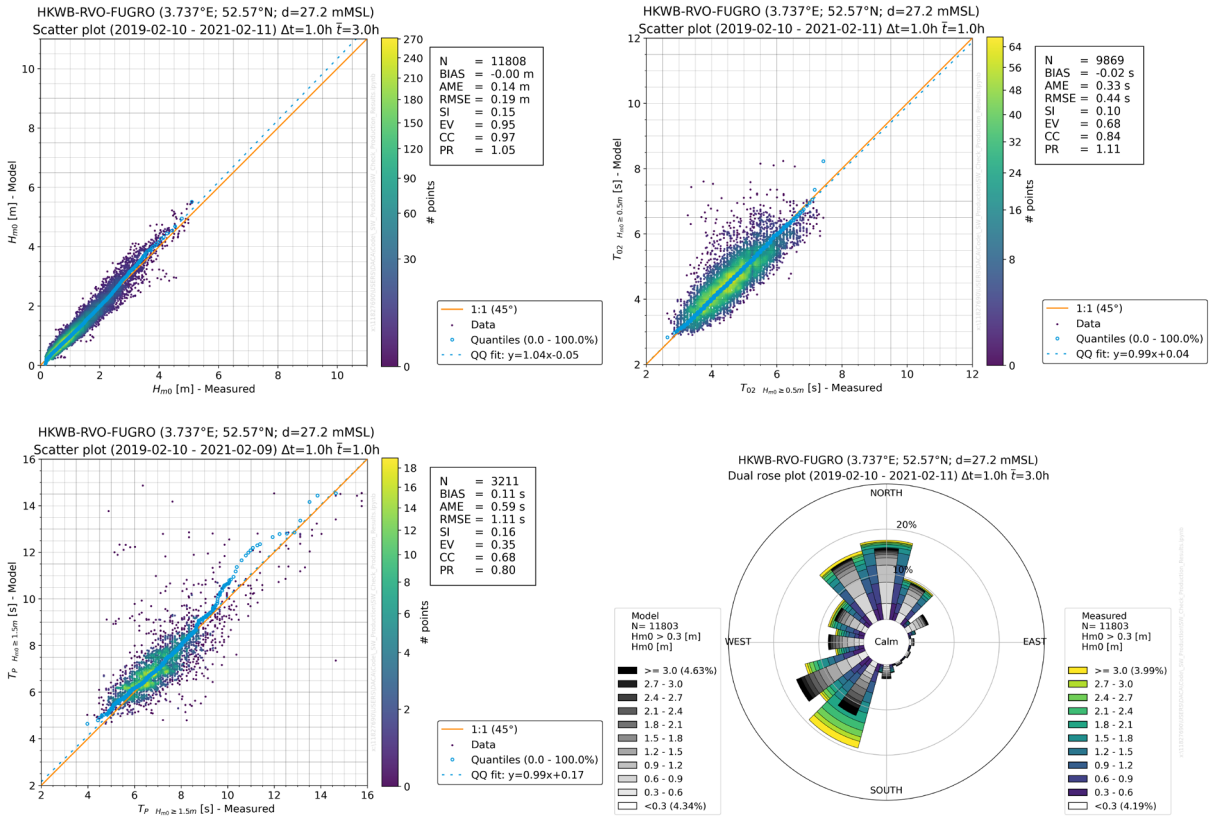

Figure G-8: SW_{DWF23} model validation at station HKWB-RVO.

Top-left figure: Hm0 validation results
Top-right figure: T02 validation results
Bottom-left figure: Tp validation results
Bottom-right figure: Wave rose validation results.

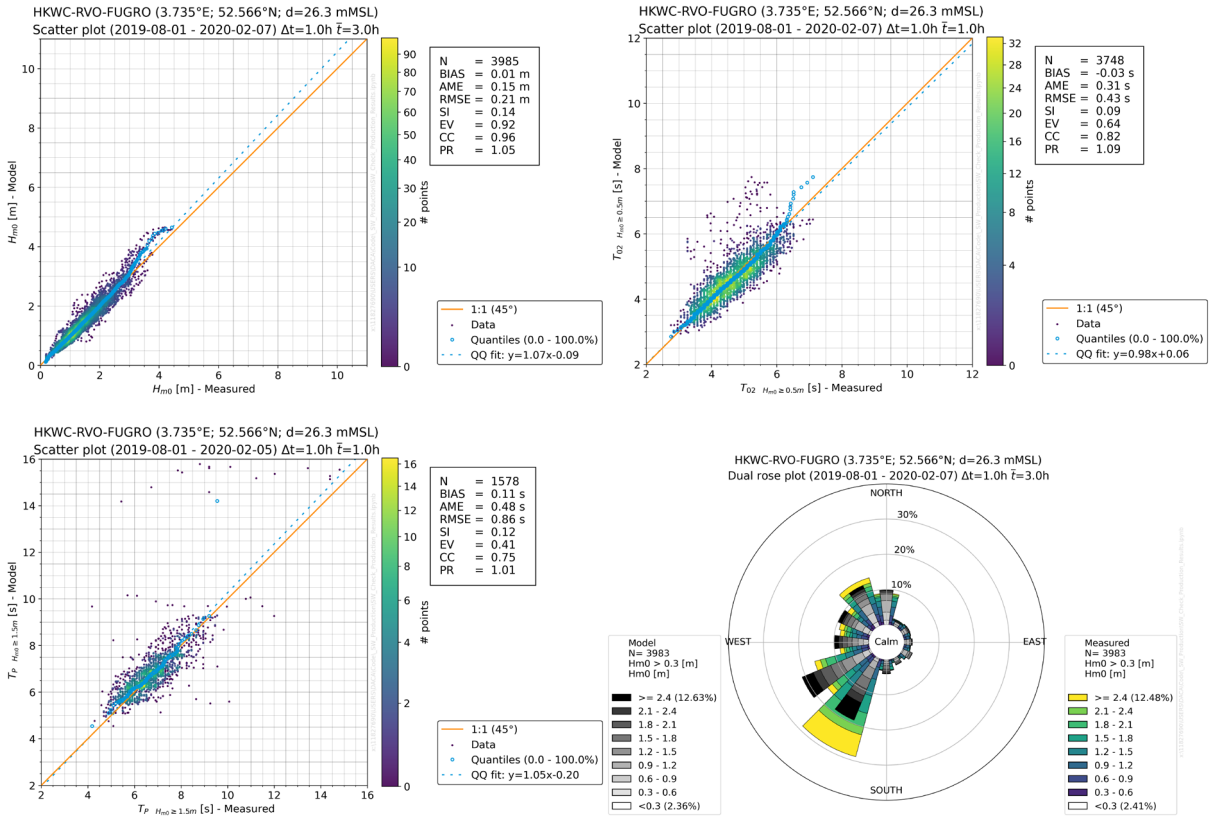

Figure G-9: SW_{DWF23} model validation at station HKWC-RVO.

Top-left figure: Hm0 validation results
Top-right figure: T02 validation results
Bottom-left figure: Tp validation results
Bottom-right figure: Wave rose validation results.

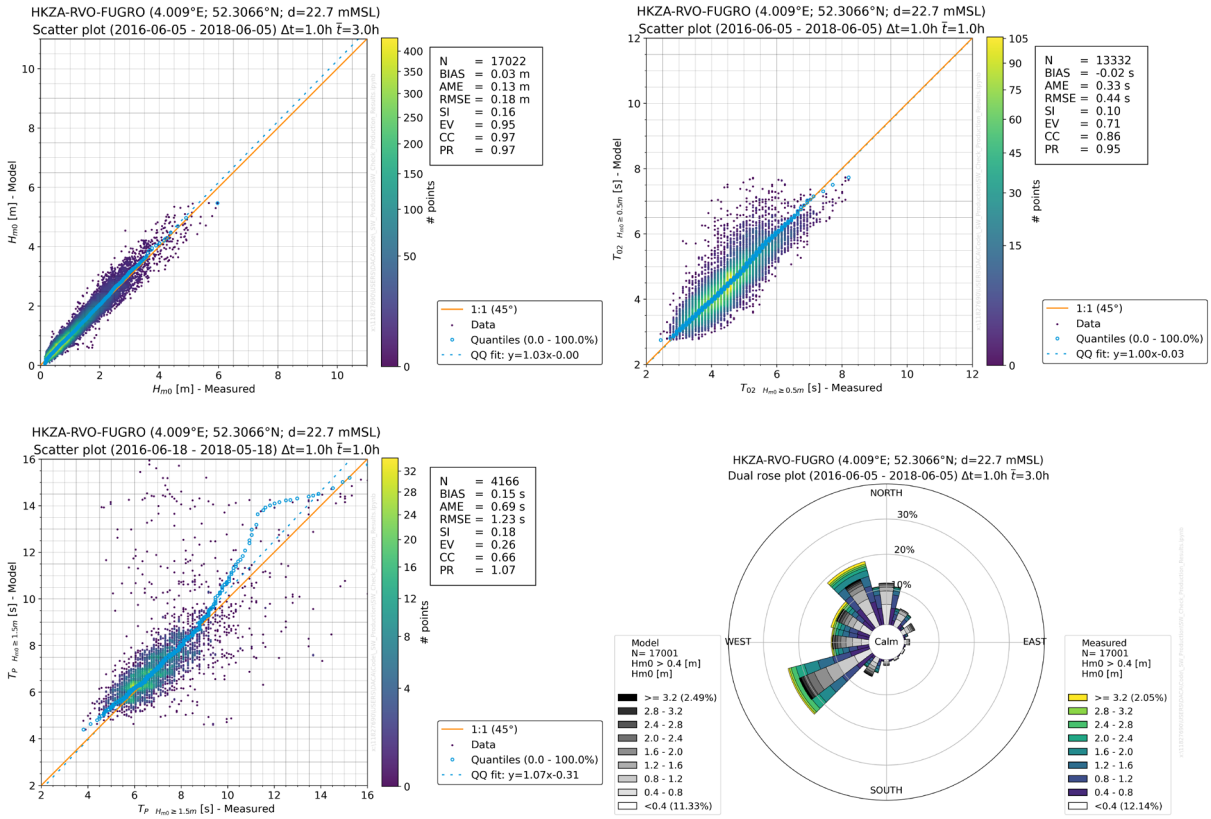

Figure G-10: SW_{DWF23} model validation at station HKZA-RVO.
Top-left figure: Hm0 validation results
Top-right figure: T02 validation results
Bottom-left figure: Tp validation results
Bottom-right figure: Wave rose validation results.

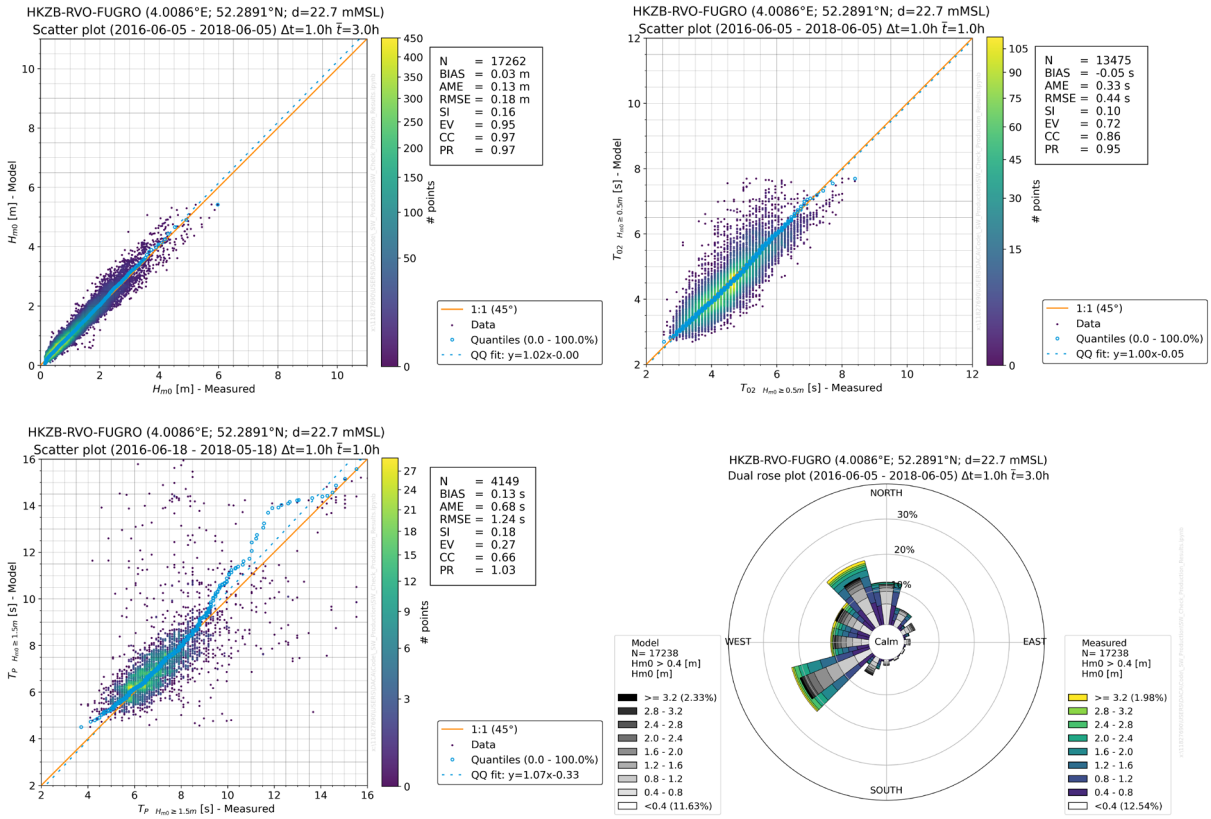

Figure G-11: SW_{DWF23} model validation at station HKZB-RVO.
Top-left figure: Hm0 validation results
Top-right figure: T02 validation results
Bottom-left figure: Tp validation results
Bottom-right figure: Wave rose validation results.

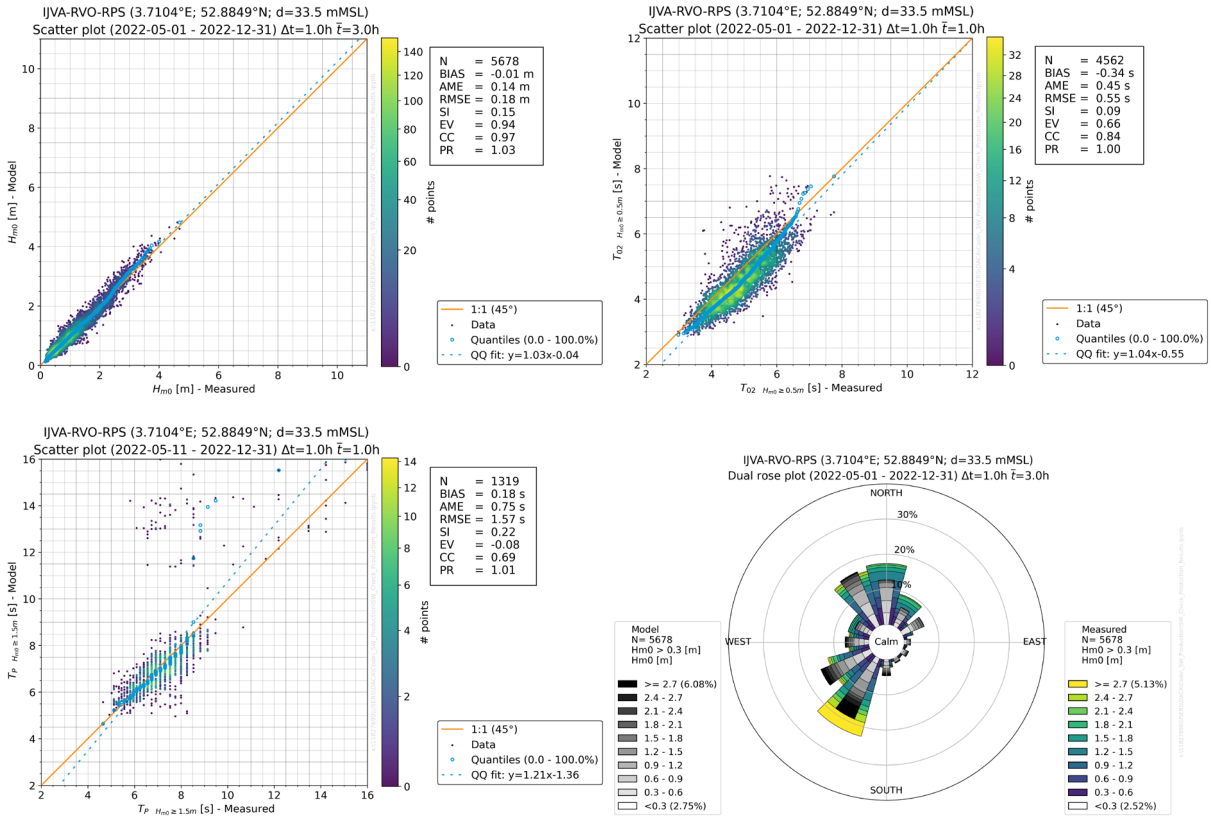

Figure G-12: SW_{DWF23} model validation at station IJVA-RVO.
Top-left figure: Hm0 validation results
Top-right figure: T02 validation results
Bottom-left figure: Tp validation results
Bottom-right figure: Wave rose validation results.

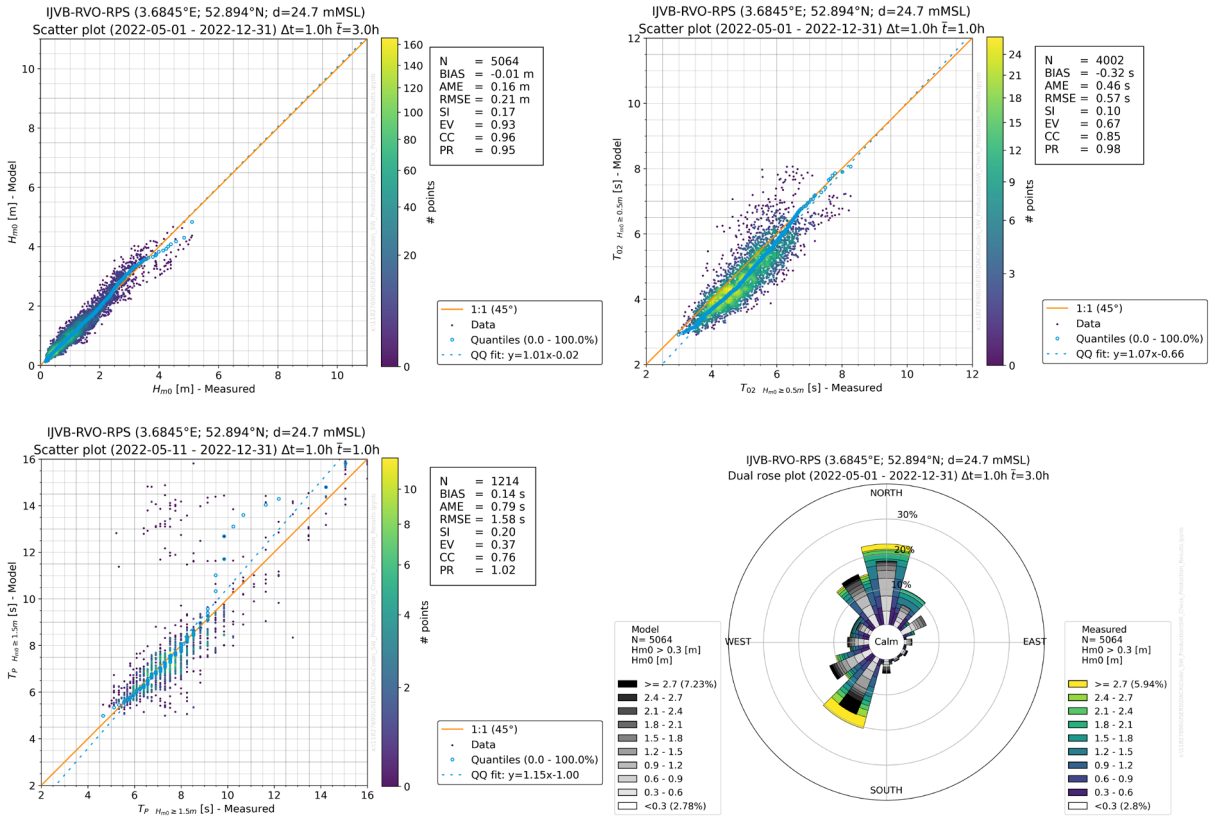

Figure G-13: SW_{DWF23} model validation at station IJVB-RVO.
Top-left figure: Hm0 validation results
Top-right figure: T02 validation results
Bottom-left figure: Tp validation results
Bottom-right figure: Wave rose validation results.

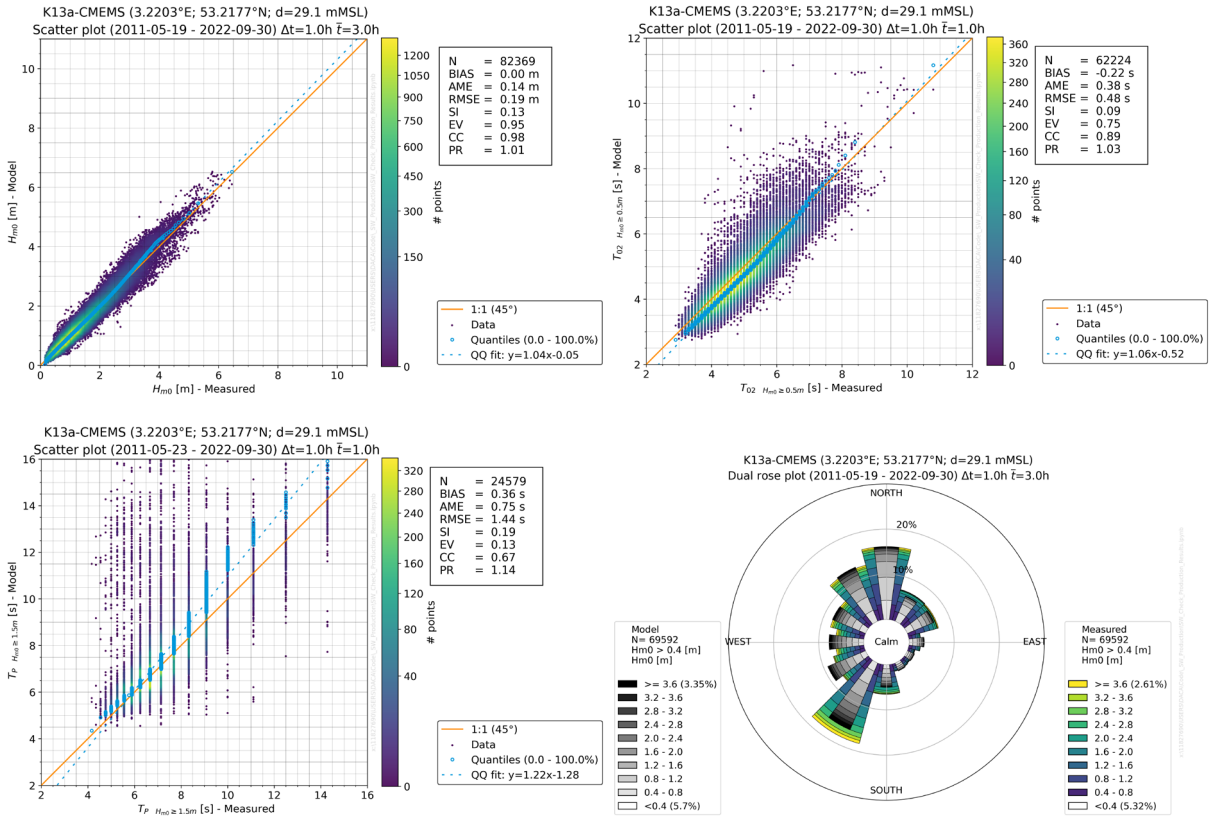

Figure G-14: SW_{DWF23} model validation at station K13a-CMEMS.
Top-left figure: Hm0 validation results
Top-right figure: T02 validation results
Bottom-left figure: Tp validation results
Bottom-right figure: Wave rose validation results.

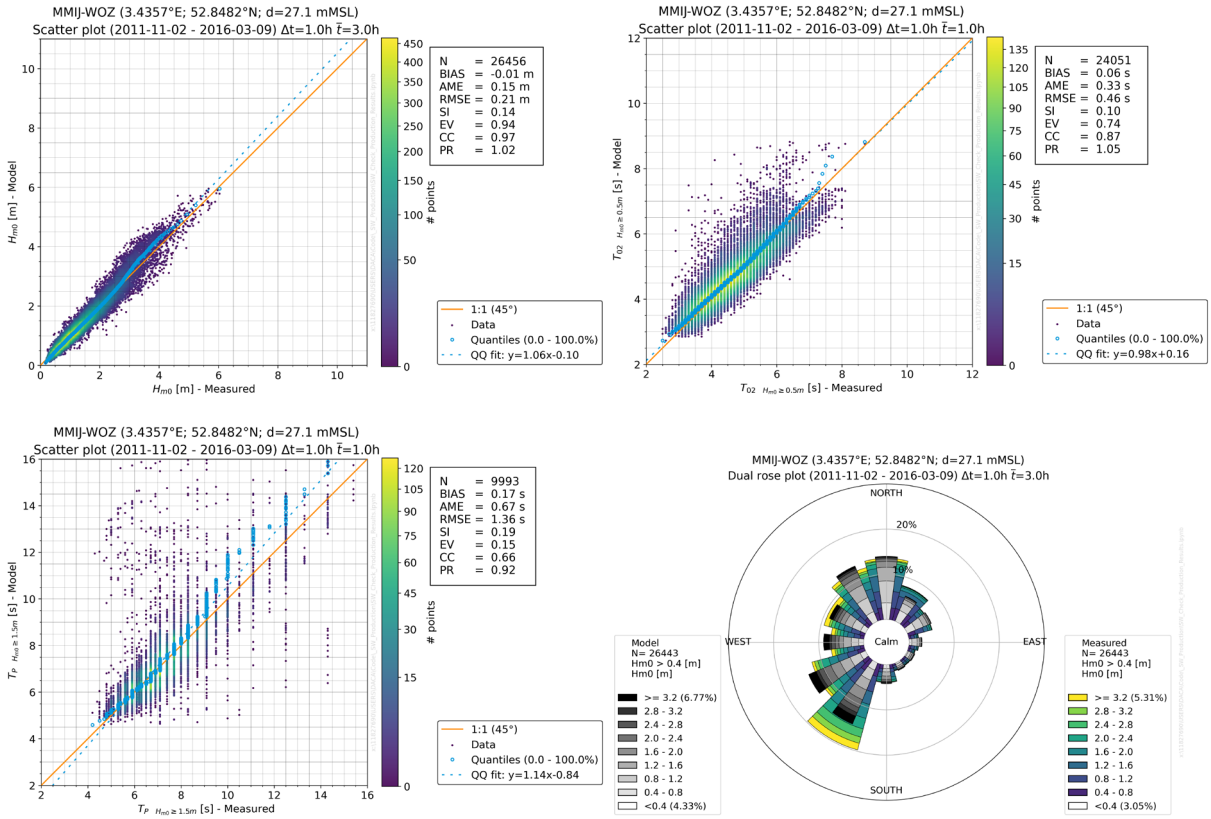

Figure G-15: SW_{DWF23} model validation at station MMIJ-WOZ.
Top-left figure: Hm0 validation results
Top-right figure: T02 validation results
Bottom-left figure: Tp validation results
Bottom-right figure: Wave rose validation results.

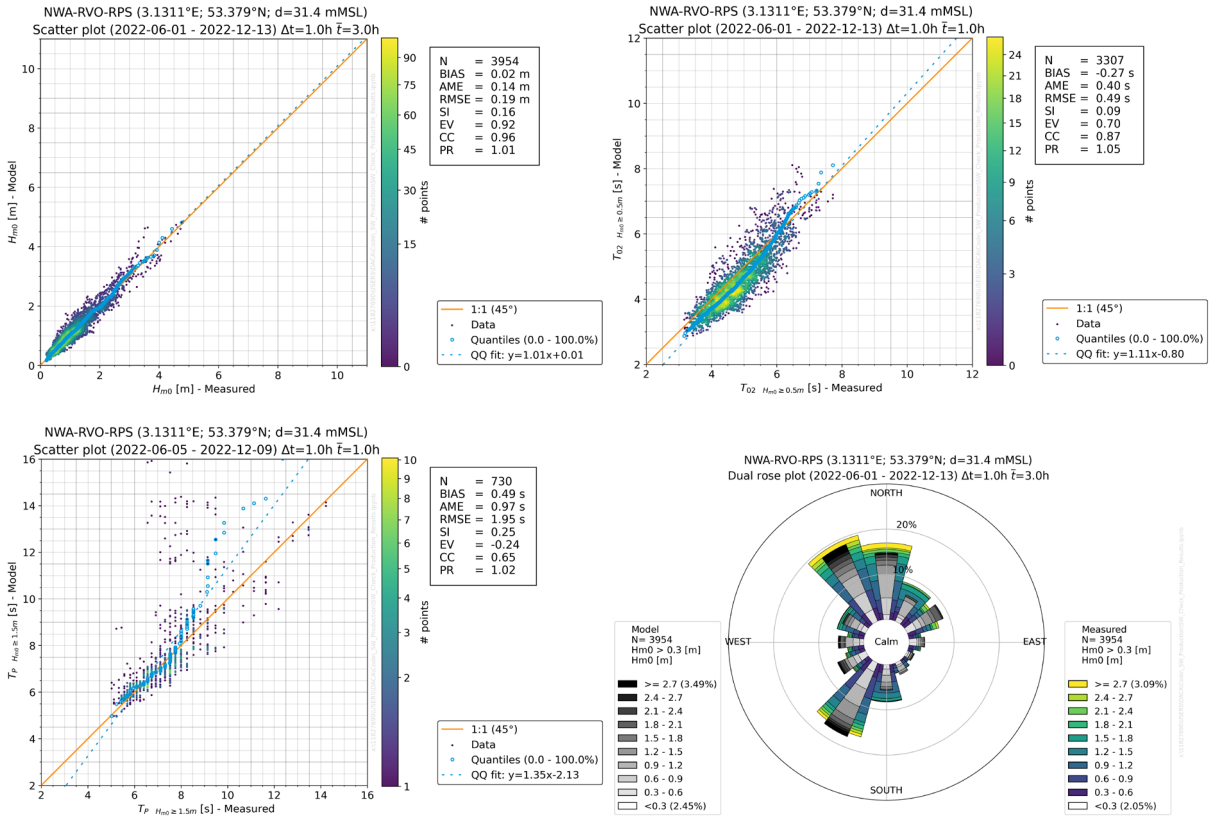

Figure G-16: SW_{DWF23} model validation at station NWA-RVO.
Top-left figure: Hm0 validation results
Top-right figure: T02 validation results
Bottom-left figure: Tp validation results
Bottom-right figure: Wave rose validation results.

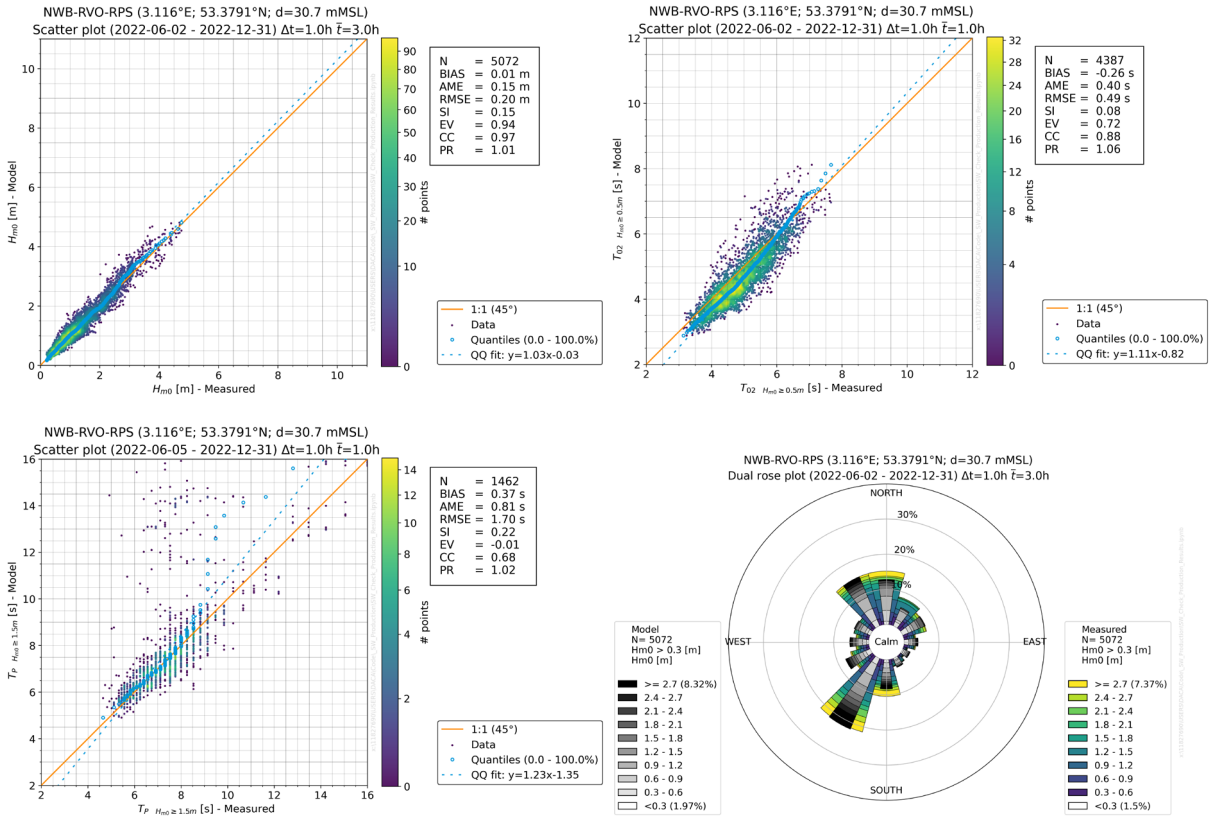

Figure G-17: SW_{DWF23} model validation at station NWB-RVO.
Top-left figure: Hm0 validation results
Top-right figure: T02 validation results
Bottom-left figure: Tp validation results
Bottom-right figure: Wave rose validation results.

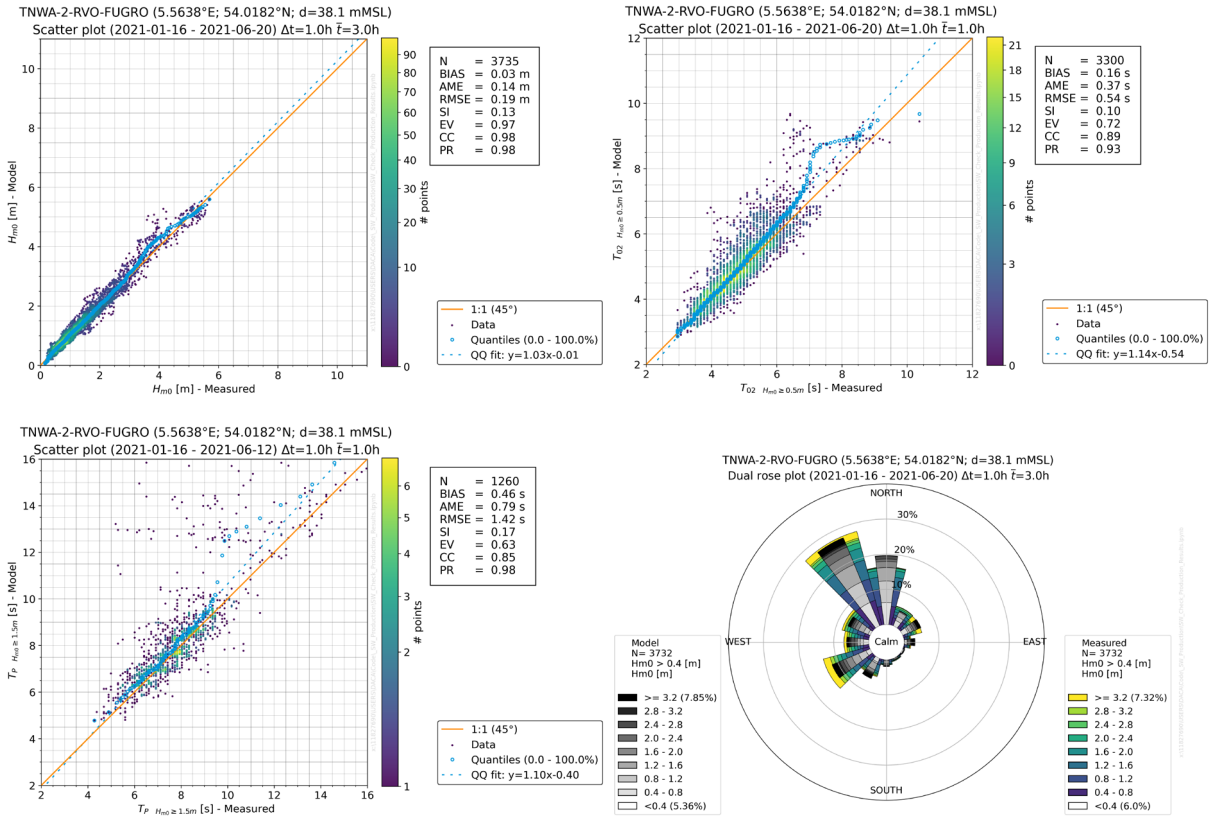

Figure G-18: SW_{DWF23} model validation at station TNWA-2-RVO.

Top-left figure: Hm0 validation results
Top-right figure: T02 validation results
Bottom-left figure: Tp validation results
Bottom-right figure: Wave rose validation results.

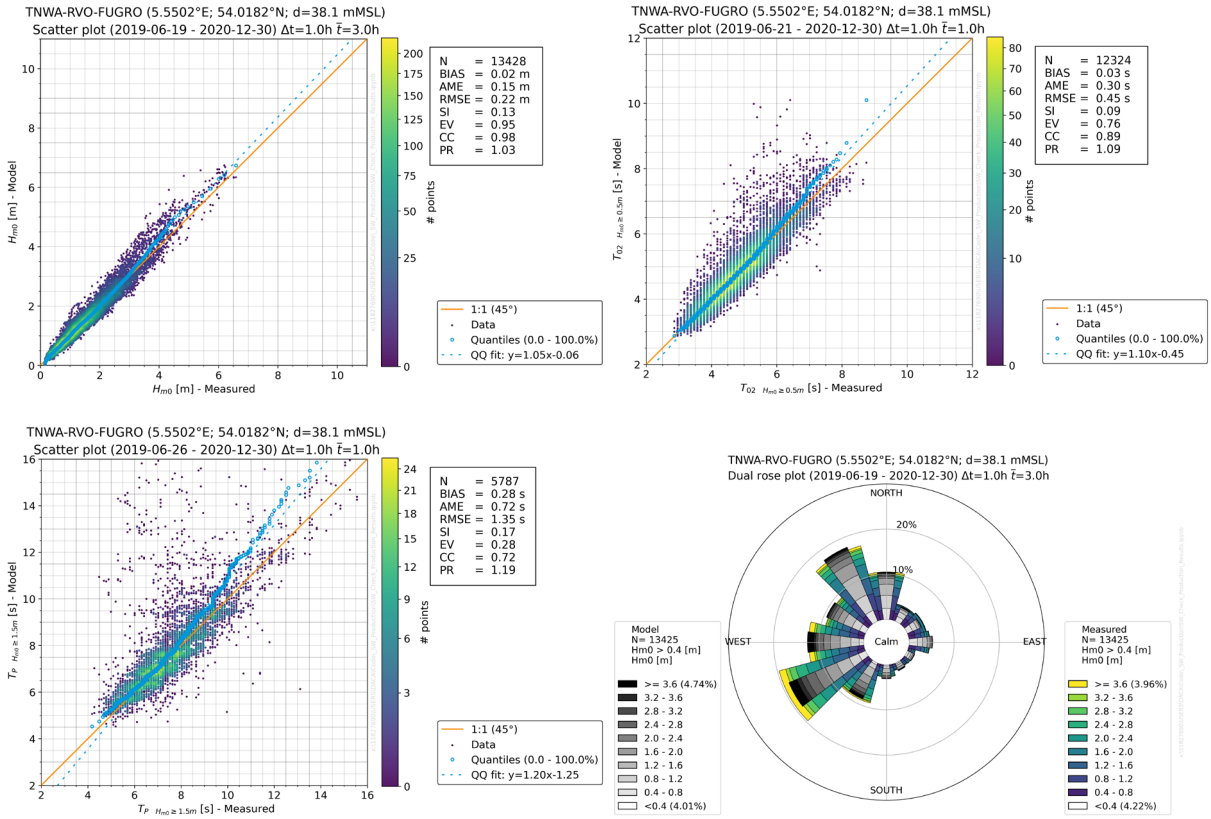

Figure G-19: SW_{DWF23} model validation at station TNWA-RVO.

Top-left figure: Hm0 validation results
Top-right figure: T02 validation results
Bottom-left figure: Tp validation results
Bottom-right figure: Wave rose validation results.

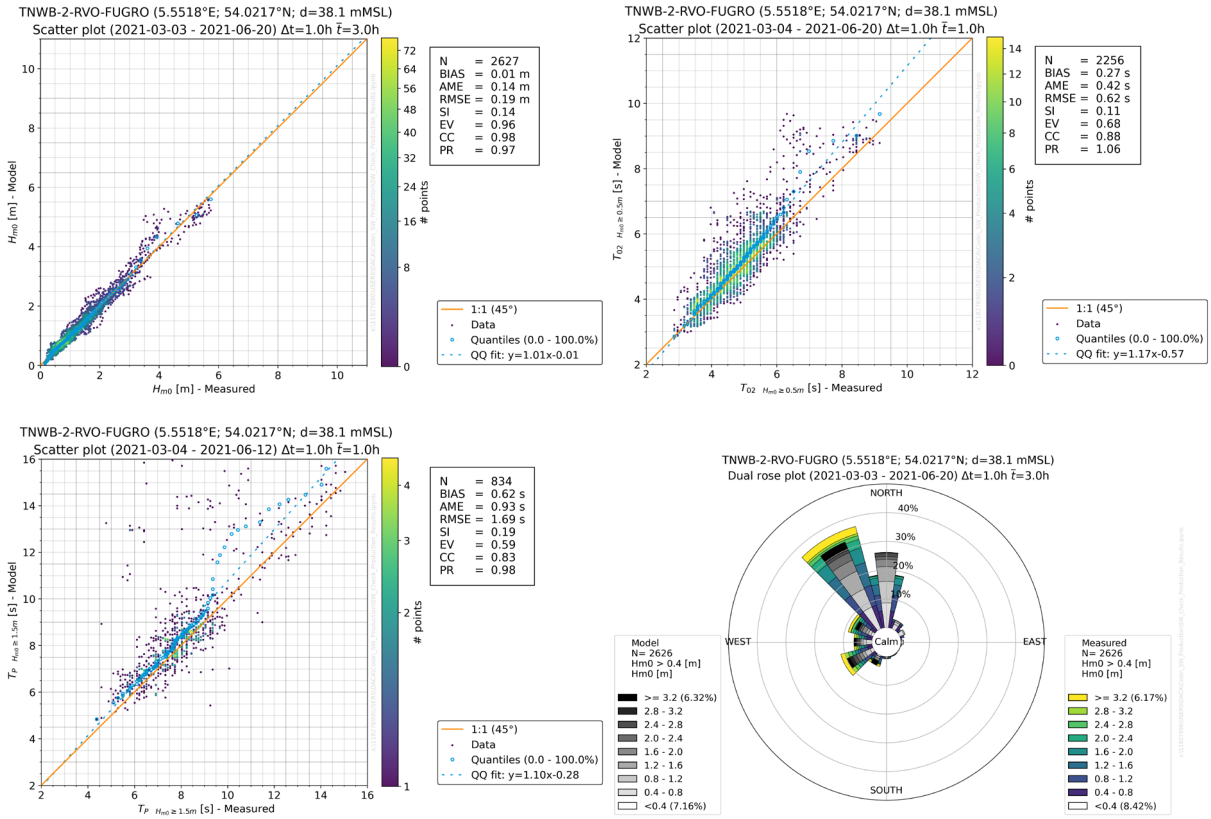

Figure G-20: SW_{DWF23} model validation at station TNWB-2-RVO.

Top-left figure: Hm0 validation results
Top-right figure: T02 validation results
Bottom-left figure: Tp validation results
Bottom-right figure: Wave rose validation results.

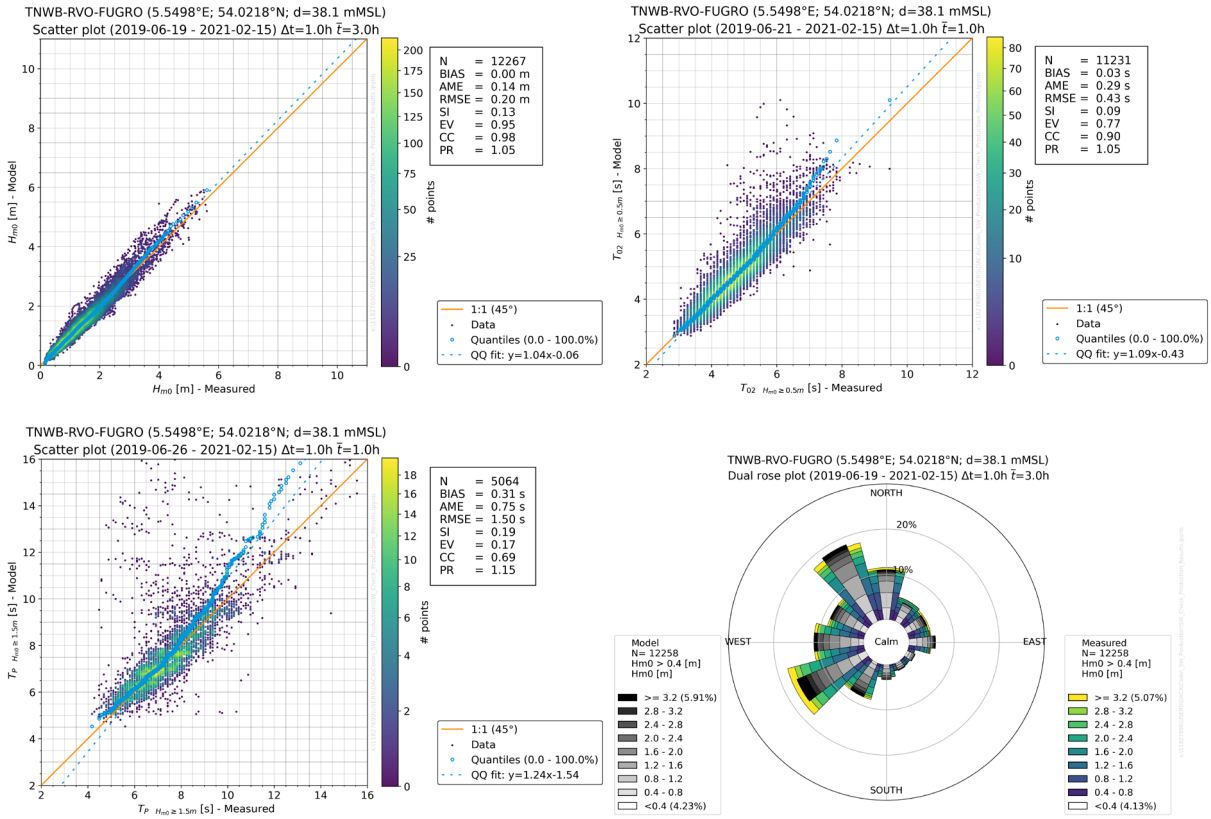

Figure G-21: SW_{DWF23} model validation at station TNWB-RVO.

Top-left figure: Hm0 validation results
Top-right figure: T02 validation results
Bottom-left figure: Tp validation results
Bottom-right figure: Wave rose validation results.

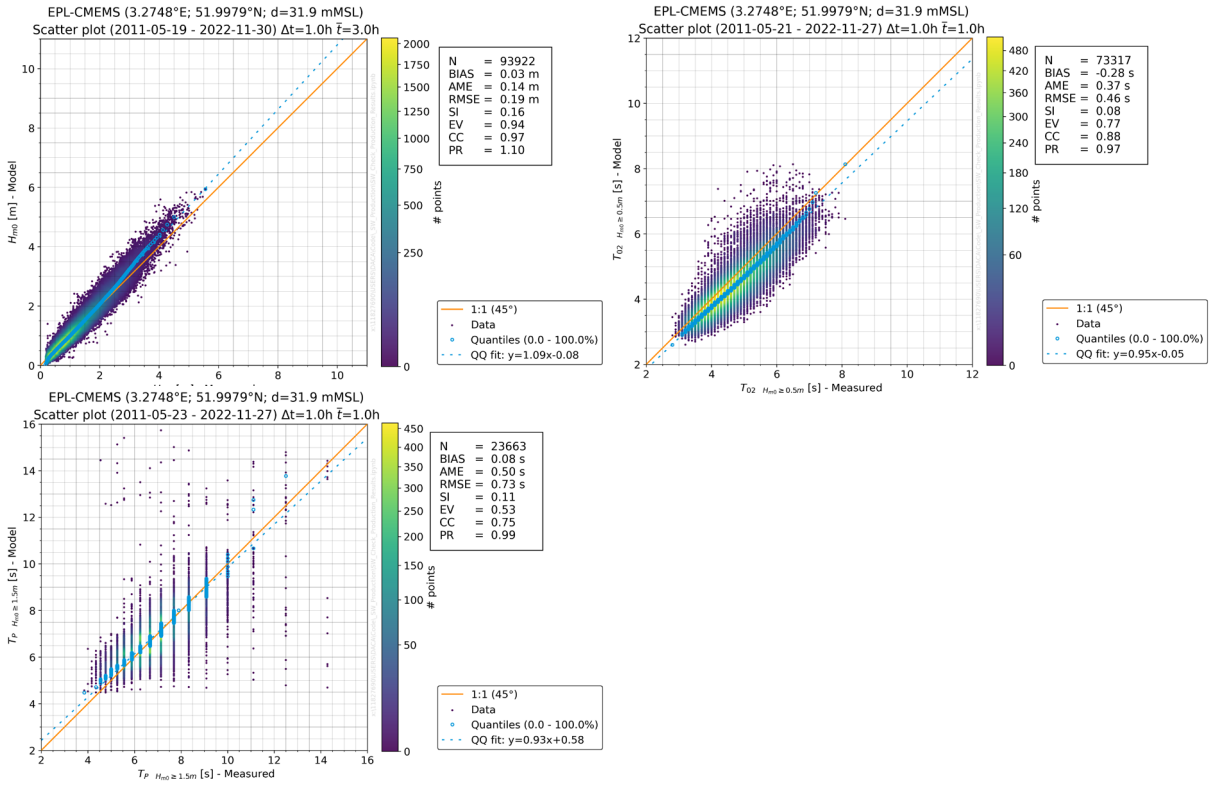

Figure G-22: SW_{DWF23} model validation at station EPL-CMEMS.
Top-left figure: Hm0 validation results
Top-right figure: T02 validation results
Bottom figure: Tp validation results.

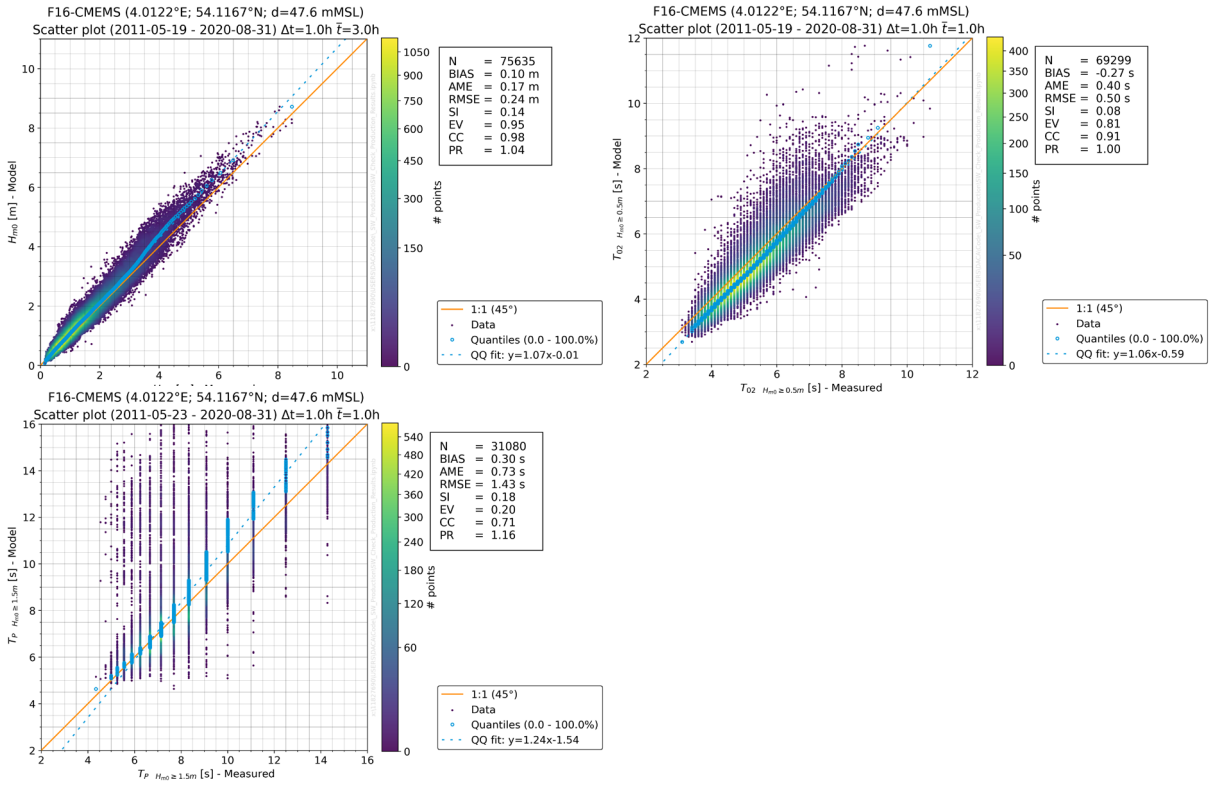

Figure G-23: SW_{DWF23} model validation at station F16-CMEMS.
Top-left figure: Hm0 validation results
Top-right figure: T02 validation results
Bottom figure: Tp validation results.

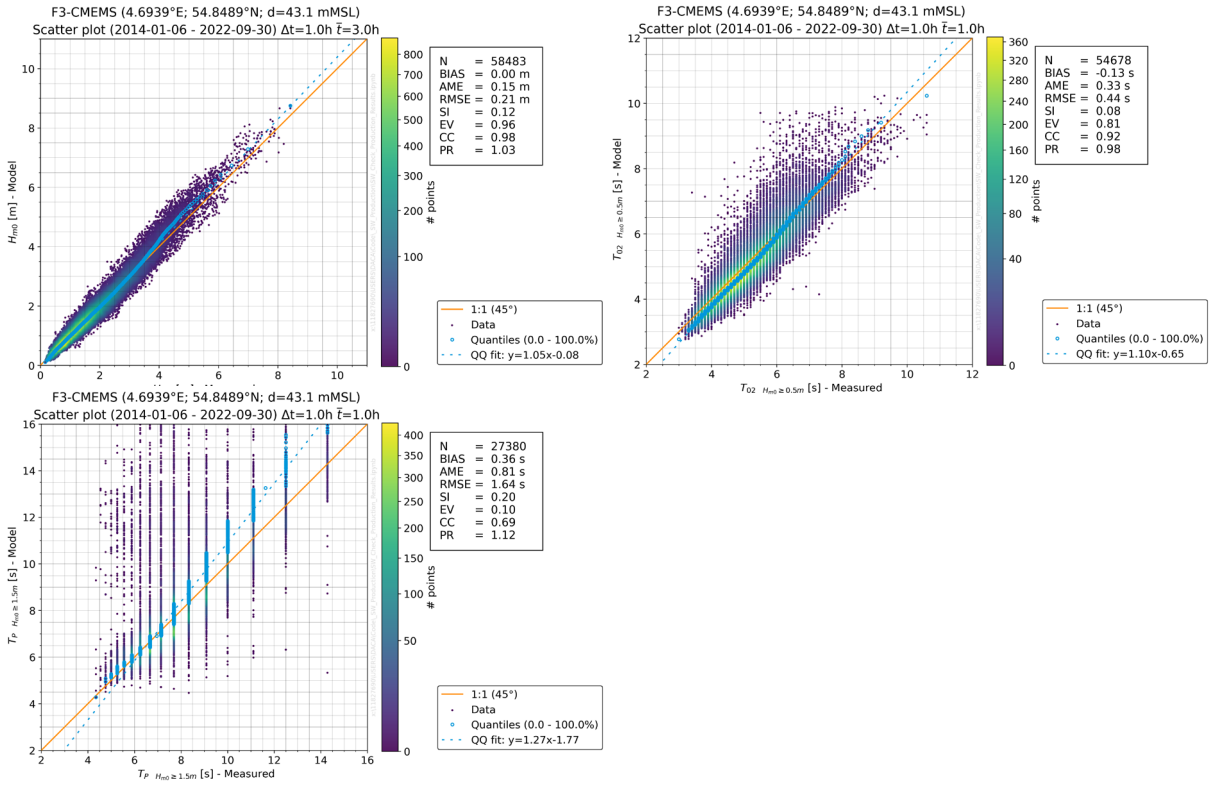

Figure G-24: SW_{DWF23} model validation at station F3-CMEMS.
Top-left figure: Hm0 validation results
Top-right figure: T02 validation results
Bottom figure: Tp validation results.

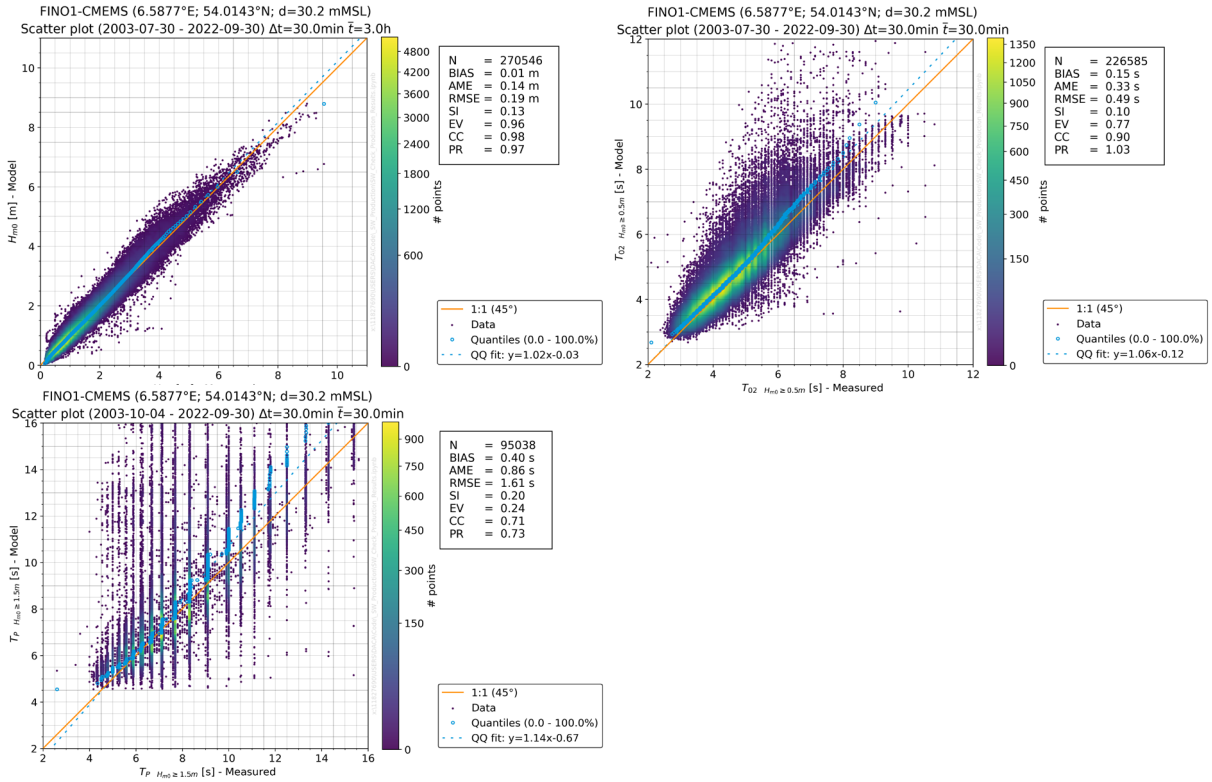

Figure G-25: SW_{DWF23} model validation at station FINO1-CMEMS.
Top-left figure: Hm0 validation results
Top-right figure: T02 validation results
Bottom figure: Tp validation results.

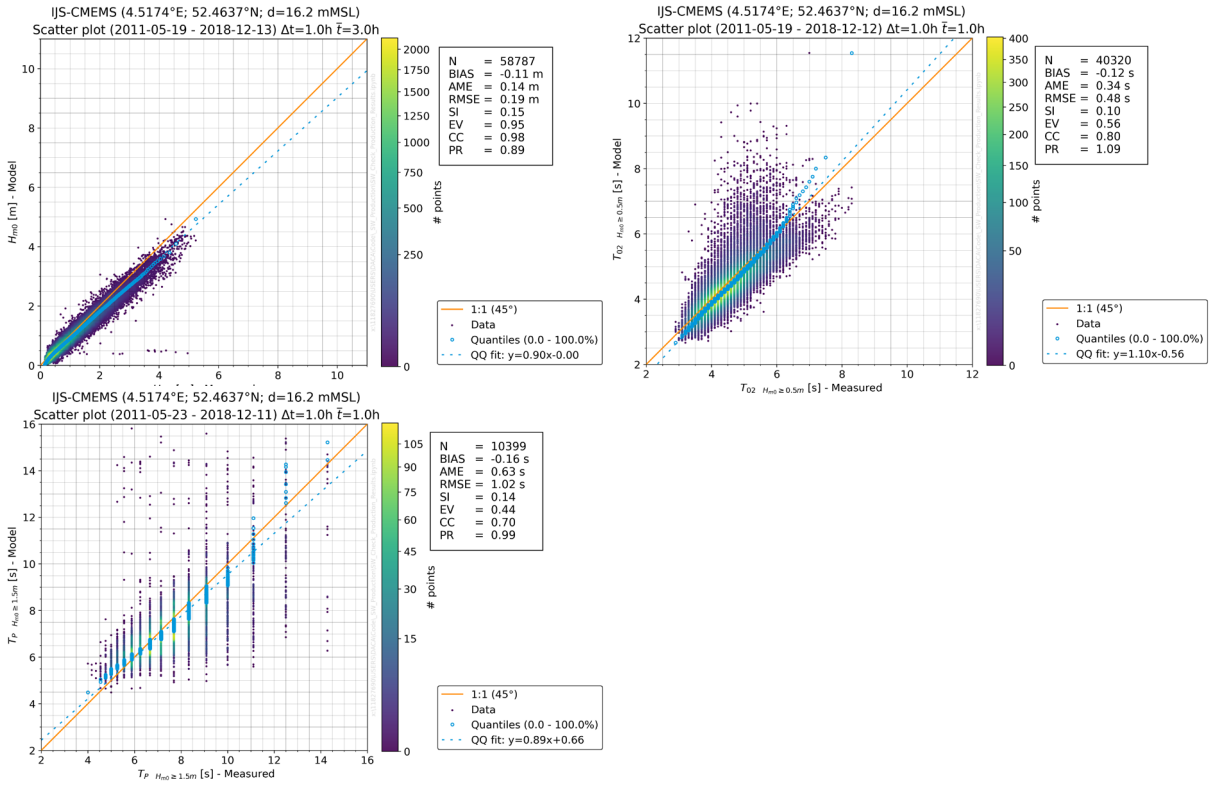

Figure G-26: SW_{DWF23} model validation at station IJS-CMEMS.
Top-left figure: Hm0 validation results
Top-right figure: T02 validation results
Bottom figure: Tp validation results.

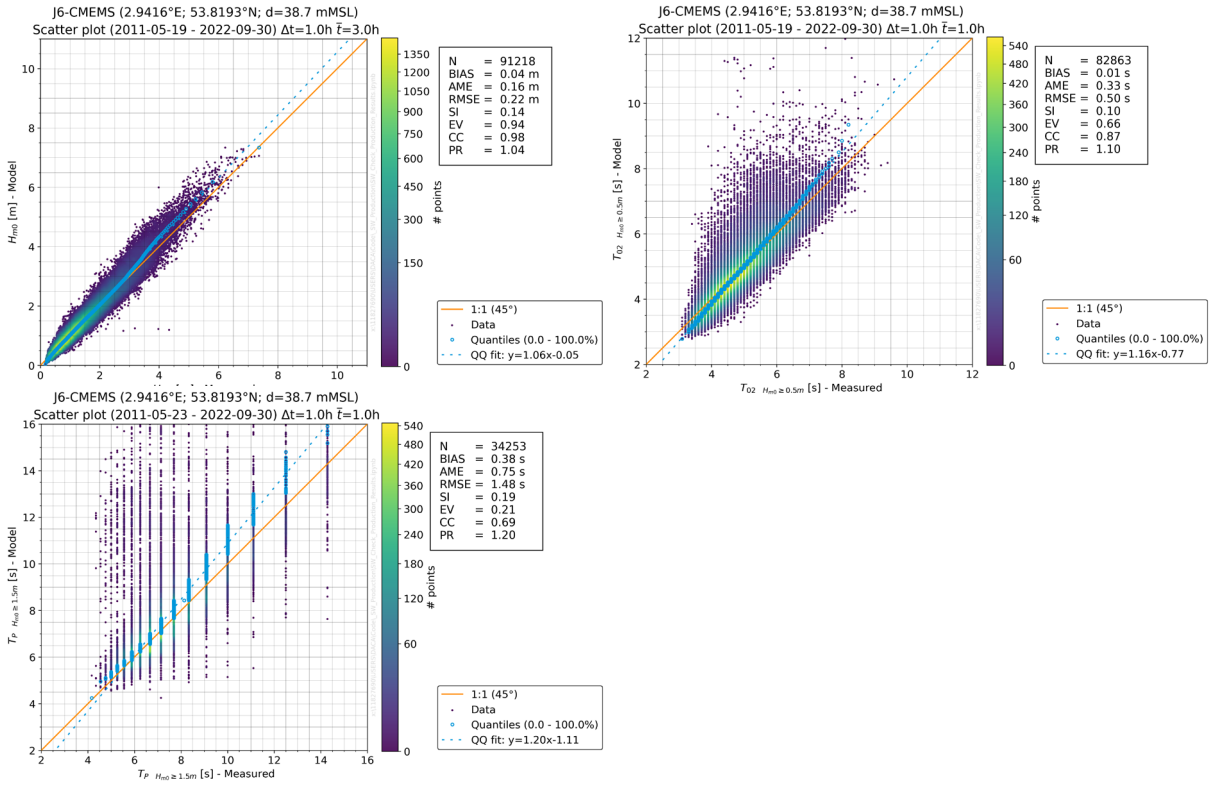

Figure G-27: SW_{DWF23} model validation at station J6-CMEMS.
Top-left figure: Hm0 validation results
Top-right figure: T02 validation results
Bottom figure: Tp validation results.

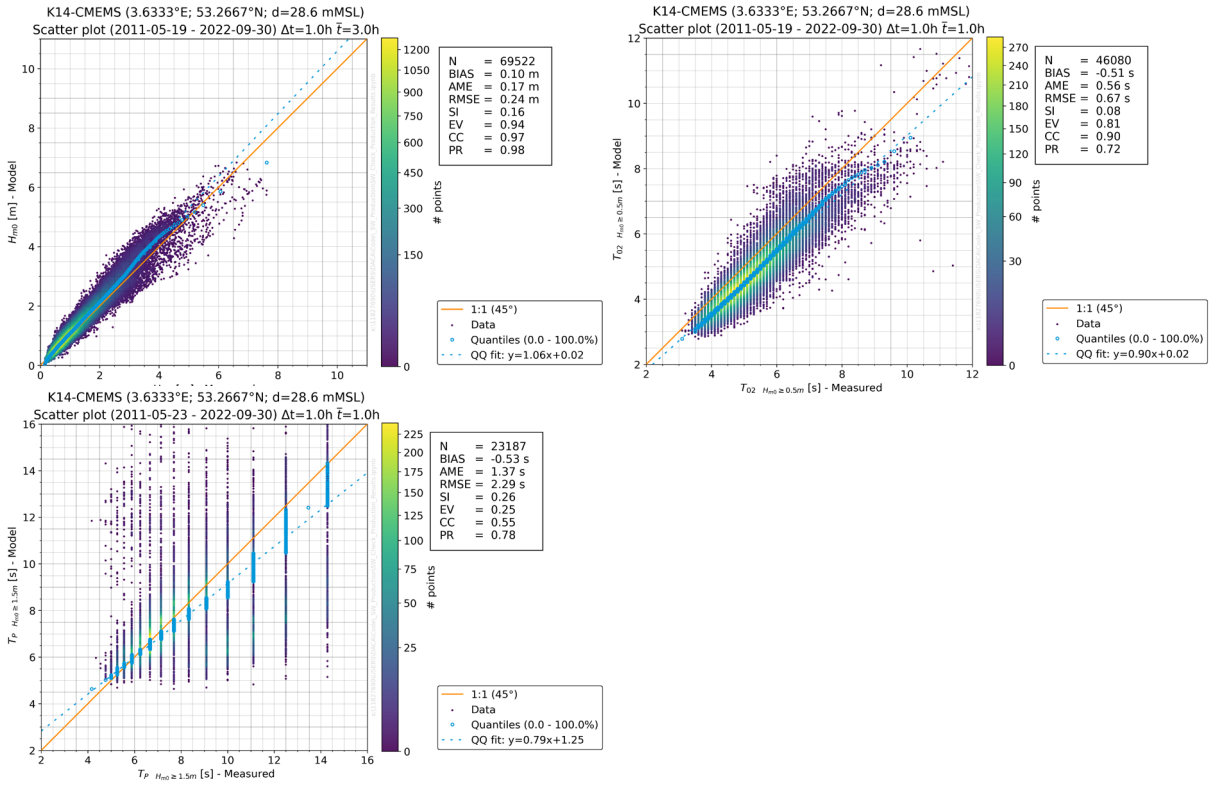

Figure G-28: SW_{DWF23} model validation at station K14-CMEMS.
Top-left figure: Hm0 validation results
Top-right figure: T02 validation results
Bottom figure: Tp validation results.

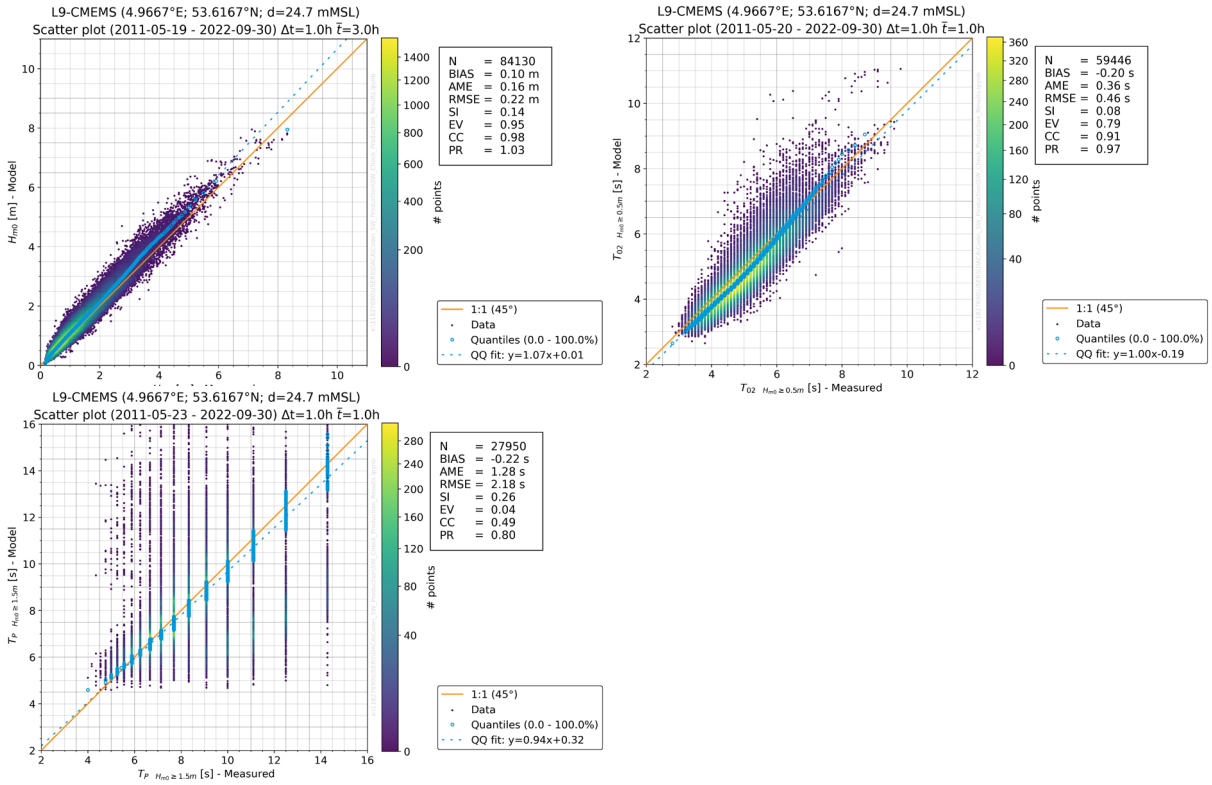

Figure G-29: SW_{DWF23} model validation at station L9-CMEMS.
Top-left figure: Hm0 validation results
Top-right figure: T02 validation results
Bottom figure: Tp validation results.

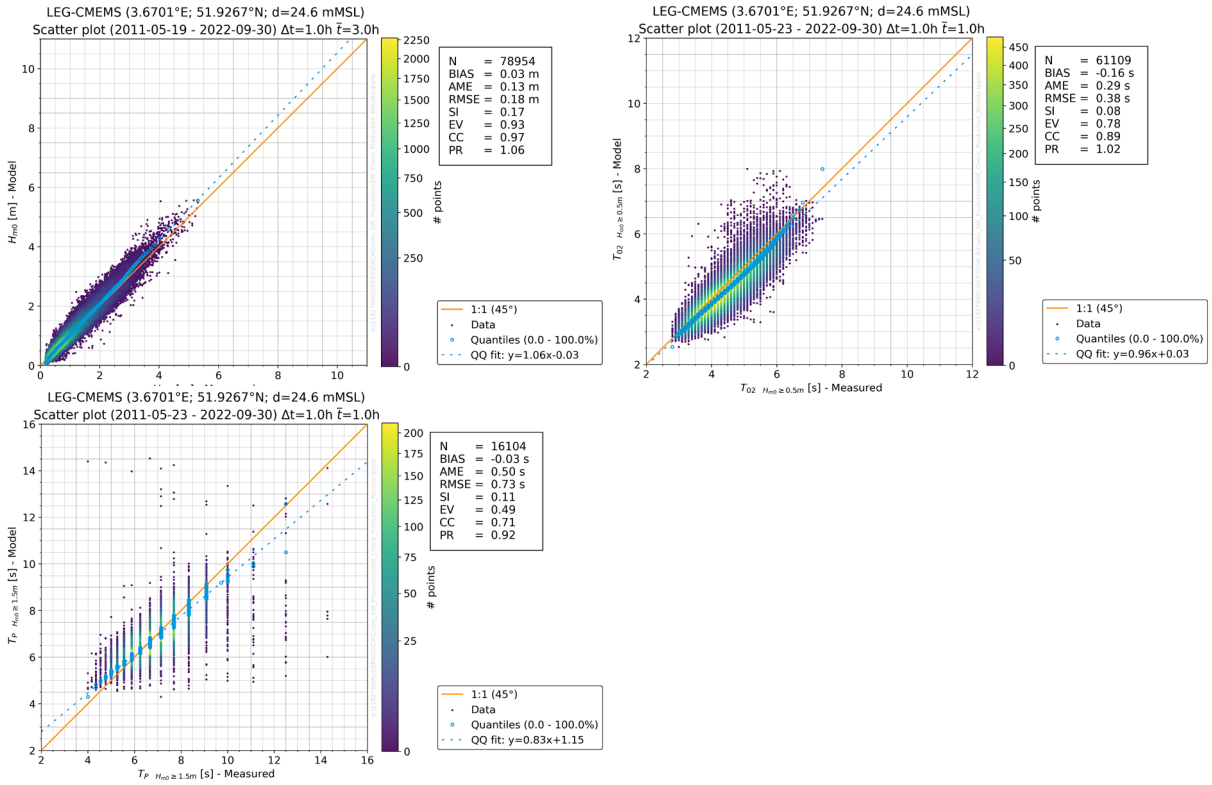

Figure G-30: SW_{DWF23} model validation at station LEG-CMEMS.
Top-left figure: Hm0 validation results
Top-right figure: T02 validation results
Bottom figure: Tp validation results.

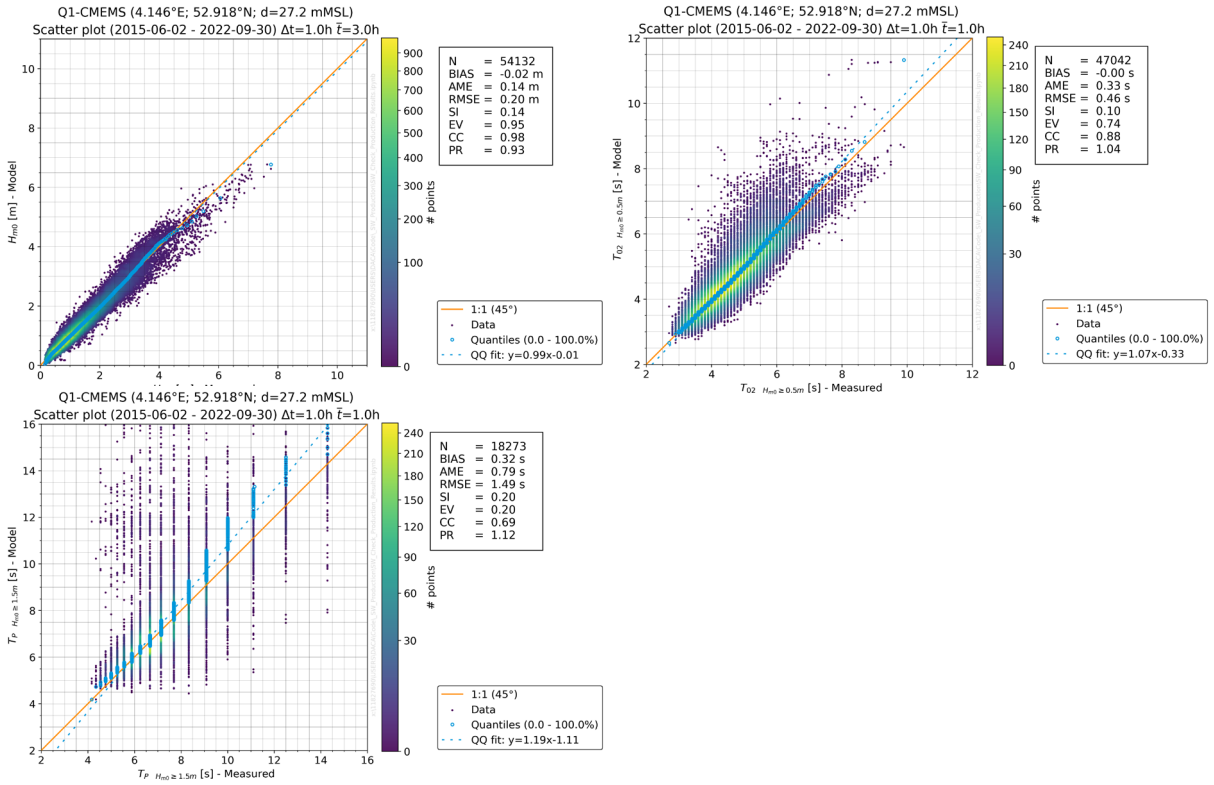

Figure G-31: SW_{DWF23} model validation at station Q1-CMEMS.
Top-left figure: Hm0 validation results
Top-right figure: T02 validation results
Bottom figure: Tp validation results.

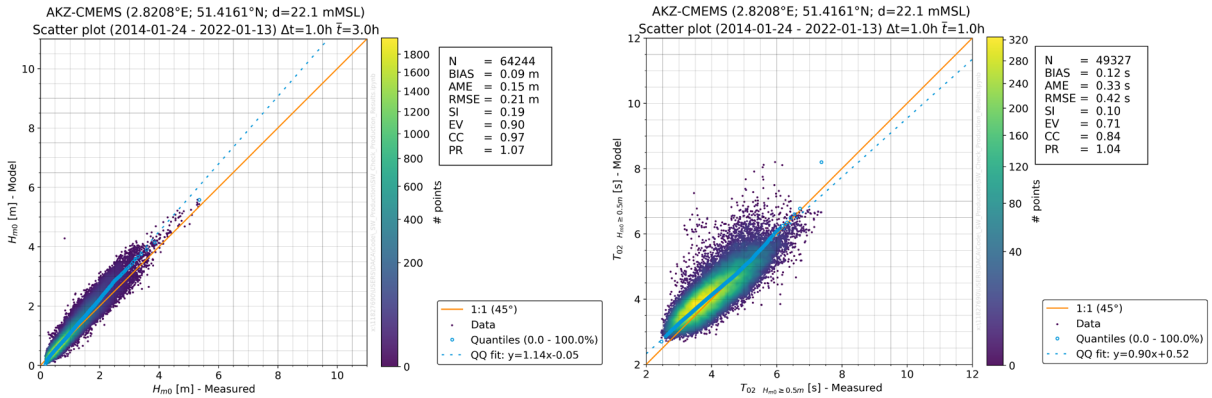

Figure G-32: SW_{DWF23} model validation at station AKZ-CMEMS.

Left figure: Hm0 validation results

Right figure: T02 validation results.

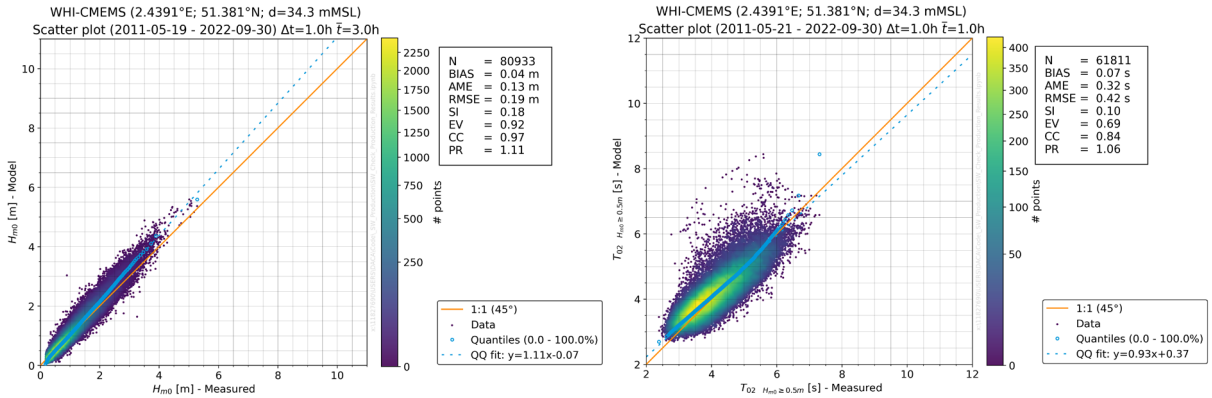

Figure G-33: SW_{DWF23} model validation at station WHI-CMEMS.

Left figure: Hm0 validation results

Right figure: T02 validation results.

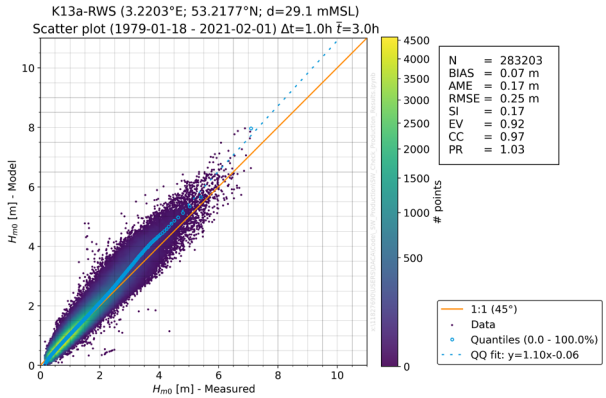

Figure G-34: SW_{DWF23} model validation at station K13a-RWS.
Hm0 validation results.

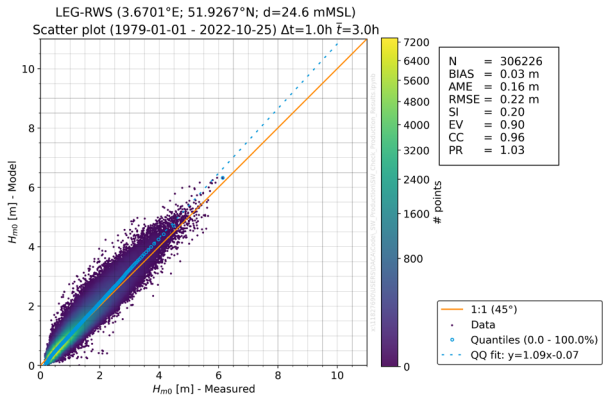

Figure G-35: SW_{DWF23} model validation at station LEG-RWS.
Hm0 validation results.

Appendix H DHI North Europe Hydrodynamic Model forced with ERA5. Validation report.

See next pages.

DHI North Europe Hydrodynamic Model forced with ERA5

Validation Report

25th October 2023

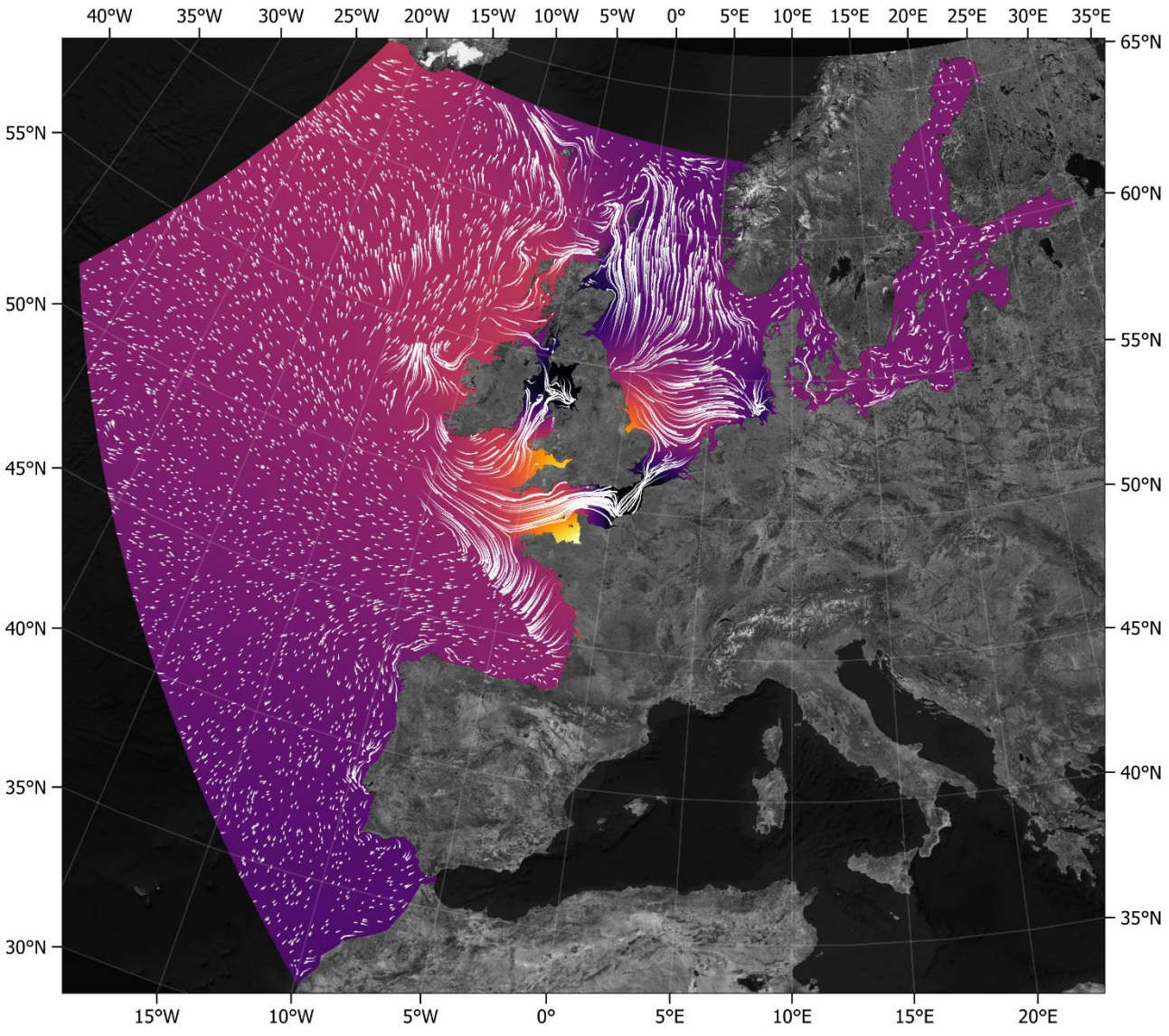

The expert in **WATER ENVIRONMENTS**

Contents

Figures

Tables

Appendices

Revision History

Revision	Date	Reviewer	Approver	Comments
Final 1.0	2023-10-25	RBOL, JTS	JUF	First revision

Nomenclature

Abbreviations	
BSH	Federal Maritime and Hydrographic Agency of Germany - Bundesamt für Seeschifffahrt und Hydrographie
CMEMS	European Centre for Medium Range Weather Forecasts
DA	Data Assimilation
DTM	Digital Terrain Model
ECMWF	European Centre for Medium-Range Weather Forecasts
EMODnet	European Marine Observation and Data Network
ERA5	ECMWF Reanalysis 5
FM	Flexible mesh
HD	Hydrodynamic
KDI	Danish Coastal Authority
LAT	Lowest Astronomical Tide
mMSL	Metres above Mean Sea Level
MOOD	DHI's Metocean-on-Demand Portal
NE	North Europe
QA	Quality Assurance
RWS	Rijkswaterstaat
SMHI	Swedish Meteorological and Hydrological Institute
UTC	Coordinated Universal Time (Universal Time Coordinated)
WL	Water Level
WOZ	Wind op Zee

Subscripts	
NE	North Europe
DA	Data Assimilation

Definitions	
Time	Times are relative to UTC
Level	Levels are relative to MSL (if not specified otherwise)

Definitions	
Coordinate system	Lon/Lat WGS84 (if not specified otherwise)
Direction	Directions are 30 bins relative to true north, i.e., 12 bins covering: 30 deg: 0° = ÷15° -15°N, 30° = 15°-45°N, etc. Clockwise from North Wind: °N coming from Current: °N going to
Time averaging	All time averages are based on a central window averaging

Symbols		Units
WL	Water Level	m
WS_{10}	Wind speed at 10 mMSL	m/s
WD_{10}	Wind direction at 10 mMSL	°N (coming from)

1 Introduction

DHI has established a new regional hydrodynamic hindcast model for the North Europe (NE) area to describe the historical hydrodynamic conditions. This technical note gives an overview of the implementation of the hydrodynamic model, including the sources of the measurements used in the water level validation process and for data assimilation.

DHI has a long-standing history of hydrodynamic and wave hindcast modelling using DHI's suite of MIKE tools, in waters around the globe including in the North Sea and the Baltic Sea. In line with this, DHI has regional models for the North Europe area, including a **hydrodynamic model (HD_{NE-DA})** established with DHI's MIKE 21 HD. The model extent can be observed in Figure 1.1.

This technical note is a validation report for the regional **DHI North Europe hydrodynamic regional model (HD_{NE-DA})**. The HD_{NE-DA} model domain extends from the deep water and encompasses the shelf-seas of north-western Europe, including the Irish and Celtic Sea, the English Channel, the North Sea, and the Baltic Sea (Figure 1.1 and Figure 2.2).

Described in this note is the model data basis and validation made against available measurement data. The measurements used in this report arise mainly from the following public sources: Federal Maritime and Hydrographic Agency of Germany - Bundesamt für Seeschifffahrt und Hydrographie (BSH[1]), Rijkswaterstaat (RWS[2]), Danish Coastal Authority (KDI[3]), Swedish Meteorological and Hydrological Institute (SMHI[4]), and Wind op Zee (WOZ[5]). Most of the data were accessed through Copernicus Marine Environment Monitoring Service (CMEMS[6]). The atmospheric model used to force HD_{NE-DA} is ERA5. ERA5, short for "ECMWF Reanalysis 5," is a state-of-the-art atmospheric reanalysis dataset created and maintained by the European Centre for Medium-Range Weather Forecasts (ECMWF[7]).

This technical note is arranged as follows:

Section 2 presents the data basis (water levels), bathymetry data source, and the applied measurement QA.

Section 3 gives a summary of the atmospheric model (ERA5) used to force HD_{NE-DA}

Section 4 provides a description of the regional North Europe hydrodynamic model, HD_{NE-DA}. Details of the model's setup and validation are presented.

Section 5 presents the concluding remarks and sums up the results obtained through the validation process.

[1] https://www.bsh.de/DE/Home/home_node.html
[2] https://www.rijkswaterstaat.nl/en
[3] https://www.kyst.dk/
[4] https://www.smhi.se
[5] https://www.windopzee.net/
[6] Dashboard - CMEMS In Situ TAC (marineinsitu.eu)
[7] ECMWF | Advancing global NWP through international collaboration

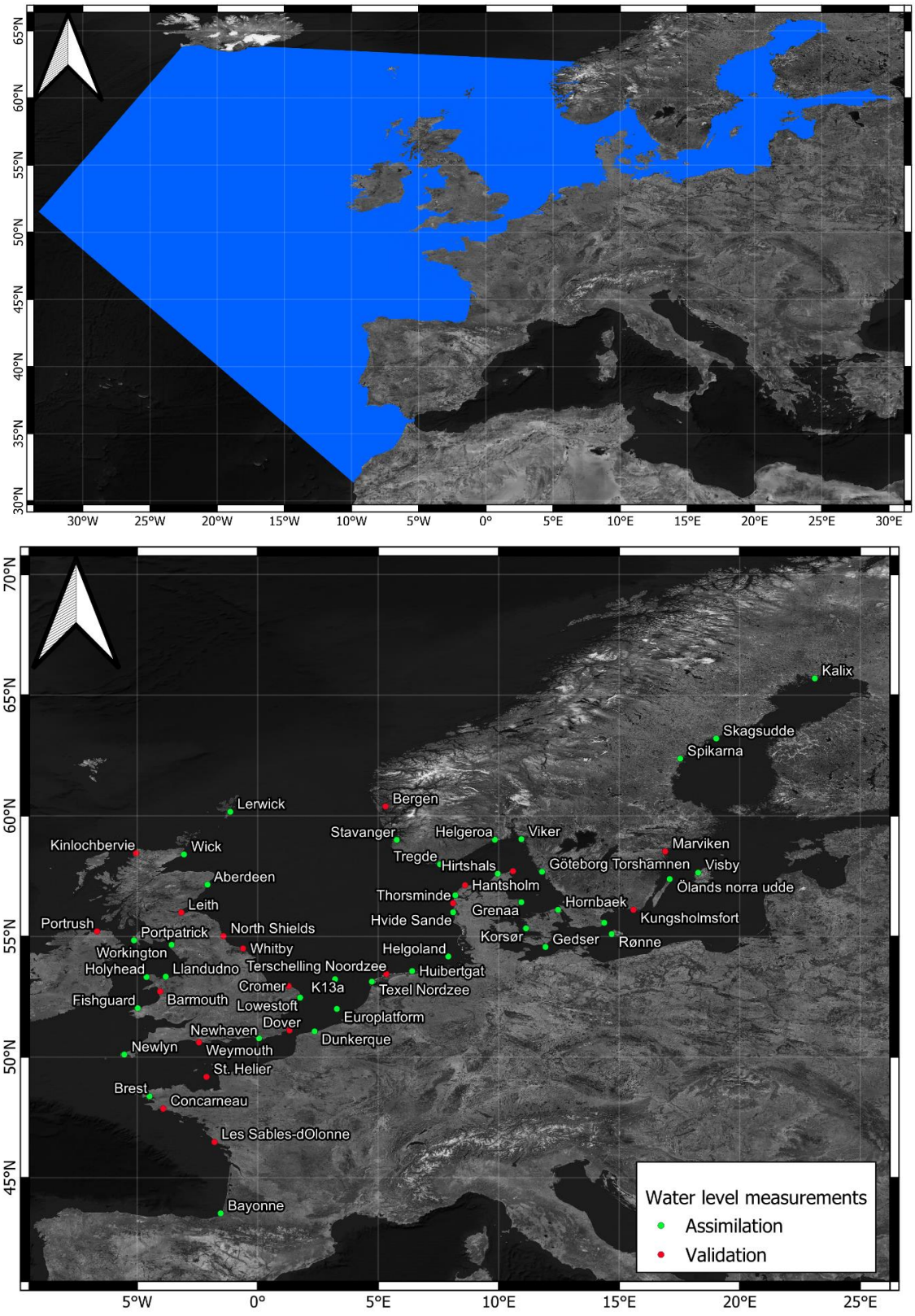

Figure 1.1 DHI North Europe Hydrodynamic Model (HD_{NE-DA}) domain and available stations

Top panel presents the model domain (blue) while the bottom panel shows the assimilation and validation stations (respectively green and red dots). The resolution of the model goes from 30 km near the offshore boundaries down to approximately 2 km in coastal areas.

2 Measurement Data

Measured data was used in two ways when establishing DHI's regional North Europe HD model, HD_{NE-DA}; Bathymetry data from regional Digital Terrain Model (DTM) was used to establish the model bathymetry; In-situ and remote sensing data were used for calibration and validation of the model. Information about the measurements used for the model validation included in this report are described in this section.

2.1 Water levels

In-situ measurements data was used to validate the regional North Europe hydrodynamic model, HD_{NE-DA}, as well as the atmospheric model used for forcing the regional hydrodynamic model. An overview of the tide gauge stations used for the model validation are presented in this report and are given in Table 2.1, and the locations are depicted in Figure 2.1.

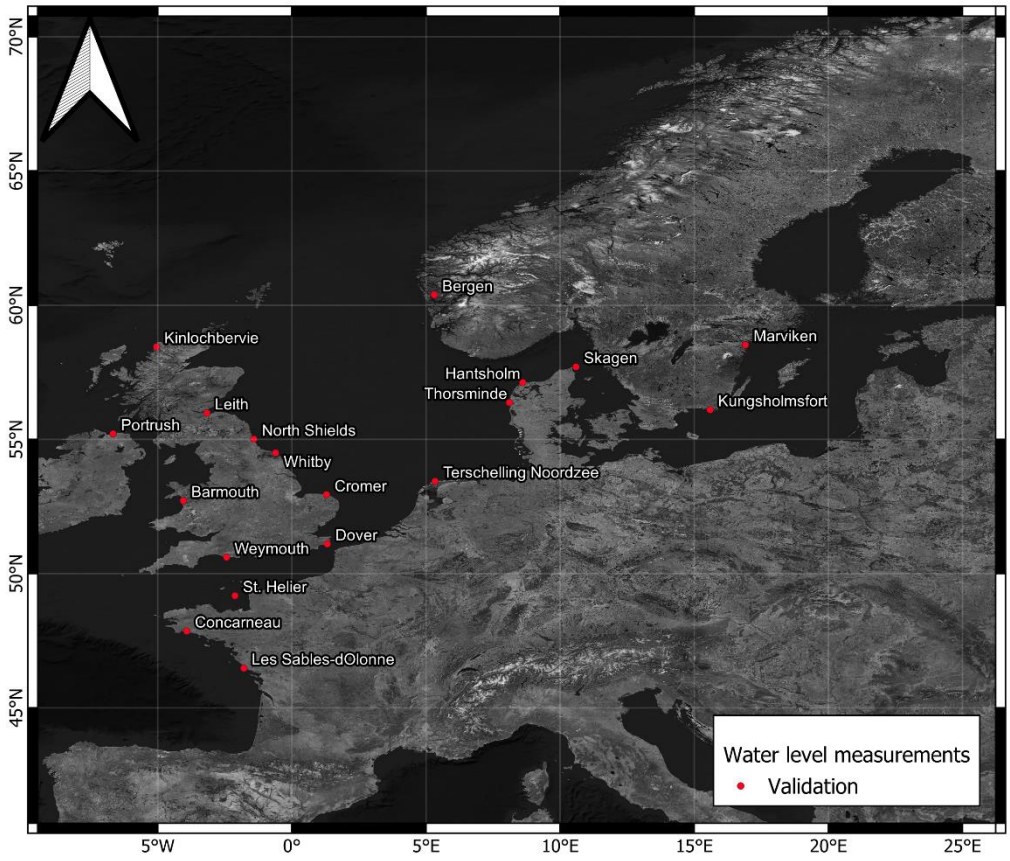

Figure 2.1 DHI North Europe hydrodynamic model (HD_{NE-DA}) validation stations
Map shows the validation stations (red dots).

Water level datasets were obtained from 20 tidal gauge station listed in Table 2.1. Measured water level (WL) was used for the validation of the HD_{NE-DA} model in this report.

Please note there may be some gaps in the measurement time series, though they are randomly distributed, and hence statistics like root-mean-square-error (RMSE) and bias are not seasonally biased.

Table 2.1 List of water level measurements stations used for model validation
List of available water level measurements containing station name, geographical coordinates, depth, and the time length of datasets. Measurements available on CMEMS[8].

Station Name	Longitude (°E)	Latitude (°N)	Depth [mMSL]	Time length
Barmouth	-4.0477	52.7172	-1.5845	1993-01-01 – 2022-04-29
Bergen	5.3042	60.3896	-84.1755	1994-01-01 – 2022-12-31
Concarneau	-3.9186	47.8603	-5.3415	1999-06-28 – 2022-09-30
Cromer	1.2872	52.9426	-4.5946	1993-12-01 – 2022-12-31
Dover	1.3187	51.1062	-14.614	1993-12-01 – 2022-12-31
Hantsholm	8.602	57.1216	-9.5426	1999-01-01 – 2022-12-31
St. Helier	9.9586	57.5965	-7.8314	1993-12-31 – 2022-12-31
Kinlochbervie	11.1311	55.3332	-3.1463	1993-01-01 – 2022-12-31
Korsør	15.5904	56.1013	-8.1665	1998-01-01 – 2022-12-31
Kungsholmsfort	-3.1695	55.9876	-3.0036	1993-12-01 – 2022-12-31
Leith	-1.1367	60.1623	-5.3692	1993-12-01 – 2022-12-31
Les Sables-dOlonne	-3.8146	53.3317	-5.0885	1994-01-01 – 2022-04-30
Marviken	0.0558	50.7772	-5.6065	1993-12-01 – 2019-10-01
North Shields	17.0923	57.3758	-12.1942	1993-01-01 – 2022-12-31
Portrush	14.6859	55.0965	-10.1277	1995-07-06 – 2022-12-31
Skagen	19.0239	63.2015	-2.6172	1993-05-03 – 2021-03-24
Terschelling Noordzee	5.3347	53.4415	-9.1777	1993-12-31 – 2022-12-31
Thorsminde	8.1062	56.3746	-5.1539	1994-10-01 – 2022-12-31
Weymouth	-2.4357	50.61	-5.526	1993-12-31 – 2022-12-31
Whitby	-0.6081	54.4989	-11.9822	1993-12-31 – 2022-12-31

2.2 Measurements QA

Third-party measurement data downloaded by DHI has been assumed to have had some level of quality assurance performed by the data provider. In addition to this, DHI also investigated the measurements to remove any spurious values (outliers, unexpected spikes, or duplicated time steps) before using the measurement data. This is of particular importance when comparing the measurements with results from the models as also for data assimilation (DA).

The following data processing were performed by DHI on the metocean water level observations:

- Visual inspection of the measurements
- Converting to UTC, time, units and conventions as used in this report

[8] Home | CMEMS (copernicus.eu)

- Removing clear outlier data outside of the tidal range of each station.

It is also important to mention that the measured water levels were averaged to 30 min.

2.3 Bathymetry

For the generation of the model's computational mesh, the bathymetry was based on data from the DTM data products adopted from the EMODnet version 2020[9]. The EMODnet digital bathymetry has been produced from bathymetric survey data and aggregated bathymetry datasets collated from public and private organisations. The data provided was pre-processed and quality-controlled at a grid resolution of 1/16 x 1/16 arc minutes (approx. 115 m x 115 m). Data can be retrieved with a vertical datum of the mean sea level (MSL).

The bathymetry interpolated in the model's computational mesh (relative to MSL) and respective mesh elements can be seen in Figure 2.1 and Figure 2.2.

[9] Bathymetry | European Marine Observation and Data Network (EMODnet) (europa.eu)

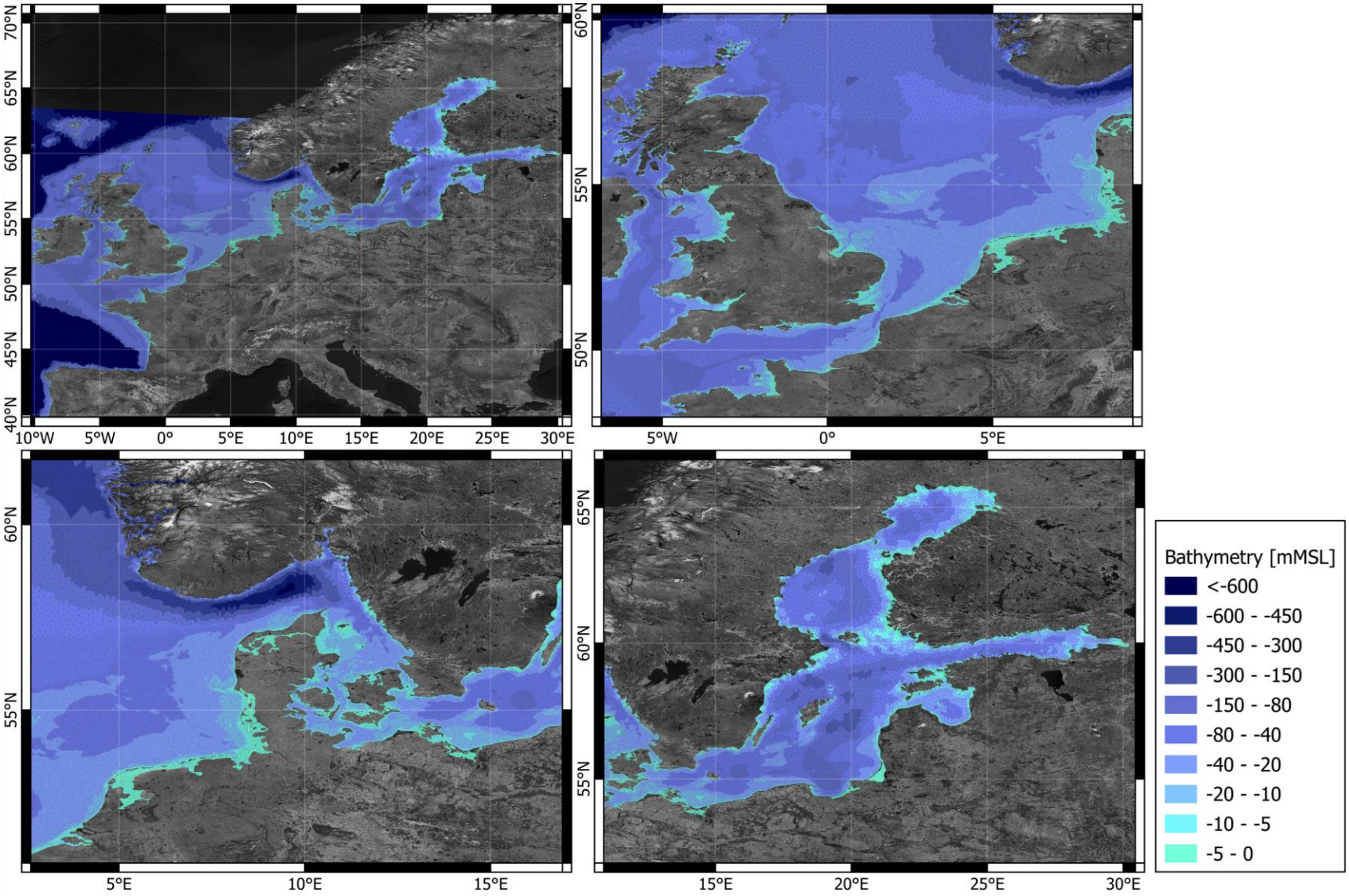

Figure 2.2 $HD_{NE\text{-}DA}$ model bathymetry (mMSL)

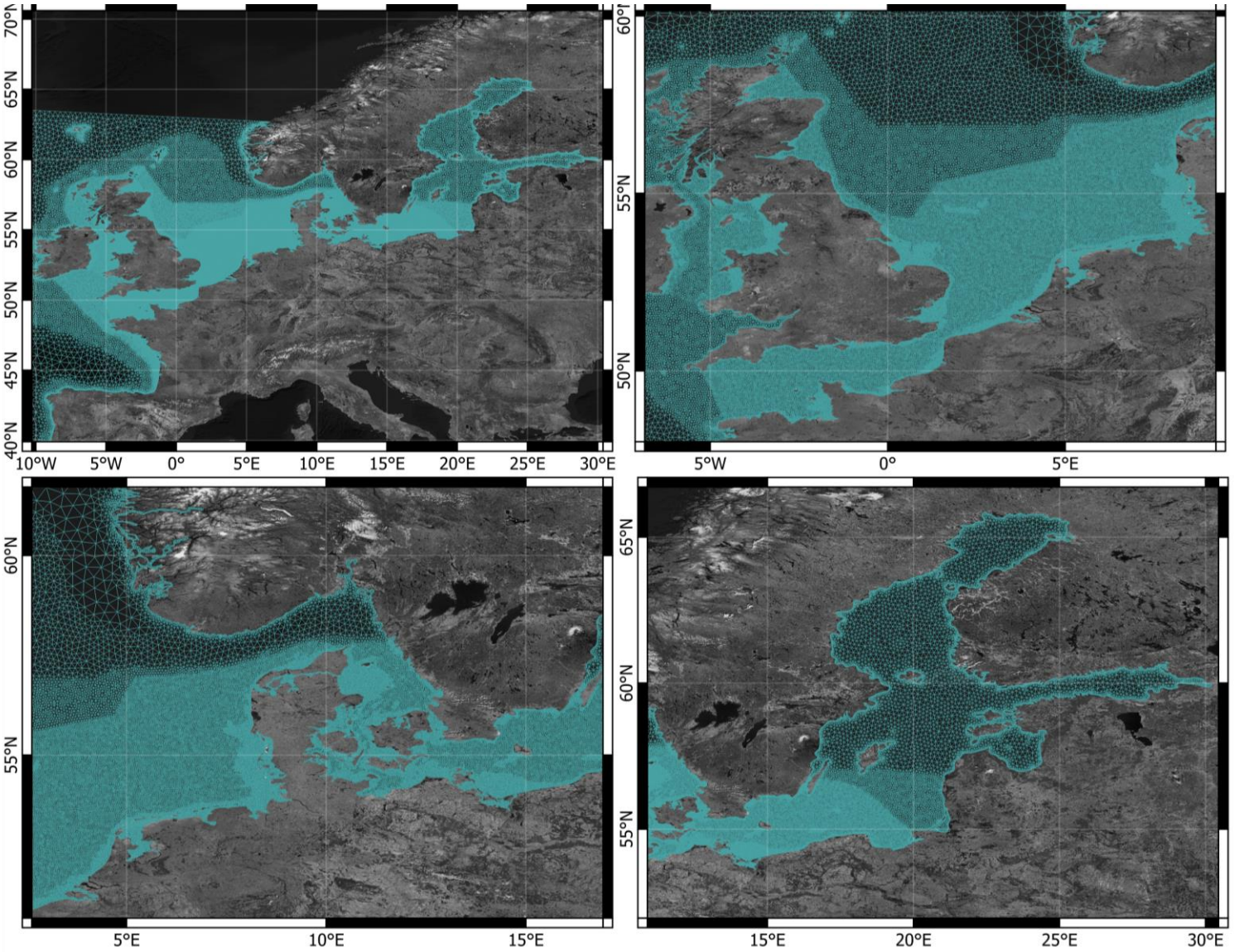

Figure 2.3 **$HD_{NE\text{-}DA}$ model mesh**

Resolution of the regional model goes from 30 km at the offshore boundaries down to approximately 2 km in coastal areas.

3 Atmospheric Model for Forcing

Atmospheric data fields are required for the numerical hydrodynamic model. In this case, the ERA5 dataset was applied to force the hydrodynamic model through wind speed and direction at 10 mMSL and surface pressure.

The wind and pressure data from the ERA5 used for this study were based on an hourly basis from 1979-01-01 to 2022-12-31. The spatial resolution of wind data is 0.25° during the full period.

ERA5 is derived from a combination of observational data, including surface and upper-air observations, satellite data, and model simulations, all integrated using advanced data assimilation techniques.

ERA5 is known for its high data quality and accuracy. It incorporates the latest advances in numerical weather prediction models and data assimilation techniques, leading to improved representation of atmospheric processes and better spatial and temporal consistency. It is widely used for a variety of applications, including weather forecasting, climate research, environmental monitoring, and climate change studies.

The ERA5 parameters utilized for analysis in this study are summarized in Table 3.1. More specifications on what consists the ERA5 can be found in MOODv2 Web App (metocean-on-demand.com).

Table 3.1 Specifications of the ERA5 10m wind parameters.
Native output parameter of the ERA5 model were used for analysis.

Parameter	Unit	Description	Comment
WS10	m/s	Wind speed at 10mMSL	Representative of 2-hour averages
WD	°	Wind direction at 10mMSL	-
MSLP	hPa	Mean sea level pressure	-

4 Hydrodynamic Model HD_{NE-DA}

This section provides a summary of the main model parameters used in the regional DHI North Europe Hydrodynamic Model (HD_{NE-DA}). Validation of the model is presented.

4.1 North Europe Hydrodynamic Model (HD_{NE-DA})

DHI's two-dimensional North Europe regional hydrodynamic model (HD_{NE-DA}) simulates water levels and depth-averaged current conditions through numerical modelling using the MIKE 21 Flow Model FM, with its 2022 version.

HD_{NE-DA} is based on an unstructured flexible mesh with refined mesh in shallow areas and covers the period 1979-01-01 to 2022-12-31 (Figure 1.1 and Figure 2.2).

The model includes tide (boundary data extracted from DHI's Global Tide Model), and surge forced by wind and air pressure from the ERA5 atmospheric model dataset (see Section 3).

For the period between 1993-01-01 and 2022-12-31, the HD_{NE-DA} model was optimised by using data assimilation of observed water levels to achieve high-quality results. An overview of the data assimilation scheme used in this period is given in Section 4.1.1.

The output data from the HD_{NE-DA} is summarised in Table 4.1. It includes water level (WL) relative to mean-sea-level, depth-averaged current speed (CS), and depth-averaged current direction (CD), which are saved for each model mesh element at intervals of 0.5 hours.

Table 4.1 Model output parameters of HD_{NE-DA}
The parameters name and specifications (symbol, unit and temporal resolution)

Parameter Name	Symbol	Unit	Temporal resolution (h)
Water level	WL	mMSL	0.5
Depth average current speed	CS	m/s	0.5
Depth average current direction	CD	°N (going-to)	0.5

Table 4.2 summarises the final $HD_{NE\text{-}DA}$ model configuration. The model setup is based on an extensive calibration and validation process against available WL measurements within the study domain (see Figure 2.1 and Table 2.1).

Table 4.2 Overview of the $HD_{NE\text{-}DA}$ model setup parameters

Setting	$HD_{NE\text{-}DA}$
Mesh resolution	~2.5 km to 30 km
Simulation period	1979-15-01 – 2021-31-12 (43 years)
Basic equations	Hydrodynamic module - 2D (depth-integrated)
Time step	30 min
Density	Barotropic
Eddy viscosity	Smagorinsky formulation with a constant value of 0.28
Bed resistance	Depth-dependent Manning map: • < 30 m: 38 $m^{1/3}/s$ • 30-100 m: 42 $m^{1/3}/s$ • > 100 m: 45 $m^{1/3}/s$
Wind forcing	ERA5 (wind field at 10 mMSL and atmospheric pressure at MSL, variable in time)
Wind drag	$C_A = 1.255 \cdot 10^{-3}$, $C_B = 2.425 \cdot 10^{-3}$, $W_A = 7\ m/s$, $W_B = 25\ m/s$ (Empirical parameters used to calculate the drag coefficient of air)
Bathymetry	EMODnet version 2020
Tidal potential	Included: 11 constituents (M2, O1, S1, K2, N2, K1, P1, Q1, MF, MM, SSA)
Boundary conditions	Tidal boundaries extracted from DHI's Global Tidal Model with surge forced by wind and air pressure from the Climate Forecast System Reanalysis (ERA5) atmospheric model.
Data Assimilation Period	1993-01-01-2022-12-31
River discharge	Not included (considered to have an insignificant influence on the water level and current in a 2D regional model where no baroclinic conditions were included)

4.1.1 Data assimilation

Data assimilation (DA) is the process of continuously improving a dynamical model by integrating and assimilating observations (measurements). It is thus not an offline, post-processing method for error correcting results after completing the simulation. Rather, it is an integral part of the simulation process where the model is updated when an observation is received, before proceeding with the next simulation time step. The main benefit of using data assimilation is that it allows the optimal combination of model and observations to give improved forecasts (model predictions) both in space and time, by considering the expected variables correlation between the different model elements.

The ocean system which is being modelled contains several physical phenomena. The two dominant phenomena in the modelled domain are 1) astronomical tides, and 2) atmosphere-driven surge, which each have different characteristic spatial

and time-scale dynamics. This can make it challenging to improve with data assimilation. In the HD_{NE-DA} model, a novel DA approach, consisting of two distinct steps addressing the above two physical phenomena separately, has been developed and applied. Firstly, the tide-component is corrected in a tidal-only model, and secondly, the surge-component is addressed in the "full" model (incorporating the atmospheric forcing). The two-step approach can be viewed as a way to introduce internal boundary conditions for tides.

Step 1 uses a simple DA method "Optimal Interpolation" (OI) integrating a large number of data points from a global tidal model. Step 2 uses a more sophisticated DA technique called the Ensemble Kalman Filter (EnKF) describing the model error covariance using perturbations of the boundary and wind forcing input.

In this model, assimilation of only one physical variable, i.e., point based water level data, was considered. The observations included were the following:

1. In-situ measurements obtained from CMEMS[10] and Rijkswaterstaat[11] data portal.
2. Points from DTU10 Global Tidal Model, which were considered as a proxy for tidal measurements.

The stations used in the model update are called "assimilation" stations, whereas the stations not included in this process but used for validation, are called "validation" stations (Figure 1.1).

Data Assimilation workflow

The data assimilation workflow applied uses two different schemes, known as Optimal Interpolation (OI) and Ensemble Kalman Filter (EnKF). The details of each data assimilation scheme (OI and EnFK) are shown in the subsequent sections. To summarise the workflow of the data assimilation procedure, a list of the steps followed is shown next, along with a flow diagram of the process.

1. Run a tidal-only model and assimilate water level data from DTU10 GTM (treated as "measurements") by means of an OI scheme.
2. Run a complete hydrodynamic model (tidal boundaries + atmospheric forcings) with an EnKF comprising 8 members for a full year, in order to get a time-invariant matrix ("best" time-averaged correction matrix). Just before applying the EnKF data-assimilation, the tidal signal is corrected by means of assimilating the water levels with the results from Step 1.

[10] Dashboard - CMEMS In Situ TAC (marineinsitu.eu)
[11] https://waterinfo.rws.nl/#!/nav/index/

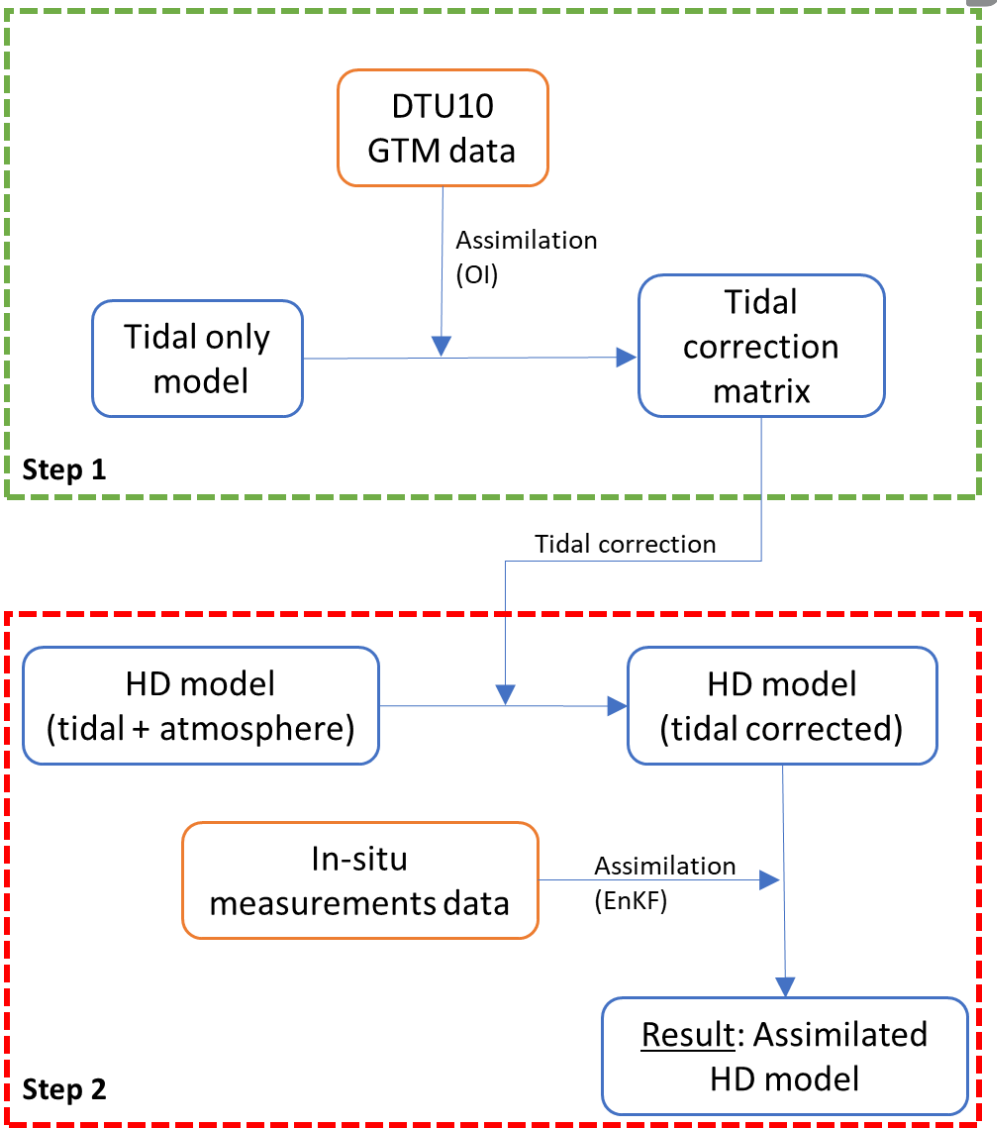

Figure 4.1 Flow diagram of the two-step DA procedure

Optimal Interpolation (OI)

Optimal Interpolation (OI or "statistical interpolation") is a relatively simple univariate data assimilation technique assuming that the model error covariance is static. In most OI implementations, including that of MIKE FMs, the so-called background error covariance describing the model error statistics is assumed to be isotropic and univariate. The implementation in MIKE FM does, however, allow for a spatially varying error covariance description given as a map of model standard deviation and horizontal correlation length scale. In this way, long-range correlations in offshore areas and short-range correlations in coastal waters can be described, or some areas may be disregarded in the model update.

In OI, a single variable (the observed) is updated directly at the point of observation. It decreases gradually away from the point of observation at a scale specified by the user. The "gain" at the observation point is a weighted estimate between the model variance P (supplied by the user) and the measurement variance R (provided by the user): gain=P/(P+R).

For the optimal interpolation scheme, a one-year run was performed of the year 2017 without atmospheric forcings, only with a tidal boundary, and as a proxy for observations, a total of 528 gridded points (1° resolution grid) obtained from DTU10 Global Tidal Model (GTM) [1] were used. Even though in principle these points

come from a model and are not measurements, that model has been corrected by data assimilation with satellite altimetry, and their water level results (tidal only) are a good proxy of the values expected in reality at offshore locations. The location of the Global Tide Model points assimilated with OI scheme are shown in Figure 4.2.

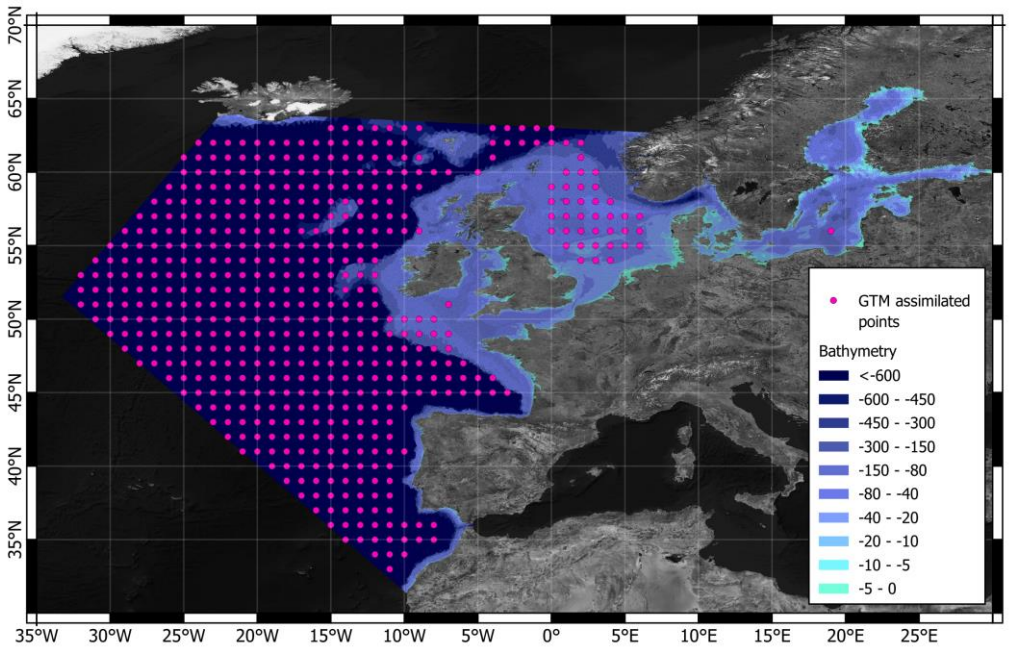

Figure 4.2 Location of water level points assimilated from DTU10-GTM

For the optimal interpolation scheme, the correlation length scale between variables and standard deviation of the model error must be defined on beforehand, and result in some additional calibration parameters. The values used for this model are the following:

- Model error correlation length scale: Between 120 km (offshore areas) to 40 km (nearshore areas)
- Model error correlation standard deviation: Between 0.02 (offshore areas) to 0.005 (nearshore areas)

The results from the run with OI scheme are used to get a near-optimal tidal result, which is then fed into the model before the application of the Ensemble Kalman Filter (explained in next section).

Ensemble Kalman Filter (EnKF)

The EnKF requires an ensemble of model realisation to represent the model error of the system. The ensemble is generally created by adding random noise (perturbations) to initial conditions, forcing data or model parameters. In this project, the primary method of model perturbation is varying the wind forcing input (perturbations both in space and time), as well as the water level boundaries.

The ensemble prescribes the model error covariance by dynamically modelling an ensemble of model simulations and thereby describes how all variables co-vary in space and across variables. The Ensemble Kalman Filter update, which is a Monte Carlo approximation of the Kalman Filter, is the “best” linear update considering the model error (the model error covariance) and measurement error in the sense that it minimises the squared error [2].

Algorithmically, the Ensemble Kalman Filter consists of two stages:

1. Forecast. Propagate all ensemble members one time-step forward.
2. Analysis. Update all ensemble members.

The Ensemble Kalman Filter was used to construct a long-term averaged Kalman gain matrix based on a run of the year 2017 (this period had high coverage of assimilation data and was considered a representative year). From this run, a time-averaged and distance-regularised (localized) Kalman gain matrix was saved. The Kalman gain was then used in all years as a so-called "steady Kalman gain" [3]. This time-constant matrix has the advantage of reducing the computational cost significantly, while preserving good assimilation skills [4] [5]. For the model presented in this report, the EnKF was setup with an 8-ensemble member.

The location of assimilation stations is shown as green points in Figure 4.4. The datum of the measurements was meters MSL. The location of the stations used for validation of the model results is shown as red points in Figure 2.1.

The improvement due to data assimilation was tested for the year 2017. Simulations were carried in the following order:

- Without data assimilation
- With tidal corrections only (ie, only applying the results of step 1 from the flow chart shown in Figure 4.1)
- With the two step approach, ie, tidal corrections and then assimilating the total water level signal (EnKF).

The skill of the model was compared in terms of RMSE and SI values of the water level for both assimilation and validation stations. The application of tidal correction, as expected, improves the results, and the two-step approach (OI + EnKF) give the best overall results. As an example, results for a validation station (North Shields) for the year 2017 is shown in the following figures[12]. For many validation stations, the model skill (RMSE and SI) was improved by 50% or more due to the data assimilation as shown in Table 4.3 for the selected representative validation stations (results of year 2017 only).

[12] The EnKF results are considering the steady-EnKF approach. Tests were done (not shown) where it was seen that results from the steady-EnKF were almost identical to the 8-member EnKF.

Table 4.3 List of measurements stations and statistics used for model validation.

List of available validation stations statistical analyses (RMSE and SI), comparing the non-data assimilation model (1st and 2nd columns), only tidal correction model (3rd and 4th columns) and full data assimilation (5th and 6th columns).

Station	No DA		Tidal Correction		Full DA	
	RMSE [m]	SI	RMSE [m]	SI	RMSE [m]	SI
Barmouth	0.25	0.25	0.17	0.16	0.17	0.15
Bergen	0.11	0.33	0.09	0.25	0.08	0.20
Concarneau	0.14	0.13	0.13	0.12	0.10	0.08
Cromer	0.29	0.27	0.14	0.13	0.10	0.09
Dover	0.38	0.25	0.31	0.20	0.14	0.09
Hantsholm	0.15	0.70	0.09	0.41	0.06	0.27
St. Helier	0.48	0.21	0.33	0.14	0.10	0.04
Kinlochbervie	0.17	0.16	0.11	0.10	0.13	0.10
Kungsholmsfort	0.08	0.57	0.07	0.49	0.05	0.11
Leith	0.35	0.22	0.26	0.12	0.22	0.07
Les Sables-dOlonne	0.15	0.14	0.14	0.13	0.12	0.10
Marviken	0.08	0.62	0.07	0.53	0.02	0.19
North Shields	0.27	0.24	0.14	0.11	0.10	0.07
Portrush	0.18	0.46	0.11	0.28	0.12	0.28
Skagen	0.15	0.90	0.09	0.52	0.04	0.21
Terschelling Noordzee	0.20	0.32	0.12	0.20	0.09	0.13
Thorsminde	0.18	0.66	0.10	0.35	0.08	0.25
Weymouth	0.18	0.39	0.12	0.26	0.08	0.18
Whitby	0.29	0.24	0.15	0.11	0.12	0.07
Mean	**0.21**	**0.37**	**0.14**	**0.24**	**0.10**	**0.14**

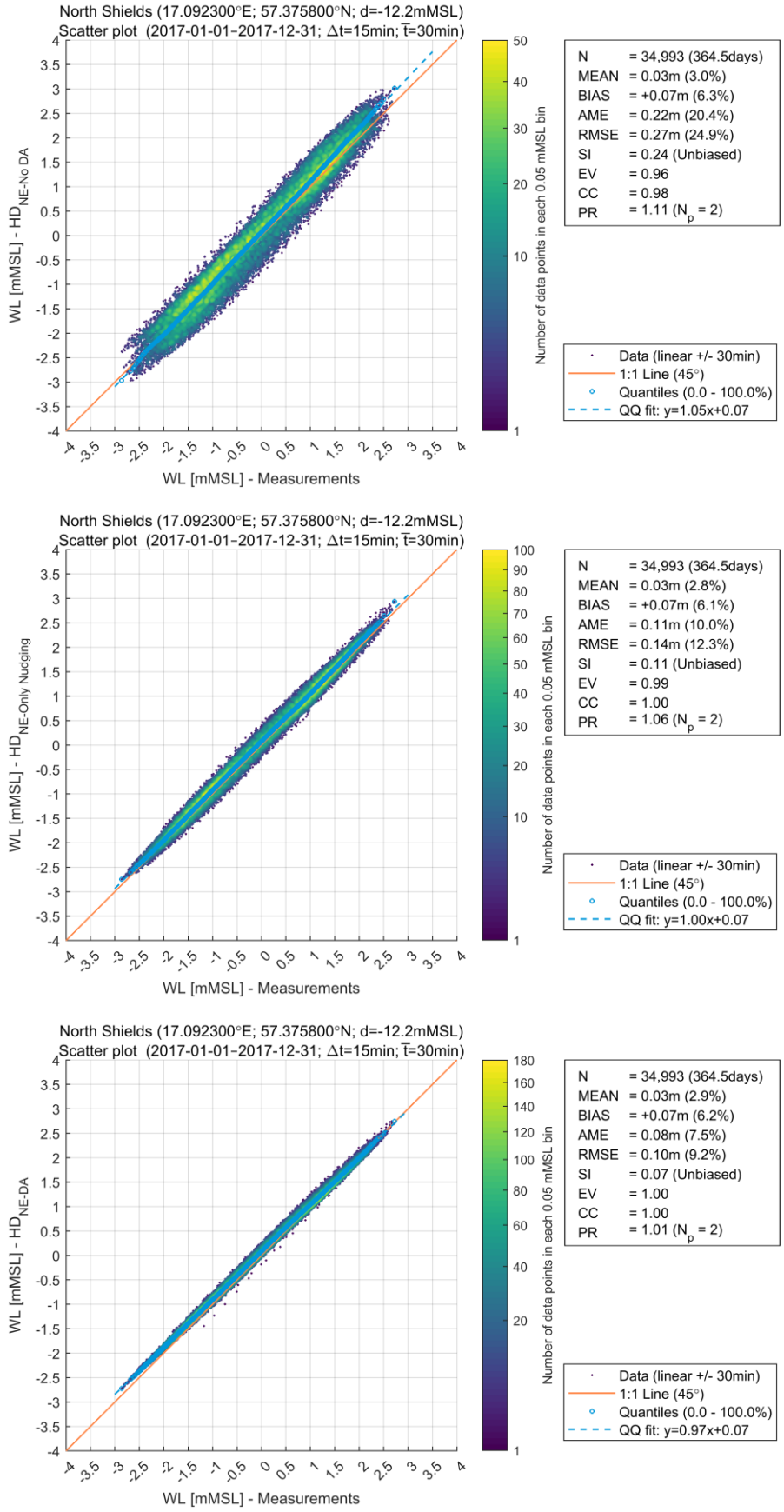

Figure 4.3 Scatter plot of modelled vs measured WL at North Shields [mMSL]
Top: Base case model without Data Assimilation.
Center: Model with tidal correction only (OI from DTU10 GTM)
Bottom: Model with two step DA approach. First, tidal correction is applied (OI), and then DA of the total signal is assimilated (EnKF)

Table 4.4 List of measurements stations used for model assimilation

List of available tide containing geographical coordinates, station name, depth, variables, and the time length of datasets. Measurements available on CMEMS[13] and RWS[14] websites.

Station Name	Longitude (°E)	Latitude (°N)	Depth [mMSL]	Time length
Aberdeen	-2.0827	57.1473	-2.3703	1993-01-01 – 2022-12-31
Bayonne	-1.5372	43.5227	-9.5183	1994-01-01 – 2022-09-30
Brest	-4.4865	48.3764	-9.8384	1993-12-01 – 2022-09-30
Dunkerque	2.36	51.0634	-0.4207	1995-07-09 – 2022-04-30
Europlatform	3.284	51.9957	-28.8943	1993-12-31 – 2022-12-31
Fishguard	-4.977	52.0243	-16.3416	1993-01-01 – 2022-12-31
Gedser	11.9382	54.5623	-3.8445	1993-06-01 – 2022-12-31
Göteborg Torshamnen	11.7952	57.6804	-6.345	1993-12-01 – 2022-12-31
Grenaa	10.9371	56.417	-6.1099	1993-12-31 – 2022-12-31
Helgeroa	9.8352	59.0074	-20.8589	1993-12-31 – 2022-12-31
Helgoland	7.9051	54.1694	-19.1149	1997-10-14 – 2022-12-31
Hirtshals	-4.6149	53.3168	-5.1936	1994-01-01 – 2022-12-31
Holyhead	12.4628	56.1017	-10.8652	1995-02-02 – 2022-12-31
Hornbaek	6.406	53.564	-6.1181	1999-04-06 – 2022-12-31
Huibertgat	8.1084	55.9996	-5.3978	1993-12-31 – 2022-12-31
Hvide Sande	3.2091	53.2235	-28.3381	1993-12-31 – 2022-12-31
K13a	23.1116	65.6922	-11.5075	1993-12-31 – 2022-12-31
Kalix	-5.0508	58.4515	-0.8406	1993-12-01 – 2022-12-31
Korsør	15.5904	56.1013	-8.1665	1998-01-01 – 2022-12-31
Lerwick	-1.7917	46.4782	-7.423	1993-12-01 – 2022-12-31
Llandudno	1.7583	52.4631	-4.8621	1994-05-17 – 2022-12-31
Lowestoft	16.9048	58.5216	-2.0346	1993-01-01 – 2022-12-31

[13] Home | CMEMS (copernicus.eu)
[14] https://waterinfo.rws.nl/#!/nav/index/

Station Name	Longitude (°E)	Latitude (°N)	Depth [mMSL]	Time length
Newhaven	-5.5349	50.1061	-2.0846	1993-01-01 – 2022-12-31
Newlyn	-1.4211	55.0123	-5.8078	1993-01-01 – 2022-12-31
Ölands norra udde	-5.134	54.8373	-16.7549	1993-12-01 – 2022-12-31
Portpatrick	-6.6655	55.2071	-13.8576	1993-01-01 – 2022-12-31
Rønne	14.3746	55.566	-20.9718	2002-04-10 – 2022-12-31
Simrishamn	10.5892	57.7045	-9.2357	1993-12-01 – 2022-12-31
Skagsudde	17.5274	62.3694	-19.9522	1993-12-01 – 04-05-2018
Spikarna	-2.1239	49.1784	-3.6966	1993-12-01 – 2022-12-31
Stavanger	5.7684	58.9986	-36.3618	1993-12-31 – 2022-12-31
Texel Nordzee	4.7369	53.1249	-9.3252	1993-12-31 – 2022-05-30
Thyborøn	8.1986	56.7044	-8.5511	1993-12-31 – 2022-12-31
Tregde	7.5642	57.9889	-40.8626	1993-12-31 – 2022-12-31
Viker	10.939	59.0301	-59.9818	1993-12-31 – 2022-12-31
Visby	18.2747	57.6394	-24.5801	1993-12-31 – 2022-12-31
Wick	-3.0583	58.3966	-44.7522	1993-01-01 – 2022-12-31
Workington	-3.571	54.6526	-1.2754	1993-12-31 – 2022-12-31

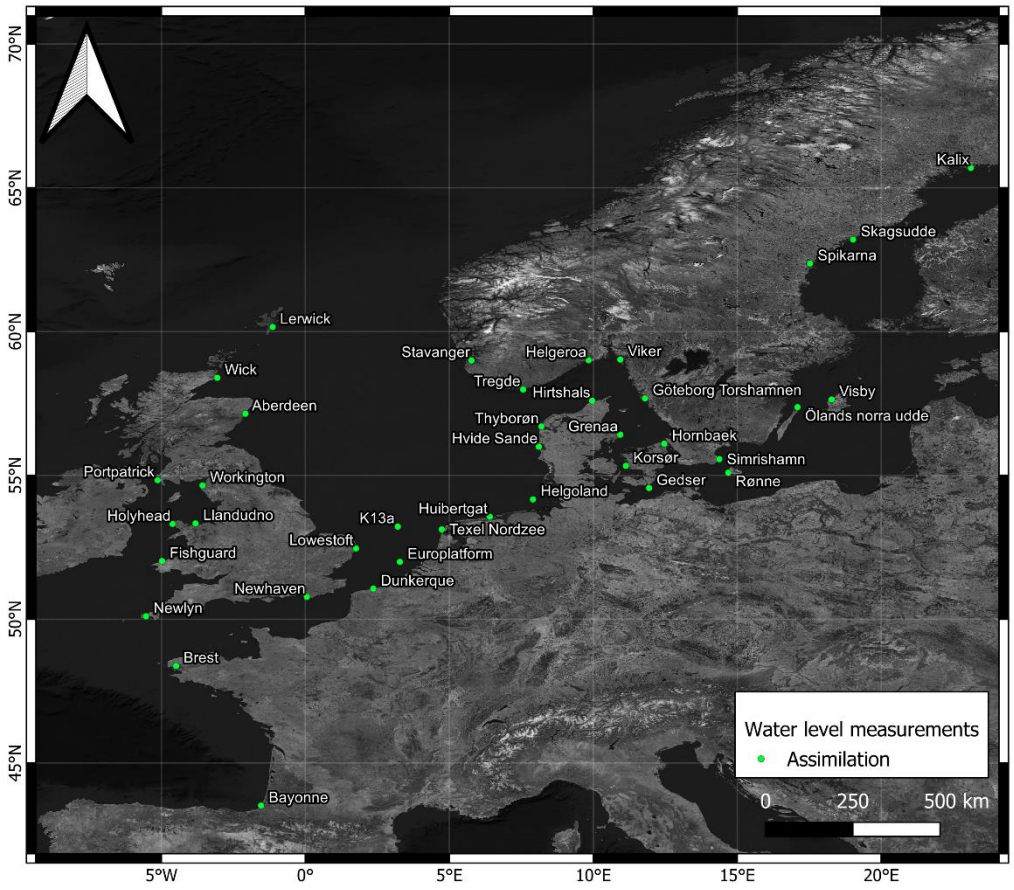

Figure 4.4 Location of water levels measurements (green dots) used in the North Europe model domain as assimilation stations.
Map of the water level measurements used for data assimilation of $HD_{NE\text{-}DA}$ model.

4.2 Assimilation stations results

The results presented here comprise time series and scatter plots for WL at Abeerden, Brest, Dunkerque and EuroPlatform. The results of the remaining stations can be seen in Appendix B.

The comparison between modelled and measured WL during the data assimilation period, for Abeerden, Brest, Dunkerque and EuroPlatform are presented in Figure 4.5, Figure 4.6, Figure 4.7 and Figure 4.8, respectively.

Figure 4.5 shows the results for Abeerden station, where an excellent agreement can be found between model and measurements with an RMSE of 0.08 m, BIAS of 0.02 m, SI of 0.09, CC of 1.00, and PR of 0.97.

Brest statistical results show an RMSE of 0.10 m, BIAS of -0.05 m, SI of 0.06, CC of 1.00, and PR of 0.99 and can be observed in Figure 4.6.

An RMSE of 0.12 m, BIAS of -0.07 m, SI of 0.06, CC of 1.00, and PR of 0.98 was obtained when considering Dunkerque station (Figure 4.7).

The latter figure, EuroPlatform station, (Figure 4.8), shows a RMSE of 0.08 m, BIAS of -0.05 m, SI of 0.13, CC of 0.99, and PR of 0.97.

Generally, the comparison during the data assimilation period is very good as the model is heavily affected by the assimilated observations.

Table 4.5 shows the statistical parameters of WL for the 39 assimilated stations. The results can be seen per station in terms of RMSE, BIAS, SI, CC, and PK. The statistics used in this validation report are described in Appendix A.

Additionally, the average statistical parameters values, considering the 39 stations used for data assimilation, are provided. Results which can be observed in the table below, were obtained through a normal averaging. A weighted average (considering the number of observations *N*) was also performed and resulted in the same results obtained when rounded to 2 decimal cases.

Considering the 39 stations in the North Europe model region, the statistical analysis showed an average RMSE of 0.08 m, BIAS of -0.03 m, SI of 0.16, CC of 0.99, and PR of 0.97.

Table 4.5 Statistical parameters of WL [m] considering the data assimilation stations

The statistics include N, RMSE, BIAS, SI, CC and PR.

Station	N	RMSE [m]	BIAS [m]	SI	CC	PR
Aberdeen	972,398	0.08	-0.02	0.09	1.00	0.97
Bayonne	837,646	0.15	-0.06	0.17	0.99	1.02
Brest	974,790	0.10	-0.05	0.06	1.00	0.99
Dunkerque	831,515	0.12	-0.07	0.06	1.00	0.98
Europlatform	1,011,053	0.08	-0.05	0.13	0.99	0.97
Fishguard	1,011,010	0.15	0.02	0.17	0.99	0.98
Gedser	952,092	0.12	-0.12	0.12	1.00	0.90
Göteborg Torshamnen	663,723	0.04	-0.01	0.25	0.98	0.91
Grenaa	928,048	0.07	-0.02	0.34	0.97	0.88
Helgeroa	1,009,907	0.02	0.00	0.13	0.99	0.97
Helgoland	860,920	0.08	-0.05	0.07	1.00	0.95
Hirtshals	948,208	0.04	0.00	0.20	0.99	1.03
Holyhead	948,208	0.04	0.00	0.20	0.99	1.03
Hornbaek	784,435	0.03	-0.02	0.18	0.99	0.94
Huibertgat	1,012,186	0.12	-0.04	0.16	0.99	0.96
Hvide Sande	896,201	0.09	-0.06	0.19	0.99	0.92
K13a	1,012,553	0.04	-0.01	0.11	1.00	0.98
Kalix	971,118	0.05	0.05	0.05	1.00	1.02
Korsør	815,815	0.09	-0.05	0.45	0.93	0.87
Lerwick	796,635	0.03	0.00	0.08	1.00	0.97
Llandudno	918,338	0.17	-0.07	0.08	1.00	1.02
Lowestoft	989,195	0.13	-0.10	0.18	0.99	0.95
Marviken	905,244	0.03	0.01	0.22	0.98	0.97
Newhaven	986,375	0.09	-0.04	0.06	1.00	1.01
Newlyn	968,420	0.10	0.01	0.09	1.00	1.01
Ölands norra udde	670,768	0.09	-0.04	0.45	0.92	0.80
Portpatrick	1,006,057	0.09	-0.07	0.06	1.00	0.95
Rønne	702,694	0.06	-0.05	0.19	0.99	0.93
Simrishamn	1,006,455	0.05	-0.05	0.04	1.00	0.93
Skagsudde	514,020	0.06	0.05	0.19	0.99	1.03
Spikarna	997,888	0.05	0.05	0.03	1.00	1.06
Stavanger	1,013,836	0.06	-0.02	0.33	0.96	0.92
Texel Nordzee	953,837	0.09	-0.04	0.14	0.99	1.00
Thyborøn	947,684	0.06	-0.02	0.20	0.99	0.92
Tregde	1,004,000	0.07	-0.05	0.32	0.96	0.94
Viker	1,002,401	0.04	0.02	0.21	0.99	0.97

Station	N	RMSE [m]	BIAS [m]	SI	CC	PR
Visby	1,005,766	0.03	0.03	0.05	1.00	1.05
Wick	962,426	0.07	-0.04	0.08	1.00	0.98
Workington	968,852	0.17	-0.07	0.09	1.00	0.99
Mean	916,993	0.08	-0.03	0.16	0.99	0.97

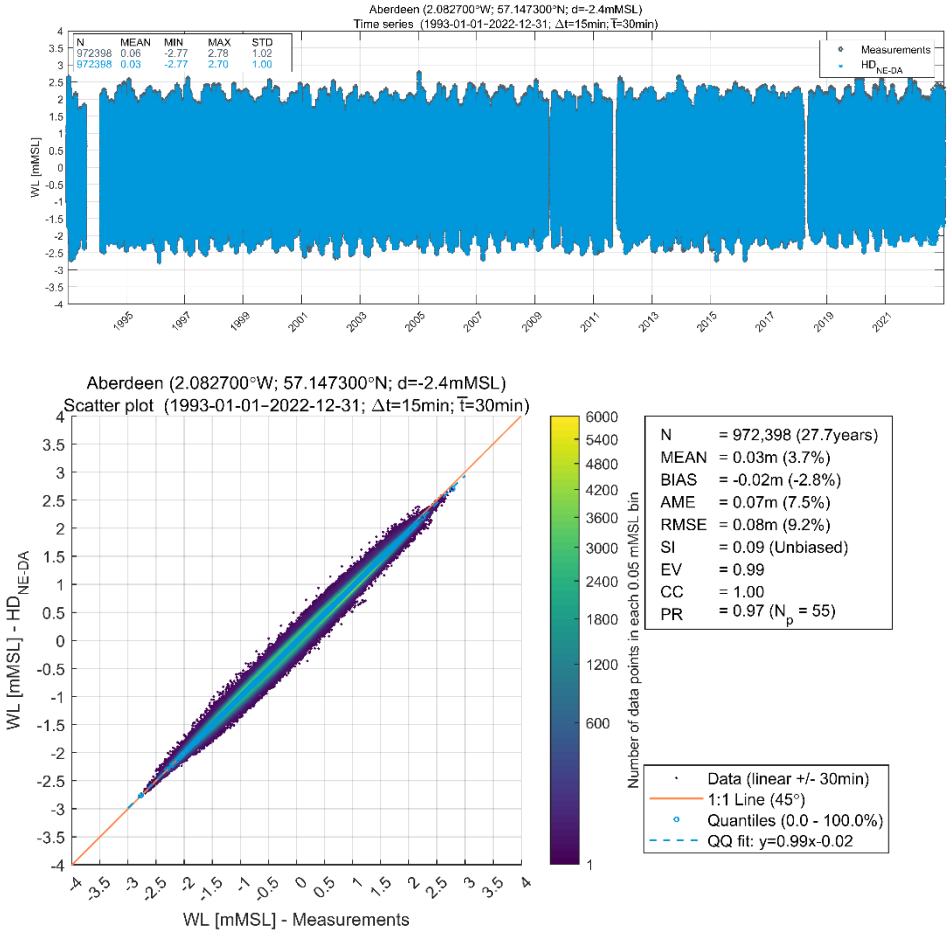

Figure 4.5 Time series plot (top) and scatter plot (bottom) of modelled against measured WL at Aberdeen [mMSL]
The model shows excellent skills in reproducing the water levels observed.

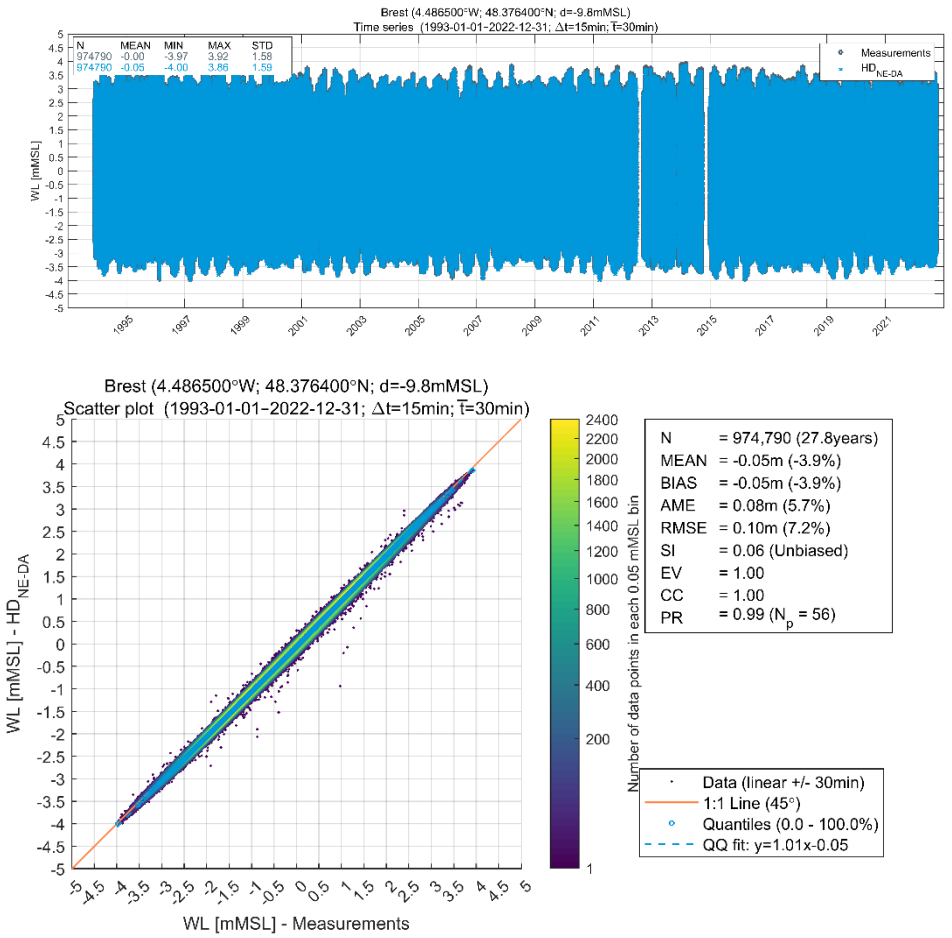

Figure 4.6 Time series plot (top) and scatter plot (bottom) of modelled against measured WL at Brest [mMSL]

The model shows excellent skills in reproducing the water levels observed.

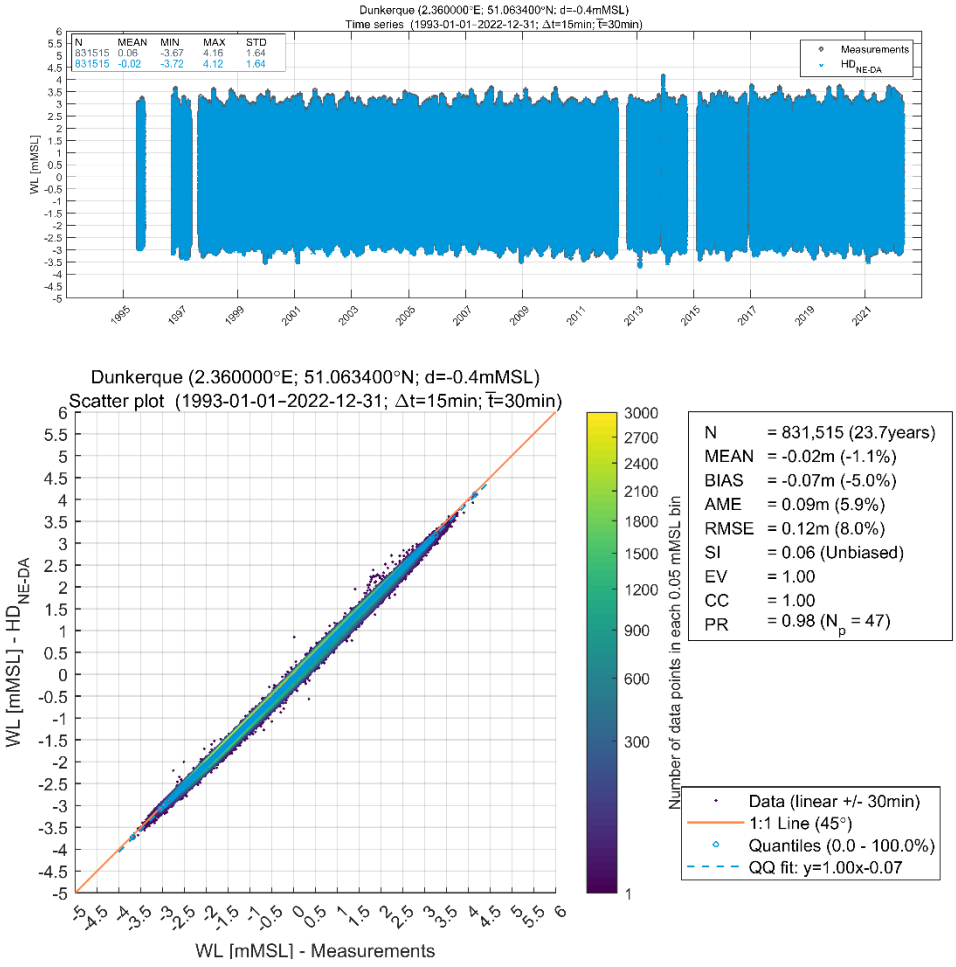

Figure 4.7 Time series plot (top) and scatter plot (bottom) of modelled against measured WL at Dunkerque [mMSL]

The model shows excellent skills in reproducing the water levels observed.

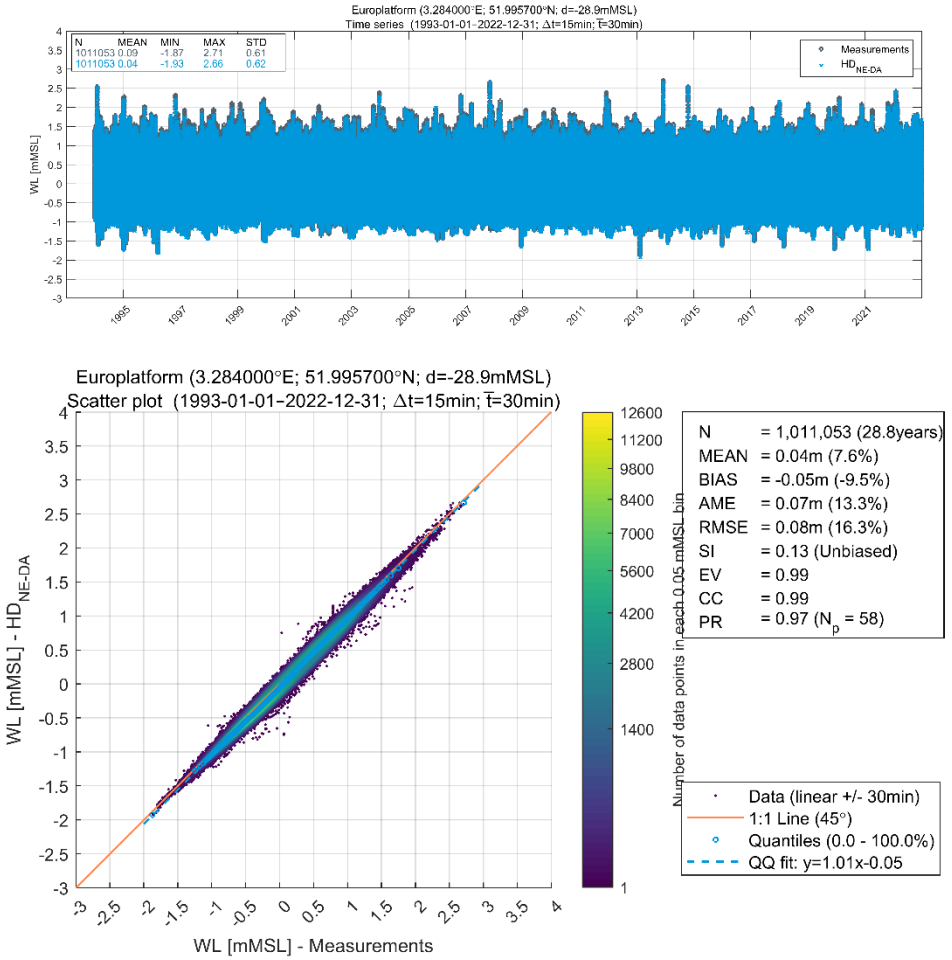

Figure 4.8 Time series plot (top) and scatter plot (bottom) of modelled against measured WL at EuroPlatform [mMSL]
The model shows excellent skills in reproducing the water levels observed.

4.3 Validation stations results

The validation presented here comprises time series and scatter plots for modelled and measured WL at North Shields, Tersch Nordzee, Witby and Skagen (Figure 4.9, Figure 4.10, Figure 4.11 and Figure 4.12, respectively). The remaining stations validation can be seen in Appendix B.

Figure 4.9 shows the results for North Shields station, where an excellent agreement can be found between model and measurements with a RMSE of 0.11 m, BIAS of 0.03 m, SI of 0.10, CC of 1.00, and PR of 0.98.

Tersch Nordzee statistical results show a RMSE of 0.11 m, BIAS of -0.03 m, SI of 0.17, CC of 0.99, and PR of 0.97 and can be observed in Figure 4.10.

A RMSE of 0.11 m, BIAS of -0.01 m, SI of 0.10, CC of 1.00, and PR of 0.96 was obtained when considering Witby station (Figure 4.11).

The latter figure, Skagen station, (Figure 4.12), shows a RMSE of 0.06 m, BIAS of 0.02 m, SI of 0.32, CC of 0.97, and PR of 0.93.

Generally, the comparisons between model with data assimilation and validation stations are good.

Table 4.6 shows the statistical parameters of WL for the 20 stations considered. The results can be seen per station in terms of RMSE, BIAS, SI, CC and PK. The statistics used in this validation report are described in Appendix A.

Additionally, it is provided the average statistical parameters values considering the 20 stations used for validation. Results can be observed in the table below and were obtained through a normal average. A weighted average (considering the number of observations *N*) was also performed and resulted in the same results obtained when rounded to 2 decimal cases.

Considering the 20 stations in the north Europe region, the average RMSE of 0.13 m, BIAS of -0.01 m, SI of 0.19, CC of 0.98, and PR of 0.98.

Table 4.6 Statistical parameters of WL [m] considering the validation stations

The statistics include N, RMSE, BIAS, SI, CC and PR.

Station	N	RMSE [m]	BIAS [m]	SI	CC	PR
Barmouth	868,164	0.16	-0.03	0.16	0.99	0.97
Bergen	1,010,970	0.17	-0.05	0.50	0.91	0.93
Concarneau	747,408	0.13	-0.06	0.11	1	0.98
Cromer	957,476	0.15	0.01	0.14	0.99	1.01
Dover	926,092	0.18	-0.06	0.11	1	1.06
Hantsholm	800,118	0.07	-0.01	0.28	0.97	1.01
St, Helier	1,017,566	0.21	0	0.09	1	1
Kinlochbervie	903,306	0.16	-0.08	0.14	0.99	0.97
Kungsholmsfort	1,006,691	0.04	-0.04	0.17	0.99	0.91
Leith	908,422	0.26	0.21	0.12	0.99	1.05
Les Sables-dOlonne	894,403	0.17	-0.05	0.16	0.99	1
Marviken	905,244	0.03	0.01	0.22	0.98	0.97
North Shields	984,105	0.11	0.03	0.10	1	0.98
Portrush	879,638	0.13	-0.03	0.31	0.97	1.03
Skagen	894,777	0.06	0.02	0.32	0.97	0.93
Terschelling Noordzee	1,005,710	0.11	-0.03	0.17	0.99	0.97
Thorsminde	913,570	0.09	-0.05	0.25	0.98	0.97
Weymouth	947,638	0.08	-0.02	0.17	0.99	0.96
Whitby	928,926	0.11	-0.01	0.10	1	0.96
Mean	921,064	0.13	-0.01	0.19	0.98	0.98

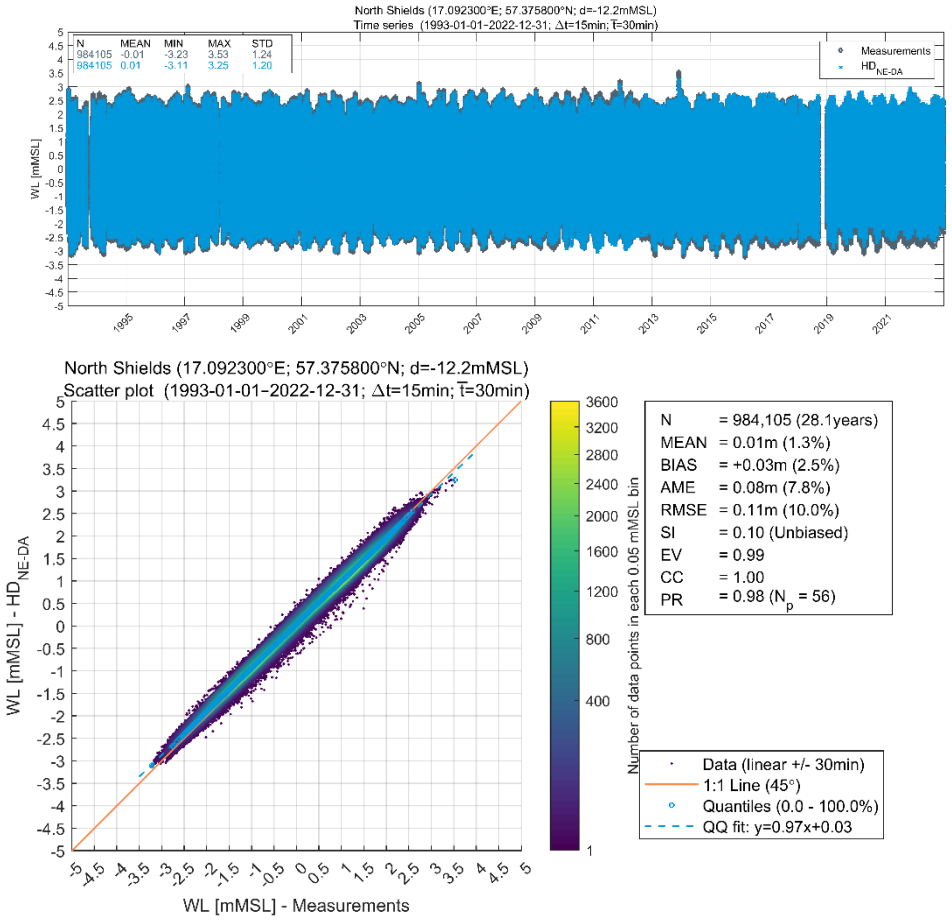

Figure 4.9 Time series plot (top) and scatter plot (bottom) of modelled against measured WL at North Shields [mMSL]
The model shows excellent skills in reproducing the water levels observed.

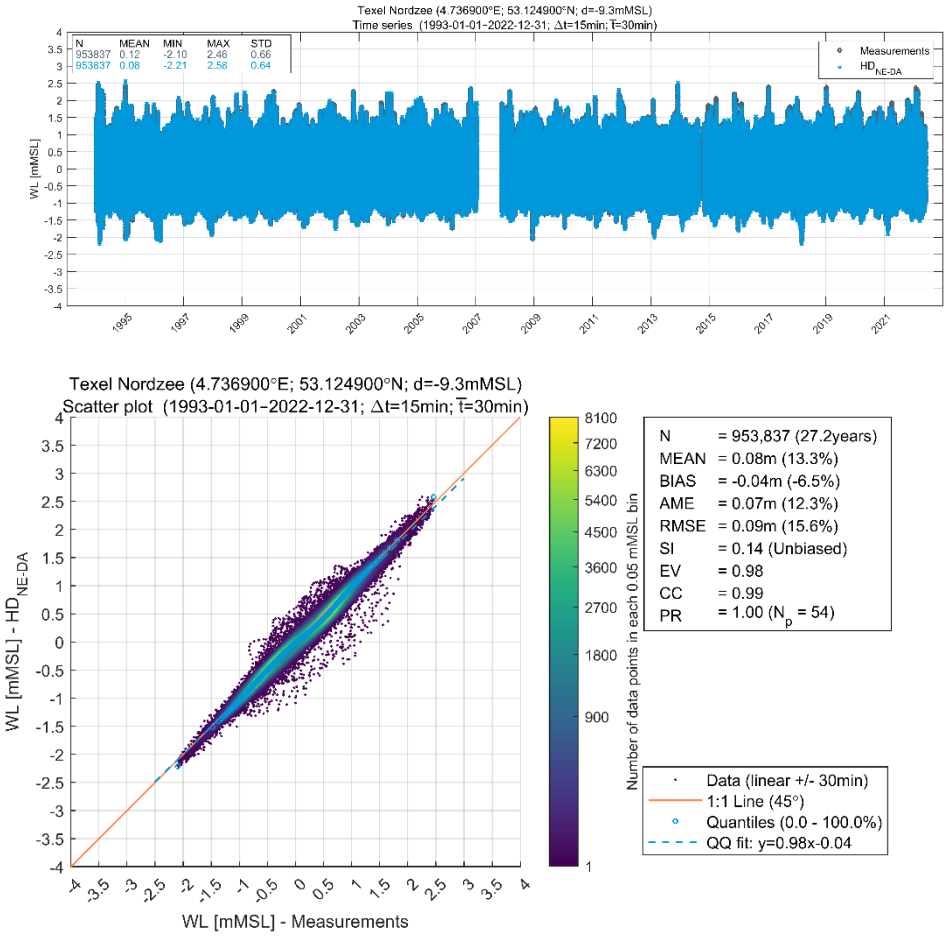

Figure 4.10 Time series plot (top) and scatter plot (bottom) of modelled against measured WL at Texel Nordzee [mMSL]
The model shows excellent skills in reproducing the water levels observed.

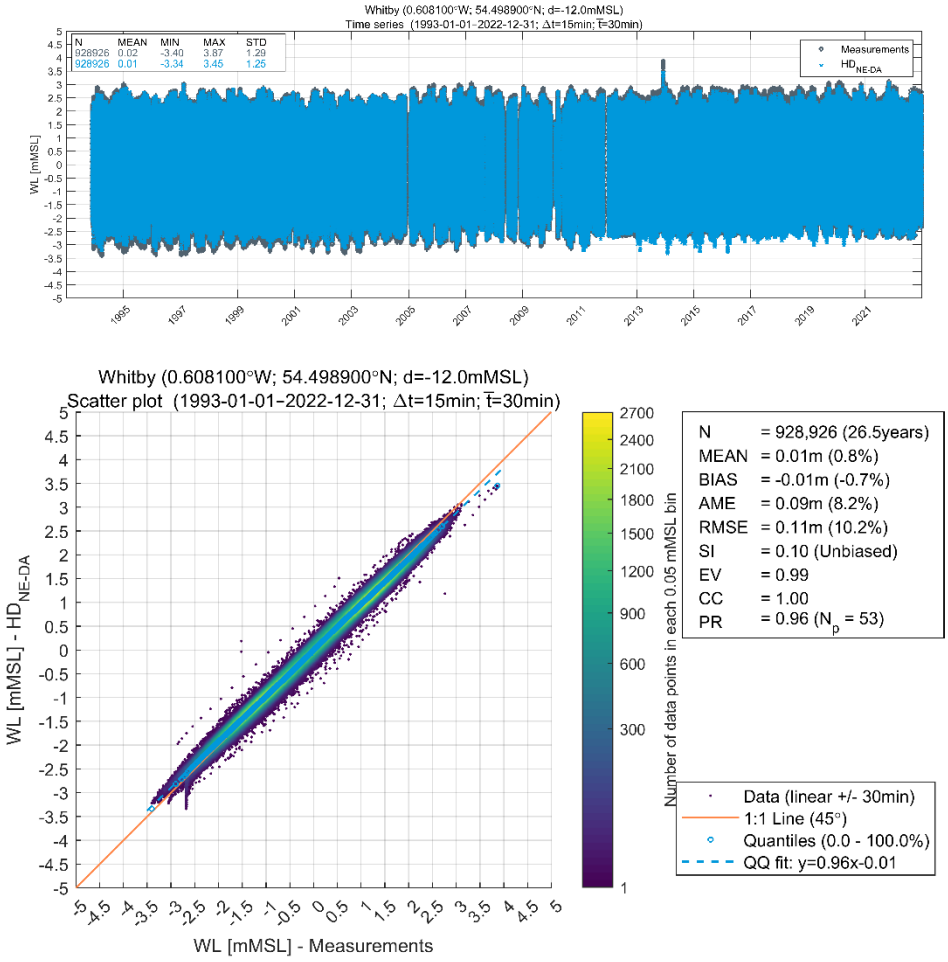

Figure 4.11 Time series plot (top) and scatter plot (bottom) of modelled against measured WL at Whitby [mMSL]

The model shows excellent skills in reproducing the water levels observed.

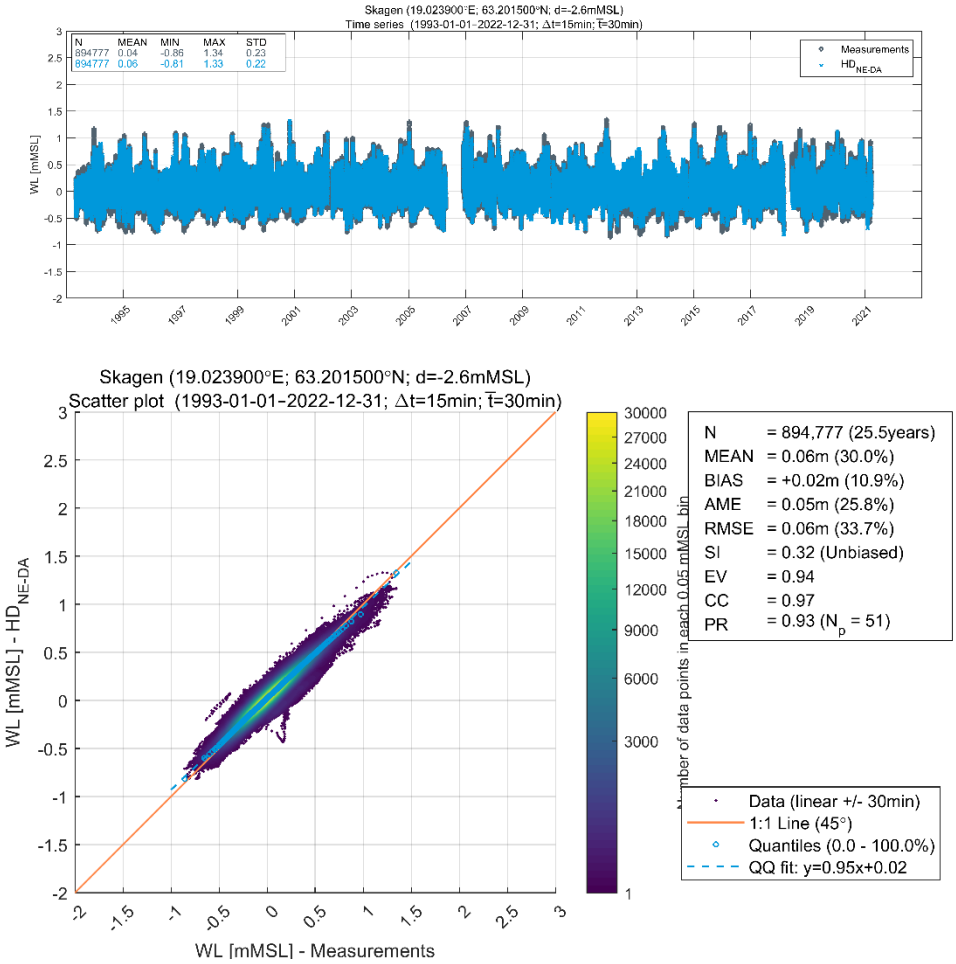

Figure 4.12 Time series plot (top) and scatter plot (bottom) of modelled against measured WL at Skagen [mMSL]
The model shows excellent skills in reproducing the water levels observed.

5 Concluding Remarks

This section presents the concluding remarks and an overall summary of the validation results obtained for the DHI North Europe regional hydrodynamic model, $HD_{NE\text{-}DA}$.

DHI implemented a dedicated state-of-the-art numerical hindcast model to establish hydrodynamic conditions for North Europe covering from 1979 to 2022 (incl.). A DA (Data Assimilation) method was implemented, which proved to be effective in reducing errors and improved the accuracy of predictions (RMSE of 0.10 and SI of 0.14 using DA versus RMSE of 0.21 and SI of 0.37 without DA – see Table 4.3). The regional model has been validated against in-situ measurements which confirms that they can accurately reproduce the observed water levels.

The quality parameters considering WL are summed up in Table 4.5 (considering stations used in the data assimilation) and Table 4.6 (considering stations used in validation), for stations across the model domain. The statistics indicate that the metocean database presented here based on ERA5 and DHI's regional North Europe model are representative of observed conditions in this area.

6 References

[1] Y. a. A. O. Cheng, “Improvement in global ocean tide model in shallow water regions (Poster, SV.1-68 45),” in *Altimetry for Oceans and Hydrology OST-ST Meeting*, Lisbon, 2010.

[2] G. Evensen, “equential data assimilation with a non-linear quasi-geostrophic model using Monte Carlo methods to forecast error statistics,” *J. Geophys. Res., Vol. 99(C5),* pp. pp 10,143-10,162, 1994.

[3] N. Assimakis and M. Adam, “Iterative and algebraic algorithms for the computation of the steady state Kalman filter gain,” *International Scholarly Research Notices,* 2014.

[4] J. Sørensen and H. Madsen, “Efficient Kalman filter techniques for the assimilation of tide gauge data in three-dimensional modeling of the North Sea and Baltic Sea system.,” 2004.

[5] K. S. H. J. T. C. Madsen, “Near-coastal satellite altimetry: Sea surface height variability in the North Sea–Baltic Sea area,” *GEOPHYSICAL RESEARCH LETTERS,* vol. 34, no. L14601, 2007.

[6] DHI, “MIKE 21 Spectral Waves FM, Spectral Wave Module User Guide,” 2022. [Online]. Available: https://manuals.mikepoweredbydhi.help//2022/Coast_and_Sea/MIKE21SW.pdf. [Accessed 09 2022].

[7] M. Golestani, P. M. Jensen and H. Kofoed-Hansen, “On the influence of atmospheric stability on the wave climate in a warm and saline water body,” St. John's, Newfoundland, Canada, 2015.

[8] DHI A/S, “Ten noorden van de Waddeneilanden (TNW) Wind Farm Zone; Metocean Desk Study Report Version 1.0,” RVO.nl, 2022. [Online]. Available: https://offshorewind.rvo.nl/cms/view/c26468f2-f44e-4d01-81c1-b0cc3de8787d/wind-en-water-tnw.

[9] DHI A/S, “Metocean Study - Wind farm zone Hollandse Kust (zuid)- Final V2.3.,” RVO.nl, September 2017. [Online]. Available: https://offshorewind.rvo.nl/cms/view/d2ab64a9-a87d-409f-92cc-15cd057b0e7d/wind-en-water-hollandse-kust-zuid.

[10] DHI A/S, “Metocean desk study and database for Dutch Wind Farm Zones; Hollandse Kust (noord) Version 2.4,” September 2019. [Online]. Available: https://offshorewind.rvo.nl/cms/view/3ce5f11f-d39c-4de4-a877-6daf6b945c5c/wind-en-water.

[11] DHI A/S, “MetOcean Desk Study - Wind farm zone Hollandse Kust (west) Version 0.6,” RVO.nl, 2021. [Online]. Available: https://offshorewind.rvo.nl/cms/view/8c258104-fbaf-4934-a6f0-1c2797d5187b/wind-en-water-hollandse-kust-west.

Appendix A Quality Indices

See next pages

DHI Model Quality Indices (QI's)

Contents

Revisions

Date	Description	Initials
2021-08-13	Version 1.0.	PDG
2022-11-24	Version 1.1; table formatting updated.	SJA

Nomenclature

Abbreviation	Explanation
QI	Quality Index
POT	Peak-Over-Threshold

1 Model Quality Indices

To obtain an objective and quantitative measure of how well the model data compared to the observed data, several statistical parameters, so-called quality indices (QI's), are calculated.

Prior to the comparisons, the model data is synchronised to the time stamps of the observations so that both time series had equal length and overlapping time stamps. For each valid observation, measured at time t, the corresponding model value is found using linear interpolation between the model time steps before and after t. Only observed values that had model values within ± the representative sampling or averaging period of the observations are included (e.g., for 10-min observed wind speeds measured every 10 min compared to modelled values every hour, only the observed value every hour is included in the comparison).

The comparisons of the synchronised observed and modelled data are illustrated in (some of) the following figures:

- Time series plot including general statistics
- Scatter plot including quantiles, QQ-fit and QI's (density-colored dots)
- Histogram of occurrence vs. magnitude or direction
- Histogram of bias vs. magnitude
- Histogram of bias vs. direction
- Dual rose plot (overlapping roses)
- Peak event plot including joint (coinciding) individual peaks

The quality indices are described below, and their definitions are listed in Table 1.1. Most of the quality indices are based on the entire dataset, and hence the quality indices should be considered averaged measures and may not be representative of the accuracy during rare conditions.

The MEAN represents the mean of modelled data, while the bias is the mean difference between the modelled and observed data. AME is the mean of the absolute difference, and RMSE is the root-mean-square of the difference. The MEAN, BIAS, AME and RMSE are given as absolute values and relative to the average of the observed data in percent in the scatter plot.

The scatter index (SI) is a non-dimensional measure of the difference calculated as the unbiased root-mean-square difference relative to the mean absolute value of the observations. In open water, an SI below 0.2 is usually considered a small difference (excellent agreement) for significant wave heights. In confined areas or during calm conditions, where mean significant wave heights are generally lower, a slightly higher SI may be acceptable (the definition of SI implies that it is negatively biased (lower) for time series with high mean values compared to time series with lower mean values (and same scatter/spreading), although it is normalised).

EV is the explained variation and measures the proportion [0 - 1] to which the model accounts for the variation (dispersion) of the observations.

The correlation coefficient (CC) is a non-dimensional measure reflecting the degree to which the variation of the first variable is reflected linearly in the variation of the second variable. A value close to 0 indicates very limited or no

(linear) correlation between the two data sets, while a value close to 1 indicates a very high or perfect correlation. Typically, a CC above 0.9 is considered a high correlation (good agreement) for wave heights. It is noted that CC is 1 (or -1) for any two fully linearly correlated variables, even if they are not 1:1. However, the slope and intercept of the linear relation may be different from 1 and 0, respectively, despite CC of 1 (or -1).

The QQ line slope and intercept are found from a linear fit to the data quantiles in a least-square sense. The lower and uppermost quantiles are not included on the fit. A regression line slope different from 1 may indicate a trend in the difference.

The peak ratio (PR) is the average of the Npeak highest model values divided by the average of the Npeak highest observations. The peaks are found individually for each dataset through the Peak-Over-Threshold (POT) method applying an average annual number of exceedance of 4 and an inter-event time of 36 hours. A general underestimation of the modelled peak events results in a PR below 1, while an overestimation results in a PR above 1.

An example of a peak plot is shown in Figure 1.1. 'X' represents the observed peaks (x-axis), while 'Y' represents the modelled peaks (y-axis), based on the POT methodology, both represented by circles ('o') in the plot. The joint (coinciding) peaks, defined as any X and Y peaks within ±36 hours[1] of each other (i.e., less than or equal to the number of individual peaks), are represented by crosses ('x'). Hence, the joint peaks ('x') overlap with the individual peaks ('o') only if they occur at the same time exactly. Otherwise, the joint peaks ('x') represent an additional point in the plot, which may be associated with the observed and modelled individual peaks ('o') by searching in the respective X and Y-axis directions, see example with red lines in Figure 1.1. It is seen that the 'X' peaks are often underneath the 1:1 line, while the 'Y' peaks are often above the 1:1 line.

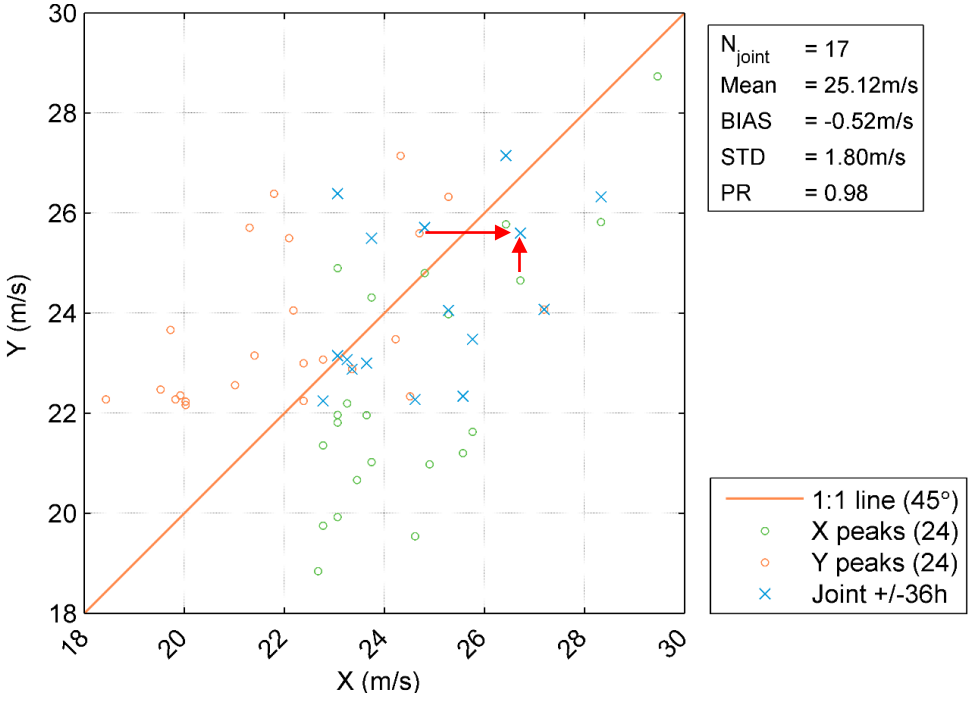

Figure 1.1 Example of peak event plot (wind speed)

[1] 36 hours is chosen arbitrarily as representative of an average storm duration. Often the measured and modelled peaks are within 1-2 hours of each other.

Table 1.1 Definitions of model quality indices (X = Observation, Y = Model)

Abbreviation	Description	Definition
N	Number of data (synchronised)	–
MEAN	Mean of Y data Mean of X data	$\frac{1}{N}\sum_{i=1}^{N} Y_i \equiv \overline{Y}$, $\frac{1}{N}\sum_{i=1}^{N} X_i \equiv \overline{X}$
STD	Standard deviation of Y data Standard deviation of X data	$\sqrt{\frac{1}{N-1}\sum_{i=1}^{N}(Y-\overline{Y})^2}$, $\sqrt{\frac{1}{N-1}\sum_{i=1}^{N}(X-\overline{X})^2}$
BIAS	Mean difference	$\frac{1}{N}\sum_{i=1}^{N}(Y-X)_i = \overline{Y}-\overline{X}$
AME	Absolute mean difference	$\frac{1}{N}\sum_{i=1}^{N}(\lvert Y-X\rvert)_i$
RMSE	Root-mean-square difference	$\sqrt{\frac{1}{N}\sum_{i=1}^{N}(Y-X)_i^{\,2}}$
SI	Scatter index (unbiased)	$\frac{\sqrt{\frac{1}{N}\sum_{i=1}^{N}(Y-X-\mathrm{BIAS})_i^{\,2}}}{\frac{1}{N}\sum_{i=1}^{N}\lvert X_i\rvert}$
EV	Explained variance	$\frac{\sum_{i=1}^{N}(X_i-\overline{X})^2-\sum_{i=1}^{N}[(X_i-\overline{X})-(Y_i-\overline{Y})]^2}{\sum_{i=1}^{N}(X_i-\overline{X})^2}$
CC	Correlation coefficient	$\frac{\sum_{i=1}^{N}(X_i-\overline{X})(Y_i-\overline{Y})}{\sqrt{\sum_{i=1}^{N}(X_i-\overline{X})^2\sum_{i=1}^{N}(Y_i-\overline{Y})^2}}$
QQ	Quantile-Quantile (line slope and intercept)	Linear least square fit to quantiles
PR	Peak ratio (of N_{peak} highest events)	$\mathrm{PR}=\frac{\sum_{i=1}^{N_{peak}} Y_i}{\sum_{i=1}^{N_{peak}} X_i}$

Appendix B Time Series, Scatter Plots

Appendix B.1 Time Series WL – DHI Regional Hydrodynamic Model 2023

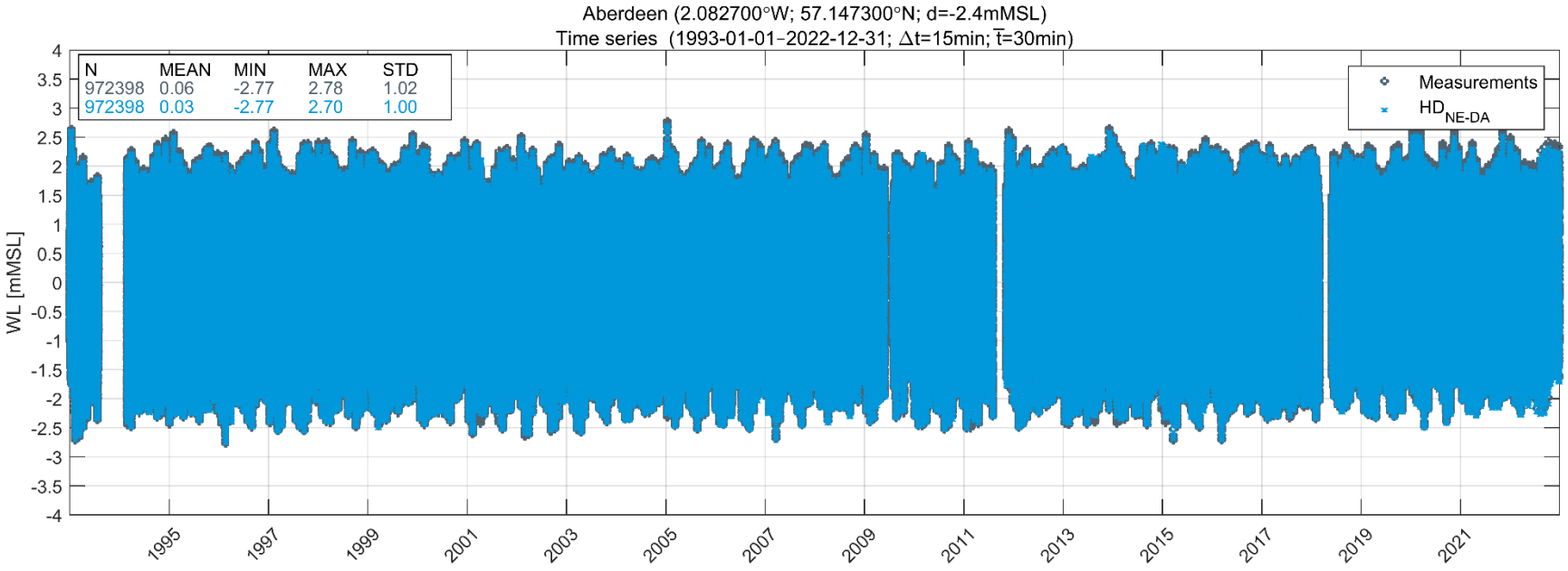
Aberdeen (2.082700°W; 57.147300°N; d=-2.4mMSL)
Time series (1993-01-01–2022-12-31; Δt=15min; t̄=30min)
N MEAN MIN MAX STD
972398 0.06 -2.77 2.78 1.02
972398 0.03 -2.77 2.70 1.00
Measurements
HD NE-DA
WL [mMSL]

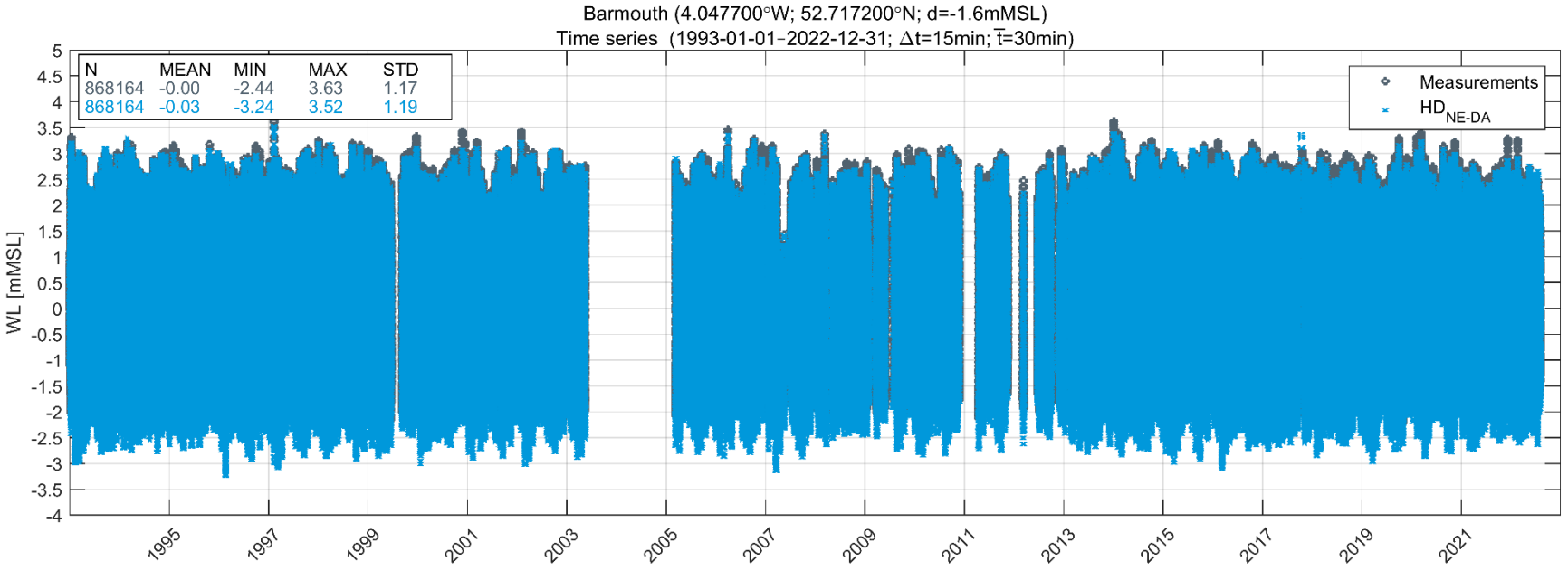
Barmouth (4.047700°W; 52.717200°N; d=-1.6mMSL)
Time series (1993-01-01–2022-12-31; Δt=15min; t̄=30min)
N MEAN MIN MAX STD
868164 -0.00 -2.44 3.63 1.17
868164 -0.03 -3.24 3.52 1.19
Measurements
HD NE-DA
WL [mMSL]

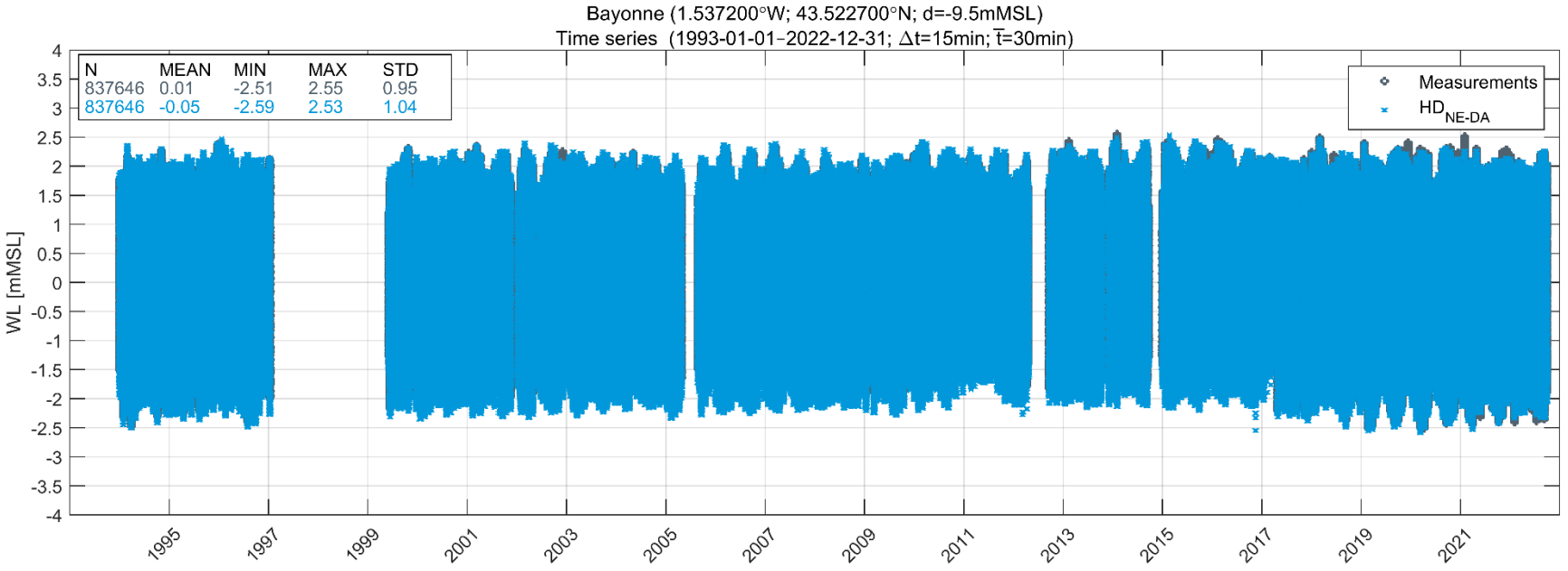
Bayonne (1.537200°W; 43.522700°N; d=-9.5mMSL)
Time series (1993-01-01–2022-12-31; Δt=15min; t̄=30min)
N MEAN MIN MAX STD
837646 0.01 -2.51 2.55 0.95
837646 -0.05 -2.59 2.53 1.04
Measurements
HD NE-DA
WL [mMSL]

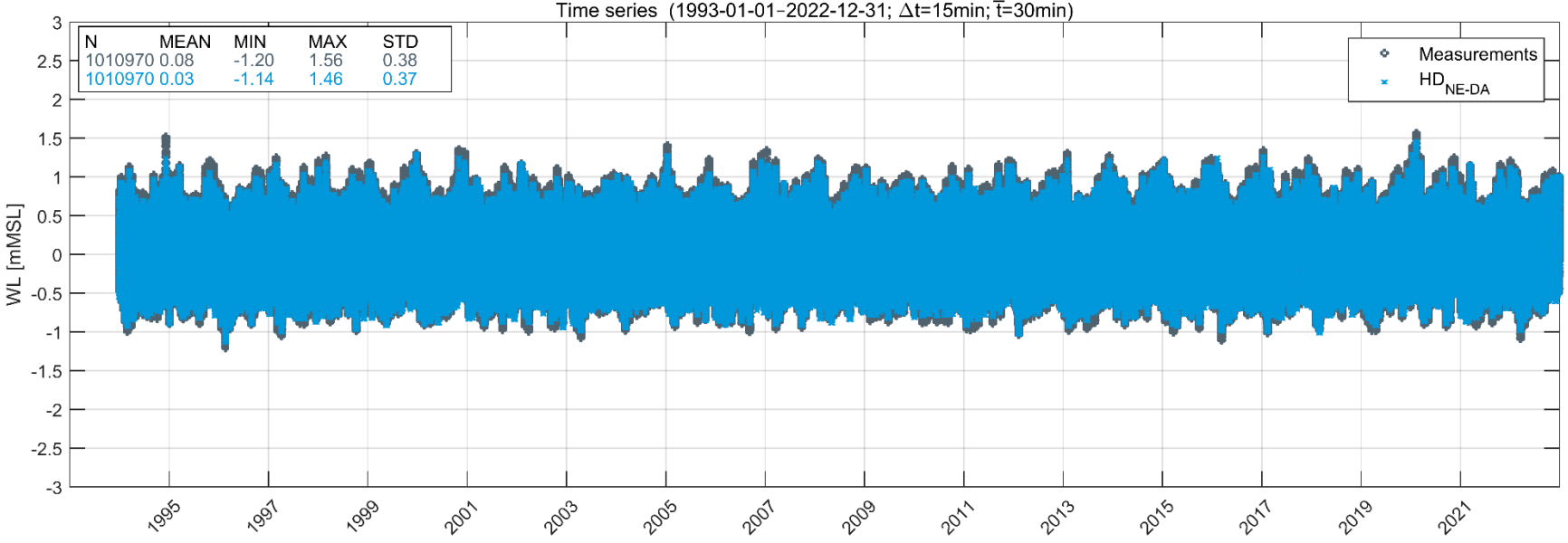
Bergen (5.304200°E; 60.389600°N; d=-84.2mMSL)
Time series (1993-01-01–2022-12-31; Δt=15min; t̄=30min)
N MEAN MIN MAX STD
1010970 0.08 -1.20 1.56 0.38
1010970 0.03 -1.14 1.46 0.37
Measurements
HD NE-DA
WL [mMSL]

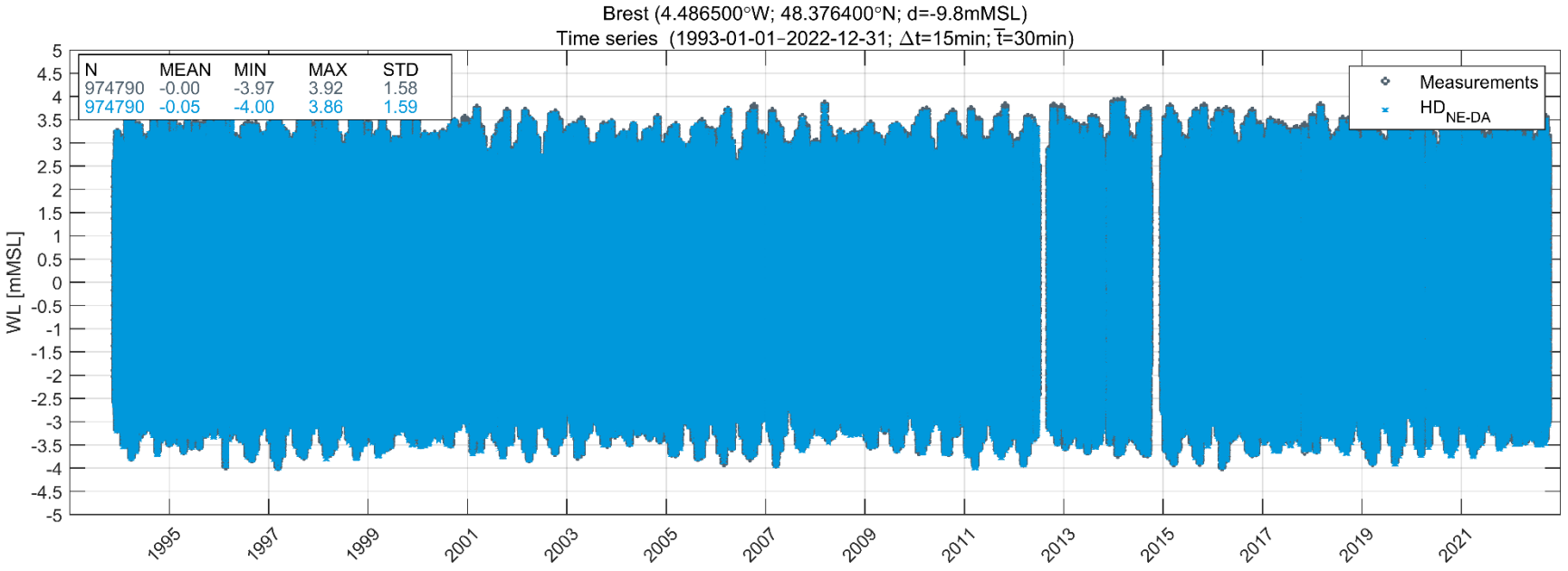
Brest (4.486500°W; 48.376400°N; d=-9.8mMSL)
Time series (1993-01-01–2022-12-31; Δt=15min; t̄=30min)
N MEAN MIN MAX STD
974790 -0.00 -3.97 3.92 1.58
974790 -0.05 -4.00 3.86 1.59
Measurements
HD NE-DA
WL [mMSL]

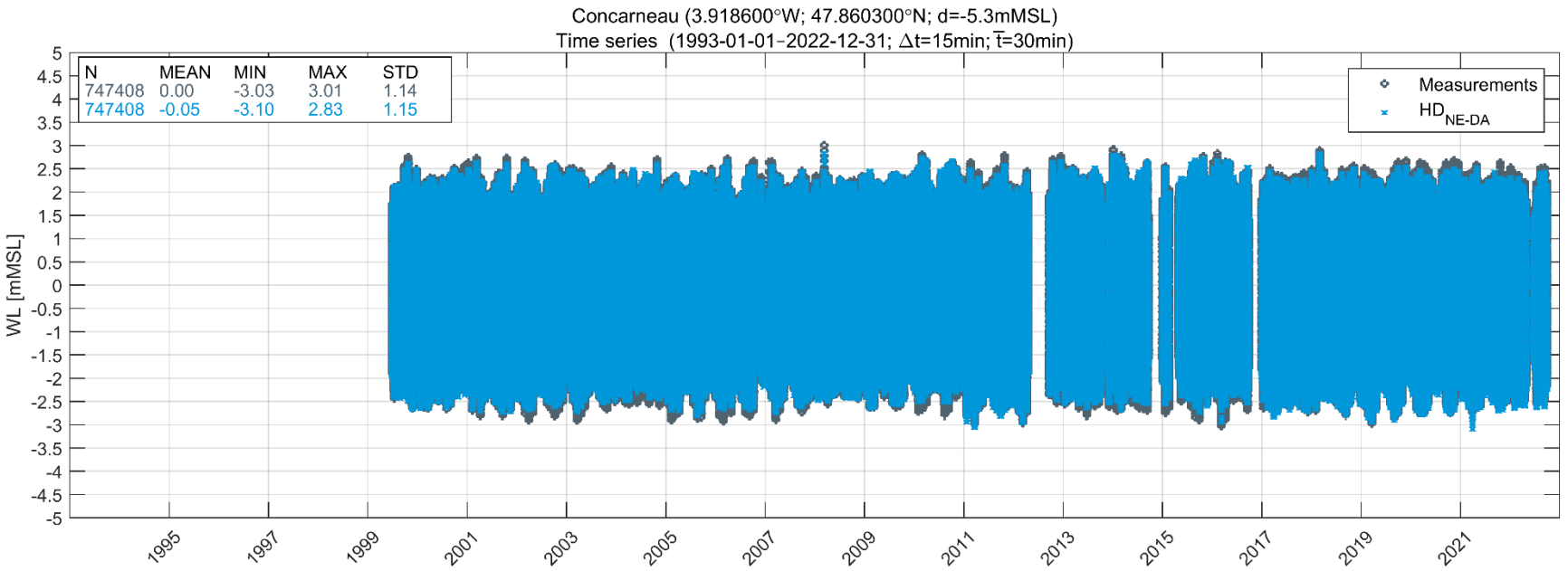
Concarneau (3.918600°W; 47.860300°N; d=-5.3mMSL)
Time series (1993-01-01–2022-12-31; Δt=15min; t̄=30min)
N MEAN MIN MAX STD
747408 0.00 -3.03 3.01 1.14
747408 -0.05 -3.10 2.83 1.15
Measurements
HD NE-DA
WL [mMSL]

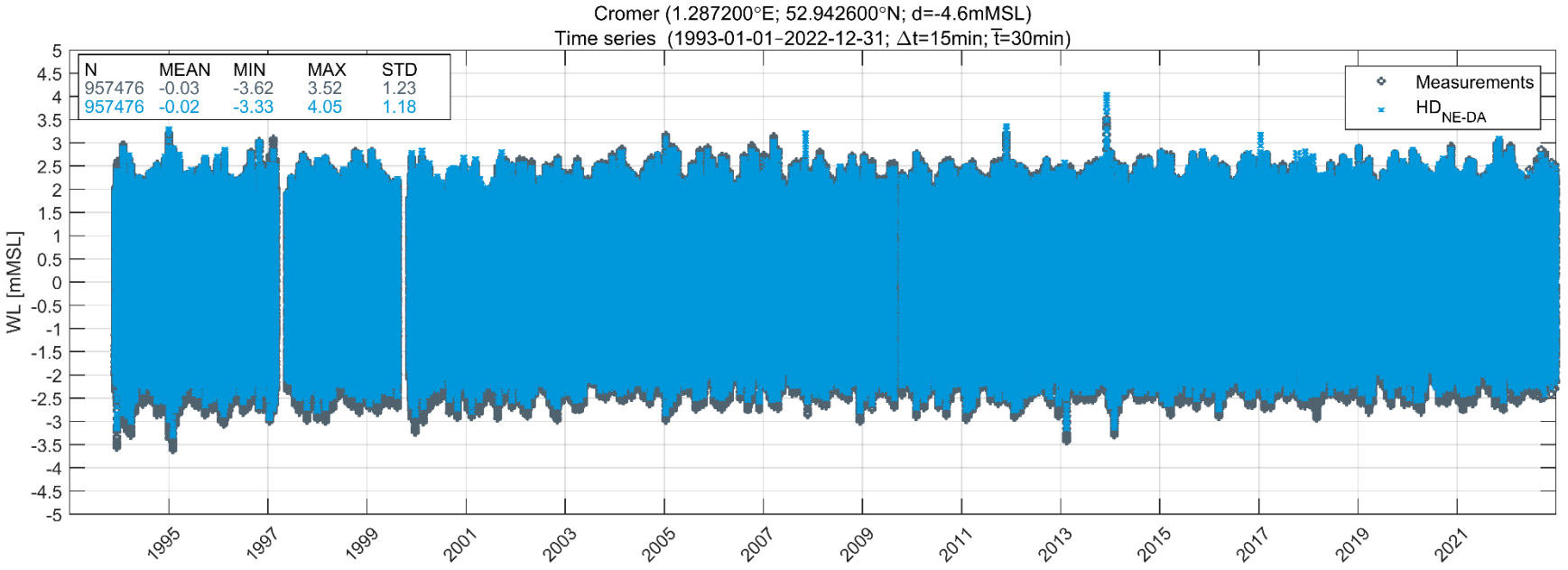
Cromer (1.287200°E; 52.942600°N; d=-4.6mMSL)
Time series (1993-01-01–2022-12-31; Δt=15min; t̄=30min)
N MEAN MIN MAX STD
957476 -0.03 -3.62 3.52 1.23
957476 -0.02 -3.33 4.05 1.18
Measurements
HD NE-DA
WL [mMSL]

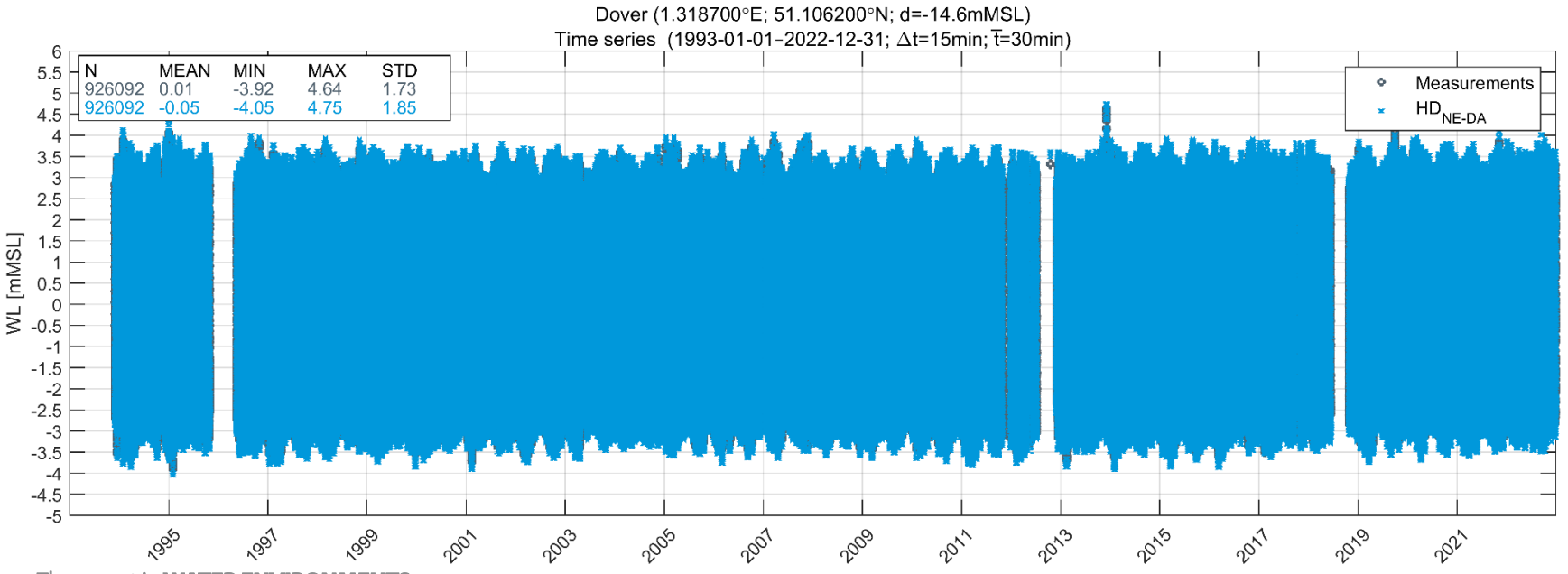
Dover (1.318700°E; 51.106200°N; d=-14.6mMSL)
Time series (1993-01-01–2022-12-31; Δt=15min; t̄=30min)
N MEAN MIN MAX STD
926092 0.01 -3.92 4.64 1.73
926092 -0.05 -4.05 4.75 1.85
Measurements
HD NE-DA
WL [mMSL]

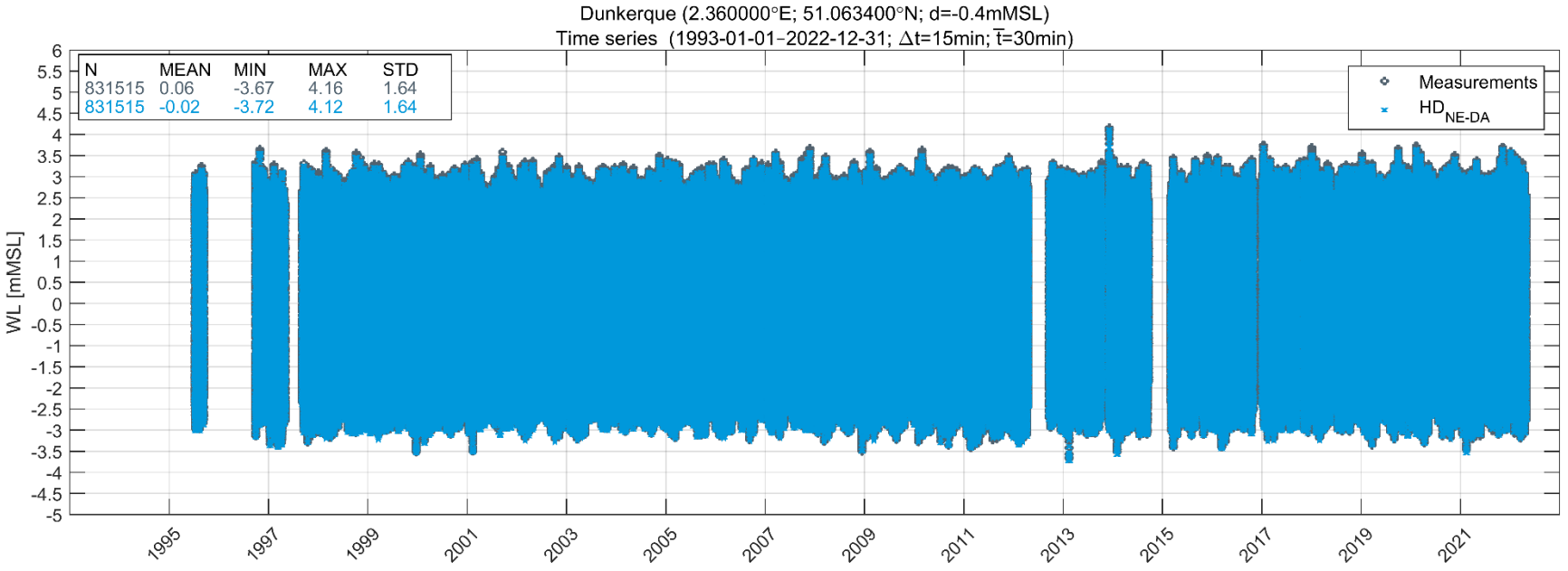
Dunkerque (2.360000°E; 51.063400°N; d=-0.4mMSL)
Time series (1993-01-01–2022-12-31; Δt=15min; t̄=30min)
N MEAN MIN MAX STD
831515 0.06 -3.67 4.16 1.64
831515 -0.02 -3.72 4.12 1.64
Measurements
HD NE-DA
WL [mMSL]

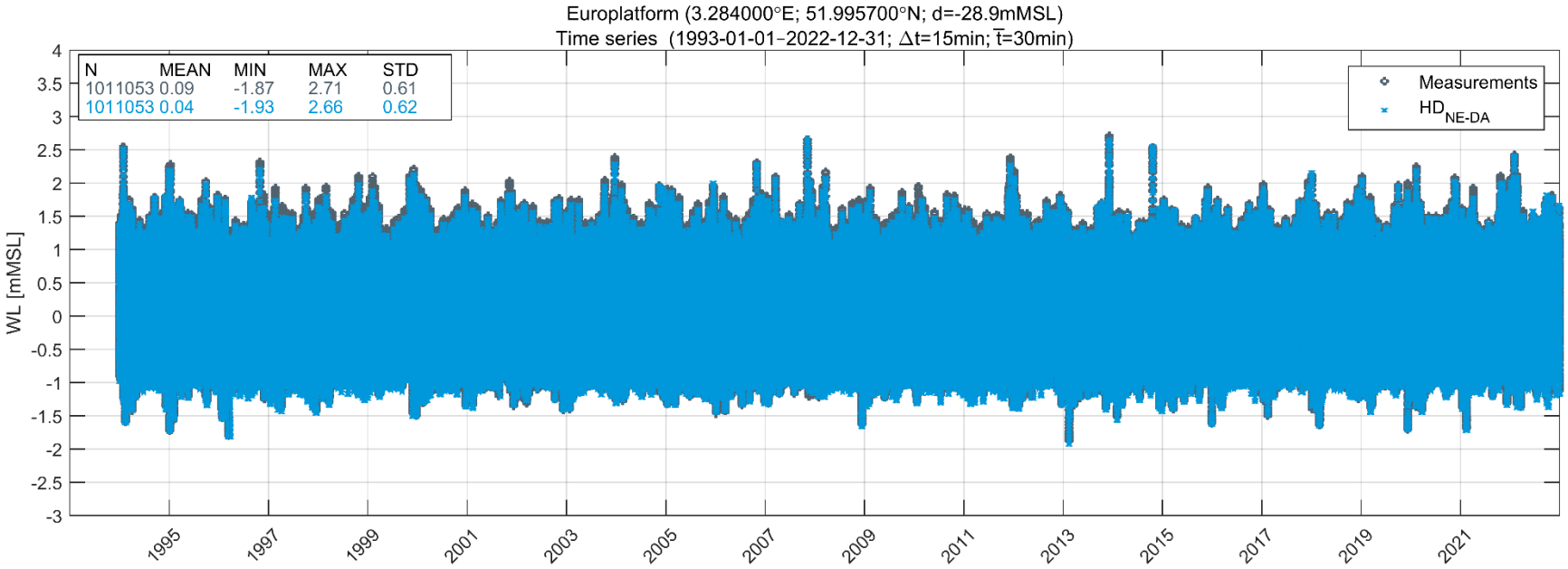
Europlatform (3.284000°E; 51.995700°N; d=-28.9mMSL)
Time series (1993-01-01–2022-12-31; Δt=15min; t̄=30min)
N MEAN MIN MAX STD
1011053 0.09 -1.87 2.71 0.61
1011053 0.04 -1.93 2.66 0.62
Measurements
HD NE-DA
WL [mMSL]

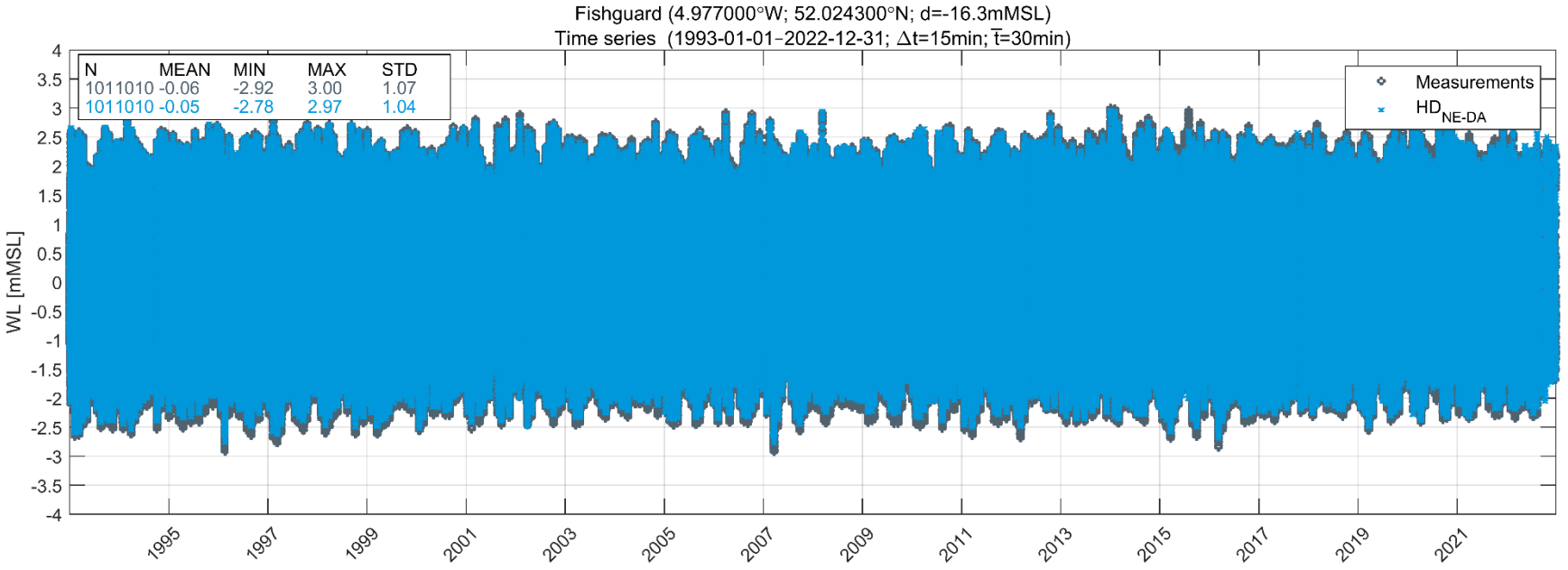
Fishguard (4.977000°W; 52.024300°N; d=-16.3mMSL)
Time series (1993-01-01–2022-12-31; Δt=15min; t̄=30min)
N MEAN MIN MAX STD
1011010 -0.06 -2.92 3.00 1.07
1011010 -0.05 -2.78 2.97 1.04
Measurements
HD NE-DA
WL [mMSL]

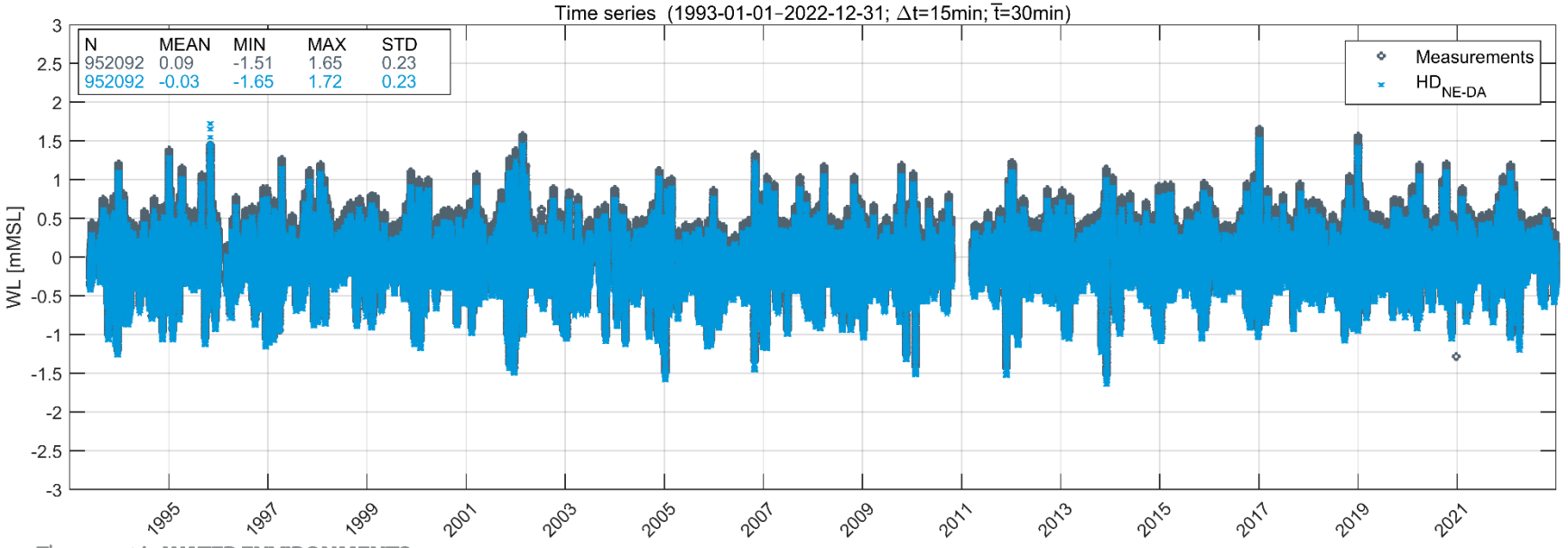
Gedser (11.938200°E; 54.562300°N; d=-3.8mMSL)
Time series (1993-01-01–2022-12-31; Δt=15min; t̄=30min)
N MEAN MIN MAX STD
952092 0.09 -1.51 1.65 0.23
952092 -0.03 -1.65 1.72 0.23
Measurements
HD NE-DA
WL [mMSL]

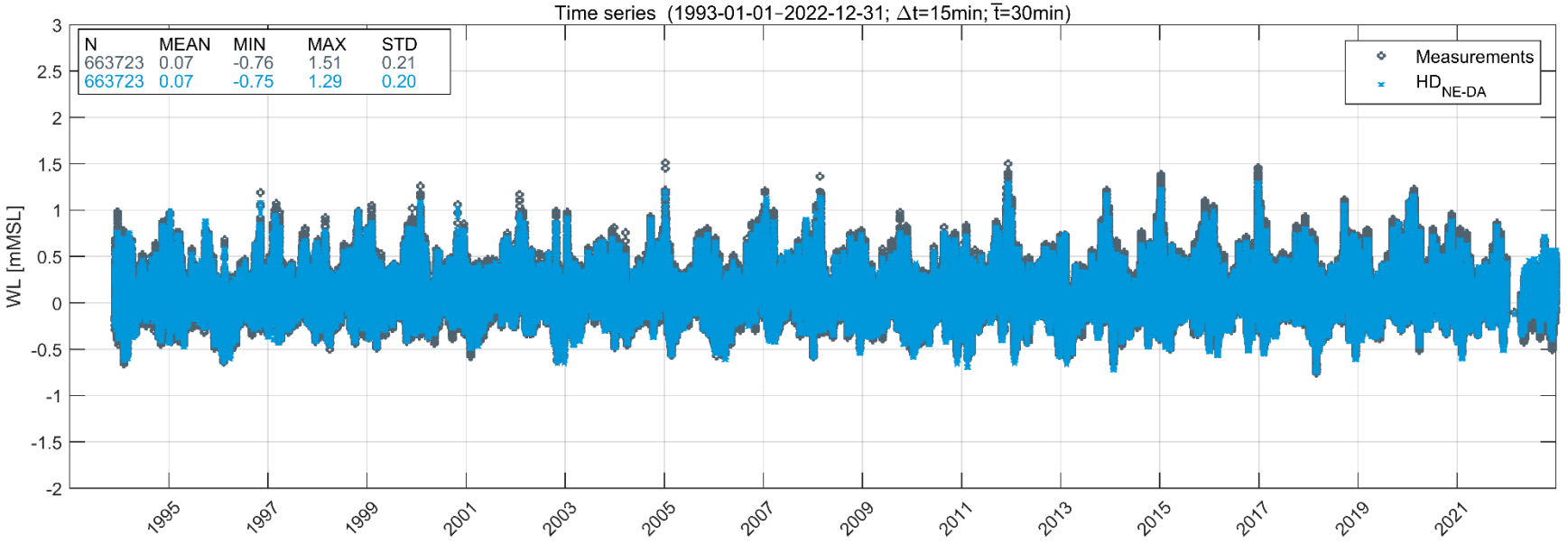
Göteborg Torshamnen (11.795200°E; 57.680400°N; d=-6.3mMSL)
Time series (1993-01-01–2022-12-31; Δt=15min; t̄=30min)
N MEAN MIN MAX STD
663723 0.07 -0.76 1.51 0.21
663723 0.07 -0.75 1.29 0.20
Measurements
HD NE-DA
WL [mMSL]

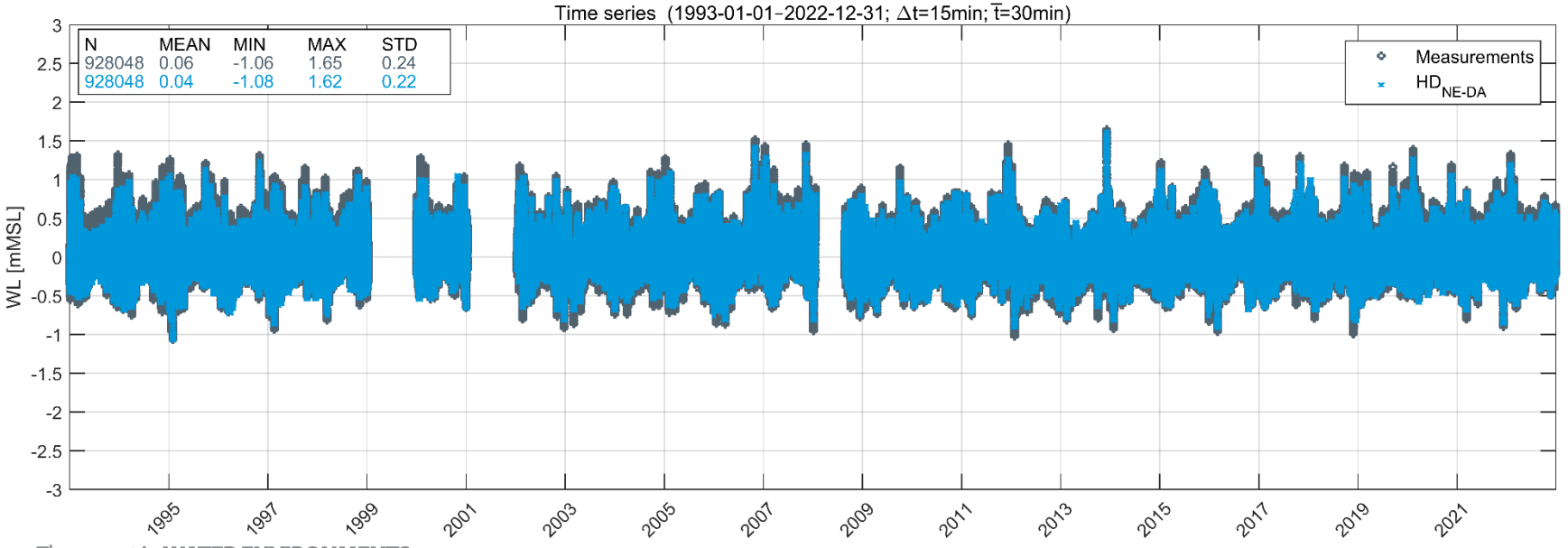
Grenaa (10.937100°E; 56.417000°N; d=-6.1mMSL)
Time series (1993-01-01–2022-12-31; Δt=15min; t̄=30min)
N MEAN MIN MAX STD
928048 0.06 -1.06 1.65 0.24
928048 0.04 -1.08 1.62 0.22
Measurements
HD NE-DA
WL [mMSL]

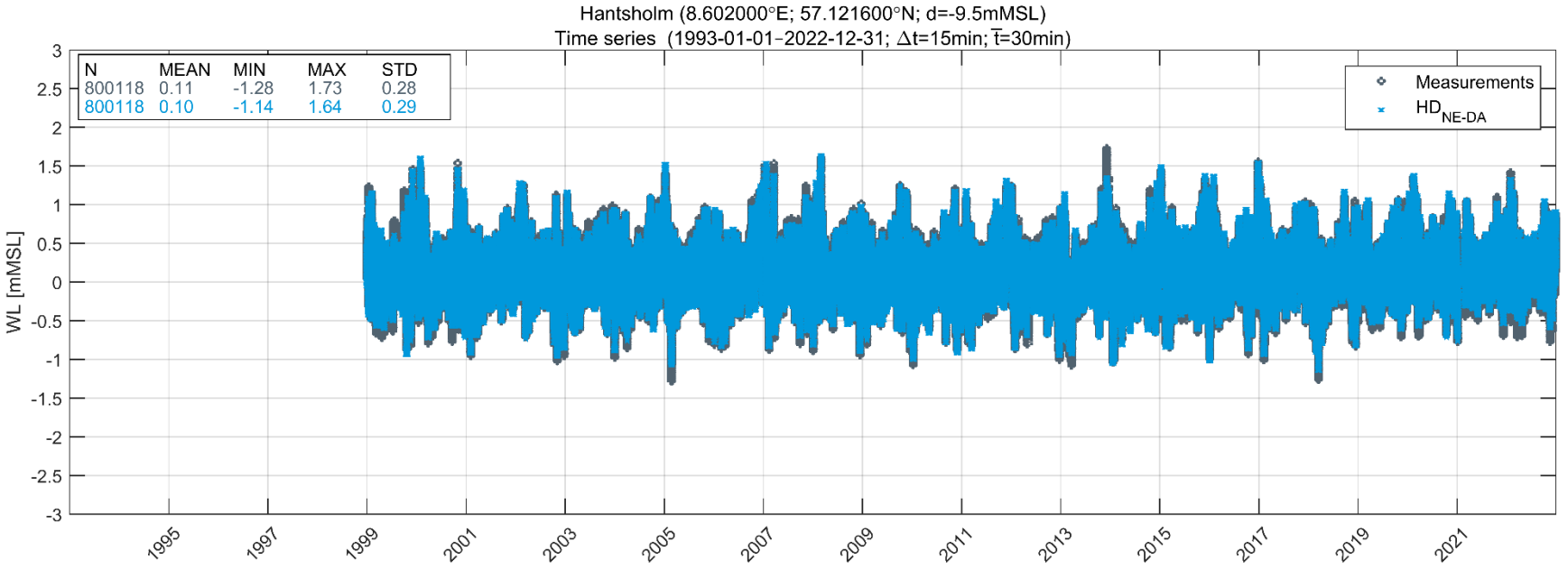
Hantsholm (8.602000°E; 57.121600°N; d=-9.5mMSL)
Time series (1993-01-01–2022-12-31; Δt=15min; t̄=30min)
N MEAN MIN MAX STD
800118 0.11 -1.28 1.73 0.28
800118 0.10 -1.14 1.64 0.29
Measurements
HD NE-DA
WL [mMSL]
3
2.5
2
1.5
1
0.5
0
-0.5
-1
-1.5
-2
-2.5
-3
1995
1997
1999
2001
2003
2005
2007
2009
2011
2013
2015
2017
2019
2021

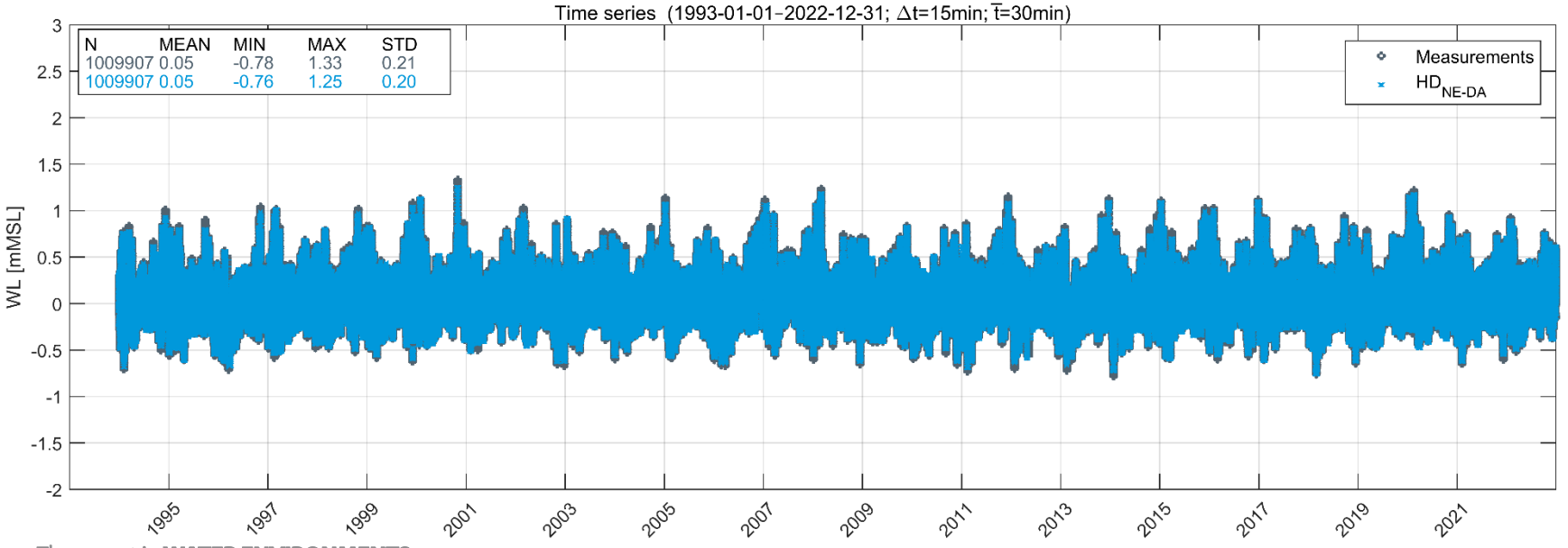
Helgeroa (9.835200°E; 59.007400°N; d=-20.9mMSL)
Time series (1993-01-01–2022-12-31; Δt=15min; t̄=30min)
N MEAN MIN MAX STD
1009907 0.05 -0.78 1.33 0.21
1009907 0.05 -0.76 1.25 0.20
Measurements
HD NE-DA
WL [mMSL]
3
2.5
2
1.5
1
0.5
0
-0.5
-1
-1.5
-2
1995
1997
1999
2001
2003
2005
2007
2009
2011
2013
2015
2017
2019
2021

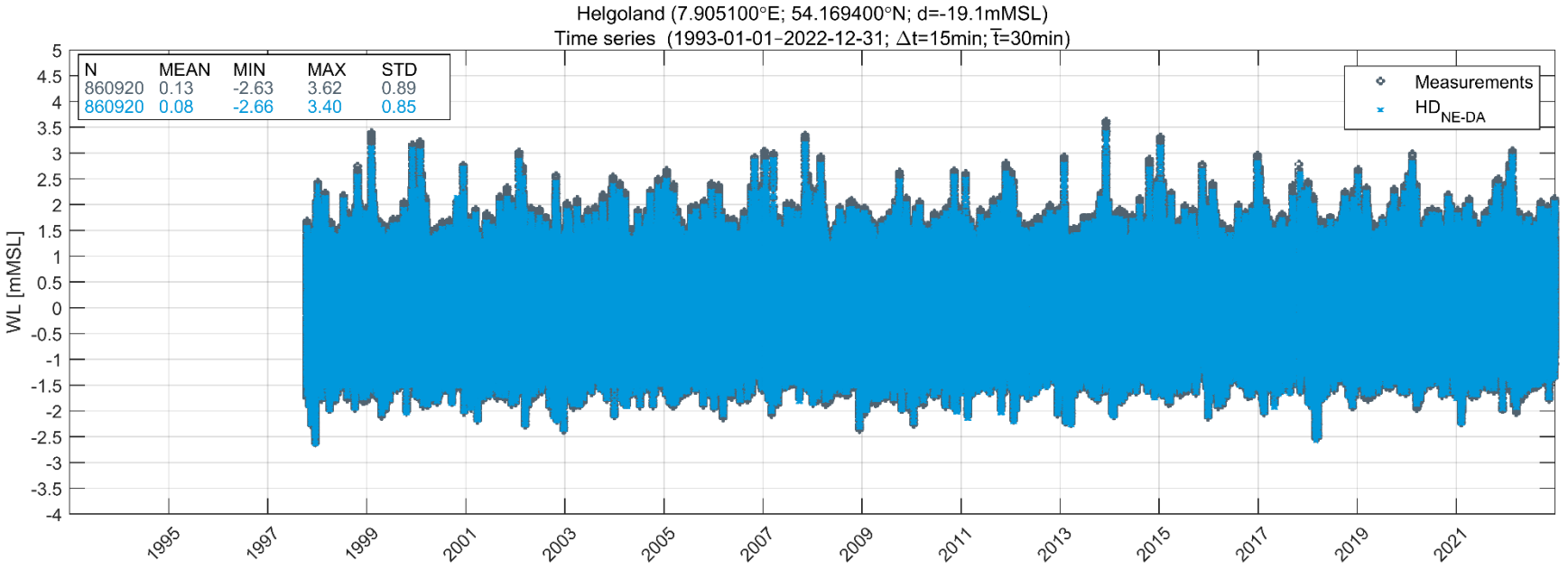
Helgoland (7.905100°E; 54.169400°N; d=-19.1mMSL)
Time series (1993-01-01–2022-12-31; Δt=15min; t̄=30min)
N MEAN MIN MAX STD
860920 0.13 -2.63 3.62 0.89
860920 0.08 -2.66 3.40 0.85
Measurements
HD NE-DA
WL [mMSL]

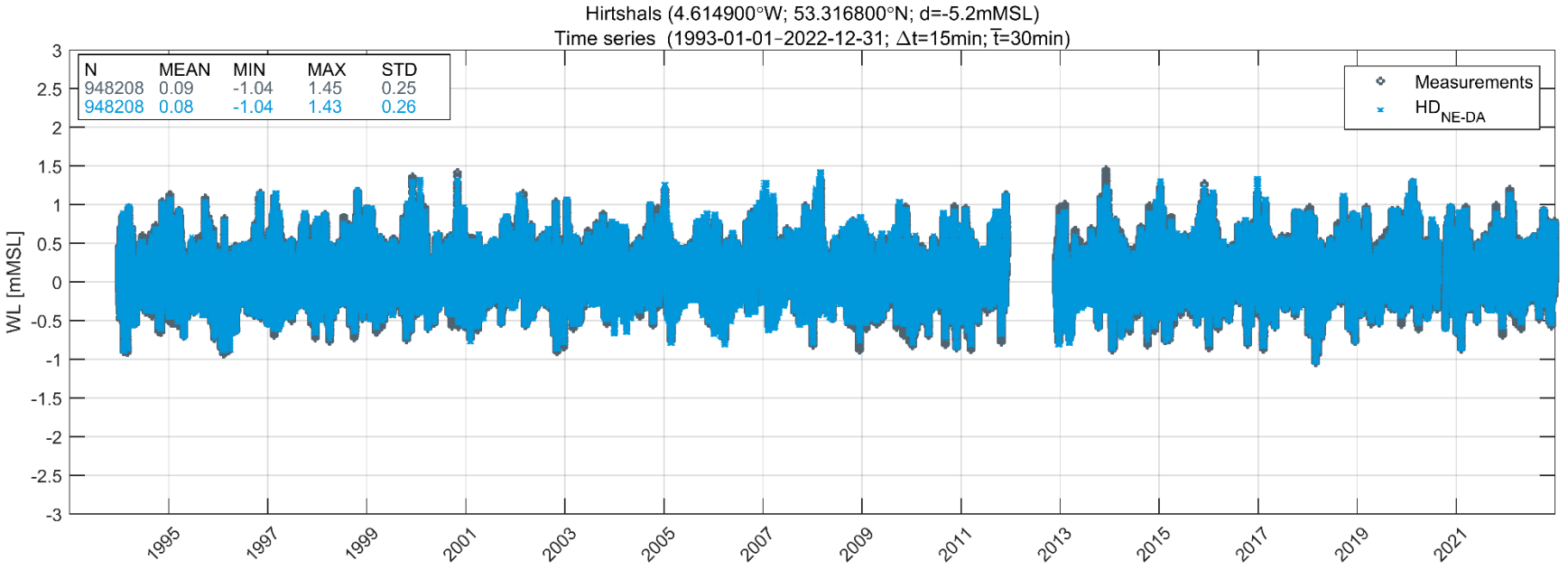
Hirtshals (4.614900°W; 53.316800°N; d=-5.2mMSL)
Time series (1993-01-01–2022-12-31; Δt=15min; t̄=30min)
N MEAN MIN MAX STD
948208 0.09 -1.04 1.45 0.25
948208 0.08 -1.04 1.43 0.26
Measurements
HD NE-DA
WL [mMSL]

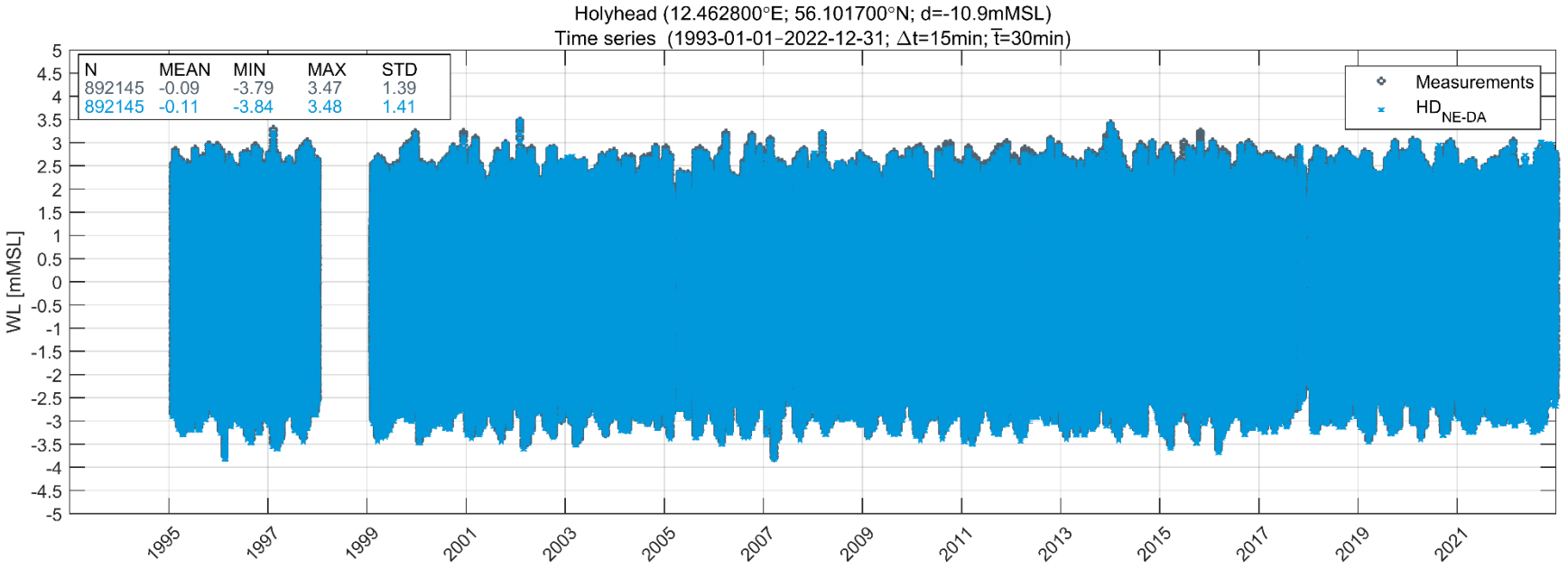
Holyhead (12.462800°E; 56.101700°N; d=-10.9mMSL)
Time series (1993-01-01–2022-12-31; Δt=15min; t̄=30min)
N MEAN MIN MAX STD
892145 -0.09 -3.79 3.47 1.39
892145 -0.11 -3.84 3.48 1.41
Measurements
HD NE-DA
WL [mMSL]

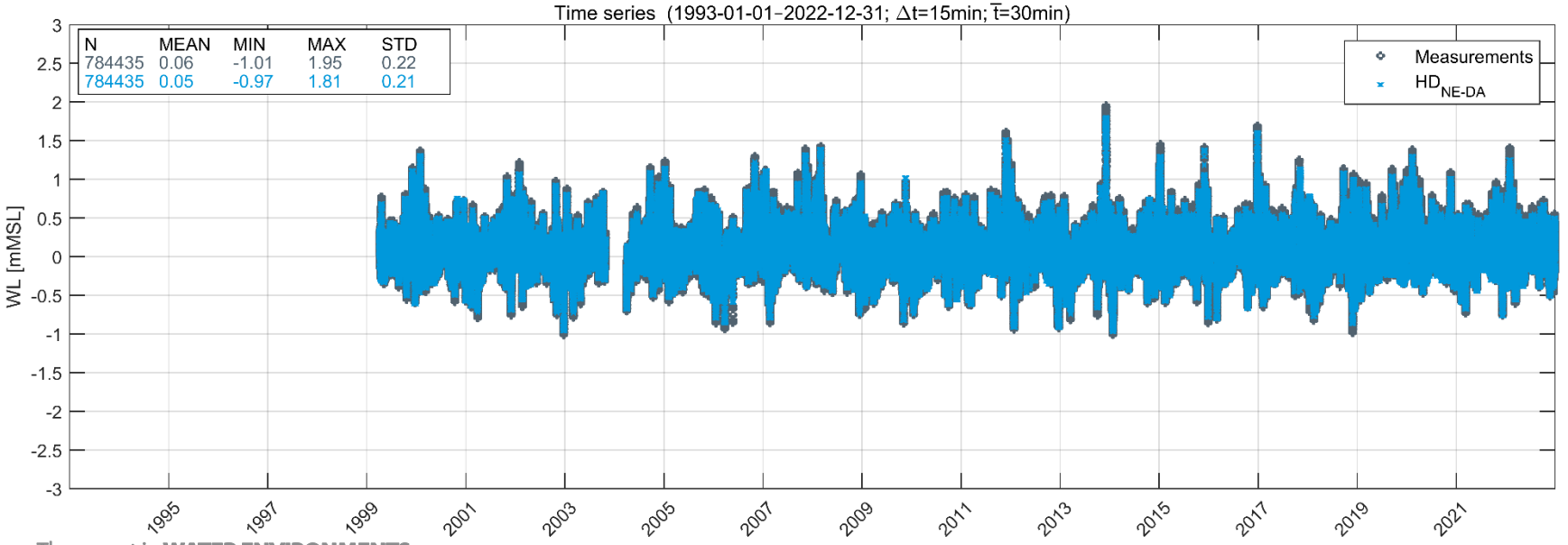
Hornbaek (6.406000°E; 53.564000°N; d=-6.1mMSL)
Time series (1993-01-01–2022-12-31; Δt=15min; t̄=30min)
N MEAN MIN MAX STD
784435 0.06 -1.01 1.95 0.22
784435 0.05 -0.97 1.81 0.21
Measurements
HD NE-DA
WL [mMSL]

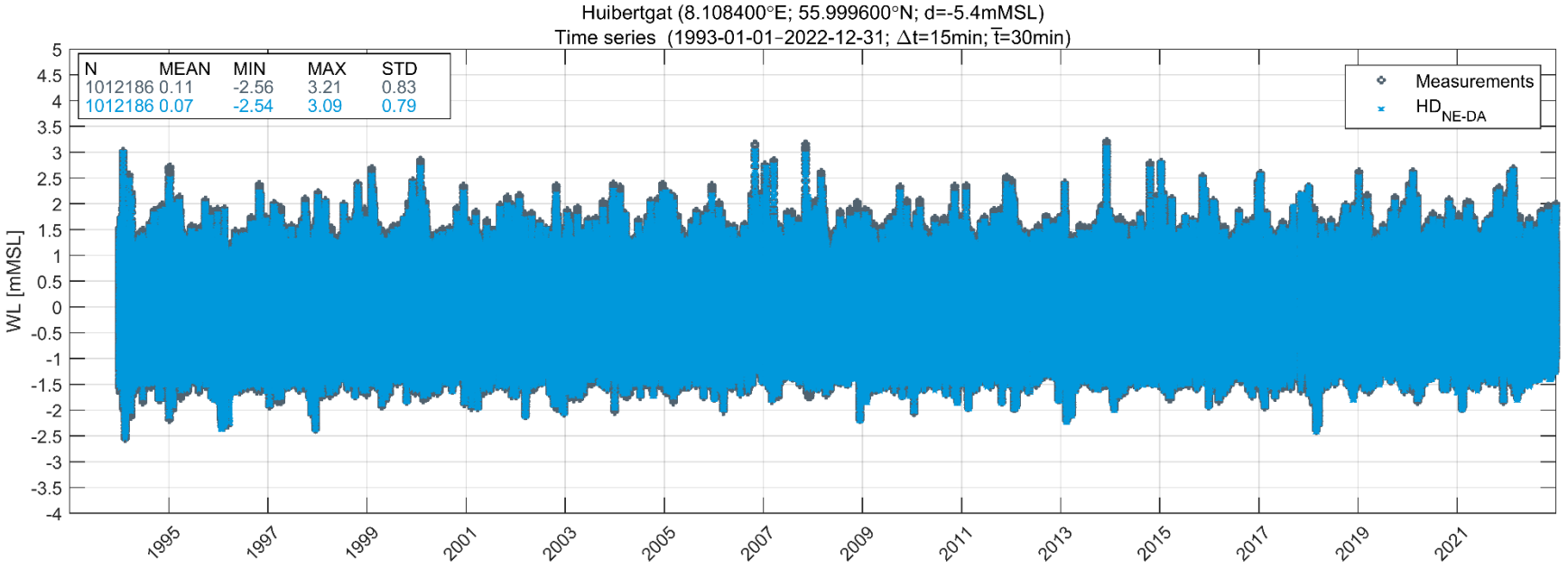
Huibertgat (8.108400°E; 55.999600°N; d=-5.4mMSL)
Time series (1993-01-01–2022-12-31; Δt=15min; t̄=30min)
N MEAN MIN MAX STD
1012186 0.11 -2.56 3.21 0.83
1012186 0.07 -2.54 3.09 0.79
Measurements
HD NE-DA
WL [mMSL]

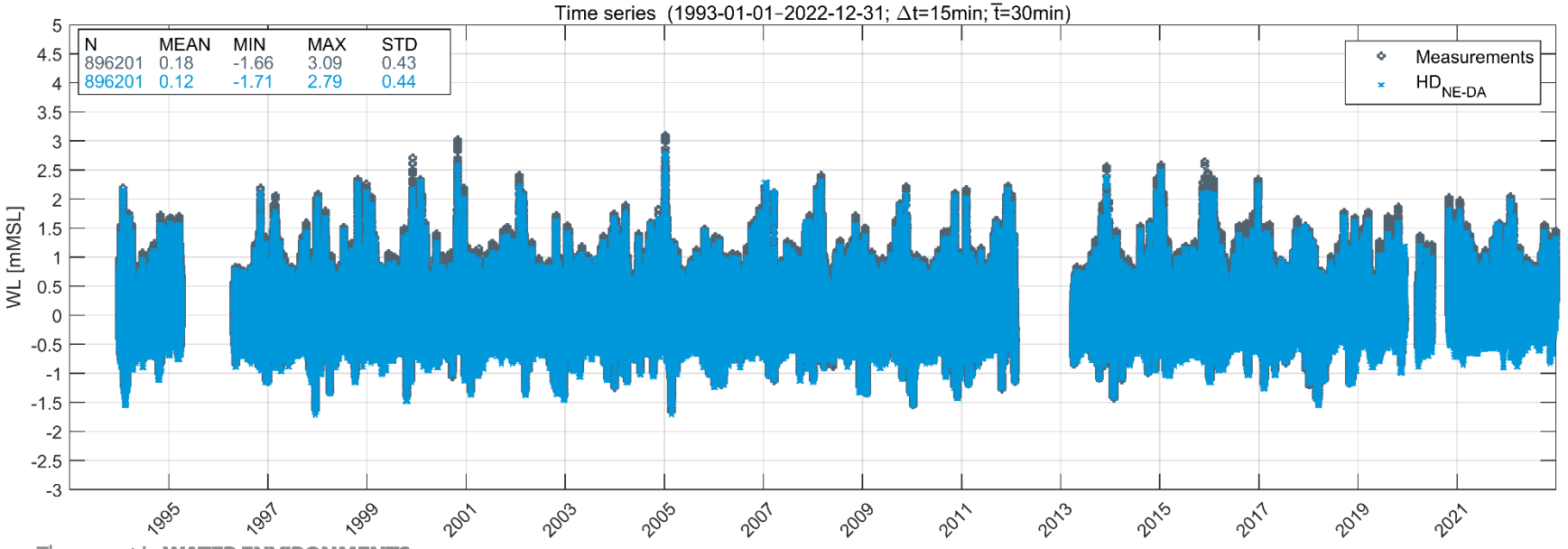
Hvide Sande (3.209100°E; 53.223500°N; d=-28.3mMSL)
Time series (1993-01-01–2022-12-31; Δt=15min; t̄=30min)
N MEAN MIN MAX STD
896201 0.18 -1.66 3.09 0.43
896201 0.12 -1.71 2.79 0.44
Measurements
HD NE-DA
WL [mMSL]

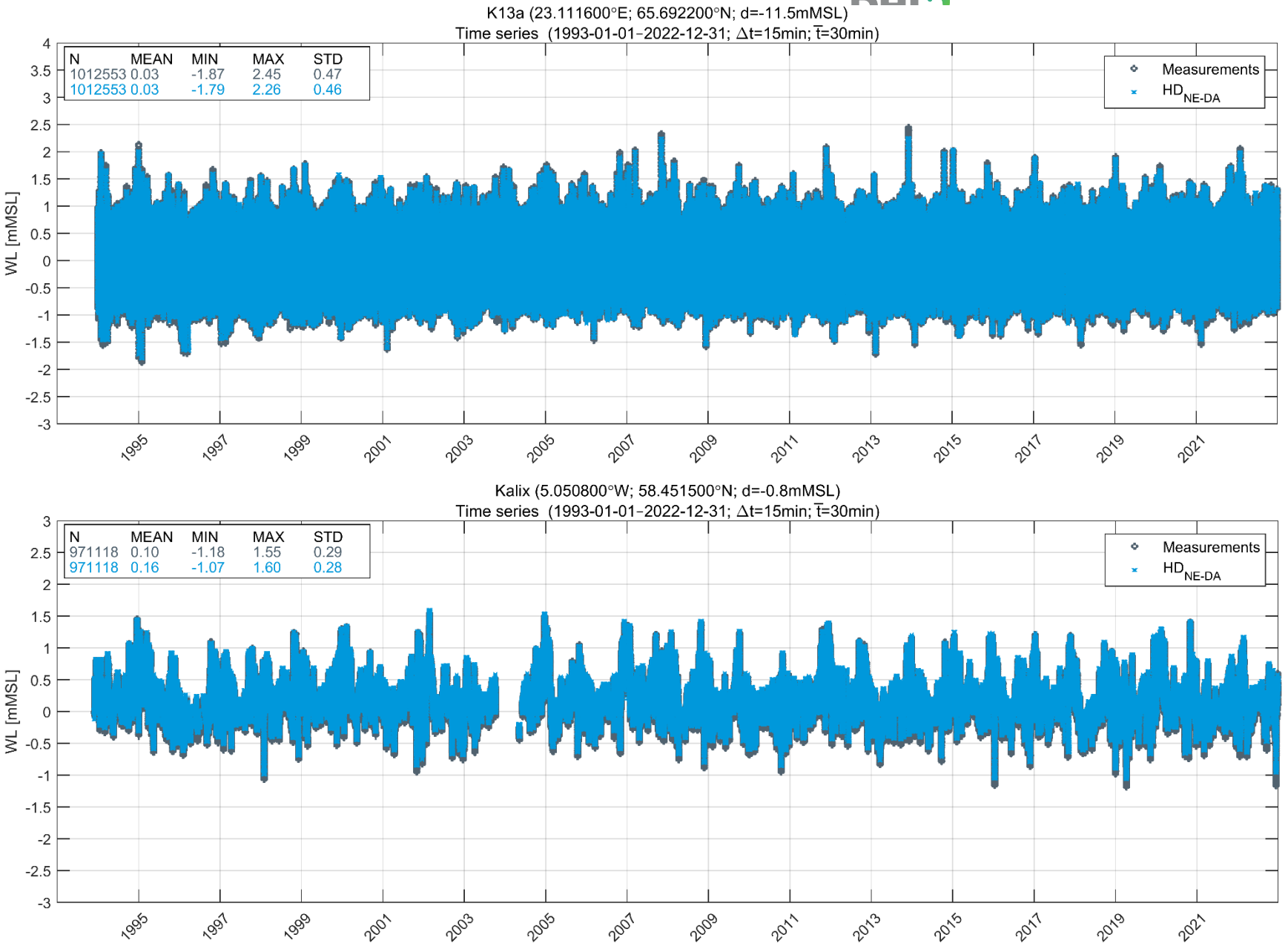
K13a (23.111600°E; 65.692200°N; d=-11.5mMSL)
Time series (1993-01-01-2022-12-31; Δt=15min; t̄=30min)
N MEAN MIN MAX STD
1012553 0.03 -1.87 2.45 0.47
1012553 0.03 -1.79 2.26 0.46
Measurements
HD NE-DA
WL [mMSL]
Kalix (5.050800°W; 58.451500°N; d=-0.8mMSL)
Time series (1993-01-01-2022-12-31; Δt=15min; t̄=30min)
N MEAN MIN MAX STD
971118 0.10 -1.18 1.55 0.29
971118 0.16 -1.07 1.60 0.28
Measurements
HD NE-DA
WL [mMSL]

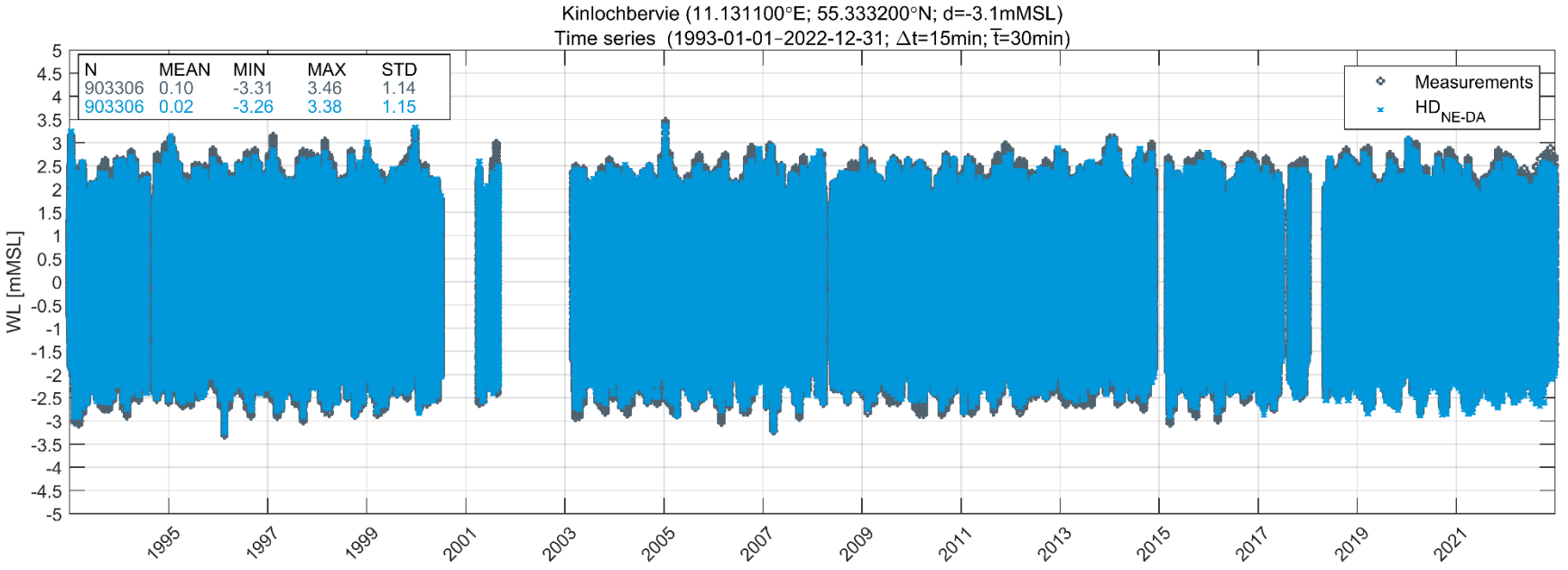
Kinlochbervie (11.131100°E; 55.333200°N; d=-3.1mMSL)
Time series (1993-01-01–2022-12-31; Δt=15min; t̄=30min)
N MEAN MIN MAX STD
903306 0.10 -3.31 3.46 1.14
903306 0.02 -3.26 3.38 1.15
Measurements
HD NE-DA
WL [mMSL]

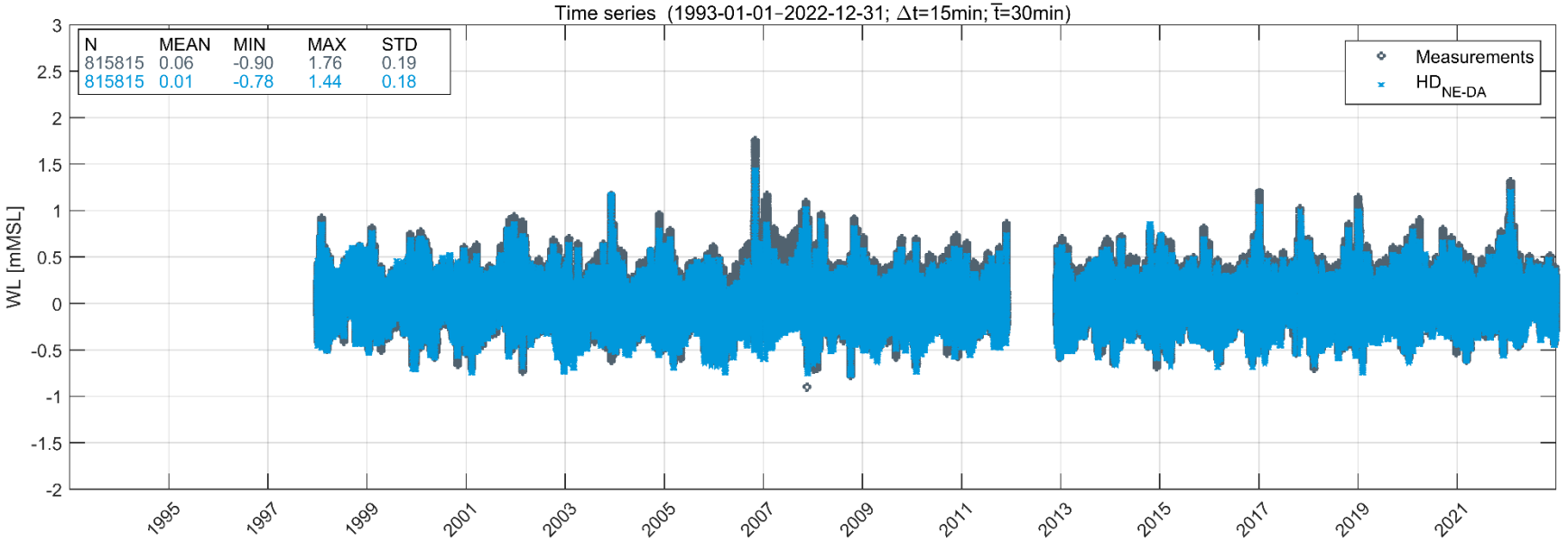
Korsør (15.590400°E; 56.101300°N; d=-8.2mMSL)
Time series (1993-01-01–2022-12-31; Δt=15min; t̄=30min)
N MEAN MIN MAX STD
815815 0.06 -0.90 1.76 0.19
815815 0.01 -0.78 1.44 0.18
Measurements
HD NE-DA
WL [mMSL]

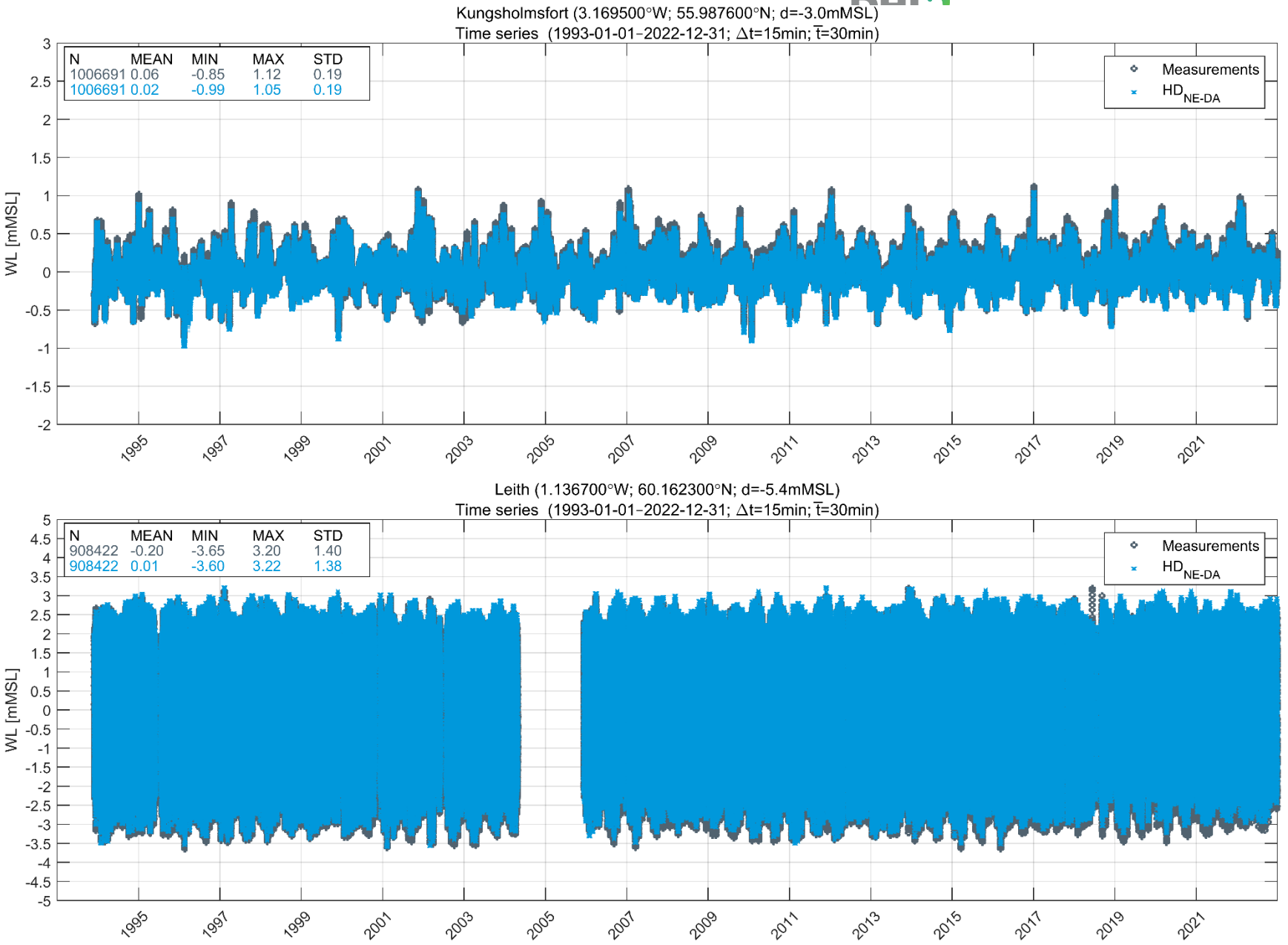
Kungsholmsfort (3.169500°W; 55.987600°N; d=-3.0mMSL)
Time series (1993-01-01–2022-12-31; Δt=15min; t̄=30min)
N MEAN MIN MAX STD
1006691 0.06 -0.85 1.12 0.19
1006691 0.02 -0.99 1.05 0.19
Measurements
HD NE-DA
WL [mMSL]
Leith (1.136700°W; 60.162300°N; d=-5.4mMSL)
Time series (1993-01-01–2022-12-31; Δt=15min; t̄=30min)
N MEAN MIN MAX STD
908422 -0.20 -3.65 3.20 1.40
908422 0.01 -3.60 3.22 1.38
Measurements
HD NE-DA
WL [mMSL]

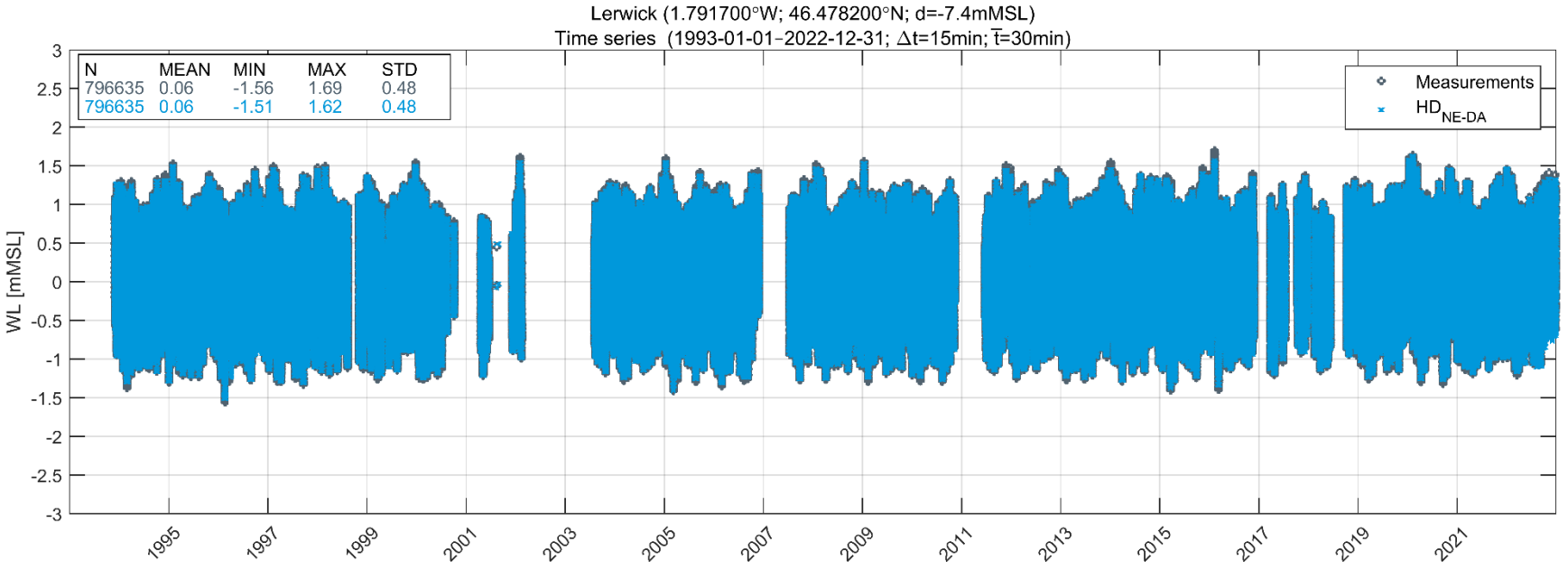
Lerwick (1.791700°W; 46.478200°N; d=-7.4mMSL)
Time series (1993-01-01–2022-12-31; Δt=15min; t̄=30min)
N MEAN MIN MAX STD
796635 0.06 -1.56 1.69 0.48
796635 0.06 -1.51 1.62 0.48
Measurements
HD NE-DA
WL [mMSL]

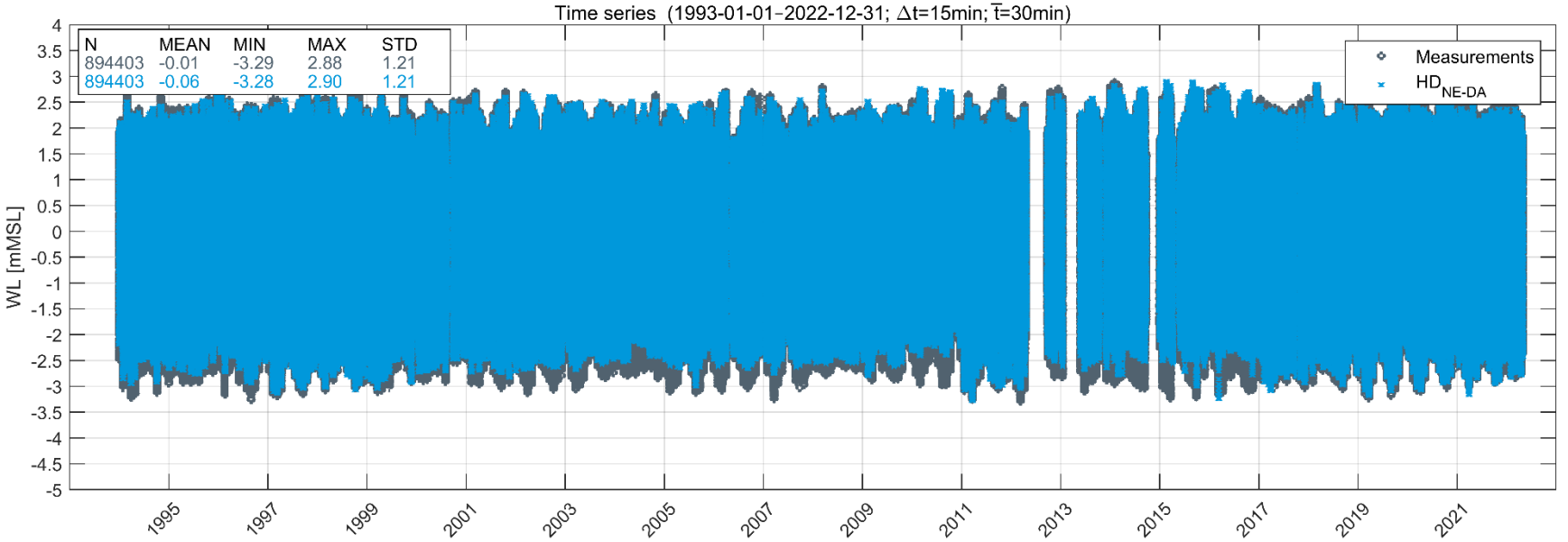
Les Sables-dOlonne (3.814600°W; 53.331700°N; d=-5.1mMSL)
Time series (1993-01-01–2022-12-31; Δt=15min; t̄=30min)
N MEAN MIN MAX STD
894403 -0.01 -3.29 2.88 1.21
894403 -0.06 -3.28 2.90 1.21
Measurements
HD NE-DA
WL [mMSL]

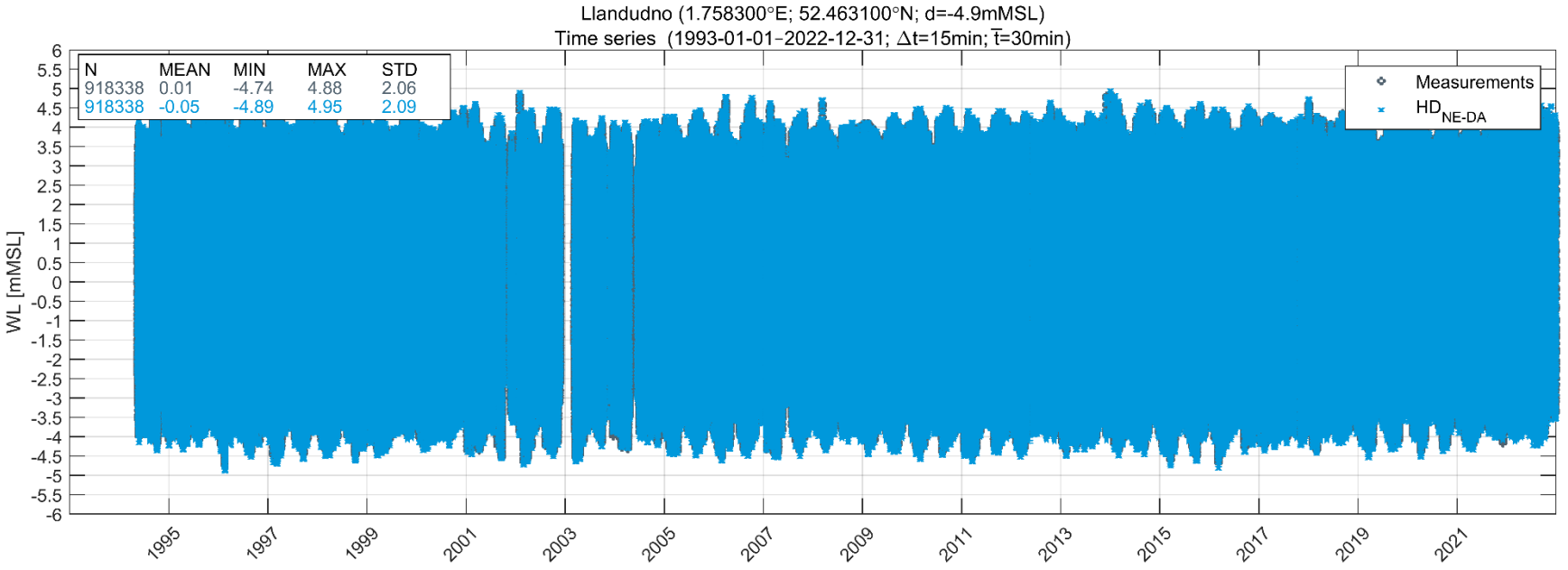
Llandudno (1.758300°E; 52.463100°N; d=-4.9mMSL)
Time series (1993-01-01–2022-12-31; Δt=15min; t̄=30min)
N MEAN MIN MAX STD
918338 0.01 -4.74 4.88 2.06
918338 -0.05 -4.89 4.95 2.09
Measurements
HD NE-DA
WL [mMSL]

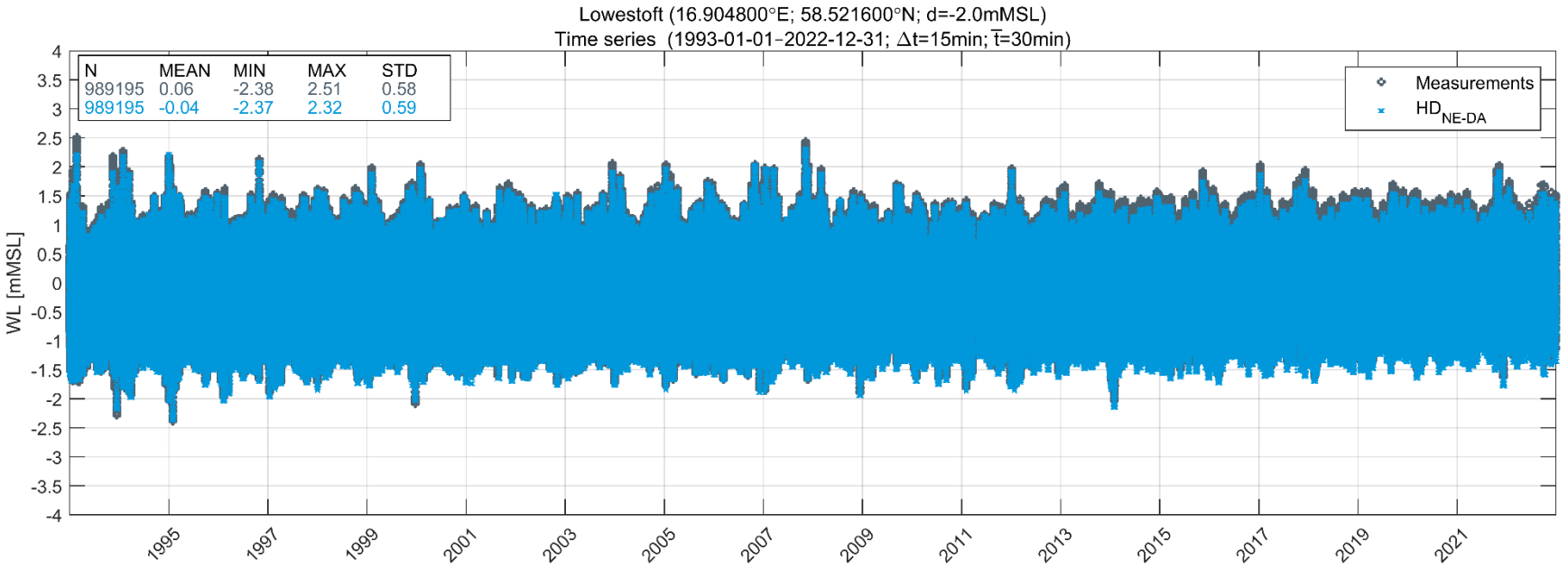
Lowestoft (16.904800°E; 58.521600°N; d=-2.0mMSL)
Time series (1993-01-01–2022-12-31; Δt=15min; t̄=30min)
N MEAN MIN MAX STD
989195 0.06 -2.38 2.51 0.58
989195 -0.04 -2.37 2.32 0.59
Measurements
HD NE-DA
WL [mMSL]

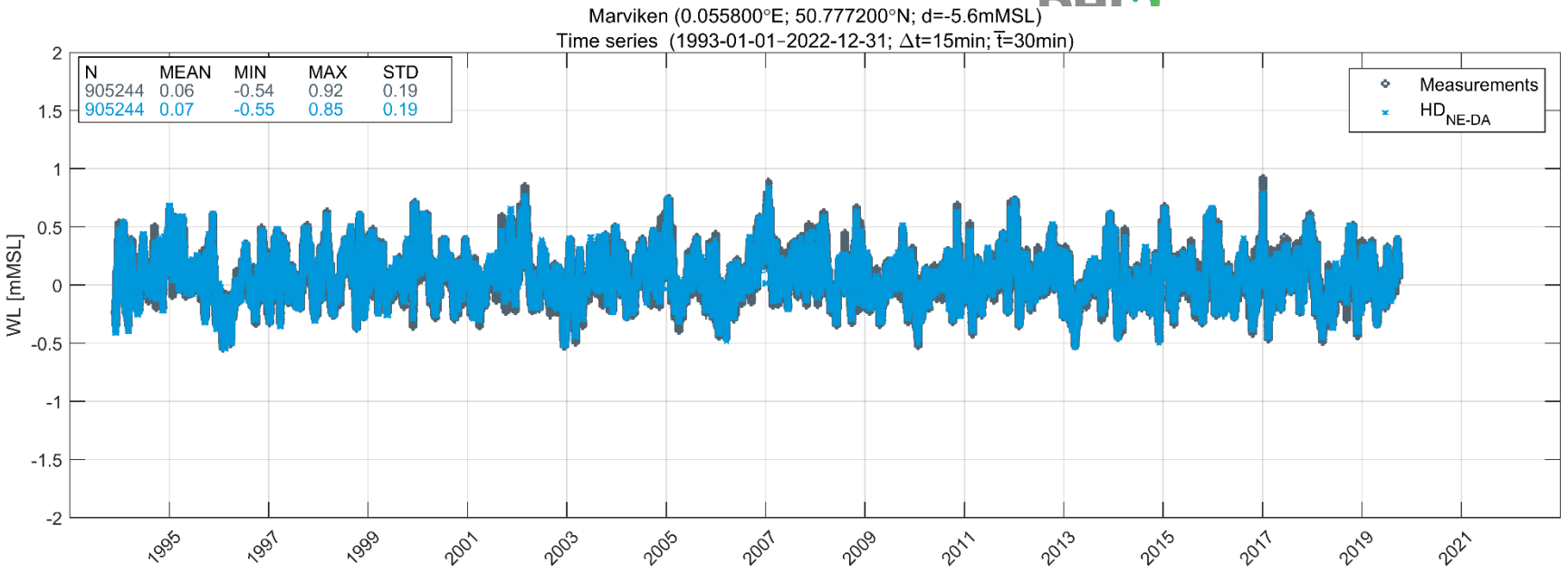
Marviken (0.055800°E; 50.777200°N; d=-5.6mMSL)
Time series (1993-01-01-2022-12-31; Δt=15min; t̄=30min)
N MEAN MIN MAX STD
905244 0.06 -0.54 0.92 0.19
905244 0.07 -0.55 0.85 0.19
Measurements
HD NE-DA
WL [mMSL]

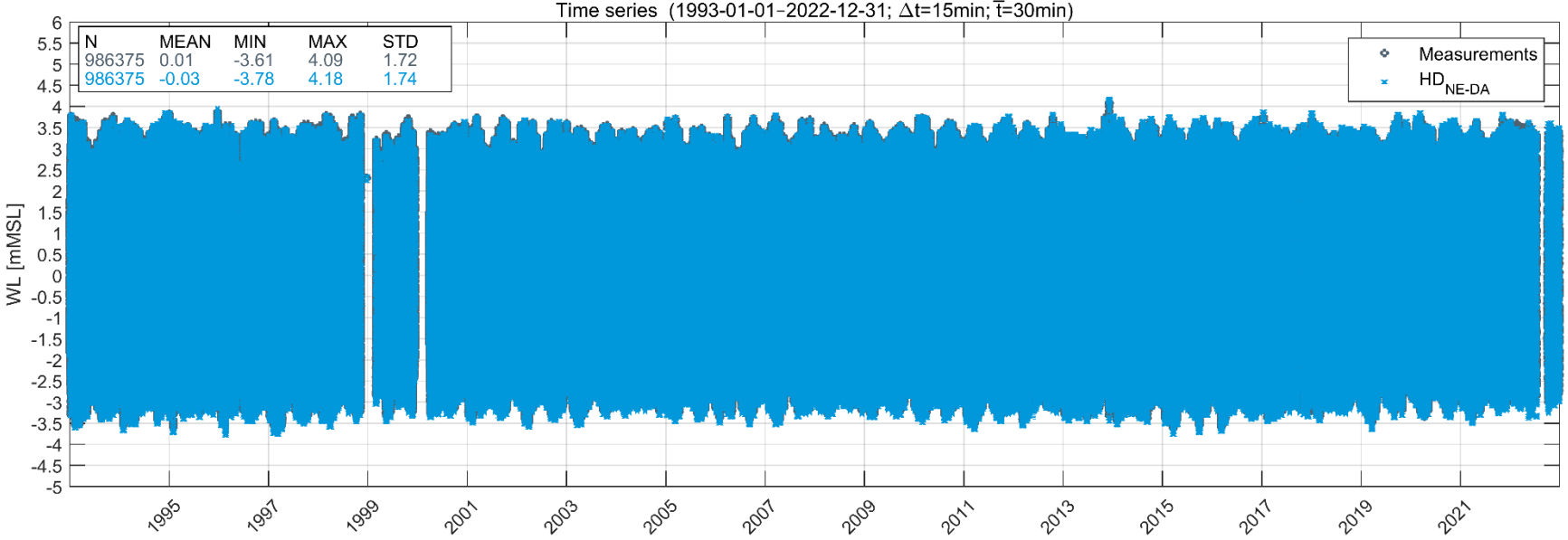
Newhaven (5.534900°W; 50.106100°N; d=-2.1mMSL)
Time series (1993-01-01-2022-12-31; Δt=15min; t̄=30min)
N MEAN MIN MAX STD
986375 0.01 -3.61 4.09 1.72
986375 -0.03 -3.78 4.18 1.74
Measurements
HD NE-DA
WL [mMSL]

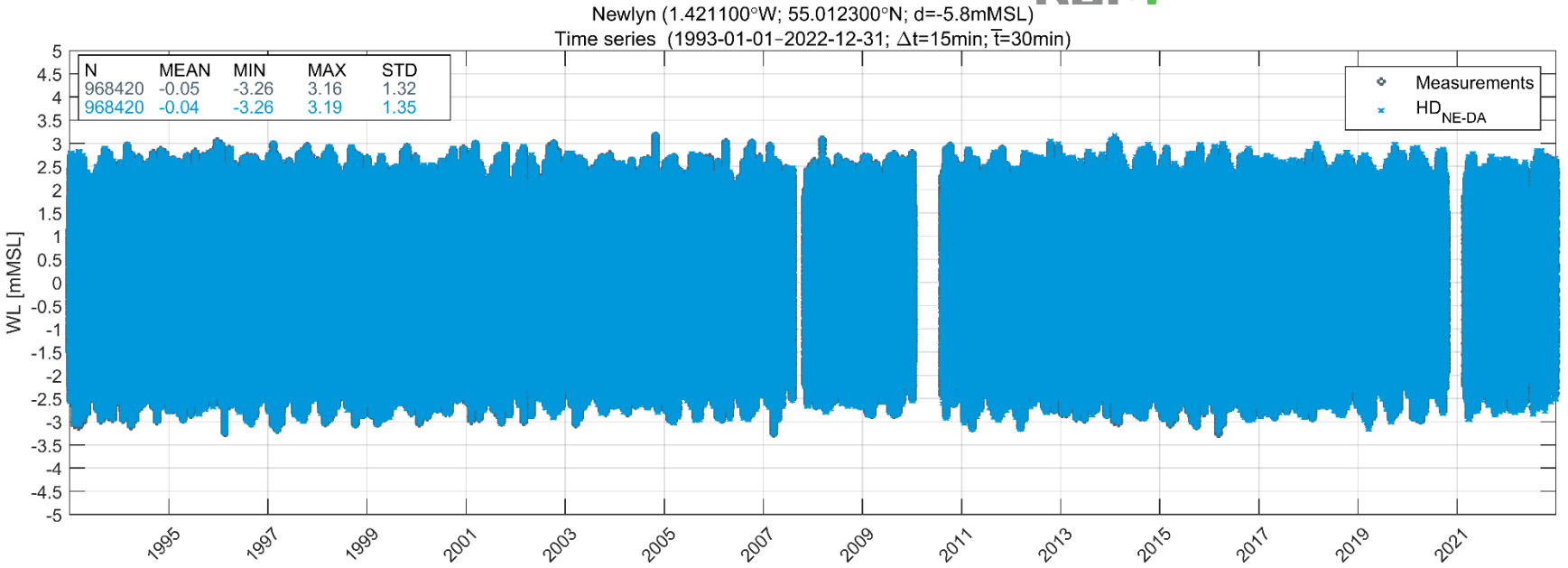
Newlyn (1.421100°W; 55.012300°N; d=-5.8mSL)
Time series (1993-01-01-2022-12-31; Δt=15min; t̄=30min)
N MEAN MIN MAX STD
968420 -0.05 -3.26 3.16 1.32
968420 -0.04 -3.26 3.19 1.35
Measurements
HD NE-DA
WL [mMSL]

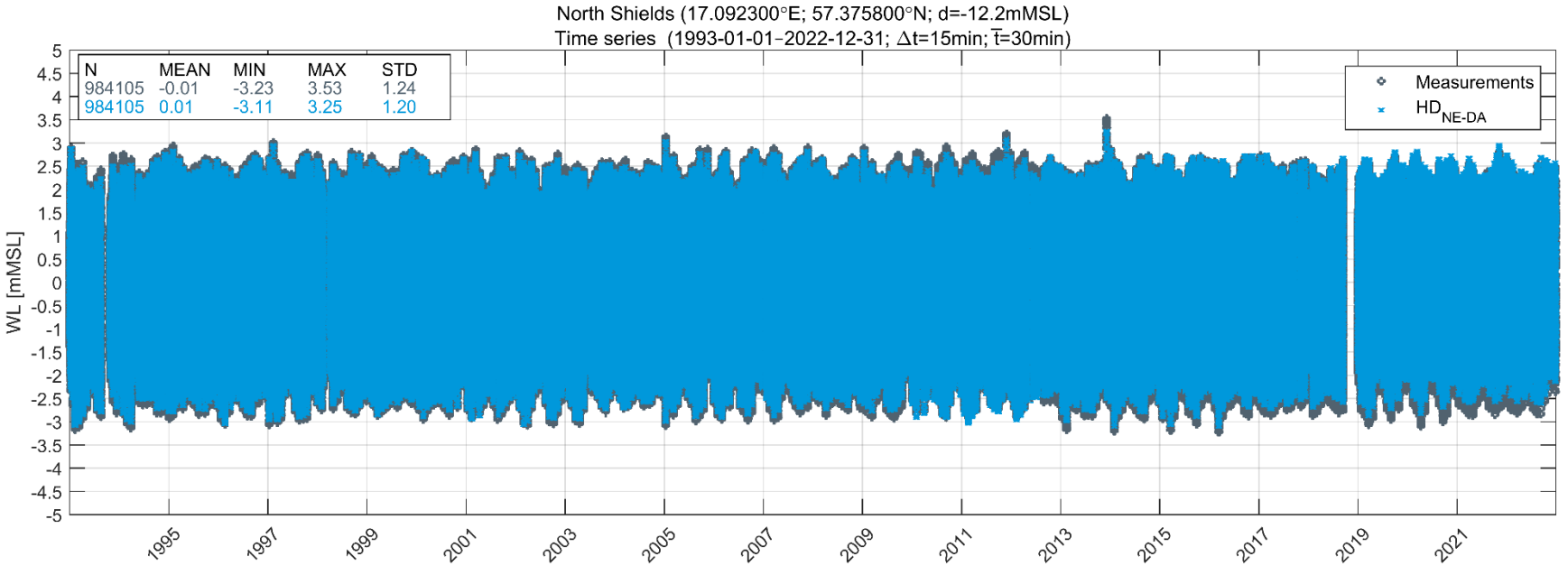
North Shields (17.092300°E; 57.375800°N; d=-12.2mSL)
Time series (1993-01-01-2022-12-31; Δt=15min; t̄=30min)
N MEAN MIN MAX STD
984105 -0.01 -3.23 3.53 1.24
984105 0.01 -3.11 3.25 1.20
Measurements
HD NE-DA
WL [mMSL]

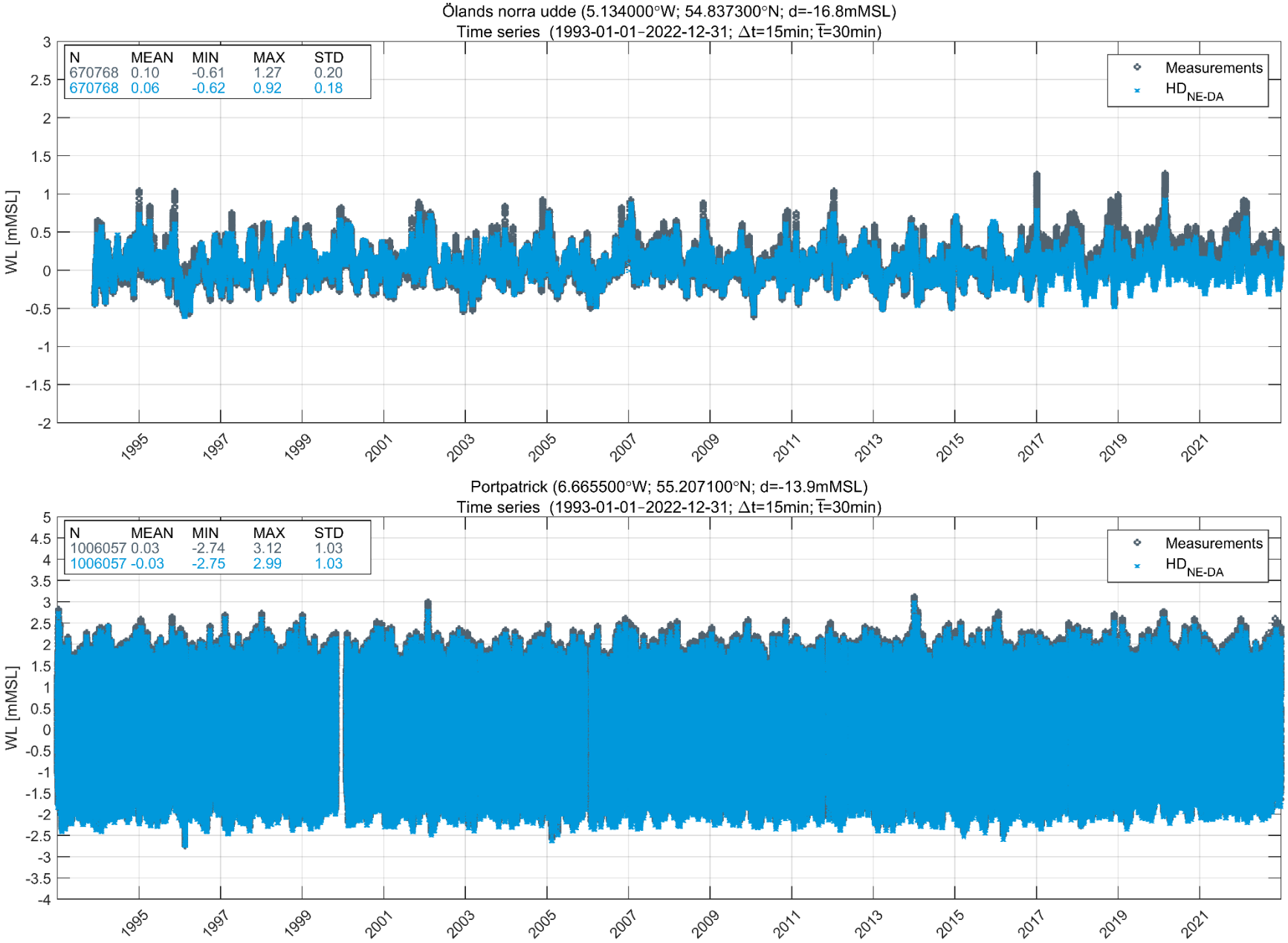
Ölands norra udde (5.134000°W; 54.837300°N; d=-16.8mMSL)
Time series (1993-01-01–2022-12-31; Δt=15min; t̄=30min)
N MEAN MIN MAX STD
670768 0.10 -0.61 1.27 0.20
670768 0.06 -0.62 0.92 0.18
Measurements
HD NE-DA
WL [mMSL]
Portpatrick (6.665500°W; 55.207100°N; d=-13.9mMSL)
Time series (1993-01-01–2022-12-31; Δt=15min; t̄=30min)
N MEAN MIN MAX STD
1006057 0.03 -2.74 3.12 1.03
1006057 -0.03 -2.75 2.99 1.03
Measurements
HD NE-DA
WL [mMSL]

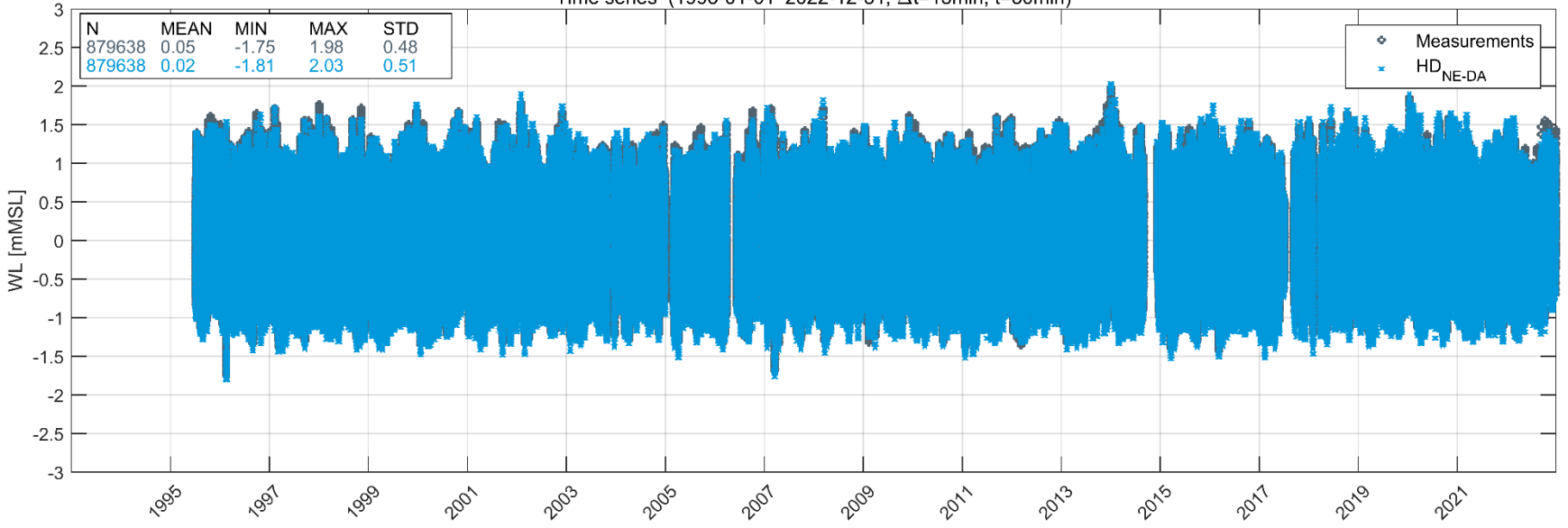
Portrush (14.685900°E; 55.096500°N; d=-10.1mMSL)
Time series (1993-01-01-2022-12-31; Δt=15min; t̄=30min)
N MEAN MIN MAX STD
879638 0.05 -1.75 1.98 0.48
879638 0.02 -1.81 2.03 0.51
Measurements
HD NE-DA
WL [mMSL]

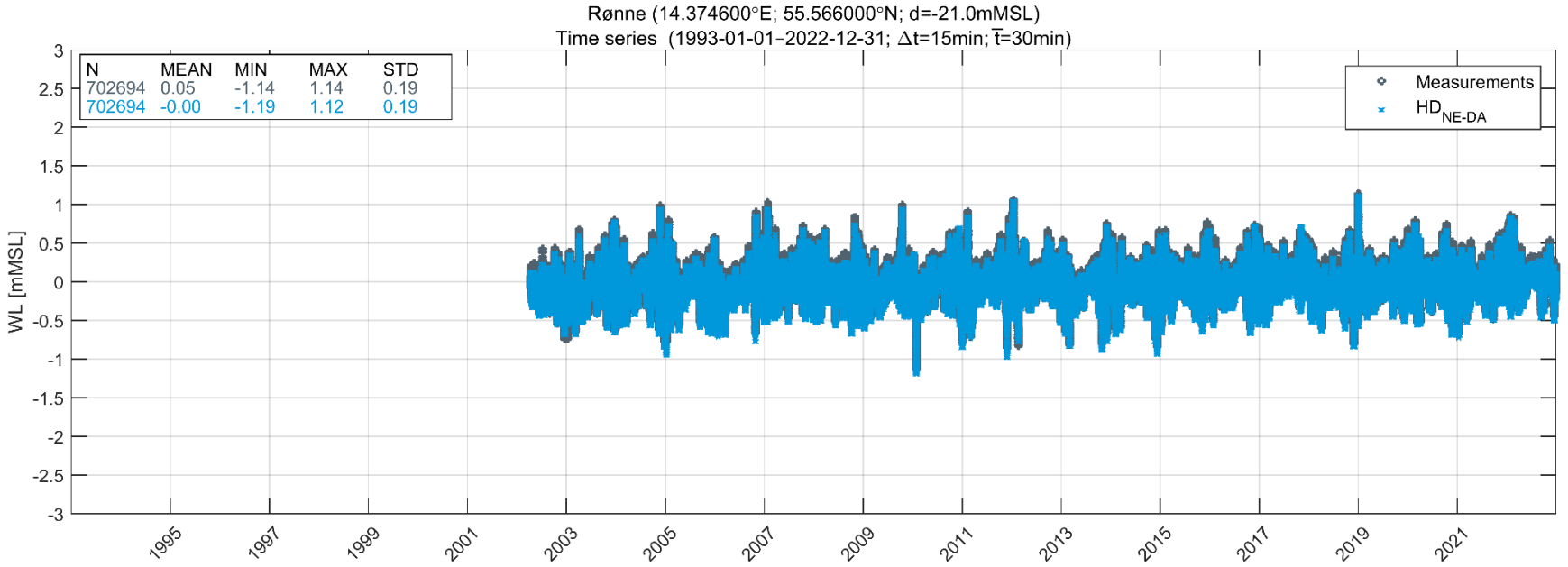
Rønne (14.374600°E; 55.566000°N; d=-21.0mMSL)
Time series (1993-01-01-2022-12-31; Δt=15min; t̄=30min)
N MEAN MIN MAX STD
702694 0.05 -1.14 1.14 0.19
702694 -0.00 -1.19 1.12 0.19
Measurements
HD NE-DA
WL [mMSL]

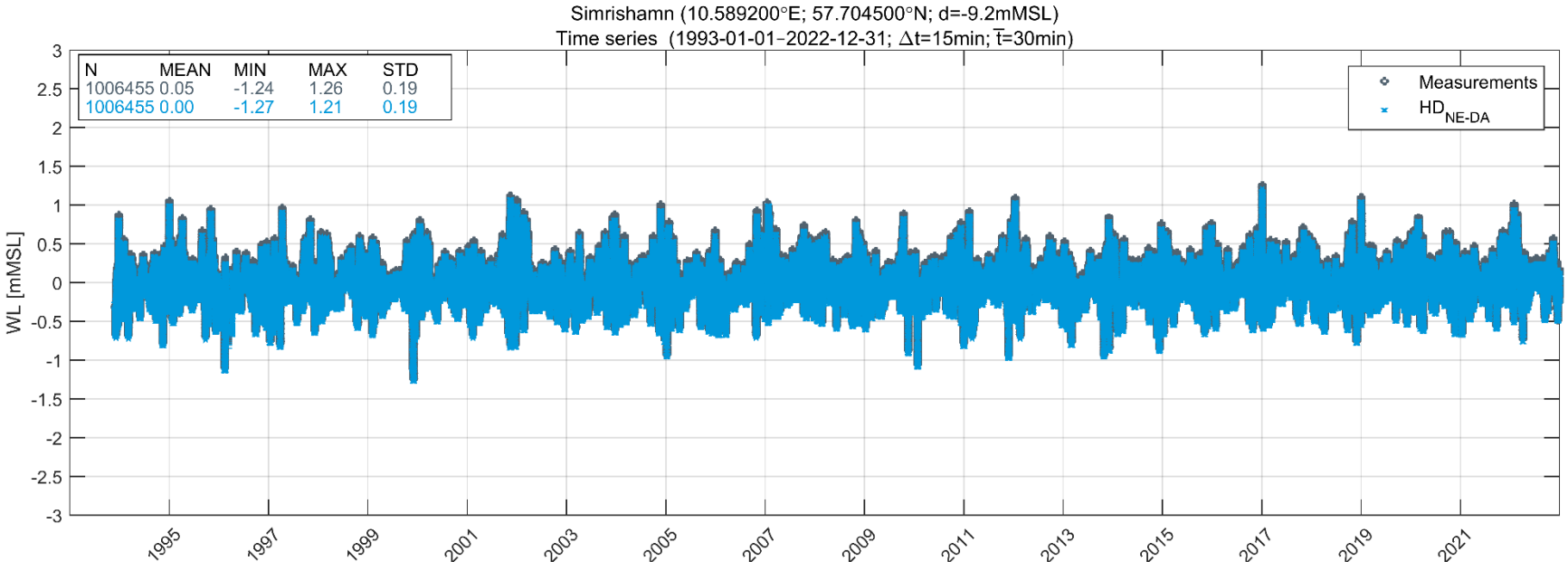
Simrishamn (10.589200°E; 57.704500°N; d=-9.2mMSL)
Time series (1993-01-01–2022-12-31; Δt=15min; t̄=30min)
N MEAN MIN MAX STD
1006455 0.05 -1.24 1.26 0.19
1006455 0.00 -1.27 1.21 0.19
Measurements
HD NE-DA
WL [mMSL]

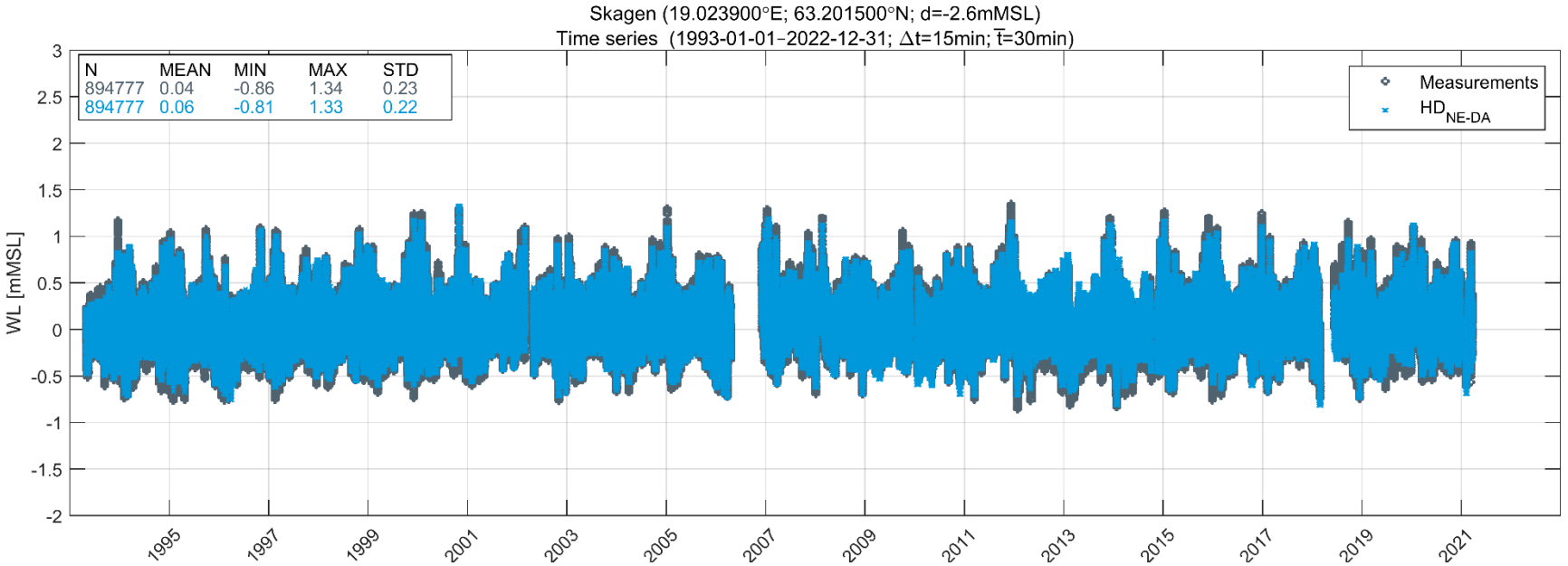
Skagen (19.023900°E; 63.201500°N; d=-2.6mMSL)
Time series (1993-01-01–2022-12-31; Δt=15min; t̄=30min)
N MEAN MIN MAX STD
894777 0.04 -0.86 1.34 0.23
894777 0.06 -0.81 1.33 0.22
Measurements
HD NE-DA
WL [mMSL]

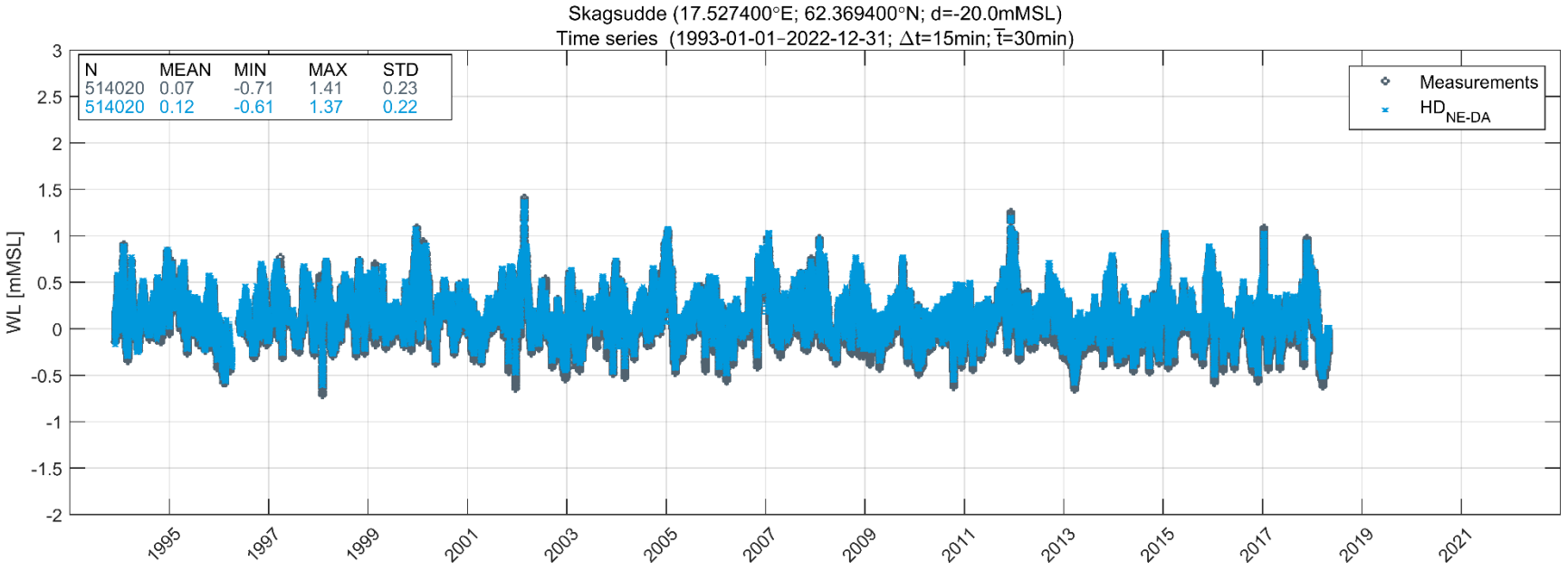
Skagsudde (17.527400°E; 62.369400°N; d=-20.0mMSL)
Time series (1993-01-01–2022-12-31; Δt=15min; t̄=30min)
N MEAN MIN MAX STD
514020 0.07 -0.71 1.41 0.23
514020 0.12 -0.61 1.37 0.22
Measurements
HD NE-DA
WL [mMSL]

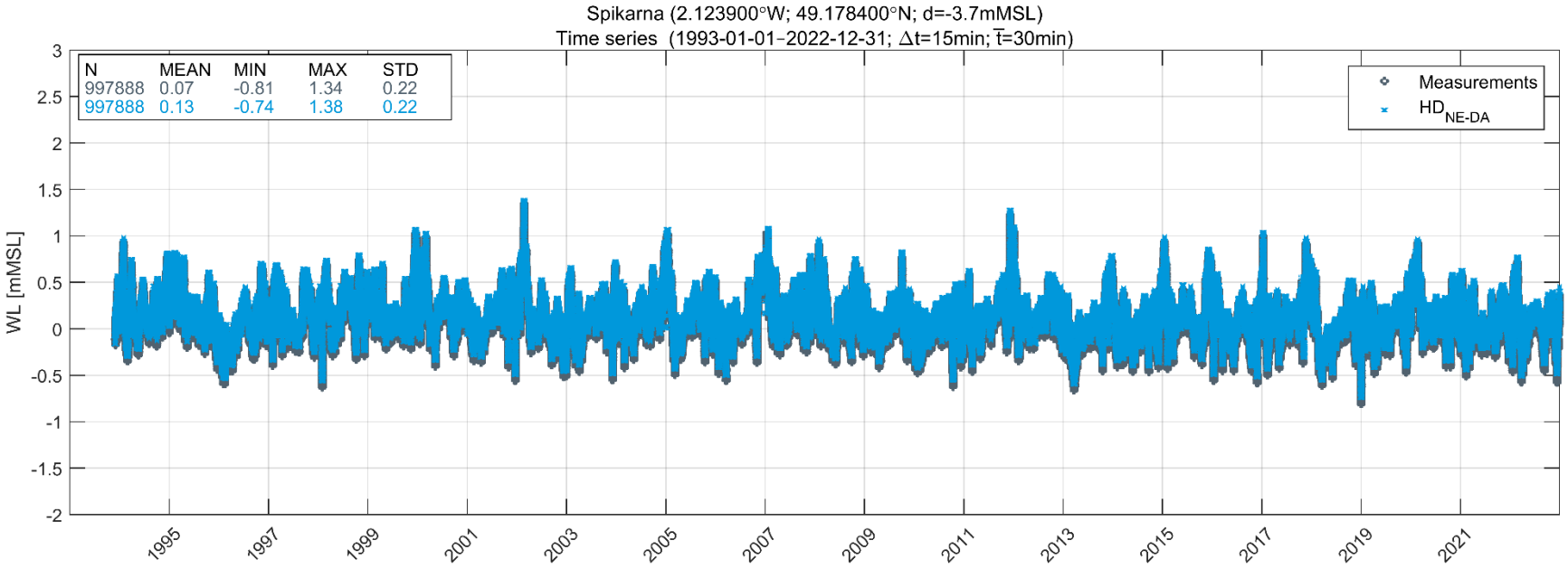
Spikarna (2.123900°W; 49.178400°N; d=-3.7mMSL)
Time series (1993-01-01–2022-12-31; Δt=15min; t̄=30min)
N MEAN MIN MAX STD
997888 0.07 -0.81 1.34 0.22
997888 0.13 -0.74 1.38 0.22
Measurements
HD NE-DA
WL [mMSL]

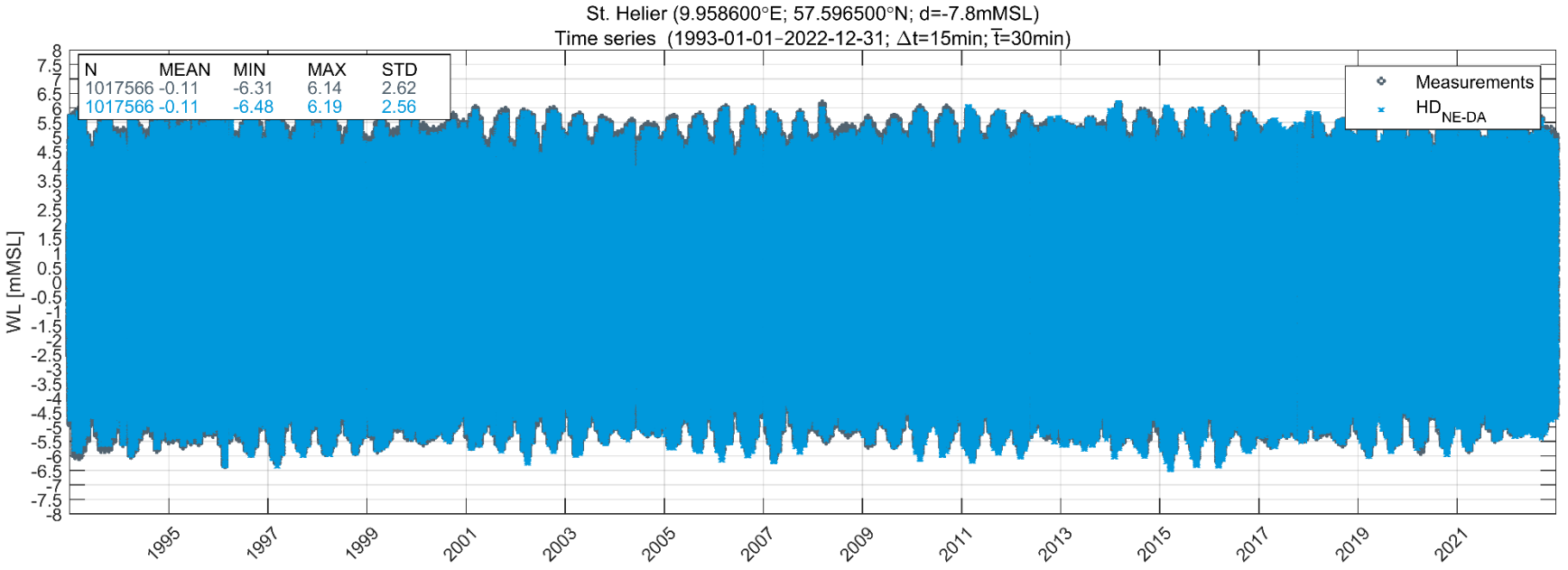
St. Helier (9.958600°E; 57.596500°N; d=-7.8mSL)
Time series (1993-01-01-2022-12-31; Δt=15min; t̄=30min)
N MEAN MIN MAX STD
1017566 -0.11 -6.31 6.14 2.62
1017566 -0.11 -6.48 6.19 2.56
Measurements
HD NE-DA
WL [mMSL]

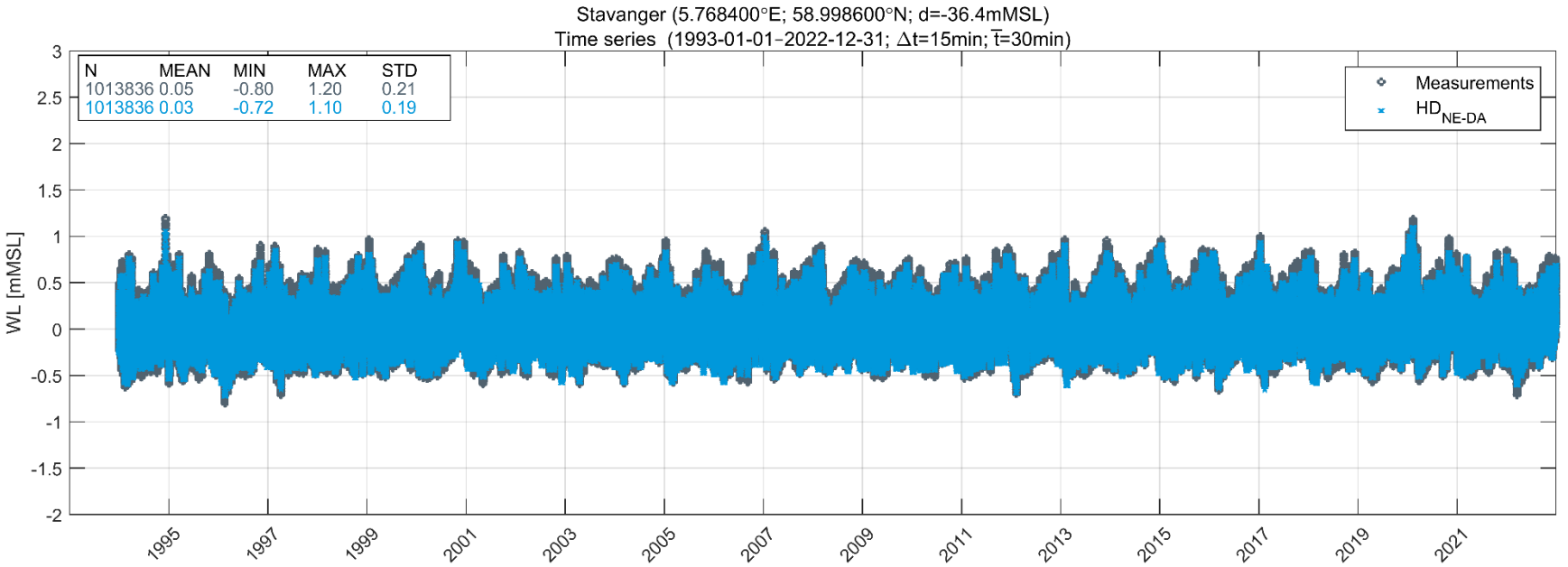
Stavanger (5.768400°E; 58.998600°N; d=-36.4mSL)
Time series (1993-01-01-2022-12-31; Δt=15min; t̄=30min)
N MEAN MIN MAX STD
1013836 0.05 -0.80 1.20 0.21
1013836 0.03 -0.72 1.10 0.19
Measurements
HD NE-DA
WL [mMSL]

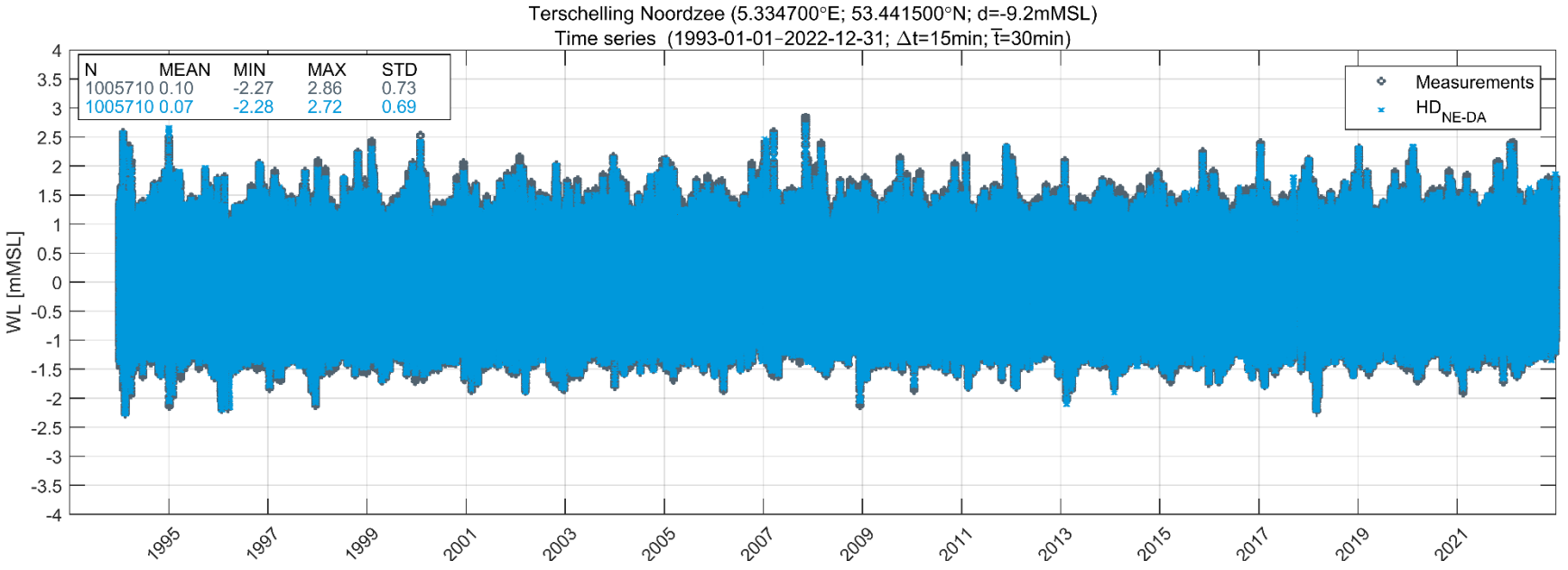
Terschelling Noordzee (5.334700°E; 53.441500°N; d=-9.2mMSL)
Time series (1993-01-01–2022-12-31; Δt=15min; t̄=30min)
N MEAN MIN MAX STD
1005710 0.10 -2.27 2.86 0.73
1005710 0.07 -2.28 2.72 0.69
Measurements
HD NE-DA
WL [mMSL]

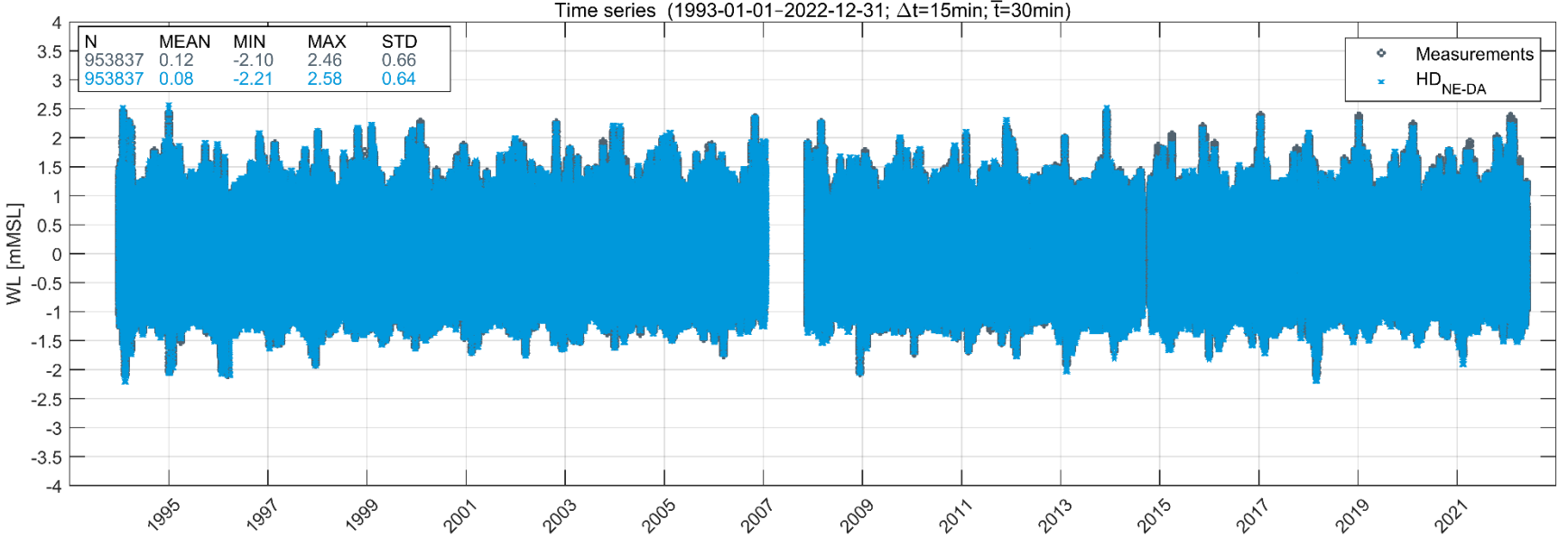
Texel Nordzee (4.736900°E; 53.124900°N; d=-9.3mMSL)
Time series (1993-01-01–2022-12-31; Δt=15min; t̄=30min)
N MEAN MIN MAX STD
953837 0.12 -2.10 2.46 0.66
953837 0.08 -2.21 2.58 0.64
Measurements
HD NE-DA
WL [mMSL]

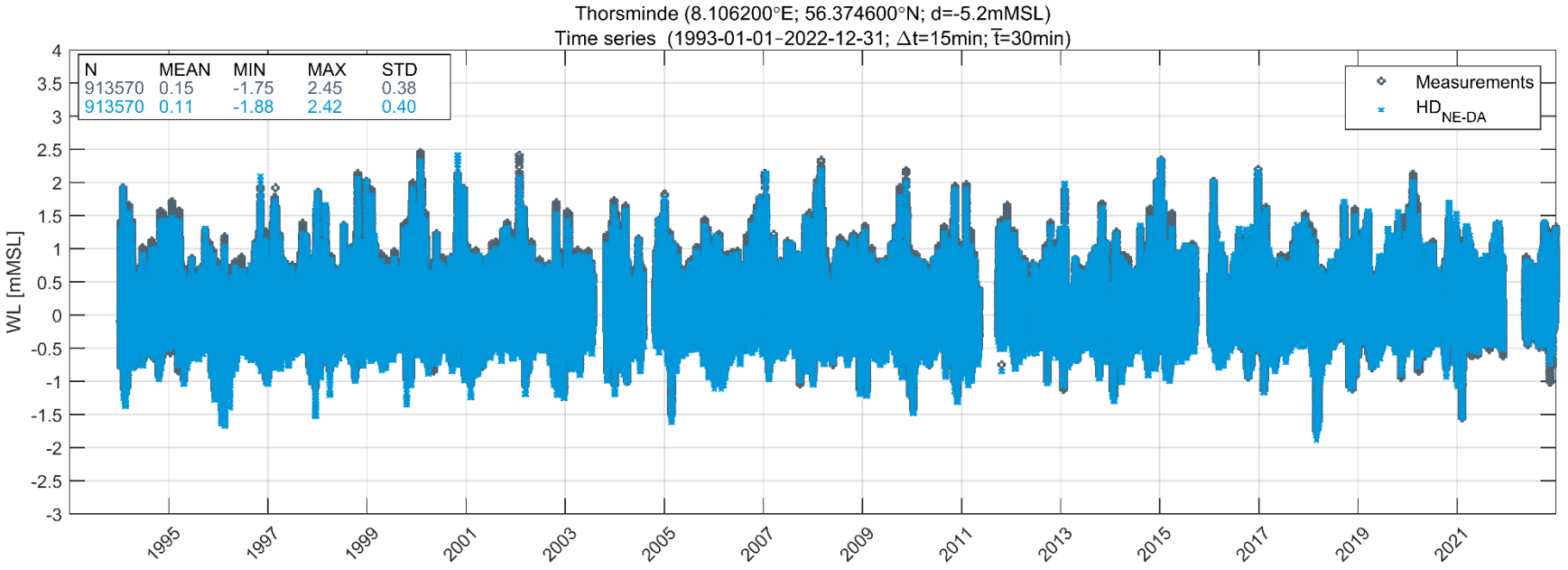
Thorsminde (8.106200°E; 56.374600°N; d=-5.2mMSL)
Time series (1993-01-01–2022-12-31; Δt=15min; t̄=30min)
N MEAN MIN MAX STD
913570 0.15 -1.75 2.45 0.38
913570 0.11 -1.88 2.42 0.40
Measurements
HD NE-DA
WL [mMSL]

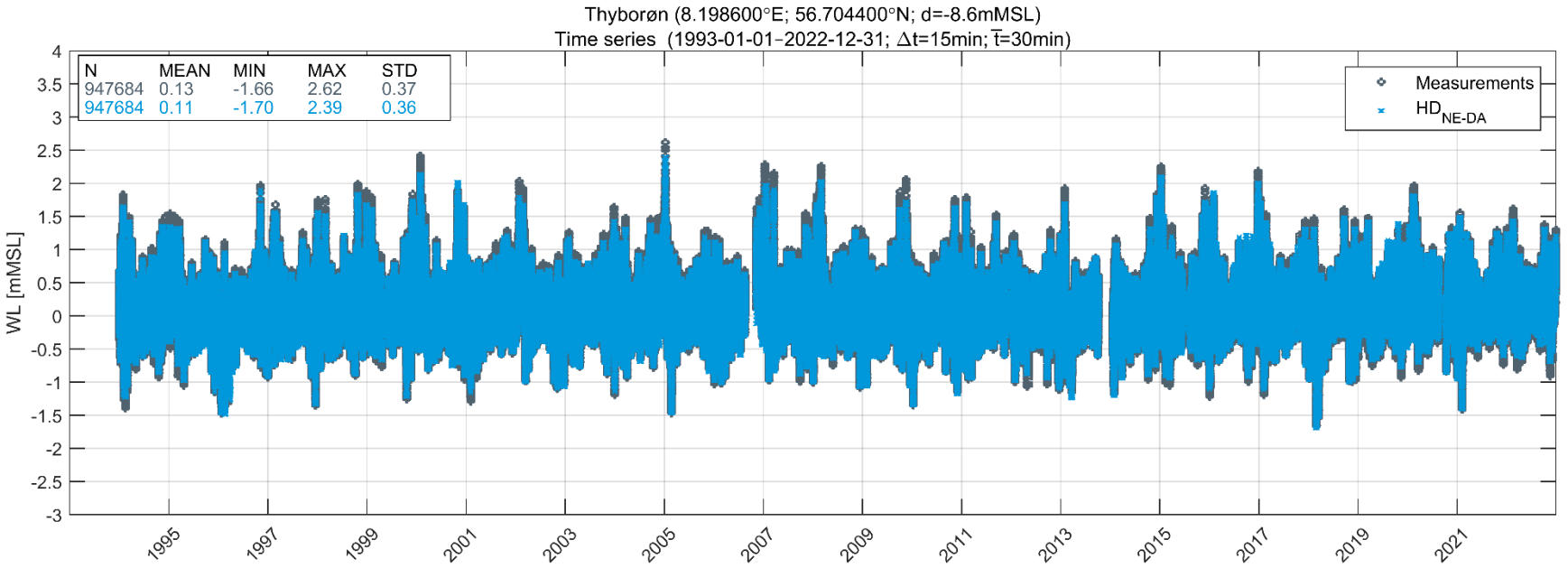
Thyborøn (8.198600°E; 56.704400°N; d=-8.6mMSL)
Time series (1993-01-01–2022-12-31; Δt=15min; t̄=30min)
N MEAN MIN MAX STD
947684 0.13 -1.66 2.62 0.37
947684 0.11 -1.70 2.39 0.36
Measurements
HD NE-DA
WL [mMSL]

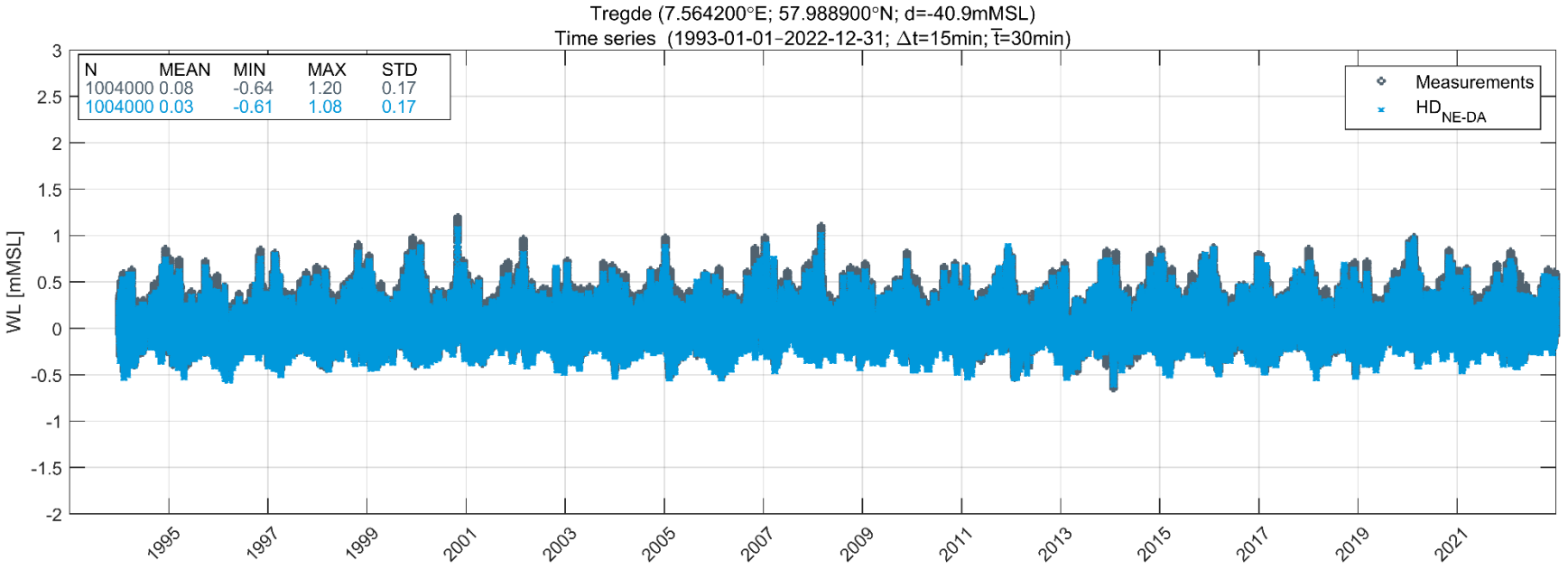
Tregde (7.564200°E; 57.988900°N; d=-40.9mMSL)
Time series (1993-01-01–2022-12-31; Δt=15min; t̄=30min)
N MEAN MIN MAX STD
1004000 0.08 -0.64 1.20 0.17
1004000 0.03 -0.61 1.08 0.17
Measurements
HD NE-DA
WL [mMSL]

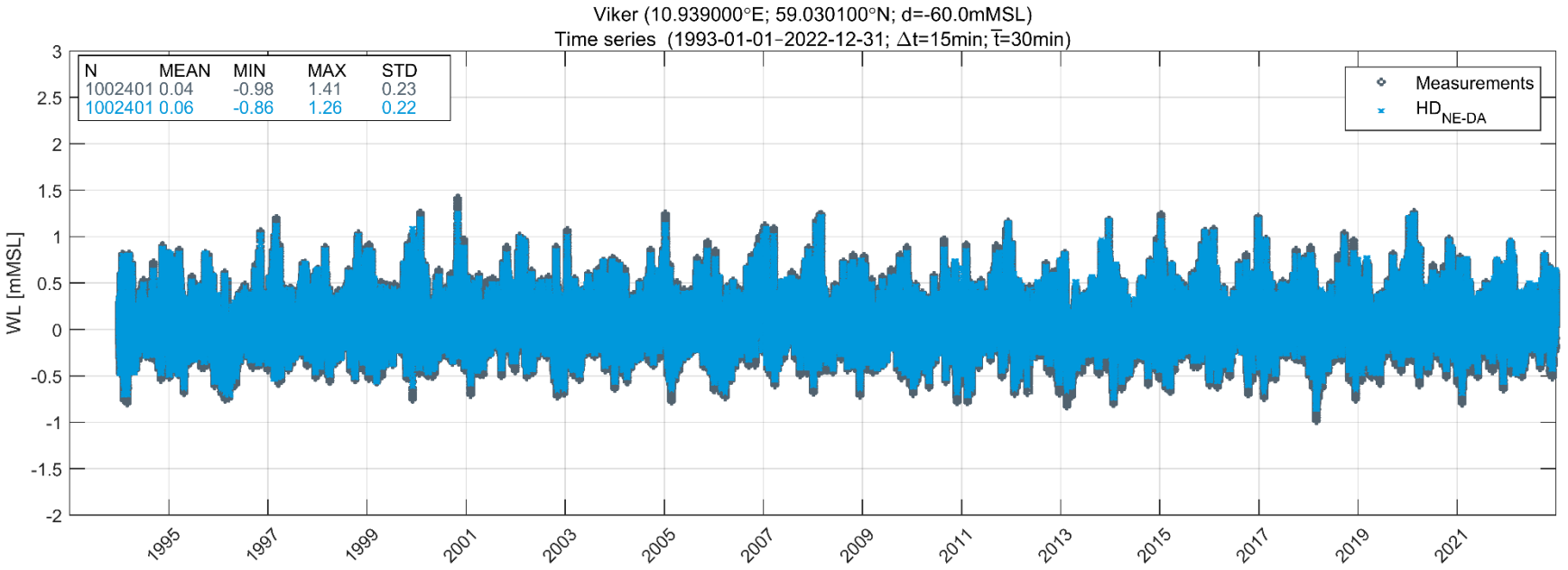
Viker (10.939000°E; 59.030100°N; d=-60.0mMSL)
Time series (1993-01-01–2022-12-31; Δt=15min; t̄=30min)
N MEAN MIN MAX STD
1002401 0.04 -0.98 1.41 0.23
1002401 0.06 -0.86 1.26 0.22
Measurements
HD NE-DA
WL [mMSL]

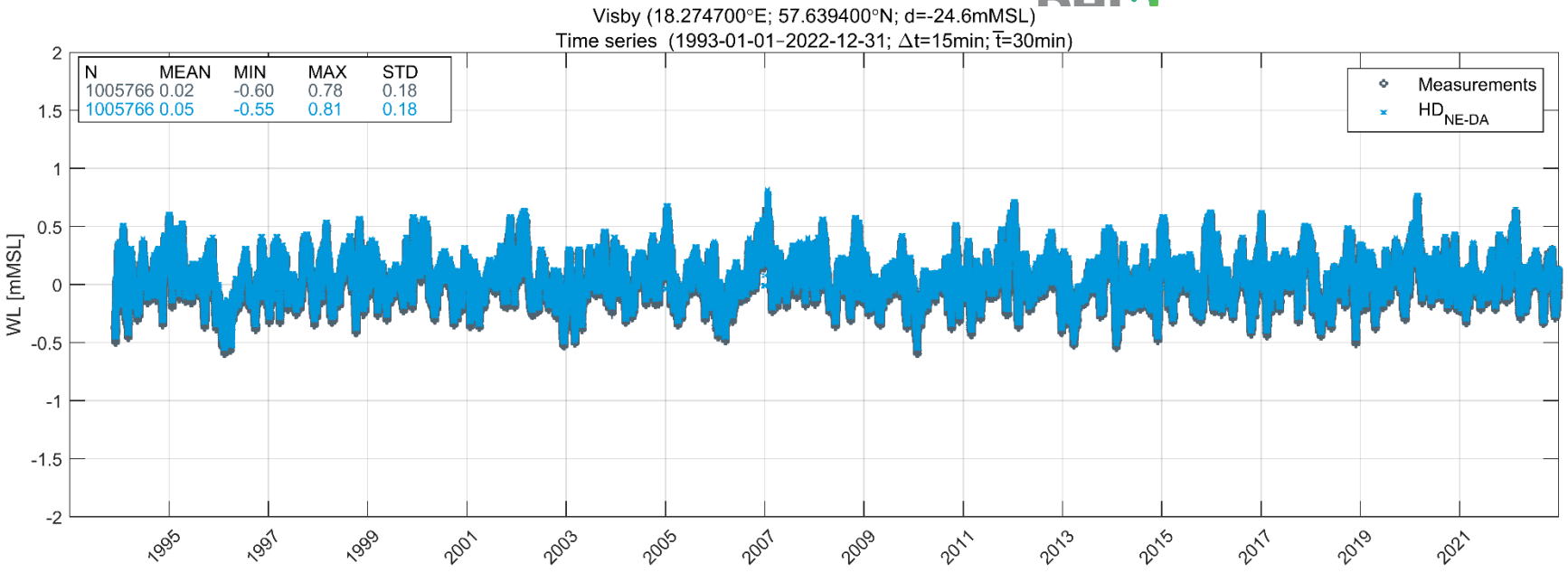
Visby (18.274700°E; 57.639400°N; d=-24.6mMSL)
Time series (1993-01-01-2022-12-31; Δt=15min; t̄=30min)
N MEAN MIN MAX STD
1005766 0.02 -0.60 0.78 0.18
1005766 0.05 -0.55 0.81 0.18
Measurements
HD NE-DA
WL [mMSL]

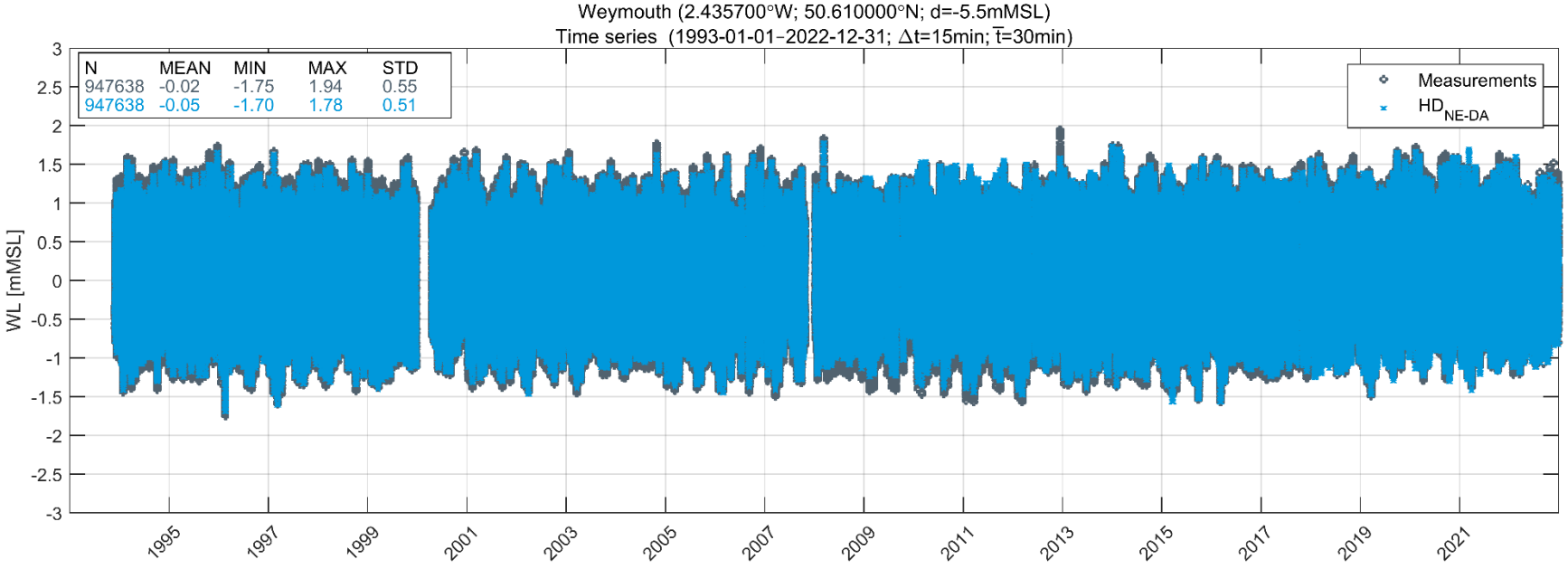
Weymouth (2.435700°W; 50.610000°N; d=-5.5mMSL)
Time series (1993-01-01-2022-12-31; Δt=15min; t̄=30min)
N MEAN MIN MAX STD
947638 -0.02 -1.75 1.94 0.55
947638 -0.05 -1.70 1.78 0.51
Measurements
HD NE-DA
WL [mMSL]

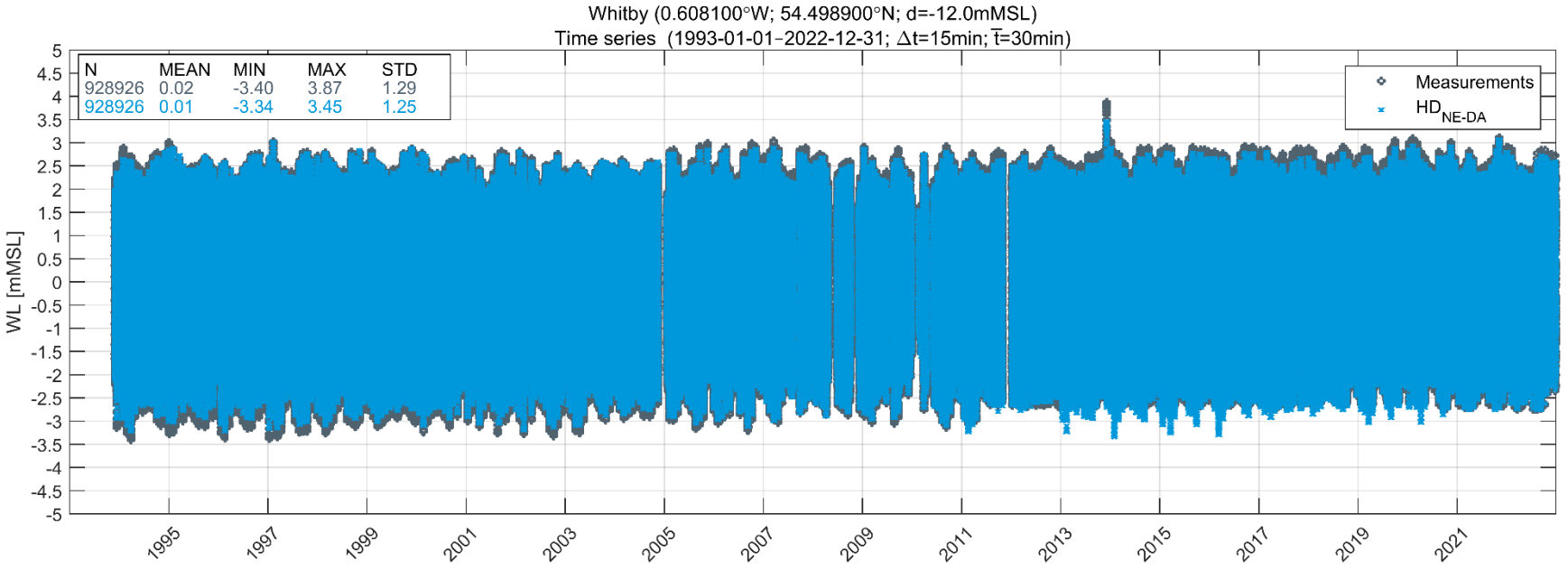
Whitby (0.608100°W; 54.498900°N; d=-12.0mMSL)
Time series (1993-01-01–2022-12-31; Δt=15min; t̄=30min)
N MEAN MIN MAX STD
928926 0.02 -3.40 3.87 1.29
928926 0.01 -3.34 3.45 1.25
Measurements
HD NE-DA
WL [mMSL]

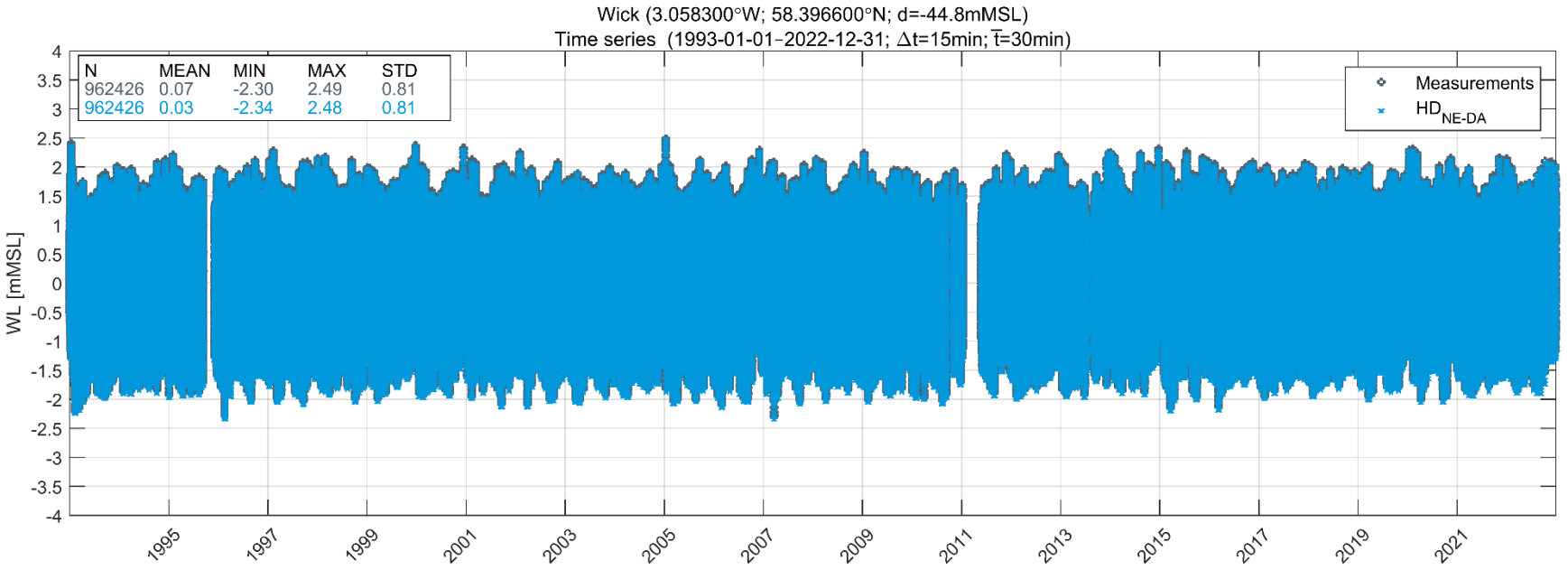
Wick (3.058300°W; 58.396600°N; d=-44.8mMSL)
Time series (1993-01-01–2022-12-31; Δt=15min; t̄=30min)
N MEAN MIN MAX STD
962426 0.07 -2.30 2.49 0.81
962426 0.03 -2.34 2.48 0.81
Measurements
HD NE-DA
WL [mMSL]

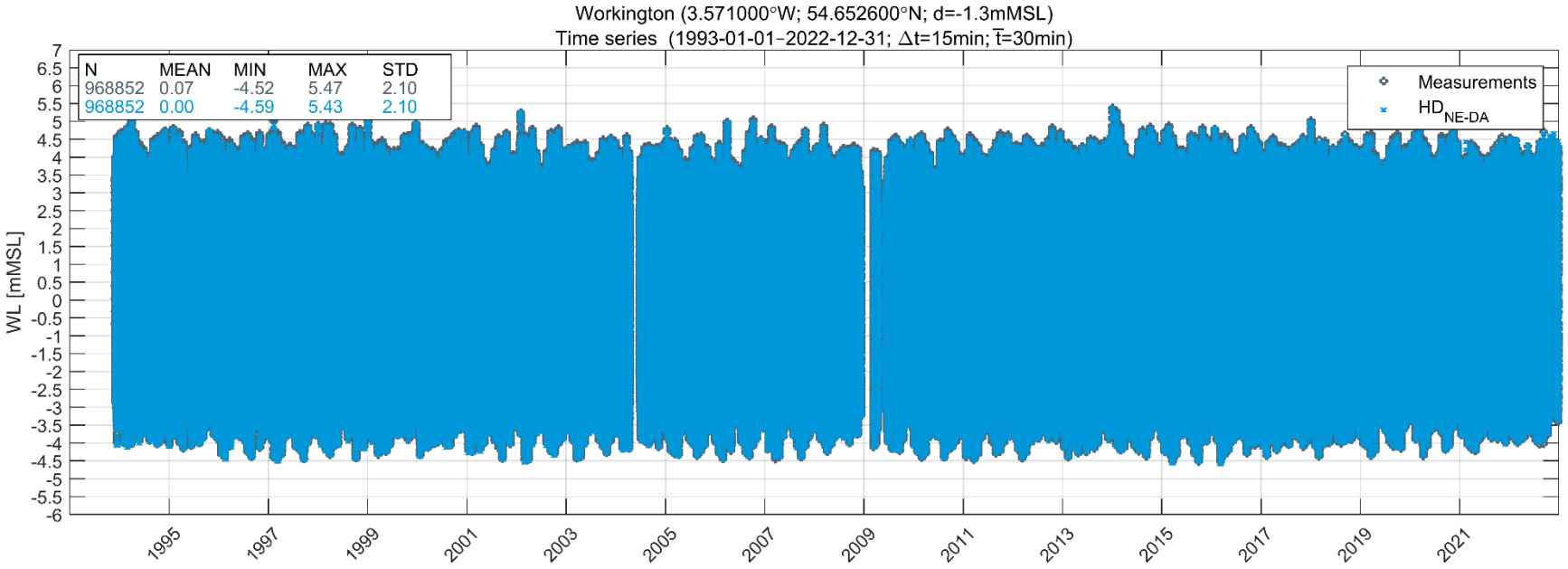
Workington (3.571000°W; 54.652600°N; d=-1.3mMSL)
Time series (1993-01-01–2022-12-31; Δt=15min; t̄=30min)
N MEAN MIN MAX STD
968852 0.07 -4.52 5.47 2.10
968852 0.00 -4.59 5.43 2.10
Measurements
HD NE-DA
WL [mMSL]
7
6.5
6
5.5
5
4.5
4
3.5
3
2.5
2
1.5
1
0.5
0
-0.5
-1
-1.5
-2
-2.5
-3
-3.5
-4
-4.5
-5
-5.5
-6
1995
1997
1999
2001
2003
2005
2007
2009
2011
2013
2015
2017
2019
2021

Appendix B.2 Scatter Plot WL - DHI Regional Hydrodynamic Model 2023

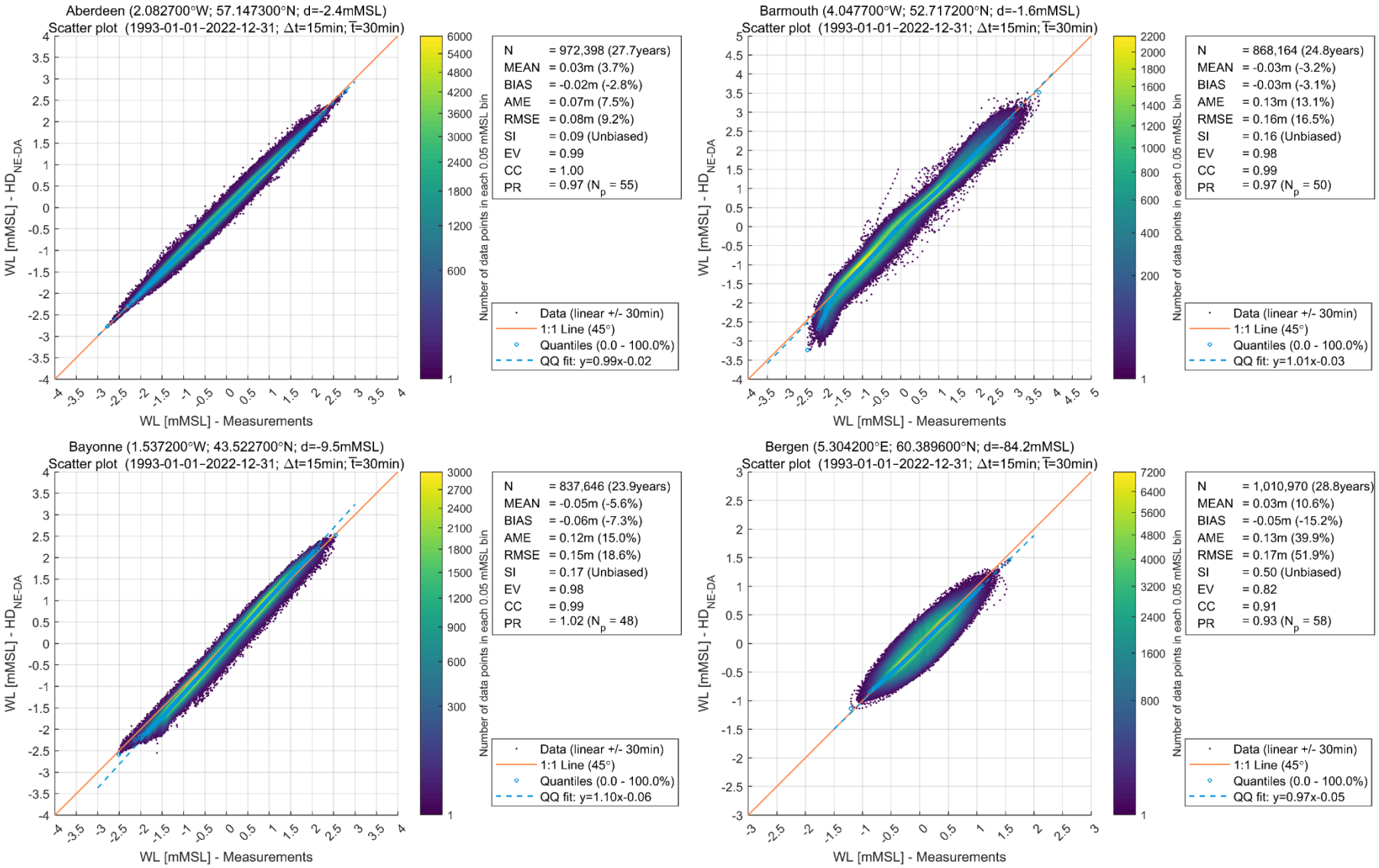

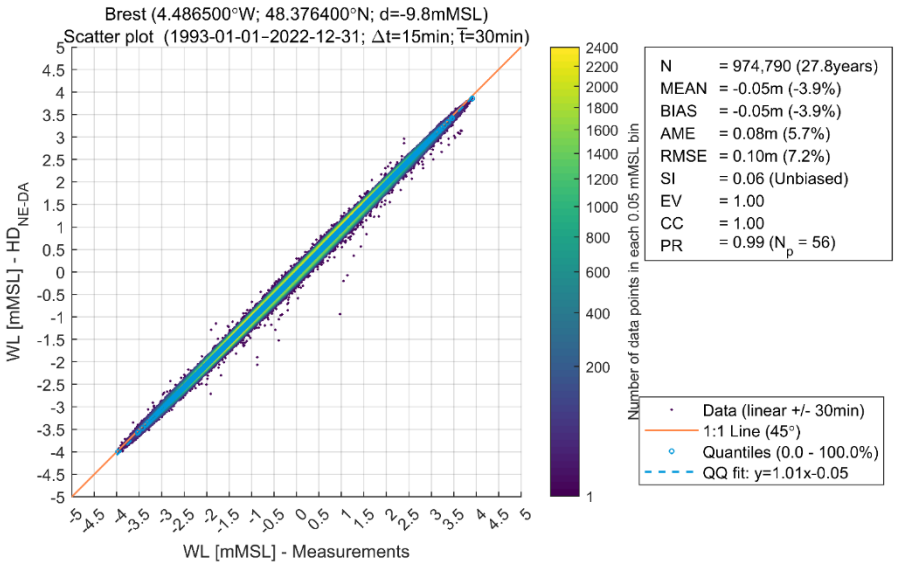
Brest (4.486500°W; 48.376400°N; d=-9.8mMSL)
Scatter plot (1993-01-01-2022-12-31; Δt=15min; t̄=30min)
WL [mMSL] - HD_NE-DA
WL [mMSL] - Measurements
Number of data points in each 0.05 mMSL bin
N = 974,790 (27.8years)
MEAN = -0.05m (-3.9%)
BIAS = -0.05m (-3.9%)
AME = 0.08m (5.7%)
RMSE = 0.10m (7.2%)
SI = 0.06 (Unbiased)
EV = 1.00
CC = 1.00
PR = 0.99 (N_p = 56)
Data (linear +/- 30min)
1:1 Line (45°)
Quantiles (0.0 - 100.0%)
QQ fit: y=1.01x-0.05

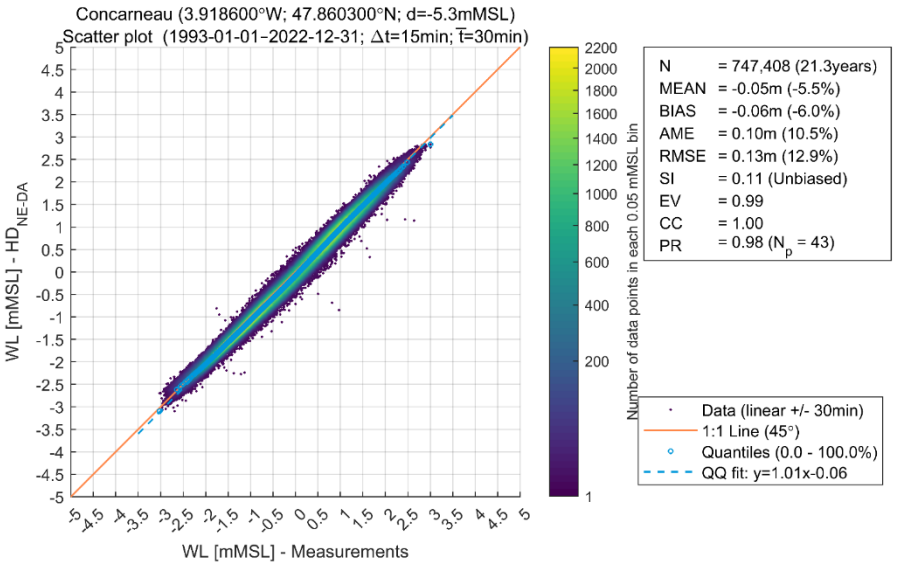
Concarneau (3.918600°W; 47.860300°N; d=-5.3mMSL)
Scatter plot (1993-01-01-2022-12-31; Δt=15min; t̄=30min)
WL [mMSL] - HD_NE-DA
WL [mMSL] - Measurements
Number of data points in each 0.05 mMSL bin
N = 747,408 (21.3years)
MEAN = -0.05m (-5.5%)
BIAS = -0.06m (-6.0%)
AME = 0.10m (10.5%)
RMSE = 0.13m (12.9%)
SI = 0.11 (Unbiased)
EV = 0.99
CC = 1.00
PR = 0.98 (N_p = 43)
Data (linear +/- 30min)
1:1 Line (45°)
Quantiles (0.0 - 100.0%)
QQ fit: y=1.01x-0.06

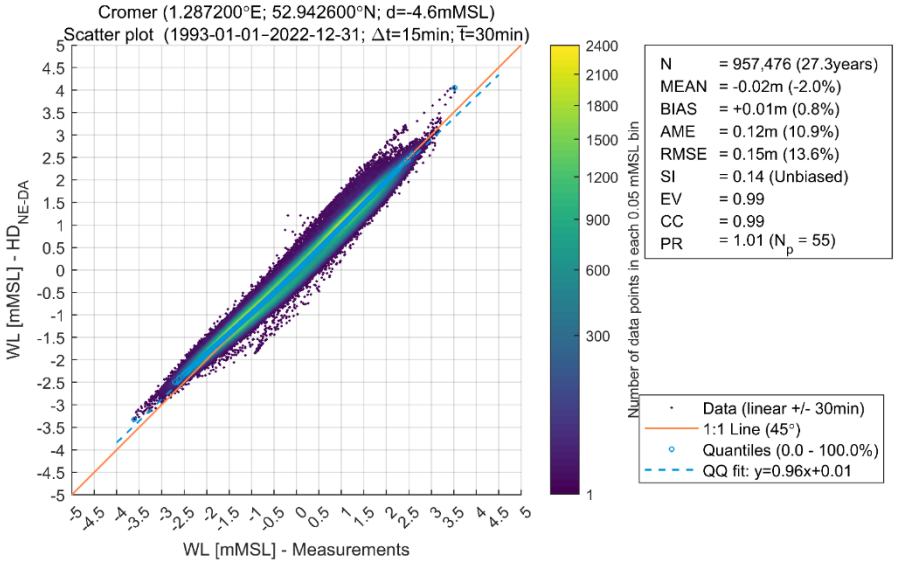
Cromer (1.287200°E; 52.942600°N; d=-4.6mMSL)
Scatter plot (1993-01-01-2022-12-31; Δt=15min; t̄=30min)
WL [mMSL] - HD_NE-DA
WL [mMSL] - Measurements
Number of data points in each 0.05 mMSL bin
N = 957,476 (27.3years)
MEAN = -0.02m (-2.0%)
BIAS = +0.01m (0.8%)
AME = 0.12m (10.9%)
RMSE = 0.15m (13.6%)
SI = 0.14 (Unbiased)
EV = 0.99
CC = 0.99
PR = 1.01 (N_p = 55)
Data (linear +/- 30min)
1:1 Line (45°)
Quantiles (0.0 - 100.0%)
QQ fit: y=0.96x+0.01

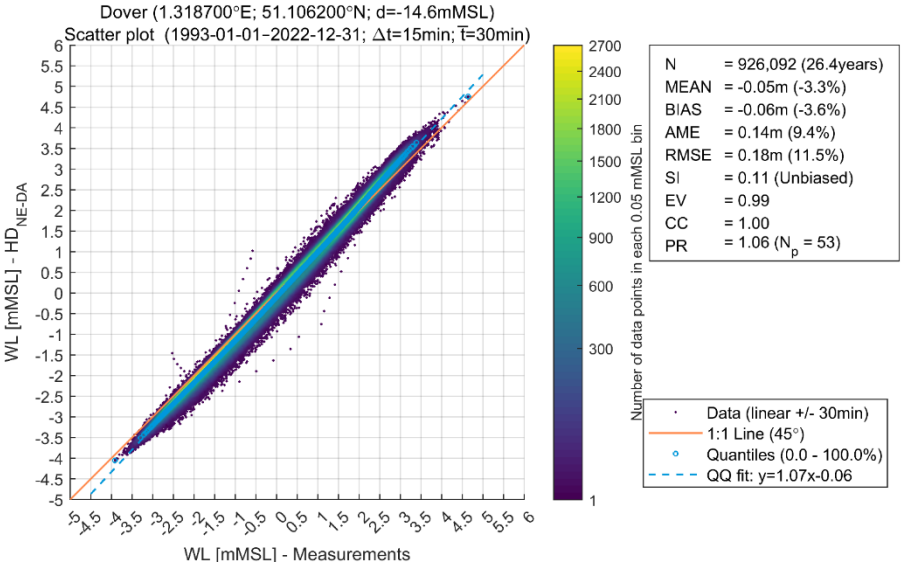
Dover (1.318700°E; 51.106200°N; d=-14.6mMSL)
Scatter plot (1993-01-01-2022-12-31; Δt=15min; t̄=30min)
WL [mMSL] - HD_NE-DA
WL [mMSL] - Measurements
Number of data points in each 0.05 mMSL bin
N = 926,092 (26.4years)
MEAN = -0.05m (-3.3%)
BIAS = -0.06m (-3.6%)
AME = 0.14m (9.4%)
RMSE = 0.18m (11.5%)
SI = 0.11 (Unbiased)
EV = 0.99
CC = 1.00
PR = 1.06 (N_p = 53)
Data (linear +/- 30min)
1:1 Line (45°)
Quantiles (0.0 - 100.0%)
QQ fit: y=1.07x-0.06

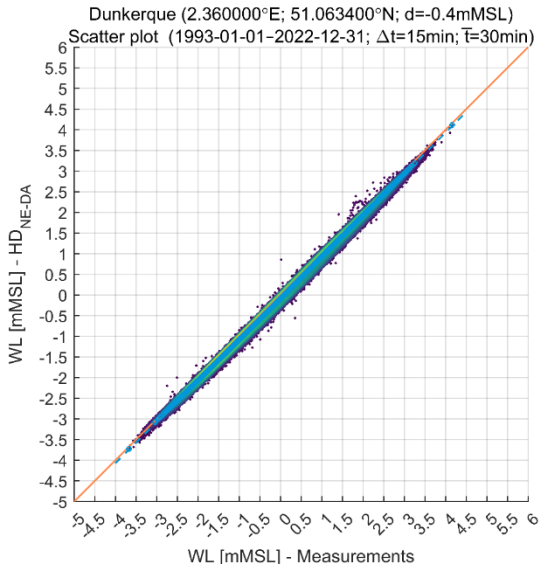
Dunkerque (2.360000°E; 51.063400°N; d=-0.4mMSL)
Scatter plot (1993-01-01-2022-12-31; Δt=15min; t̄=30min)
WL [mMSL] - HD_NE-DA
WL [mMSL] - Measurements
Number of data points in each 0.05 mMSL bin
N = 831,515 (23.7years)
MEAN = -0.02m (-1.1%)
BIAS = -0.07m (-5.0%)
AME = 0.09m (5.9%)
RMSE = 0.12m (8.0%)
SI = 0.06 (Unbiased)
EV = 1.00
CC = 1.00
PR = 0.98 (N_p = 47)
Data (linear +/- 30min)
1:1 Line (45°)
Quantiles (0.0 - 100.0%)
QQ fit: y=1.00x-0.07

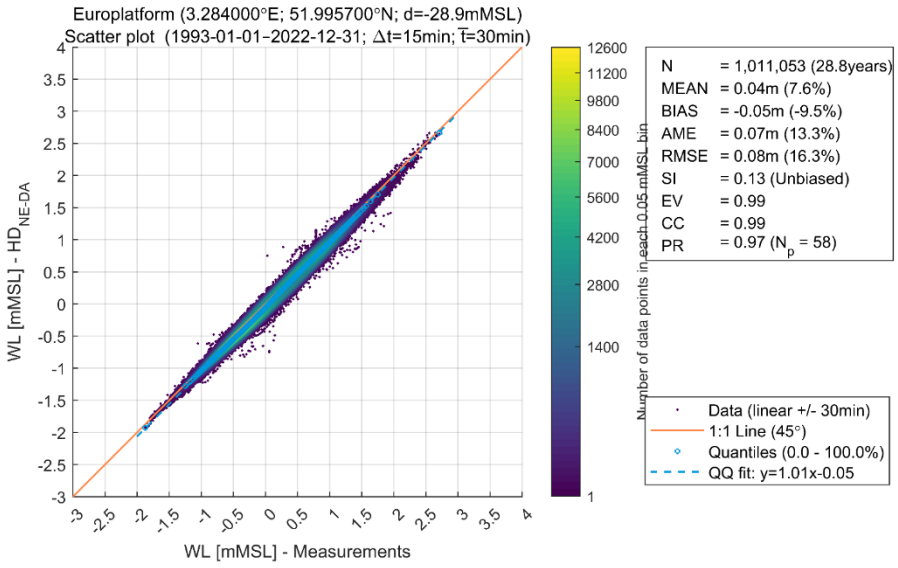
Europlatform (3.284000°E; 51.995700°N; d=-28.9mMSL)
Scatter plot (1993-01-01-2022-12-31; Δt=15min; t̄=30min)
WL [mMSL] - HD_NE-DA
WL [mMSL] - Measurements
Number of data points in each 0.05 mMSL bin
N = 1,011,053 (28.8years)
MEAN = 0.04m (7.6%)
BIAS = -0.05m (-9.5%)
AME = 0.07m (13.3%)
RMSE = 0.08m (16.3%)
SI = 0.13 (Unbiased)
EV = 0.99
CC = 0.99
PR = 0.97 (N_p = 58)
Data (linear +/- 30min)
1:1 Line (45°)
Quantiles (0.0 - 100.0%)
QQ fit: y=1.01x-0.05

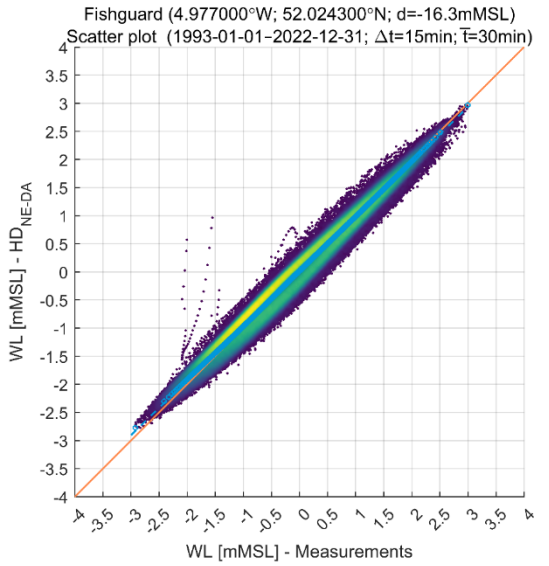
Fishguard (4.977000°W; 52.024300°N; d=-16.3mMSL)
Scatter plot (1993-01-01-2022-12-31; Δt=15min; t̄=30min)
WL [mMSL] - HD_NE-DA
WL [mMSL] - Measurements
Number of data points in each 0.05 mMSL bin
N = 1,011,010 (28.8years)
MEAN = -0.05m (-5.1%)
BIAS = +0.02m (1.8%)
AME = 0.13m (14.6%)
RMSE = 0.15m (16.8%)
SI = 0.17 (Unbiased)
EV = 0.98
CC = 0.99
PR = 0.98 (N_p = 58)
Data (linear +/- 30min)
1:1 Line (45°)
Quantiles (0.0 - 100.0%)
QQ fit: y=0.97x+0.01

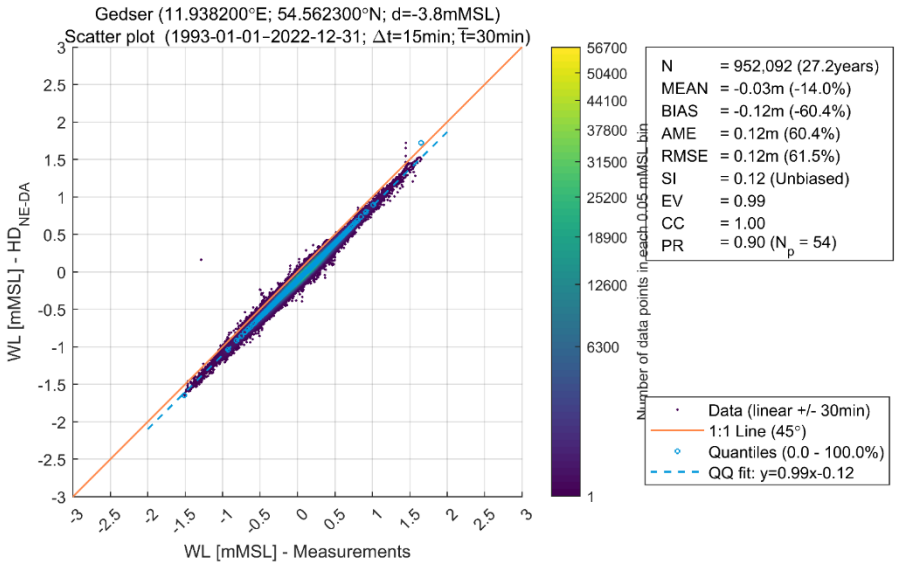
Gedser (11.938200°E; 54.562300°N; d=-3.8mMSL)
Scatter plot (1993-01-01-2022-12-31; Δt=15min; t̄=30min)
WL [mMSL] - HD_NE-DA
WL [mMSL] - Measurements
Number of data points in each 0.05 mMSL bin
N = 952,092 (27.2years)
MEAN = -0.03m (-14.0%)
BIAS = -0.12m (-60.4%)
AME = 0.12m (60.4%)
RMSE = 0.12m (61.5%)
SI = 0.12 (Unbiased)
EV = 0.99
CC = 1.00
PR = 0.90 (N_p = 54)
Data (linear +/- 30min)
1:1 Line (45°)
Quantiles (0.0 - 100.0%)
QQ fit: y=0.99x-0.12

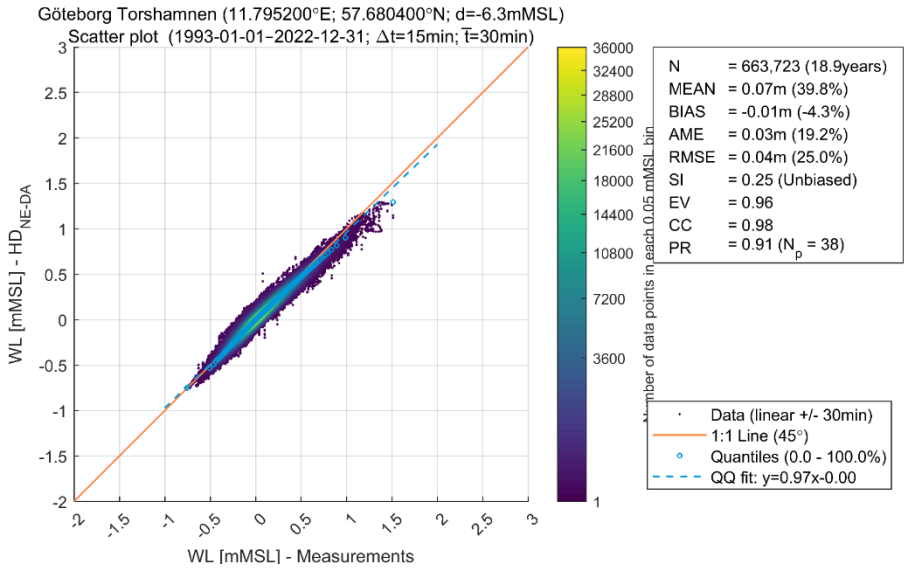
Göteborg Torshamnen (11.795200°E; 57.680400°N; d=-6.3mMSL)
Scatter plot (1993-01-01-2022-12-31; Δt=15min; t̄=30min)
WL [mMSL] - HD_NE-DA
WL [mMSL] - Measurements
Number of data points in each 0.05 mMSL bin
N = 663,723 (18.9years)
MEAN = 0.07m (39.8%)
BIAS = -0.01m (-4.3%)
AME = 0.03m (19.2%)
RMSE = 0.04m (25.0%)
SI = 0.25 (Unbiased)
EV = 0.96
CC = 0.98
PR = 0.91 (N_p = 38)
Data (linear +/- 30min)
1:1 Line (45°)
Quantiles (0.0 - 100.0%)
QQ fit: y=0.97x-0.00

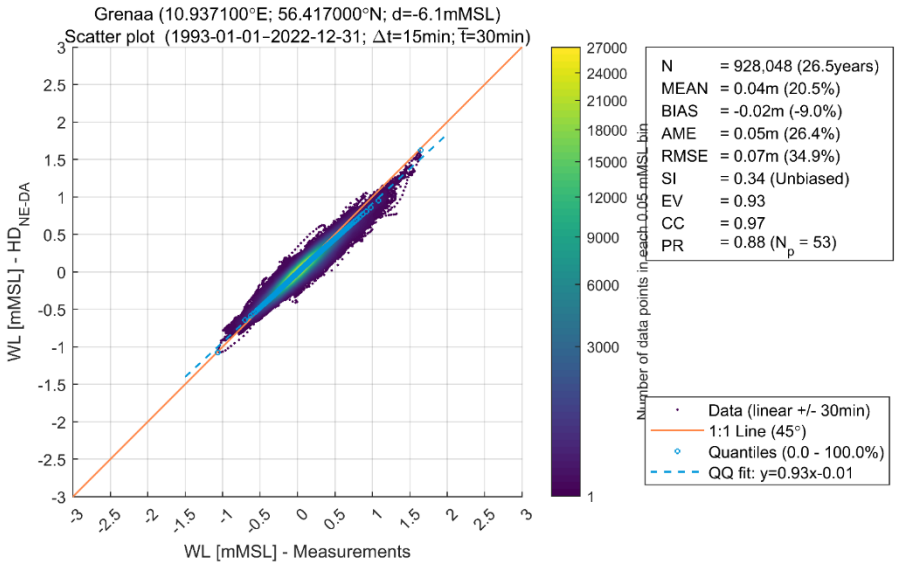
Grenaa (10.937100°E; 56.417000°N; d=-6.1mMSL)
Scatter plot (1993-01-01-2022-12-31; Δt=15min; t̄=30min)
WL [mMSL] - HD_NE-DA
WL [mMSL] - Measurements
Number of data points in each 0.05 mMSL bin
N = 928,048 (26.5years)
MEAN = 0.04m (20.5%)
BIAS = -0.02m (-9.0%)
AME = 0.05m (26.4%)
RMSE = 0.07m (34.9%)
SI = 0.34 (Unbiased)
EV = 0.93
CC = 0.97
PR = 0.88 (N_p = 53)
Data (linear +/- 30min)
1:1 Line (45°)
Quantiles (0.0 - 100.0%)
QQ fit: y=0.93x-0.01

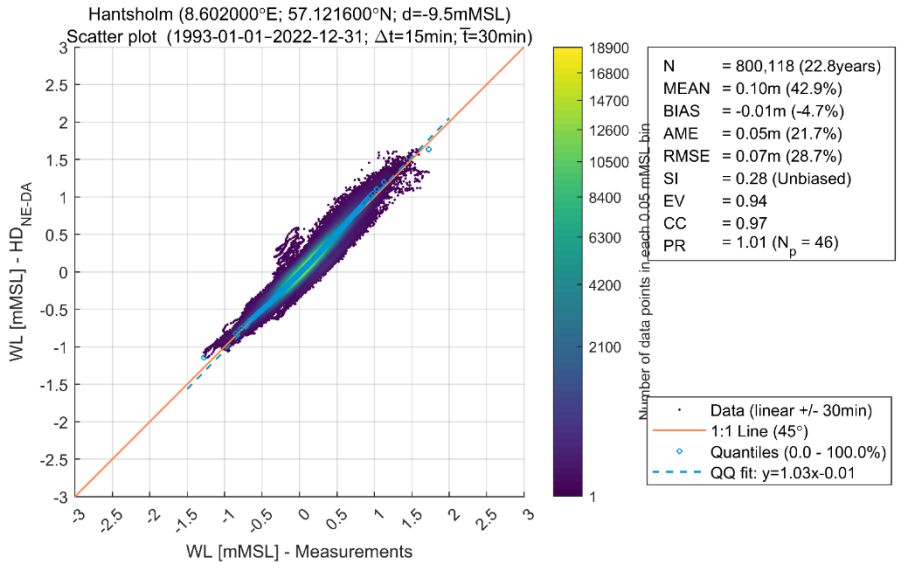
Hantsholm (8.602000°E; 57.121600°N; d=-9.5mMSL)
Scatter plot (1993-01-01-2022-12-31; Δt=15min; t̄=30min)
WL [mMSL] - HD_NE-DA
WL [mMSL] - Measurements
Number of data points in each 0.05 mMSL bin
N = 800,118 (22.8years)
MEAN = 0.10m (42.9%)
BIAS = -0.01m (-4.7%)
AME = 0.05m (21.7%)
RMSE = 0.07m (28.7%)
SI = 0.28 (Unbiased)
EV = 0.94
CC = 0.97
PR = 1.01 (N_p = 46)
Data (linear +/- 30min)
1:1 Line (45°)
Quantiles (0.0 - 100.0%)
QQ fit: y=1.03x-0.01

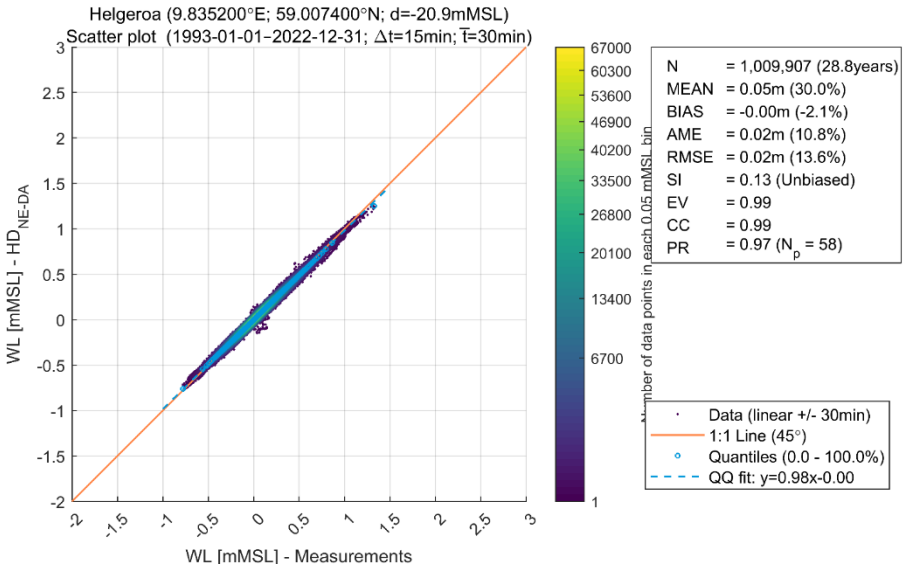
Helgeroa (9.835200°E; 59.007400°N; d=-20.9mMSL)
Scatter plot (1993-01-01-2022-12-31; Δt=15min; t̄=30min)
WL [mMSL] - HD_NE-DA
WL [mMSL] - Measurements
Number of data points in each 0.05 mMSL bin
N = 1,009,907 (28.8years)
MEAN = 0.05m (30.0%)
BIAS = -0.00m (-2.1%)
AME = 0.02m (10.8%)
RMSE = 0.02m (13.6%)
SI = 0.13 (Unbiased)
EV = 0.99
CC = 0.99
PR = 0.97 (N_p = 58)
Data (linear +/- 30min)
1:1 Line (45°)
Quantiles (0.0 - 100.0%)
QQ fit: y=0.98x-0.00

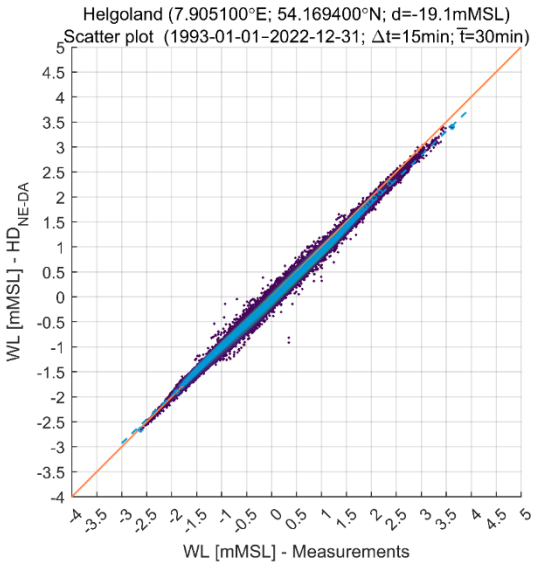
Helgoland (7.905100°E; 54.169400°N; d=-19.1mMSL)
Scatter plot (1993-01-01-2022-12-31; Δt=15min; t̄=30min)
WL [mMSL] - HD_NE-DA
WL [mMSL] - Measurements

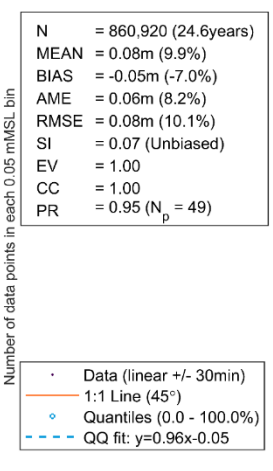
N = 860,920 (24.6years)
MEAN = 0.08m (9.9%)
BIAS = -0.05m (-7.0%)
AME = 0.06m (8.2%)
RMSE = 0.08m (10.1%)
SI = 0.07 (Unbiased)
EV = 1.00
CC = 1.00
PR = 0.95 (N_p = 49)
Number of data points in each 0.05 mMSL bin
Data (linear +/- 30min)
1:1 Line (45°)
Quantiles (0.0 - 100.0%)
QQ fit: y=0.96x-0.05

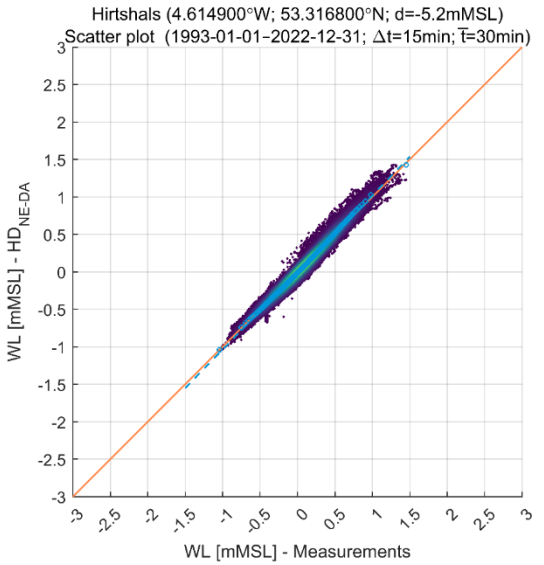
Hirtshals (4.614900°W; 53.316800°N; d=-5.2mMSL)
Scatter plot (1993-01-01-2022-12-31; Δt=15min; t̄=30min)
WL [mMSL] - HD_NE-DA
WL [mMSL] - Measurements

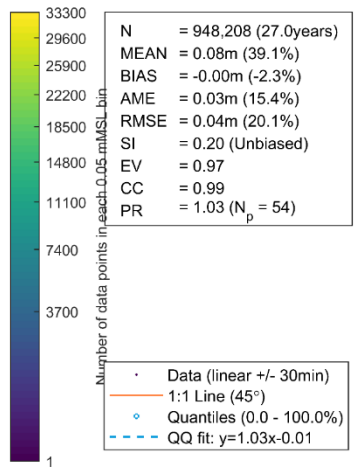
N = 948,208 (27.0years)
MEAN = 0.08m (39.1%)
BIAS = -0.00m (-2.3%)
AME = 0.03m (15.4%)
RMSE = 0.04m (20.1%)
SI = 0.20 (Unbiased)
EV = 0.97
CC = 0.99
PR = 1.03 (N_p = 54)
Number of data points in each 0.05 mMSL bin
Data (linear +/- 30min)
1:1 Line (45°)
Quantiles (0.0 - 100.0%)
QQ fit: y=1.03x-0.01

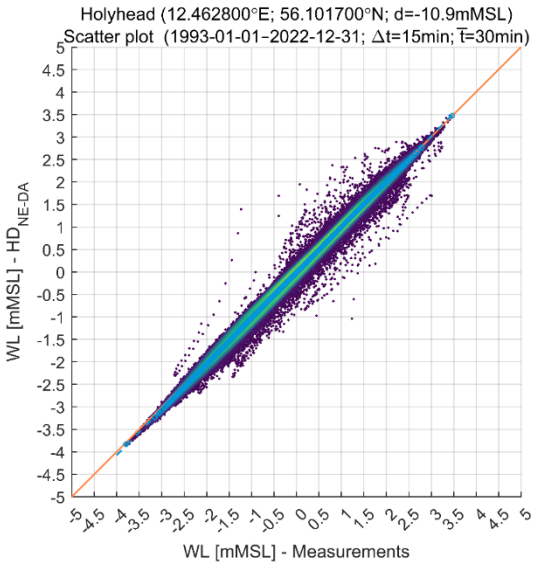
Holyhead (12.462800°E; 56.101700°N; d=-10.9mMSL)
Scatter plot (1993-01-01-2022-12-31; Δt=15min; t̄=30min)
WL [mMSL] - HD_NE-DA
WL [mMSL] - Measurements

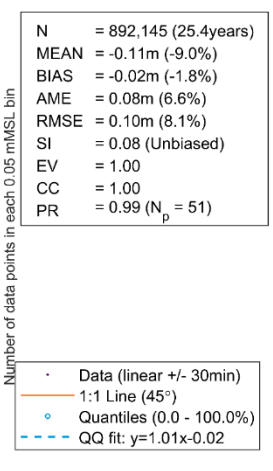
N = 892,145 (25.4years)
MEAN = -0.11m (-9.0%)
BIAS = -0.02m (-1.8%)
AME = 0.08m (6.6%)
RMSE = 0.10m (8.1%)
SI = 0.08 (Unbiased)
EV = 1.00
CC = 1.00
PR = 0.99 (N_p = 51)
Number of data points in each 0.05 mMSL bin
Data (linear +/- 30min)
1:1 Line (45°)
Quantiles (0.0 - 100.0%)
QQ fit: y=1.01x-0.02

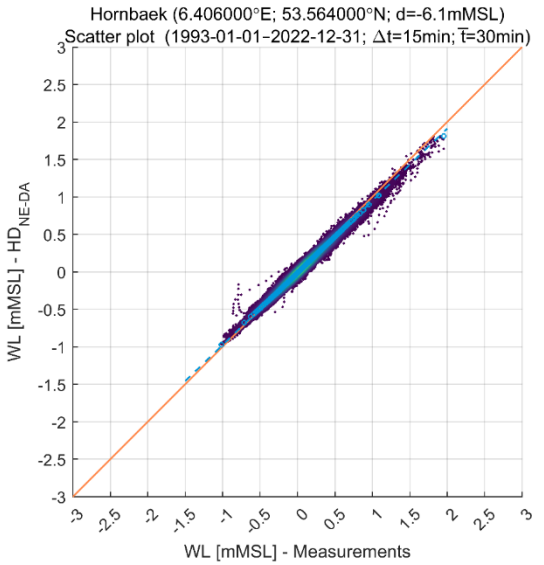
Hornbaek (6.406000°E; 53.564000°N; d=-6.1mMSL)
Scatter plot (1993-01-01-2022-12-31; Δt=15min; t̄=30min)
WL [mMSL] - HD_NE-DA
WL [mMSL] - Measurements

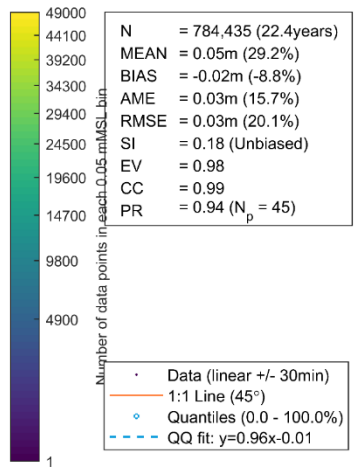
N = 784,435 (22.4years)
MEAN = 0.05m (29.2%)
BIAS = -0.02m (-8.8%)
AME = 0.03m (15.7%)
RMSE = 0.03m (20.1%)
SI = 0.18 (Unbiased)
EV = 0.98
CC = 0.99
PR = 0.94 (N_p = 45)
Number of data points in each 0.05 mMSL bin
Data (linear +/- 30min)
1:1 Line (45°)
Quantiles (0.0 - 100.0%)
QQ fit: y=0.96x-0.01

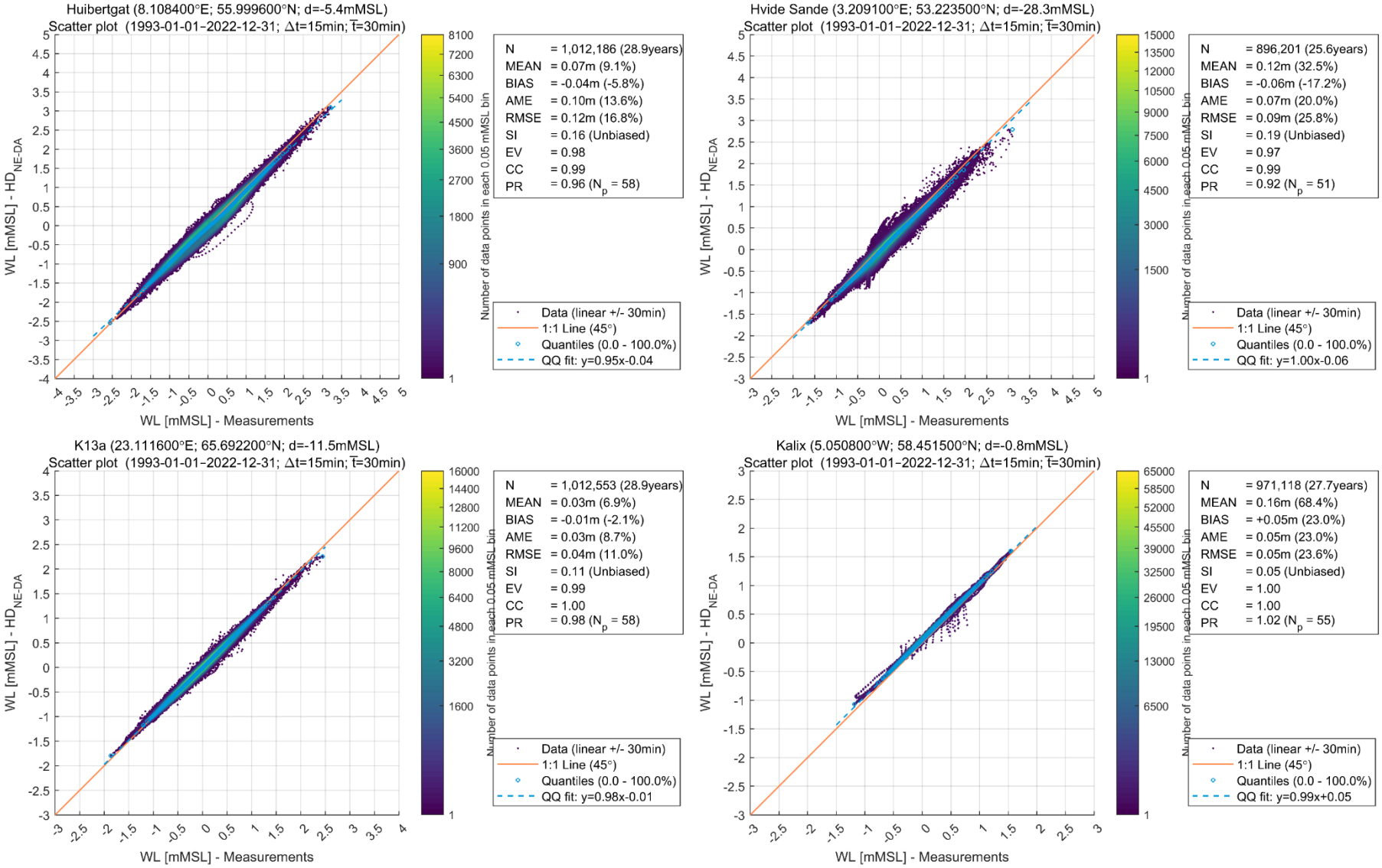
Huibertgat (8.108400°E; 55.999600°N; d=-5.4mMSL)
Scatter plot (1993-01-01-2022-12-31; Δt=15min; t̄=30min)
WL [mMSL] - HD_NE-DA
WL [mMSL] - Measurements
Number of data points in each 0.05 mMSL bin
N = 1,012,186 (28.9years)
MEAN = 0.07m (9.1%)
BIAS = -0.04m (-5.8%)
AME = 0.10m (13.6%)
RMSE = 0.12m (16.8%)
SI = 0.16 (Unbiased)
EV = 0.98
CC = 0.99
PR = 0.96 (N_p = 58)
Data (linear +/- 30min)
1:1 Line (45°)
Quantiles (0.0 - 100.0%)
QQ fit: y=0.95x-0.04
Hvide Sande (3.209100°E; 53.223500°N; d=-28.3mMSL)
Scatter plot (1993-01-01-2022-12-31; Δt=15min; t̄=30min)
WL [mMSL] - HD_NE-DA
WL [mMSL] - Measurements
Number of data points in each 0.05 mMSL bin
N = 896,201 (25.6years)
MEAN = 0.12m (32.5%)
BIAS = -0.06m (-17.2%)
AME = 0.07m (20.0%)
RMSE = 0.09m (25.8%)
SI = 0.19 (Unbiased)
EV = 0.97
CC = 0.99
PR = 0.92 (N_p = 51)
Data (linear +/- 30min)
1:1 Line (45°)
Quantiles (0.0 - 100.0%)
QQ fit: y=1.00x-0.06
K13a (23.111600°E; 65.692200°N; d=-11.5mMSL)
Scatter plot (1993-01-01-2022-12-31; Δt=15min; t̄=30min)
WL [mMSL] - HD_NE-DA
WL [mMSL] - Measurements
Number of data points in each 0.05 mMSL bin
N = 1,012,553 (28.9years)
MEAN = 0.03m (6.9%)
BIAS = -0.01m (-2.1%)
AME = 0.03m (8.7%)
RMSE = 0.04m (11.0%)
SI = 0.11 (Unbiased)
EV = 0.99
CC = 1.00
PR = 0.98 (N_p = 58)
Data (linear +/- 30min)
1:1 Line (45°)
Quantiles (0.0 - 100.0%)
QQ fit: y=0.98x-0.01
Kalix (5.050800°W; 58.451500°N; d=-0.8mMSL)
Scatter plot (1993-01-01-2022-12-31; Δt=15min; t̄=30min)
WL [mMSL] - HD_NE-DA
WL [mMSL] - Measurements
Number of data points in each 0.05 mMSL bin
N = 971,118 (27.7years)
MEAN = 0.16m (68.4%)
BIAS = +0.05m (23.0%)
AME = 0.05m (23.0%)
RMSE = 0.05m (23.6%)
SI = 0.05 (Unbiased)
EV = 1.00
CC = 1.00
PR = 1.02 (N_p = 55)
Data (linear +/- 30min)
1:1 Line (45°)
Quantiles (0.0 - 100.0%)
QQ fit: y=0.99x+0.05

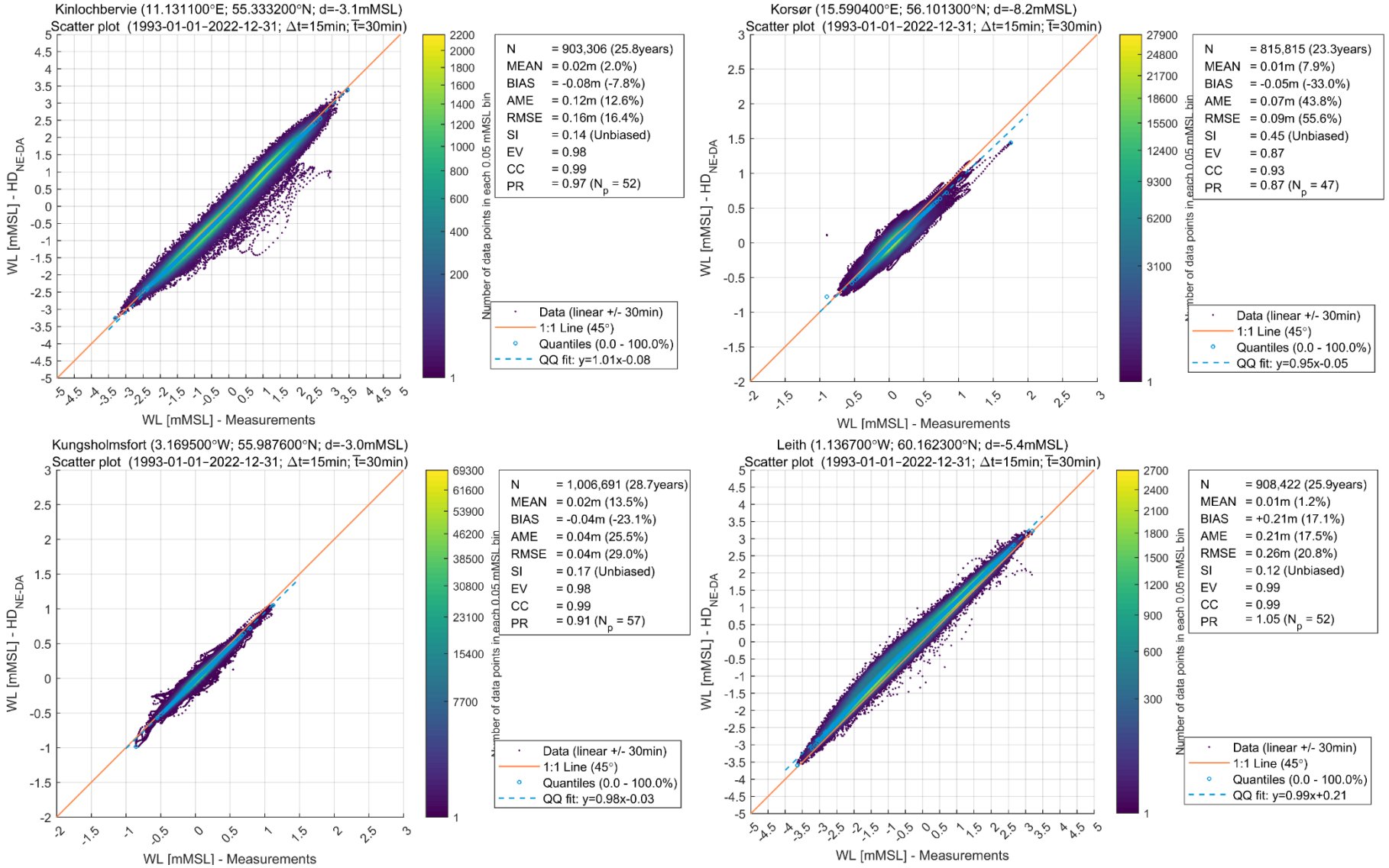
Kinlochbervie (11.131100°E; 55.333200°N; d=-3.1mMSL)
Scatter plot (1993-01-01-2022-12-31; Δt=15min; T̄=30min)
WL [mMSL] - HD_NE-DA
WL [mMSL] - Measurements
Number of data points in each 0.05 mMSL bin
N = 903,306 (25.8years)
MEAN = 0.02m (2.0%)
BIAS = -0.08m (-7.8%)
AME = 0.12m (12.6%)
RMSE = 0.16m (16.4%)
SI = 0.14 (Unbiased)
EV = 0.98
CC = 0.99
PR = 0.97 (N_p = 52)
Data (linear +/- 30min)
1:1 Line (45°)
Quantiles (0.0 - 100.0%)
QQ fit: y=1.01x-0.08
Korsør (15.590400°E; 56.101300°N; d=-8.2mMSL)
Scatter plot (1993-01-01-2022-12-31; Δt=15min; T̄=30min)
WL [mMSL] - HD_NE-DA
WL [mMSL] - Measurements
Number of data points in each 0.05 mMSL bin
N = 815,815 (23.3years)
MEAN = 0.01m (7.9%)
BIAS = -0.05m (-33.0%)
AME = 0.07m (43.8%)
RMSE = 0.09m (55.6%)
SI = 0.45 (Unbiased)
EV = 0.87
CC = 0.93
PR = 0.87 (N_p = 47)
Data (linear +/- 30min)
1:1 Line (45°)
Quantiles (0.0 - 100.0%)
QQ fit: y=0.95x-0.05
Kungsholmsfort (3.169500°W; 55.987600°N; d=-3.0mMSL)
Scatter plot (1993-01-01-2022-12-31; Δt=15min; T̄=30min)
WL [mMSL] - HD_NE-DA
WL [mMSL] - Measurements
Number of data points in each 0.05 mMSL bin
N = 1,006,691 (28.7years)
MEAN = 0.02m (13.5%)
BIAS = -0.04m (-23.1%)
AME = 0.04m (25.5%)
RMSE = 0.04m (29.0%)
SI = 0.17 (Unbiased)
EV = 0.98
CC = 0.99
PR = 0.91 (N_p = 57)
Data (linear +/- 30min)
1:1 Line (45°)
Quantiles (0.0 - 100.0%)
QQ fit: y=0.98x-0.03
Leith (1.136700°W; 60.162300°N; d=-5.4mMSL)
Scatter plot (1993-01-01-2022-12-31; Δt=15min; T̄=30min)
WL [mMSL] - HD_NE-DA
WL [mMSL] - Measurements
Number of data points in each 0.05 mMSL bin
N = 908,422 (25.9years)
MEAN = 0.01m (1.2%)
BIAS = +0.21m (17.1%)
AME = 0.21m (17.5%)
RMSE = 0.26m (20.8%)
SI = 0.12 (Unbiased)
EV = 0.99
CC = 0.99
PR = 1.05 (N_p = 52)
Data (linear +/- 30min)
1:1 Line (45°)
Quantiles (0.0 - 100.0%)
QQ fit: y=0.99x+0.21

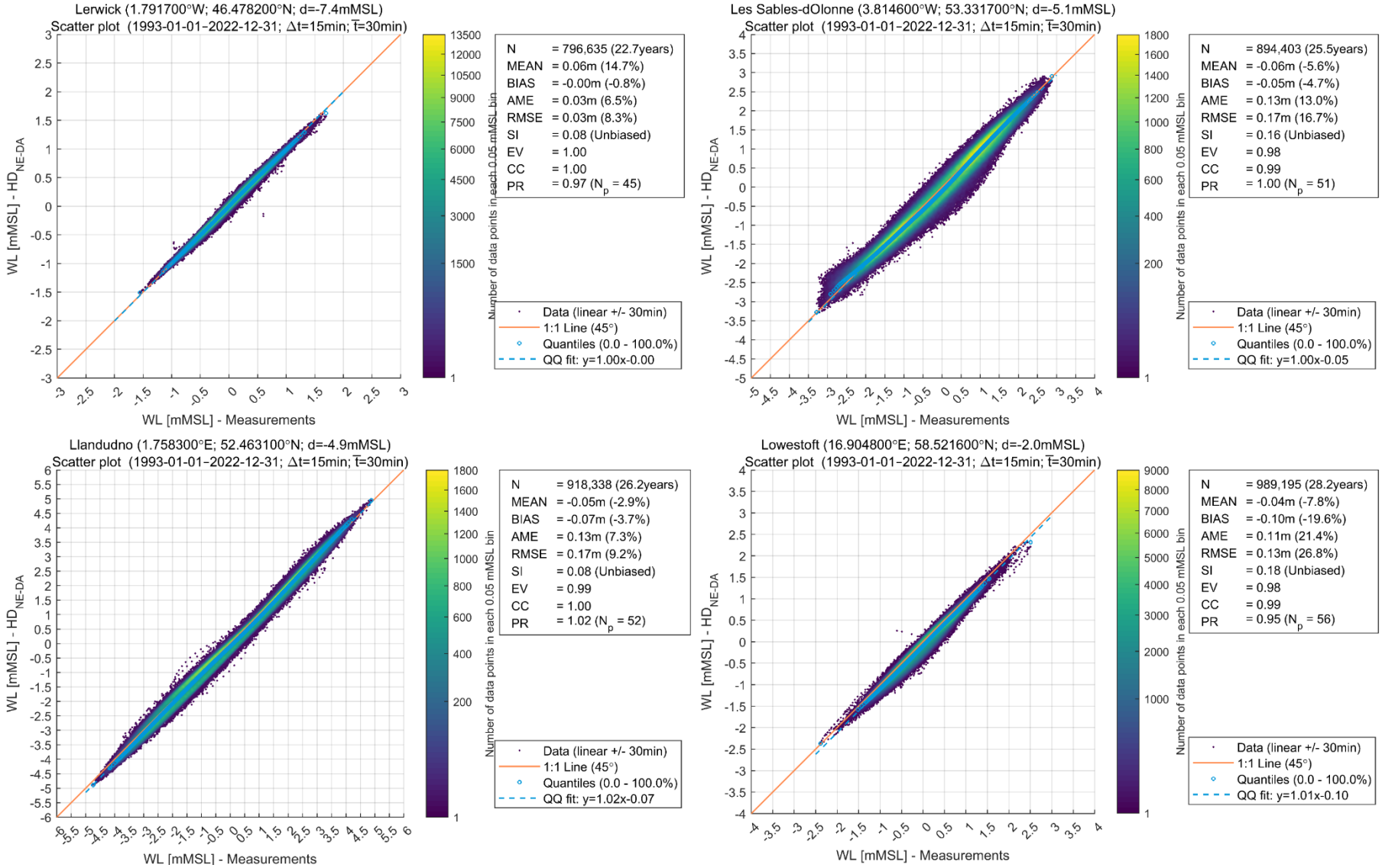
Lerwick (1.791700°W; 46.478200°N; d=-7.4mMSL)
Scatter plot (1993-01-01-2022-12-31; Δt=15min; t̄=30min)
WL [mMSL] - HD_NE-DA
WL [mMSL] - Measurements
Number of data points in each 0.05 mMSL bin
N = 796,635 (22.7years)
MEAN = 0.06m (14.7%)
BIAS = -0.00m (-0.8%)
AME = 0.03m (6.5%)
RMSE = 0.03m (8.3%)
SI = 0.08 (Unbiased)
EV = 1.00
CC = 1.00
PR = 0.97 (N_p = 45)
Data (linear +/- 30min)
1:1 Line (45°)
Quantiles (0.0 - 100.0%)
QQ fit: y=1.00x-0.00
Les Sables-dOlonne (3.814600°W; 53.331700°N; d=-5.1mMSL)
Scatter plot (1993-01-01-2022-12-31; Δt=15min; t̄=30min)
WL [mMSL] - HD_NE-DA
WL [mMSL] - Measurements
Number of data points in each 0.05 mMSL bin
N = 894,403 (25.5years)
MEAN = -0.06m (-5.6%)
BIAS = -0.05m (-4.7%)
AME = 0.13m (13.0%)
RMSE = 0.17m (16.7%)
SI = 0.16 (Unbiased)
EV = 0.98
CC = 0.99
PR = 1.00 (N_p = 51)
Data (linear +/- 30min)
1:1 Line (45°)
Quantiles (0.0 - 100.0%)
QQ fit: y=1.00x-0.05
Llandudno (1.758300°E; 52.463100°N; d=-4.9mMSL)
Scatter plot (1993-01-01-2022-12-31; Δt=15min; t̄=30min)
WL [mMSL] - HD_NE-DA
WL [mMSL] - Measurements
Number of data points in each 0.05 mMSL bin
N = 918,338 (26.2years)
MEAN = -0.05m (-2.9%)
BIAS = -0.07m (-3.7%)
AME = 0.13m (7.3%)
RMSE = 0.17m (9.2%)
SI = 0.08 (Unbiased)
EV = 0.99
CC = 1.00
PR = 1.02 (N_p = 52)
Data (linear +/- 30min)
1:1 Line (45°)
Quantiles (0.0 - 100.0%)
QQ fit: y=1.02x-0.07
Lowestoft (16.904800°E; 58.521600°N; d=-2.0mMSL)
Scatter plot (1993-01-01-2022-12-31; Δt=15min; t̄=30min)
WL [mMSL] - HD_NE-DA
WL [mMSL] - Measurements
Number of data points in each 0.05 mMSL bin
N = 989,195 (28.2years)
MEAN = -0.04m (-7.8%)
BIAS = -0.10m (-19.6%)
AME = 0.11m (21.4%)
RMSE = 0.13m (26.8%)
SI = 0.18 (Unbiased)
EV = 0.98
CC = 0.99
PR = 0.95 (N_p = 56)
Data (linear +/- 30min)
1:1 Line (45°)
Quantiles (0.0 - 100.0%)
QQ fit: y=1.01x-0.10

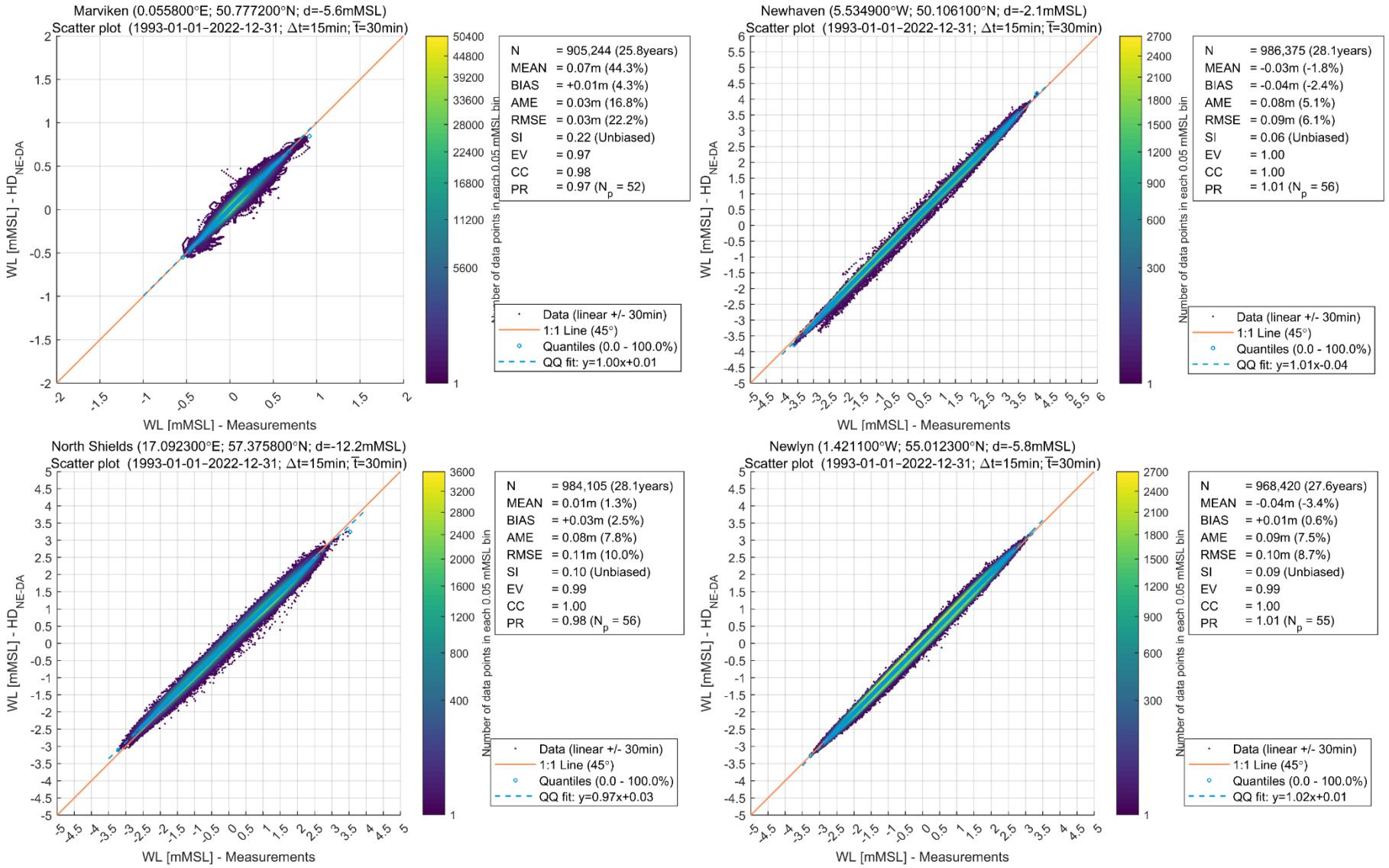
Marviken (0.055800°E; 50.777200°N; d=-5.6mMSL)
Scatter plot (1993-01-01-2022-12-31; Δt=15min; T̄=30min)
WL [mMSL] - HD_NE-DA
WL [mMSL] - Measurements
Number of data points in each 0.05 mMSL bin
N = 905,244 (25.8years)
MEAN = 0.07m (44.3%)
BIAS = +0.01m (4.3%)
AME = 0.03m (16.8%)
RMSE = 0.03m (22.2%)
SI = 0.22 (Unbiased)
EV = 0.97
CC = 0.98
PR = 0.97 (N_p = 52)
Data (linear +/- 30min)
1:1 Line (45°)
Quantiles (0.0 - 100.0%)
QQ fit: y=1.00x+0.01
Newhaven (5.534900°W; 50.106100°N; d=-2.1mMSL)
Scatter plot (1993-01-01-2022-12-31; Δt=15min; T̄=30min)
WL [mMSL] - HD_NE-DA
WL [mMSL] - Measurements
Number of data points in each 0.05 mMSL bin
N = 986,375 (28.1years)
MEAN = -0.03m (-1.8%)
BIAS = -0.04m (-2.4%)
AME = 0.08m (5.1%)
RMSE = 0.09m (6.1%)
SI = 0.06 (Unbiased)
EV = 1.00
CC = 1.00
PR = 1.01 (N_p = 56)
Data (linear +/- 30min)
1:1 Line (45°)
Quantiles (0.0 - 100.0%)
QQ fit: y=1.01x-0.04
North Shields (17.092300°E; 57.375800°N; d=-12.2mMSL)
Scatter plot (1993-01-01-2022-12-31; Δt=15min; T̄=30min)
WL [mMSL] - HD_NE-DA
WL [mMSL] - Measurements
Number of data points in each 0.05 mMSL bin
N = 984,105 (28.1years)
MEAN = 0.01m (1.3%)
BIAS = +0.03m (2.5%)
AME = 0.08m (7.8%)
RMSE = 0.11m (10.0%)
SI = 0.10 (Unbiased)
EV = 0.99
CC = 1.00
PR = 0.98 (N_p = 56)
Data (linear +/- 30min)
1:1 Line (45°)
Quantiles (0.0 - 100.0%)
QQ fit: y=0.97x+0.03
Newlyn (1.421100°W; 55.012300°N; d=-5.8mMSL)
Scatter plot (1993-01-01-2022-12-31; Δt=15min; T̄=30min)
WL [mMSL] - HD_NE-DA
WL [mMSL] - Measurements
Number of data points in each 0.05 mMSL bin
N = 968,420 (27.6years)
MEAN = -0.04m (-3.4%)
BIAS = +0.01m (0.6%)
AME = 0.09m (7.5%)
RMSE = 0.10m (8.7%)
SI = 0.09 (Unbiased)
EV = 0.99
CC = 1.00
PR = 1.01 (N_p = 55)
Data (linear +/- 30min)
1:1 Line (45°)
Quantiles (0.0 - 100.0%)
QQ fit: y=1.02x+0.01

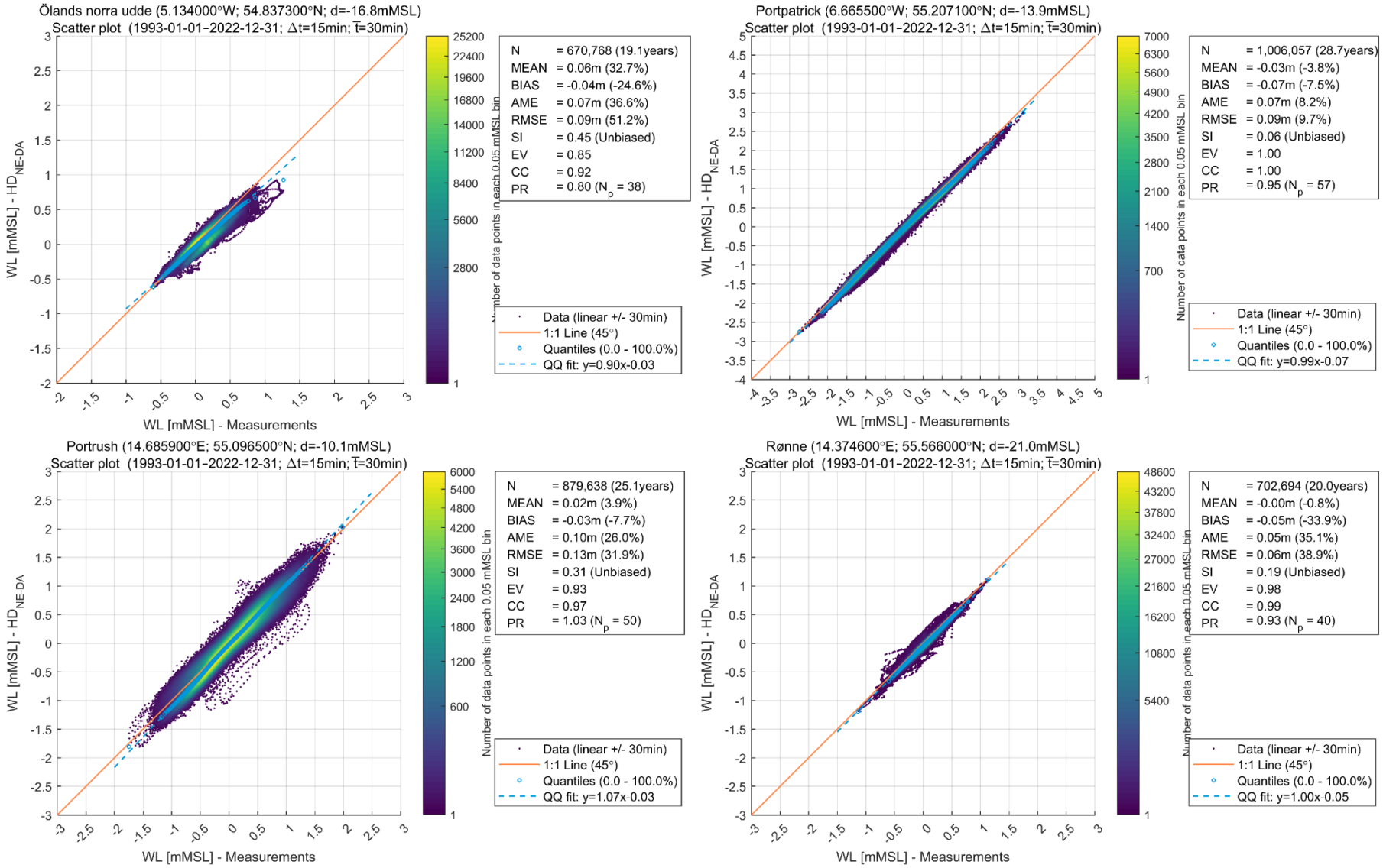
Ölands norra udde (5.134000°W; 54.837300°N; d=-16.8mMSL)
Scatter plot (1993-01-01-2022-12-31; Δt=15min; t̄=30min)
WL [mMSL] - HD_NE-DA
WL [mMSL] - Measurements
Number of data points in each 0.05 mMSL bin
N = 670,768 (19.1years)
MEAN = 0.06m (32.7%)
BIAS = -0.04m (-24.6%)
AME = 0.07m (36.6%)
RMSE = 0.09m (51.2%)
SI = 0.45 (Unbiased)
EV = 0.85
CC = 0.92
PR = 0.80 (N_p = 38)
Data (linear +/- 30min)
1:1 Line (45°)
Quantiles (0.0 - 100.0%)
QQ fit: y=0.90x-0.03
Portpatrick (6.665500°W; 55.207100°N; d=-13.9mMSL)
Scatter plot (1993-01-01-2022-12-31; Δt=15min; t̄=30min)
WL [mMSL] - HD_NE-DA
WL [mMSL] - Measurements
Number of data points in each 0.05 mMSL bin
N = 1,006,057 (28.7years)
MEAN = -0.03m (-3.8%)
BIAS = -0.07m (-7.5%)
AME = 0.07m (8.2%)
RMSE = 0.09m (9.7%)
SI = 0.06 (Unbiased)
EV = 1.00
CC = 1.00
PR = 0.95 (N_p = 57)
Data (linear +/- 30min)
1:1 Line (45°)
Quantiles (0.0 - 100.0%)
QQ fit: y=0.99x-0.07
Portrush (14.685900°E; 55.096500°N; d=-10.1mMSL)
Scatter plot (1993-01-01-2022-12-31; Δt=15min; t̄=30min)
WL [mMSL] - HD_NE-DA
WL [mMSL] - Measurements
Number of data points in each 0.05 mMSL bin
N = 879,638 (25.1years)
MEAN = 0.02m (3.9%)
BIAS = -0.03m (-7.7%)
AME = 0.10m (26.0%)
RMSE = 0.13m (31.9%)
SI = 0.31 (Unbiased)
EV = 0.93
CC = 0.97
PR = 1.03 (N_p = 50)
Data (linear +/- 30min)
1:1 Line (45°)
Quantiles (0.0 - 100.0%)
QQ fit: y=1.07x-0.03
Rønne (14.374600°E; 55.566000°N; d=-21.0mMSL)
Scatter plot (1993-01-01-2022-12-31; Δt=15min; t̄=30min)
WL [mMSL] - HD_NE-DA
WL [mMSL] - Measurements
Number of data points in each 0.05 mMSL bin
N = 702,694 (20.0years)
MEAN = -0.00m (-0.8%)
BIAS = -0.05m (-33.9%)
AME = 0.05m (35.1%)
RMSE = 0.06m (38.9%)
SI = 0.19 (Unbiased)
EV = 0.98
CC = 0.99
PR = 0.93 (N_p = 40)
Data (linear +/- 30min)
1:1 Line (45°)
Quantiles (0.0 - 100.0%)
QQ fit: y=1.00x-0.05

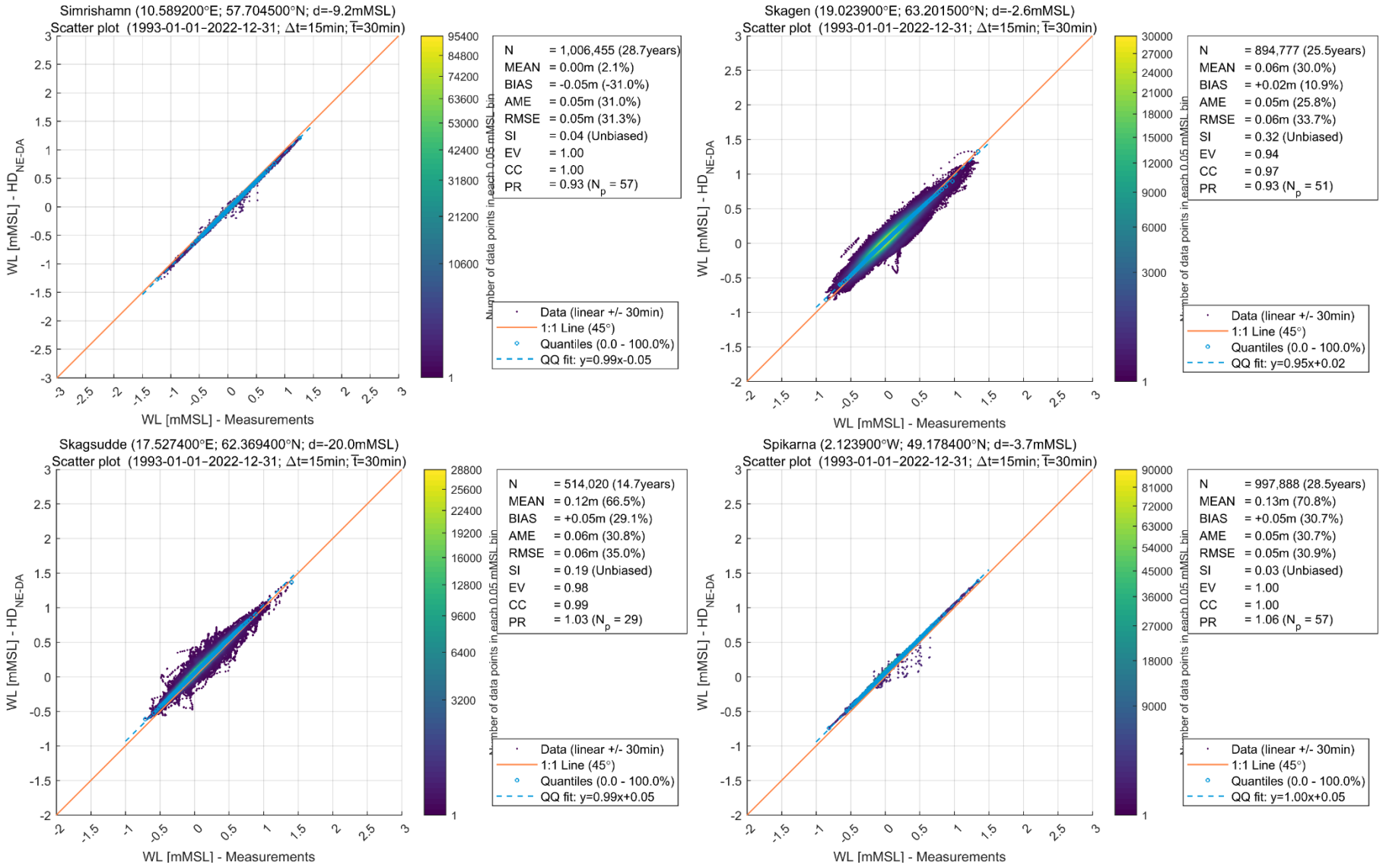
Simrishamn (10.589200°E; 57.704500°N; d=-9.2mSL)
Scatter plot (1993-01-01-2022-12-31; Δt=15min; T̄=30min)
WL [mMSL] - HD_NE-DA
WL [mMSL] - Measurements
Number of data points in each 0.05 mMSL bin
N = 1,006,455 (28.7years)
MEAN = 0.00m (2.1%)
BIAS = -0.05m (-31.0%)
AME = 0.05m (31.0%)
RMSE = 0.05m (31.3%)
SI = 0.04 (Unbiased)
EV = 1.00
CC = 1.00
PR = 0.93 (Np = 57)
Data (linear +/- 30min)
1:1 Line (45°)
Quantiles (0.0 - 100.0%)
QQ fit: y=0.99x-0.05
Skagen (19.023900°E; 63.201500°N; d=-2.6mSL)
Scatter plot (1993-01-01-2022-12-31; Δt=15min; T̄=30min)
WL [mMSL] - HD_NE-DA
WL [mMSL] - Measurements
Number of data points in each 0.05 mMSL bin
N = 894,777 (25.5years)
MEAN = 0.06m (30.0%)
BIAS = +0.02m (10.9%)
AME = 0.05m (25.8%)
RMSE = 0.06m (33.7%)
SI = 0.32 (Unbiased)
EV = 0.94
CC = 0.97
PR = 0.93 (Np = 51)
Data (linear +/- 30min)
1:1 Line (45°)
Quantiles (0.0 - 100.0%)
QQ fit: y=0.95x+0.02
Skagsudde (17.527400°E; 62.369400°N; d=-20.0mSL)
Scatter plot (1993-01-01-2022-12-31; Δt=15min; T̄=30min)
WL [mMSL] - HD_NE-DA
WL [mMSL] - Measurements
Number of data points in each 0.05 mMSL bin
N = 514,020 (14.7years)
MEAN = 0.12m (66.5%)
BIAS = +0.05m (29.1%)
AME = 0.06m (30.8%)
RMSE = 0.06m (35.0%)
SI = 0.19 (Unbiased)
EV = 0.98
CC = 0.99
PR = 1.03 (Np = 29)
Data (linear +/- 30min)
1:1 Line (45°)
Quantiles (0.0 - 100.0%)
QQ fit: y=0.99x+0.05
Spikarna (2.123900°W; 49.178400°N; d=-3.7mSL)
Scatter plot (1993-01-01-2022-12-31; Δt=15min; T̄=30min)
WL [mMSL] - HD_NE-DA
WL [mMSL] - Measurements
Number of data points in each 0.05 mMSL bin
N = 997,888 (28.5years)
MEAN = 0.13m (70.8%)
BIAS = +0.05m (30.7%)
AME = 0.05m (30.7%)
RMSE = 0.05m (30.9%)
SI = 0.03 (Unbiased)
EV = 1.00
CC = 1.00
PR = 1.06 (Np = 57)
Data (linear +/- 30min)
1:1 Line (45°)
Quantiles (0.0 - 100.0%)
QQ fit: y=1.00x+0.05

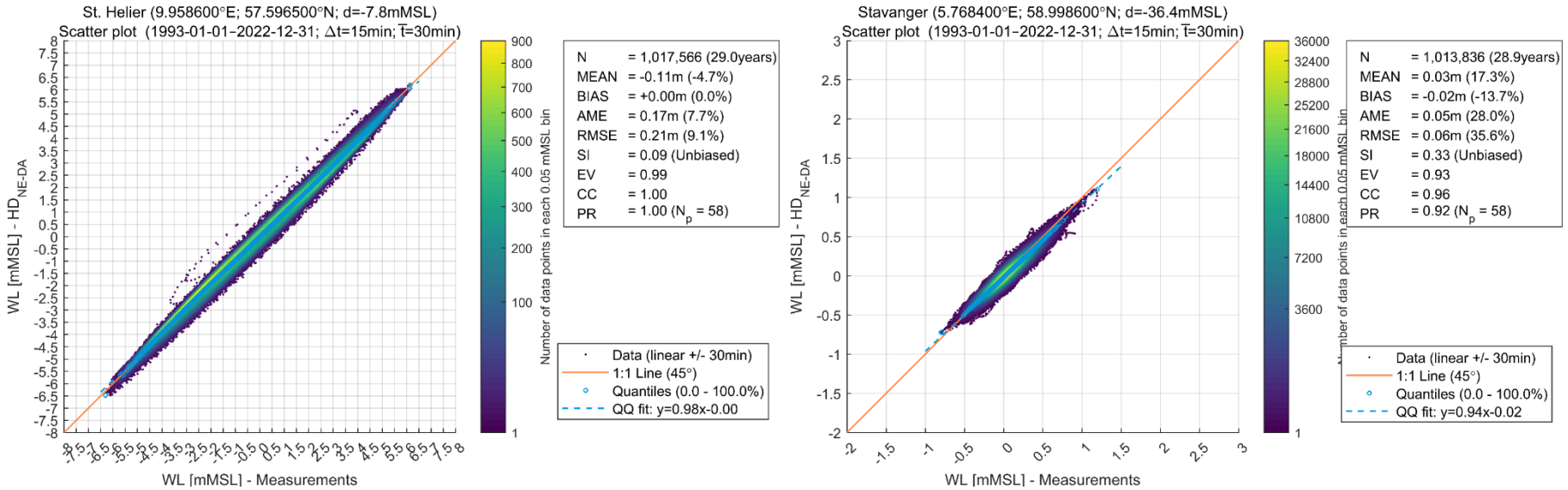
St. Helier (9.958600°E; 57.596500°N; d=-7.8mMSL)
Scatter plot (1993-01-01-2022-12-31; Δt=15min; t̄=30min)
WL [mMSL] - HD NE-DA
WL [mMSL] - Measurements
Number of data points in each 0.05 mMSL bin
N = 1,017,566 (29.0years)
MEAN = -0.11m (-4.7%)
BIAS = +0.00m (0.0%)
AME = 0.17m (7.7%)
RMSE = 0.21m (9.1%)
SI = 0.09 (Unbiased)
EV = 0.99
CC = 1.00
PR = 1.00 (Np = 58)
Data (linear +/- 30min)
1:1 Line (45°)
Quantiles (0.0 - 100.0%)
QQ fit: y=0.98x-0.00
Stavanger (5.768400°E; 58.998600°N; d=-36.4mMSL)
Scatter plot (1993-01-01-2022-12-31; Δt=15min; t̄=30min)
WL [mMSL] - HD NE-DA
WL [mMSL] - Measurements
Number of data points in each 0.05 mMSL bin
N = 1,013,836 (28.9years)
MEAN = 0.03m (17.3%)
BIAS = -0.02m (-13.7%)
AME = 0.05m (28.0%)
RMSE = 0.06m (35.6%)
SI = 0.33 (Unbiased)
EV = 0.93
CC = 0.96
PR = 0.92 (Np = 58)
Data (linear +/- 30min)
1:1 Line (45°)
Quantiles (0.0 - 100.0%)
QQ fit: y=0.94x-0.02
Terschelling Noordzee (5.334700°E; 53.441500°N; d=-9.2mMSL)
Scatter plot (1993-01-01-2022-12-31; Δt=15min; t̄=30min)
WL [mMSL] - HD NE-DA
WL [mMSL] - Measurements
Number of data points in each 0.05 mMSL bin
N = 1,005,710 (28.7years)
MEAN = 0.07m (10.8%)
BIAS = -0.03m (-4.4%)
AME = 0.09m (14.2%)
RMSE = 0.11m (17.5%)
SI = 0.17 (Unbiased)
EV = 0.98
CC = 0.99
PR = 0.97 (Np = 57)
Data (linear +/- 30min)
1:1 Line (45°)
Quantiles (0.0 - 100.0%)
QQ fit: y=0.95x-0.02
Texel Nordzee (4.736900°E; 53.124900°N; d=-9.3mMSL)
Scatter plot (1993-01-01-2022-12-31; Δt=15min; t̄=30min)
WL [mMSL] - HD NE-DA
WL [mMSL] - Measurements
Number of data points in each 0.05 mMSL bin
N = 953,837 (27.2years)
MEAN = 0.08m (13.3%)
BIAS = -0.04m (-6.5%)
AME = 0.07m (12.3%)
RMSE = 0.09m (15.6%)
SI = 0.14 (Unbiased)
EV = 0.98
CC = 0.99
PR = 1.00 (Np = 54)
Data (linear +/- 30min)
1:1 Line (45°)
Quantiles (0.0 - 100.0%)
QQ fit: y=0.98x-0.04

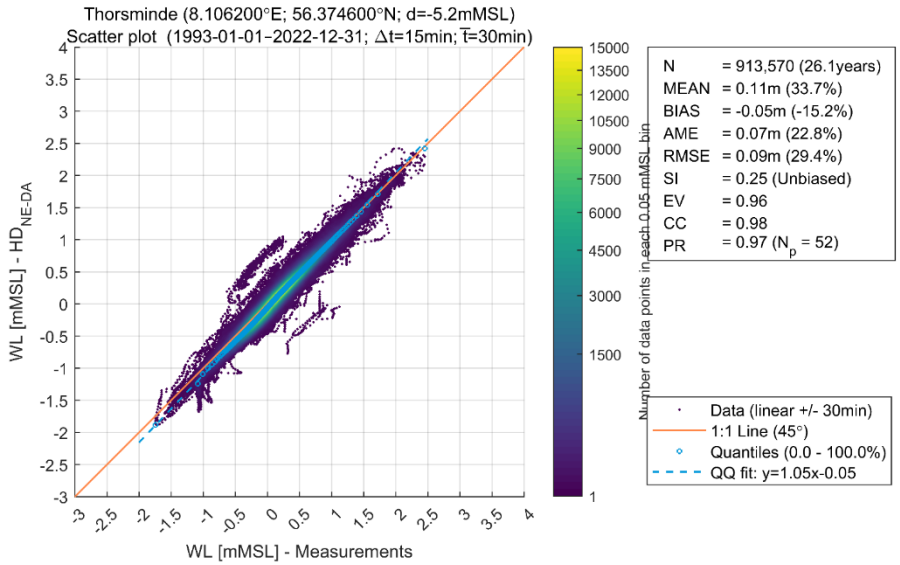
Thorsminde (8.106200°E; 56.374600°N; d=-5.2mMSL)
Scatter plot (1993-01-01-2022-12-31; Δt=15min; t̄=30min)
WL [mMSL] - HD_NE-DA
WL [mMSL] - Measurements
Number of data points in each 0.05 mMSL bin
N = 913,570 (26.1years)
MEAN = 0.11m (33.7%)
BIAS = -0.05m (-15.2%)
AME = 0.07m (22.8%)
RMSE = 0.09m (29.4%)
SI = 0.25 (Unbiased)
EV = 0.96
CC = 0.98
PR = 0.97 (N_p = 52)
Data (linear +/- 30min)
1:1 Line (45°)
Quantiles (0.0 - 100.0%)
QQ fit: y=1.05x-0.05

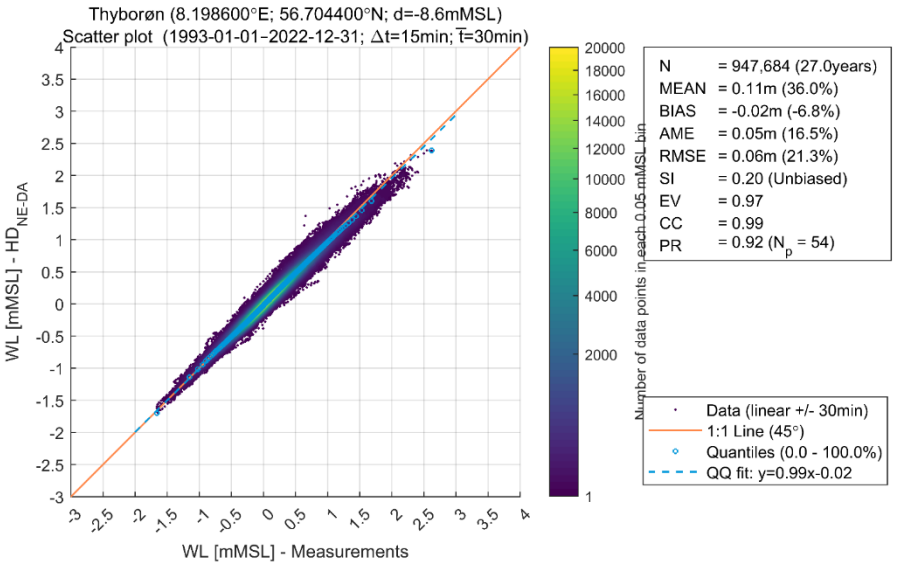
Thyborøn (8.198600°E; 56.704400°N; d=-8.6mMSL)
Scatter plot (1993-01-01-2022-12-31; Δt=15min; t̄=30min)
WL [mMSL] - HD_NE-DA
WL [mMSL] - Measurements
Number of data points in each 0.05 mMSL bin
N = 947,684 (27.0years)
MEAN = 0.11m (36.0%)
BIAS = -0.02m (-6.8%)
AME = 0.05m (16.5%)
RMSE = 0.06m (21.3%)
SI = 0.20 (Unbiased)
EV = 0.97
CC = 0.99
PR = 0.92 (N_p = 54)
Data (linear +/- 30min)
1:1 Line (45°)
Quantiles (0.0 - 100.0%)
QQ fit: y=0.99x-0.02

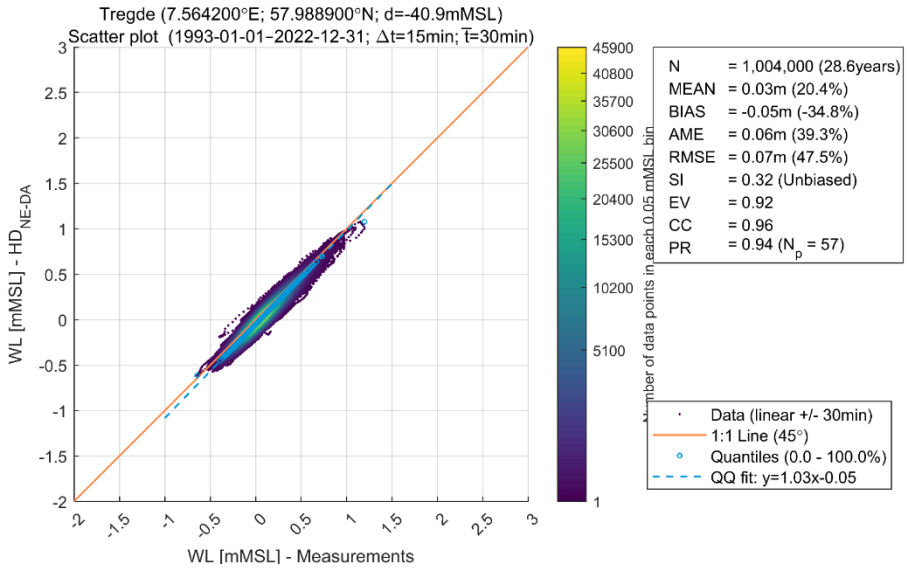
Tregde (7.564200°E; 57.988900°N; d=-40.9mMSL)
Scatter plot (1993-01-01-2022-12-31; Δt=15min; t̄=30min)
WL [mMSL] - HD_NE-DA
WL [mMSL] - Measurements
Number of data points in each 0.05 mMSL bin
N = 1,004,000 (28.6years)
MEAN = 0.03m (20.4%)
BIAS = -0.05m (-34.8%)
AME = 0.06m (39.3%)
RMSE = 0.07m (47.5%)
SI = 0.32 (Unbiased)
EV = 0.92
CC = 0.96
PR = 0.94 (N_p = 57)
Data (linear +/- 30min)
1:1 Line (45°)
Quantiles (0.0 - 100.0%)
QQ fit: y=1.03x-0.05

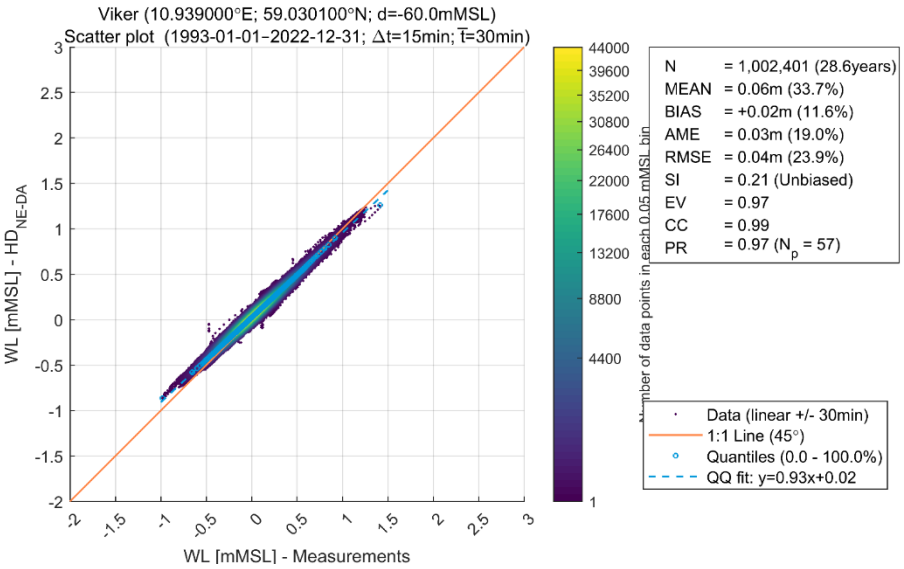
Viker (10.939000°E; 59.030100°N; d=-60.0mMSL)
Scatter plot (1993-01-01-2022-12-31; Δt=15min; t̄=30min)
WL [mMSL] - HD_NE-DA
WL [mMSL] - Measurements
Number of data points in each 0.05 mMSL bin
N = 1,002,401 (28.6years)
MEAN = 0.06m (33.7%)
BIAS = +0.02m (11.6%)
AME = 0.03m (19.0%)
RMSE = 0.04m (23.9%)
SI = 0.21 (Unbiased)
EV = 0.97
CC = 0.99
PR = 0.97 (N_p = 57)
Data (linear +/- 30min)
1:1 Line (45°)
Quantiles (0.0 - 100.0%)
QQ fit: y=0.93x+0.02

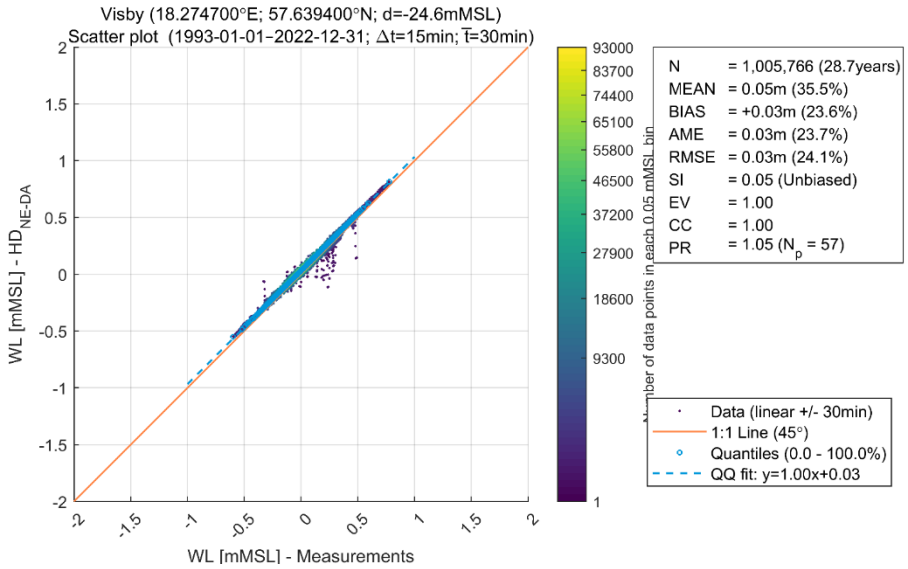
Visby (18.274700°E; 57.639400°N; d=-24.6mMSL)
Scatter plot (1993-01-01-2022-12-31; Δt=15min; t̄=30min)
WL [mMSL] - HD_NE-DA
WL [mMSL] - Measurements
Number of data points in each 0.05 mMSL bin
N = 1,005,766 (28.7years)
MEAN = 0.05m (35.5%)
BIAS = +0.03m (23.6%)
AME = 0.03m (23.7%)
RMSE = 0.03m (24.1%)
SI = 0.05 (Unbiased)
EV = 1.00
CC = 1.00
PR = 1.05 (N_p = 57)
Data (linear +/- 30min)
1:1 Line (45°)
Quantiles (0.0 - 100.0%)
QQ fit: y=1.00x+0.03

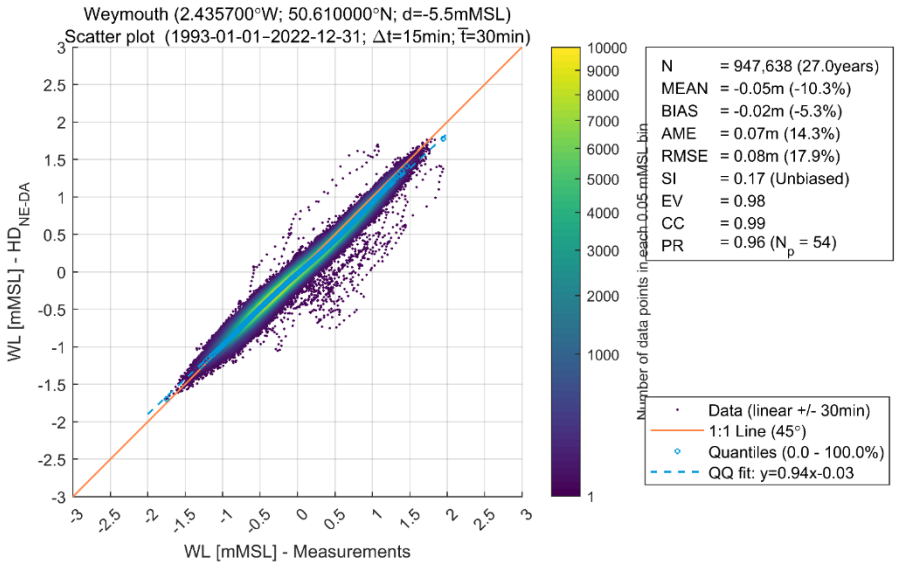
Weymouth (2.435700°W; 50.610000°N; d=-5.5mMSL)
Scatter plot (1993-01-01-2022-12-31; Δt=15min; t̄=30min)
WL [mMSL] - HD_NE-DA
WL [mMSL] - Measurements
Number of data points in each 0.05 mMSL bin
N = 947,638 (27.0years)
MEAN = -0.05m (-10.3%)
BIAS = -0.02m (-5.3%)
AME = 0.07m (14.3%)
RMSE = 0.08m (17.9%)
SI = 0.17 (Unbiased)
EV = 0.98
CC = 0.99
PR = 0.96 (N_p = 54)
Data (linear +/- 30min)
1:1 Line (45°)
Quantiles (0.0 - 100.0%)
QQ fit: y=0.94x-0.03

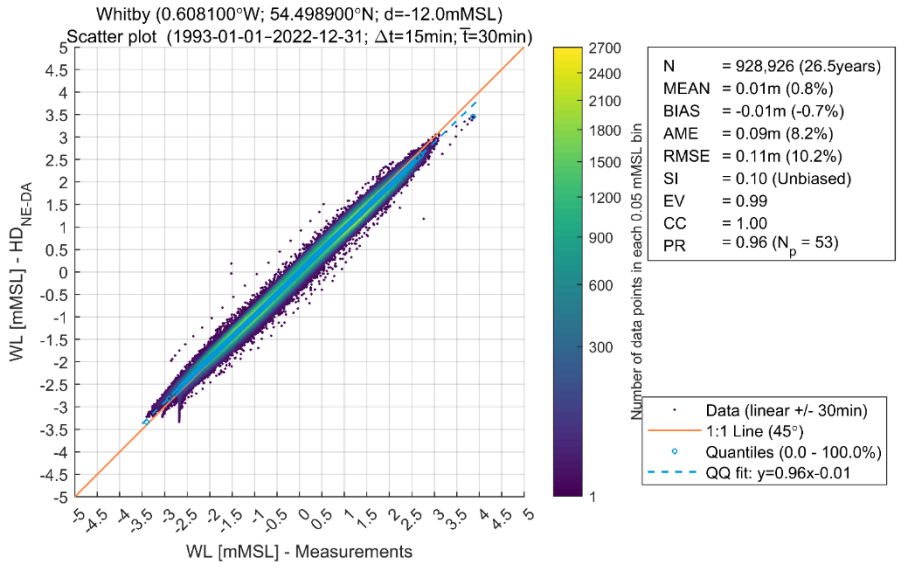
Whitby (0.608100°W; 54.498900°N; d=-12.0mMSL)
Scatter plot (1993-01-01-2022-12-31; Δt=15min; t̄=30min)
WL [mMSL] - HD_NE-DA
WL [mMSL] - Measurements
Number of data points in each 0.05 mMSL bin
N = 928,926 (26.5years)
MEAN = 0.01m (0.8%)
BIAS = -0.01m (-0.7%)
AME = 0.09m (8.2%)
RMSE = 0.11m (10.2%)
SI = 0.10 (Unbiased)
EV = 0.99
CC = 1.00
PR = 0.96 (N_p = 53)
Data (linear +/- 30min)
1:1 Line (45°)
Quantiles (0.0 - 100.0%)
QQ fit: y=0.96x-0.01

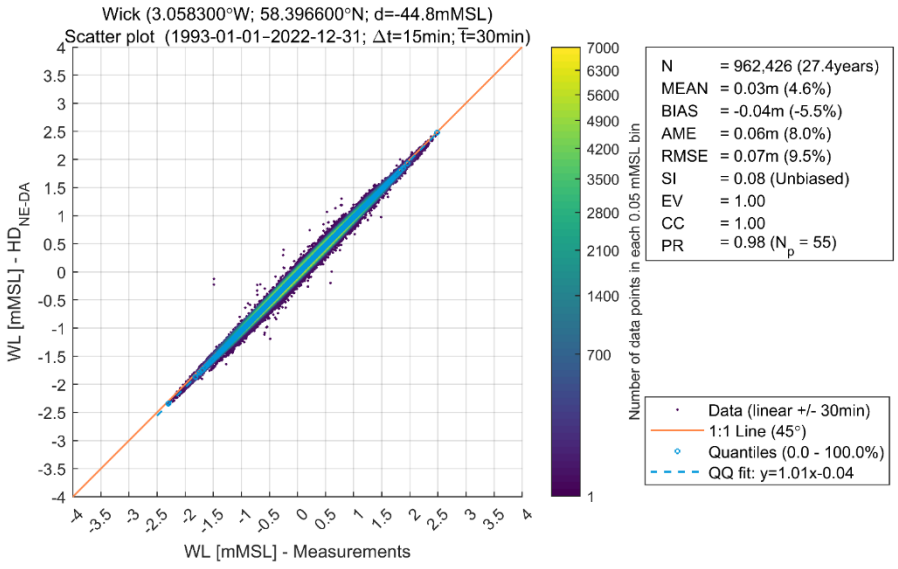
Wick (3.058300°W; 58.396600°N; d=-44.8mMSL)
Scatter plot (1993-01-01-2022-12-31; Δt=15min; t̄=30min)
WL [mMSL] - HD_NE-DA
WL [mMSL] - Measurements
Number of data points in each 0.05 mMSL bin
N = 962,426 (27.4years)
MEAN = 0.03m (4.6%)
BIAS = -0.04m (-5.5%)
AME = 0.06m (8.0%)
RMSE = 0.07m (9.5%)
SI = 0.08 (Unbiased)
EV = 1.00
CC = 1.00
PR = 0.98 (N_p = 55)
Data (linear +/- 30min)
1:1 Line (45°)
Quantiles (0.0 - 100.0%)
QQ fit: y=1.01x-0.04

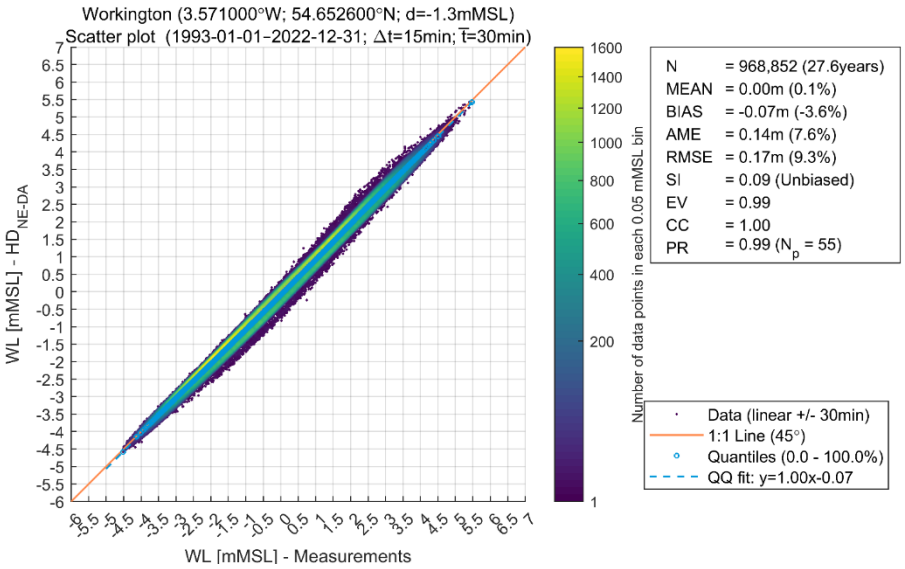
Workington (3.571000°W; 54.652600°N; d=-1.3mMSL)
Scatter plot (1993-01-01-2022-12-31; Δt=15min; T=30min)
WL [mMSL] - HD NE-DA
WL [mMSL] - Measurements
Number of data points in each 0.05 mMSL bin
N = 968,852 (27.6years)
MEAN = 0.00m (0.1%)
BIAS = -0.07m (-3.6%)
AME = 0.14m (7.6%)
RMSE = 0.17m (9.3%)
SI = 0.09 (Unbiased)
EV = 0.99
CC = 1.00
PR = 0.99 (N p = 55)
Data (linear +/- 30min)
1:1 Line (45°)
Quantiles (0.0 - 100.0%)
QQ fit: y=1.00x-0.07

This investigation was carried out by DHI Consortium, commissioned by RVO, an agency of the Ministry of Economic Affairs and Climate Policy.

The information in this document is valid at the time of publishing (see month/year). Updates will be published on the website https://offshorewind.rvo.nl, at the relevant sitemap, General Information, submap Revision Log and Q&A. In the Revision Log is indicated which versions are the latest and what the changes are in relation to previous versions. The documents can be found at the relevant sites, indicated in the List of all reports and deliverables.

Contacts
Netherlands Enterprise Agency (RVO)
Graadt van Roggenweg 200 | 3531 AH | Utrecht
P.O. Box 8242 | 3503 RE | Utrecht
www.rvo.nl / https://english.rvo.nl

Netherlands Enterprise Agency (RVO) | December 2023